Chapter 7

Liquid Scintillation Analysis: Principles and Practice

Michael F. L'Annunziata
The Montague Group, P.O. Box 5033, Oceanside, CA 92052-5033, USA

Michael J. Kessler[1]

Chapter Outline

[1] This chapter is dedicated to the memory of Michael J. Kessler, who contributed to the First Edition of the Handbook of Radioactivity Analysis in 1997 and provided the author with much encouragement during the preparation of that First Edition. His sudden passing in April of 1997 was a great loss to all who knew him and to the world scientific community. He was a dear friend and esteemed colleague.

Handbook of Radioactivity Analysis. DOI: http://dx.doi.org/10.1016/B978-0-12-384873-4.00007-4

I. INTRODUCTION

Liquid scintillation counting (LSC) or liquid scintillation analysis (LSA) has been a very popular technique for the detection and quantitative measurement of radioactivity since the early l950s. The technique has been most useful in studies of the life sciences and the environment, and it is also a powerful tool in the chemical and physical sciences. Many of the principles of liquid scintillation analysis overlap into the fields of low-level environmental radioactivity monitoring, the detection of singular decay events in basic nuclear physics, and the measurement of higher levels of radioactivity used in research, radioisotope applications, and nuclear power. However, the techniques and principles used in the LSA of environmental radioactivity *per se* will not be covered in detail in this chapter. The reader is directed to Chapter 9 for additional information on the use of LSA for the measurement of either natural levels of radionuclides or low-levels of man-made radionuclides found in the environment.

Applications of liquid scintillation analysis to the measurement of radionuclides used as tracers in research has led to a large number of cutting-edge and Nobel-prize-winning discoveries in the life sciences over the past 50 years. The LSA technique in scientific research remains one of the most popular experimental tools used for the quantitative analysis of radionuclides. These include principally the analysis of alpha- and beta-particle-emitting nuclides, and may also include nuclides that emit gamma radiation, as well as atoms that decay with the emission of X-radiation, and those that emit Auger and internal conversion electrons. Included in this chapter are also advances that continue to be made in the application of liquid scintillation to the analysis of neutrons, and the discrimination of neutron and gamma radiation, the analysis of high-energy charged particles, and the detection and measurement of unique events, such as π^+ decay, μ^+ decay, $\beta\beta$ decay, and the detection of neutrinos.

Some advances in the use of liquid scintillation analysis in the standardization of radionuclides will be included in this chapter. A more comprehensive treatment of radionuclide standardization by means of all available radiation detection and measurement methods will be included in Chapter 14.

The wide popularity of liquid scintillation analysis is a consequence of numerous advantages, which are high efficiencies of detection, improvements in sample preparation techniques, automation including computer data processing, and the spectrometer capability of liquid scintillation analyzers permitting the simultaneous assay of different radionuclides.

II. BASIC THEORY

A. Scintillation Process

The discovery of scintillation in organic compounds was documented in a thesis by Lieselott Herforth (1948) under the leadership of Hartmut Kallmann, which is related in a historical account by Niese (2003, 1999). In her thesis presented on September 13, 1948 at the Technical University Berlin − Charlottenburg, Herforth reported that aromatic compounds could convert absorbed energy of nuclear radiation into light photons. Herforth coauthored a subsequent publication together with Kallmann and Immanuel Broser, another student of Kallmann, on the scintillation process in naphthalene (Broser et al., 1948) as well as a paper on the fluorescence from liquid (molten) naphthalene, diphenyl, and phenanthrene as a consequence of interaction with alpha particles, fast electrons, and gamma rays (Herforth and Kallmann, 1948). Both Herforth and Broser were fellow students, who had researched radioactivity counters under Hans Geiger. Herforth's thesis and publications with Kallmann were followed by papers authored by Kallmann (1950) and Reynolds et al. (1950) on liquid scintillation counting that demonstrated certain organic compounds in solution emitted fluorescent light when bombarded by nuclear radiation. The origin of liquid scintillation analysis as a technique for the quantification of radioactivity is attributed to the original papers by Kallmann and Reynolds in 1950. The fluorescence or emission of photons by organic compounds (fluors) as a result of excitation can be readily converted to a burst of electrons with the use of a photomultiplier tube (PMT), and subsequently measured as an electric pulse.

The technique of liquid scintillation counting involves placing the sample containing the radioactivity into a glass or plastic container, called a scintillation vial, and adding a special scintillation cocktail containing organic fluors dissolved into suitable solvents. Samples may also be analyzed by high-sample-throughput LSA in plastic microplates containing 24, 96, or 384 sample wells per microplate, which accept sample−fluor cocktail volumes in the range of 20−150 μL. High-sample-throughput microplate liquid scintillation counting is described in Section XIII. Common capacities of scintillation vials that can be easily accommodated in conventional automatic liquid scintillation analyzers vary from 4 to 20 mL; however, microfuge tubes of 0.5−1.5 mL capacity can also be counted directly in a conventional LSA with the use of special microtube holders.

Both plastic and glass liquid scintillation counting vials have certain advantages and disadvantages in terms of background, solvent permeability, fragility, and transparency, etc. Polyethylene plastic vials are permeable when stored containing fluor solvents such as benzene, toluene, and xylene; however, these vials do not display solvent diffusion when more environmentally safe commercial fluor cocktails are used (*e.g.*, Ultima Gold™, Pico-fluor™, and Opti-fluor™), which use diisopropylnaphthalene (DIN), pseudocumene, or linear alkylbenzene solvents. The plastic vials are also unbreakable, less expensive, and display lower backgrounds than the glass vials.

Glass vials, however, provide the advantage of transparency to visualize the sample and fluor cocktail solution to permit inspection for undesirable properties such as color, residue, or sample inhomogeneity.

The scintillation cocktail may be composed of a solvent such as DIN, or a linear alkylbenzene together with a fluor solute such as 2,5-diphenyloxazole (PPO) dissolved in a concentration of approximately 2−10 g/L. Many liquid fluor cocktails are available commercially, and these are made to be compatible and mixable with radioactive samples dissolved in either organic solvents or aqueous media. When samples are dissolved in aqueous media, three different chemical components are required in the fluor cocktail solution: the organic solvent, organic scintillator, and a surfactant (emulsifier). The choice of solvent, scintillator, and surfactant for the preparation of contemporary fluor cocktails is dictated by the need for efficient energy transfer and light output in the scintillation process even under very high aqueous sample loads exceeding 50% water as well as the need for environmentally safe solutions with low toxicity, high flash point, and low disposal costs. To meet these needs, some commercially available formulations use diisopropylnaphthalene or a linear alkylbenzene solvent. A few of these commercial fluor cocktails were noted in the previous paragraph. The properties and performance of the modern environmentally safe solvents and some of the commercially available cocktails made from these solvents have been reviewed and tested by Verrezen et al. (2008), Medeiros et al. (2003), DeVol et al. (1996), Neumann and Roessler (1991), Thomson (1991), Takiue et al. (1990a), and Elliott and van Mourik, (1987). The findings of these studies, as summarized by Verrezen et al. (2008), are that no specific liquid scintillation cocktail can be identified to fit all radioanalytical needs, and cocktail formulations are designed to provide between a performance aspect (*e.g.*, high sample load or sample compatibility) at the expense of another (*e.g.*, counting efficiency or stability). Chapter 8 provides detailed information on the composition and performance of many liquid scintillation fluor cocktails and sample preparation techniques.

Unique scintillation cocktails may be prepared to meet special detection needs, such as the detection of neutrinos, neutron/gamma discrimination, alpha/beta discrimination, and the detection of neutrinos or unique decay events, such as muon-, pion-, and double-beta decay. The characteristics of the liquid scintillation media or cocktails used for these specific detection needs are noted within the chapter.

A sample, that is to be analyzed for its radioactivity or disintegration rate, is placed into the scintillation cocktail to form a homogeneous counting solution. The liquid scintillation process that occurs in a scintillation cocktail is shown in Fig. 7.1. The first step in the process is the interaction of the radioactivity with the solvent molecules of the liquid scintillation cocktail. These solvent molecules, as seen in Fig. 7.1, are organic in nature and contain at least one aromatic ring. Because the solvent molecules are in greater concentration than the solute fluor molecules in the fluor cocktail, the solvent molecules will absorb the major portion of the nuclear radiation energy emitted by the radionuclides in the cocktail

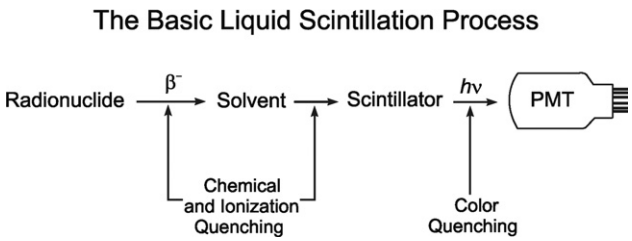

FIGURE 7.1 An illustration of the sequence of events in the basic liquid scintillation process. A radionuclide will dissipate its energy of decay (*e.g.*, β^-−particle energy) in the liquid scintillation cocktail containing solvent and fluor. The aromatic solvent absorbs most of the energy of the beta particle. The energy of excitation of the solvent is then transferred to the scintillator (fluor) molecules, which upon deexcitation emit photons of visible light. The light photons are detected by a photomultiplier tube (PMT), which converts the light photons into a flow of electrons and further amplify the current pulse. Points of interference caused by chemical, ionization, and color quench are also indicated.

solution. The result is the formation of activated organic solvent molecules, which transfer their energy to the organic scintillator or fluor, as illustrated in Fig. 7.1. Organic scintillators are chosen because they are soluble in the organic solvent, they can easily accept the energy from the activated solvent molecule, and they produce an activated or excited scintillator molecule. These excited scintillator molecules rapidly lose their energy and return to their original ground state by way of a fluorescence mechanism. The energy is released as a flash of light in the wavelength range of 375−430 nm for each radioactive decay process occurring in the fluor cocktail. The wavelength of emission depends on the scintillator dissolved in the fluor cocktail. The intensity or brightness of the light flash, that is produced, is a function of the energy and the type of nuclear decay.

The entire process of liquid scintillation counting can be described by using the following analogy. The original nuclear decay energy absorbed in the fluor cocktail can be thought of as a battery, and the fluor cocktail itself can be considered as a light source or lamp fueled by the battery. The amount of energy in the battery cannot be determined by sight, touch, taste, or smell; however, the battery energy will govern the light intensity emitted by the lamp. This is the scintillation cocktail's purpose. It converts the original nuclear decay energy to flashes of light by way of the process shown in Fig. 7.1. The intensity of the light flashes is directly proportional to the original nuclear energy dissipated in the fluor cocktail. The higher the energy absorbed by the fluor cocktail, the brighter the resultant light flash. For example, tritium, which is a low-energy beta-particle emitter ($E_{max} = 18.6$ keV), would produce relatively very low intensity light flashes for each beta particle absorbed in the fluor cocktail, such as dim light from a lamp. However, ^{32}P, which is a high-energy beta-particle emitter ($E_{max} = 1710$ keV), would produce a light intensity approximately 100 times brighter in the fluor cocktail (like a large spotlight). Thus, the light intensity emitted by a scintillation fluor cocktail reflects the original nuclear decay energy, and the number of light flashes per unit time is proportional to the number of nuclear decays in that time unit or, in other words, the sample radioactivity (*e.g.*, disintegrations per minute or DPM).

A liquid scintillation analyzer may also be used to measure the fluorescence produced when radioactive nuclides are adsorbed onto or in close proximity to the surface of a plastic or glass scintillator (solid scintillator) located within a conventional liquid scintillation counting vial or well of a microplate scintillation analyzer. The solid scintillation counting process uses a solid inorganic scintillator (*e.g.*, yttrium silicate) to produce the light flashes, which are quantified by the liquid scintillation counter. The light flashes are produced directly by the interaction of the decaying nuclear event with the inorganic scintillator. The intensities of the light flashes produced are proportional to the energies of the radiation emitted from the nuclear decay that are absorbed by the scintillator, similar to that for the liquid scintillation process. This technique, known as scintillation proximity assay (SPA), is used to measure binding reactions, commonly studied in the fields of medicine, biochemistry, and molecular biology, without the need to separate bound from free fractions. It uses glass or plastic solid scintillation microspheres together with a low-energy-emitting isotope-labeled (^{3}H or ^{125}I) ligand. The method is described briefly in Section XIII and in more detail in Chapter 16, "Solid Scintillation Analysis," as it is a solid scintillation technique, which utilizes a liquid scintillation counter.

B. Alpha-, Beta-, and Gamma-Ray Interactions in the LSC

The scintillation process and light output are different for the alpha, beta, and gamma decay. These decay processes are described in detail in Chapter 1. Only a brief treatment is provided here. The alpha-decay process is illustrated by Eqn 1.83 and Fig. 1.27 of Chapter 1. During the alpha-decay process, a helium nucleus, which is composed of two protons and two neutrons, is released with a specific energy (monoenergetic) from the atomic nucleus. The general decay energy range for alpha particles is 2−8 MeV. When alpha decay occurs in a liquid scintillation cocktail, the alpha particles interact with the fluor cocktail to produce light (approximately 1 photon/keV of original decay energy). The light intensity is converted into an electric pulse of magnitude proportional to the light intensity via a photomultiplier tube described in Section III.

If we compare the linear range (R_{cm}) in centimeters of a 5.5-MeV alpha particle from ^{241}Am in water ($R_{cm} = 0.0048$ cm) to the range of a 0.55-MeV beta particle from ^{90}Sr in water ($R_{cm} = 0.178$ cm), we see that the alpha particle travels a much shorter distance, only 2.7 hundredths (0.0048/0.178) that of the beta particle, regardless of the fact that the alpha particle possessed ten times the energy of the beta particle (see Chapter 1 for calculations of range and energy for alpha and beta particles). The higher charge and mass of the alpha particle compared with the beta particle are responsible for the reduced range of the alpha particle (see Chapter 1) and less efficient excitation energy transfer to solvent and fluor. Alpha particles produce light in the liquid scintillation cocktail at about one-tenth the light intensity per unit of particle energy of beta particles (Horrocks, 1974). Therefore, in the case of alpha particles, which are monoenergetic, a single pulse height peak is seen for each alpha decay, at a pulse height equivalent to approximately one-tenth its original nuclear decay energy. A 5-MeV alpha particle, therefore, would be detected by a pulse height equivalent to approximately 500 keV in a liquid scintillation cocktail. Consequently, the pulse heights of alpha particles and beta particles in the same sample often overlap even when the alpha particles emitted from certain radioactive nuclides are of energy about 10 times greater than the E_{max} of beta particles emitted by other radionuclides in the same sample. The overlapping liquid scintillation pulse height spectra of ^{210}Po and ^{90}Sr(^{90}Y) in the same sample are illustrated in Fig. 7.2.

The pulse decay times of the light emissions from alpha and beta events are also different. A pulse in the scintillation process produced by an alpha particle can be about 35−40 nsec longer than a pulse event produced by a beta particle. Using this characteristic, simultaneous analysis of alphas and betas in the

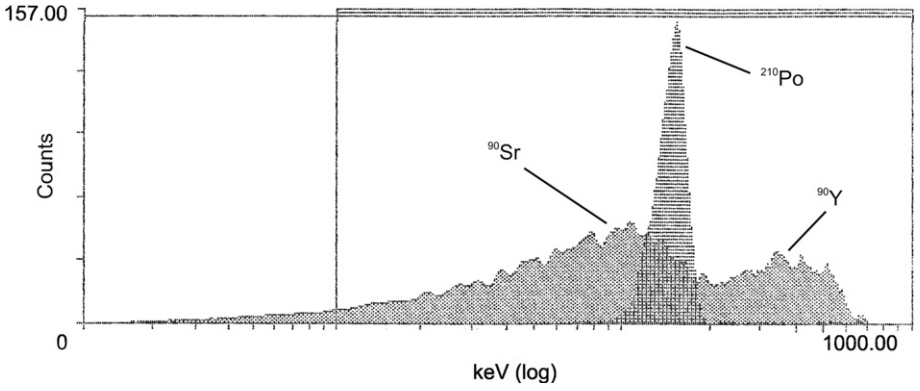

FIGURE 7.2 The overlapping pulse height spectra produced by a mixture of the 5.30-MeV alpha particles of ^{210}Po and the 0.55-MeV beta particles of ^{90}Sr in a PerkinElmer 2750TR liquid scintillation analyzer. The sample contains a mixture of ^{210}Po + ^{90}Sr (^{90}Y) in a scintillation cocktail of 50% water (1:1 mixture of water and Ultima Gold AB™ fluor cocktail) and displayed a tSIE of 277. Notice the relatively sharp peak of the 5.3-MeV alpha-particle pulse-height spectrum overlapping with the 0.55-MeV beta-particle pulse-height spectrum. The ^{90}Y daughter is in secular equilibrium with its parent ^{90}Sr. The α-peak of ^{210}Po and the β peaks of ^{90}Sr (^{90}Y) appear in a separate α-MCA and β-MCA, The two pulse-height spectra of the MCAs are overlapped to demonstrate the overlapping pulse heights produced by the ^{210}Po and ^{90}Sr. *(From L'Annunziata, M. F., 1997, unpublished work)*

same pulse height energy range can be performed. The discrimination of alpha and beta particles, which produce overlapping pulse height intensities, will be described in Section XV.

The counting efficiency (*i.e.*, how efficiently the nuclear decay is detected) is approximately 100% for almost all alpha decays using a liquid scintillation cocktail. Because of the unique pulse height spectral characteristics of alpha detection in a liquid scintillation counter (see Fig. 7.2) and their slower pulse decay times, alpha particles can be distinguished easily from most other nuclear decay radiations with the liquid scintillation analyzer.

A very common radionuclide decay process is the production and emission of beta particles. Beta decay can take place by either negatron (β^-) or positron (β^+) emission. The production of a negative beta particle (negatron) is described by Eqns 1.101 and 1.103 of Chapter 1, and several examples are given in Eqns 1.105−1.110 of that chapter. During the beta-decay process with negatron emission, a neutron is converted to a proton and an electron (negative beta particle) and an antineutrino. The beta particle (negatron) is equivalent to an electron in property, and the antineutrino is a particle of zero charge and near zero mass. The total decay energy that is released in the beta-decay process is shared between the beta particle and the antineutrino. This total decay energy is usually expressed as the E_{max}, which is the maximum energy that is released in the decay process. The decay energy is shared between the beta particle and antineutrino, but only the beta particle can be detected by the scintillation process. Thus, the resultant spectrum for all beta decays starts at zero and goes to the maximum decay energy (E_{max}) as illustrated in Fig. 1.30 of Chapter 1. Approximately 10 photons of light per keV of beta-particle decay energy are produced in the liquid scintillation process. Because of the broad spectrum of beta-particle energies emitted by a given radionuclide sample, beta decays can easily be recognized by this distinct broad spectral pattern as illustrated in Fig. 1.30 of Chapter 1 on the linear energy scale or Fig. 7.2 of this chapter illustrating the pulse height spectra of ^{90}Sr(^{90}Y) on a logarithmic energy scale.

The second type of beta decay produces a positron or positive beta particle. This beta-decay process converts a proton to a neutron and a positively charged electron (positron) accompanied by the emission of a neutrino. Positron emission is described by Eqns 1.130 and 1.131 of Chapter 1, and an example is provided by Eqn 1.132 of the same chapter. The positron is an antiparticle of an electron; it possesses an opposite charge and a spin in the opposite direction to that of the electron. The total energy released in the positron decay process is shared between the positron and the neutrino similar to the negatron decay process. The positron will lose its kinetic energy in matter via ionization. When it comes to a near stop, it comes into contact with an electron, its antiparticle, and is annihilated with the simultaneous production of two gamma-ray photons of 0.51 MeV energy equivalent to the two annihilated electron rest masses. See Chapter 1 for more detailed information on both the negatron and positron decay processes.

The liquid scintillation counting efficiency for beta particles (negatrons or positrons) is dependent on the original energy of the beta decay. For most beta particles with a decay energy above 100 keV, the counting efficiency is 80−100%, but for lower-energy beta decays (*e.g.*, ^{3}H, $E_{max} = 18.6$ keV) the counting efficiency is normally in the range of 10−60% depending upon the degree of quench in the sample. The phenomenon of quench and its effect on liquid scintillation counting efficiency are described in Sections IV and V.

Another common nuclear decay process is gamma-ray emission. In this process, a gamma ray is emitted from the nucleus of the decaying atom. The gamma ray is an electromagnetic radiation or, in other respects, a photon particle. The general energy range for gamma rays is 50−1500 keV. Gamma-ray emission often accompanies alpha, beta, or electron capture (EC) decay processes. Bremsstrahlung or X-radiation, which is electromagnetic radiation originating from electron energy transitions, also accompanies the EC decay process. When gamma-emitting radionuclides are detected by the liquid scintillation counter, it is not the gamma ray that is detected to a very significant degree, but rather the alpha particles, beta particles, or atomic electrons (Auger and internal-conversion electrons) that may be produced during decay processes occurring in the liquid scintillation fluor cocktail. Gamma rays from sample radionuclides in the scintillation cocktail can produce Compton electrons, although these interactions are less significant in magnitude in the liquid fluors. In general, electromagnetic radiation makes only a minor contribution to excitation in liquid scintillation fluor compared to charged-particle radiation. For example, if we consider the liquid scintillation analysis of ^{125}I, which decays by electron capture with the emission of gamma rays and daughter X-radiation, liquid scintillation counting efficiencies as high as 85% are reported. However, the excitations in the liquid scintillation fluor are due mainly to the absorption of Auger and internal-conversion electrons and only a minor contribution (~8%) is the result of X-rays produced during the decay process (L'Annunziata, 1987).

C. Cherenkov Photon Counting

Beta particles of energy in excess of 263 keV can be detected and quantified in water or other liquid medium using the liquid scintillation analyzer without the use of scintillation fluor cocktail. The sample is simply placed in a clear liquid solution (often aqueous) and detected by the light produced by the Cherenkov effect. Charged particles, such as beta particles, that possess sufficient energy can travel at a velocity exceeding the speed of light in media such as water, organic solvents, plastic, and glass. When this occurs, the charged particle will produce Cherenkov photons, which extend from the ultraviolet into the visible wavelengths. The light, that is produced, is of low intensity, and it is normally detected in the low-energy counting region with pulse heights equivalent to those produced by beta particles of 0−50 keV. High-energy beta-particle emitters, which emit a significant number of beta particles in excess of 263 keV, can be analyzed by counting the Cherenkov photons in the liquid scintillation analyzer without fluor cocktail. Some examples are ^{32}P ($E_{max} = 1710$ keV), ^{90}Sr(^{90}Y) where the E_{max} of ^{90}Y beta particles is 2280 keV, ^{86}Rb ($E_{max} = 1770$ keV

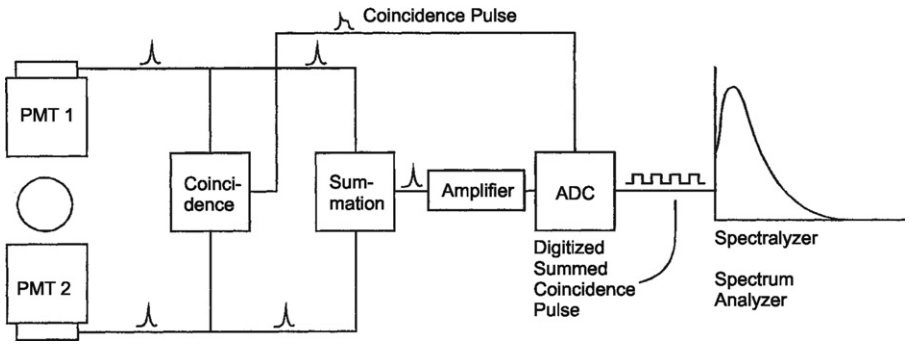

FIGURE 7.3 Schematic diagram of the components of a basic liquid scintillation analyzer. The circle between photomultiplier tubes PMT 1 and PMT2 represents a vial containing the sample and scintillation fluor cocktail. *(From Kessler, 1989, ©1998–2010, PerkinElmer, Inc. Printed with permission)*

occurring at an 88% intensity (probability per decay) or 680 keV at a 12% intensity), and ^{89}Sr ($E_{max} = 1490$ keV). The Cherenkov counting efficiency of these radionuclides in water is in the range of approximately 35–70% depending on color quench. The process of Cherenkov counting is treated in detail in Chapter 15, and a thorough treatment of the origin, principles, and theory of Cherenkov radiation and the Cherenkov effect is provided in a previous book by the writer (L'Annunziata, 2007). In general, it is important to remember that when quantifying radionuclides by Cherenkov counting, the counting region should be set to encompass only the low pulse height spectra produced by Cherenkov photons, which is equivalent to the pulse heights produced by low-energy (0–50 keV) beta particles, and no fluor cocktail is required.

III. LIQUID SCINTILLATION COUNTER (LSC) OR ANALYZER (LSA)

As described previously, the scintillation process involves the conversion of nuclear decay energy into light flashes. Therefore, to quantify the nuclear decay event and to satisfy needs for automation and multiple user programs a liquid scintillation counter must be able to perform the following functions: (1) it must be able to detect light flashes that occur in the scintillation vial with fluor cocktail or solid scintillator (SPA) and be able to determine the number of light flashes and their intensity; (2) it must be able to hold a large number of scintillation vials (>400) of various sizes (*e.g.*, 20 mL, 8 mL, 7 mL, 4 mL, and microfuge or Eppendorf tubes); (3) it must have the ability to process automatically various types of samples using different counting conditions and counting programs (*e.g.*, single radionuclides, multiple radionuclides, quench corrections, direct DPM, or Cherenkov counting) using programmable counting setups or counting protocols; (4) it must be able to process the data from flashes of light per minute to counts per minute (CPM) and then convert these count rates to actual nuclear disintegration rates or nuclear decay events per minute (DPM) using a quench-correction method or direct DPM method; and (5) it must perform data analysis and reduction, special computer-managed data application programs, and instrument performance assessment.

The first and most important task of the liquid scintillation analyzer is the detection and quantification of the number of light flashes and their corresponding intensities. This is accomplished by the heart of the LSC, the light detection and quantification components. A simple block diagram of a conventional LSC with two photomultipliers is illustrated in Fig. 7.3. Three basic components are found in this part of the LSC, namely, the detector(s), a counting circuit, and a sorting circuit. Liquid scintillation analyzers with three photomultiplier tubes (PMTs) are also available, but yet less common. LSAs operating with three PMTs provide unique methods of activity analysis, and these are discussed in Section IX.C.

In order to quantify the radioactivity in the sample, the sample is loaded into the counting chamber using either an uploading or a downloading elevator mechanism. The downloading mechanism is able to prevent any external light from entering the counting chamber by using a double light seal mechanism. The double light seal is implemented by automatic loading of the sample vial from the sample chamber deck to a holding area, where the sample is sealed from external light. The sample is subsequently moved into the counting chamber, which is below the holding area. Because of this unique downloading mechanism, the photomultiplier tube (PMT) high voltage can remain on at all times and the PMT background stabilized. Once the sample has been loaded into a light-tight chamber, the light is detected using two photomultiplier tubes (PMT 1 and PMT 2 of Fig. 7.3).

The photomultiplier tubes (PMTs) convert the light photons emitted from the liquid scintillation vial to electrons when the light photons hit a bialkali photocathode located inside the face of the PMT, as illustrated in Fig. 7.4. The photoelectrons produced at the PMT photocathode are amplified through a series of positively charged dynodes, each dynode having an increasing positive voltage along the series. The increasing voltage accelerates the initial photoelectrons produced at the PMT photocathode to yield an avalanche of secondary electrons, resulting in a pulse amplification. A photon, which is produced in the scintillation vial, is thereby converted to a corresponding electronic signal. Because the amount of light produced in the scintillation vial is normally very low (~10 photons per keV energy absorbed in the liquid fluor cocktail), the PMT must be able to amplify the pulse resulting from secondary electrons produced by a single photon of light by a large factor. This pulse amplification factor or gain is $>10^6$ for the standard PMT used in the LSC.

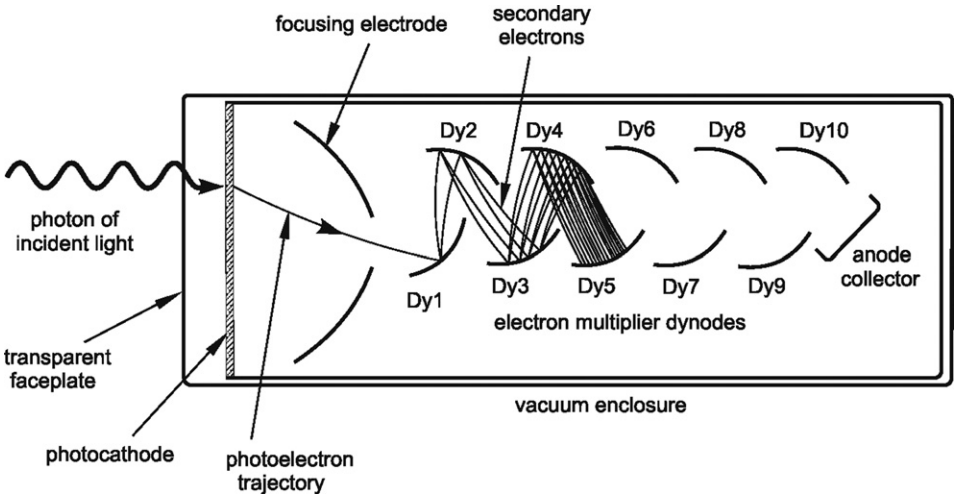

FIGURE 7.4 Schematic of a photomultiplier tube. The drawing is based on a schematic by Itaya et al. (2004). A photon of visible light emitted from a liquid scintillation vial collides with a bialkali photocathode producing a photoelectron. The trajectory of the photoelectron is focused and accelerated toward a positive dynode (Dy1). The impact of the photoelectron onto the first dynode (Dy1) produces secondary electrons that are accelerated toward a second dynode (Dy2) of higher positive voltage. The secondary electrons are accelerated sequentially toward dynodes of increasing potential difference (Dy3 to Dy10), which result in an avalanche of secondary electrons. The avalanche of electrons (not illustrated with dynodes Dy6 to Dy10) is collected at the anode, yielding a pulse amplification $>10^6$, with a typical rise time of ~2 ns. The rise time is the time for the anode output pulse to rise from 10% to 90% of the peak amplitude. The faceplate is made generally of borosilicate glass with a diameter of ~5 cm.

As illustrated in the block diagram of Fig. 7.3 two PMTs are used for the measurement of the light intensity from the nuclear decay processes in the sample vial. The two PMTs permit coincidence light detection and coincidence pulse summation required for the LSC to be able to detect low-energy radionuclides such as tritium ($E_{max} = 18.6$ keV) and to distinguish instrument background from true nuclear events. If only a single PMT were used in the LSC, the background level would be approximately 10,000 CPM for a 0−2000-keV counting region. This high background is normally due to the large amplification factor from the PMT. This high background count rate mainly occurs in the 0−10-keV region (thermal and electronic background noise). In the LSC, two PMTs and a coincidence circuit are used to help differentiate background signals from true nuclear decay events in the scintillation vial, which is referred to as coincidence counting. The principle behind coincidence counting is based upon the fact that, when a nuclear decay event occurs in the scintillation vial, light is produced which is isotropic (*i.e.*, is emitted equally in all directions). Since the decay process and resultant scintillation process produce multi-photon events (about 10 photons per keV of nuclear energy dissipated in a liquid scintillation cocktail), light is emitted in all directions from the scintillation vial. The decay process and resultant scintillation are very rapid (approximate light decay time is 2−10 nsec). Because the scintillation process produces multi-photon events and the events decay rapidly, we can distinguish most background from true nuclear decay in the scintillation vial. If light is produced in the scintillation vial inside the analyzer detection area, it will be emitted in all directions and be detected by the two PMTs in the very short pulse decay time of 2−10 ns. When a signal is detected in both the PMTs within a coincidence resolving time of 18 nanoseconds, it is accepted as a true nuclear decay event. If on the other hand, a background event occurs in one of the PMTs or in the electronic circuitry (*e.g.*, thermal or electronic noise), it will produce a single event, which will be detected by only one of the two PMTs in the 18-ns time frame. Such a single event is rejected as occurring external to the sample or, in other words, a background event. By using two PMTs and the coincidence circuit, the instrument background is reduced from 10,000 CPM with a single PMT to about 30 CPM with two PMTs for a wide-open 0−2000-keV pulse height counting region. The PMT signal that is sent to the coincident circuit is an analog signal with a pulse height that reflects and is proportional to the original nuclear decay energy.

The next part of the detection area, illustrated in Fig. 7.3, is the summation circuit. This circuit has a dual purpose. The first is to reassemble the original two coincident signals into an individual signal with the summed intensity. This helps to optimize the signal-to-noise ratio in the instrument. The second purpose is to compensate for the light intensity variations due to the position of the nuclear decay in the vial that would occur when samples containing color are counted. If only one of the two PMT signals were used in counting a colored sample, the signal height would be dependent on where in the scintillation vial the light was produced. If the light was produced near the edge of the scintillation vial, a brighter flash of light would be detected by the PMT that is in closer proximity to that edge of the vial. However, with two PMTs and a summed signal, the final pulse height produced by the PMT is not affected by the position of the nuclear decay in the presence of color in the sample counting vial.

Subsequent to pulse summation in the LSC, the signal is further amplified and sent to the analog-to-digital converter (ADC). The ADC converts the signal from an analog signal, which is a pulse with a certain height, to a single number that represents its pulse height or intensity. The digital pulses are finally sorted on the basis of their magnitude or pulse height

number. The sorting can be accomplished by one of two methods: pulse height analysis (PHA) or multichannel analysis (MCA).

PHA, which is the older of the two methods, utilizes only two discriminators, an upper- and a lower-energy discriminator. An upper-level discriminator is set such that all of the pulses with a certain energy of interest are always lower than this upper level. A lower-level discriminator is also set to reject pulse magnitudes that are below the lower-level discriminator setting, thereby reducing background and other counting interferences of low pulse height. When an event is detected, its pulse height is measured; if it has an intensity lower than the upper discriminator and higher than the lower discriminator, it is accepted as a true nuclear event. If any of the pulses fall outside this range, they are rejected and lost by the counting circuitry. All of the pulses that fall into the accepted range are counted, hence the term liquid scintillation counting (LSC).

The second and more contemporary method of sorting pulses is MCA. The multichannel analyzer is a series of bins or slots, where different pulse height magnitudes are placed once they have been detected. Two types of MCAs are commonly used: linear and logarithmic. The linear MCA provides data with pulse heights calibrated to represent decay energy in keV on a linear scale. For a common 4000-channel linear MCA, each channel may represent approximately 0.5 keV of energy. The logarithmic MCA displays the pulse heights in channels plotted along a logarithmic scale as illustrated in Fig. 7.2.

All of the pulses collected in MCAs are not only counted but also analyzed in terms of their number and height; therefore, the liquid scintillation counter is now more often referred to as the liquid scintillation analyzer (LSA). A linear MCA output with a typical beta-particle pulse height spectrum is illustrated in Fig. 7.5.

The second function of the modern LSA is to count automatically various types and sizes of samples in vials containing scintillation fluor cocktail. Most modern LSAs are cassette based. This means that sample vials are placed in racks holding between 12 and 18 individual scintillation vials or samples. Specific cassettes are available for holding scintillation vials of different volumes up to 20 mL.

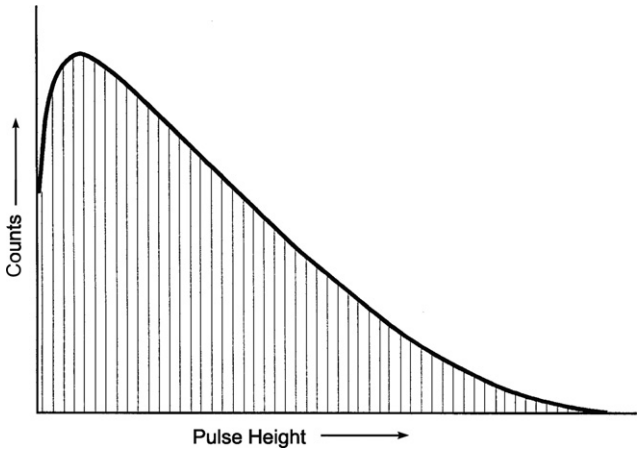

FIGURE 7.5 Illustration of a typical liquid scintillation beta-particle pulse-height spectrum collected in the many channels of a multichannel analyzer (MCA). A typical linear MCA will have as many as 4000 channels within which pulses of certain heights are collected and counted. The channels are calibrated over the energy range of 0–2000 keV. *(©1998–2010, PerkinElmer, Inc. Printed with permission)*

Many persons can use the same instrument by establishing counting protocols to analyze different radionuclides under different counting conditions and sample sizes. The key functions of the LSA – analyzing sample data by determining sample quench levels, converting count rate (*e.g.*, counts per minute or CPM) to disintegration rate (*e.g.*, disintegrations per minute or DPM) for unknown samples, and automatic monitoring of the performance of the instrument (instrument performance assessment) – will be described in detail later in this chapter.

The majority of liquid scintillation analyzers in use today contain two photomultipliers, and these are installed with large-capacity sample changers as nonportable equipment in laboratories around the world. A portable and very compact single-photomultiplier liquid scintillation analyzer with multichannel analyzer has been developed, which is very applicable to mobile laboratories (Theodórsson, 2006, Theodórsson and Jónsson, 2006, Theodórsson et al., 2006, Jónsson et al., 2006, and Gudjónsson et al., 2009). The photomultiplier tube measures the scintillation photons from the bottom of the counting vial. Such a small portable liquid scintillation analyzer can find numerous applications in mobile-laboratory on-site monitoring of radionuclides. The application of the single-photomultiplier LSA for the monitoring of environmental tritium and radon has been demonstrated (Theodórsson and Skripkin, 2003, Theodórsson and Gudjónsson, 2003, and Gudjónsson et al., 2009). An example of such a portable liquid scintillation analyzer and luminescence counter is the Triathler™ (Hidex, Inc., Turku, Finland).

IV. QUENCH IN LIQUID SCINTILLATION COUNTING

In scintillation counting the sample is either dissolved in a liquid scintillation cocktail or adsorbed onto a solid scintillator in a sample vial or microplate well. In order to quantify the nuclear events as activity in terms of disintegrations per minute (DPM), the LSA counts the number of flashes of light in a preselected time period to provide a count rate (CPM) of the sample. The sample count rate is dependent on how efficiently the nuclear decay events are converted to light flashes that are detected and quantified by the LSA. Because the sample solution is always present, it can absorb nuclear decay energy, thereby preventing this energy from being absorbed by the solvent and chemical fluor molecules, or the solution can absorb photons of light emitted by the fluor molecules, thus reducing the light intensity measured by the PMT. This causes the phenomenon called quench. We can define quench as interference in the conversion of nuclear decay energy to photons of light emitted from the sample vial. Quenching can be the result of three phenomena, namely, (1) chemical quenching, (2) ionization quenching, and (3) color quenching. These interference phenomena are discussed in more detail subsequently.

Many texts refer only to chemical and color quench phenomena as mechanisms to be considered for the determination of radionuclide detection efficiency with little or no reference to ionization quenching. This may be due to the much smaller effect that ionization quenching has compared to chemical and color quenching in liquid scintillation counting (Bagán et al., 2008). However, much attention has been given in recent years to the ionization quenching phenomena by researchers in scintillation counting, particularly in the field of radionuclide standardization (Grau Carles, et al., 2004, 2006a,b, Kossert and Grau Carles, 2006, Grau Malonda and Grau Carles, 2008, and Bignell et al., 2010) and in the measurement of radiotracers particularly with the use of plastic scintillators (Bagán et al., 2008, 2009). The points of interference of chemical, ionization, and color quenching in the liquid scintillation process are illustrated in Fig. 7.1.

The three quenching phenomena, which interfere with the liquid scintillation measurement of radionuclides, are described in more detail as follows:

1. *Chemical quenching*. This is the most common quench mechanism and the one that generally can have the most deleterious effect on the liquid scintillation detection efficiency. Chemical quench is caused by the presence of chemical substances in the sample, including the sample solution, which absorbs nuclear decay energy in the scintillation process, thereby obstructing to a certain degree the transfer of nuclear decay energy to the scintillation cocktail solvent. A chemical quenching agent can be thought of as a sponge that absorbs energy before it can produce light in the scintillation process. In addition to reducing the number of light flashes resulting in a reduction of radiation counts, the quenching process can, and often does, decrease the light intensity, thereby reducing the pulse heights as measured by the scintillation process. Chemical quenching occurs to some degree in most liquid scintillation counting samples.
2. *Ionization quenching*. The second mechanism of quench, ionization quenching, as described by Grau Carles et al. (2004), is related to the density of excited solvent molecules in the scintillation fluor cocktail. The response of a liquid scintillator to the interaction of charged particles is not linear with the energy deposited. The nonlinearity of the photon intensity output by the scintillator and the energy deposited by the charged particles increases with the mass of the particle, and the nonlinearity is a function of the linear energy transfer (LET) of the particle. Also, as defined by Bignell et al. (2010a), ionization quenching in scintillators is the reduction of luminosity associated with a high density of excited molecules caused by a large LET to the scintillant. Thus, low-energy beta particles, such as those emitted from ^{3}H, exhibit a greater nonlinearity of light output versus energy deposited than high-energy beta particles or electrons, because the LET of low-energy beta particles or electrons is higher than the LET of high-energy beta particles or electrons (see Table 1.25 of Chapter 1). The cause of this nonlinearity is ionization quenching, which is a consequence of the density of excited solvent molecules in the scintillation fluor cocktail. Charged particles, which exhibit a high LET, will create a higher number of excited solvent molecules. When the concentration of the excited molecules is high, there is a higher probability of interaction between two excited molecules whereby one molecule can lose its energy of excitation to the other, resulting in one molecule becoming super-excited. The super-excited molecule has a high probability of reaching the state of ionization. The overall outcome of this process is two solvent molecules, which were originally excited by the charged particle (*e.g.*, β-particle or electron), lose their energy of excitation and thereby do not transfer this energy to the fluor molecules or transfer only a diminished portion of that excitation energy. This results in a loss of excitation energy and a reduction of the photon intensity from the scintillation fluor, which may manifest itself by a reduced count rate or a reduction in the magnitude of the pulse height measured by the photomultiplier from the photon intensity output. Grau Carles et al. (2004) explain that this process is observed clearly in the interaction of α-particles with liquid scintillator. Also, radionuclides decaying by low-energy β transitions, such as ^{3}H, as well as those decaying by electron capture with the emission of Auger or Coster−Kronig electrons are those that display this ionization quenching, that is, the nonlinearity between the intensity of the fluorescent emissions from the scintillation counting vial and the energy deposited by the β particle or electron. Electron-capture decay results in the emission of X-rays from subsequent atomic electron rearrangements following EC decay, which can produce X-ray Compton electrons and photoionization, all of which are low-energy electrons exhibiting a relative high LET compared to the higher-energy beta particles from most beta-emitting radionuclides.
3. *Color quenching*. The phenomenon of color quench occurs when color is visible in the sample that is being counted. The color quench phenomenon normally acts by absorbing photons of light in the scintillation vial before they can be detected and quantified by the PMT. This is similar to what happens when a colored filter is used on a camera to filter out certain wavelengths of light. Chemical quench absorbs nuclear decay energy and color quench absorbs photons of light. Color quenching is often less a problem than chemical quenching, because samples most often can be decolorized easily with minute quantities of bleaching agent or other means (see Chapter 8).

The quenching phenomena reduce the photon intensities emitted from a scintillation counting vial and consequently reduce the magnitudes of the pulse heights measured by the liquid scintillation analyzer; in addition, the quenching phenomena can also reduce the count rate of a sample measured by the liquid scintillation analyzer (*i.e.*, counts per minute, CPM). To compensate for the count rate loss due to quench and to determine the sample activity or DPM (nuclear decay rate), it is necessary to know the counting efficiency, defined by the following equation:

$$\%\ \text{efficiency} = \text{CPM}/\text{DPM} \times 100 \qquad (7.1)$$

where CPM is the count rate of the sample determined by the LSA, and DPM is the actual disintegration rate of the sample. The relationship between CPM and DPM of the sample varies according to the energy of the nuclear decay at a given degree of quench. The lower the energy of the decay, the greater is the effect of quench on the counting efficiency for beta-emitting radionuclides. This is illustrated in Fig. 7.6, which shows the liquid scintillation pulse height spectra of seven tritium samples ($E_{max} = 18.6$ keV) that were prepared with the same activity (DPM), but with different amounts of 5.0 M HNO_3, which acts as a chemical quenching agent. The liquid scintillation analyzer determined the CPM for each sample by summing the area under the pulse height spectrum of each sample. As illustrated in Fig. 7.6, the least quenched sample is that which contains no HNO_3. The area under the pulse height spectrum of the first sample had 126,287 CPM and the highest pulse heights with a maximum equivalent to approximately 18.6 keV. The counting efficiency for this sample is calculated as 126,287 CPM/210,000 DPM or 60.1%. The second sample is quenched by the added 0.05 mL of HNO_3, and, as a result, (1) the CPM is reduced to 115,834, (2) the endpoint or maximum intensity of the pulse height spectrum of this sample is reduced, and (3) the counting efficiency of the sample is reduced to 55%. As illustrated in Fig. 7.6, when the sample is quenched more and more, the maximum observed pulse height is reduced further and the CPM collected under the pulse height spectrum is reduced. For example, the last sample listed, which contains the highest amount of quenching agent, gave the lowest count rate of 16,091 CPM and a calculated counting efficiency of only 7.7%. Thus, as the quench increases for tritium, both the maximum pulse height and the total CPM are reduced significantly. We can conclude that chemical quenching agents, although dilute and small in quantity, can have a significant effect on the counting efficiency of tritium.

On the other hand, in an isotope such as carbon-14, which emits beta particles of energy almost 10 times higher ($E_{max} = 156$ keV) than tritium, quenching agents cause a significant reduction in the maximum pulse heights but have a less significant effect on the pulse counts collected than was observed in the case of tritium. Table 7.1 shows the effect of the quenching agent on five samples of carbon-14. The five samples contained the same activity (100,000 DPM), but increasing amounts of quenching agent. The quenching agent is not given here, but a common quenching agent used for these studies is nitromethane over the range of 0−100 μL per 20 mL of fluor cocktail. The endpoint of the pulse height spectra (maximum pulse height expressed in keV) of each sample listed in Table 7.1 changed significantly from sample 1 to sample 5 as chemical quench increased; however, the sample count rates (total counts collected under the pulse height spectra per given period of time) did not change as drastically as for tritium. As can be seen from Table 7.1, pulse height spectral intensity (maximum pulse height) changes as the sample is quenched, but the efficiency or CPM value (area of energy spectrum) changes only slightly. The overall conclusion is that for beta-particle emitters, the lower the energy (E_{max}) of the beta decay, the greater is the effect of quench on the counting efficiency of the radionuclide.

For alpha-emitting radionuclides, the phenomenon of quench does not significantly affect the counting efficiency as shown in Fig. 7.7. As the quench of the sample is increased, the monoenergetic alpha peak is simply shifted to lower pulse heights, but the total area under the pulse height spectrum or detection efficiency (equivalent to counting efficiency) is not changed significantly. Also, as illustrated in Fig. 7.7, the alpha-particle pulse height spectrum in the LSA undergoes some peak broadening (reduced resolution) proportional to the level of quench, although this will have no significant effect on detection efficiency. The resolution is determined by the percent full width at half maximum as described in Chapter 16. Vera Tomé et al. (2002) studied alterations in alpha-peak shape in liquid scintillation with the potential of utilizing LSA for alpha spectrometry.

For gamma emitters, the quenching phenomenon is very similar to that observed with beta emitters (Ishikawa and Takiue, 1973), as Compton electrons produced by γ-photon

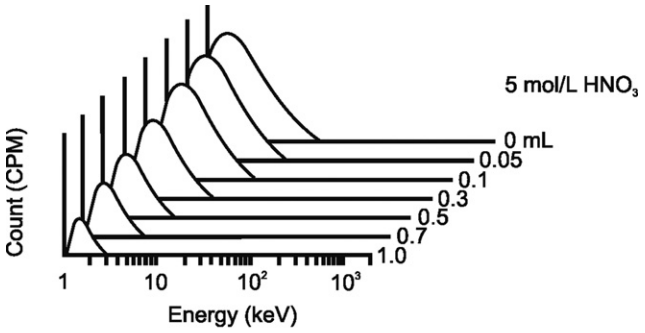

HNO_3 (0.5M) (mL)	^3H (CPM)	^3H (DPM)	^3H (%E)
0.00	126,287	210,000	60.1
0.05	115,834	210,000	55.1
0.10	102,218	210,000	48.7
0.30	61,211	210,000	29.1
0.50	39,846	210,000	19.0
0.70	25,239	210,000	12.0
1.00	16,091	210,000	7.7

FIGURE 7.6 Pulse-height spectra of seven samples of ^3H of equal activity containing varying amounts of 0.5-M HNO_3 quenching agent. The pulse-height spectra are plotted on a logarithmic scale with pulse heights calibrated to equivalence in keV energy. The liquid scintillation counting (detection) efficiencies for each sample are listed as percentages. *(©1998−2010, PerkinElmer, Inc. Printed with permission)*

TABLE 7.1 Effect of Quench on Carbon-14 Counting Efficiency in Liquid Scintillation Analysis

Sample	Maximum pulse height (keV)	CPM	DPM	Efficiency (%)
1	156	95,000	100,000	95.0
2	112	94,500	100,000	94.5
3	71	92,500	100,000	92.5
4	43	90,500	100,000	90.5
5	32	87,000	100,000	87.0

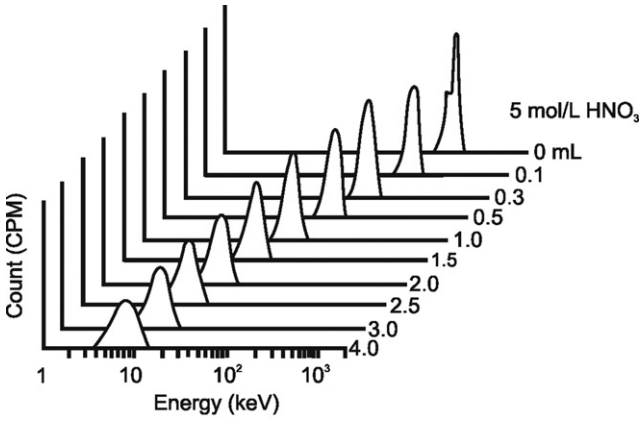

HNO_3 (0.5M) (mL)	^{241}Am (CPM)	^{241}Am (DPM)	^{241}Am (%E)	^{241}Am %FWHM
0.00	46,660	46,700	100	42
0.05	46,632	46,700	100	a
0.10	46,692	46,700	100	a
0.30	46,149	46,700	99	47
0.50	46,234	46,700	99	a
0.70	46,371	46,700	99	a
1.00	46,394	46,700	99	a
1.50	46,448	46,700	99	53
2.00	46,256	46,700	99	a
3.00	46,148	46,700	99	a
4.00	46,080	46,700	99	a

[a]% FWHM not calculated

FIGURE 7.7 Liquid scintillation pulse-height spectra of 11 samples of ^{241}Am of equal activity containing varying amounts of 0.5-M HNO_3 quenching agent. The pulse-height spectra are plotted on a logarithmic scale with pulse height calibrated to equivalence in keV energy. The liquid scintillation counting (detection) efficiencies for each sample are listed as percentages. The alpha peak resolutions are measured as percent full width at half-maximum. *(©1998 PerkinElmer, Inc. Printed with permission.)*

interactions in scintillation fluor cocktail will undergo similar quenching effects as beta particles. See Section VI for a treatment on the liquid scintillation analysis of gamma-emitting radionuclides.

The effect of quench using solid scintillators in a liquid scintillation analyzer is described in Chapter 16. When using solid scintillators, the sample is normally placed directly on the solid scintillator and dried or the sample is counted adsorbed onto the solid scintillator as in a scintillation proximity assay (SPA). See Chapter 16 for more detailed information on SPA. The sample is in direct intimate contact with the solid scintillator, and therefore no chemical quenching exists for these types of samples. Under these circumstances, color quench can occur with colored samples. Also, ionization quench may occur when plastic scintillators are used external to the sample (Bagán et al., 2009).

For the Cherenkov counting of samples containing high-energy beta-emitting radionuclides, color quench can occur; however, neither chemical quench nor ionization quench are possible. See Chapter 15 for a detailed treatment of Cherenkov counting.

All chemical substances that either dilute the solvent of the fluor cocktail or compete with it for nuclear decay energy will cause quench. Even dissolved oxygen from the air is a chemical quenching agent (Takiue and Ishikawa, 1974); its effect can be seen in the LSA of weak (low-energy) beta-particle-emitting radionuclides such as tritium. More information on chemical quenching agents and their classifications can be obtained from a previous book (L'Annunziata, 1987). As chemical quenching agents in the samples we analyze generally cannot be avoided and the effect of quench on detection efficiency is significant with many radionuclides, it is important to correct for quench when necessary. This will permit accurate measurement of sample activities in disintegration rate (*e.g.*, DPM).

V. METHODS OF QUENCH CORRECTION IN LIQUID SCINTILLATION COUNTING

Because some type of quenching exists in almost all samples, which are quantified by the liquid scintillation counting process, it is important to understand the methods that can be used to correct for quench. These methods allow us to relate and even convert the count rate (CPM) to the actual number of nuclear decays or disintegration rate (DPM) of a sample. This can be accomplished by one of the following techniques: (1) internal standard method, (2) sample spectrum method, (3) external standard method, and (4) direct DPM method. These techniques can be used for quench correction and DPM determination. Each has distinct advantages for various sample types and/or radionuclides. These will be discussed subsequently together with explanations of the when and why of using these techniques.

A. Internal Standard (IS) Method

The internal standard (IS) method is the oldest and most tedious, and it can be the most accurate method if great care is taken in its implementation. The technique involves a series of steps for each sample. The first step is to count each sample and obtain an accurate count rate (CPM) value for each. Then the samples are removed from the LSC, and a known activity (DPM) of a radionuclide standard is added to each sample; hence, the term internal standard is applied to this technique. After the addition of the internal standard and thorough mixing of the standard and sample, the samples are recounted to obtain the CPM of the sample plus the internal standard. Once the CPM of the sample and the CPM of the sample plus internal standard are obtained, the following equation is applied to determine the counting efficiency of the sample:

$$E = \frac{C_{s+i} - C_s}{D_i} \tag{7.2}$$

where C_{s+i} is the count rate of the sample after the addition of the internal standard, C_s is the count rate of the sample before the addition of the internal standard, and D_i is the disintegration rate of the added aliquot of internal standard. The disintegration rate of the sample, D_s, may then be calculated as follows:

$$D_s = C_s/E \tag{7.3}$$

For example, if the counting efficiency for a given sample was found to be 0.25 according to Eqn 7.2 and the sample count rate

was found to be 25,000 CPM, the activity of the sample can be calculated to be 25,000 CPM/0.25 = 100,000 DPM.

Several assumptions and restrictions are made for the internal standard method, some of which may be intuitively obvious. These are described as follows: (1) The same radionuclide must be used for the internal standard as the sample radionuclide; for example, a tritium-labeled standard must be used with samples containing tritium. Hendee et al. (1972) showed that [^{3}H]toluene and [^{3}H]hexadecane are good internal standards for organic-compatible fluor cocktails and [^{3}H]water or [^{3}H]hexadecane serve well for aqueous-compatible fluor cocktails when assaying for tritium. The organic standards labeled with ^{14}C are good internal standards for counting efficiency determinations of samples containing ^{14}C. (2) The internal standard added to the sample must have a count rate at least 100 times that of the sample. (3) The addition of the internal standard to the sample must not alter the quench in the sample to any significant degree. (4) The activity (DPM) of the internal standard must be accurately known, as with a National Institute of Standards and Technology (NIST) traceable standard. (Commercially available ^{3}H and ^{14}C standards, as well as mixtures of the two radionuclides, designed specifically for application in the internal standard quench-correction technique for either aqueous or organic solutions are available from PerkinElmer, Inc.) (5) This method of determining sample activities requires accurate sample transfer procedures, which can be tedious when working with many samples and small volumes of internal standard. Dobbs (1965) and Thomas et al. (1965) have investigated syringe-dispensing techniques for the addition of internal standards to samples in scintillation counting vials.

This method, if performed properly, can provide accurate activity measurements. Some examples of the internal standard quench-correction technique applied to the analysis of ^{3}H may be obtained from the works of Alongi et al. (2003), Sweet et al. (2004), Batistoni et al. (2005, 2007), and Eikenberg et al. (2011), and to the analysis of ^{14}C from the works of Alongi et al. (2003), Martins and Boekel (2003), TenBrook and Tjeerdema (2006), and Eikenberg et al. (2011). The major disadvantages of this technique are the time and the number of sample-handling steps required for each sample.

B. Sample Spectrum Characterization Methods

Sample spectrum characterization methods of quench correction involve the use of some characteristic of the sample spectrum as a measure of quench in the sample. Some of these methods are described subsequently.

1. Sample Channels Ratio (SCR)

The sample channels ratio (SCR) method was applied often during the early generations of liquid scintillation counters that were equipped with only the pulse height analysis (PHA) or single-channel analyzer for data storage and analysis. Nevertheless, the method is applicable with most commercial liquid scintillation analyzers today. It also remains a useful method for modern liquid scintillation analyzers not equipped with external standards, and the SCR method has other applications described further on in this chapter. The method involves counting the sample in two counting regions defined by lower-level (LL) and upper-level (UL) pulse discriminator settings. The count rate in each counting region varies according to the level of quench in the sample due to the pulse height spectral shift from higher to lower magnitudes caused by sample quench. An example of the pulse height shift according to quench level is illustrated in Fig. 7.8. As illustrated, a sample that is more highly quenched will produce pulse events of lower magnitude (height) than a sample that is lesser quenched.

The SCR quench-correction method requires first defining the widths of two counting regions also referred to as counting channels or windows. The lower and upper discriminator levels of one region are selected so as to provide a narrow counting

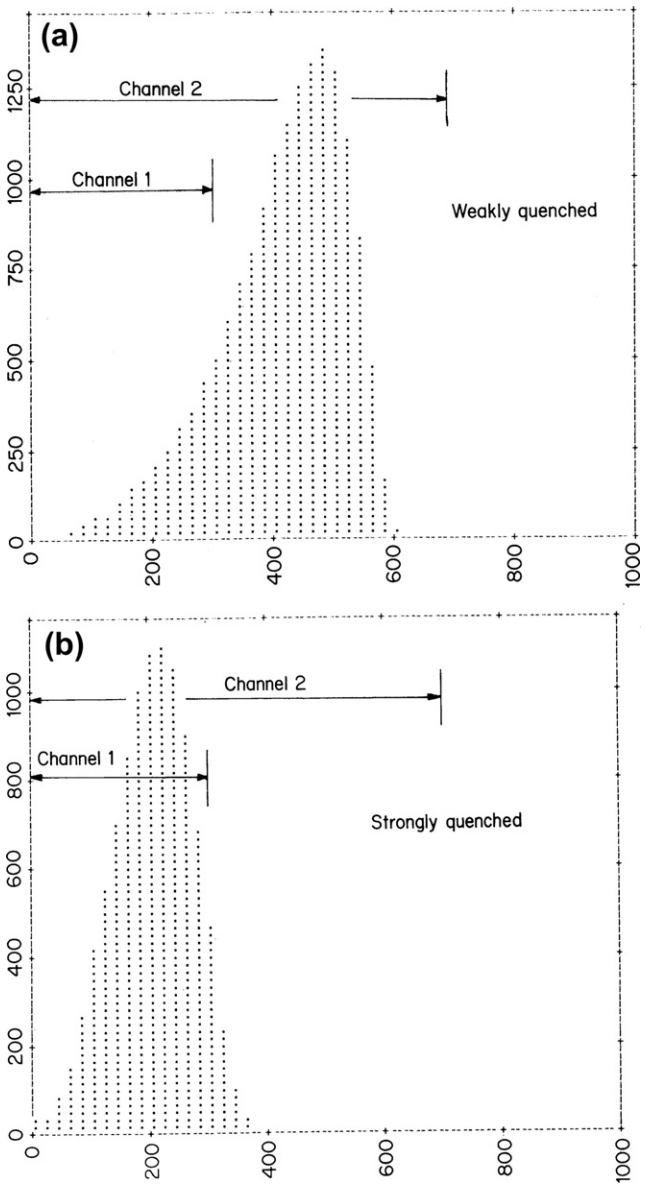

FIGURE 7.8 a) Weakly quenched and (b) strongly quenched pulse-height spectra produced by ^{33}P in relation to two overlapping counting regions (channels 1 and 2) of a Beckman LQ 7800 liquid scintillation analyzer. The counting channels 1 and 2 are defined by lower- and upper-level discriminator settings of 0–300 and 0–700, respectively. *(L'Annunziata, M. F., 1986, unpublished work.)*

region, which can register pulses of only low magnitude (*e.g.*, Channel 1, 0−300 of Fig. 7.8). The discriminator levels of the second counting region are set to provide a wider counting region, which can register most of the pulses of both low and high magnitude (*e.g.*, channel 2, 0−700 of Fig. 7.8).

A shift in pulse height due to quenching produces a change in the ratio of the pulses registered (counts) by the two regions. The degree of spectral shift and magnitude of change in the sample channels ratio (SCR), such as CPM_1/CPM_2 or sample count rate in channel 1 over the sample count rate in channel 2, are dependent on the severity of quench. Consequently, if a series of quenched standards consisting of scintillation vials each containing the same amount of radioactive standard but increasing amounts of quenching agent were counted, they would show a variation in the channels ratio and counting efficiency, such as that illustrated in Fig. 7.9. The procedures used to prepare sets of quenched standards are described in Section V.D. The quench-correction curve, once prepared for a given radionuclide and fluor cocktail, may be used as a standard curve for determining the counting efficiency of a sample from its channels ratio. The values of counting efficiency for the standard curve are calculated according to

$$E = C_{\text{std}}/D_{\text{std}} \tag{7.4}$$

where E is the counting or detection efficiency with values between 0 and 1.0, C_{std} is the count rate of the quenched standard in units of counts per minute (CPM) or counts per second (CPS), and D_{std} is the disintegration rate of the quenched standard in units of disintegrations per minute (DPM) or disintegrations per second (DPS). The activities of the unknown samples are determined from the count rate of the sample in the wider channel divided by the detection efficiency obtained from the SCR quench-correction curve or

$$D_s = C_s/E \tag{7.5}$$

where D_s is the disintegration rate of the sample, C_s is the count rate of the sample in the wide-open channel (*i.e.*, the wider channel from which the detection efficiencies of the quenched standards were determined), and E is the detection efficiency obtained from the SCR quench-correction curve.

A more detailed treatment of this method can be found in reviews by L'Annunziata (1984a, 1984b, 1987). The method is less often used with modern liquid scintillation analyzers due to the advent of multichannel analyzers (MCAs) in commercial LSA instrumentation, which utilize sample spectrum quench-indicating parameters or external standard quench-correction methods. Tarancón et al. (2004) used the SCR quench measurement technique as well as an internal standard quench measurement in the evaluation of plastic scintillation beads in a conventional liquid scintillation analyzer. The SCR technique is generally not useful with samples of low count rate or high quench, because the counts in one or both of the channels may be so low that a channels ratio becomes meaningless, or long periods of counting time would be required to achieve acceptable levels of statistical accuracy.

2. Combined Internal Standard and Sample Channels Ratio (IS-SCR)

Dahlberg (1982) devised a combination of the IS and SCR methods (IS-SCR), which ameliorates the disadvantages of the

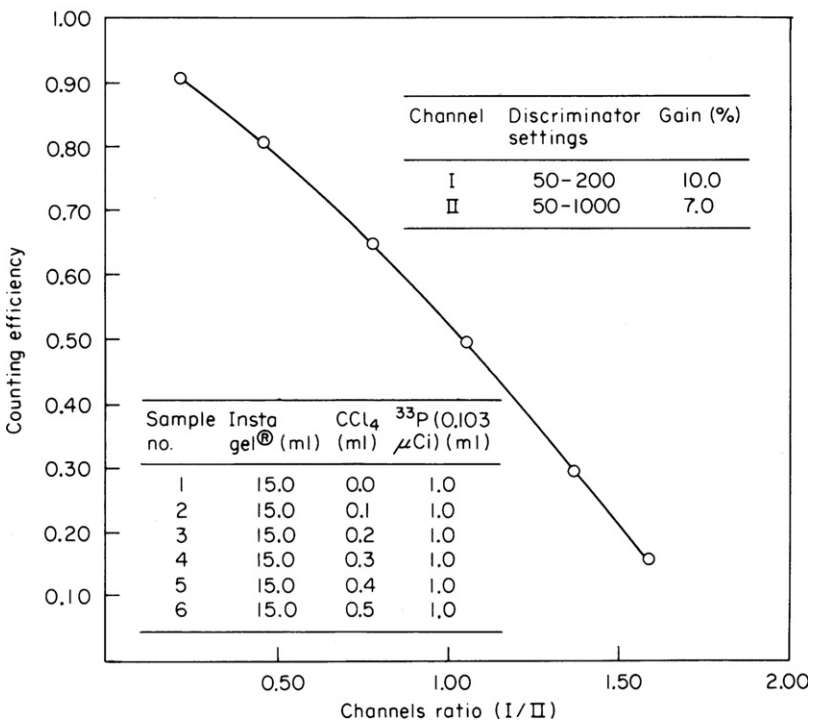

FIGURE 7.9 Typical channels ratio quench-correction curve. The channels ratio (I/II) represents the count rate of ^{33}P from channel I divided by the count rate from channel II. The discriminator and gain settings for each channel are given. The data were obtained from six samples, each containing 15 mL of commercial scintillation cocktail (Insta Gel) and 1.0 mL of [^{33}P]orthophosphate of known activity (0.103 μCi equivalent to 3.81 kBq). Each sample contained increasing amounts of quenching agent (CCl_4) as described in the table inset. *(L'Annunziata, M. F., 1986, unpublished work.)*

two techniques. The high dependence on accurate dispensing of internal standards in the IS technique and the high errors encountered at low count rates in the SCR technique have been eliminated in the combined IS-SCR method for quench correction. In the combined IS-SCR method, the disadvantage of the SCR method at low count rates is avoided by the addition of internal standard (IS) to low radioactivity samples. The SCR values are then taken for quench correction, instead of calculating the efficiency by the 'classical' IS method of measuring the contribution to count rate by the known amount of standard added. As only an SCR value is required after adding an internal standard, the dependence of the 'classical' IS method on accurate dispensing of standard to sample is also eliminated.

A similar combined IS-SCR technique was devised by McQuarrie and Noujaim (1983) for the counting efficiency determinations of either ^{3}H, ^{14}C, or both nuclides as a mixture. The unique characteristic of this method is the use of ^{67}Ga as the internal standard for either ^{3}H, ^{14}C, or the dual nuclide mixture. The liquid scintillation pulse-height spectrum of ^{67}Ga is characterized by two peaks (Fig. 7.10) corresponding to 8-keV Auger electrons and 93-keV conversion electrons, which are similar in energy to the average beta-particle energy of 5.7 keV for ^{3}H and 49 keV for ^{14}C. A ratio of the measured activity of the two ^{67}Ga peaks is used to reflect the degree of quenching in the sample. The sample is easily recovered after the internal standard ^{67}Ga decays $(t_{1/2} = 78$ hours$)$ and accurate dispensing of the internal standard to sample is not required, because only the ratio of activity between the two peaks is used to monitor quench.

3. Sample Spectrum Quench-Indicating Parameters

With the development of the multichannel analyzer (MCA), sample spectrum quench-indicating parameters (QIPs) have become more sophisticated, as all of the channels of the MCA can be used simultaneously to measure quench. Examples of quench-indicating parameters that measure quench by sample spectrum characterization are the spectral index of the sample (SIS), the spectral quench parameter of the isotope, SQP(I), and the asymmetric quench parameter of the isotope, AQP(I).

a. Spectral Index of the Sample (SIS)

The SIS is a measure of the mean pulse height or center of gravity of the sample pulse-height spectrum, which is utilized in the Tri-Carb liquid scintillation analyzers of PerkinElmer, Inc. The pulses produced from photon events are linearly amplified, digitized, and stored in a multichannel analyzer to produce a complete sample pulse-height spectrum in a region of pulse heights calibrated to represent the energy scale from 0 to 2000 keV. The SIS is a measure of the first moment of the pulse-height spectrum proportional to the average energy of the beta spectrum times a factor K or

$$\mathrm{SIS} = K\frac{\sum_{X=L}^{U} X\cdot n(x)}{\sum_{X=L}^{U} n(x)} \tag{7.6}$$

where X is the channel number (see the beta-particle pulse-height spectrum with respect to the numerous channels of the MCA in Fig. 7.5), $n(x)$ is the number of counts in channel X, L and U are the lowest and uppermost limits of the pulse-height spectrum, and K is a factor, which fixes the SIS of unquenched ^{3}H and ^{14}C at 18.6 and 156, respectively, corresponding to the respective maximum beta-particle energies of ^{3}H and ^{14}C in keV. Therefore, the SIS reflects the endpoint or maximum energy of the sample pulse-height spectrum as well as the magnitude and shape of the spectrum. From Eqn 7.6 we see that the value of SIS is (1) unitless, (2) always greater than 1.0, (3) becomes smaller in magnitude as quench increases for a given radionuclide, and, (4) at a given level of quench, beta-emitters of higher $E_{\max}$ will produce higher values of SIS.

An example of count rate (CPM) and quench-indicating parameter (SIS) data collected for a series of ten quenched tritium standards is given in Table 7.2. These data were collected by the liquid scintillation analyzer when the instrument counted each tritium quenched standard to provide a count rate (CPM) for each standard, which is listed in column 2 of Table 7.2. After the count rate of each standard is obtained, the

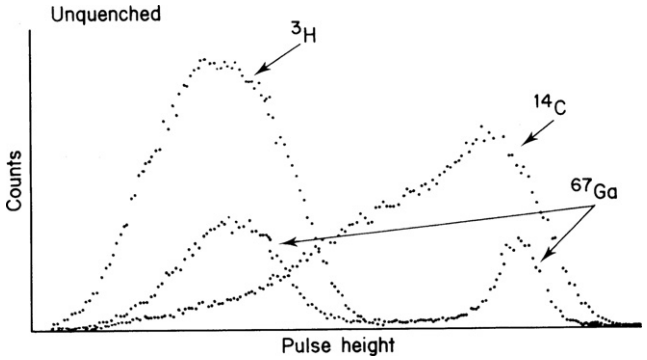

FIGURE 7.10 Liquid scintillation spectra of ^{3}H, ^{14}C, and ^{67}Ga. *(From McQuarrie and Noujaim, 1983. Reprinted with permission from Faculty of Pharmacy and Pharmaceutical Sciences © 1983 University of Alberta, Edmonton)*

TABLE 7.2 Data Collected for the Preparation of a ^{3}H Quench-Correction Curve of Counting Efficiency Versus the Quench-Indicating Parameter SIS

Standard	CPM	DPM	Efficiency (%)[a]	SIS
1	68,000	100,000	68	18.6
2	64,000	100,000	64	16.0
3	58,000	100,000	58	14.8
4	52,000	100,000	52	13.6
5	48,000	100,000	48	12.0
6	38,000	100,000	38	11.0
7	29,000	100,000	29	10.5
8	23,000	100,000	23	9.2
9	18,000	100,000	18	8.5
10	13,000	100,000	13	8.0

[a]*The % efficiency here refers to the % counting efficiency calculated according to Eqn 7.1. For the calculation of sample activities from count rate, the decimal equivalent of percent counting efficiency is used (e.g., 0.68 for 68%).*

LSA measures the QIP of each standard, in this case SIS, according to Eqn 7.6. The next step required for the preparation of the quench-correction curve is the calculation of the % counting efficiency for each standard according to Eqn 7.1. The instrument makes this calculation by taking the CPM (column 2) and dividing by the DPM (column 3) of each quenched standard and multiplying by 100 to obtain the percent counting efficiency.

The data of counting efficiency and quench-indicating parameter, SIS, listed in Table 7.2 is then taken automatically by the instrument to plot the quench-correction curve for tritium illustrated in Fig. 7.11. Another quench-correction curve, that for ^{14}C, is also plotted in Fig 7.11. The ^{14}C quench-correction curve was prepared in a fashion similar to the procedure described above for ^{3}H with the exception that ^{14}C quenched standards were used. Fig. 7.11, therefore, illustrates plots of the quench-correction curves for two radionuclides on the same graph. Several observations can be made from these two curves. The first observation is that for ^{14}C, which is a beta-particle-emitting radionuclide of intermediate energy ($E_{max} = 156$ keV), quench has a marked effect on the endpoint or maximum energy, as the SIS decreases from 156 to 25. However, the count rate (area under the pulse-height spectrum of each standard) or counting efficiency (CPM/DPM) decreases only slightly (0.95−0.83) as illustrated in Fig. 7.11. Therefore, for midrange to higher-energy beta-particle-emitting radionuclides, quench does not have as marked effect on the counting efficiency of the sample as on the apparent endpoint energy. The second observation is related to the tritium quench-correction curve. In the case of tritium, both the pulse-height spectrum endpoint and the counting efficiency are dramatically reduced as a result of quench. The curve of percent counting efficiency versus SIS is very steep for tritium. This dramatic slope can result in a rather large error in DPM values, if accurate SIS values are not obtained. Also, it is intuitively obvious, that the spectrum characterization method of determining the quench-indicating parameter is dependent on the counts in the sample. The larger the number of counts, the more accurate is the measurement of sample spectrum quench parameter (*e.g.*, SIS). From these observations, it is clear that the sample spectrum characterization method of determining the QIP should be used only when mid- to high-energy radionuclides are being quantified and when the count rate of the sample is well above background (>~1000 CPM). We shall see further on in this chapter that quench-indicating parameters derived from an external standard are more versatile and applicable to samples of both low and high activity (see Section V.C.). However, quench-indicating parameters derived from the sample spectrum are particularly useful when external standards cannot be applied such as in color quench correction for Cherenkov counting as demonstrated by L'Annunziata and coworkers (see Noor et al., 1996a). The SIS parameter was used by Vincze et al. (2007) in tests on the applicability of plastic scintillator beads in lieu of scintillation cocktail in a conventional liquid scintillation analyzer. The SIS is also a valuable tool in spectrum unfolding for the analysis of a mixture of two beta-particle-emitting radionuclides (L'Annunziata, 1997b, and Lee et al., 2002a,b) described further on in this chapter.

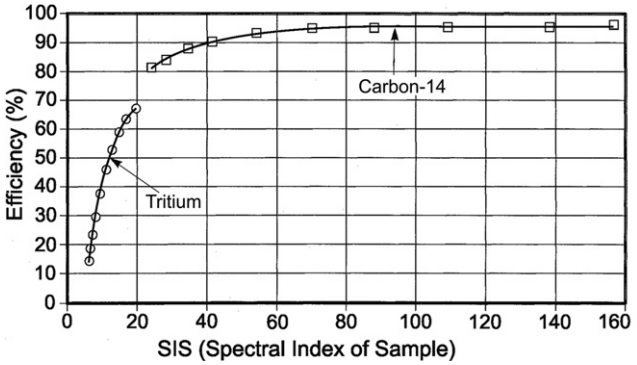

FIGURE 7.11 Quench-correction curves for ^{3}H and ^{14}C based on the quench-indicating parameter SIS, a sample pulse-height spectrum characterization method. *(© 1998 PerkinElmer, Inc. Printed with permission)*

Once a quench-correction curve is plotted by the liquid scintillation analyzer (LSA) and stored in its memory, it can be applied by the instrument computer to calculate the activity (DPM) of an unknown sample. For example, an unknown sample is counted and the LSA provides a count rate of 36,000 CPM and an SIS value of 12. The radionuclide is known to be tritium. A tritium quench curve of percent efficiency versus SIS, as illustrated in Fig. 7.11, is used by the LSA to determine the percent counting efficiency of that unknown sample. The instrument is programmed to read the stored quench curve and obtains the percent counting efficiency of 48% from the curve. The sample activity is calculated by the LSA according to the equation

$$\mathrm{DPM}_s = \frac{\mathrm{CPM}_{\mathrm{net}}}{E} \tag{7.7}$$

where DPM_S is the sample activity in disintegrations per minute, $\mathrm{CPM}_{\mathrm{net}}$ is the net count rate (i.e., background-subtracted count rate) of the unknown sample, and E is the counting efficiency obtained from the quench-correction curve as a decimal, not as a percent. The value of E should generally be in the range between 0 and 1.0, as the decimal representation of the percent counting efficiency over the range of 0−100%. Therefore, in this example, the instrument calculates the activity of the unknown sample as 36,000 CPM/0.48 and the resultant value of 75,000 DPM is obtained. The LSA can perform this type of analysis for all samples of unknown activities.

b. Spectral Quench Parameter of the Isotope Spectrum or SQP(I)

The spectral quench parameter of the isotope or SQP(I) is also referred to as the mean pulse height of the isotope spectrum (Rundt, 1991). It is utilized as a sample quench-indicating parameter with liquid scintillation analyzers of Wallac Oy (PerkinElmer, Inc.). The SQP(I) is measured by the liquid scintillation analyzer in a similar fashion as the previously described quench-indicating parameter SIS. As described by Grau Malonda (1999), the SIS provides a value for the center of gravity of the sample pulse-height spectrum plotted on a linear pulse-height scale, while the SQP(I) is a calculation of the

sample pulse-height spectrum plotted on a logarithmic scale according to the equation

$$\mathrm{SQP(I)} = \frac{\sum_{i=L}^{U} iN_i}{\sum_{i=L}^{U} N_i} \tag{7.8}$$

where i is the channel number of the MCA (see Fig. 7.5), N_i is the number of counts in channel i, and L and U are lowest and uppermost limits, respectively, of the sample pulse-height spectrum. By comparing Eqns 7.6 and 7.8, we can see the close similarities of the sample spectrum quench-indicating parameters, SIS and SQP(I).

The sample spectrum quench-indicating parameter SQP(I) has the same applications and limitations as SIS described previously. All methods of characterizing the sample spectrum to define the degree of quench in a sample require the use of quenched standards for the preparation of a standard quench-correction curve of counting efficiency plotted against the QIP. The procedures used to prepare a standard quench-correction curve are described in Section V.D.

c. Asymmetric Quench Parameter of the Isotope or AQP(I)

The asymmetric quench parameter of the isotope [AQP(I)] is a sample spectrum quench-indicating parameter employed with certain microplate scintillation counters of PerkinElmer, Inc. (Hughes et al., 2001). Quench-correction curves based on AQP(I) provide an improvement over the SQP(I) sample spectrum quench-correction curves for low-energy beta emitters such as tritium. The previously described SQP(I) is a quench-indicating parameter, which provides an MCA channel number equating the midpoint of the isotope spectrum. When quench occurs in tritium samples the shift in the MCA channel number according to quench is limited because of the small (low-energy range) of the tritium beta-particle pulse-height spectrum. The AQP(I) makes use of two multichannel analyzers, $\mathrm{MCA_1}$ and $\mathrm{MCA_2}$, providing two pulse-height spectra of the sample. The $\mathrm{MCA_1}$ produces a pulse-height spectrum of the sample of beta events detected by the two photomultiplier tubes in coincidence. The $\mathrm{MCA_2}$ records the beta events from only one MCA where pulse events of low height (*e.g.*, below channel number 150) are discarded. The setting of the channel discriminator can be adjusted to optimize quench-correction curves. The AQP(I) is then calculated from the ratio of the counts in the two MCAs or $\mathrm{AQP}(I) = \mathrm{MCA_1}/\mathrm{MCA_2}$. Since the pulse-height spectrum of $\mathrm{MCA_1}$ is always greater than that of $\mathrm{MCA_2}$, the value of the quench-indicating parameter is greater than one, and its value reduces in magnitude as quench increases.

A major advantage of the AQP(I) quench-indicating parameter is a very broad range of QIP values over a broad range of quench levels providing more accurate determination of detection efficiencies for low-energy beta emitters, such as tritium. For example, ^{3}H samples with counting efficiencies over the range of approximately 2.5−35% will yield AQP(I) values over the broad range of approximately 5−120, respectively. Therefore, a tritium quench-correction curve based on a plot of % counting efficiency of ^{3}H versus AQP(I) can be used to provide more accurate measurements of counting efficiency as a function of AQP(I).

C. External Standard Quench-Indicating Parameters

A method of quench correction more popular than the aforementioned sample spectral methods is the external standard method. This method uses an external source of gamma radiation to create a Compton spectrum in the scintillation cocktail as a tool to facilitate the measurement of quench in the sample. The sample with fluor cocktail in its scintillation counting vial is counted first in the absence and subsequently in the presence of the external gamma-ray source. This external gamma-ray source is located within the instrument and it is positioned into close proximity of the counting vial when needed. The general interaction of the gamma rays with the scintillation vial material and cocktail is mainly via the Compton effect (see Chapter 1). The external gamma radiation produces Compton electrons with a wide spectrum of energies within the scintillation cocktail. The Compton electrons produce a scintillation effect in the fluor cocktail and a characteristic pulse-height spectrum. The pulse-height spectrum produced by the external standard is used to create a quench-indicating parameter (QIP) for the measurement of quench in homogeneous samples in fluor cocktail. A series of radionuclide quenched standards are prepared generally as described in Section V.D, and a quench-correction curve of percent counting efficiency versus a QIP created by the external gamma-ray source is plotted. Once the quench-correction curve is prepared, the quench levels and activities of experimental samples are determined automatically by the LSA. The instrument determines the count rate of the sample and then uses the external standard gamma-ray source to measure the QIP of the sample. The value of the QIP is then used to obtain the radionuclide counting efficiency from the quench-correction curve. The counting efficiency, in turn, is used to convert the sample count rate to disintegration rate according to Eqn 7.7.

Some external standard gamma-ray sources used in liquid scintillation analyzers are ^{133}Ba ($t_{1/2} = 10.6\ y$), ^{137}Cs ($t_{1/2} = 30\ y$), ^{152}Eu ($t_{1/2} = 13.2\ y$), ^{226}Ra ($t_{1/2} = 1559\ y$), and ^{241}Am ($t_{1/2} = 432\ y$). The QIPs that are measured against the ^{133}Ba, ^{137}Cs, and ^{152}Eu external standards are defined as the tSIE (transformed spectral index of the external standard), H# (Horrock's number), and SQP(E) (*i.e.*, spectral quench parameter of the external standard), respectively. These quench-indicating parameters (QIPs) are determined differently and with different gamma sources. These will be described subsequently in addition to a quench-indicating parameter common to all external standard sources, namely, the external standard channels ratio (ESCR) technique.

1. External Standard Channels Ratio (ESCR)

The external standard channels ratio (ESCR) technique for the determination of counting efficiencies is similar to the SCR method described previously. The principal difference is that the channels ratio produced by the external standard Compton pulse-height spectrum is utilized rather than that produced by the sample pulse-height spectrum. The ESCR was once a very popular quench-indicating parameter before the advent of modern liquid scintillation analyzers equipped with more

versatile QIPs, such as *H*#, SQP(E), and tSIE; however, the ESCR method is still used with the older-generation instruments.

The ESCR technique offers the advantage that the optimum channel widths (counting regions) and gains for the channels ratio determinations are often factory set to monitor the scintillation events produced by Compton electrons, which result from the interaction of gamma rays of the external standard with the scintillation cocktail and vial wall. In the previously described SCR technique, the channel widths and gain settings, which produce the best (most linear) quench-correction curve, must be determined experimentally and will differ from radionuclide to radionuclide.

In practice, the ESCR quench-correction curve is prepared first by counting a series of variably quenched radionuclide standards in a preselected counting region from which counting efficiency values are obtained. After each of the above counts is obtained, an additional count is made for each sample exposed to the external gamma-ray source. The external standard counts are collected in two other preselected counting channels, and the net count rate in these two channels due to the external standard is computed by subtracting from both channels those pulses or counts contributed by the sample nuclide. The ESCR is obtained from the external standard count rates in these two channels. A plot of counting efficiency versus ESCR is then made as illustrated in Fig. 7.12.

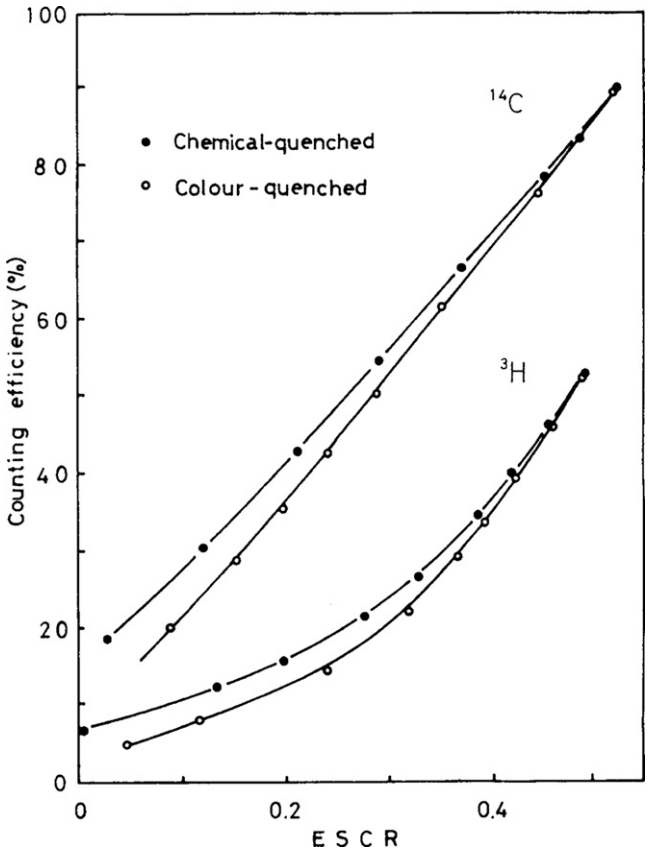

FIGURE 7.12 Color and chemical quench-correction curves based on the external standard channels ratio. *(From Takiue et al., 1983, reprinted with permission from Elsevier ©1983)*

Because the channels ratio in the ESCR method arises from counts produced by an external source, the ratio determination does not suffer from poor statistical accuracy for samples with low count rates, as does the SCR method. However, the ESCR technique has certain disadvantages among which are (1) the quench-correction curves are dependent on sample volume, (2) the quench-correction curves display a greater difference for color and chemical quenching, and (3) at least one minute additional counting time is required to count each sample exposed to the external standard. Wigfield and Cousineau (1978) found excellent agreement between counting efficiencies and various combinations of chemical and color quenching. They advise that the user investigate his/her own counting system and scintillation cocktail to evaluate the acceptability of this technique within acceptable error for samples with chemical and color quenching before discarding the use of this technique. Although the method currently is not commonly used in lieu of the more versatile external standard QIPs to be discussed subsequently, the ESCR method was used successfully by Lin et al. (2008) and Liu et al. (2005) for the measurement of ^{45}Ca, Wells et al. (2001) for the measurement of ^{32}P, and Al-Haddad et al. (1999) for the measurement of ^{3}H.

2. *H*-number (*H*#)

The *H*-number (*H*#), as a quench-indicating parameter, was first proposed by Horrocks (1976a, 1976b, 1977, 1978a), and it remains a versatile method for quench correction in liquid scintillation analysis with Beckman Instruments (Laureano-Perez, et al., 2010, Ray et al., 2009, Bonardi et al., 2004, Zimmerman et al., 1998, Zimmerman and Collé, 1997a,b, Sinor et al., 1997, Samuels and Scott, 1995, Newell and Krambeck, 1995, and L'Annunziata, 1987).

The technique involves the irradiation of liquid scintillation counting vials containing standards in scintillation cocktail, varying in their degree of quench, with an external radionuclide source ^{137}Cs (^{137m}Ba) emitting monoenergetic gamma radiation. The radiation reaching the scintillation vials and samples consists exclusively of 0.662-MeV gamma rays, as the 0.032-MeV X-rays from ^{137m}Ba are absorbed by the source container. Via the Compton effect, the gamma radiation produces a spectrum of Compton scatter electrons of varying energies between zero and E_{max} in the scintillation fluor cocktail.

The spectrum of energies of the Compton electrons is constant from sample to sample. However, the scintillation photon intensities and concomitant pulse heights produced by the Compton electrons will vary depending on the amount and type of quenching agent in each sample. The Compton scatter electrons produce a spectrum of pulse events as illustrated in Fig. 7.13. If only those Compton scatter electrons with energy E_{max} are considered, these would produce pulse heights of maximum magnitude as a peak referred to as the Compton edge. The magnitude of the pulse-height spectrum at the Compton edge is maximum for a sample free of quenching agents and saturated with nitrogen gas (nonquenched sample). The Compton edge of quenched samples is encountered at lower pulse heights than that of the non-quenched sample, and the degree of spectral shift is a function of the amount of quench in the sample. A measure of the degree of spectral shift or

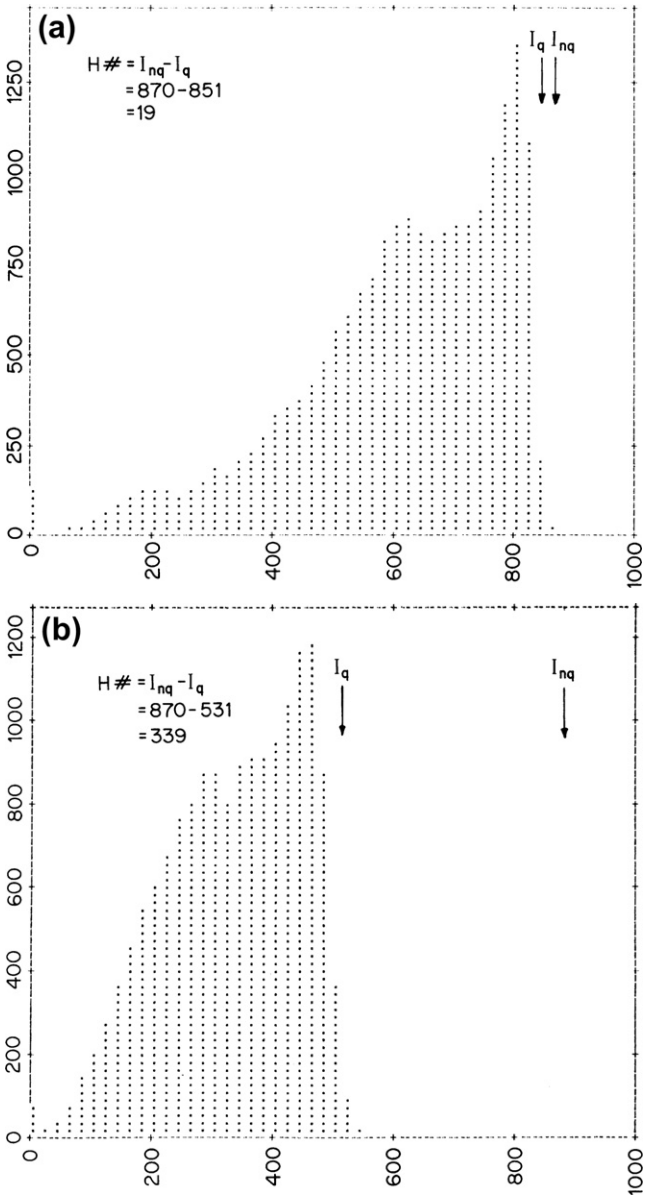

FIGURE 7.13 Effect of quenching on the inflection point of the external standard ^{137}Cs Compton edge for (a) a weakly quenched sample ($H\# = 19$) and (b) a strongly quenched sample ($H\# = 339$) in a Beckman LS 7800 liquid scintillation analyzer. *(L'Annunziata, M. F., 1986, unpublished work)*

difference in E_{max} pulse response is called the $H\#$, and it is a measure of the amount of quench in a sample.

In practice, the $H\#$ concept is applied to the quench correction of samples counted with liquid scintillation analyzers with logarithmic pulse-height conversion. Such systems convert the initial pulse-height response to the logarithm of the pulse height. Thus, initial pulse responses, which may differ by a factor of 1000, may be handled by a single amplifier and pulse-height analyzer and, as reported by Horrocks (1978b), there is a constant logarithmic difference between response relationships at different quench levels. For example, a 50-percent reduction in photon yield or an increase in quench by a factor of two represents a constant difference of 0.301 or the logarithm of two between the logarithmic response relationships of different quench levels. This is illustrated in Fig. 7.14.

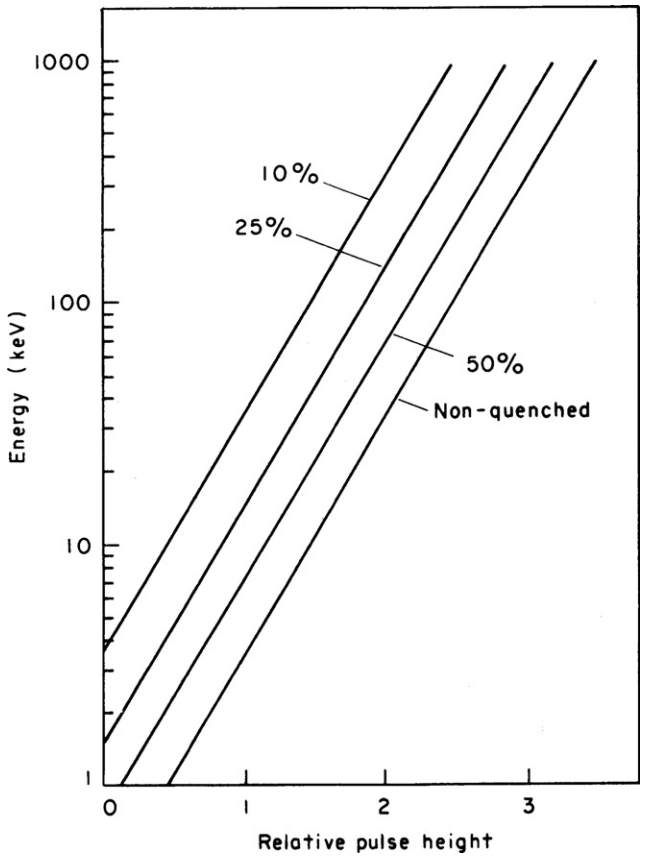

FIGURE 7.14 Relative quench effect on the logarithmic response for different electron energies. Curves are marked to indicate logarithmic response at quench levels of 50, 25, and 10 percent compared to the pulse-height response from nonquenched scintillation media. Curves marked '25%', '50%', and 'nonquenched' are separated by a constant value of 0.301 relative pulse height. *(From Horrocks, 1980. reprinted with permission from Elsevier © 1980)*

With logarithmic response relationships, the measured pulse height, H, may be defined using the notation of Horrocks as

$$H = a + b \log E \tag{7.9}$$

where H is commonly expressed in discriminator division, a is the pulse-height response for a 1-keV electron, and b is the slope of the energy response curve. For different levels of quench, the slope b will remain constant, but the value a will differ. For a nonquenched sample the measured pulse height, H_o, may be defined as

$$H_o = a_o + b \log E \tag{7.10}$$

Likewise, for a quenched system the measured pulse height, H_q, may be written as

$$H_q = a_q + b \log E \tag{7.11}$$

The difference between the measured pulse-height responses for electrons of the same energy (*e.g.*, E_{max} from ^{137}Cs Compton edge) in nonquenched and quenched systems is defined as the H # or

$$H\# = H_0 - H_q \tag{7.12}$$

$$= a_0 - a_q + b \log E - b\log E \tag{7.13}$$

$$= a_0 - a_q \tag{7.14}$$

The *H#* is determined by taking the difference between the relative pulse heights at the inflection points of the ^{137}Cs Compton spectra of nonquenched and quenched samples, as illustrated in Fig. 7.13. In the examples presented in Fig. 7.13, *H#* values of 19 and 339 are illustrated. Greater and lesser degrees of quench will result in a corresponding variation in the magnitude of the *H#*. The inflection points of the quenched and non-quenched samples are determined automatically by multichannel analysis while exposing the samples to an external ^{137}Cs(^{137m}Ba) source. The multichannel analyzer divides the pulse-height scale into narrow channels and accumulates the counts in each channel over a given period of time. A microprocessor then compares the counts in each channel to define the Compton spectra and precisely locate the inflection points.

With certain liquid scintillation spectrometers, for example, those of Beckman Instruments, the inflection point of the external standard Compton edge produced by a nonquenched fluor cocktail is factory set at 870 discriminator units. Quenched samples produce Compton edges with inflection points at lower discriminator levels, and the magnitude of the difference defines the *H#* (see the examples in Fig. 7.13).

In practice, a standard curve is prepared to relate counting efficiency to *H#*. This requires the preparation of a set of standards in liquid scintillation vials containing the same and known activity (DPM) of radionuclide and increasing amounts of quenching agent in scintillation fluor cocktail (see Section V.D for procedures for preparing quenched standards). These standards are then counted in optimal region settings (LL and UL discriminator settings) and the counting efficiency (E = cpm/dpm or cps/Bq) for each quenched standard is plotted against the *H#* as illustrated in Fig. 7.15. The counting efficiency of specific radionuclide samples of unknown activity is determined from their *H#* and the standard curve for that radionuclide.

The *H#* technique offers certain advantages over the 'classical' quench-correction methods such as SCR and ESCR. These advantages are (1) any sample can have only one *H#* value, contrary to channels ratio techniques, (2) the *H#* technique results in less variable quench-correction curves over a wider range of counting efficiency, (3) if the *H#* of a nonquenched standard is properly calibrated, the *H#* of any given sample would be constant from instrument to instrument, although the counting efficiency may not necessarily be constant.

3. Relative Pulse Height (RPH) and External Standard Pulse (ESP)

The relative pulse height (RPH) and external standard pulse (ESP) quench-correction techniques are similar in concept to the previously described *H#* quench monitor procedure.

In the ESP technique, reported by Laney (1976, 1977) and evaluated by McQuarrie et al. (1980), the liquid scintillation spectrometer measures the degree of quench in a sample by the shift in the average pulse height, P_s, originating from Compton electrons produced by an external ^{133}Ba gamma-ray source as compared to the average pulse height, P_r, produced in a sealed nonquenched reference vial stored in the elevator mechanism of the counter. The shift in the average pulse heights is defined by the ratio

$$\text{ESP} = \frac{P_r - P_\infty}{P_s - P_\infty}, \tag{7.15}$$

where P_∞ is a correction term corresponding to Compton electrons produced by the external gamma-ray source under 'infinite' quenching. In ESP determinations, the entire external standard pulse-height spectrum of quenched and non-quenched samples is stored in a multichannel analyzer from which the average pulse height is determined.

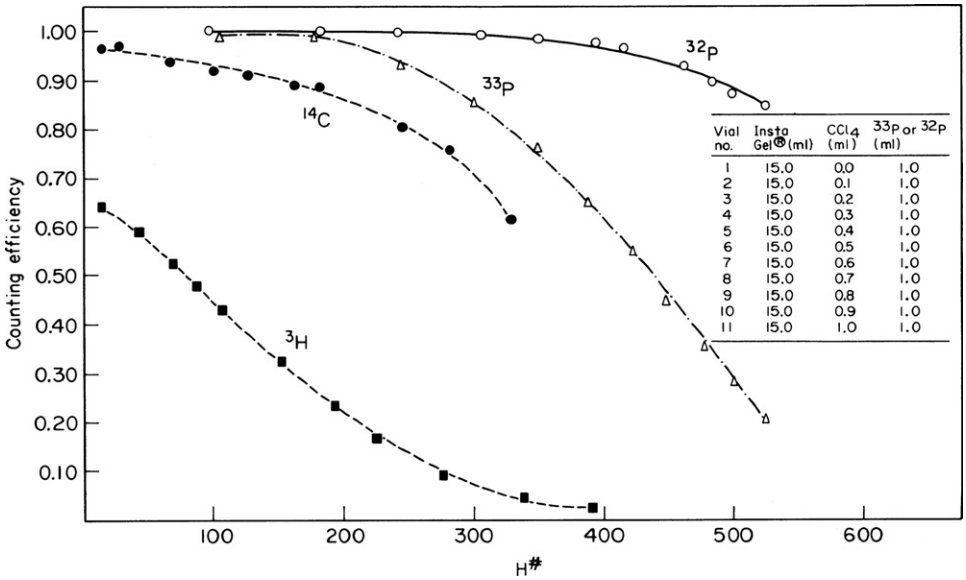

FIGURE 7.15 Quench-correction curves for ^{3}H, ^{14}C, ^{33}P, and ^{32}P based on the quench-indicating parameter *H#*. The ^{3}H and ^{14}C plots were obtained from commercially obtained quenched standards. Those of ^{33}P and ^{32}P were obtained from standards prepared with Insta Gel scintillation cocktail and CCl_4 quenching agent according to the table inset. *(L'Annunziata, M. F., 1986, unpublished work)*

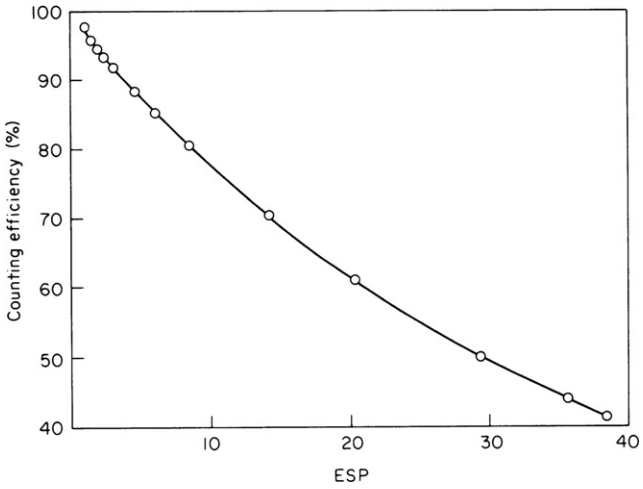

FIGURE 7.16 Variations in counting efficiency with ESP using quenched ^{14}C standards. *(Plotted from data of McQuarrie et al., 1980)*

As described in the case of *H#*, a quench-correction curve is prepared relating counting efficiency with ESP, using a set of quenched standards containing the same activity of radionuclide and varying amounts of quenching agent in fluor cocktail. A quench-correction curve is obtained by plotting counting efficiency against ESP as illustrated in Fig. 7.16. Laney (1976) defined the relative pulse height (RPH) as the reciprocal of the ESP. Both can serve as quench-indicating parameters, but ESP produces quench-correction curves with more linearity (Grau Malonda, 1999).

4. Spectral Quench Parameter of the External Standard or SQP(E)

The quench-indicating parameter SQP(E) is measured with ^{226}Ra or ^{152}Eu (Günther, 1998) as the external standard source in liquid scintillation analyzers of the LKB and Wallac instruments (Kouru, 1991 and Grau Malonda, 1999). These instruments are now manufactured by PerkinElmer, Inc. A multichannel analyzer with 1024 logarithmic channels is used to determine the position of 99.5% of the endpoint of the external standard Compton spectrum to define the value of the SQP(E). As described by Grau Carles (2006b), the endpoint of the Compton spectrum is a well-defined point for spectrometers with logarithmic amplifiers. The SQP(E) parameter, like all quench-indicating parameters (QIPs), is a relative number, and it is a meaningful number when compared to other SQP(E) values. As a QIP in liquid scintillation analysis, SQP(E) remains a robust and widely used parameter to monitor and correct for sample quench levels for the determination of detection efficiencies (Chmeleff et al., 2010; Jörg et al., 2010; Kossert and Grau Carles, 2010, 2008 and 2006; Wanke et al., 2010; Kossert et al., 2009; Krajcar Bronić et al, 2009; Varlam et al. 2009; Kossert et al., 2009; Werth and Kuzyakov, 2008; Laureano-Pérez et al., 2007; Tarancón et al., 2007; Grau Carles et al., 2006; Grau Malonda et al., 2006; Hou, 2005; and Hou et al., 2005).

The gamma source for the SQP(E) determination is positioned below the counting vial containing scintillation fluor cocktail. The SQP(E) defines the uppermost channel number (endpoint) that comprises 99.5% of the total counts of the external standard pulse-height spectrum. Only a small portion of the endpoint, the remaining 0.5% of the total counts or area under the pulse-height spectrum, is excluded (Kessler, 1989). As described by Grau Malonda (1999), the SQP(E) for a non-quenched sample is defined as

$$\text{SQP(E)} = P - 400 \tag{7.16}$$

where SQP(E) corresponds to the i value of the equation

$$\sum_{j=1}^{n} N_j \geq (1-r) \sum_{j=400}^{n} N_j > \sum_{j=i+1}^{n} N_j \tag{7.17}$$

where N_j is the total number of external standard counts in channel j, $r = 0.995$, $n =$ the total number of channels $= 1024$, and $\sum_{j=400}^{n} N_j = N_{\text{tot}}$ is the total number of external standard counts or area under the external standard pulse-height spectrum above channel 400. The above formula indicates that the first 400 channels of the external standard pulse-height spectrum are excluded from the calculations. The 400 channels at the lower end of the pulse-height spectrum corresponds to approximately 0−20-keV events, and the objective of the exclusion is to reduce that portion of the spectrum that could vary from any 'wall effect' that would occur whenever scintillation fluor solvent penetrates into the plastic wall of the counting vial. The wall effect is enhanced scintillation resulting from organic solvents such as benzene or toluene penetrating into the plastic vial wall. However, this effect generally does not occur to any appreciable extent with the modern solvents based on linear alkyl benzene and diisopropylnaphthalene (see Chapter 8.). In the elucidation by Grau Malonda (1999), the value of P is obtained from the equation

$$P = i + \frac{1}{N_i}\left[\sum_{j=i}^{n} N_j - (1-r)N_{\text{tot}}\right] \tag{7.18}$$

where N_i is obtained from the equation

$$N_i = \frac{1}{3}\left[\sum_{j=i-1}^{i+1} N_j\right] \tag{7.19}$$

As required with other quench-indicating parameters, it is necessary to count a set of quenched standards all having a known and constant activity of radionuclide but varying levels of quench. From the count rates of each standard and SQP(E) value measured by the liquid scintillation analyzer, a standard curve of counting efficiency for a given radionuclide versus SQP(E) is plotted, such as illustrated in Fig. 7.17 for the radionuclides ^{3}H and ^{14}C. When a sample of unknown activity of a given radionuclide is analyzed in the liquid scintillation analyzer, the instrument will determine the SQP(E) value of the sample, and subsequently extract the counting efficiency of that radionuclide from the standard curve.

5. Transformed Spectral Index of the External Standard (tSIE)

The external standard quench-correction methods previously described define specific characteristics of the external standard pulse-height spectrum as quench-indicating parameters, such as

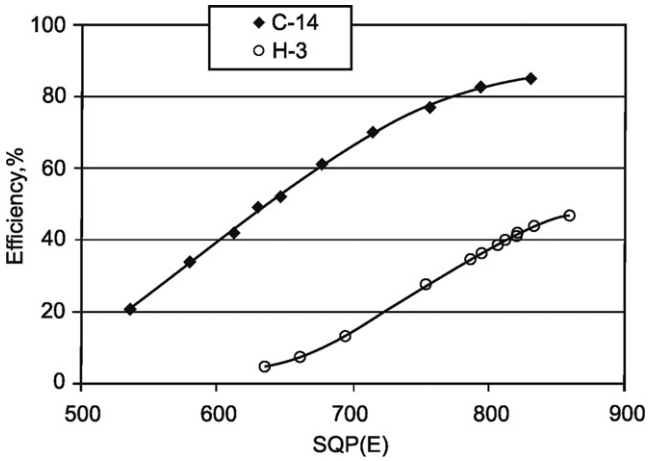

FIGURE 7.17 Quench-correction curves for ^{3}H and ^{14}C with SQP(E) as the quench-indicating parameter measured with a Quantulus™ 1220 liquid scintillation counter. *(From Hou, 2005, reprinted with permission from Elsevier © 2005)*

(1) the magnitude of the average pulse heights of the external standard Compton spectrum (*e.g.*, ESP and RPH), (2) the inflection point at the Compton edge (*e.g.*, *H*#), and (3) the endpoint of the external standard pulse-height spectrum [*e.g.*, SQP(E)]. Another popular external standard quench-indicating parameter was first reported by Everett et al. (1980) and Ring et al. (1980) under the designation of spectral index of the external standard (SIE). The SIE is similar to the SIS previously described with the exception that the SIE characterizes the external standard pulse-height spectrum in the same fashion as the SIS characterizes the sample pulse-height spectrum (Kessler, 1989). The objective of SIE is to characterize the external standard pulse-height spectrum to the extent of quantifying the various features of the pulse-height distribution and any changes in these features, which could occur as a result of quench. Features such as the spectral peak, slope at various points of the spectrum, and maximum pulse height will govern the center of gravity of the pulse-height spectrum, which will obviously change according to quench level (L'Annunziata, 1987). The SIE is calculated as

$$\mathrm{SIE} = k\frac{\sum_{X=L}^{U} X \cdot n(x)}{\sum_{X=L}^{U} n(x)} \tag{7.20}$$

where k is a factor assigned to provide a maximum value to the SIE of a nonquenched standard, X is the channel number, $n(x)$ is the number of counts or pulse events in channel X, and L and U are lower and upper limits that encompass the pulse-height spectrum. The lower limit L is set above zero sufficient to eliminate changes in pulse events of low magnitude produced by the 'wall effect'. That could occur if fluor cocktail solvent were to penetrate the plastic wall of the scintillation counting vial. Notice the close similarity of the above equation for SIE to that used to calculate SIS (Eqn 7.6). The values of SIE are unitless, always greater than 1.0, and of magnitude that will vary according to quench (*i.e.*, the higher the quench level in the sample, the lower will be the SIE value.

A further development based on the SIE is the transformed spectral index of the external standard (tSIE) introduced by

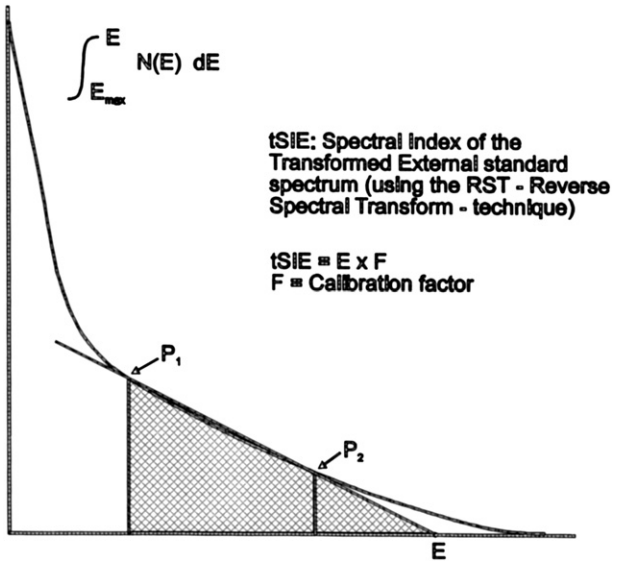

FIGURE 7.18 Transformed liquid scintillation pulse-height spectrum of an external ^{133}Ba standard. The tSIE is calculated by the extrapolated value E times a calibration factor F to provide a quench-indicating parameter in the range of zero to 1000. The highest value of tSIE = 1000 is set using an unquenched ^{14}C standard. *(©1998 PerkinElmer, Inc. Printed with permission.)*

Packard Instruments and now a product of PerkinElmer, Inc. The tSIE method of quench correction uses ^{133}Ba as the external gamma-ray source or standard. The Compton spectrum of this external standard is obtained in an MCA, such as the SIE described previously and transformed by performing a reverse back sum on the spectrum to obtain the transformed spectrum as illustrated in Fig. 7.18. From the transformed spectrum, an endpoint energy is determined by a reverse spectral transform (RST) technique using two points on the spectrum and extrapolating to the energy axis (Kessler, 1989). The simplified mathematical expression of the reversed spectral transform is

$$\int_{\hat{E}_{\max}}^{\hat{E}} N(\hat{E})d\hat{E} = \left(\int_{\hat{E}_{\max}}^{\hat{E}_2} N(\hat{E})d\hat{E} - \int_{\hat{E}_{\max}}^{\hat{E}_1} N(\hat{E})d\hat{E}\right) \times \frac{\hat{E} - \mathrm{tSIE}}{\hat{E}_2 - \hat{E}_1} \tag{7.21}$$

where $\hat{E}$ is the transformed energy and tSIE is calculated as one of the parameters of the RST function as

$$\mathrm{tSIE} = \hat{E} - (\hat{E}_2 - \hat{E}_1)\frac{\int_{\hat{E}_{\max}}^{\hat{E}} N(\hat{E})d\hat{E}}{\int_{\hat{E}_{\max}}^{\hat{E}_2} N(\hat{E})d\hat{E} - \int_{\hat{E}_{\max}}^{\hat{E}_1} N(\hat{E})d\hat{E}} \tag{7.22}$$

The final tSIE (extrapolated endpoint times a calibration factor) is calculated on the basis of the tSIE being equal to 1000 for a nonquenched ^{14}C sample, that is used for instrument calibration and normalization. Additional information on the measurement of tSIE and its applications is given by Kessler (1991a,b). The ^{133}Ba gamma-ray source for the measurement of the tSIE is positioned below the sample vial. The positioning of the external standard under the sample produces a quench

measurement that compensates for variations of sample volume. The value of tSIE, therefore, can be accurately determined even for small (<1 mL) sample−fluor cocktail mixtures.

The major advantages of using the external standard quench-indicating parameter tSIE rather than the QIP based on the sample spectrum (SIS) can be ascertained from Fig. 7.19, which shows quench-correction curves for tritium, ^{14}C, and ^{32}P plotted on the same graph. These plots of percent efficiency versus tSIE were obtained with a PerkinElmer 2700TR LSA using three sets of quenched standards, one set of standards for each radionuclide. The plots illustrate the dynamic range of the quench-indicating parameter from 1000 for the non-quenched cocktail mixtures to less than 100 for the highly quenched samples of the three radioisotopes. Also, we can note from Fig. 7.19 that, for a given level of quench, the counting efficiencies are higher for radionuclides that emit beta particles of higher energy, and quench has less effect on the counting efficiencies of radionuclides that emit beta particles of higher energy. It is important to recall that tSIE, like other external standard QIPs, is radioisotope independent; it is a function of the quality or quench level of the fluor cocktail. The second advantage of the external standard method over the sample spectrum characterization method for the determination of QIP is that the external standard method is sample count-rate independent. The external standard quench-indicating parameter (QIP) does not depend on the count rate of the sample; rather it depends on the counts created by the external gamma-ray source and the resultant Compton electrons produced within the scintillation fluor cocktail. The only disadvantage of the external standard method is that each sample must be counted alone and then counted again with the external standard present. This extra counting step usually requires about 6−120 seconds additional counting time, depending on the sample volume and quench level. This disadvantage is of little significance, because sample counting with and without the presence of the external standard and the measurement of the QIP are fully automated.

The quench-indicating parameter tSIE is, like the previously described SQP(E) external standard QIP, a very robust and commonly employed parameter for the measurement of quench and the determination of radionuclide detection efficiencies. Numerous examples are found in the literature, and a few examples covering a wide range of applications are the following: Chmeleff et al. (2010), Ishimori et al. (2010), Jörg et al. (2010), Kossert and Grau Carles (2010, 2008 and 2006), Stamoulis et al. (2010), Wanke et al. (2010), Zhilin, et al. (2010), Alamelu and Aggarwal (2009), Kossert et al. (2009), Lazare et al. (2009), Laureano-Pérez et al. (2007), Mikelic et al. (2007), Grau Carles et al. (2006), Grau Malonda et al. (2006), Mingote et al. (2006), Altzitzoglou (2004), Harms and Jerome (2004), and Johansson et al. (2004 and 2003).

Low-energy beta emitters, such as tritium ($E_{max} = 18.6$ keV), will exhibit a more significant variability in detection efficiency as a function of quench when compared to radionuclides that have higher beta-decay energies, such as ^{14}C ($E_{max} = 156$ keV), ^{33}P ($E_{max} = 249$ keV), and ^{32}P ($E_{max} = 1710$ keV). This is illustrated clearly in Figs. 7.11, 7.15, and 7.19. A maximum liquid scintillation detection efficiency for nonquenched tritium (*i.e.*, a sample containing no quenching agent) in modern liquid scintillation analyzers is ~68 % (see Table 7.2 and Figs. 7.11, 7.15, and 7.19), which is achievable with a nonquenched tritium

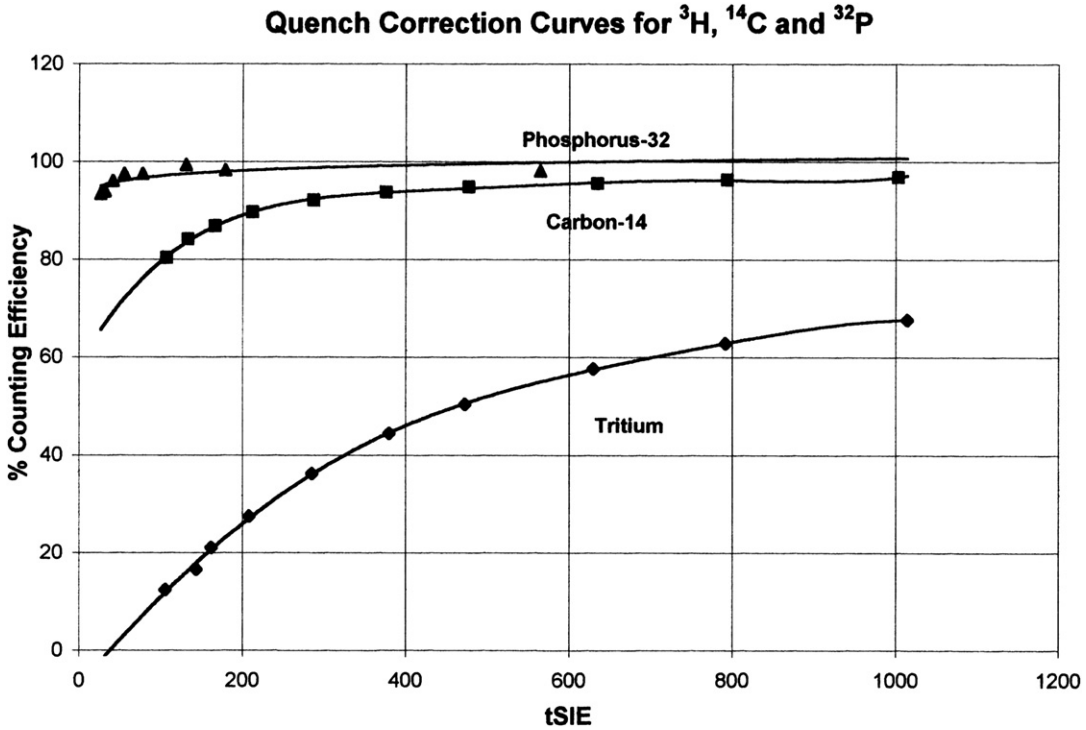

FIGURE 7.19 Quench-correction curves for ^{3}H ($E_{max} = 18.6$ keV), ^{14}C ($E_{max} = 156$ keV), and ^{32}P ($E_{max} = 1710$ keV) using tSIE as the external standard quench-indicating parameter with a PerkinElmer 2700TR LSA. The optimum counting efficiencies for the unquenched samples of ^{3}H, ^{14}C, and 5% water-quenched ^{32}P were 67.6, 96.9, and 98.1%, respectively. *(L'Annunziata, M. F., 1996, unpublished work)*

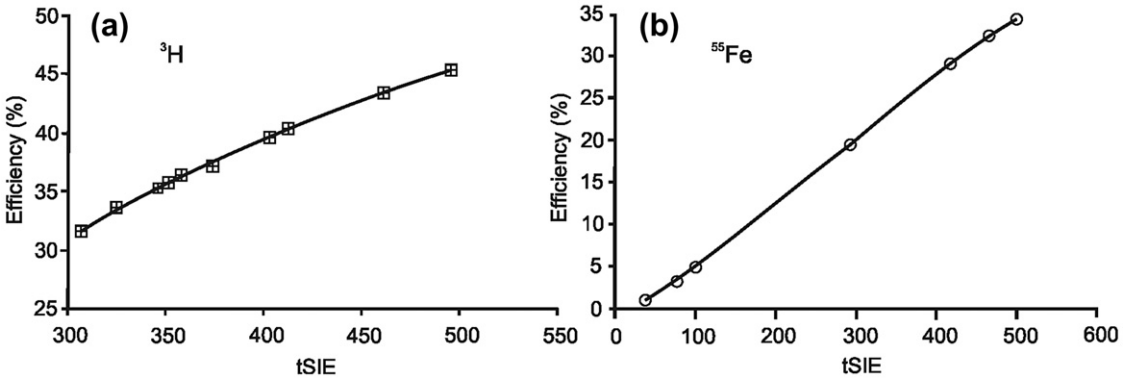

FIGURE 7.20 Quench-correction curves of detection efficiency (%) versus the quench-indicating parameter tSIE for (a) tritium (from Harms and Jerome, 2004, reprinted with permission from Elsevier © 2004) and (b) for ^{55}Fe. *(from Mikelic et al., 2007, reprinted with permission from Elsevier © 2007)*

standard generally used for instrument calibration. However, in practice, unquenched samples are not encountered, as the sample solution (*e.g.*, H_2O is a quenching agent as well as dissolved oxygen gas in the counting solutions). Thus, a typical quench-correction curve for tritium is one reported by Harms and Jerome (2004) and illustrated in Fig. 7.20a, which was prepared from a series of tritium quenched standards in counting vials containing the same and known activity of tritiated water (1 mL of HTO), 10 mL of scintillation fluor cocktail, and increasing amounts of up to 0.3 g of 10% nitromethane in ethanol as quenching agent. Fig. 7.20a clearly illustrates an optimum detection efficiency of ~45% for the tritiated water containing no nitromethane. Now, if we consider a radionuclide, such as ^{55}Fe, which emits Auger electrons of energy well below the E_{max} of the tritium beta particles, we will observe yet lower detection efficiencies for samples with similar quench levels as those previously discussed for tritium. The radionuclide ^{55}Fe decays by electron capture (EC) to stable ^{55}Mn with the emission of 5.2-keV Auger *K* electrons and Mn *K*-series X-rays of 5.9 and 6.5 keV (NNDC, 2011). A quench-correction curve for ^{55}Fe, illustrated in Fig. 7.20b, reported by Mikelic et al. (2007), was prepared from a series of quench standards of ^{55}Fe in fluor cocktail containing increasing amounts of nitromethane quenching agent. Although quenching agents can have a very significant affect on the liquid scintillation detection efficiencies of low-energy beta-emitting nuclides (*e.g.*, ^{3}H) and on the detection efficiencies of radionuclides that emit Auger electrons (*e.g.*, ^{55}Fe), the quench-indicating parameter tSIE as well as the previously described SQP(E) are robust QIPs capable of measuring accurately very low detection efficiencies (<10% E).

6. G-number (G#)

The G# is a quench indicating parameter (QIP) first described in detail by Grau Carles and Grau Malonda (1992) as a patent and subsequently reported by Grau Carles et al. (1993a). The method was designed to provide an accurate QIP regardless of the level of quench in a sample, even when the quench level is so high that the counting efficiency of the beta-emitting radionuclide is reduced to less than 1%. The idea behind this approach of Grau Carles and Grau Malonda is based on the use of an external standard which emits considerable quantities of high-energy gamma radiation sufficient to produce appreciable numbers of Compton electrons in the sample scintillation cocktail that have energies above the Cherenkov threshold of 263 keV. The LKB Rack Beta liquid scintillation analyzers (PerkinElmer, Inc.) are equipped with such a gamma source, namely ^{226}Ra; and the development of this technique was therefore demonstrated with the LKB instrument. The Compton electrons produced by the ^{226}Ra external standard will generate a pulse height spectrum, which is a result of photons emitted by the sample originating from a combination of scintillation and Cherenkov events. As explained by Grau Carles and Grau Malonda (1992), both scintillation and Cherenkov photons are detected simultaneously within the 18 ns time window of the coincidence circuitry of the liquid scintillation analyzer. However, when samples are very highly quenched in the liquid scintillation cocktail, the liquid scintillation diminishes considerably to the point that the pulse height spectrum produced by the ^{226}Ra external standard becomes the result of mostly Cherenkov photons produced by the portion of Compton electrons of energy in excess of 263 keV. In this fashion, regardless of the level of quench, a characteristic of the pulse height spectrum of the ^{226}Ra can be measured to provide an accurate QIP even when the scintillation process is quenched to the extent that beta-particle emitting radionuclides are counted at an efficiency of less than 1%.

Like all other methods of quench correction, this technique requires the preparation of a set of quenched standards of the radionuclide of interest. The quenched standards are counted in a suitable counting region defined by lower-level and upper-level discriminator settings. The count rate of each quenched standard is determined in this counting region, and the counting efficiency is calculated. The quenched standards are also exposed to the ^{226}Ra external standard gamma-ray source, and the resulting ^{226}Ra pulse-height spectrum is produced in the channel or counting region between 10 and 500. Fig. 7.21 illustrates pulse-height spectra produced by eight quenched standards exposed to ^{226}Ra external standard. The spectra show how the pulse heights shift from higher to lower magnitudes (higher channels to lower channels) as quench increases. At very high levels of quench (standards # 4 to # 8 of Fig. 7.21) the pulse-height spectra from ^{226}Ra are the consequence of mainly Cherenkov photons produced by the Compton electrons in excess of 263-keV energy.

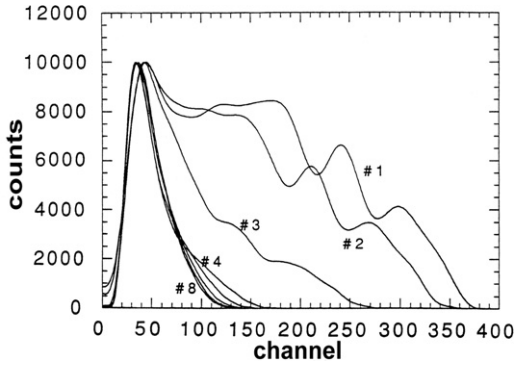

FIGURE 7.21 Compton spectra from ^{226}Ra adjusted and normalized for different quench levels. *(From Grau Carles and Grau Malonda, 1992, printed with permission)*

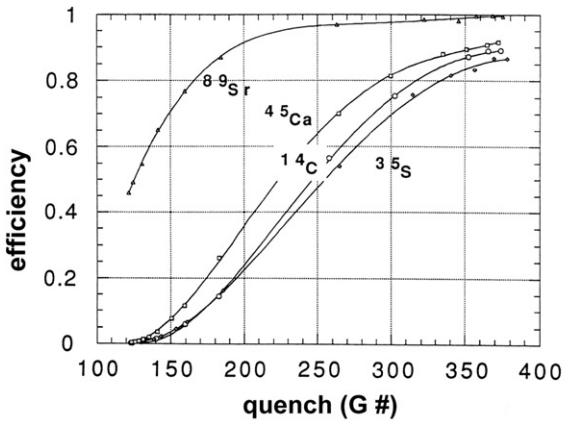

FIGURE 7.22 Calibration or quench-correction curves of counting efficiency as a function of the G-number for ^{35}S, ^{14}C, ^{45}Ca, and ^{89}Sr. *(From Grau Carles and Grau Malonda, 1992, printed with permission)*

The G-number is based on the analysis of the displacement of the final part (endpoint) of the ^{226}Ra external standard pulse-height spectra as a function of quench. According to Grau Carles et al. (1993a), Fourier series are fitted to the pulse-height spectra produced by the ^{226}Ra external standard to enable their normalization to the number of counts, y_N, of the first peak in the pulse-height spectra due to Cherenkov light created by the most energetic Compton electrons (*i.e.*, the left-most peaks in Fig. 7.21). The spectral interval within the limits $y_N/10$ and $y_N/500$ is taken from the final part of each external standard pulse-height spectrum. A linear relationship in the selected interval is obtained by raising the number of counts y to the power α or

$$y \rightarrow y^{\alpha} \quad 0 < \alpha < 1 \tag{7.23}$$

where α is the value, that provides the best regression coefficient in the line

$$y^{\alpha} = ax + b \tag{7.24}$$

For the channel with a number of counts $y = y_N/100$ the G-number is given by

$$G = \frac{(y_N/100)^{\alpha} - b}{a} \tag{7.25}$$

Examples of typical quench-correction curves obtained with quenched standards of ^{35}S, ^{14}C, ^{45}Ca, and ^{89}Sr are illustrated in Fig. 7.22, where it is clearly illustrated that the G-number serves as an excellent quench-indicating parameter over the widest possible range of counting efficiency from the highest detection efficiency to the lowest (<1%). This is clearer from the expanded quench-correction curve for highly quenched ^{45}Ca illustrated in Fig. 7.23 over the counting efficiency range of 1% to approximately 27%.

There is no documented rationale for the selection of the name 'G-number' for the identification of this quench-indicating parameter. However, the writer can only assume that the letter 'G' calls to mind the first letter of the family names Grau Carles and Grau Malonda, who devised this technique. Consequently, this QIP could likewise be called the 'Grau-number'. There exists a similar corollary in the previous development of the *H*-number by D. L. Horrocks, described

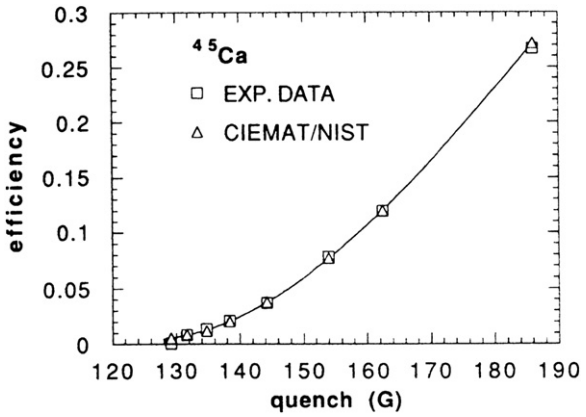

FIGURE 7.23 Experimental and CIEMAT/NIST computed efficiencies for ^{45}Ca. *(From Grau Carles et al., 1993a, reprinted with permission from Elsevier ©1993)*

previously in Section V.C.2. In recognition of its founder, the *H*-number is also referred to as the Horrocks-number.

D. Preparation and Use of Quenched Standards and Quench-Correction Curves

A quench-correction curve is a calibration curve of percent efficiency versus a quench-indicating parameter (*e.g.*, *H*#, SQP(E), tSIE, and G#). Examples of quench-correction curves are found in Figs. 7.9, 7.11, 7.12, 7.15–7.17, 7.19, and 7.20, 7.22 and 7.23. The quench-correction curve is prepared from a set of quenched standards, which is a series of samples containing the same radionuclide in scintillation cocktail, all with the same activity (DPM) but different levels of quench.

1. Preparation of Quenched Standards

There are two methods used for obtaining a set of quenched standards. The first method is to purchase a set of sealed standards for the radionuclide of interest and scintillation cocktail

type that one plans to use, and with the quenched standards, prepare a quench-correction curve of percent counting efficiency versus a suitable QIP. Quenched standards of ^{3}H and ^{14}C are available commercially, because of their relatively long half-lives. Some suppliers (*e.g.*, PerkinElmer, Inc.) can provide the quenched standards according to specification including variables such as (1) radionuclide standard activity, (2) scintillation cocktail, (3) quenching agent, (4) counting vial size and type, and (5) sample volume. Also, sets of quenched standards for ^{3}H and ^{14}C are sold on the market without customer specifications. If a user is interested in procuring these, it is important that he or she procures the set of quenched standards with vial size, sample volume, and scintillation cocktail compatible with their experimental samples. The second method is to prepare a series of quenched standards in the laboratory and to prepare the quench-correction curve from these quenched standards. This method can be the most reliable when very accurate DPM values are required, because the user can control all aspects of the preparation of the quenched standards to most closely represent the chemistry of his or her experimental samples. A detailed description of the procedure for the preparation of quenched standards and a quench-correction curve from the quenched standards is provided next. An outline of the steps is as follows:

a. **Choose the type and size of counting vial and sample volume that will be used.** Counting vials come in various sizes (*e.g.*, 4, 6, 8, and 20 mL) and as glass or plastic. Although glass and plastic vials may perform similarly (Elliott, 1984), there can be differences depending on the cocktail used and radionuclide analyzed. Also, background counts can be lower with plastic vials. The size of the vial can have a significant effect on counting geometry and the quench-correction curve could vary significantly according to this variable. The vial size and type, scintillation cocktail-sample volume, and cocktail composition of the quenched standards should be the same as the experimental samples (Collé, 1997a,b).
b. **Choose the scintillation cocktail that will be used.** Commercial scintillation cocktails come in various chemical compositions with differing properties, some miscible with organic solutions and others with aqueous sample solutions (see also Chapter 8.). Scintillation cocktails that use solvents such as toluene, xylene, pseudocumene, or linear alkylbenzene may be used with samples in organic solvents, while cocktails using diisopropylnaphthylene (DIN) or phenylxylylethane (PXE) as solvents may be mixed with aqueous samples. Most accurate results are obtained when the chemistry of the quenched standards are the same as the experimental samples. Detection efficiencies can vary between different scintillation cocktail compositions. Error can be introduced when determining the activity (*e.g.*, DPM) of an experimental sample mixed in a scintillation cocktail different from that from which the quenched standards were prepared. The error is particularly pronounced in the case of the LSA of low-energy radionuclides such as tritium (Collé, 1997a,b). It is best therefore to prepare quenched standards with the same scintillation cocktail to be used with the experimental samples.
c. **Prepare a stock solution to contain the radionuclide standard of interest of known activity (DPM) in the scintillation cocktail.** The radionuclide standard should have an activity that is accurately known such as one traceable to a primary standard (*e.g.*, NIST traceable standard) or a radionuclide standardized according to a known method of standardization. The standard used must be compatible and thoroughly miscible with the cocktail. The stock solution should be of sufficient volume to prepare more vials than standards that are needed to allow for the possibility of discarding some standard vials for reasons described subsequently. For example, if 10 quenched standards each containing 10 mL of scintillation cocktail are desired, than prepare a stock solution of more than 150 mL of scintillation cocktail containing radionuclide standard to allow the testing of 15 standards with the possibility of discarding 5 as described in step (5) below. The level of the radioactivity in the stock scintillation cocktail should be high enough to require counting the standards for only a short period of time and still achieve good or acceptable counting statistics. Activities of approximately 200,000 DPM per vial of low-energy-emitting radionuclide, such as ^{3}H, or approximately 100,000 DPM per vial of higher-energy-emitting radionuclide, such as ^{14}C, should be adequate.
d. **Transfer the exact aliquot of radionuclide standard−scintillation cocktail stock solution into each of the vials to be used for the preparation of the quench-correction curve.** The stock solution may be added by pipette or gravimetrically. Gravimetric addition can be the most accurate. The volume of the quenched standards should be similar to the volume of the experimental samples against which the quench-correction curve will be used. Counting geometry due to volume differences can affect the counting efficiency.
e. **Count each of the standards and determine whether the count rate (CPM) of each is within acceptable counting statistics.** A counting region that encompasses the entire radionuclide pulse-height spectrum can be used or other suitable counting region that would encompass a large part of the pulse-height spectrum and avoiding most background pulse events at the low-energy end of the background spectrum. The standards are of high activity and background counts can be subtracted or ignored if insignificant. Replicate counts of each standard (*e.g.*, count each standard from 5 to 10 times). Obtain a mean count for all of the standards. As an excess number of standards are prepared, any of the standards that deviate more than 2% from the mean count rate can be discarded. This provides us with a set of standards of equal activity in scintillation cocktail.
f. **Select a suitable quenching agent and add increasing amounts of the quenching agent to each standard.** In this step, the amounts of quenching agent do not have to be added with precision. Only the amount of

radionuclide standard in each vial, prepared in the previous step, must be exact. With respect to the quenching agent added, it is only important that each vial has increasing amounts of quenching agent so that a quench-correction curve of counting efficiency versus QIP can be established over a broad range of quench levels. Nitromethane is a popular quenching agent, because it is a strong quencher and only small increments are required. For example, if the scintillation cocktail uses toluene as a solvent and there are ten quenched standards of either ^{3}H or ^{14}C, than the following increments of nitromethane can be added to the vials: 0, 1, 5, 10, 18, 25, 35, 45, 55, and 65 μL to provide a broad range of quench levels. Notice that the first vial contains no added quenching agent. It would be the least-quenched standard. Radionuclide standards that emit higher-energy beta particles (higher E_{max}) generally require larger increments of quenching agent to provide a quench curve, which displays a significant reduction in counting efficiency against a QIP. For example, Fig. 7.15 shows ^{33}P ($E_{max} = 249$ keV) and ^{32}P ($E_{max} = 1710$ keV) undergo little change in counting efficiency over a wide range of quench level. Quenching agents have less effect on counting efficiency as the E_{max} of the beta-emitter increases, as illustrated in Figs. 7.15 and 7.19, using ^{3}H, ^{14}C, ^{33}P, and ^{32}P as examples. Other scintillation cocktails respond differently to nitromethane. For example, cocktails containing DIN or PXE solvent may require larger increments of nitromethane quenching agent. In such cases, the following increments of nitromethane for a set of 10 quenched standards may be appropriate: 0, 5, 10, 15, 28, 45, 70, 110, 150, and 230 μL. Other popular quenching agents are CCl_4, chloroform, acetone, and water, which are not as strong quenchers as nitromethane, also display differing degrees in their relative strength of quench. The amounts of quenching agent required will differ, because not all agents quench equally, *e.g.*, CCl_4 is a stronger quencher than water by two orders of magnitude (Grau Carles, 2006b). Classification of quenching agents according to their quenching power is given by L'Annunziata (1987). The quenching agent used should be soluble and not react with the scintillation cocktail. A color dye can be selected as a quenching agent for a set of quenched standards when color quench is expected in the experimental samples.

g. **If in doubt concerning the amounts of quenching agents to add, predetermine this experimentally.** Whenever the amounts of quenching agent required are in doubt, it is easy to predetermine this by adding various amounts of quenching agent to scintillation cocktail in counting vials without radionuclide standard. The vials can then be counted without radionuclide only to determine the external standard quench-indicating parameter (QIP) for each vial. Adjustments can be made with more or less quenching agent in order to achieve a wide range of quench levels according to the QIP.

h. **Label the quenched standards by number or letter (*e.g.*, 1 to 10 or A to J) and isotope, date, etc.** The quenched standards can be labeled only on the top of the counting vial cap. A round self-adhesive label may be placed on the cap or the information written on the top of the cap with a fine-tipped indelible pen.

i. **Store the quenched standards in the dark for a day or more for stability against any possible photo- or chemiluminescence.** Photo- and chemiluminescence are possibilities that can occur either when the counting vials are open or when quenching agent is added, respectively. The samples can be counted on a daily basis to observe if there is any reduction in count rate with time as evidence of luminescence. Once stability is confirmed, the quenched standards can be used to prepare a quench-correction curve.

A procedure alternative to the above for the preparation of a set of quenched standards would be to dispense the desired volume of scintillation cocktail to a set of counting vials. The volume would depend on the combined volume of sample and scintillation cocktail planned for the experimental counting vials (*e.g.*, 10, 15, or even 20 mL depending on vial size and capacity). The radionuclide standard is then added to each vial in equal amounts using a very precise microliter syringe with an adapter to help assure the addition of the same amounts to each vial. A Hamilton syringe equipped with a Cheney adapter (Hamilton Company, Reno, NV 89502, USA or CH-7402 Bonaduz, Switzerland) may be suitable. The writer finds it easier and more precise to prepare standards of equal activity by preparing a stock solution of radionuclide standard in scintillation cocktail and dispensing this solution into counting vials as described in steps c and d above.

If stored under refrigeration (5−10 °C), sets of quenched standards may be stable for two to three years. It is best to keep records of the quench-correction curves prepared from a given set of quenched standards from time to time (*e.g.*, monthly basis) to check their stability.

2. Preparation of a Quench-Correction Curve

The quench-correction curve or plot of counting efficiency versus quench-indicating parameter (QIP) must be determined with a set of quenched standards, and this curve stored in the memory of the liquid scintillation analyzer. The preparation of the quench-correction curve is described as follows:

a. **Set up a counting protocol on the LSC to plot a quench-correction curve of percent counting efficiency versus a quench-indicating parameter**. One of the QIPs that uses a sample spectrum characterization method may be used, although an external standard QIP is more often preferred for reasons described in Section V.C. Some modern liquid scintillation analyzers store the entire pulse-height spectrum of the sample counted onto the memory of the hard disk. With these instruments, it is often not necessary to set the counting region defined by lower-level (LL) and upper-level (UL) discriminator settings. Once the pulse-height spectrum of each quenched standard is stored in the instrument, the count rate in any counting region defined by LL and UL

discriminator settings can be extracted. However, in older-generation instrumentation it is necessary to first define the counting region according to LL and UL discriminator settings prior to counting the set of quenched standards. The counting efficiency can vary according to counting region settings, and consequently quench-correction curves of counting efficiency versus QIP can also differ according to counting region settings.

b. Count the quenched standards at a statistical accuracy of at least 0.5% 2s. Due to high activities of standards in each vial (100,000−200,000 DPM) the counting time required to reach the 0.5% 2s statistics should not exceed 5 minutes per quenched standard.

c. Obtain a plot of the percent counting efficiency of the radionuclide standards versus the QIP. Modern liquid scintillation analyzers will store these data in computer memory. When experimental samples are counted, the instrument should use the QIP measured for the sample and determine the counting efficiency from the correction curve.

3. Use of a Quench-Correction Curve

The objective of the quench-correction curve (also referred to as a calibration curve) is to determine the counting efficiency of experimental samples. From the counting efficiency the count rate (*e.g.*, CPM) of the sample is converted to radionuclide activity (*e.g.*, DPM) according to Eqn 7.7 described previously. When using a quench-correction curve, it is important to keep in mind certain rules, some of which may be intuitively obvious. These are the following:

a. A quench-correction curve is good for only one radionuclide and instrument.

b. The quench-correction curve is dependent on counting region defined by lower-level and upper-level pulse-height discriminator settings.

c. The quench-correction curve is scintillation cocktail dependent (Collé, 1997a,b). It is important to be certain that the scintillation cocktail used for the experimental samples is the same as that used for the preparation of the quench-correction curve. If a different cocktail is used for experimental samples compared to that used to prepare the quench-correction curve, it is necessary to confirm that there is no significant difference between the cocktails in performance for a given radionuclide. Differences in performance of cocktails are more pronounced when analyzing for relatively low-energy beta emitters such as ^{3}H and ^{14}C.

d. Quench-correction curves using an external standard QIP are preferred, because these are independent of sample activity.

E. Combined Chemical and Color Quench Correction

When there are significant quantities of chemical or color quench in scintillation cocktail there can be a significant difference in the chemical or color quench-correction curve

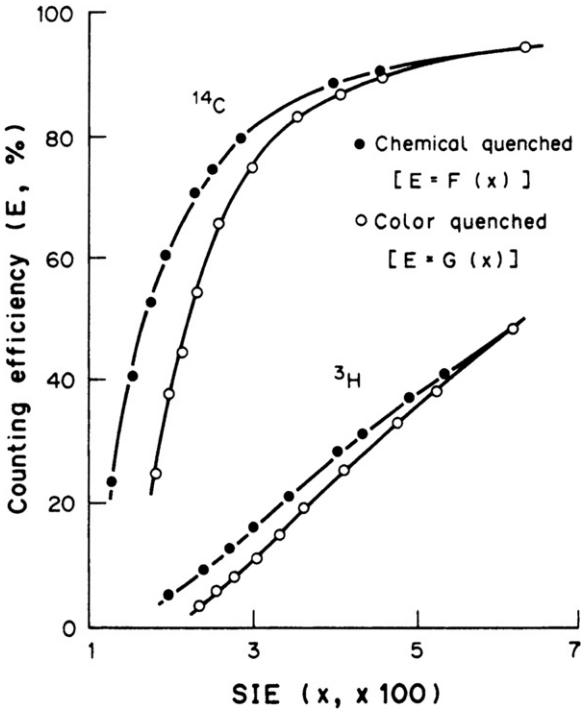

FIGURE 7.24 Chemical and color quench-correction curves based on an external standard. *(From Takiue et al., 1991a, reprinted with permission from Elsevier © 1991)*

obtained. This is particularly the case when there is a high degree of either chemical or color quench (high quench level) and for the liquid scintillation analysis of relatively weak beta-particle-emitting radionuclides such as ^{3}H ($E_{max} = 18.6$ keV) or ^{14}C ($E_{max} = 156$ keV). Examples of differences between chemical and color quench-correction curves can be seen in Figs. 7.12 and Fig. 7.24. Such differences can be observed regardless of the quench-indicating parameter used. The differences in the two curves is based on the two different mechanisms of quench, namely chemical quench that entails the inhibition of energy transfer from cocktail solvent to fluor molecules and color quench that entails the absorption of light photons emitted by the scintillation cocktail (see Fig. 7.1). As noted by Takiue et al. (1991b), the liquid scintillation pulse-height distribution of a color-quenched sample is different from that of a chemical-quenched sample, even if both the samples have the same activity and counting efficiency (see Fig. 7.25). Therefore, the pulse-height distribution of the external standard can be different for either color- or chemical-quenched samples producing different QIPs and different quench-correction curves. The difference can be more significant at high levels of quench as depicted on Figs. 7.12 and 7.24, and it becomes less significant as the beta-particle energy (E_{max}) of the radionuclide increases. The colors (*e.g.*, blue, red, green, and yellow) can have different effects on the degree of color quenching, as the photocathodes of the photomultiplier tubes within the liquid scintillation analyzer (LSA) vary in their degree of sensitivity or response to certain wavelengths. If samples to be counted are colored, it is best to prepare two series of quenched standards, namely, one set of standards that have increasing intensities of coloring agent (color quencher) and another set of standards

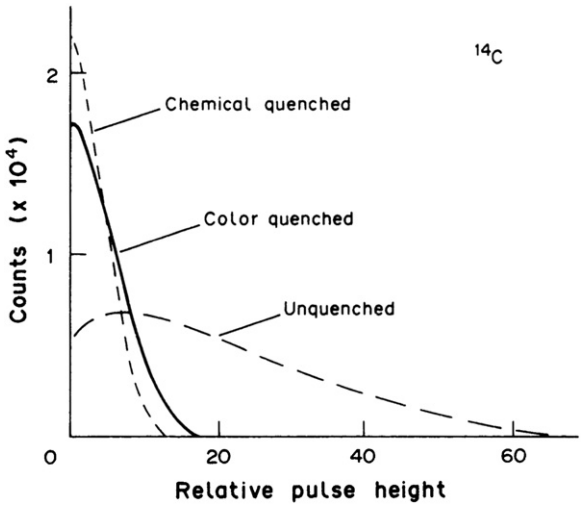

FIGURE. 7.25 Liquid scintillation pulse-height distributions of chemical- and color-quenched ^{14}C samples. Both samples have identical activity and counting efficiencies. *(From Takiue et al., 1991a, reprinted with permission from Elsevier © 1991)*

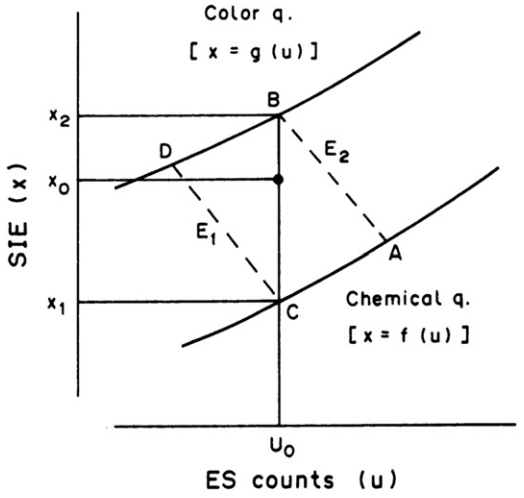

FIGURE 7.26 DESR curves for chemical- and color-quenched radionuclide used for the calculation of the counting efficiency of an experimental combined chemical- and color-quenched sample, where x_o and u_o are the quench-indicating parameter and external standard (ES) counts for the experimental combined chemical- and color-quenched sample. *(From Takiue et al., 1991a, reprinted with permission from Elsevier © 1991)*

containing varying amounts of chemical quencher. A comparison of the two quench-correction curves derived from these standards would provide evidence for any significant differences that might exist between the two types of quenching. Certain modern liquid scintillation analyzers are programmed to correct for color quenching (PerkinElmer, Inc.). Bukowski et al. (1992) found no differences between color and chemical quench-correction curves for ^3H when either picric acid (yellow color quencher) or CCl_4 (chemical quencher) was used as a quenching agent and the H# was measured as the external standard quench-indicating parameter (QIP). Also, Effertz et al. (1993) demonstrated identical quench-correction curves for the measurement of ^3H when either nitromethane (chemical quencher) or yellow, red, or green (color-quenching agents) were used as color quenchers and tSIE was utilized as the external standard QIP.

The best alternative when color exists in the sample is to decolorize (*e.g.*, sample bleaching or oxidation of organic samples to CO_2 and H_2O, see Chapter 8), because color causes quench, and it can reduce the detection efficiency. Decolorizing the sample eliminates the problem of color quench leaving behind only chemical quench, which is present in all samples to be analyzed. The works of Warwick et al. (2010), Williams and Kookana (2010), Sirelkhatim et al. (2008), and Hou et al. (2005) are excellent examples of the use of sample decolorization prior to liquid scintillation analysis of ^3H, ^{14}C, ^{63}Ni, and ^{55}Fe, thereby eliminating color quenching. If decolorization is not possible, most modern liquid scintillation analyzers are equipped with color-correction programs or algorithms that will correct for the difference between chemical and color quench. When both color and chemical quench are significant and cannot be avoided, it is recommended that the color-correction program provided with the instrumentation be utilized, if available, at high quench levels (e.g. tSIE < 400).

An example of a practical program for the correction of the difference between color and chemical quench-correction curves, whenever these are significant, was formulated by Takiue et al. (1991a). This method entails the preparation of two sets of quenched standards of a given radionuclide. One set of standards is prepared with a color-quenching agent (*e.g.*, bromothymol blue, methyl red, or bromocresol green) that produces minimal chemical quench, and another set of standards is prepared using a chemical-quenching agent (*e.g.*, nitromethane or CCl_4). The sets of quenched standards are used to plot two curves consisting of a color- and chemical-quench-correction curve of counting efficiency versus any external standard quench-indicating parameter (*e.g.*, *H*#, SQP(E), or tSIE, see Fig. 7.24). In addition, the color- and chemical-quenched standards are used to plot a second set of curves consisting of the external standard quench-indicating parameter plotted against the external standard counts, referred to as double external standard relation curves (DESR curves; see Fig. 7.26). When an experimental sample, that is quenched by both chemical and color constituents, is counted, the counting efficiency of the unknown sample has the value between E_1 and E_2, which corresponds to the external standard (ES) counts of u_o of the DESR curves illustrated in Fig. 7.26. Hence, as demonstrated by Takiue et al. (1991a), according to the geometry depicted in Fig. 7.26, the counting efficiency (E_0) is defined as

$$E_0 = E_1 + \frac{x_0 - x_1}{x_2 - x_1}(E_2 - E_1) \tag{7.26}$$

where x_1 and x_2 are obtained from the chemical and color DESR curves, respectively (Fig. 7.26) where $x_1 = f(u_0)$ and $x_2 = g(u_0)$. The efficiency values E_1 and E_2 are obtained from the chemical and color-quench-correction curves, respectively (Fig. 7.24) where $E_1 = F(x_1)$ and $E_2 = G(x_2)$. Eqn 7.26 is then written as

$$E_o = F(x_1) + \frac{x_o - f(u_o)}{g(u_o) - f(u_o)}[G(x_2) - F(x_1)]. \tag{7.27}$$

Takiue et al. (1991a) used polynomial curve fitting with the least squares method to define the coefficients of the quench-correction and DESR curves. This color-correction method is

easily applied with the computer application programs of most modern liquid scintillation analyzers. Nevertheless, the problem of combined color and chemical quench in samples is best averted by decolorization of samples prior to the addition of scintillation cocktail.

F. Direct DPM Methods

The Direct DPM methods entail the LSA measurement of the disintegration rates of radionuclides, particularly beta emitters, under various levels of quench without the use of quench-correction curves. These methods are described subsequently.

1. Conventional Integral Counting Method (CICM)

During the early years of liquid scintillation counting, it was discovered that an extrapolation of integral counting curves to zero discriminator bias could be used to determine the disintegration rates (DPM) of alpha emitters (Basson and Steyn, 1954) and beta emitters (Steyn, 1956) without interference from gamma emission. The method applied to alpha emitters received little attention, because the LSA counting efficiency of alpha emitters was close to 100% even in these early years of liquid scintillation development. As far as beta emitters are concerned, this technique, known as integral counting, received some popular attention and applications in the late 1950s and during the 1960s. Further developments made this technique a practical and accurate method for the activity measurement of beta-emitting radionuclides.

The work of Goldstein (1965) demonstrated the broad range of radionuclides that may be analyzed by integral counting as well as the simplicity of the procedure involved. In the development and testing of integral counting, Goldstein (1965) used the first and only commercial LSA available at that time, which was a Packard 314 liquid scintillation spectrometer. The procedure involved three pulse-height discriminators labeled AA', B, and C. The AA' discriminator was set just above the noise level to reject noise pulses. The C discriminator (upper-level discriminator) was turned off or disengaged so that all of the pulses of magnitude above the B discriminator would be registered and counted. The height of the B discriminator was varied in the range of 10−30 volts in 5-volt increments. The count rates for a given beta-emitting sample in scintillation cocktail were collected for each setting of the B discriminator. With the B discriminator at its lowest setting, the count rate is highest. With each incremental increase in the height of the B discriminator, the count rate diminishes, because fewer and fewer pulses are detected. The resulting plot of count rate on a logarithmic scale versus the B discriminator bias (volts) setting on a linear scale would be linear with negative slope, which could be extrapolated back to zero bias volts. At this point of extrapolation, the count rate (CPM) at zero bias would be the disintegration rate (DPM) of the sample. This extrapolation method is currently referred to as the conventional integral counting method (CICM). It is an effective method for extrapolating to sample DPM for beta emitters or beta−gamma emitters, which emit beta particles with an $E_{max} > 200$ keV, including ^{147}Pm, ^{45}Ca, ^{99}Tc, ^{36}Cl, ^{204}Tl, ^{89}Sr, ^{90}Sr(^{90}Y), ^{91}Y, ^{32}P, ^{131}I, ^{85}Kr, ^{131m}Xe, and ^{60}Co, among others, regardless of quench level. Corrections for quench in the sample scintillation cocktail mixtures are not necessary, because the quench level in the sample affects only the slope of the integral curve, and extrapolation of the curve to zero discriminator bias ends at the same count rate for all quench levels with expected statistical deviations (<2% error). Homma and Murakami (1977) also applied the conventional integral counting method to determine the activity of ^{226}Ra after separating the equilibrated ^{222}Rn in a liquid scintillator. The disintegration rates of ^{222}Rn and its daughters, which include both alpha and beta emitters, were determined by this method at various quench levels.

The conventional integral counting method for sample DPM determinations generally cannot be applied to the measurement of beta-emitting radionuclides of $E_{max} <$ about 200 keV. However, Homma et al., (1994a) developed the technique into the modified integral counting method (MICM), which can be used to determine the activities of all beta-particle emitters including ^{3}H of very low energy ($E_{max} = 18.6$ keV) and with higher accuracy.

2. Modified Integral Counting Method (MICM)

The modified integral counting method was reported by Homma et al. (1993a, 1993b), who modified the conventional integral counting method by extrapolating the integral counting curves, not to the zero pulse height as described above for the CICM, but to the zero detection threshold of the liquid scintillation spectrometer, which refers to the average energy required to produce a measurable pulse. They applied the new method to analyze the activity of alpha and beta emitters including ^{222}Rn and its daughters as well as the low-energy beta emitters ^{3}H, ^{14}C, ^{35}S, and ^{45}Ca with 100% detection efficiency. The method is described subsequently in more detail.

The modified integral counting method as was determined by Homma et al. (1994a) is carried out by the following procedure:

a. The first step requires the determination of the zero detection threshold of the particular liquid scintillation analyzer utilized for the analysis. This is carried out by measuring a standardized nonquenched ^{3}H sample according to the integral counting method described earlier. The observed integral count rates of the ^{3}H standard are plotted at several pulse heights and the curve is then extrapolated to the count rate, which is equivalent to the disintegration rate (DPM) of the ^{3}H standard. The keV value (pulse height) at this count rate represents the zero detection threshold. The zero detection threshold was found by Homma et al. (1994b) to vary from instrument to instrument over the range of 2.4−3.5 ± 0.2 keV.

b. Once the zero detection threshold is determined for the particular instrument, the absolute disintegration rate of any low-energy beta emitter ($E_{max} <$ about 200 keV) including ^{3}H as well as high-energy beta emitter ($E_{max} >$ about 200 keV) is determined by extrapolating the integral pulse height spectrum of the radionuclide of interest to the previously determined zero detection threshold.

Examples of results obtained from the modified integral counting method applied to the activity determination of ^{35}S

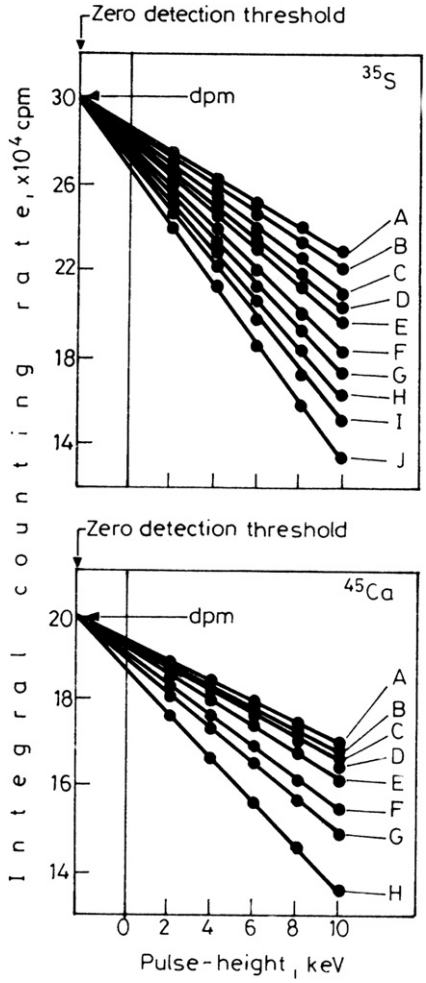

FIGURE 7.27 Extrapolation plots of the integral count rates of quenched ^{35}S and ^{45}Ca to the zero detection threshold for determination of the radionuclide disintegration rates. Letters A, B, C … denote samples with increasing quench levels. Deviations from actual DPM values were <1% for all plots *(From Homma et al., 1994b with kind permission from Springer Science + Business Media © 1994 Akadémiai Kiadó, Budapest.)*

and ^{45}Ca are illustrated in Fig. 7.27. As noted by Homma et al. (1994a,b), it is obvious from the plots illustrated, that extrapolation of the integral pulse-height spectrum to only the zero pulse height leads to an intercept value that is lower than the actual DPM of the radionuclide. However, extrapolation of the integral counting curve to the zero detection threshold leads to the actual disintegration rate of the sample.

The modified integral counting method was reported also by Homma et al. (1993a,b, 1994c) for the determination of ^{222}Rn and its daughters ^{218}Po, ^{214}Pb, ^{214}Bi, and ^{214}Po. Total α and β activity was determined with 100% counting efficiency. The MICM can be applied to the activity measurements of α- and β-emitters as single radionuclide samples or mixtures, and γ-emission does not interfere in most cases (Homma et al., 1994a). Measurements of ^{222}Rn with activity ranges of 0.2−22.9 Bq/L in natural water samples obtained from private wells and springs were carried out by Murase et al. (1998) with the MICM applying 100-minute counting times, which provided activities with an overall uncertainty of 3.1%. An integral counting method was carried out together with improvements in alpha liquid scintillation spectrometry by Yoshikawa et al. (2006) to determine ^{220}Rn/^{222}Rn ratios. For low-activity ratios, they developed a liquid scintillation alpha spectrometry method to measure ^{220}Rn with reduced error. The modified integral counting method has a practical simplicity similar to the efficiency tracing (ET) method described next. The ET method is most often used to determine the activity of single and multiple β- and β−γ-emitters; it can be applied also to the activity measurements of mixtures of α- and β- emitters (see Fujii and Takiue, 1988, and Chapter 15).

3. Efficiency Tracing with ^{14}C (ET)

Efficiency tracing (ET) with ^{14}C is another practical and simple extrapolation method applied generally to the activity measurements of β-emitting radionuclides with the exception of tritium. This method should not be confused with the CIEMAT/NIST efficiency tracing method described in Section IX.A, which is used for radionuclide standardization. The ET method was demonstrated by Takiue and Ishikawa (1978) to provide accurate DPM values for 14 radionuclides. A subsequent study by Ishikawa et al. (1984) showed that the technique provided accurate DPM measurements of 11 additional β- and β−γ-emitting radionuclides, namely, ^{14}C, ^{32}P, ^{36}Cl, ^{46}Sc, ^{59}Fe, ^{60}Co, ^{63}Ni, ^{86}Rb, ^{90}Sr (^{90}Y), ^{131}I, ^{134}Cs, and ^{147}Pm, regardless of quench level. The method was demonstrated by Fujii et al. (1986) in a study whereby the efficiency tracing DPM measurements of ^{14}C, ^{35}S, ^{32}P, ^{36}Cl, ^{45}Ca, and ^{131}I were determined for radionuclides on filter disks in LSA counting vials.

The efficiency tracing with ^{14}C (ET) technique involves the following steps:

a. A ^{14}C nonquenched standard is counted in six separate counting regions, such as counting regions defined by lower-level discriminators set at 0, 2, 4, 6, 8, and 10, and upper-level discriminators set at the upper limit of the pulse-height scale. For example, counting regions, such as 0−2000, 2−2000, 4−2000, 6−2000, 8−2000, and 10−2000 keV for lower-level (LL) to upper-level (UL) pulse-height discriminator settings on a linear keV equivalent scale, may serve as one example of workable counting regions. However, other similar counting regions may be used. Also, equivalent discriminator settings for liquid scintillation analyzers equipped with a logarithmic scale for pulse-height analysis may be determined. See L'Annunziata (1997a,b) and L'Annunziata and coworkers [Noor et al. (1996a)].

b. The percent counting efficiency values of the non-quenched ^{14}C standard in each of the six counting regions are calculated according to Eqn 7.1.

c. A sample of unknown activity is subsequently counted in the same six regions as the non-quenched ^{14}C standard.

d. The six CPM values of the sample of unknown activity are plotted against the six percent counting efficiency values of the non-quenched ^{14}C standard.

e. The curve is then extrapolated to 100% counting efficiency, where the CPM of the unknown sample is equal to its DPM. Extrapolation may require a linear or multilinear regression least-squares best fit of the data points and definition of the equation to the line or curve to most accurately determine

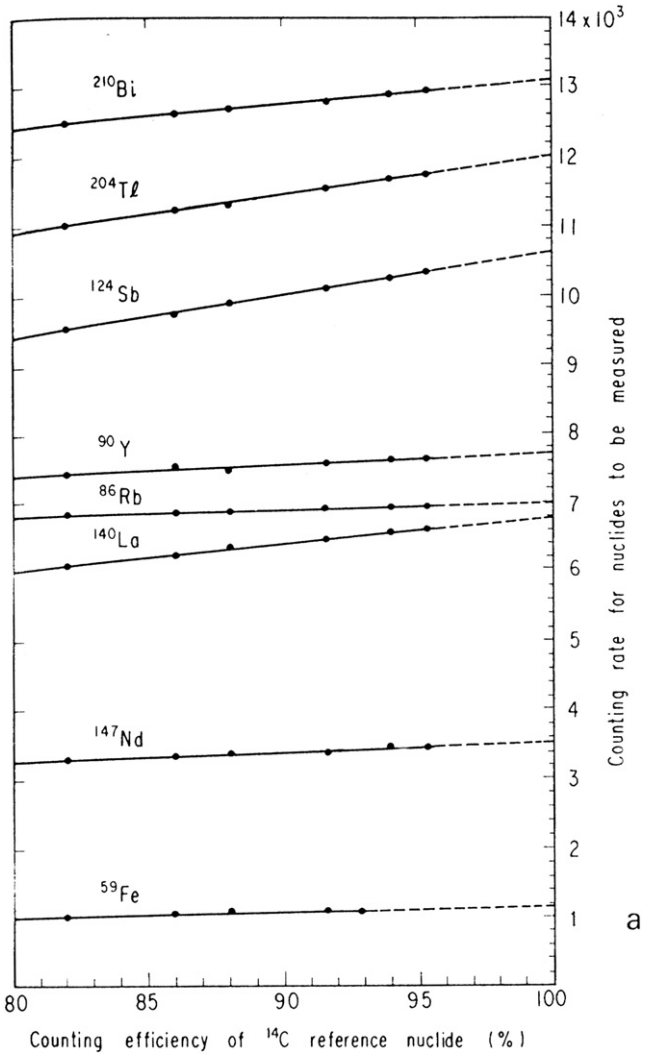

FIGURE 7.28 Efficiency tracing curves of eight radionuclide samples. The dashed portion of the plots represents the extrapolated segments to 100% counting efficiency. Extrapolated values indicate the counting rates at 100 % counting efficiency or DPM of each nuclide. *(From Takiue and Ishikawa, 1978, reprinted with permission from Elsevier © 1978)*

the point of intersection at 100 % counting efficiency. An example of eight efficiency tracing curves for the DPM determination of eight radionuclides is illustrated in Fig. 7.28, and an example of an efficiency tracing curve for the analysis of ^{35}S from the writer's work is illustrated in Fig. 7.29.

Variables such as sample scintillation cocktail volumes over the range of 1−20 mL, composition of the scintillation cocktail, amount or kind of quenching agent, or size and material of the counting vial may affect the slope of the efficiency tracing curve of the sample of unknown activity. At low quench levels the curves are often linear, as illustrated in Fig, 7.28. Linear regression analysis in these cases will define the equation to the line permitting extrapolation of the curve to 100% detection efficiency and DPM of the sample. At higher quench levels, the efficiency tracing curves may not be linear, such as illustrated in Fig. 7.29. In these cases quadratic regression may be needed to fit the data to a second-order polynomial $y = ax^2 + bx + c$, where the independent variable x is the % counting efficiency and the dependent variable y is the sample count rate (CPM). When x of the regression curve is given the value of 100%, the calculated value of y provides the extrapolated sample activity or disintegration rate (DPM). Examples of radionuclide activity recoveries that have been reported by this method are given in Table 7.3. The table indicates that at very high levels of sample quench (*e.g.*, SIS $<$ 1000 for ^{86}Rb and SIS $<$ 69 for ^{33}P) error can creep into the dpm calculation. This is due to the fact that the efficiency tracing curves lose their linearity and even take on a marked concave shape complicating the mathematical extrapolation to 100% efficiency.

An additional attribute of the efficiency tracing technique is the possibility of determining the total DPM of mixtures of β-emitting radionuclides (with the exception of ^{3}H) and α/β-emitters as demonstrated by Fujii and Takiue (1988a,b) and L'Annunziata and coworkers [see Noor et al. (1996a)]. The activity of ^{3}H cannot be measured by this method, as the efficiency tracing curves for ^{3}H are too concave yielding inaccurate extrapolation to 100% detection efficiency. Table 7.4 illustrates the excellent recoveries obtained for total DPM measurements of mixtures of ^{86}Rb + ^{35}S + ^{33}P. It should be noted, however, that the technique provides the total DPM of the mixture and not the activities of the individual radionuclide components of the mixture.

This direct DPM method is very useful for the determination of activities of radionuclides of relatively short half-life for which NIST-traceable standards are not available commercially. The ET-DPM method is an automatic radionuclide activity analysis option available with some Packard liquid scintillation analyzers (now manufactured by PerkinElmer, Inc.). With these liquid scintillation analyzers, the DPM of any β-emitting radionuclide of $E_{max} > 70$ keV is determined with a homogeneous radionuclide sample in scintillation cocktail using a preprogrammed ET-DPM counting mode. The instrument automatically determines the DPM of the sample. Older Packard models manufactured during the previous decade would provide the user with a plot of the efficiency tracing curve. However, newer models do not provide the efficiency curve printouts.

The efficiency tracing DPM technique was reviewed by Kessler (1991b). Some practical examples of the application of the efficiency tracing method can be found in the literature including the analysis of ^{222}Rn by Yasuoka et al. (2005), ^{14}C and ^{45}Ca by Takiue et al. (2004), ^{32}P by Liyanage and Yonezawa (2003), and ^{14}C by Wakabayashi et al. (1999). The method was tested by L'Annunziata (1997a) and Edler (2004) for β-emitting radionuclide samples over a wide range of quench and levels of sample activity. On the basis of these tests, the following conclusions and recommendations are made:

1. The efficiency tracing DPM (ET-DPM) technique is an accurate method for the determining the total activity (DPM) of β-emitting and $\beta-\gamma$-emitting radionuclide samples with the exception of ^{3}H.
2. The ET-DPM method can be used to determinate the total activity (DPM) of a mixture of β-emitting radionuclides.
3. No quench-correction curves are needed, for either chemical or color quench, when using the ET-DPM method.

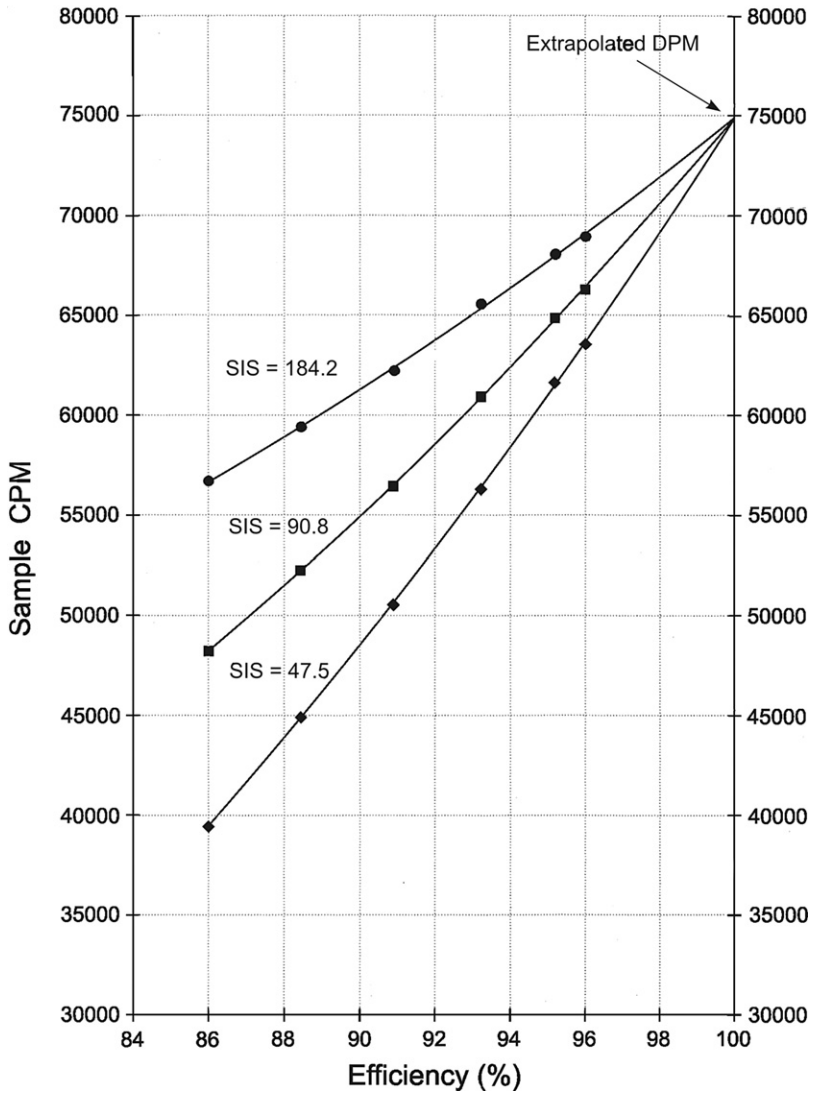

FIGURE 7.29 Efficient tracing (ET) curves for the activity determinations of three samples of ^{35}S at three levels of quench. The degree of quench is measured by the sample quench-indicating parameter SIS where the uppermost curve is that produced by the least-quenched of the three samples. *(From the work of L'Annunziata and coworkers, See Noor et al. (1996). Reprinted with permission from Elsevier © 1996)*

4. For best results samples should be counted for a duration sufficient to achieve a count rate with a % 2 sigma standard deviation (*i.e.*, % 2s) of 1% or lower.
5. The ET-DPM method is very useful for the determination of activities (DPM) of radionuclides of short half-life for which quenched standards are not available. When the activity of a nuclide is required within the limits established by a national bureau of standards (*e.g.*, NIST) for what is classified as a primary standard, the CIEMAT/NIST, TDCR, or other liquid scintillation method of radionuclide standardization is recommended. These methods are described in Section IX and in Chapter 14.
6. The ET-DPM method may be used to determine the activity of a source radionuclide prior to initiating a tracer experiment with that nuclide. Before beginning an experiment with a radionuclide as a tracer, it is best not to accept blindly the cited activity provided by the radioisotope supplier on the label of the source container. It is best to prepare replicate samples of the radionuclide source and use the ET-DPM method or other suitable method to confirm the activity (DPM) of the radionuclide source before beginning an experiment with that source.

Liquid scintillation analyzers previously manufactured by Packard and now by PerkinElmer, Inc. provide a counting mode called 'Direct-DPM'. This counting mode determines for the user the activities of beta-emitting samples in units of DPM. No quench-correction curves are needed. The user needs only to select the 'Direct DPM' counting mode and count the sample in a suitable liquid scintillation cocktail. In this 'Direct DPM' count mode the liquid scintillation analyzer first determines whether or not the sample is that of ^{3}H, which it can establish after measuring the tSIE and pulse-height spectrum of the sample. If the sample is ^{3}H, the analyzer will determine the DPM of the ^{3}H via a coded assay method, which involves the use of a quench-correction curve for ^{3}H, that is contained in

TABLE 7.3 Calculated Recoveries of Efficiency Tracing (ET) for the Determination of Activities of ^{86}Rb, ^{35}S, ^{33}P and a Composite Mixture of the Three Radionuclides under Various Levels of Quench[a]

Radionuclide	SIS	ET calculated DPM	Recovery (%)[b]
^{86}Rb	1568[c]	43,629[d]	100.0
	1043	43,077[d]	98.7
	83	45,293[d]	103.8
	41	42,563[d]	97.6
	28	42,729[d]	97.9
^{35}S	113.8 [c]	74,862[e]	100.0
	82.8	74,087[e]	99.0
	70.6	74,893[e]	100.0
	57.8	75,702[e]	101.1
	50.0	74,822[e]	99.9
	40.3	76,174[e]	101.8
^{33}P	184.2[c]	63,819[f]	100.0
	120.7	64,054[f]	100.4
	90.8	64,370[f]	100.8
	69.5	64,436[f]	100.9
	56.2	65,325[f]	102.4
	47.5	64,868[f]	101.6
^{86}Rb + ^{35}S + ^{33}P	463[c]	176,028[e]	100.0
	358	176,346[e]	100.2
	278	176,643[e]	100.3
	231	175,489[e]	99.7
	198	175,881[e]	99.9
	176	176,836[e]	100.4

[a] *From L'Annunziata and coworkers (See Noor et al., 1996a). Reprinted with permission from Elsevier © 1996.*
[b] *The % recoveries are calculated for those samples containing nitromethane quenching agent on the basis of the efficiency tracing DPM determined for those samples containing no added quenching agent.*
[c] *No quenching agent added.*
[d] *Linear regression extrapolation to 100% counting efficiency, mean correlation coefficient r = 0.985.*
[e] *Linear regression extrapolation to 100% counting efficiency, mean correlation coefficient r = 0.9997.*
[f] *Quadratic regression fitting of data to second order polynomial and extrapolation to 100% efficiency.*

TABLE 7.4 Percent Recoveries of Calculated Activities of Five Composite Mixtures of ^{86}Rb–^{35}S–^{33}P Determined by the Efficiency Tracing (ET) Technique[a]

Sample DPM (in hundreds) ^{86}Rb:^{35}S:^{33}P	Total DPM (actual)	Total DPM (ET)	Total DPM recovery (%)
4326:7294:7194	18,814	18,671	99.2
2146:3620:3424	9,190	9,185	99.9
1042:1794:1550	4,386	4,408	100.5
3113:5510:4620	13,243	13,237	100.0
432.3:742.6:646.1	1,821	1,819	99.9

[a] *From L'Annunziata and coworkers (see Noor et al. (1996a), reprinted with permission from Elsevier © 1996.*

the computer program of the analyzer (personal communication with Packard BioScience Co.; now PerkinElmer, Inc.). If the sample is a beta emitter other than ^{3}H, the liquid scintillation analyzer will determine the DPM of the sample using the efficiency tracing (ET) method described above in this section. The older models of Packard liquid scintillation analyzers manufactured in the 1990s were programmed to provide the user with a printout of the ET curve for each sample counted in the 'Direct DPM' count mode. These curves were plotted in the format depicted in Figs. 7.28 and 7.29. The modern Packard liquid scintillation analyzers, now manufactured by PerkinElmer, do not provide the ET curves in the 'Direct DPM' count mode; they provide simply the DPM of each sample counted and analyzed according to the ET method. Many examples in the scientific literature, particularly in the biological sciences (*e.g.*, Hawkins et al., 2010, Kobbe et al., 2009, Borthwick et al., 2008, Dianu and Podină, 2007, Mordaunt et al., 2005, Little and Rodríguez, 2005, Breitholtz and Wollenberger, 2003, Eardly et al., 2001, Roberts et al., 2001, and Holst et al., 2000), can be found where researchers utilize this 'Direct DPM' count mode. This is due to the fact, that the 'Direct DPM' count mode is very convenient, as there is no need to prepare a quench-correction curve for the beta-emitting radionuclide to be analyzed. Nevertheless, the writer would like to delineate some recommendations to the user of the 'Direct DPM' count mode, which are the following:

1. The use of a quench-correction curve to determine the DPM of the radionuclide of interest, such as one consisting of the % detection efficiency of the radionuclide of interest plotted against an external standard quench-indicating parameter [*e.g.*, tSIE, SQP(E), or H#] is preferred over the use of the 'Direct DPM' count mode. The rationale for this recommendation is based on the fact that, in the 'Direct DPM' count mode, the user is provided with the DPM of the sample; however, no curve or plot is available to the user to confirm the results obtained. If the user prepares a quench-correction curve, that curve is established, stored in the counting protocol of the instrument computer, used by the LSA computer to calculate the detection efficiency and DPM of each sample from the QIP [*i.e.*, tSIE, SQP(E), or H#], and the curve is available to the user to confirm the detection efficiency of each sample from its QIP. Once the quench-correction curve is established with the scintillation cocktail and nuclides of interest, the measurement of sample activities in units of DPM are automated by the LSA; and the quench curve provides important confirmation of the results.

2. If the 'Direct DPM' counting mode is used, it is recommended that standards containing the radionuclide of interest be prepared in the same formula of liquid scintillation cocktail used for the experimental samples of unknown activity. These standards should be of a similar count rate as the unknown samples, and these can be placed among the unknown samples as the samples are counted in the 'Direct DPM' mode. If the standards, which are of similar count rate and prepared in the same formula of scintillation cocktail as the samples of unknown activity, yield DPM values for the standards that are within acceptable error limits, then it can be assumed with confidence that the DPM values of the unknown samples counted together with the standards are acceptable within the same error limits. It is important that the standards be made of the same nuclide, have a similar magnitude of count rate, and be prepared in the same formula of scintillation cocktail as the samples of unknown activity.
3. For best results samples should be counted for a duration sufficient to achieve a count rate with a % 2 sigma standard deviation (*i.e.*, % 2s) of 1% or lower.
4. When analyzing for the activity (DPM) of ^{3}H, it is best to prepare a quench-correction curve for ^{3}H based on an external standard QIP as described in Section V.D. The ^{3}H standards should be prepared with a scintillation cocktail equivalent to the cocktail containing the samples of unknown ^{3}H activity.

4. Multivariate Calibration

The principles of multivariate calibration, including the multivariate methods of multiple linear regression (MLR), principal component regression (PCR), and partial least squares (PLS), among others, are described in detail by Varmuza and Filmoser (2009), Næs (2002), Martens and Næs (1992), Thomas and Haaland (1990), and Beebe and Kowalski (1987). The practical applications of MLR are indisputable, as this statistical method is of widespread use. The authors noted that PCR and PLS is gaining acceptance in chemistry, as the laboratory computer can facilitate data collection and processing required for multivariate calibration. As a statistical mathematical tool, multivariate calibration can be applied to a chemical or physical analysis when more than one measurement is acquired for each sample. Mathematical data matrices are written according to the numbers of samples and variables implicated in an analytical result. As explained by Beebe and Kowalski (1987), PLS is a factor-based modeling procedure in which factors are defined for any linear combination of the variables in the data matrices. The PLS algorithm estimates the factors in these matrices to provide a prediction of the observation on an unknown sample. Information on the mechanics of calibration and prediction using the PLS algorithm can be obtained from Gelaldi and Kowalski (1986) and a rigorous treatment of the methodology from Lorber et al. (1986).

García et al. (1996) applied partial least squares (PLS) as a multivariate calibration to determine (predict) ^{14}C activities in samples over the activity range of 1.48−15.16 DPM per sample-scintillation cocktail mixture. They used a Packard Tri-Carb® 2000 CA/LL liquid scintillation analyzer (now PerkinElmer Tri-Carb LSA) and samples with variable quench levels using a quenching agent in the concentration range of 0−0.6% CCl_4. For the multivariate calibration, they applied PLS regression using the PLS-Toolbox package for MATLAB devised by Wise (1992). The factors considered in two models constructed by García et al. (1996) consisted of ^{14}C content, quenching, blank, and spectral variability in one model, with blank omitted from the second model. They obtained slightly improved results omitting the blank (background) among the factors considered. Among 16 samples tested over the activity range of 1.48−15.16 DPM per sample, they obtained predicted activities with a relative error in the range of 0−5.4% (average = 1.09% relative error). This is the first application of multivariate calibration to activity determinations for single radionuclide samples. The multivariate calibration approach has been applied by several researchers to the simultaneous liquid scintillation analysis of mixtures of radionuclides, and these studies are discussed further on in this chapter. The multivariate calibration approach to the analysis of ^{14}C is yet to be applied routinely. However, it offers the advantage of being a time-saving approach to low-level liquid scintillation counting, because background information would not be needed and, therefore, total counting time reduced.

VI. ANALYSIS OF X-RAY, GAMMA-RAY, ATOMIC ELECTRON AND POSITRON EMITTERS

Liquid scintillation analysis (LSA) is not restricted to the activity analysis of pure beta- and alpha-particle-emitting nuclides. However, liquid scintillation is also applied to the analysis of nuclides decaying by electron capture and certain gamma-ray emitters (Grau Malonda, 1999). The electron-capture (EC) decay process often competes with positron emission, as described in Chapter 1. Consequently, radionuclides that decay by electron capture may also decay by positron emission. In addition, EC decay is generally accompanied by the emission of inner bremsstrahlung radiation, X-rays, Auger electrons, and gamma radiation when the daughter nuclide is left in an excited energy state, as illustrated in the following general EC decay process taken from Eqn 1.151 of Chapter 1 and presented here again for convenience:

$$e^{-} + p^{+} \rightarrow n + \nu + \text{inner bremsstrahlung} + \text{x-rays} + \text{Auger electrons} + \gamma \qquad (7.28)$$

The electron-capture decay process depicted above, often referred to as *K* capture, is described in detail in Chapter 1. Nuclides emitting gamma rays may also emit internal conversion (IC) electrons, as described in Section VIII.C of Chapter 1. Because electron capture often competes with positron emission, radionuclides that decay by positron emission also decay by electron capture. These nuclides are therefore grouped into this section of the chapter, as nuclides that may emit X-rays, gamma rays, atomic electrons (*i.e.*, Auger and IC electrons), and positrons. This broad potential of liquid scintillation analysis was illustrated previously in this chapter (see Fig. 7.10) where the 8-keV Auger electrons and 93 keV conversion electrons emitted from ^{67}Ga produce pulse-height spectra with peaks that coincide closely to those produced by ^{3}H and ^{14}C (McQuarrie and Noujaim, 1983). In addition to the emission of

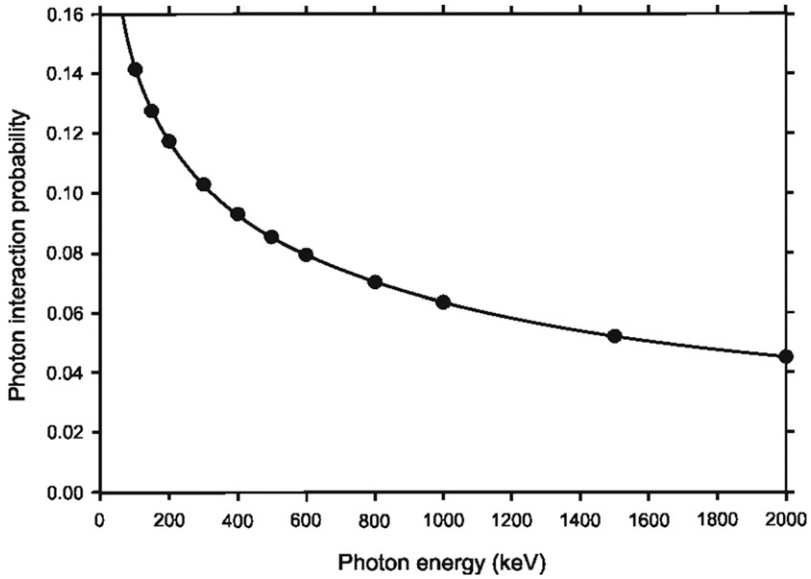

FIGURE 7.30 Simulated photon interaction probability determined at the indicated energies (closed circles) for a counting vial containing 12 mL of *Quicksafe A* liquid scintillator. The solid line is a regression fit to the data. *(From Simpson and Morris, 2004a, reprinted with permission from Elsevier © 2004)*

Auger and IC electrons ^{67}Ga displays major gamma-ray emissions at 93, 184, 296, and 388 keV. Altogether, the atomic electrons and gamma-ray photons interact with liquid scintillation cocktail, and efficiencies between 44 and 76% are reported by Bobin et al. (2007). Gamma-ray and X-ray photon interactions with liquid scintillation cocktail are a function of the photon energy as depicted in Fig. 7.30. Photon energies of low energy have greater probability of interaction with liquid scintillator, as the linear energy transfer (LET) of the photon is inversely proportional to its energy as illustrated in Table 1.25 of Chapter 1. In general, the lower the X-ray or gamma-ray energy, the higher will be the LET in the scintillation cocktail. As illustrated in Fig. 7.30, the photon interaction probabilities in liquid scintillator are high at photon energies below 100 keV. This is in agreement with the data of Zimmerman (2006a), who demonstrated very high photon interaction probabilities of >0.25 in toluene, >0.35 in Ultima Gold™ scintillation cocktail, and >0.5 in Hionic Fluor™ for photon energies of 20 keV.

Vanadium-49 is another radionuclide that decays solely by pure electron capture. It emits X-rays and Auger electrons of very low energy (<5 keV). Rodríguez et al. (1998) and Rodríguez Barquero and Los Arcos (2000) demonstrate that liquid scintillation analysis is the preferred method, because LSA is not affected by self-absorption problems that would otherwise be prevalent with such low-energy electron emitters. They report liquid scintillation counting efficiencies between 8% and 25% for ^{49}V.

In certain cases, the counting efficiencies of radionuclides that decay by electron capture emitting X-rays and Auger electrons may be higher with the liquid scintillation technique than those attainable with the thin-walled NaI(Tl) solid scintillation crystal detector. The liquid scintillation analyzer with its automatic sample changer and computer is more commonly encountered in laboratories than its solid scintillation counterpart. This reflects the driving force behind finding broader ranges of application of liquid scintillation counting.

The interaction of X- and gamma-ray photons with liquid scintillation cocktail (Fig. 7.30) is principally the result of the Compton effect, whereby part of the energy of the X- or gamma-ray photon is imparted to orbital electrons. An ejected electron (Compton electron) imparts its energy in material in a fashion similar to that of a beta particle. The absorption of its energy by the liquid scintillation cocktail results in fluorescence with the emission of photons of visible light. In liquid scintillation cocktail, the photoelectric effect usually does not occur over 30 eV. However, the photoelectric interaction is significant and accounted for in the liquid scintillation standardization of radionuclides (particularly low-*Z* nuclides) decaying by electron capture and emitting low-energy X-rays (Kossert and Grau Carles, 2010, 2008, 2006, Grau Carles, 2006a,b, and Grau Carles et al., 2006, Grau Malonda and Grau Carles, 2000). Bransome (1973) reports that the photoelectric effect can be evident at higher gamma-ray energies in the glass vial walls or, in the sample-scintillation cocktail mixture, if the scintillator is loaded with heavy elements.

Cherenkov photons will be produced in liquid scintillators to a significant extent if gamma-ray energies are high enough to produce Compton electrons of sufficient energy to cause the Cherenkov Effect (Grau Carles and Grau Malonda, 1992, and Grau Carles et al., 1993a,b). The Cherenkov Effect is discussed in detail in Chapter 15.

Numerous studies have been undertaken on the liquid scintillation analysis of ^{55}Fe, which decays exclusively by electron capture emitting X-rays and Auger electrons of low energy, 0.6−6.5 keV. Some examples that can be cited are Gudelis et al. (2010), Ratel (2008), Razdolescu et al. (2008), Fischer et al. (2007), Mikelic, et al. (2007), Grau Carles and Grau Malonda (2006), Grau Malonda et al. (2006), Grahek and Mačefat (2006, 2004), Warwick and Croudace (2006), Hou et al. (2005), Grau Malonda and Grau Carles (2000), Ceccatelli and De Felice (1999), Günther (1998), Ortiz et al. (1993), Grau Malonda (1982a,b), Cramer et al. (1971), Horrocks (1971),

Miller et al. (1969), Cosolito et al. (1968), Eakins and Brown (1966), Perry and Warner (1963), and Dern and Hart (1961a,b). Electron capture decay gives rise to the emission of X-rays, Auger electrons, and internal conversion electrons, which interact with the liquid scintillation cocktail to cause fluorescence. Recent papers report counting efficiencies of up to 62% for ^{55}Fe (Mikelic et al., 2007, Ortiz et al., 1993, Günther, 1998, and Grau Malonda and Grau Carles, 1999, 2000). A liquid scintillation detection efficiency in the range of 10−45% for ^{55}Fe, as a function of quench level using the external standard quench-indicating parameter SQP(E), was reported by Hou et al. (2005). A liquid scintillation quench-correction curve for ^{55}Fe is provided earlier in Fig. 7.20.

Another popular radionuclide, which decays exclusively by electron capture, is ^{125}I. The radionuclide is very useful as a tracer in the biological sciences (*e.g.*, Malkov et al., 2000, Teresa et al., 2000, and Larsson et al., 2001) and liquid scintillation is a very convenient and efficient means of analysis. The electron-capture decay results in the emission of 35-keV gamma radiation in 6.7% of the transitions and the emission of converted electrons in 93.3% of the transitions; this is accompanied with the emission of X-ray photons and Auger electrons (NNDC, 2011, Grau Malonda et al., 2006, and Grau Malonda, 1999). Early studies reported a liquid scintillation counting efficiency of 56% for ^{125}I by standard liquid scintillation counting techniques (Rhodes, 1965), and later yet higher counting efficiencies of over 80% were reported by Jordan et al. (1974), Horrocks (1976c), Ring et al. (1980), Chandrasekaran (1981), Kits et al. (1985), and Grau Carles et al. (1994c). Subsequent studies by Grau Malonda and Grau Carles (2000) report counting efficiencies of over 88% for ^{125}I in Insta Gel Plus and Ultima Gold liquid scintillation cocktail. The liquid scintillation detection efficiency is dependent on the quench level, and an example of an ^{125}I quench-correction curve taken from the work of Kim et al. (2006) is illustrated in Fig. 7.31.

As discussed in Chapter 1, either the electron-capture decay process or the emission of an internal conversion electron leaves an orbital electron vacancy. For the case of ^{125}I this vacancy may be filled by electrons from outer shells giving rise to the emission of X-rays of the Te daughter nuclide and Auger electrons. Horrocks (1976c) explained that the electron-capture process in ^{125}I involves capture of a *K*-shell electron in 80 percent of the decay transitions and an *L*-shell in the remaining 20 percent. The Te *L* X-ray is 3.5 keV in energy (NNDC, 2011) and totally absorbed by the liquid scintillation cocktail, whereas the Te *K* X-ray is emitted with 27.7-keV energy and has a high probability of escape. He concluded that the excitations in the liquid scintillation cocktail are due mainly to the absorption of Auger and internal conversion electrons, and only a minor contribution (about 8% of the fluor excitations) is the result of X-rays produced during the decay process. Liquid scintillation remains a common method of analysis for ^{125}I (Ogata, 2007, Grau Malonda et al., 2006, Kossert, 2006, Van Wyngaardt and Simpron, 2006a,b, and Pommé et al., 2005). An interesting approach taken by Ogata (2007) was the analysis of ^{125}I in solution within a microtube inserted inside a Bicron (BC-400) plastic scintillator with dimensions suitable to fit within a standard plastic liquid scintillation vial. No liquid scintillator

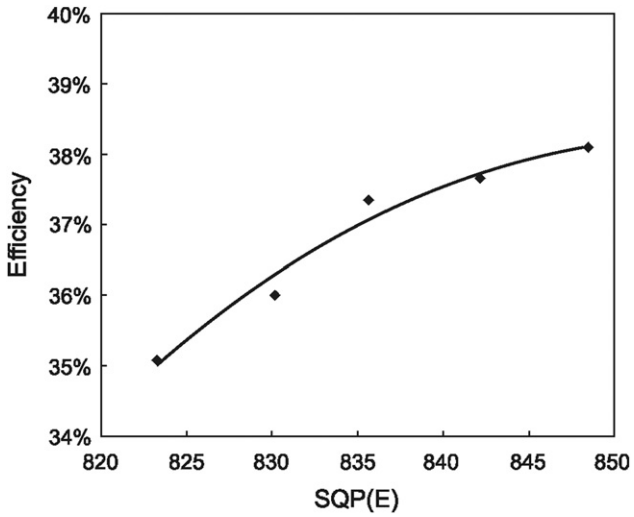

FIGURE 7.31 Quench-correction curve for ^{125}I based on the external standard quench-indicating parameter, SQP(E). The photon emissions from ^{125}I in scintillation cocktail are due to cocktail interactions with 35-keV gamma-ray emissions in 6.7% of the transitions, internal conversion electrons in 93.3% of the transitions and abundant Auger electron and Te K X-ray emissions (NNDC, 2011, see also Table of Radioactive Isotopes in the Appendix). *(From Kim et al. (2006), reprinted with permission from Radiocarbon, the University of Arizona, © 2006 Arizona Board of Regents on behalf of the University of Arizona)*

solution is used, there is no fluor waste to contend with, and the sample remains unadulterated and may be reused after counting in a conventional liquid scintillation counter. Ogata (2007) reported a detection efficiency of 4−8% for the electron-capture nuclide ^{125}I and a detection efficiency of 10−40% for the high-energy beta-emitting nuclide ^{32}P. The detection efficiency is a function of the sample volume.

Zinc-65 is another radionuclide used in the biological sciences as a tracer (Huntington et al., 2008 and Wolterbeek et al., 2002). It decays by electron capture and positron emission (see Table of Radioactive Isotopes in the Appendix). Günther (1998) and Sandhya and Subramanian (1998) report liquid scintillation counting efficiencies up to 76%. Only 1.5% of the ^{65}Zn nuclide transitions to stable ^{65}Cu occur via β^+ emission ($E_{max} = 325$ keV). Consequently, positron interaction with scintillation cocktail contributes only a small portion to the overall detection efficiency. About 50.5% of the transitions occur via electron capture (EC) to the ground state of ^{65}Cu and the remaining 48% by EC with accompanying gamma emission (Günther, 1998). Consequently, the abundant atomic electron and low-energy (1−9 keV) X-ray photons (NNDC, 2011), which accompany the EC decay process of ^{65}Zn, are the emissions that generate significant liquid scintillator excitation and light emission. Liquid scintillation analysis is employed for the standardization of ^{65}Zn (Kossert, 2006, Van Wyngaardt and Simpson, 2006b, and Simpson and Morris, 2004a).

Chromium-51 decays by electron capture and 10 percent of the excited daughter nuclei simultaneously undergo decay to the ground state with the emission of gamma radiation of 320-keV energy or the emission of internal conversion electrons of 315 keV (NNDC, 2011). Internal conversion electron emission competes with the emission of gamma radiation, and the conversion electrons are always slightly lower in energy than the gamma radiation. The energy difference is equivalent to the

binding energy of the atomic electron as described in Chapter 1. X-ray and Auger-electron emission, which accompany electron-capture decay, also must be considered among the processes that generate scintillation fluor excitation. Chromium-51 decays with the emission of 5-keV X-rays in 22 % of the transitions and 4.4 keV Auger electrons in 66 % of the transitions (NNDC, 2011). The double radionuclide tracer ^{59}Fe–^{51}Cr was assayed by Barosi et al. (1980) in red blood-cell kinetic studies. If the double-label is assayed by NaI(Tl) solid scintillation counting of the gamma-ray photopeaks of the two nuclides, optimum counting efficiencies of 15% and 3% are reported for ^{59}Fe and ^{51}Cr, respectively. However, if liquid scintillation counting is used, optimum counting efficiencies of 20% and 15% are reported for the ^{59}Fe and ^{51}Cr double label, respectively. The five-fold increase in the counting efficiency of ^{51}Cr is due mainly to the liquid scintillation cocktail absorption of X-ray and Auger electron energy. More recent work by Bradshaw et al. (2006) and Kumblad et al. (2005) provide examples of the application of ^{51}Cr as a tracer nuclide, and 5% detection efficiency for the liquid scintillation analysis of ^{51}Cr was reported (Kumblad et al., 2005).

Positron-emitting nuclides can be assayed by liquid scintillation analysis with a high detection efficiency when positron emission is the principal mode of decay. As described in Chapter 1, positrons have similar interactions, ranges, and stopping powers as negatrons of similar energy; however, in addition, positrons will produce annihilation radiation (0.511-keV gamma rays) when the positrons come to rest in the proximity of atomic electrons. The liquid scintillation pulse-height spectra produced by positrons are similar to those of negatrons as expected (see Fig. 7.32). Roteta et al. (2006) report a liquid scintillation detection efficiency close to 100% for the positron emissions from ^{18}F. The radionuclide ^{18}F decays by to the stable nuclide ^{18}O by positron emission with a positron $E_{max} = 634$ keV in 96.7 % of the transitions and by electron capture in the remaining 3.3 % of the transitions (NNDC, 2011). Positron annihilation radiation of 511-keV gamma-ray photons (See Chapter 1) always accompanies positron emission, and, as pointed out by Schrader et al. (2007), the liquid scintillation pulse-height spectrum illustrated in Fig. 7.32 will have some contribution from the secondary Compton electrons of the

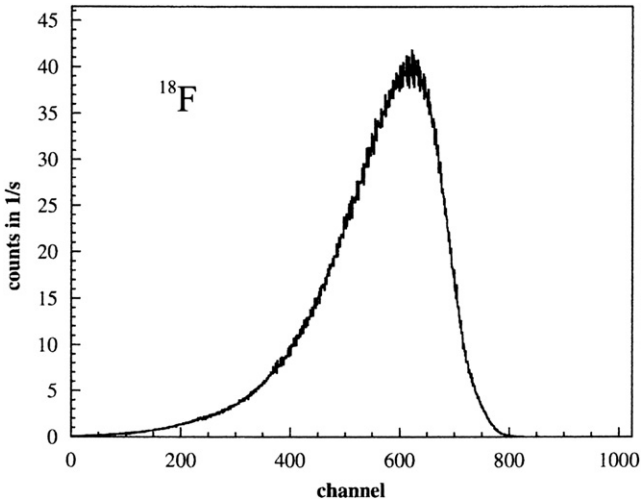

FIGURE 7.32 Pulse-height spectrum of a ^{18}F sample measured with a *Wallac 1414 Guardian*™ liquid scintillation spectrometer with logarithmic amplifier. Background has been subtracted. *(From Schrader et al., 2007, reprinted with permission from Elsevier © 2007)*

annihilation radiation. When the E_{max} of the positrons are sufficiently above the Cherenkov threshold in water (See Chapter 15.), these may be analyzed by Cherenkov counting (Table 7.5).

Wiebe et al. (1980) and McQuarrie et al. (1981) measured the Compton electron contribution to the count rate resulting from the interactions of 511-keV annihilation gamma rays with the liquid scintillation cocktail. Thus, in addition to positron–scintillation cocktail interactions, they point out that as much as 24% of the observed count rate is due to scintillation cocktail interactions with Compton electrons originating from annihilation radiation. Wiebe et al. (1980) showed that the largest amount of energy that may be deposited in a liquid scintillation cocktail is equivalent to the sum of the highest positron energy and the energy deposited by the annihilation gamma rays or

$$E_{max} = E_{\beta^+} + 2E_{e^-} \tag{7.29}$$

where E_{max} is the maximum energy deposited by the positron in the scintillation cocktail, $E_{\beta^+}$is the maximum positron

TABLE 7.5 Liquid Scintillation (LS) and Cherenkov Counting Efficiencies of a Few Positron-emitting nuclides[a]

Nuclide	$E_{\beta^+ max}$	Half-life	LS counting efficiency (%)	Cherenkov counting efficiency in water (%)
^{18}F	0.635 (96.9%)[b]	109.7 m	100	3.7
^{68}Ga	0.80 (1.3%)	68.3 m	100	47
	1.889 (89%)			
^{34m}Cl	1.35 (24%)	32.0 m	100	57
^{34}Cl	2.47 (28%)	1.5 s		
	4.50 (47%)[c]			

[a] *From McQuarrie et al. (1981); Reprinted by permission © 1981 by the American Nuclear Society, La Grange Park, Illinois.*
[b] *Energy values are in MeV and the intensities of the decay mode are given alongside in parenthesis.*
[c] *Of ^{34m}Cl.*

energy, and E_{e^-} is the energy of the Compton edge associated with 511-keV annihilation gamma radiation (341 keV). For example, in the case of ^{18}F, $E_{max} = 635$ keV + 2(341 keV) = 1317 keV. Two times the energy of the annihilation radiation Compton edge must be accounted for, because a positron annihilates with the simultaneous emission of two gamma rays of 511-keV energy.

Numerous radionuclides, that decay by electron capture and/or the competing positron decay mode with the emission of gamma radiation, X-rays, and atomic electrons, may be measured by liquid scintillation. Among these are ^{18}F, ^{54}Mn, ^{85}Sr, ^{88}Y, ^{109}Cd, ^{111}In, ^{123}I, ^{125}I, ^{133}Ba, and ^{139}Ce (Bignell et al., 2010b, Grau Carles and Kossert, 2009, Nejjari et al., 2008, Cassette et al., 2006, Wolterbeek and van der Meer, 2002, Grau Malonda and Grau Carles, 1999, Grau Carles et al., 1994c, and Los Arcos et al., 1991). Liquid scintillation counting efficiencies of over 60% and 70% are reported for ^{85}Sr and ^{109}Cd, respectively (Grau Carles et al., 1994c).

VII. COMMON INTERFERENCES IN LIQUID SCINTILLATION COUNTING

The counting interferences most commonly found in liquid scintillation analysis and how each can be recognized and/or corrected to obtain accurate and reproducible DPM values must be considered. Six major counting interferences exist in the scintillation counting of samples: (1) background radiation, (2) quench (color, chemical, and ionization), (3) multiple radionuclides in the same sample, (4) luminescence, (5) static, and (6) wall effect. Each of these interferences will be considered here and in other parts of this chapter with special attention given to their identification, elimination, or means of correcting for any errors that these may generate.

A. Background

Background is defined as counts arising from sources external to the sample, such as cosmic or environmental radiation, and from instrument noise and PMT crosstalk. When determining sample count rates (CPM_s) from which sample disintegration rates (DPM_s) will be determined according to procedures described previously in Section V, it is necessary to obtain an accurate measure of the background count rate (CPM_{bkg}) whenever background counts are significant relative to the sample counts. Background count rates are determined by counting a blank counting vial containing the scintillation cocktail plus all other chemical constituents used in the preparation of samples with the exception of the radionuclide of interest. In other words, the blank should have the same quench level as the radioactive samples to be analyzed. For example, if the radioactive samples are measured in a sample−scintillation cocktail mixture of 50% water (1:1 water load), the background count rate should be determined in the blank sample 1:1 water−scintillation cocktail mixture. Ideally, any other quenching agents that may be present in the sample should also be present in the background blank counting vial. Such a blank can be obtained by preparing a sample containing no radionuclide of interest in a fashion similar to the preparation of the experimental samples. Once a blank is prepared, it must be counted for a sufficient period of time to get an accurate measurement of its count rate. The time required for counting background blanks can be decided by using statistical criteria presented in Chapter 2, and this is discussed in the later part of this chapter concerning measurements of lower limits of detection (LLD).

Once the background count rate is determined, most modern liquid scintillation analyzers store the background pulse-height spectrum in computer memory. The background counts for any given counting region of the pulse-height spectrum can then be subtracted automatically from the sample count rates to provide a net count rate according to the following equation:

$$CPM_{net} = CPM_s - CPM_{bkg} \tag{7.30}$$

If the background count rate (CPM_{bkg}) is significant compared to the sample count rate (CPM_s), it is necessary to subtract the background contribution according to the above equation. The net count rate (CPM_{net}) is then used to determine disintegration rates according to Eqn 7.7 described in Section V.B. The majority of the background counts are found in the low end of the liquid scintillation pulse-height spectrum, such as 0−5.0 keV for instruments that have pulse-height spectra calibrated over the energy range of 0−2000 keV.

Methods of reducing background to optimize instrument performance are provided in Section XX.

B. Quench

Color, chemical, and ionization quench are described in detail in Section IV. In brief, quench affects the scintillation photon intensity and efficiency of detection of radionuclides in the liquid scintillation cocktail. The lower the radiation energy of the radionuclide, the greater is the effect of quench on the counting efficiency of the sample. Four common methods of quench correction are (1) internal standardization, (2) sample spectrum quench correction, (3) external standard quench correction, and (4) direct DPM methods. The mechanisms of quench and methods of quench correction are treated in detail in Section V.

C. Radionuclide Mixtures

Multiple radionuclides in samples can present an interference when the pulse-height spectra of the two radionuclides overlap. In the case of beta-particle-emitting nuclides, this is due to the fact that all beta-emitting radionuclides produce a continuous spectrum of beta-particle energies from zero to the E_{max}, as illustrated in Fig. 1.30 of Chapter 1. If two beta-emitting radionuclides are present in the same sample (*e.g.*, ^{3}H and ^{14}C of E_{max} 18.6 and 156 keV, respectively), the pulse-height spectrum produced by the beta-particles of one of the radionuclides (*e.g.*, tritium) produces a broad spectrum of pulse heights created by a broad range of beta-particle energies from zero to the most energetic 18.6 keV beta particle, as illustrated in Fig. 7.33. The magnitude and shape of the spectrum will also depend upon the level of quench in the

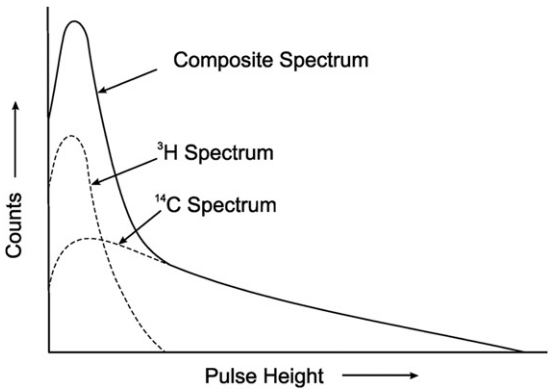

FIGURE 7.33 Overlapping liquid scintillation pulse-height spectra of ^{3}H (beta-particle $E_{max} = 18.6$ keV) and ^{14}C (beta-particle $E_{max} = 156$ keV). The composite spectrum is that produced by the two radionuclides as a mixture. *(© 1998 PerkinElmer, Inc. Printed with permission)*

sample. The second radionuclide ^{14}C, which has a higher decay energy than tritium, emits beta particles of higher energy maximum (E_{max}), produces a pulse-height spectrum overlapping that of tritium, and the spectrum of pulse heights produced by the beta particles emitted by ^{14}C extends from zero to a maximum produced by the most energetic ^{14}C beta particles of 156 keV. Figure 7.33 is a graphic composite spectrum of a sample with both ^{3}H and ^{14}C. In order to quantify the separate radionuclide activities (DPM) of a mixture of two beta-emitting nuclides in a sample, the count rates and counting efficiency of each radionuclide must be determined. Several methods may be employed for the measurement of two, three, or even more beta-emitting radionuclides in a mixture by liquid scintillation analysis. These methods are described in detail in Section VIII.

D. Luminescence

Luminescence in liquid scintillation fluor cocktails or in aqueous buffer media refers to the emission of light photons as a consequence of energy absorption and concomitant molecular excitation from origins other than nuclear radiation. Luminescence can be a practical tool in the study of biochemical reactions or an interference in liquid scintillation analysis. This section will provide a treatment of the various types of luminescence encountered in liquid scintillation analysis and recommendations on how to avoid or minimize any interference that some types of luminescence can present.

1. Bioluminescence

Bioluminescence occurs when a biochemical reaction produces photons, which is a desirable reaction when used as a tool to study certain biochemical assays. Some examples are the biochemical reactions catalyzed by avidin–alkaline phosphatase, horseradish peroxidase, β-galactosidase, luciferase, xanthine oxidase, and ATP assays via luciferin-luciferase. The liquid scintillation analyzer can be utilized to count all luminescent events when these are used to study certain biochemical reactions. Under such circumstances, the LSA counting protocol should be set to count the experimental samples in the single-photon counting (SPC) mode. In this counting mode, only a single PMT is used without the coincidence counting circuitry. SPC is used, because all luminescent events are single photon in nature and would be eliminated by the two PMTs and the coincidence counting circuitry. Therefore, in the SPC mode the coincidence counting circuit is disabled and only one PMT is operational. In addition, because bioluminescence normally produces a higher intensity of light compared to a radioactive event, the high voltage on the PMT is automatically lowered in the SPC mode to prevent saturation of the PMT. The counting region for bioluminescent samples in the liquid scintillation analyzer is generally 0–10 keV for pulse-height scales calibrated in keV energy equivalence.

2. Photoluminescence and Chemiluminescence

There are primarily two types of luminescence, which can interfere in the assay of radioactive samples in scintillation cocktail. These are photoluminescence and chemiluminescence.

Photoluminescence is the result of the exposure of the sample–scintillation cocktail mixture to ultraviolet light. Photoluminescence is normally single photon in nature and decays in a matter of minutes. Therefore, letting freshly prepared samples in scintillation cocktail remain in the dark of the liquid scintillation analyzer for 10–15 minutes completely eliminates any photoluminescence that may occur. A precount delay time can also be used with counting protocols of certain liquid scintillation analyzers.

The second type of luminescence, chemiluminescence, is a frequent interference in the liquid scintillation assay of radioactive samples. This is the production of light within the scintillation cocktail due to a chemical reaction. Chemical reactions that cause chemiluminescence often occur when scintillation cocktail is added to the sample solution in the liquid scintillation counting vial. A chemical reaction can occur, for example, when scintillation cocktail is added to a basic sample solution (pH 8–14) or when a chemical substance, such as hydrogen peroxide, is present in the sample. The pH effects and chemical interactions with some component of the scintillation cocktail can cause molecular excitation and light emission. Some types of samples that can produce a considerable chemiluminescence are tissue or cell digests with inorganic bases (*e.g.*, NaOH, KOH, Solvable™) or organic bases (*e.g.*, Soluene 350™).

During the chemiluminescent reaction, single photons are produced in the scintillation cocktail and, because of their large number, they may bypass the coincidence circuit and be registered as counts together with counts produced by the radionuclides in the sample. The counting of single-photon chemiluminescence events by the coincidence (dual PMT) circuitry can be demonstrated from the equation of Horrocks and Kolb (1981), which is written as

$$N_C = 2\tau_R(N_1N_2) \tag{7.31}$$

where N_C is the coincidence count rate, τ_R is the coincidence resolving time (*e.g.*, 30 ns), and N_1 and N_2 are the single-event count rates from photomultiplier tubes 1 and 2, respectively. As the single-photon events from chemiluminescence increase in

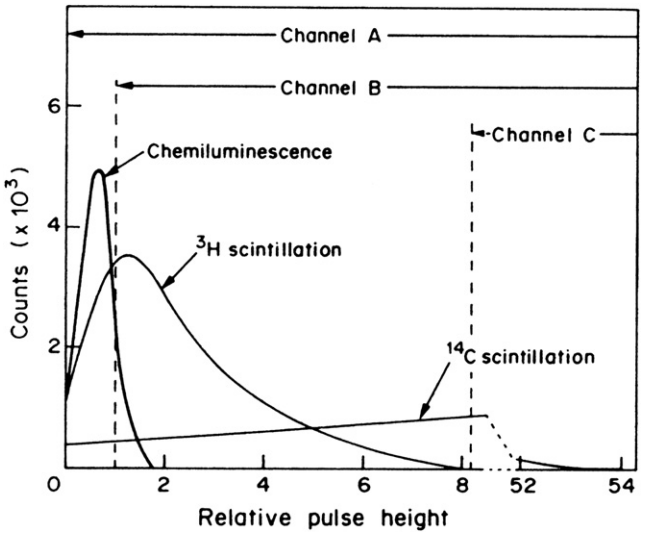

FIGURE 7.34 Pulse-height distributions of ^{3}H and ^{14}C scintillation pulses and of chemiluminescence pulses, and channel settings for the analytical measurement of each activity and chemiluminescence count rate. *(From Takiue et al., 1985, reprinted with permission from Elsevier ©1985)*

frequency, the probability that they produce a coincidence count rate correspondingly increases according to Eqn 7.31. Horrocks and Kolb (1981) calculated the coincidence count rate, N_C, that would be measured by a liquid scintillation analyzer with a resolving time of 30 ns for various single-photon event levels according to Eqn 7.31. For example, they demonstrated that, if photomultiplier tubes 1 and 2 measured the same number of single-photon events to be 50,000 (*i.e.*, $N_1 = N_2$), the coincidence count rate, N_C, would be calculated to be

$$N_C = [2(30 \times 10^{-9})/60](N_1 N_2) = 10^{-9}(N_1 N_2) = 2.5 \text{ CPM}$$

They elaborate further that, if $N_1 = N_2 = 500{,}000$, the coincidence count rate, N_C, would calculate to be 250 CPM, and for $N_1 = N_2 = 5{,}000{,}000$, the coincidence count rate, N_C, would calculate to be 25,000 CPM. Thus, it is obvious from the above calculation, that if sample count rates are low, luminescence can be a source of serious error. Luminescence count rates can be very high, depending on the chemical constituents and/or pH of the sample. In any event, luminescence should be identified, if it occurs, and it should be eliminated before counting to avoid error in the activity determinations of experimental samples.

Luminescence, which may occur in sample−scintillation cocktail mixtures, can be detected easily when counting relatively high-energy β-emitting radionuclides ($E_{max} > 70$ keV). For example, Fig. 7.34 illustrates the pulse-height spectrum of a luminescent sample, a tritium sample, and a ^{14}C sample. As illustrated in Fig. 7.34, the luminescence spectrum occurs at the very low-energy portion of the pulse-height spectrum occurring generally in the 0−6-keV region for pulse-height spectra on an energy equivalent scale. Luminescence in a sample can be recognized easily by one of three methods, namely (1) spectral display, (2) counting region settings, and (3) instrumental detection and measurement. As illustrated in Fig. 7.34, a sample containing appreciable chemiluminescence produces a pulse-height spectral peak in the 0−6-keV region on top of (overlapping) the main radioactivity pulse height peak. The figure illustrates the chemiluminescence pulse-height spectrum overlapping with ^{3}H and ^{14}C pulse-height spectra. When counting single-radionuclide samples, two counting regions can be used to detect luminescence. For example, when counting ^{14}C the following counting regions may be used: region A: 0−156 keV and region B: 4.0−156 keV. If the counts in these regions are similar, then little, if any, luminescence would be expected. If, on the other hand, the counts in region A (0−156 keV) are much higher (25−500%), luminescence may be predicted. In addition, many modern liquid scintillation analyzers are able to determine the magnitude of luminescence in a sample and print the percent luminescence on the same page as the CPM and DPM values of each sample. The percent luminescence is calculated by the instrument according to the equation

$$\%\ \text{luminescence} = \frac{\text{chance coincidence events}}{\text{true coincidence events}} \times 100 \tag{7.32}$$

When luminescence is detected or even suspected in experimental samples, it can be controlled, corrected for, or even eliminated as discussed subsequently.

3. Luminescence Control, Compensation, and Elimination

Once luminescence is recognized as a problem with a particular set of samples, it can be controlled by using proper sample preparation procedures and even eliminated or compensated for by certain liquid scintillation counter controls. The five most common methods of reducing or correcting sample luminescence are (1) dark adaptation of samples, (2) chemical methods, (3) temperature control, (4) counting region settings, and (5) delayed coincidence counting also referred to as random coincidence counting. A liquid scintillation analyzer equipped with three photomultiplier tubes (*e.g.*, Hidex 300 SL), which can operate in coincidence, is reported to avoid sample luminescence (Haaslahti, 2010).

a. Dark adaptation of Samples

The most straightforward method of removing luminescence from liquid scintillation sample−cocktail mixtures is to dark-adapt the samples overnight or until the luminescence decays to the point of not contributing to erroneous sample activities (Warwick et al., 2010; Wiesenberg et al., 2010; Cheng and Wong, 2008; Ren and Mahon, 2007; Warwick and Croudace, 2006; and Groppi et al., 2005a). Photoluminescence generally decays rapidly, and dark adaptation of the samples for an hour or two should suffice for photoluminescence to disappear. The liquid scintillation analysis of samples of low activity require low background counting, and dark adaptation of samples overnight or for more than a day is a practice. Chemiluminescence has a much slower decay rate, and significant levels may persist beyond a day depending on sample temperature (Kessler, 1989). Dark adaptation of samples for three days in the liquid scintillation analyzer was reported by Yamada et al. (2004) to suppress chemical luminescence. Some liquid

scintillation cocktails are manufactured to be resistant to chemiluminescence (see Part b. Chemical Methods discussed subsequently and Chapter 8). Dark adaptation of samples exhibiting chemiluminescence, together with other methods described subsequently, may be used to eliminate interference from this phenomenon.

b. Chemical Methods

Chemical methods used to avoid or suppress chemiluminescence are reviewed by Peng (1976). Among these, neutralization of alkaline sample solutions with a nonoxidizing acid is recommended, as basic sample solutions are often the main cause of chemiluminescence. This can be accomplished by (1) adding 10 mL of acetic acid to a gallon (3.8 L) of scintillation cocktail provided this does not alter the performance of the fluor cocktail, (2) neutralizing the basic sample solution before adding the scintillation cocktail to the sample counting vial, or (3) using a special scintillation cocktail designed to reduce or suppress luminescence such as Insta-Fluor, which contains a chemiluminescence inhibitor or Hionic-Fluor, which displays a very fast chemiluminescence decay property. See Chapter 8 for scintillation cocktail properties and characteristics. This normally reduces the amount of chemiluminescence. A problem associated with sample neutralization may occur when counting large macromolecules found in certain biological samples, in which acidification of samples may cause precipitation. Precipitation of sample most often includes precipitation of the radioactive material and, therefore, loss of counting efficiency and incorrect DPM values.

c. Temperature Control

Acidification of sample solution, as already described, followed by heating to 40°C is often recommended to reduce chemiluminescence, or acidification may be omitted when it causes precipitation and the sample solution only heated. Heating the sample to 40°C helps drive the chemiluminescence reaction to its endpoint. This is possible because the reaction is a chemical reaction and every 10°C increase in temperature doubles the reaction rate. Another procedure, alternative to heating, is to cool the reaction using a liquid scintillation analyzer with temperature control. Cooling slows the reaction rather than accelerating its termination. Cooling reduces counts from chemiluminescence. In addition, chemiluminescence can be eliminated altogether by counting-region setting or by delayed-coincidence counting, discussed subsequently in this section.

d. Counting-Region Settings

This is the recommended method for all radionuclides with the exception of tritium and some nuclides that decay by electron capture (EC) to stable daughter nuclides with the emission of X-rays and Auger electrons. The use of "counting-region settings" to remove pulse events from luminescence is not possible in the measurement of tritium or EC nuclides emitting only X-rays and Auger electrons (*e.g.*, ^{37}Ar, ^{49}V, ^{68}Ge, and ^{131}Cs), because their liquid scintillation pulse-height spectra overlap significantly with that of luminescence (see Fig. 7.34 for the case of tritium.). Auger electrons and X-rays following electron capture are of low energy, as noted in Chapter 1, and the liquid scintillation pulse heights from the monochromatic Auger electrons or from X-ray Compton electrons would occur in the same counting region as tritium (Takiue and Ishikawa, 1979). Nuclides that decay by electron capture with the emission of gamma radiation from unstable daughter nuclei emit also internal conversion electrons that produce generally pulse heights significantly higher than that of tritium. Consequently, the method of "counting-region settings", which is described in the following, could be applicable in these cases.

The method of "counting-region settings" to remove erroneous luminescence pulse events from the sample count rate is relatively simple, but not often used. If the counting region for a mid- to high-energy β-emitting radionuclide (*e.g.*, ^{14}C and higher energy β emitters) is set at approximately 10 keV or above, no luminescence of any kind will be observed in the sample counts and, therefore, no correction will be necessary. The only precaution when performing DPM determination is to set the same counting region for the quench-correction curve and for the experimental samples. A counting region for ^{14}C to avoid error from luminescence would be, for example, 10.0−156 keV for lower-level and upper-level discriminator settings when using instruments that have pulse-height discriminator settings calibrated to keV energy equivalence. In the case of tritium, a counting region cannot be set to avoid luminescence, because tritium emits very low energy beta particles ($E_{max} = 18.6$ keV) producing a pulse-height spectrum that greatly overlaps that of luminescence. In the case of tritium, chemiluminescence must be eliminated or measured and subtracted from the sample counts for accurate activity calculations (Takiue et. al., 1984). Fig. 7.34 illustrates other discriminator settings to define three counting regions, proposed by Takiue et al., (1985), which permit the simultaneous counting of chemiluminescence, ^{3}H, and ^{14}C, when the DPM analysis of dual-radionuclide samples containing chemiluminescence is required. Equations for calculating the activities (DPM) of the dual-radionuclide samples and the count rates due to chemiluminescence are given by Takiue et al., (1985, 1986). Detailed information on multiple-radionuclide analysis is provided in Section VIII.

e. Delayed Coincidence Counting

Most modern liquid scintillation analyzers are equipped with delayed coincidence counting, also referred to random coincidence counting, as a method for the elimination of error resulting from luminescence, that can be applied to the liquid scintillation analysis of all radionuclides including tritium (Varlam et al., 2009, and Palomo et al., 2007). For this method to work, a delayed coincidence circuit with a 20-ns delay is added to one of the two PMTs. The sample containing the radioactivity is counted simultaneously with and without the delay coincidence circuit enabled. If the coincident circuit is used without the delay or random coincidence circuit, both the luminescence and radioactive decays will be detected. The radioactive decay events are accepted by the coincidence counting circuit, because they

are isotropic multiphoton events, and luminescent single-photon events are also accepted by the coincidence counting circuit, because they occur at a high count rate in the sample and are detected within the resolving time of the counting circuit. Now, if the coincident circuit is used with a delay mode added to one of the PMTs, only the single-photon luminescence events will be detected, because of their high count rate of occurrence. Radioactive decay, which produces isotropic multiphoton events, will not be detected by the coincidence circuit due to a 20-ns delay in one of the two PMTs. Finally, the counts collected from the two readings with and without the delay circuit enabled are subtracted channel by channel of the MCA over the pulse-height region equivalent to 0–6.0 keV. The resultant spectrum will be a product of the actual nuclear decay events without chemiluminescence. This special delay method is known as the luminescent detection and correction method. It can be applied to all radionuclides independent of radioisotope decay energy. Luminescence detection and correction are available with most state-of-the-art liquid scintillation analyzers (Kessler, 1989); however, caution is recommended in the application of this instrumental method of correction. The user should confirm that the luminescence subtraction is working properly for their samples. For example, Warwick and Croudace (2006) confirmed that the delayed coincidence counting option was not reliable for their particular samples, and they decided that dark adaptation of the samples was necessary to ensure against erroneously high activities due to chemiluminescence-derived scintillations.

E. Static

Electrostatic discharge is a photon-producing interference in liquid scintillation counting. Static electricity may be generated by friction or pressure between two materials. When nonconductive materials are separated, one material develops a positive and the other a negative charge. Static consists of charged ions, positive or negative, which are atoms electrically out of balance due to the removal or addition of electrons. The intensity of static electricity can be measured as positive or negative voltage on the surface of matter in magnitudes of tens of thousands of volts. The discharge of static electricity is a random event; but the phenomenon commonly occurs with many materials we may come into contact with when preparing samples for counting, including scintillation counting vials. Static electricity is produced easily in low-humidity rooms during the time of the year when dry heat is used to warm laboratories. A common characteristic of static electricity is its stability; it can remain on the surface of scintillation counting vials for relatively long periods of time. When the scintillation vial is placed in the counting chamber and electrostatic discharges occur, it is like an electrical lightning storm occurring in or on the surface of the scintillation vial producing random pulse events. The static charge buildup can have many causes, including shipping, handling, use of plastic gloves, and low humidity in the sample preparation area. Plastic vials tend to build up more of a static charge than glass vials.

There are primarily four methods of reducing or eliminating static from sample vials for liquid scintillation counting: (1) the use of an electrostatic controller, (2) selection of vial type, (3) antistatic wipes, and (4) humidification of the sample preparation and counting area. A brief description of each method is given.

The electrostatic controller is a circular donut-shaped device located in the elevator tube through which the counting vial must pass before it is moved into the counting chamber. In certain instruments it contains eight geometrically located electrodes, which generate a 360° field of electrically produced ions. When the counting vial passes through the electrostatic controller it enters the field of electrically produced counterions, which can neutralize static electricity on the counting vial surface in a matter of 2 seconds. This process occurs just before the robotic positioning of the vial into the counting chamber located between the two PMTs. Contemporary state-of-the-art liquid scintillation analyzers are equipped with an electrostatic controller (*e.g.*, Mendonça et al., 2006). Although the electrostatic controller offers no guarantee of removing all static from the counting vial surface, there may be no need to take any other steps to control static on the surface of counting vials before placing them in the LSA sample changer.

Further measures may be taken to guard against static charge collection and discharge from counting vial surfaces. One step is to select a type of counting vial that would tend to collect less static electricity. Because plastic tends to hold a static charge more than glass, the use of glass vials helps to reduce the static charge for most samples. The disadvantages of using glass vials are that they are more expensive, more difficult to dispose of, and can yield higher background count rates. The alternative to glass vials is to use special "antistatic" plastic vials (Nakanishi et al., 2009). These vials are manufactured with a special plastic treatment that greatly reduces the amount of static on the vial surfaces compared with standard plastic vials. Yamada et al. (2004) reports that the use of Teflon counting vials with acryl resin caps with the inside wall of the caps lined with aluminum foil could suppress effectively the static electricity. Yoon et al., (2010) took the added precaution of locating the liquid scintillation analyzer 30 cm. away from any other electrical devices, ventilation ducts, or air conditioner. Another technique is to wipe each vial with an "antistatic" wipe or with a moist cloth just before placing the vial into the sample changer of the liquid scintillation counter. This readily removes the static charge on the surface of the vial just before counting. The final step that may be taken to reduce static is to increase the humidity in the room where the samples are prepared as well as in the counting area.

F. Wall Effect

The 'wall effect' can be classified into two types, namely (1) the effect of certain traditional organic solvents that penetrate into the walls of plastic counting vials and (2) a loss of detection efficiency in the liquid scintillation standardization of radionuclides due to the interaction of beta particles with the glass walls of the scintillation counting vial. These two types of 'wall

effect' are encountered only in unique modes of liquid scintillation analysis and are thus treated separately as follows:

1. *Wall effect from solvent penetration into plastic counting vial.* When samples are counted in plastic vials with traditional cocktails, the organic scintillator from the cocktail can penetrate the wall of the plastic vial. Traditional cocktails are those made with solvents such as toluene, xylene, and pseudocumene. This can cause a problem when external standard quench-correction methods are used, because certain plastic vials with solvent penetration can scintillate causing a distortion of the external standard pulse-height spectrum. The result would be inaccurate quench-indicating parameters, which would give erroneous counting efficiencies and, as a consequence, error in the DPM measurements of samples. This problem can be overcome easily by always using environmentally safer cocktails. The newer environmentally safer cocktail solvents, such as diisopropylnaphthalene and linear alkylbenzene will not penetrate into the wall of the plastic vial and cause the wall effect. As a general rule, always use glass vials when using traditional scintillation cocktails, and use either plastic or glass vials with the environmentally safer cocktails.
2. *Wall effect in the liquid scintillation standardization of radionuclides.* In the liquid scintillation standardization of radionuclides, discussed further on in this chapter, calculations may include a wall effect, that is, a reduction in detection efficiency due to nuclear decays that occur at the walls of the scintillation vial (Cassette, 2003). In the wall effect, it is assumed that a 10-μm layer next to the vial wall will have only a 50% counting efficiency, as electrons interact with the glass envelope of the counting vial (Jaubert and Cassette, 2004, Johansson et al., 2003, Cassette, 2003). The influence of this wall effect is considered negligible in the standardization of high-energy beta-emitting radionuclides [*e.g.*, ^{89}Sr ($E_{max} = 1490$ keV) or ^{90}Y ($E_{max} = 2280$ keV)] by the CIEMAT/NIST or TDCR methods, if the source is unquenched or only moderately quenched (Jaubert and Cassette, 2004 and Cassette, 2003). For lower-energy beta-emitting radionuclides and for alpha-emitting nuclides, the wall effect must be corrected for in the standardization of radionuclides (Cassette, 2003). In the liquid scintillation standardization of ^{238}Pu an uncertainty of 0.25% on the efficiency was attributed to the wall effect (Johansson et al., 2003). A similar uncertainty to the detection efficiency of 0.2% for ^{210}Po was attributed to the wall effect (Laureano-Pérez et al., 2007). The significance of the wall effect was demonstrated by Hurtado et al. (2009) by their comparison of the theoretical beta spectrum of ^{90}Y with the spectrum that is produced by the ^{90}Y beta-particle energy deposited in a liquid scintillator (see Fig. 7.35). The comparison was made using a Monte Carlo simulation using GEANT4 code, as a tool for efficiency calculations in radionuclide standardization and stopping power calculations, etc. Figure 7.35 illustrates how the low-energy portion of the beta spectrum is distorted by the wall effect, as the low-energy beta particles are absorbed in the walls of the liquid scintillation counting vial. DeVries and Griffen (2008) point out that the high LET of alpha particles in the scintillation cocktail reduce the wall effect, and assigned a liquid scintillation alpha detection efficiency of 100% in the measurement of ^{237}Np.

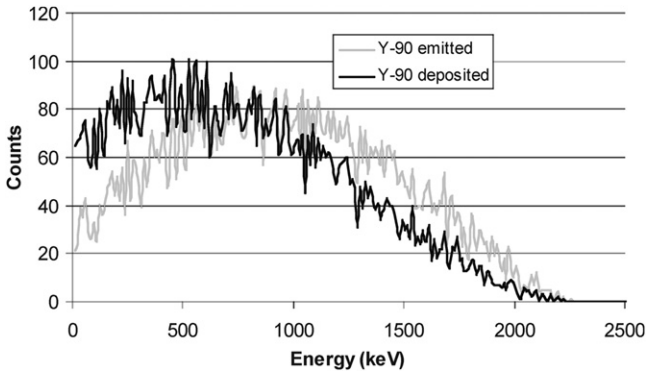

FIGURE 7.35 Theoretical and wall-effect-distorted beta spectra of ^{90}Y. *(From Hurtado et al., 2009, Reprinted with permission from Radiocarbon, the University of Arizona, © 2009 Arizona Board of Regents on behalf of the University of Arizona)*

VIII. MULTIPLE RADIONUCLIDE ANALYSIS

There is a wide-ranging need in the scientific community to analyze multiple radionuclides as mixtures. These include dual-, triple-, and multiple radionuclide mixtures stemming from research in the chemical, biological, nuclear power, and environmental sciences, among others, as reviewed by L'Annunziata (1984b), Bukowski et al. (1992), Takiue et al. (1991b,c, 1992, 1995, 1999), Toribo et al. (1995, 1996, 1997, 1999), Fujii et al. (2000), Kashirin et al. (2000), Nayak (2001), and Reddy et al. (2009). Several methods are available for analyzing the activity of more than one β-emitting radionuclide in the same sample. Because of the broad spectrum of β-particle energies emitted by any given radionuclide anywhere between zero and E_{max}, we always observe a broad pulse-height spectrum in the liquid scintillation analyzer from zero to a maximum pulse height. Therefore, all liquid scintillation pulse-height spectra from different β-emitting radionuclides overlap to some degree. Because of this spectral overlap and the very broad characteristics of β-particle pulse-height spectra, it was traditionally considered feasible to analyze by LSA at most three β-emitting radionuclides in the same sample provided their β-particle energy maxima differed by a factor of three or four (L'Annunziata, 1979, 1984, and 1987). However, advances in LSA have revealed new regionless spectral unfolding and deconvolution methods capable of analyzing several β-emitting radionuclides in the same sample with the aid of computer processing. Even radionuclide mixtures of ^{14}C ($E_{max} = 156$ keV) and ^{35}S ($E_{max} = 167$ keV), which for decades were thought to be impossible to resolve by LSA, because of their similar β-particle energies, can now be identified and quantified as mixtures. A description of the techniques used to resolve and quantify mixtures of β-, and α-emitting radionuclides by LSA is provided in this section.

A. Conventional Dual- and Triple-Radionuclide Analysis

The conventional methods described in detail in this section refer, for the most part, to the analysis of two β-emitting radionuclides in a mixture. However, the same principles can apply to the analysis of three beta-emitting radionuclides as a mixture, which is included in this section.

1. Exclusion Method

The exclusion method is one of the original methods applied to the analysis of a dual-radionuclide mixture by liquid scintillation analysis. It is described in detail by Okita et al. (1957), Kobayashi and Maudsley (1970), and L'Annunziata (1979). The technique is rarely used today, because of the availability of more efficient methods of dual- or triple-radionuclide analysis. Nevertheless, it is presented briefly here, as the reader will encounter occasional reference to this method in the current literature.

The dual-radionuclide mixture of ^{3}H ($E_{max} = 18.6$ keV) and ^{14}C ($E_{max} = 156$ keV) will be taken as an example to describe this method, which requires a relatively large difference in β-particle energies between the two radionuclides. It is recommended generally that the E_{max} of the two radionuclides differ by a factor of 3 or 4. Two counting regions or windows are defined using lower-level (LL) and upper-level (UL) pulse-height discriminators such that in counting region 1, also referred to as counting region A and in this case, we can refer to it as the tritium region (*e.g.*, LL = 0.0 and UL = 18.6 keV), where both the tritium spectrum and the spilldown of the carbon-14 spectrum into the tritium region are found. In this example, the pulse-height analyzer is one that utilizes a multichannel analyzer with channel numbers calibrated to approximate keV energy of the ^{3}H and ^{14}C beta particles (see Fig. 7.36). In such a case, a nonquenched sample of ^{3}H will not produce calibrated pulse heights beyond 18.6 keV. In counting region 2, also referred to as region B and in this case the carbon-14 region, pulse-height discriminators are set (*e.g.*, LL = 18.6 and UL = 156 keV) to allow only pulses from the carbon-14 spectrum. The name exclusion method is derived from the fact that region 2 excludes all tritium pulses. When counting a mixture of ^{3}H and ^{14}C, count rates (CPM) will be collected in each region, and the following equations are used to calculate the activity or disintegration rate (DPM) for ^{3}H and ^{14}C:

$$H = \frac{N_1 - Cc_1}{h_1} \tag{7.33}$$

$$\text{and } C = \frac{N_2}{c_2} \tag{7.34}$$

where H and C are the activities or DPM of ^{3}H and ^{14}C, respectively, in the mixed radionuclide sample, N_1 and N_2 are the net count rates (CPM), *i.e.*, background-subtracted count rates, in regions 1 and 2 of the liquid scintillation analyzer, h_1 and c_1 are the counting efficiencies of ^{3}H and ^{14}C in counting region 1, and c_2 is the counting efficiency of ^{14}C in counting region 2.

From these equations it is clear that five parameters are needed to calculate the DPM for both the tritium and ^{14}C dual-labeled samples. The net CPM in regions 1 and 2 are determined automatically by the LSC. The three efficiency factors are determined using three quench-correction curves, which consist of plots made from a series of tritium and ^{14}C quenched standards. The three curves are constructed by plotting % counting efficiency for tritium and ^{14}C in region 1 and ^{14}C in region 2 versus an external standard quench-indicating parameter.

This method is less commonly used today for low-energy beta emitters, such as ^{3}H-^{14}C, because scintillations from beta-particle emissions from both nuclides are highly quenchable, and the counting region of the higher-energy beta emitter (*e.g.*, ^{14}C in the above example) is restricted to include only pulse events from that nuclide. Under high levels of quench, the detection efficiency of ^{14}C drops significantly, and the pulse events can spill down excessively from region B to region A. This can yield very low detection efficiencies for the ^{14}C in region B; however, modern liquid scintillation analyzers equipped with automatic efficiency control (AEC) or automatic quench compensation (AQC) can automatically shift counting region settings according to quench level. With respect to relatively high-energy beta emitters, such as ^{90}Sr ($E_{max} = 546$ keV) and ^{90}Y ($E_{max} = 2280$ keV), which are less easily quenched, the exclusion method is more easily utilized. Eikenberg et al. (In Press) report the successful application of this technique for the analysis of ^{3}H and ^{14}C mixtures. They report the use of one of the internal standards to determine the detection efficiencies of ^{3}H and ^{14}C or quench-correction curves. Eikenberg et al. (2011) found the use of internal standards to yield more precise results (see Section V.A for the use of internal standards.). Xiques Castillo et al. (2009, 2010) applied the exclusion method for the analysis of ^{90}Sr(^{90}Y) for clinical applications. They used counting regions defined by channels 5−700 for region A and 701−1014 for region B of a Wallac (PerkinElmer) 1029 Rackbeta™ liquid scintillation analyzer. The upper region (region B) registers pulse events arising exclusively from ^{90}Y beta-particle interactions with

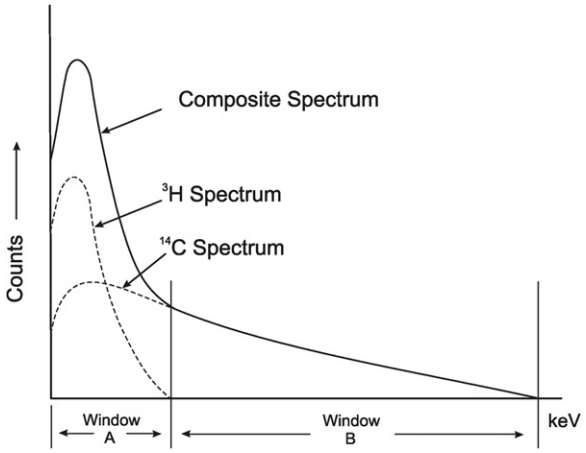

FIGURE 7.36 Typical component and composite liquid scintillation analyzer pulse-height spectra produced by approximately equal activities of ^{3}H and ^{14}C. Two counting windows (counting regions) are illustrated, namely, window A (or region A), which registers count rates originating from beta emissions of ^{3}H and ^{14}C, whereas window B (or region B) registers a count rate originating only from beta emissions of ^{14}C. *(© 1998 PerkinElmer, Inc. Printed with permission)*

liquid scintillator, and these interactions with such a very-high-energy beta emitter are not easily quenched and any spilldown of pulse events from region B to region A would be minimal. Another application of the exclusion method is reported by Huntington et al. (2008) for the dual-nuclide liquid scintillation analysis of ^{65}Zn and ^{69m}Zn. The inclusion method, which is described subsequently, is the most popular method, as it assures, particularly with low-energy beta emitters, a less variable detection efficiency for both nuclides over a wide range of quench.

2. Inclusion Method

In this method, the counting regions are set such that there are spillup and spilldown of pulse events in each region from both of the radionuclides when two beta-emitting radionuclides are analyzed as a mixture. When three beta-emitting radionuclides are analyzed, three counting regions are employed.

a. Dual-Radionuclide Analysis

Again, we will use ^{3}H and ^{14}C as an example of a typical dual mixture, keeping in mind that the procedure presented here and equations used will work for any dual mixture of β-emitting radionuclides, provided the β-particle energies (E_{max} values) of the two radionuclides differ significantly. Also, in this discussion we will refer to lower-energy and higher-energy radionuclides to distinguish between nuclides that differ in their beta-decay energies. In this example, ^{3}H ($E_{max} = 18.6$ keV) is the lower-energy radionuclide and ^{14}C ($E_{max} = 156$ keV) the higher-energy radionuclide of the mixture.

For this method to work it is necessary that two counting regions (regions A and B) are established by setting the lower-level and upper-level pulse-height discriminators to assure that there will be significant spillup of pulse events from ^{3}H into region B and the unavoidable spilldown of pulse events from ^{14}C into region A. An illustration of pulse-height discriminator settings, which establish the counting regions for the analysis of two radionuclides by this inclusion method, is given in Fig. 7.37.

Some modern liquid scintillation analyzers are available with preset dual counting regions for the activity analysis of dual mixtures such as ^{3}H−^{14}C, ^{3}H−^{32}P, and ^{3}H−^{125}I. For other radionuclide combinations, it is necessary to establish the LL and UL discriminators settings for the appropriate spillup and spilldown of pulse events from the two radionuclides. The procedure used to establish these regions will be discussed later on in this section. For the case of the ^{3}H−^{14}C mixtures, counting region A is normally set by discriminators LL = zero and UL = 12.0 keV, while region B is defined by the discriminator settings LL = 12.0 and UL = 156 keV, when the pulse height spectra are displayed on a linear scale in β-particle energy equivalents (*e.g.*, Fig, 7.37). Some liquid scintillation analyzers simply make use of channel numbers, and the counting regions are defined by the channel numbers (see Fig. 7.42 further on in this section).

After the two counting regions are defined, it is necessary to prepare quench-correction curves, which can be used to determine the counting efficiencies of the ^{3}H and ^{14}C (or lower-energy and higher-energy radionuclides) in the two counting regions. Two sets of quench standards are required, one set of ^{3}H and one set of ^{14}C quenched standards. If two other radionuclides need to be analyzed, a set of quenched standards of the lower-energy radionuclide and a set of quenched standards of the higher-energy radionuclide are required. The procedure for preparing a series of quenched standards was given in Section V.D. Each series of quenched standards is counted in regions A and B and, as a result, four quench-correction curves are created, as illustrated in Fig. 7.38.

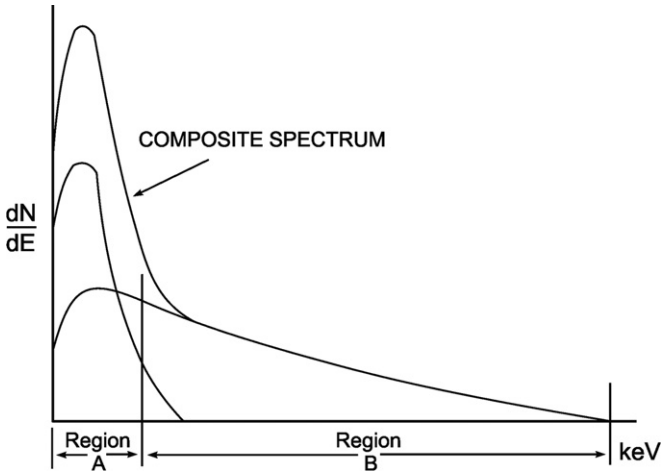

FIGURE 7.37 Typical component and composite pulse-height spectra observed for two β-emitting radionuclides (*e.g.*, ^{3}H and ^{14}C) in an approximately 1:1 mixture and having significantly different β-particle energy maxima. The pulse-height spectra are plotted as dN/dE, *i.e.*, the number of events or counts per energy channel versus channels of a multichannel analyzer calibrated in keV. Two counting regions are illustrated (regions A and B also referred to as windows A and B) for use in the inclusion method, which are set to allow spillup of the lower energy radionuclide from region A into region B, whereby counts from both radionuclides appear in both counting regions. *(© 1998 PerkinElmer, Inc. Printed with permission)*

When using quench-curve correction, determination of the radionuclide activities becomes more difficult as spillover of ^{14}C into the tritium region (region A) increases with quench or, in other words, when the ratio of ^{14}C to tritium increases in region A. If the number of counts from ^{14}C into the tritium region becomes large, the correction of the tritium counts can result in a small number that is less accurate. Likewise, as quench increases, the spillover of ^{3}H pulse events into region B (^{14}C region) diminishes and can even disappear, which makes the calculations for the ^{3}H and ^{14}C activities invalid. Therefore, to maintain optimal counting conditions, it is necessary to keep the amount of spillover of the ^{14}C pulse events in the tritium region A at a fairly constant level as well as the spillup of tritium events into region B. This is accomplished using an automatic windows tracking method called AEC (automatic efficiency control) or AQC (automatic quench compensation). As the sample is counted, the liquid scintillation analyzer determines the level of quench of the experimental sample using a quench-indicating parameter (*e.g.*, *H#*, or tSIE), and the counting regions are adjusted automatically so that the spillover of the ^{14}C into the tritium region (region A) is kept at a fairly constant level (10−15%), and the spillup of ^{3}H into the ^{14}C region (region B) is also preserved. Fig. 7.39 illustrates that the liquid

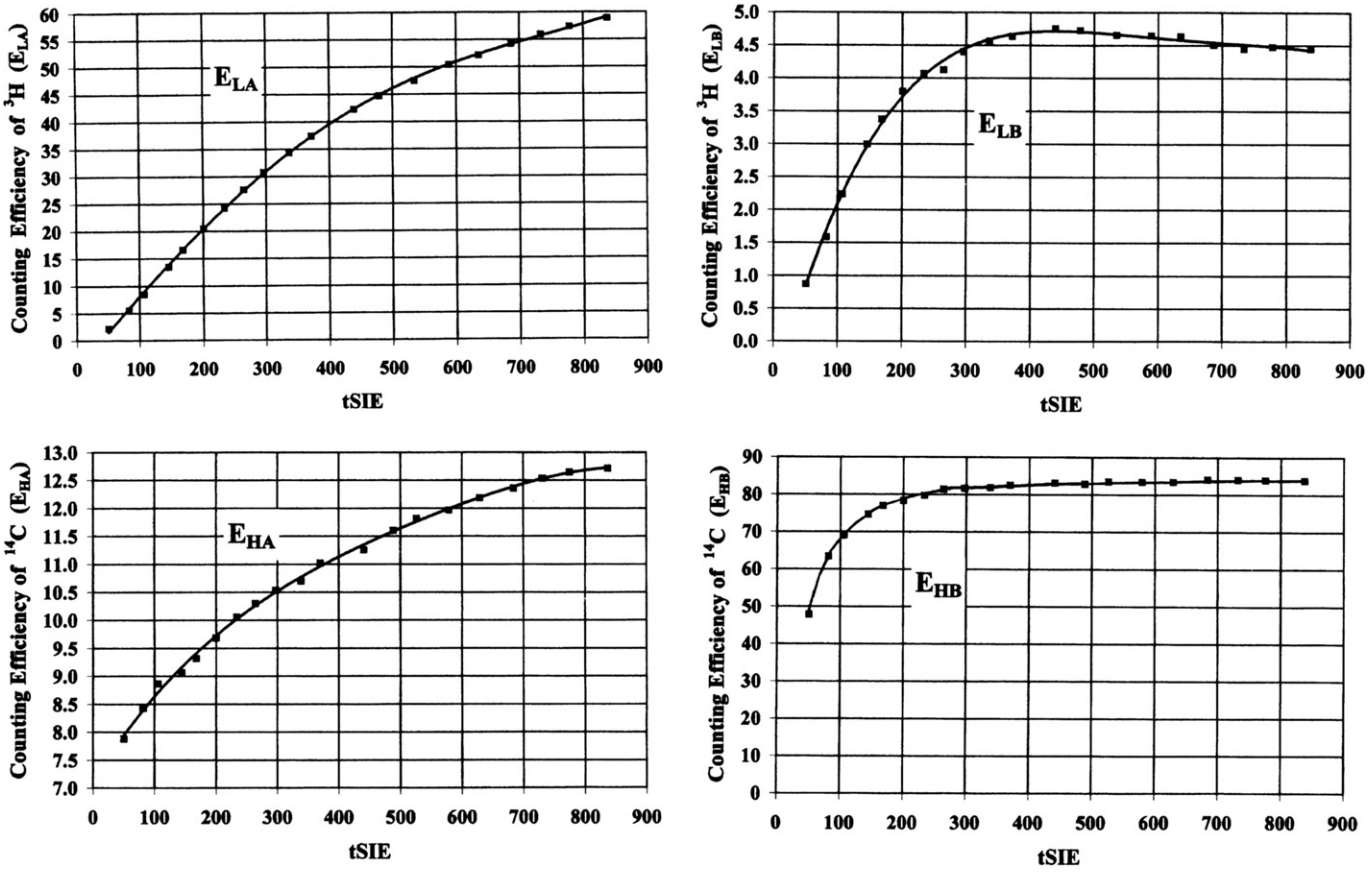

FIGURE 7.38 Quench-correction curves of counting efficiency versus tSIE/AEC for ^{3}H and ^{14}C in region A (LL−UL: 0−12.0 keV) and region B (LL−UL: 12.0−156 keV) for the dual-radionuclide analysis of ^{3}H−^{14}C. The notations E_{LA}, E_{LB}, E_{HA}, and E_{HB} are the counting efficiency factors defined in Eqns 7.35 and 7.36. The quench-correction curves were obtained with ^{3}H and ^{14}C quenched standards counted in regions A and B with a PerkinElmer 2770TR/SL liquid scintillation analyzer.

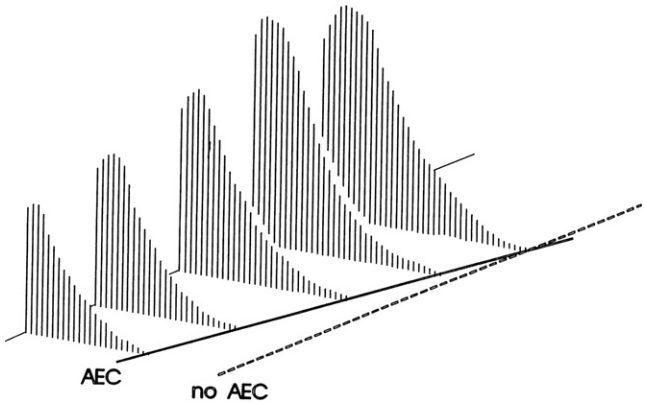

FIGURE 7.39 Illustration of automatic region tracking. Using automatic efficiency control (AEC), the liquid scintillation analyzer automatically moves the upper-level discriminator of a counting region from pulse heights of higher magnitude to those of lower magnitude (right to left of the pulse-height spectrum) according to the degree of quench in a sample. The pulse-height spectra of five samples are illustrated, each at different levels of quench. The samples of higher quench level are those of smallest pulse number and magnitude. *(© 1998 PerkinElmer, Inc. Printed with permission)*

scintillation pulse-height spectrum of a radionuclide diminishes as quench increases, and AEC automatically moves a discriminator setting according to the degree of quench in the sample. If dual-radionuclide samples of tritium and ^{14}C are counted using quench curves and automatic window tracking methods (*e.g.*, AEC or AQC) are employed, the resultant quench-correction curves shown in Figure 7.38 can be used to determine the counting efficiency of each radionuclide in each counting region. As illustrated, four curves are created, one for each of the two nuclides in each of the two counting regions. The major feature to note is that the amounts of spilldown of ^{14}C into the ^{3}H region and the spillup of ^{3}H into the ^{14}C region are kept constant.

The equations used to calculate the DPM for each radionuclide are derived from the following equations, which describe the count rate in the two counting regions:

$$CPM_A = D_L E_{LA} + D_H E_{HA} \tag{7.35}$$

$$\text{and } CPM_B = D_L E_B + D_H E_{HB} \tag{7.36}$$

where CPM_A and CPM_B are the net (background-subtracted) count rates of a dual-radionuclide sample in regions A and B, respectively; D_L and D_H are the disintegration rates (DPM) of the lower-energy radionuclide (*e.g.*, ^{3}H) and higher-energy radionuclide (*e.g.*, ^{14}C), respectively; E_{LA} and E_{LB} are the counting efficiencies of the lower-energy radionuclide in regions A and B, respectively; and E_{HA} and E_{HB} are the counting efficiencies of the higher-energy radionuclide in regions A and B, respectively. The four counting efficiency factors in Eqns.

7.35 and 7.36 are obtained automatically by the liquid scintillation analyzer from the four quench-correction curves (Fig. 7.38) stored in the computer memory of the LSA. Therefore, the preceding two equations still have two unknowns, namely, D_L and D_H, which are solved for simultaneously to obtain

$$D_L = \frac{CPM_A E_{HB} - CPM_B E_{HA}}{E_{LA} E_{HB} - E_{LB} E_{HA}} \quad (7.37)$$

$$\text{and } D_H = \frac{CPM_B E_{LA} - CPM_A E_{LB}}{E_{LA} E_{HB} - E_{LB} E_{HA}} \quad (7.38)$$

For the activity determinations of a dual nuclide mixture, the liquid scintillation analyzer determines the net count rates of the sample in regions A and B, and the quench-indicating parameter of the sample. From the value of the quench-indicating parameter, the LSA automatically extracts the needed four counting efficiency factors from the quench-correction curves (*e.g.*, Fig. 7.38) and then automatically calculates the disintegration rates of the two radionuclides in the mixture according to Eqns 7.37 and 7.38. All of the calculations are performed by the software of the liquid scintillation analyzer.

Because the discriminator settings defining the counting regions A and B will move automatically according to the amount of quench in the sample, as measured by the QIP, it is important to note that varying the counting region settings changes the quench-correction curves (efficiency versus QIP). This is generally of little concern to the analyst, because most modern liquid scintillation analyzers save, on the hard disk of the computer, the entire pulse-height spectra of the quenched radionuclide standards. Consequently, as the counting regions are changed automatically by the instrument according to quench level, so are the resultant new quench-correction curves automatically determined by the instrument.

Often it is necessary to analyze radionuclide mixtures for which no preset counting regions have been established in the liquid scintillation analyzer. In such a case, it is necessary to find and select the optimum LL and UL discriminator settings to define counting regions A and B. The procedure used to obtain the proper discriminator settings is as follows, using the ^{33}P–^{32}P dual-radionuclide mixture as an example:

1. To find the appropriate LL and UL discriminator settings for the inclusion method for dual-radionuclide activity analysis, we must count first a known activity (DPM) of the lower-energy radionuclide (*e.g.*, ^{33}P, $E_{max} = 249$ keV) as a pure radioisotope sample in a wide range of counting regions starting at an LL discriminator setting of zero and progressively increasing the UL discriminator in small increments (*e.g.*, 10 eV). Certain liquid scintillation analyzers (*e.g.*, PerkinElmer Tri-Carb) display the pulse-height discriminator settings in units of eV (0–2000 eV); others (*e.g.*, PerkinElmer Quantulus) display the discriminator settings in channel numbers (0–1024). A net count rate (CPM) for each region setting is recorded.
2. This procedure is repeated with a known activity (DPM) of the higher-energy radioisotope (*e.g.*, ^{32}P, $E_{max} = 1700$ keV), which is counted in the same regions selected in the above step 1. The net count rates (CPM) of the higher energy radionuclide in the counting regions are recorded. Both samples of the low-energy radionuclide (e.g., ^{33}P, $E_{max} = 249$ keV) and the higher-energy radionuclide (e.g., ^{32}P, $E_{max} = 1700$ keV) used for this exercise should be at similar and low levels of quench, that is, the lowest level of quench expected for any given unknown mixture.
3. The counting efficiencies of the separate low- and high-energy radionuclides (*e.g.*, ^{33}P and ^{32}P) standards in the various counting regions are then calculated according to the equation %E = (CPM/DPM)(100).
4. The counting efficiencies of the low-energy radionuclide in the individual counting regions are plotted against the counting efficiencies of the high-energy radionuclide in the same counting regions as illustrated in Fig. 7.40.
5. The objective of this exercise is to find discriminator settings at which there will be significant overlap (spill-over) of counts from both radionuclides in the two counting regions required for the inclusion method. These conditions are found in the "knee" section of the curve. Hence, a counting region is selected arbitrarily from the knee section of the curve as the counting region A for the dual-radionuclide analysis. In the example using the ^{33}P and ^{32}P radionuclide standards a counting region (LL–UL) of 0–100 keV from the knee of the curve was selected from the eighth data point counting from left to right of Fig. 7.40.

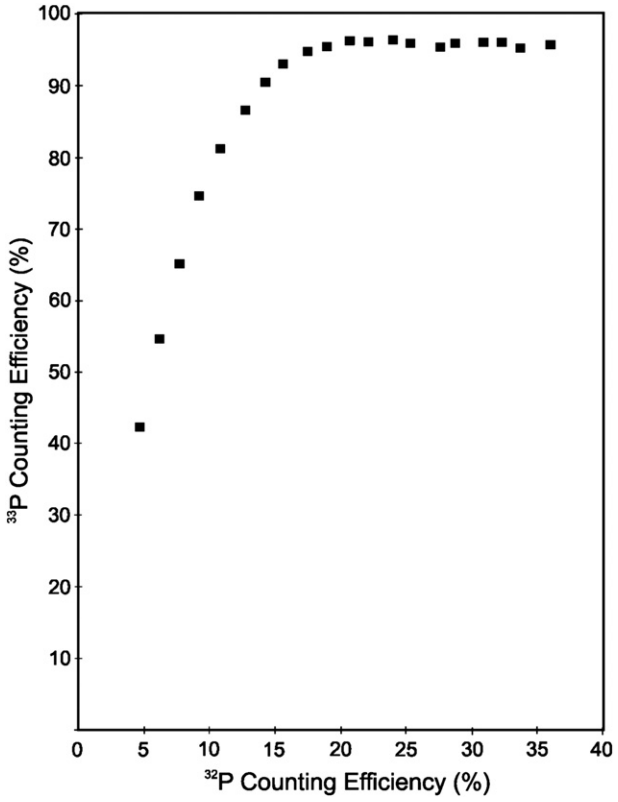

FIGURE 7.40 Effect of region settings on ^{33}P and ^{32}P counting efficiencies over the range of LL–UL, 0–30 to 0–220 keV. The data points represent increasing counting region widths in increments of 10 keV. *(From L'Annunziata, 1997b, © 1997 PerkinElmer, Inc. Printed with permission)*

6. Having defined in this way one of the counting regions (region A), we can then proceed to select the discriminator settings for the second counting region (region B). The discriminator settings for region B are defined by selecting its LL discriminator setting to be equivalent to the upper limit of region A (*e.g.*, 100 keV for the $^{33}P-^{32}P$ double label) and selecting the UL discriminator setting to encompass all pulses of highest magnitude arising from the higher-energy radionuclide. In this example, the UL discriminator setting of 1700 keV was selected, because no pulses from this double-radionuclide mixture can reach beyond 1700 keV. The second counting region (region B) for the case of the $^{33}P-^{32}P$ dual radionuclide was therefore defined by the LL and UL discriminator settings of 100−1700 keV.

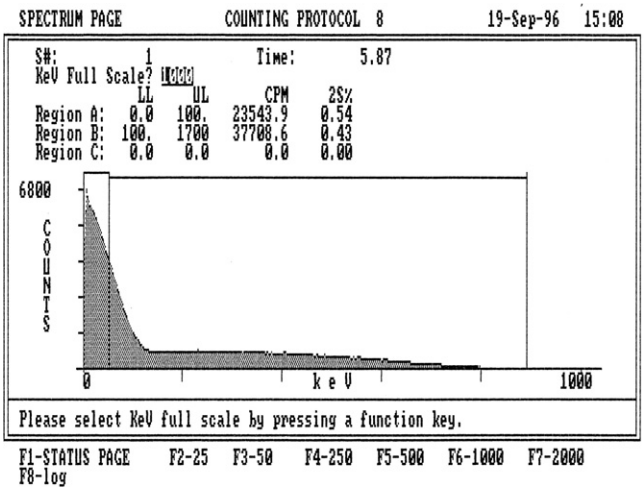

FIGURE 7.41 A composite pulse-height spectrum of a $^{33}P-^{32}P$ dual-radionuclide sample as displayed on the computer screen of a PerkinElmer Tri-Carb 2300TR liquid scintillation analyzer. Counting regions A and B are set for the dual-radionuclide analysis by the conventional inclusion method. *(L'Annunziata, M.F., 1996, unpublished work)*

Figure 7.41 illustrates the composite pulse-height spectrum of a dual-isotope sample of $^{33}P-^{32}P$ with an approximate 1:1 activity ratio as seen on the LSA computer screen. The discriminator settings established for regions A and B, as required for the analysis of these two isotopes in the same sample, are also seen in the figure. Data illustrating typical recoveries obtainable by this inclusion method for the analysis of a dual nuclide combination of $^{33}P-^{32}P$ are provided in Table 7.6. The inclusion method has been found to provide excellent recoveries of the $^{3}H-^{14}C$, $^{3}H-^{45}Ca$, $^{14}C-^{36}Cl$, $^{33}P-^{32}P$, $^{55}Fe-^{59}Fe$, $^{90}Sr-^{90}Y$, and other double radionuclide mixtures, for a wide range of activity ratios of the two radionuclides (Hui et al., 2012, Nebelung et al., 2009, Nakanishi et al., 2009, Reddy et al., 2009, Shaffer and Langer, 2007, Rodríguez et al., 2006, Zheng and Bobich, 2004, Zheng et al., 2004, Lee et al., 2002b, Benitez-Nelson and Buesseler, 1998, L'Annunziata, 1984b, 1987, 1997b, Viteri and Kohaut, 1997, and Kessler, 1989). Reddy et al., (2009) made extensive tests of this dual nuclide analysis method for $^{3}H-^{14}C$ combinations at low-activity levels. They obtained minimum detectable activities of 2100 DPM/L for ^{3}H and 1200 DPM/L for ^{14}C with a counting time of 300 minutes and found the accuracy of results to be within ± 10% for ^{3}H:^{14}C activity ratios ranging from 1:1 to 1:18. Fujii and Takiue (2001) report the unique analysis of airborne ^{3}H and ^{14}C in activity concentrations as low as 0.01 Bq/cm^3 by suspension of the radionuclides in a "foggy scintillator" created with an ultrasonic wave generator. The radionuclides could be analyzed as single- or dual-radionuclide mixtures. Nebelung et al. (2009) evaluated this dual-radionuclide analysis technique with activity ratios of up to 1/50 for

TABLE 7.6 DPM Recoveries for $^{33}P-^{32}P$ Dual-Nuclide Combinations[a] by the Dual Region Inclusion Method

Sample[b]	Ratio[c]					% Recovery[d]	
^{33}P:^{32}P	^{33}P:^{32}P	SIS	tSIE	DPM (^{33}P)	DPM (^{32}P)	DPM (^{33}P)	DPM (^{32}P)
1.0 mL: 0.0 mL	1:0	130	470	63056	188	99.5	0.3
0.0 mL: 1.0 mL	0:1	1039	476	28	63047	0.0	98.1
0.5 mL: 0.5 mL	1:1	589	472	32426	32867	102.2	99.1
1.0 mL: 0.5 mL	2:1	419	444	63311	32602	100.0	98.3
0.5 mL: 1.0 mL	1:2	707	445	31699	65550	100.1	98.8
1.0 mL: 0.2 mL	5:1	279	457	65012	13352	102.6	100.7
0.2 mL: 1.0 mL	1:5	869	460	12744	65011	100.6	98.0
1.0 mL: 0.1 mL	10:1	215	464	63499	6613	100.2	99.7
0.1 mL: 1.0 mL	1:10	936	466	6770	65194	106.9	98.3

[a] *Activity of ^{33}P = 63361 DPM/mL, activity of ^{32}P = 66328 DPM/mL. Instrumentation: PerkinElmer TriCarb 2300TR liquid scintillation analyzer.*
[b] *Triplicate samples were counted for a duration of ten minutes or until a % 2 sigma standard deviation of 1.0% was reached.*
[c] *Ratios listed are only approximate. The exact ratios can be calculated from the isotope activities (DPM/mL) and sample sizes (mL) of each isotope.*
[d] *The standard deviation of the mean of all triplicate measurements ranged from 0.13% to 2.77%.*
(From L'Annunziata, 1997b © 1997 PerkinElmer, Inc. Printed with permission)

several combinations of nuclides and, including $^{3}H/^{14}C$, $^{14}C/^{60}Co$, $^{14}C/^{90}Sr$, $^{14}C/^{99}Tc$, $^{137}Sc/^{60}Co$, $^{55}Fe/^{3}H$, and $^{99}Tc/^{60}Co$ with good accuracy. They used a PerkinElmer Tri-Carb 3100 TR liquid scintillation analyzer, which requires the establishment of quench-correction curves using the quench-indicating parameter, tSIE, with automatic efficiency control (tSIE/AEC), as described previously.

b. Dual-Radionuclide Analysis with Daughter Ingrowth

When two beta-emitting radionuclides are analyzed in two counting regions or windows, and there occurs ingrowth of a radionuclide daughter during the analysis, we have essentially the need to analyze simultaneously three radionuclides in the two counting windows. An excellent example is that of the liquid scintillation analysis of ^{89}Sr ($E_{max} = 1490$ keV) and ^{90}Sr ($E_{max} = 546$ keV) in two counting windows after the separation of ^{89}Sr and ^{90}Sr from other nuclides in the sample by chemical means, such as ion exchange. When the strontium is separated from other nuclides on an ion-exchange column, activity of the ^{90}Y daughter of ^{90}Sr will appear immediately after the isolation of strontium, and the ^{90}Y activity will increase with time due to daughter nuclide ingrowth until the ^{90}Y activity reaches the activity of the ^{90}Sr parent nuclide, *i.e.*, secular equilibrium (L'Annunziata, 1971 and Fig. 1.97 of Chapter 1). Thus, the liquid scintillation analysis of radiostrontium, *i.e.*, ^{89}Sr and ^{90}Sr, in two counting windows must also include the measurement of the high-energy ^{90}Y ($E_{max} = 2280$ keV) daughter activity, which will produce liquid scintillation events in the same counting windows within which the ^{89}Sr and ^{90}Sr events are counted. Thus, in this case, there is the need to analyze the activities of three beta-emitting radionuclides in two counting regions. The measured activity of the ^{90}Y will be a function of the ^{90}Sr parent nuclide activity and the time in hours since the time of isolation or separation of the strontium from other nuclides (t_0) and the time of measurement or counting (t_1). The recorded time of separation of strontium from other radionuclides and the time of counting will provide the duration in hours during which ^{90}Y ingrowth would have occurred. The calculated ingrowth of ^{90}Y allows for the mathematical correction of the contribution of ^{90}Y to the sample count rates in the two counting windows and permits the final calculated activities of ^{89}Sr and ^{90}Sr.

An excellent example of the dual counting region method with correction for daughter nuclide ingrowth, described previously, was reported by Kim et al. (2009) for the analysis of ^{89}Sr and ^{90}Sr in milk, which is based on the method of Eikenberg et al., (2006). The method of Eikenberg et al., (2006) utilized three counting windows to include the simultaneous analysis of an additional radionuclide, ^{85}Sr, which is used as a tracer nuclide to calculate the chemical recovery of strontium. Kim et al. (2009) isolated strontium including the ^{89}Sr and ^{90}Sr from milk using a column of ion-exchange resin that removed all other radionuclides including the ^{90}Y daughter nuclide of ^{90}Sr. The time of collection of the radiostrontium was taken as t_0, which is the time that the ^{90}Y daughter nuclide of ^{90}Sr is removed and when ingrowth of ^{90}Y with its parent will begin. The isolated radiostrontium was counted in a liquid scintillation analyzer in two counting windows illustrated in Fig. 7.42. When counting a sample of radiostrontium, *i.e.*, ^{89}Sr and ^{90}Sr, isolated from other nuclides in the counting windows, illustrated in Fig. 7.42, window A will yield a total count rate, which will be sum of count rates from pulse events arising from beta emissions of $^{89}Sr + {}^{90}Sr +$ ingrown $^{90}Y +$ background events,

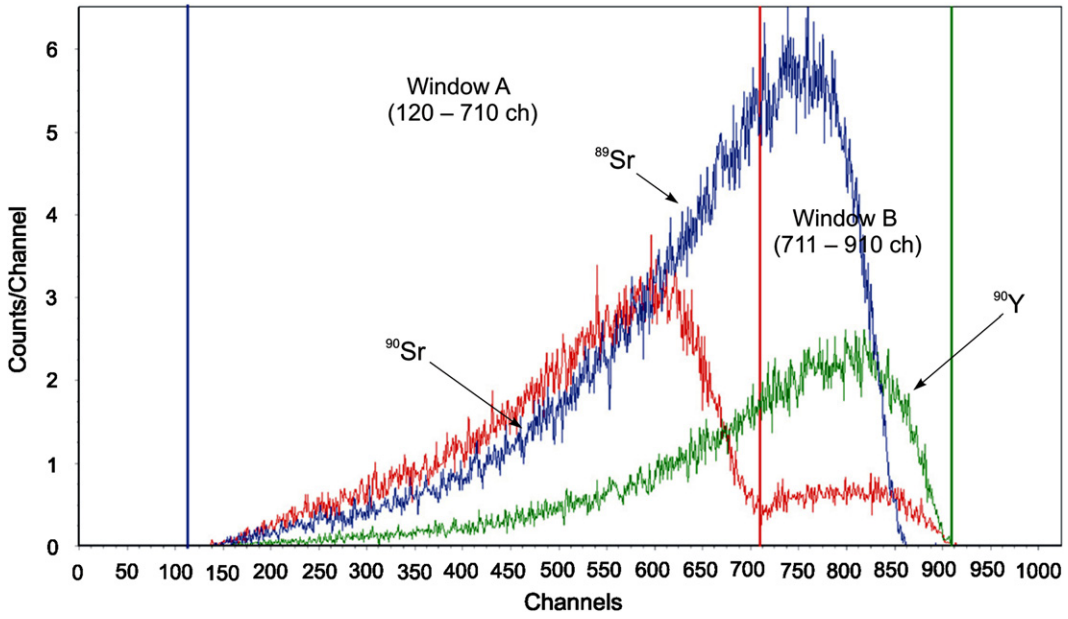

FIGURE 7.42 The liquid scintillation beta pulse-height spectra of ^{89}Sr, ^{90}Sr, and ^{90}Y. Two counting regions or windows are illustrated, namely, window A defined by lower-level (LL) and upper-level (UL) discriminator settings set at channel 120−710, respectively, and window B with LL and UL discriminator settings at channel 711−910, respectively. A relatively weak and broad peak of pulse events due to ^{90}Y ingrowth with ^{90}Sr parent can be seen in window B. For the color version of the figure, the reader is referred to the online version of the book. *(From Kim et al., 2009, reprinted with permission from Elsevier © 2009)*

whereas window B will yield a summed count rate arising from beta emissions from ^{89}Sr + ingrown ^{90}Y + background events.

Using the notation of Eikenberg et al., (2006), Kim et al. (2009) calculated the net (background-subtracted) count rates in the two counting windows A and B, which are defined as

$$N(t)^A = N(t)^A_{Sr-89} + N(0)^A_{Sr-90} + N(t)^A_{Y-90} \quad (7.39)$$

$$\text{and } N(t)^B = N(t)^B_{Sr-89} + N(t)^B_{Y-90} \quad (7.40)$$

where in Eqn 7.39, $N(t)^A$ is the net count rate (CPS) in window A, $N(t)^A_{Sr-89}$ is the net count rates in window A due to ^{89}Sr at the time t of counting (^{89}Sr can undergo appreciable decay from the time of separation from the other nuclides to the time of counting; half-life of ^{89}Sr is 50.5 days), $N(0)^A_{Sr-90}$ is the count rate due to ^{90}Sr in window A at the time of counting and the time of separation from other nuclides (^{90}Sr undergoes no observable decay; half-life of ^{90}Sr is 28.8 years), and $N(t)^A_{Y\text{-}90}$is the count rate in window A due to ingrowth of ^{90}Y at the time t of counting. Also in Eqn 7.40, $N(t)^B$ is the net count rate (CPS) in window B, $N(t)^B_{Sr\text{-}89}$ is the net count rate in window B due to ^{89}Sr at the time t of counting, and $N(t)^B_{Y\text{-}90}$ is the count rate in window B due to ingrowth of ^{90}Y at the time t of counting. According to Eqn 7.7 it is obvious that the count rate (e.g., CPS) of a radionuclide is the product of the activity or disintegration rate (DPS) and detection efficiency ε of the nuclide, where $0 \leq \varepsilon \leq 1$ for detection efficiencies in the range of 0 and 100%. Thus, Kim et al. (2009) expressed Eqns. 7.39 and 7.40 as

$$N(t)^A = A(t)_{Sr-89} \cdot \varepsilon^A_{Sr-89} + A(0)_{Sr-90} \cdot \varepsilon^A_{Sr-90} + A(0)_{Sr-90} \cdot f_1 \cdot \varepsilon^A_{Y-90} \quad (7.41)$$

$$\text{and } N(t)^B = A(t)_{Sr-89} \cdot \varepsilon^B_{Sr-89} + A(0)_{Sr-90} \cdot f_1 \cdot \varepsilon^B_{Y-90} \quad (7.42)$$

where $A(t)_{Sr-89} \cdot \varepsilon^A_{Sr-89}$is the product of the activity in disintegrations per second (DPS) of ^{89}Sr at the time t of counting and the detection efficiency of ^{89}Sr in counting window A, $A(0)_{Sr\text{-}90} \cdot \varepsilon^A_{Sr\text{-}90}$is the product of the activity of ^{90}Sr at the time of its separation from ^{90}Y and other radionuclides and the detection efficiency of ^{90}Sr in counting window A, and $A(0)_{Sr\text{-}90} \cdot f_1 \cdot \varepsilon^A_{Y\text{-}90}$ represents the contribution to the count rate in window A arising from the ingrowth of ^{90}Y from the time t_0 of separation of the ^{90}Sr from yttrium to the time t of counting and

$$f_1 = (1 - e^{-\lambda_{Y\text{-}90} t_1}) \quad (7.43)$$

where $\lambda_{Y\text{-}90}$ is the decay constant of ^{90}Y and $t_1$is the interval of time from the time of separation of ^{90}Sr from ^{90}Y, t_0, and the time t of counting, i.e., $t_1 = t - t_0$. Thus, the term $A(0)_{Sr\text{-}90} \cdot f_1$ of Eqn 7.42 represents the activity of the ^{90}Y ingrown with the isolated ^{90}Sr, and the activity of the ^{90}Y will grow according to the time interval t_1 to a maximum activity (A_{max}) equivalent to that of isolated ^{90}Sr (L'Annunziata, 1971), or

$$A_{Y-90} = A_{Y-90,\,max}(1 - e^{-\lambda_{Y\text{-}90} t_1}) = A(0)_{Sr-90}(1 - e^{-\lambda_{Y\text{-}90} t_1}) \quad (7.44)$$

Eqn 7.44 is equivalent to that expressed by Eqn 1.442 of Chapter 1.

From Eqns 7.41 and 7.42, Kim et al. (2009) arrive at the final expressions for calculating the activities of ^{90}Sr and ^{89}Sr in units of Bq/L when the strontium recovery, r_{sr}, and sample volume, V, are included, which are

$$A(0)_{Sr-90} = \frac{(N(t)^A - A(t)_{Sr-89} \cdot \varepsilon^A_{Sr-89})}{(\varepsilon^A_{Sr-90} + f_1 \cdot \varepsilon^A_{Y-90}) \cdot r_{sr} \cdot V} \quad (7.45)$$

$$A(t)_{Sr-89} = \frac{(N(t)^B - A(0)_{Sr-90} \cdot f_1 \cdot \varepsilon^B_{Y-90})}{\varepsilon^B_{Sr-89} \cdot r_{sr} \cdot V} \quad (7.46)$$

Quench-correction curves are not needed in this case to determine the detection efficiencies of ^{90}Sr, ^{89}Sr, and ^{90}Y in the two counting windows, because all samples are prepared uniformly with the same level of quench, and minor variations of quench level have negligible effect on the detection efficiencies of these relatively high-energy beta emitters. The determination of the detection efficiencies by the use of internal standards of ^{90}Sr, ^{89}Sr, and ^{90}Y, as carried out by Kim et al. (2009), does suffice in this case.

c. Triple-Radionuclide Analysis

In triple-radionuclide analysis (*e.g.*, a mixture of $^3H + ^{14}C + ^{32}P$ or $^3H + ^{14}C + ^{131}I$), three counting regions and three sets of quench standards would be required to prepare quench-correction curves for each radionuclide in each counting region. Consequently, three CPM values, one for each of the three counting regions, are obtained and three equations solved to calculate the DPM of each of the three radionuclides. For example, Bukowski et al. (1992) describe the liquid scintillation analysis of mixtures of ^3H, ^{14}C and ^{131}I in three counting windows, namely, window 1 defined by channel numbers 5−300, window 2 defined by channel numbers 300−550, and window 3 defined by channel numbers 550−800. The channel numbers (LL and UL discriminator settings) are selected by determining the pulse-height spectra of the lowest-quenched sample of each individual radionuclide with the LSA multichannel analyzer, as illustrated in Fig. 7.43. The upper limits of the pulse-height spectra of the lowest-quenched samples were selected as the upper-level (UL) discriminator settings for each counting window, as illustrated in Fig. 7.43. Modern liquid scintillation analyzers equipped with automatic efficiency control (AEC) or automatic quench compensation (AQC) will automatically shift the upper-level discriminator setting to lower channel numbers according to the level of quench in the sample, as the uppermost levels of the spectra shift with quench.

When three sets of quenched standards, *i.e.*, quenched standards for each radionuclide, are counted in each of the three counting windows, separate quench-correction curves of % detection efficiency versus a quench-indicating parameter for each radionuclide in each counting window are obtained, as illustrated in Fig. 7.44. In the example given here the detection efficiency of ^3H in windows 2 and 3 are zero, and the detection efficiency of ^{14}C in window 3 is zero. This is so, because there is no spillover of ^3H into window 2 or 3 as well as no spillover of ^{14}C into window 3. However, other counting windows can be selected to permit some spillover of pulse events from the ^3H into

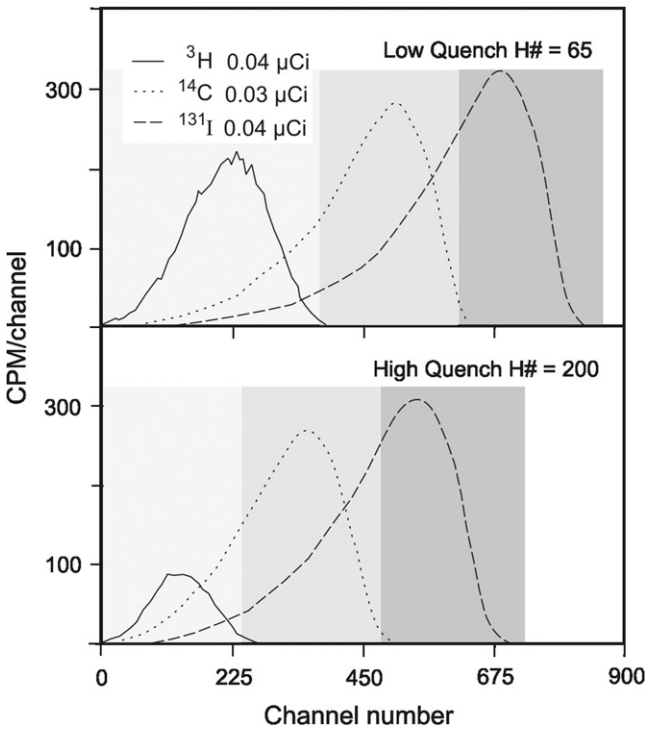

FIGURE 7.43 Liquid scintillation pulse-height spectra of ^{3}H, ^{14}C, and ^{131}I at low and high quench levels. As quench increases, the pulse-height spectra are reduced in intensity (fewer counts/per channel) and pulse height (shift from higher to lower channel numbers). *(From Bukowski et al., 1992. Reprinted with permission from Elsevier © 1992)*

window 2 or the ^{14}C into window 3, as the three equations used to calculate the radionuclide activities can be solved with spillover.

For the analysis of experimental samples the liquid scintillation analyzer (LSA) will determine the count rate in each counting window, the quench-indicating parameter [*e.g.*, H#, tSIE, SQP(E)] of that sample and then determine the nine detection efficiencies for the three radionuclides in each counting window. The LSA will also determine the background count rate in each counting window. With these data collected by the LSA, the follow equations can be analyzed according to the notation used by Bukowski et al. (1992) to calculate the activity or disintegration rate of each of the three radionuclides in the sample:

$$\begin{aligned} W_1 &= e_{11}D_1 + e_{12}D_2 + e_{13}D_3 + B_1 \\ W_2 &= e_{21}D_1 + e_{22}D_2 + e_{23}D_3 + B_2 \\ W_3 &= e_{31}D_1 + e_{32}D_2 + e_{33}D_3 + B_3 \end{aligned} \tag{7.47}$$

Bukowski et al. (1992) used a standard Gaussian elimination matrix inversion method to solve the above three equations for D_j, which is the activity (DPM) of radionuclide j, where Wi is the count rate (CPM) in window i, e_{ij} is the counting efficiency of radionuclide j in window i, and B_i is the background count rate (CPM) in counting window i. For the calculation of the activities of three radionuclides utilizing three counting windows according to Eqn 7.47, there is the need for 9 counting efficiency values, one for each of the three radionuclides in each counting window (Nebelung et al. 2009). Fig. 7.44 illustrates 8 of the 9 quench-correction curves, the missing 9th curve is that of ^{14}C in window 3; this curve would be similar to that of ^{3}H in window 3, when there is no spillover of pulse events from ^{14}C into window 3.

For another excellent example of a triple-radionuclide analysis (^{3}H, ^{22}Na, and ^{36}Cl) of this type and the calculations and quench curves involved, the reader should refer to Schneider and Verbrugge (1993). Nebelung et al. (2009) tested the above method of triple-radionuclide analysis with a PerkinElmer TriCarb 3100 TR liquid scintillation analyzer requiring the preparation of quench-correction curves based on the quench-indicating parameter tSIE/AEC. They obtained excellent recoveries from the following combination of radionuclides with activity ratios of up to 1/50: ^{55}Fe/^{3}H/^{14}C, ^{55}Fe/^{14}C/^{99}Tc, ^{3}H/^{14}C/^{60}Co, ^{3}H/^{14}C/^{137}Cs, ^{3}H/^{14}C/^{90}Sr, and ^{14}C/^{99}Tc/^{60}Co.

Triple-radionuclide liquid scintillation analysis is utilized for the analysis of radiostrontium, because ^{89}Sr and ^{90}Sr are encountered generally together, and with that comes the unavoidable ^{90}Y daughter nuclide of ^{90}Sr. An exception would be pure ^{90}Sr(^{90}Y), which is used in nuclear medicine free of ^{89}Sr as a source of ^{90}Y for clinical applications. The liquid scintillation analysis of ^{89}Sr and ^{90}Sr(^{90}Y) utilizing three counting regions or counting windows was studied in detail by Chobola

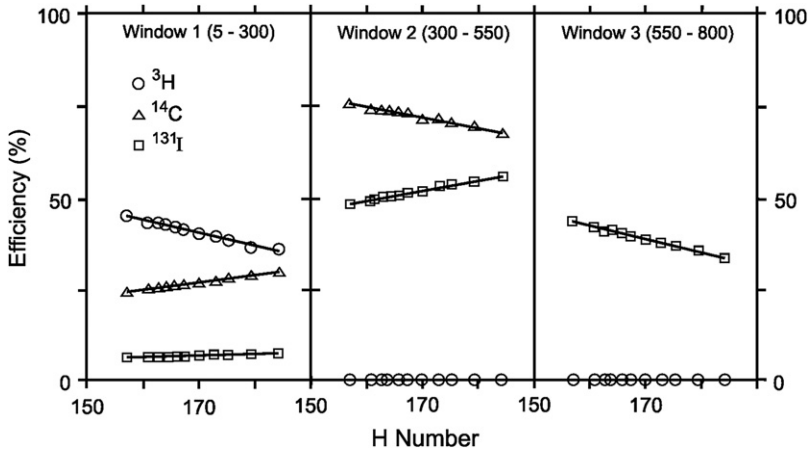

FIGURE 7.44 Quench-correction curves of % detection efficiency versus the quench-indicating parameter, H #, for ^{3}H, ^{14}C, and ^{131}I in three counting windows defined by LL and UL discriminator settings at channel numbers 5−300 for window 1, 300−550 for window 2, and 550−800 for window 3. The detection efficiency of ^{3}H is zero in windows 2 and 3, and the detection efficiency of ^{14}C is zero in window 3. *(From Bukowski et al., 2009. Reprinted with permission from Elsevier © 1992)*

et al. (2006). They calculated the theoretical beta distributions for ^{90}Sr ($E_{max} = 546$ keV), ^{89}Sr ($E_{max} = 1490$ keV), and ^{90}Y ($E_{max} = 2280$ keV) and compared these with the experimental pulse-height spectra produced by the three radionuclides with a PerkinElmer TriCarb 2275 liquid scintillation analyzer. They found the composite pulse-height spectrum provided by the LSA to approximate closely to the calculated beta distributions of each radionuclide. Figure 7.45 illustrates the approximate beta distributions of equal activities of each radionuclide, and a composite spectrum, as depicted by the writer from their work. For the precise spectral distributions, see Chobola et al. (2006). They selected three counting windows, as depicted in Fig. 7.45, to be defined by lower-level (LL) and upper-level (UL) discriminator settings of channel 23−200 for window A, 201−800 for window B, and 801−4000 for window C. They counted the radiostrontium after passing the sample to be counted through a strontium-specific ion-exchange column (SrSpec™, Eichrom Technologies) that would remove all radionuclides other than strontium including the ^{90}Y daughter nuclide of ^{90}Sr.

As depicted in Fig. 7.45, window A registers pulse events from ^{90}Sr, ^{89}Sr, and ^{90}Y, window B registers pulse events from ^{89}Sr and ^{90}Y, and window C register pulse events from ^{90}Y. Chobola et al. (2006) defined three equations for the net (background-subtracted) count rates in each counting window using the matrix

$$\begin{bmatrix} I_A \\ I_B \\ I_C \end{bmatrix} = \begin{bmatrix} A \\ B \\ C \end{bmatrix} \cdot \begin{bmatrix} \eta_{AA}\ \eta_{BA}\ \eta_{CA} \\ \eta_{AB}\ \eta_{BB}\ \eta_{CB} \\ \eta_{AC}\ \eta_{BC}\ \eta_{CC} \end{bmatrix} \tag{7.48}$$

where I_A, I_B, and I_C are the net intensities or net count rates (CPM) obtained in counting windows A, B, and C, and the sample activities (DPM) of each radionuclide are $A = {}^{90}$Sr activity, $B = {}^{89}$Sr activity, and $C = {}^{90}$Y activity. Within the matrix are the detection efficiencies of each radionuclide in the three counting windows or counting regions where η_{XY} denotes the counting efficiency of radionuclide X in counting region Y. Chobola et al. (2006) solved for activities A, B, and C including the constraint imposed by the ^{90}Y ingrowth. The activity C, that is the activity of ^{90}Y, will depend on the activity of ^{90}Sr in the sample and the time interval in hours from the time of isolation of strontium from the ion-exchange column to the time of sample counting, which would govern ^{90}Y ingrowth according to the following:

$$^{90}\mathrm{Y}_{\mathrm{DPM}} = {}^{90}\mathrm{Sr}_{\mathrm{DPM}}[1 - e^{-\lambda t}] = A\left[1 - e^{-\frac{0.693}{64.1\ \mathrm{h}}(t - t_0)}\right] \tag{7.49}$$

The above Eqn 7.49 is identical to Eqn 7.44 discussed previously in this chapter and that expressed by Eqn 1.442 of Chapter 1. The various detection efficiencies of the three radionuclides required to solve the radionuclide activities need not be determined by quench-correction curves, as the radiostrontium nuclides as well as ^{90}Y are not easily quenched and the samples do not vary significantly in their chemistry or quench level. Internal standards can be used conveniently to determine the detection efficiencies, and internal standards can yield very precise detection efficiencies, if utilized properly, as described in Section V.A.

Eikenberg et al. (2006) included a ^{85}Sr yield tracer in the three-window approach to the simultaneous liquid scintillation analysis of ^{89}Sr−^{90}Sr(^{90}Y). Like most analytical preparations for radiostrontium analysis, they separated the radiostrontium from other radionuclides (including ^{90}Y) in the sample by use of cation exchange with a column of SrSpec™ resin (Eichrom Technologies). Ingrowth of the ^{90}Y daughter nuclide of ^{90}Sr would begin immediately after the radionuclide separation (L'Annunziata, 1971). During the radiostrontium separation process, Eikenberg et al. (2006) allowed for the isolation of the ^{90}Y from the sample for subsequent Cherenkov counting and extrapolation of the ^{90}Y curve to time t_0, the time of separation of the ^{90}Y from the sample when it was in secular equilibrium with the ^{90}Sr.

For liquid scintillation analysis, Eikenberg et al. (2006) selected a three-window counting arrangement in a PerkinElmer TriCarb 2270TR/AB liquid scintillation analyzer, which is equipped with a pulse-height analyzer calibrated in keV (See Fig. 7.46). The counting regions were window A: 0−12 keV, window B: 12−300 keV, and window C: 300−1200 keV. Window A would register pulse events mostly from the ^{85}Sr yield tracer. The ^{85}Sr, which decays by electron capture, will produce abundant relatively low-energy Auger and conversion electron interactions with the liquid scintillation fluor cocktail, and there are, in addition, X-ray and gamma photon Compton electron interactions. Window B would register mostly ^{89}Sr and ^{90}Sr beta emissions in addition to ^{90}Y ingrowth.

Eikenberg et al. (2006) expressed the count rates (CPM) in the three counting regions as

$$\begin{aligned} N(t)_m^A &= A(t)_{85} \cdot \varepsilon_{85}^A + A(t)_{89} \cdot \varepsilon_{89}^A + A(0)_{90\mathrm{Sr}} \cdot \varepsilon_{90\mathrm{Sr}}^A \\ &\quad + A(0)_{90\mathrm{Sr}} \cdot f_1 \cdot \varepsilon_{90\mathrm{Y}}^A \\ N(t)_m^B &= A(t)_{85} \cdot \varepsilon_{85}^B + A(t)_{89} \cdot \varepsilon_{89}^B + A(0)_{90\mathrm{Sr}} \cdot \varepsilon_{90\mathrm{Sr}}^B \\ &\quad + A(0)_{90\mathrm{Sr}} \cdot f_1 \cdot \varepsilon_{90\mathrm{Y}}^B \\ N(t)_m^C &= A(t)_{89} \cdot \varepsilon_{89}^C + A(0)_{90\mathrm{Sr}} \cdot f_1 \cdot \varepsilon_{90\mathrm{Y}}^C \end{aligned} \tag{7.50}$$

where $N(t)_m^A$, $N(t)_m^B$, and $N(t)_m^C$ are the net (background-subtracted) count rates at time $t(m)$, i.e., time of measurement,

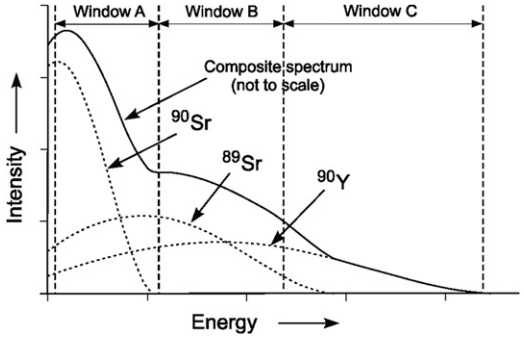

FIGURE 7.45 Approximate relative beta distributions of equal activities of ^{90}Sr, ^{89}Sr, and ^{90}Y and the approximate composite spectrum resulting from a mixture of equal activities the three radionuclides. Sketched from the work of Chobola et al. (2006). See reference for more precise distributions. *(Reprinted with kind permission from Springer Science + Business Media © 2006 Akadémiai Kiadó Budapest)*

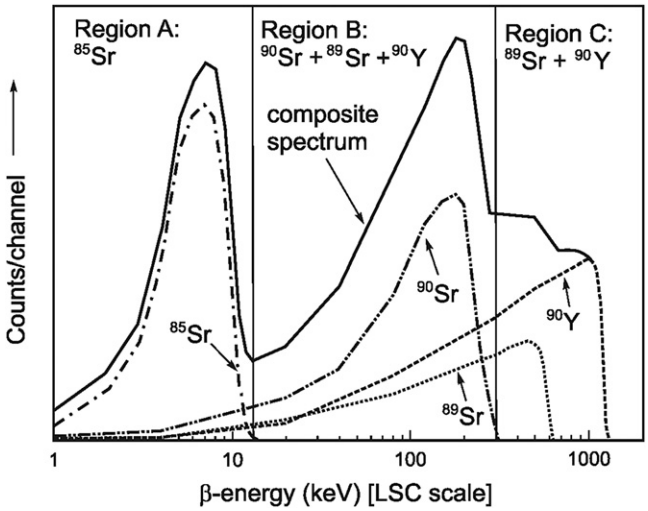

FIGURE 7.46 Approximate LSC beta spectra of ^{85}Sr, ^{90}Sr, ^{89}Sr, and ^{90}Y with the composite spectrum of the four radionuclides. Three counting windows are shown for the more precise measurement of each of the radionuclides. Sketched from the work of Eikenberg et al., (2006). See reference for more precise distributions. *(Reprinted with permission of Radiocarbon, University of Arizona, ©2006 Arizona Board of Regents on behalf of the University of Arizona)*

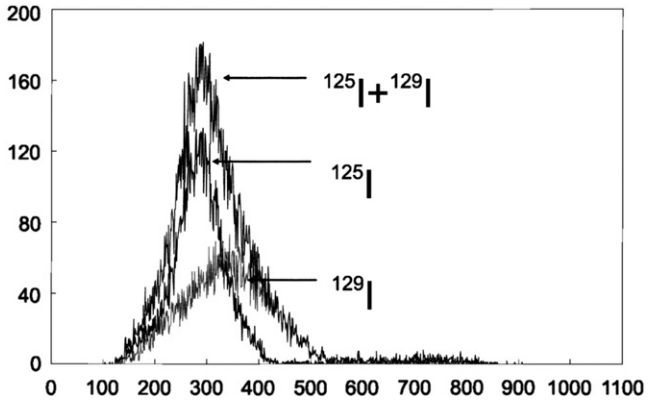

FIGURE 7.47 Pulse-height spectra (counts per channel vs. channel number) of ^{125}I and ^{129}I obtained with a PerkinElmer Quantulus 1220 liquid scintillation analyzer. *(From Kim et al., 2006, reprinted with permission of Radiocarbon, University of Arizona, ©2006 Arizona Board of Regents on behalf of the University of Arizona)*

in counting regions A, B, and C, respectively, $A(t)_{85}$, $A(t)_{89}$, and $A(0)_{90Sr}$ are the activities (DPM) of the added ^{85}Sr tracer at the time of measurement, the activity of ^{89}Sr at the time of measurement, and the activity of ^{90}Sr at the time of its separation from ^{90}Y on the ion-exchange SrSpec™ column, respectively, ε_{85}, ε_{89}, ε_{90Sr}, and ε_{90Y} are the detection efficiencies of ^{85}Sr, ^{89}Sr, ^{90}Sr, and ^{90}Y in counting windows A, B, or C, and f_1 is the ^{90}Y ingrowth term described previously (see Eqn 7.43). From the three equations describing the count rates in each counting region (Eqn 7.50), Eikenberg et al. (2006) derived the equation for calculating the activities of ^{85}Sr, ^{89}Sr, and ^{90}Sr. They obtained highly accurate ^{90}Sr activities by collecting the ^{90}Y extracted from the original sample during the ion-exchange separation of radiostrontium from ^{90}Y and other nuclides on the SrSpec™ exchange column. By Cherenkov counting of the ^{90}Y in a counting window of 0−25 keV, they could follow the ^{90}Y decay over a few half-lives and extrapolate the decay curve back to the time of separation from ^{90}Sr to determine the equal activities of ^{90}Sr and ^{90}Y, which were at secular equilibrium at the time of their separation (see Section XV.C and Fig. 1.97 of Chapter 1.).

B. Three-Over-Two Fitting and Digital Overlay Technique (DOT)

The three-over-two method and the digital overlay techniques are described by Kouru and Rundt, (1991). The three-over-two method, as noted in a previous paper by the writer (Noor et al., 1995), involves the counting of samples containing two radionuclides with three counting regions or windows. The count rate of each radionuclide is determined by solving a set of three equations for the two unknowns. By this technique, three and even more radionuclides in composite samples could be determined by using the number of counting windows greater than the number of radionuclides. This three-over-two fitting method was applied by Kim et al. (2006) to determine the activities of ^{129}I and ^{125}I, which display closely overlapping liquid scintillation pulse-height spectra (see Fig. 7.47). Iodine-125 decays by electron capture with the emission of 23-keV Auger electrons (20% intensity), 30-keV conversion electrons (13% intensity), as well as 30-keV X- and 35-keV gamma radiations of the daughter nuclide. Iodine-129 undergoes beta decay with an endpoint energy (E_{max}) of 154 keV and mean beta energy of 40.9 keV, 40 keV gamma, and 30-keV X-radiation (NNDC, 2011). The beta emissions of ^{129}I (average 40 keV) are slightly higher than the Auger and conversion electron emissions of ^{125}I producing a ^{129}I liquid scintillation pulse-height spectrum with a peak at higher channel numbers illustrated in Fig. 7.47. Kim et al. (2006) were able to accurately determine the activities of both nuclides in a mixture using the three-over-two fitting method included with the EasyView™ software (Wallac, PerkinElmer) installed in a PerkinElmer Quantulus 1220 liquid scintillation analyzer.

The three-over-two fitting method developed into the digital overlay technique (DOT) whereby, in principle, the number of windows approaches the resolution of the multichannel analyzer of the liquid scintillation counter. This digital overlay technique uses an external standard to measure quench and a specimen overlay to obtain the DPM for single or multiple-radionuclide samples. The shape of the sample spectrum is used to resolve dual or triple radionuclide samples by fitting the spectrum of each component to the measured composite spectrum. The fitting of a reference spectrum to the sample spectrum can give a measure of the level of quench. Spectral fitting is accomplished by the instrument (*e.g.*, Wallac RackBeta PerkinElmer, Inc.), which maintains a spectrum library that covers a large quench region of both chemical and color quench for the radionuclides. The technique is reviewed and tested by Kouru and Rundt (1991) and described in patents by Rundt and Kouru (1989, 1992). They demonstrate the method to perform as well as the counting region method previously described. The method is applied also in very specific models of Wallac (PerkinElmer, Inc.) liquid scintillation analyzers for quench correction and activity measurements of samples containing

only one beta-emitting radionuclide. Kouru (1991), Leppänen and Kukkonen (2006), Wiegand et al. (2007), and Hueber-Becker et al. (2007) report the use of DOT for quench correction and activity analysis of ^{14}C.

C. Full Spectrum DPM (FS-DPM)

Full Spectrum DPM is a user-friendly method available with PerkinElmer TriCarb liquid scintillation analyzers for the measurement of many dual-radionuclide combinations including ^{3}H–^{14}C, ^{3}H–^{32}P, ^{3}H–^{35}S, ^{14}C–^{32}P, ^{33}P–^{32}P, ^{35}S–^{32}P, ^{3}H–^{125}I, ^{125}I–^{131}I, ^{51}Cr–^{14}C, ^{67}Ga–^{68}Ga, ^{55}Fe–^{59}Fe, ^{125}I–^{14}C, ^{59}Fe–^{51}Cr, and ^{89}Sr–^{90}Sr, among others. The analysis protocol for FS-DPM is easy to set up, because no counting regions need to be defined. The full-spectrum DPM method utilizes the spectral index of the sample (SIS) of the double radionuclide sample to "unfold" the separate pulse-height spectra of the composite spectrum. This is possible because the SIS of the composite spectrum is a function of the individual distributions and the fractional counts of each radionuclide as well as the level of quench in the sample. The direct proportionality of SIS to the radionuclide composition in the sample was demonstrated by L'Annunziata and coworkers (see Noor et al., 1995, 1996b), who determined the activity ratios of ^{3}H:^{14}C and ^{35}S:^{32}P from only the spectral index of the sample.

The key to spectrum unfolding used in the full-spectrum DPM method is the SIS. At a given level of quench, each radionuclide has a defined pulse-height-energy distribution and hence a unique SIS value. When two radionuclides are combined into a single sample, the resultant pulse height is the sum of the two individual distributions. The SIS of the total distribution is a function of the SIS of the individual distributions and the fractional counts of each radionuclide. If the SIS_L and the SIS_H are the spectral index values of the low- and high-energy radionuclides of a dual-radionuclide sample, then the SIS of the total distribution SIS_T can be calculated as

$$SIS_T = \frac{(SIS_L)(\sum N_L E + SIS_H)(\sum N_H E)}{\sum N_L E + \sum N_H E} \tag{7.51}$$

where $\sum N_L E =$ accumulated counts from the low-energy radionuclide (*e.g.*, ^{3}H) and $\sum N_H E =$ accumulated counts from the high-energy radionuclide (*e.g.*, ^{14}C).

From Eqn 7.51 the following equations are derived, which define the count rates of the low-energy radionuclide (CPM_L) and the high-energy radionuclide (CPM_H) of a composite sample:

$$CPM_L = \frac{SIS_H - SIS_T}{SIS_H - SIS_L}(CPM_T) \tag{7.52}$$

$$\text{and } CPM_H = \frac{SIS_T - SIS_L}{SIS_H - SIS_L}(CPM_T) \tag{7.53}$$

For a detailed treatment on the derivation of Eqns 7.52 and 7.53, the reader may refer to Kessler (1989) and van Cauter and Roessler (1991).

To determine the count rates and disintegration rates of unknown dual-radionuclide samples, four quench-correction curves must be prepared with two sets of quenched standards. Quenched standards of the low-energy radionuclide and of the high-energy radionuclide are needed. The quenched standards are counted in a regionless environment, that is, no counting region discriminator settings need to be established. The data collected by the liquid scintillation analyzer from the counting of each of the quenched standards are the quench-indicating parameters (tSIE), the SIS values of the low- and high-energy radionuclide standards (SIS_L) and (SIS_H), respectively, and the percent counting efficiency of the low- and high-energy radionuclide standards. The LSA then plots automatically the four quench-correction curves such as the curves illustrated in Fig. 7.48.

For the analysis of unknown activities of the radionuclide components of a dual-radionuclide sample, the liquid scintillation analyzer will first determine the total count rate (CPM_T) and the tSIE of the sample. From the one value of tSIE, the instrument extracts automatically the values of SIS_L and SIS_H for the composite sample using two of the quench-correction curves (Fig. 7.48), which are maintained in computer memory. The LSA then calculates the count rate values of the low- and high-energy radionuclides CPM_L and CPM_H respectively, according to Eqns 7.52 and 7.53. The instrument then automatically converts these count rates to the disintegration rates of the low- and high-energy radionuclide DPM_L and DPM_H respectively, according to the equations

$$DPM_L = CPM_L/E_L \tag{7.54}$$

$$\text{and } DPM_H = CPM_H/E_H \tag{7.55}$$

where E_L and E_H, the counting efficiencies of the low- and high-energy radionuclides, respectively, are obtained from the respective quench-correction curves illustrated in Fig. 7.48.

This DPM method provides accurate DPM values for dual radionuclides when the endpoint energies (E_{max}) of the two radionuclides differ by a factor of 3 and the activity ratios are in the range of 1:25 and 25:1. For additional information on this technique, see Kessler (1989), De Filippis (1991), van Cauter and Roessler (1991), and L'Annunziata (1997b). The method was utilized for the analysis of ^{89}Sr–^{90}Sr mixtures by Hong et al. (2001) within 4 hours after strontium separation from liquid waste. For low-level counting they report a counting efficiency of 95% for ^{89}Sr and 92% for ^{90}Sr with the full-spectrum DPM method and lower limits of detection of 37 mBq/L for ^{90}Sr and 32 mBq/L for ^{89}Sr with a 60-minute counting time. An excellent illustration of the spectral unfolding power of the full-spectrum DPM method is provided in Fig. 7.49 using the ^{89}Sr–^{90}Sr combination as an example.

Altzitzoglou et al. (1998) and Lee et al. (2002a,b) also report the use of the method for the analysis of ^{90}Sr with its ^{90}Y daughter. Lee et al. (2002b) compared the full-spectrum DPM method and inclusion method (Section VIII.A.2) for the ^{90}Sr–^{90}Y analysis and found equal performance for both. The full-spectrum DPM method is easier to carry out for the less experienced analyst, as no counting regions need to be established. Lee et al. (2002b) tested the FS-DPM method for the analysis of ^{90}Sr in liquid waste, and the method should also be applicable to the analysis of trace activities of ^{90}Sr in samples of ^{90}Y, that are used in clinical applications where ^{90}Sr would be an

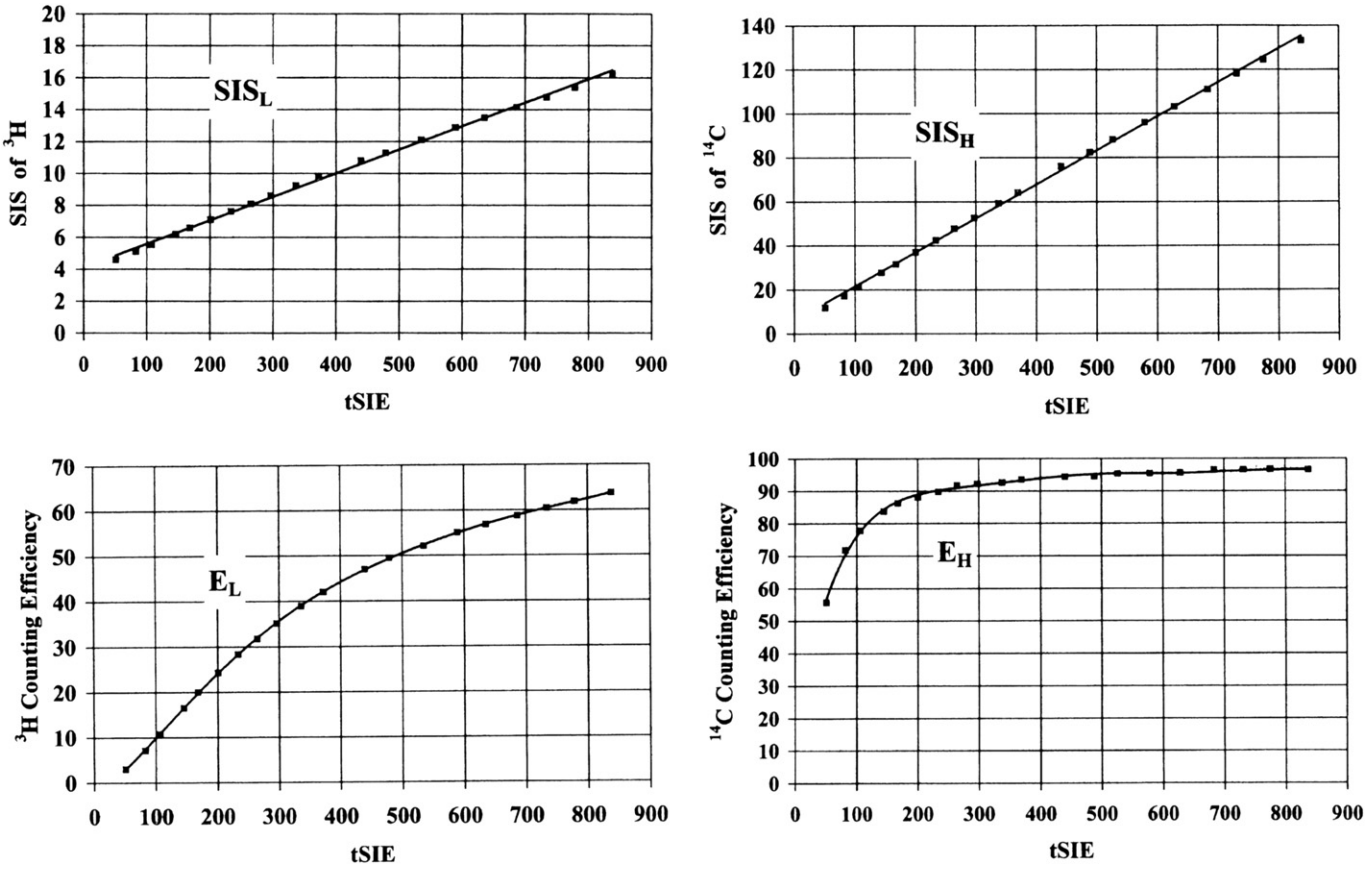

FIGURE 7.48 Quench-correction curves for full-spectrum DPM (FS-DPM) analysis of ^{3}H and ^{14}C mixtures. From the tSIE of a given sample, the liquid scintillation analyzer obtains from these curves the SIS of the lower- and higher-energy radionuclides, SIS_L and SIS_H, respectively, and the percent counting efficiency of the lower- and higher-energy radionuclides, E_L and E_H, respectively. The above curves were obtained from ^{3}H and ^{14}C quenched standards with a PerkinElmer TriCarb 2770TR/SL liquid scintillation analyzer.

undesirable contaminant. Fig. 7.50 illustrates the ^{90}Sr and ^{90}Y spectra in the FS-DPM counting mode at various times after the separation of ^{90}Sr. The figure illustrates the potential of this counting mode at any stage of ^{90}Y ingrowth, or for the analysis of traces of ^{90}Sr activity in isolated ^{90}Y.

Excellent recoveries were reported by Lee et al. (2002b) for the determination or ^{90}Sr activities. The measured activities in DPM were within 5% from the expected values with ingrowth of ^{90}Y measured over intervals from 0 to 15 days following the separation of ^{90}Sr. Reddy et al., (2009) made extensive tests of this FS-DPM analysis method for ^{3}H—^{14}C combinations at low-activity levels. They obtained minimum detectable activities of 2100 DPM/L for ^{3}H and 1200 DPM/L for ^{14}C with a counting time of 300 minutes and found the accuracy of results to be within ± 10% for ^{3}H:^{14}C activity ratios ranging from 1:1 to 1:18. Also, good recoveries of ^{33}P—^{32}P combinations were obtained by the writer using the FS-DPM method, and these are illustrated in Table 7.7.

D. Recommendations for Multiple Radionuclide Analysis

The following are a few suggestions to follow when performing DPM determinations for multiple- radionuclide samples by one of the methods previously described: (1) for the preparation of quench-correction curves, prepare the sets of quenched standards in the same cocktail, vial size, and total sample volume as the samples to be analyzed; (2) use of automatic region tracking (AEC or AQC) is recommended for dual- or triple-radionuclide analysis when using the counting-window inclusion methods of DPM analysis to maintain constant spillover of the radionuclides in the required counting regions; and (3) DOT or full-spectrum DPM methods require an accurate measurement of the sample pulse-height spectra by the instrument pulse height analyzer following automatic subtraction of the background. When sample counts are low, long counting times will be needed to obtain well-defined sample pulse-height spectra. As noted previously, Reddy et al., (2009) made extensive tests of the FS-DPM as well as the dual-window inclusion method of analysis for ^{3}H—^{14}C combinations at low-activity levels. They obtained minimum detectable activities of 2100 DPM/L for ^{3}H and 1200 DPM/L for ^{14}C with a counting time of 300 minutes and found the accuracy of results to be within ± 10% for ^{3}H:^{14}C activity ratios ranging from 1:1 to 1:18.

E. Complex Spectral Analysis

The multiple-radionuclide analysis methods previously discussed are limited to the analysis of not more than three β-emitting radionuclides in the same sample. From the

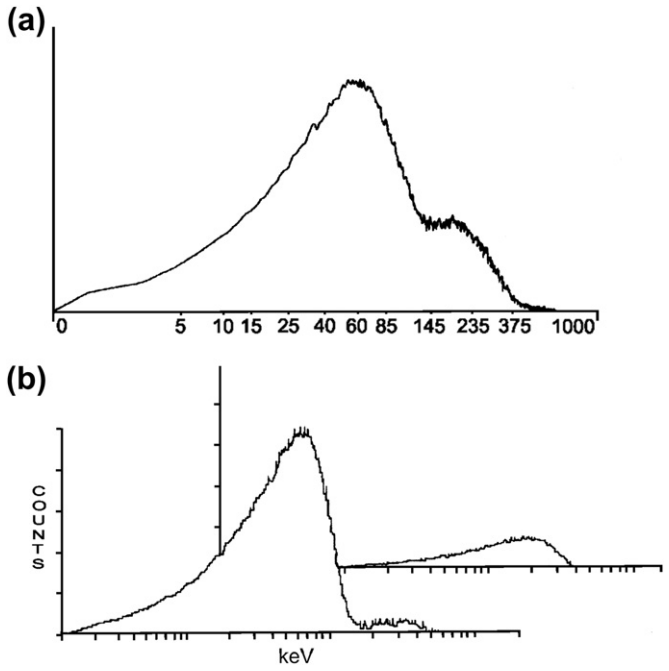

FIGURE 7.49 Unfolded spectrum of ^{90}Sr and ^{89}Sr (b) from mixture spectrum (a) by full-spectrum (FS-DPM) method with a PerkinElmer TriCarb 2770 TR liquid scintillation analyzer. The pulse-height spectra are plotted as counts versus pulse heights calibrated on a liquid scintillation keV scale. The unfolded spectrum of ^{89}Sr is illustrated in the rear of (b) and the unfolded ^{90}Sr spectrum in the front of (b). A very weak peak of ^{90}Y is seen together with the strong ^{90}Sr spectrum. The ^{90}Y peak was due to the ingrowth of ^{90}Y two hours after the separation of ^{90}Y from the sample using an SrSpec™ ion-exchange column. *(From Hong et al., 2001. Reprinted with permission from Elsevier © 2001)*

beginning of liquid scintillation analysis in the 1950s up to about 1990, the regionless analysis of more than three β-emitting radionuclides in the same sample was considered to be impracticable or not feasible. The broad pulse-height spectra produced by β-particles made the task of deconvoluting the pulse-height spectra of more than three radionuclides in the same sample appear daunting. However, with the advent of technological advances including applications of multichannel analyzers in liquid scintillation analysis and direct computer processing of LSA data, it has become possible to analyze simultaneously numerous α-, β-, and $\alpha-\beta$-emitting radionuclides in a mixture, including nuclides decaying by electron-capture emitting relatively low-energy Auger electrons and X-rays. This was evidenced by the early research reported by Takiue et al. (1990b, 1991b,c, 1992, 1995, 1999), Matsui and Takiue (1991), and Fujii et al. (1999, 2000) on the application of the most-probable-value theory to simultaneous multiple-radionuclide (as many as seven) analysis and the work of Grau Carles et al. (1993c), Grau Malonda et al. (1994), and Grau Carles (1996) on the use of spectral deconvolution and interpolation methods to multiple radionuclide (as many as six) activity analysis. These techniques can be applied also to mixtures of α- and β-emitters in one multichannel analyzer by spectral unfolding without α/β discrimination as demonstrated by Grau Carles et al. (1996). Subsequent research advances in liquid scintillation spectral deconvolution for multiple radionuclide analysis were reported by Heilgeist (2000), Kashirin et al. (2000), Verrezen and Hurtgen (2000), Malinovsky et al. (2002a,b), Nebelung (2003), Nebelung and Baraniak (2007), Nebelung et al. (2001, 2009), Ermakov et al. (2006),

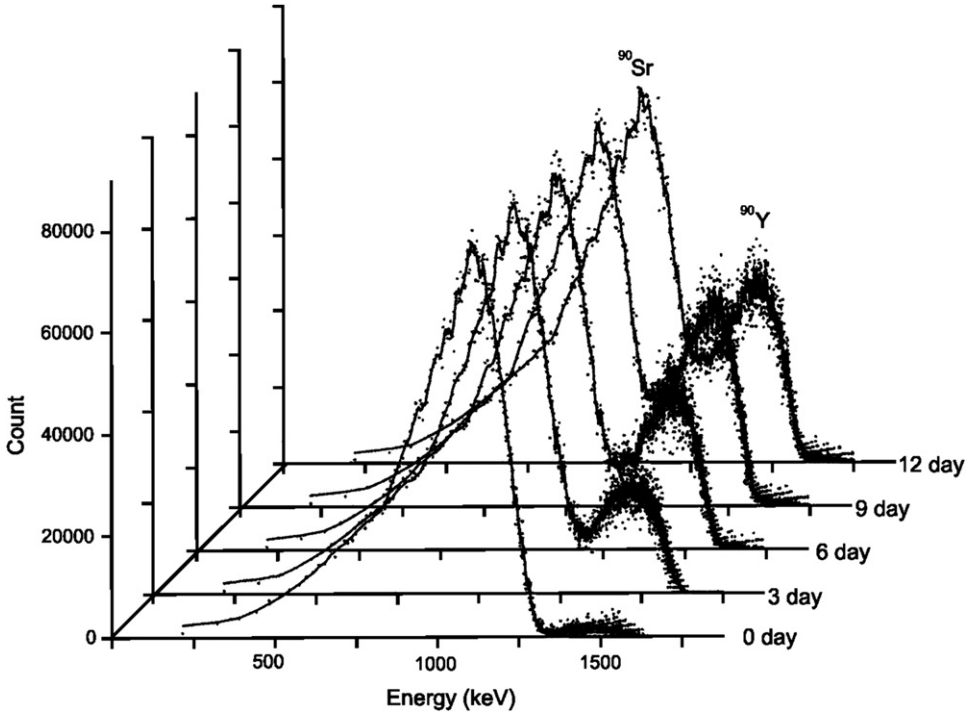

FIGURE 7.50 Spectra of ^{90}Sr and ^{90}Y in FS-DPM counting mode with time after the separation of ^{90}Sr obtained with a PerkinElmer TriCarb 2770 liquid scintillation analyzer. *(From Lee et al., 2002b. Reprinted with permission from Elsevier © 2002)*

TABLE 7.7 DPM Recoveries for ^{33}P—^{32}P Dual Nuclide Combinations[a] by the FS-DPM Method

Sample[b]	Ratio[c]					% Recovery[d]	
^{33}P:^{32}P	^{33}P:^{32}P	SIS	tSIE	DPM (^{33}P)	DPM (^{32}P)	DPM (^{33}P)	DPM (^{32}P)
1.0 mL: 0.0 mL	1:0	130	472	72167	47	99.5	0.06
0.0 mL: 1.0 mL	0:1	1043	476	28	82686	0.04	98.2
0.5 mL: 0.5 mL	1:1	612	472	37184	41596	102.7	98.6
1.0 mL: 0.5 mL	2:1	441	445	72493	41615	100.2	98.7
0.5 mL: 1.0 mL	1:2	729	449	36400	83117	100.6	98.5
1.0 mL: 0.2 mL	5:1	292	458	74487	16912	102.9	100.2
0.2 mL: 1.0 mL	1:5	885	462	14521	82860	100.3	98.2
1.0 mL: 0.1 mL	10:1	234	465	72319	8584	99.9	101.8
0.1 mL: 1.0 mL	1:10	951	469	7777	82708	107.4	98.0

[a]*Activity of ^{33}P = 72373 DPM/mL, activity of ^{32}P = 84357 DPM/mL. Instrumentation: PerkinElmer TriCarb 2300TR liquid scintillation analyzer.*
[b]*Triplicate samples were counted for a duration of ten minutes or until a % 2 sigma standard deviation of 1.0% was reached.*
[c]*Ratios listed are only approximate. The exact ratios can be calculated from the isotope activities (DPM/mL) and sample sizes (mL) of each isotope.*
[d]*The standard deviation of the mean of all triplicate measurements ranged from 0.085% to 2.97%.*

(From L'Annunziata, 1997b, Printed with permission. © 1997 PerkinElmer, Inc.).

Altzitzoglou (2008), Remetti and Sessa (2011), and Dobrin et al. (2011).

It was traditionally believed that ^{14}C ($E_{max} = 156$ keV) and ^{35}S ($E_{max} = 167$ keV) in the same sample could be neither identified nor analyzed by liquid scintillation counting, because of the very close similarities of the β-particle endpoint energies (E_{max}) of these two radionuclides. However, work first reported by Grau Carles and Grau Malonda (1991) demonstrated the accurate analysis of these two radionuclides in a mixture using spectral dilatation—interpolation and least-squares fitting. Activity ratios of $^{14}C/^{35}S$ were analyzed with an accuracy within about 3%. Grau Carles with Rodríguez Barquero and Grau Malonda (1993a) reported further improvements to this methodology, and Malinovsky et al. (2002a) demonstrated the deconvolution of 1:8 ratios of ^{14}C:^{35}S.

Another advancement is the application of chemometrics including multivariate calibration (MVC) to the deconvolution of α-, β-, and α—β-emitting radionuclides (without the need for α/β discrimination) in the same sample including nuclides decaying by electron capture, as reported by Toribio et al. (1995, 1996, 1997, 1999), Mellado et al. (2005), and Khayatzadeh Mahani et al. (2008, 2009). These techniques were successfully applied to the analysis of α—β-emitting radionuclide mixtures using plastic scintillator microspheres in an LSC (Bagán et al., 2011a).

These advances in the development of techniques for the analysis of several radionuclides in the same sample will be discussed here. The reader is invited to refer to the literature cited for more details on the techniques involved.

1. Most-Probable-Value Theory

Takiue et al. (1990a,b) and Matsui and Takiue (1991) reported the application of the most-probable-value theory as a new technique applied to the simultaneous liquid scintillation analysis of four β-emitting radionuclides in the same sample. This technique was expanded to the simultaneous analysis of six β-emitting radionuclides by Takiue et al. (1991c, 1992) and even seven β- and β—γ-emitting radionuclides (Takiue et al., 1995).

The technique requires only a contemporary liquid scintillation analyzer equipped with a multichannel analyzer, sets of quenched standards for the radionuclides to be measured, and a personal computer for data processing. The approach to this technique, as it was first devised for the analysis of samples containing mixtures of ^{3}H, ^{14}C, ^{32}P and ^{45}Ca, calls for more counting regions than the number of nuclides to be measured. According to Takiue et al. (1990b) and Matsui and Takiue (1991) the method may be described using the four radionuclide composite sample consisting of ^{3}H, ^{14}C, ^{32}P, and ^{45}Ca, as an example. The count rates of a sample observed in each counting region are defined by the following equations:

$$\begin{aligned} n_1 &= Aa_1 + Bb_1 + Cc_1 + Dd_1 \\ &\vdots \\ n_i &= Aa_i + Bb_i + Cc_i + Dd_i \\ &\vdots \\ n_m &= Aa_m + Bb_m + Cc_m + Dd_m \end{aligned} \tag{7.56}$$

where $n_1, \cdots n_i, \cdots n_m$ are the count rates of a sample in different counting regions ($m >$ number of nuclides in the sample), A, B, C, and D are the activities of ^{3}H, ^{14}C, ^{32}P, and ^{45}Ca, respectively, and a_i, b_i, c_i, and d_i are the respective counting efficiencies in the i th counting region.

The counting efficiencies of a radionuclide in each counting region are determined by means of external standard quench-correction curves plotted using sets of quenched standards for each radionuclide. Sets of quenched standards are not

commercially available for many radionuclides. These can be prepared in the laboratory in advance by first determining the activities of separate pure β- and $\beta-\gamma$-emitting radionuclides using a direct DPM method, such as efficiency tracing DPM (ET-DPM) as described in Section V.F or a more precise radionuclide standardization according to the techniques described in Section IX. Even radionuclides procured commercially should be analyzed to confirm their exact activities by a direct DPM method. Once the DPM values of the separate radionuclide standards are known, sets of quenched standards can be prepared according to the procedure described in Section V.D.

From the series of equations listed in Eqn 7.56 and following the derivations of Takiue et al. (1990b) and Matsui and Takiue (1991), the most probable values of A, B, C, and D, that is, the activities of ^{3}H, ^{14}C, ^{32}P, and ^{45}Ca must be determined, and the following equation is derived to search a minimum value (S):

$$S = \sum_{i=1}^{m} w_i\{n_i - (Aa_i + Bb_i + Cc_i + Dd_i)\}^2 \tag{7.57}$$

where w_i is the arithmetic weight of the measurement in the ith counting region, which is calculated by $1/N_i$ where N_i is the total number of counts in the ith counting region.

The most probable value, that is, the activities of each radionuclide A, B, C, and D should satisfy the following condition:

$$\frac{\partial S}{\partial A} = \frac{\partial S}{\partial B} = \frac{\partial S}{\partial C} = \frac{\partial S}{\partial D} = 0. \tag{7.58}$$

The following normal equations are then derived:

$$A\sum w_i a_i^2 + B\sum w_i a_i b_i + C\sum w_i a_i c_i + D\sum w_i a_i d_i = \sum w_i a_i n_i, \tag{7.59}$$

$$A\sum w_i b_i a_i + B\sum w_i b_i^2 + C\sum w_i b_i c_i + D\sum w_i b_i d_i = \sum w_i b_i n_i, \tag{7.60}$$

$$A\sum w_i c_i a_i + B\sum w_i c_i b_i + C\sum w_i c_i^2 + D\sum w_i c_i d_i = \sum w_i c_i n_i, \tag{7.61}$$

$$A\sum w_i d_i a_i + B\sum w_i d_i b_i + C\sum w_i d_i c_i + D\sum w_i d_i^2 = \sum w_i d_i n_i. \tag{7.62}$$

These equations can be solved for radionuclide activities A, B, C, and D, *i.e.*, the disintegration rate (DPM) of ^{3}H, ^{14}C, ^{32}P, and ^{45}Ca, respectively, using the determinant calculated by a personal computer. For example, as given by Matsui and Takiue (1991), the determinant for the calculation of the ^{3}H activity from the above equations is the following:

$$H = \frac{1}{K}\begin{vmatrix} \sum w_i a_i n_i & \sum w_i a_i b_i & \sum w_i a_i c_i & \sum w_i a_i d_i \\ \sum w_i b_i n_i & \sum w_i b_i^2 & \sum w_i b_i c_i & \sum w_i b_i d_i \\ \sum w_i c_i n_i & \sum w_i c_i b_i & \sum w_i c_i^2 & \sum w_i c_i d_i \\ \sum w_i d_i n_i & \sum w_i d_i b_i & \sum w_i d_i c_i & \sum w_i d_i^2 \end{vmatrix} \tag{7.63}$$

where

$$K = \begin{vmatrix} \sum w_i a_i^2 & \sum w_i a_i b_i & \sum w_i a_i c_i & \sum w_i a_i d_i \\ \sum w_i b_i a_i & \sum w_i b_i^2 & \sum w_i b_i c_i & \sum w_i b_i d_i \\ \sum w_i c_i a_i & \sum w_i c_i b_i & \sum w_i c_i^2 & \sum w_i c_i d_i \\ \sum w_i d_i a_i & \sum w_i d_i b_i & \sum w_i d_i c_i & \sum w_i d_i^2 \end{vmatrix} \tag{7.64}$$

For this case, six counting regions were used in the multichannel pulse-height analyzer for the measurement of the four nuclides. The discriminator settings of counting regions 1, 2, 3, and 4 are set to receive significant pulses from ^{3}H, ^{14}C, ^{45}Ca, and ^{32}P, respectively, with overlapping pulse-height distributions. Channels 5 and 6 were set to receive pulses mostly from the medium-energy β-emitting radionuclides ^{14}C and ^{45}Ca, as the use of double channel settings for the medium-energy β-emitters produces more accurate data. The counts of the quenched standards collected in the various counting regions should exceed 10^4 to keep error at a minimum. The mean percent recovery was 2.4 % for eight samples containing different proportions of ^{3}H, ^{14}C, ^{45}Ca, and ^{32}P at different quench levels, which represent 32 radionuclide analyses (8 samples $\times$ 4 radionuclides). Matsui and Takiue (1991) modified the technique by using only three counting regions for the analysis of the four radionuclides in a mixture. This required counting the unknown sample at two quench levels determined by the quench-indicating parameter tSIE. The sample was counted twice, that is, before and after the addition of quenching agent. Mean recoveries by this modified approach for 28 radionuclide analyses (7 samples $\times$ 4 radionuclides) was 3.6 %.

The approach described above can be applied to the simultaneous liquid scintillation analysis of six different β-emitting radionuclides in a mixture as demonstrated by Takiue et al. (1991c, 1992). They demonstrated the activity analysis of ^{3}H–^{63}Ni–^{14}C–^{45}Ca–^{36}Cl–^{32}P by application of the most-probable-value theory. A PerkinElmer Tri-Carb Model 4000 was used, and the samples were counted in 12 counting regions as illustrated in Fig. 7.51. Thus, the measurement of an unknown sample requires 12 observation equations of the general type described in Eqn 7.56. The series of 12 equations are written according to the following:

$$n_i = Aa_i + Bb_i + Cc_i + Dd_i + Ee_i + Ff_i \quad (i = 1 - 12), \tag{7.65}$$

where n_i is the count rate of a sample in the i th counting region. A, B, C, D, E, and F are the activities of the six radionuclides, namely ^{3}H, ^{63}Ni, ^{14}C, ^{45}Ca, ^{36}Cl, and ^{32}P, and a_i, b_i, c_i, d_i, e_i, and f_i are the respective radionuclide counting efficiencies in the ith channel. Because six radionuclide activities must be determined simultaneously, a six-by-six matrix is derived and written similarly to the case of a four-by-four matrix (Eqn 7.63) written for the analysis of four radionuclides. The mean recovery for 60 analyses (*i.e.*, 10 samples $\times$ 6 radionuclides per sample) was 3.9 %.

The technique can be applied to the liquid scintillation analysis of low-level $\beta-\gamma$-emitting radionuclides together with β-emitters as demonstrated by Takiue et al. (1995). In this case, mixtures of the following seven radionuclides were determined by application of the most-probable-value theory: ^{51}Cr–^{3}H–^{125}I–^{14}C–^{45}Ca–^{22}Na–^{32}P. In this case, 14 counting

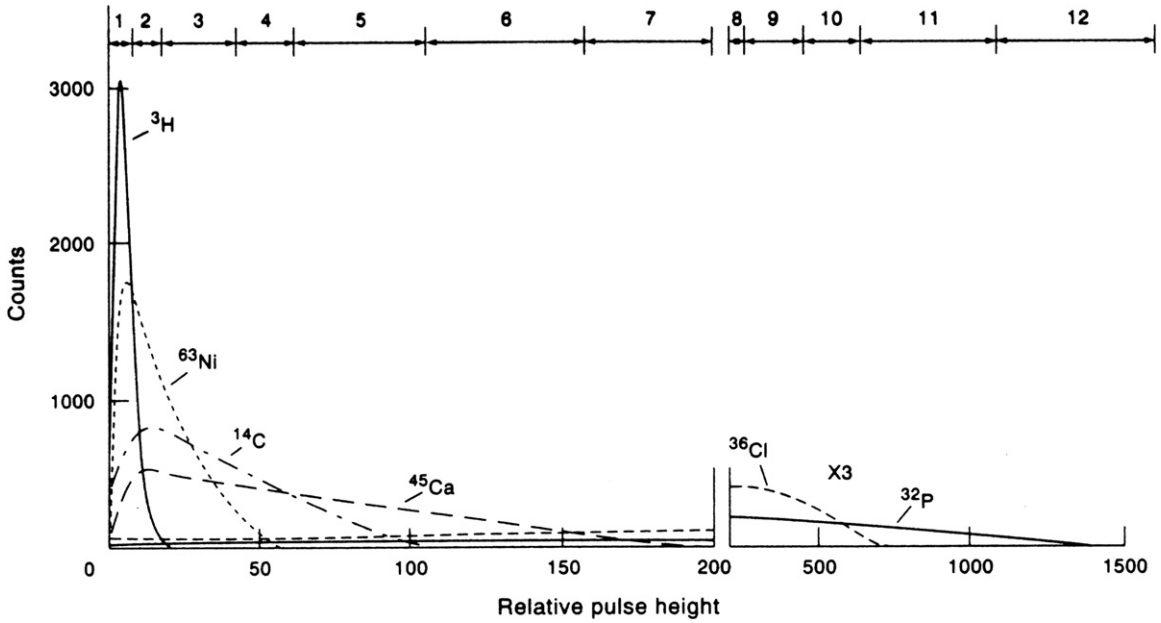

FIGURE 7.51 Liquid scintillation pulse-height distributions of six pure beta emitters and region settings for analytical measurements. *(From Takiue et al., 1992, reprinted with permission from Elsevier © 1992)*

regions were used. The lower limits of detection based on the analysis of 30 samples were calculated as 0.01 Bq/mL for higher-energy radionuclides and 0.05 Bq/mL for lower-energy radionuclides in the mixtures.

A further development of this technique is its application to the analysis of radionuclide combinations with similar pulse-height distributions, such as ^{3}H—^{125}I and ^{3}H—^{51}Cr, regardless of the different decay modes of these radionuclides, that is, β decay with ^{3}H and electron-capture (EC) decay with ^{125}I and ^{51}Cr. Takiue et al. (1991b) demonstrated the successful application of this procedure to the analysis of combinations ^{3}H—^{14}C—^{125}I and ^{3}H—^{14}C—^{51}Cr in a wide range of activity ratios and quench levels.

Subsequent work by Takiue et al. (1999) and Fujii et al. (1999, 2000) included the combined use of liquid scintillation and NaI(Tl) spectrometers to permit the simultaneous determination of the activities of many more nuclides in only one calculation process and, at the same time, enhance the accuracy of the radionuclide activity determinations. This method is referred to as a hybrid radioassay technique, because both liquid and solid scintillation spectrometers are used for a given sample. The NaI(Tl) solid scintillation detector provides additional sensitivity, as it would be particularly sensitive to X- and gamma-ray-photon emitters and high-energy beta emitters, which produce considerable Bremsstrahlung radiation. For example, Takiue et al. (1999) and Fujii et al. (2000) analyzed a mixture of seven radionuclides (*i.e.*, ^{3}H, ^{14}C, ^{22}Na, ^{32}P, ^{45}Ca, ^{51}Cr, and ^{125}I) using 12 counting regions defined, as illustrated in Figs. 7.52 and 7.53. The hybrid radioassay technique was applied by Fujii et al. (2000) to the analysis of the seven radionuclides in waste solutions with a detection limit of approximately 0.005 Bq/mL.

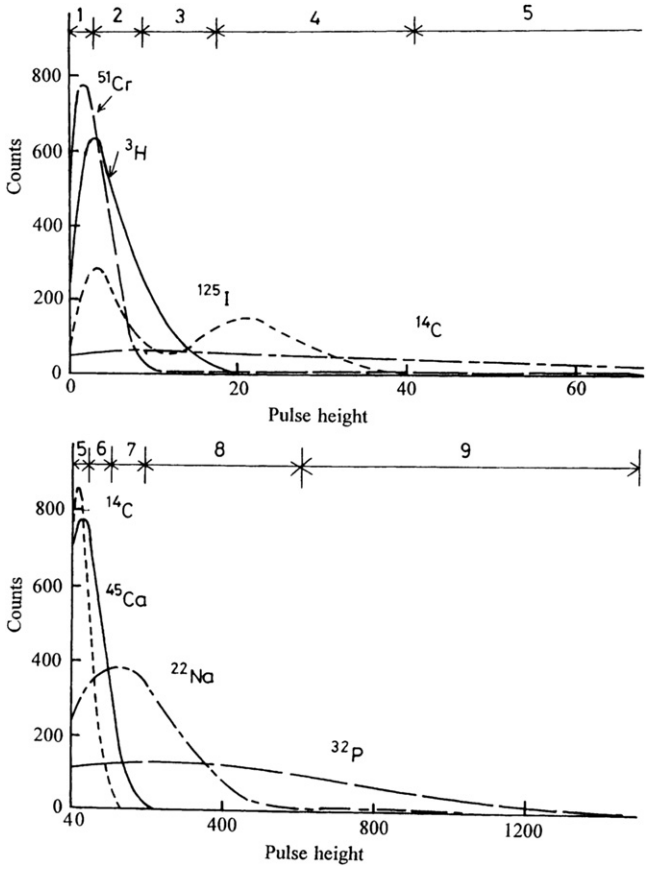

FIGURE 7.52 Liquid scintillation pulse-height distributions of seven nuclides and channel settings for analysis. *(From Takiue et al., 1999, reprinted with permission from Elsevier © 1999)*

The procedures outlined in this section are carried out easily with any liquid scintillation analyzer equipped with an MCA or, for the hybrid radioassay, data provided by conventional liquid and solid scintillation analyzers without any modification of the equipment and with a personal computer for data processing. If the counting protocols of the LSA allow for only three counting

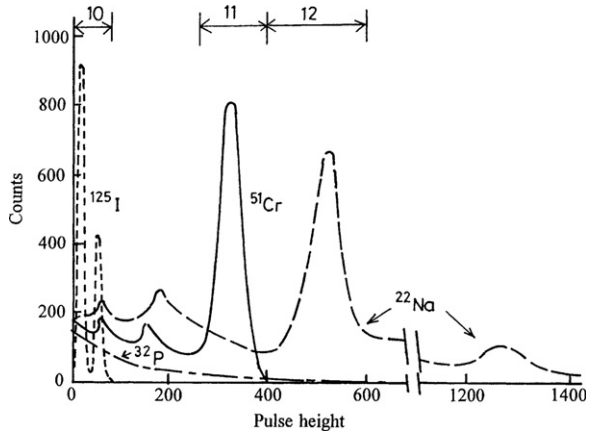

FIGURE 7.53 NaI(Tl) scintillation pulse-height distributions of ^{125}I, ^{51}Cr, ^{22}Na, and ^{32}P and channel settings for analysis. *(From Takiue et al., 1999, reprinted with permission from Elsevier © 1999)*

regions with upper- and lower-level discriminator settings, more counting regions can be established by using additional counting protocols. However, this calls for counting the samples in more than one protocol. The liquid scintillation analyzer is classified as a radionuclide spectrometer, because numerous X-ray, β- and $\beta-\gamma$-emitting radionuclides can be identified and analyzed simultaneously. Beta spectrometry applications of the liquid scintillation analyzer currently play a role of increased importance in the analysis of radionuclides.

2. Spectral Fitting, Unfolding, and Interpolation

Over the period of 1991−1996, a new technique was reported and developed by researchers at CIEMAT, Madrid, which is a powerful spectral unfolding method for the simultaneous activity analysis of numerous β-emitting radionuclides, including β-emitting nuclides of very similar energy maxima (*e.g.*, ^{14}C and ^{35}S) and even some α/β-emitting radionuclides in the same MCA without α/β discrimination. A description of these techniques is provided here. References are cited for additional information.

The procedure involved, as described by Grau Carles (1993), for two types of liquid scintillation analyzers, namely, the LSA that analyzes pulse-height spectra on a logarithmic scale and the LSA that uses a linear pulse-height scale. As explained by Grau Carles (1993), the method has three key components: spectral fitting, spectrum unfolding, and spectral interpolation. These components to the analysis are described next.

a. Spectral Fitting

As noted by Grau Carles and Grau Malonda (1991), pulse-height spectra are generally defined in terms of discrete pulse heights or energy values; however, they are histograms. It is therefore necessary to have a continuous mathematical function defining the spectra. For pulse-height spectra on a logarithmic scale, the spectral function is obtained by fitting Fourier series to the experimental spectra according to the following function:

$$f_F(\omega) = \begin{cases} a + b\omega + \sum_{k=1}^{N} c_k \sin\dfrac{k\pi\omega}{M} & 0 \le \omega < \omega^* \\ 0 & \omega > \omega^* \end{cases} \quad (7.66)$$

where $\omega = 0$ and $\omega = \omega^* = M$ are the first and the last values of the spectrum and N is the number of harmonics. The coefficients a, b, and c_k are:

$$a = y_0$$

$$b = \frac{y_M - y_0}{M}$$

$$c_k = \frac{2}{M}\sum_{j=0}^{M} y'_j \sin\frac{\pi k\omega_j}{M} \quad (7.67)$$

where $y'_j = y_j - (a + b\omega_j)$

$$\omega_j = j = 1, 2, \ldots, M.$$

For the case of a liquid scintillation analyzer that uses a linear pulse-height scale the spectral function is obtained by fitting the Chebyshev series to the experimental spectra determined by the following:

$$f_c(\omega) = \begin{cases} \left[\sum_{k=1}^{N} c_k T_{k-1}(\omega)\right] - \dfrac{1}{2}c_1 & 0 \le \omega < \omega^* \\ 0 & \omega > \omega^* \end{cases} \quad (7.68)$$

where $\omega = 0$ and $\omega = \omega^* = M$ are the first and the last values of the spectrum, $T_k(\omega)$ are the Chebyshev functions defined in the interval $[0,\omega^*]$ and c_k are the coefficients given by

$$c_k = \frac{2}{N}\sum_{j=1}^{N} f(\lambda_j) T_{k-1}(\lambda_j) \quad (7.69)$$

where the values λ_j are the zeros of the function $T_k(\omega)$.

b. Spectrum Unfolding

According to descriptions by Grau Carles (1993) and Grau Carles et al. (1993b), the spectral deconvolution method is a simultaneous standardization technique, providing radionuclide activities, based on spectral shape analysis of the component nuclides in the mixture. The spectrum unfolding is based on minimizing the expression:

$$\min\left\{\sum (y_i(X+Y) - a y_i(X) - b y_i(Y))^2\right\} \quad (7.70)$$

For a dual-radionuclide mixture, where y_i is the number of counts in channel i for the nuclide in brackets, X and Y are the two radionuclides, and a and b are the parameters obtained from the least-squares fit. This minimum condition, as explained by Grau Carles (1993) and Grau Carles et al. (1994a), can be applied only when all spectra $y_i(X+Y)$, $y_i(X)$, and $y_i(Y)$ have the same quench value, that is, the same quench-indicating parameter. Therefore, it is necessary to obtain the spectra $y_i(X)$ and $y_i(Y)$, at the same quench value of the radionuclide mixture. This is achieved by the spectral interpolation described subsequently in the next part of the analysis procedure. The activities in DPM for the two nuclides X and Y are obtained from the following:

$$A(X) = \frac{a y_i(X)}{t\varepsilon(X)} \quad (7.71)$$

$$\text{and } A(Y) = \frac{b y_i(Y)}{t\varepsilon(Y)} \quad (7.72)$$

where t is the counting time in minutes and $\varepsilon(X)$ and $\varepsilon(Y)$ are the counting efficiencies of radionuclide X and Y, respectively.

When a mixture of more than two radionuclides is analyzed, Eqn 7.70 is written as

$$\min\left\{\sum_i\left(y_i\left(\sum_j X_j\right)-\sum_j a_j y_i(X_j)\right)^2\right\} \tag{7.73}$$

where X_j are the component nuclides, a_j the coefficients that make the condition minimum, and y_i the number of counts in channel i.

c. Spectral Interpolation

Spectra at different quench levels have different endpoints or maxima. Therefore, as noted earlier, all spectra are interpolated to the same endpoint and maxima to validate the application of Eqns 7.70 or 7.73 for spectral unfolding of dual or multiple (three or more) radionuclides, respectively. Interpolation of spectra, as explained by Grau Carles et al. (1993c), is carried out in the following steps: (1) a mathematical transformation is found that makes all spectra pass through common maxima, inflection, and endpoints; (2) the transformed spectra are then interpolated channel by channel; and (3) the required spectrum is found by inverse transformation.

As explained by Grau Carles (1993), the spectral function, such as the Chebyshev fitting described previously by Eqn 7.68, is a mathematical manipulation of the spectra that smoothes the spectra and eliminates all superfluous statistical fluctuations. If $f_i(\omega)$ $(i=1,\ 2,\ 3)$ are the spectral functions, these may be divided into two regions, such as

$$f_i(\omega) = \begin{cases} g_i(\omega) & 0 \le \omega \prec \omega_{i\alpha} \\ h_i(\omega) & \omega_{i\alpha} \le \omega \le \omega_{i\beta} \end{cases} \tag{7.74}$$

where $\omega_{i\alpha}$ is the position of the maximum and $\omega_{i\beta}$ is the endpoint for spectrum i. As explained by Grau Carles (1993), the following mathematical transformation:

$$\omega' = a\omega \tag{7.75}$$

$$a = \frac{\omega_{1\alpha}}{\omega_{i\alpha}} \tag{7.76}$$

allows the transformation of all $g_i(\omega)$ functions, making them pass through the maximum of the spectral function $f_1(\omega)$. In the same way, the transformation

$$\omega' = b\omega + c \tag{7.77}$$

$$\text{where}\quad b = \frac{\omega_{1\alpha}-\omega_{1\beta}}{\omega_{i\alpha}-\omega_{i\beta}} \tag{7.78}$$

$$c = \frac{\omega_{i\alpha}\omega_{1\beta}-\omega_{1\alpha}\omega_{i\beta}}{\omega_{i\alpha}-\omega_{i\beta}} \tag{7.79}$$

takes the maximum and the endpoint of the function $f_1(\omega)$ as common points for each function $h_i(\omega)$.

When the spectral functions are transformed, a channel-by-channel interpolation provides a spectrum y_i^*. As explained by Grau Carles (1993), the following step determines the inverse equation, which transforms the spectrum y_i^* into the spectrum y_i:

Let $f_p^*(\omega)$ be the spectral function for y_i^* distribution and divide the function into the two regions:

$$f_p^*(\omega) = \begin{cases} g_p^*(\omega) & 0 \le \omega \prec \omega_{1\alpha} \\ h_p^*(\omega) & \omega_{1\alpha} \le \omega \le \omega_{i\beta} \end{cases} \tag{7.80}$$

The positions of the maximum $\omega_{p\alpha}$ and the endpoint $\omega_{p\beta}$ of the spectrum y_i for Q_p (quench value or quench-indicating parameter) can be found by interpolation in quench-correction curves of channel number versus quench-indicating parameter, such as one illustrated for ^{14}C in Fig. 7.54. An example of interpolated spectra of ^{14}C and ^{35}S with overlapping spectral maxima, inflection points, and endpoints, is illustrated in Fig. 7.55.

Then the inverse transformation

$$\omega' = a'\omega \tag{7.81}$$

$$\text{where}\quad a' = \frac{\omega_{p\alpha}}{\omega_{1\alpha}} \tag{7.82}$$

transforms $g_p^*(\omega)$ into $g_p(\omega)$, and

$$\omega' = b'(\omega) + c' \tag{7.83}$$

$$\text{where}\quad b' = \frac{\omega_{p\alpha}-\omega_{p\beta}}{\omega_{1\alpha}-\omega_{1\beta}} \tag{7.84}$$

$$c' = \frac{\omega_{1\alpha}\omega_{p\beta}-\omega_{p\alpha}\omega_{1\beta}}{\omega_{1\alpha}-\omega_{1\beta}} \tag{7.85}$$

transforms $h_p^*(\omega)$ into $h_p(\omega)$. The functions $g_p(\omega)$ and $h_p(\omega)$ define the spectral function $f_p(\omega)$, the spectrum y_i for the particular quench level Q_p.

The power of this method can be evidenced in the spectral deconvolution of ^{14}C ($E_{max}=156$ keV) and ^{35}S ($E_{max}=167$ keV), which have very close β-particle energy maxima with a ratio of the energy maxima of only 1.07. The spectral unfolding of a 2.2:1 mixture of ^{14}C and ^{35}S is illustrated in Fig. 7.56. The difference spectrum illustrated is a result of subtracting the actual ^{14}C–^{35}S pulse height spectrum from the fitted Fourier spectral function $f_F(\omega)$. As explained by Grau Carles (1993), the difference spectrum shows that the fluctuations are statistical, that is, Fourier spectral function fits the empirical data well. For the deconvoluted ^{14}C–^{35}S sample

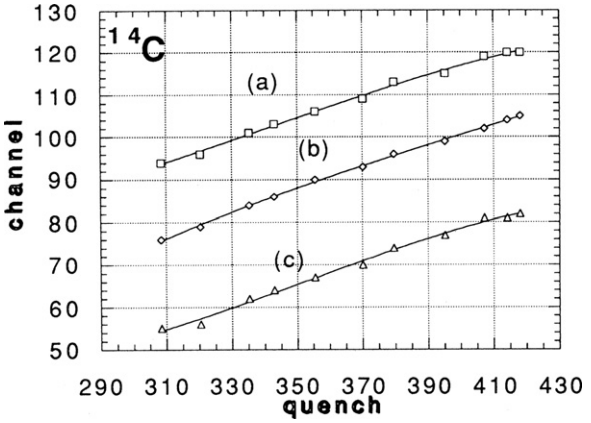

FIGURE 7.54 Fitted curves of ^{14}C local parameters versus quench: (a) endpoints of the spectra, (b) inflection points, and (c) position of the spectral maxima. The quench-indicating parameter is SQP(E). *(From Grau Carles et al., 1993a, reprinted with permission from Elsevier © 1993)*

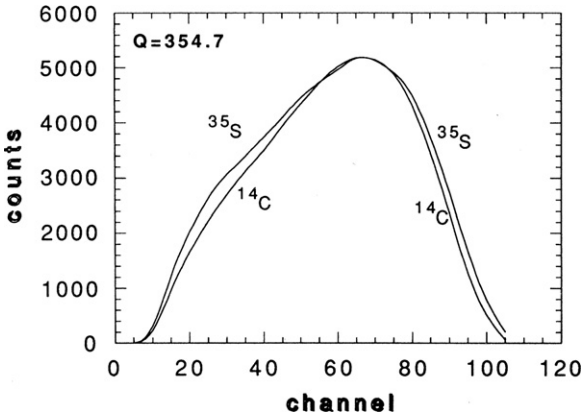

FIGURE 7.55 Computed ^{14}C and ^{35}S spectra for the quench value Q = 354.7, where Q is the SQP(E). *(From Grau Carles et al., 1993a, reprinted with permission from Elsevier © 1993)*

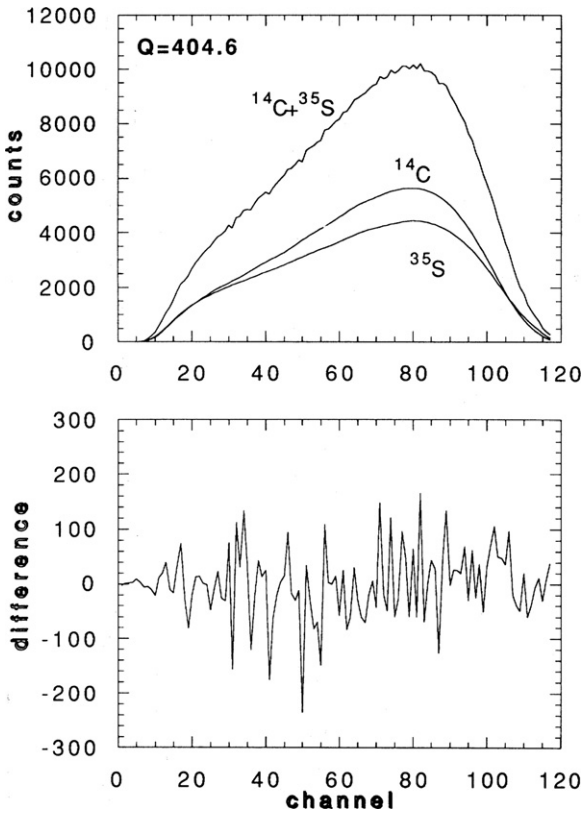

FIGURE 7.56 Spectrum unfolding of a sample containing $^{14}C/^{35}S$ with an activity ratio of 2.2:1 and the difference spectrum. *(From Grau Carles et al., 1993a, reprinted with permission from Elsevier © 1993)*

spectrum illustrated in Fig. 7.56, Grau Carles et al. (1993b) determined the ^{14}C and ^{35}S activities with a 1.3 and 3.6 % discrepancy, respectively, from the true DPM values. The $^{14}C-^{35}S$ dual mixture was considered traditionally inseparable spectrometrically by liquid scintillation analysis. Another radionuclide pair with very similar pulse-height spectral endpoints is $^{3}H-^{55}Fe$. Grau Carles et al. (1993c) again demonstrated the potential of this spectrum unfolding method with this nuclide pair. The power of the method is also demonstrated in the analysis of the traditional $^{14}C-^{3}H$ radionuclide mixtures, as low discrepancies from the true activity values are reported by Grau Carles et al. (1991) at various levels of quench and high-count-rate ratios of $^{14}C-^{3}H$ up to 100:1. Grau Carles et al. (1993f) demonstrated that this spectral deconvolution method will also provide good recoveries for multiple-radionuclide activity determinations in scintillation cocktails consisting of aqueous gel suspensions, such as aqueous $^{45}Ca-^{35}S$ in Insta-Gel. Mean recoveries expressed as percent discrepancy between computed and actual radionuclide DPM values for a wide range of $^{45}Ca-^{35}S$ activity ratios from 10.3:1 to 1:8.1 were 2.3 and 3.1% for ^{45}Ca and ^{35}S, respectively.

In addition to dual-radionuclide mixtures, this spectral unfolding method is applicable to the activity analysis of numerous β-emitting radionuclides. When numerous radionuclides are in the mixture, the previously described Eqn 7.73 is the general expression upon which spectrum unfolding is based. The spectral unfolding and activity analysis of up to six different β-emitting radionuclides in the same mixture are reported by Grau Carles et al. (1993d,e), Grau Malonda et al. (1994), and Grau Carles (1996). Among the radionuclides analyzed by this technique are mixtures of ^{89}Sr, ^{90}Sr, and ^{90}Y even before secular equilibrium was reached between the ^{90}Sr and ^{90}Y. The percent recoveries, that is, percent discrepancy or uncertainty, of the analyzed activities are amazingly low in many circumstances. An example is given in Fig. 7.57, which illustrates the spectral unfolding of a $^{3}H-^{14}C-^{125}I-^{131}I-^{32}P$ mixture and the computer output with activity analysis and percent uncertainties of the activity determinations for each radionuclide.

The spectrum unfolding technique has been tested by Grau Carles et al. (1996) with a mixture of α- and β-emitting radionuclides consisting of $^{234}Th + ^{234m}Pa + ^{230}Th$. The activities of the α- and β-emitting radionuclides could be determined by the spectrum unfolding method without pulse shape analysis (PSA) for α/β separation. Percent discrepancies for activity determinations of the radionuclides in the mixture by spectrum unfolding were much lower than discrepancies obtained by the traditional PSA method.

The computer program MLOG is described by Grau Carles (1996) for the spectrum unfolding methods previously described. The MLOG program was applied by Grau Carles et al. (1998) to determine the separate activities of the parent–daughter nuclides, ^{125}Sb and ^{125m}Te and, thereby, determine the ^{125}Sb to ^{125m}Te beta branching ratio.

3. Spectral Fitting and Subtraction

Early work by Heilgeist (2000) applied a spectral-subtraction method to resolve mixed liquid scintillation spectra of ^{85}Sr, ^{89}Sr, and $^{90}Sr/^{90}Y$ with a PerkinElmer Quantulus 1220 liquid scintillation analyzer. Strontium-85 was included in these measurements, as it is commonly used as a tracer nuclide in the determination of chemical recoveries of strontium. The calibration of the liquid scintillation spectrometer and the evaluation of the sample spectrum required the measurement of the pulse-height spectra from reference standards of the separate nuclides ^{85}Sr, ^{89}Sr, and $^{90}Sr/^{90}Y$, and isolated ^{90}Y. The reference standards are prepared at the same quench level as the experimental samples.

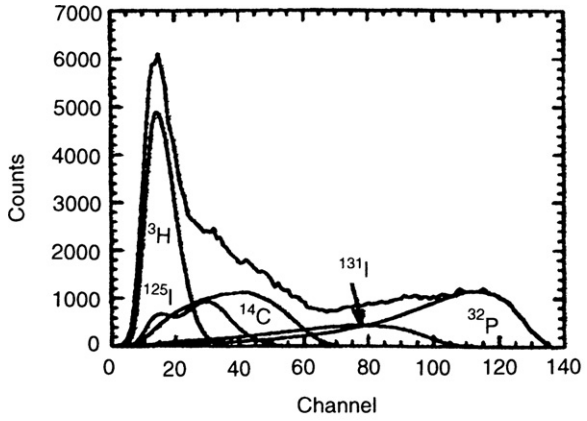

Local Quench Parameters and Efficiency

Nuclide	Quench	Maximum	End	Efficiency
P32	280.8	112.0	136.8	0.9964
I131	280.8	76.6	113.4	0.9620
I125	280.8	29.1	54.1	0.6115
C14	280.8	40.5	71.9	0.8647
H3	280.8	13.7	35.5	0.2129

Nuclide	Counting rate (cpm)
P32	27291.9
I131	12298.1
I125	11669.4
C14	21525.8
H3	28965.3

Nuclide	Activity (dpm)	Uncertainty (%)
P32	27391.1	0.5
I131	12784.0	2.3
I125	19083.2	3.4
C14	24893.0	1.9
H3	136049.3	2.2

FIGURE 7.57 Separated components of a mixture of $^{3}H + ^{14}C + ^{125}I + ^{131}I + ^{32}P$ by spectrum unfolding and the underlying computer output of activity analysis. *(From Grau Carles, 1996, reprinted with permission from Elsevier © 1996)*

Pulse-height spectra from the separate reference standards permit a determination of the spectral endpoints corresponding to the beta-energy maxima of each radionuclide as illustrated in Fig. 7.58. Window discriminators (pulse-height discriminators) are defined, namely, E1, E2, and E3, which are set at the endpoints of the abundant low pulse-height events from ^{85}Sr, and the endpoints of the pulse events from ^{90}Sr and ^{89}Sr, respectively. The ^{90}Sr endpoint (E2) was set at channel 690, and the ^{89}Sr endpoint at channel 815. Pulse events originating from ^{90}Y extend beyond channel 815 (E3) to channel 950. The ^{85}Sr, which decays by electron capture produces a large peak of low pulse heights due to Auger, conversion-electron, and X-ray Compton electron interactions with scintillation cocktail. It also produces a very weak smear of events at higher pulse heights up to discriminator E2 due to gamma−photon Compton interactions.

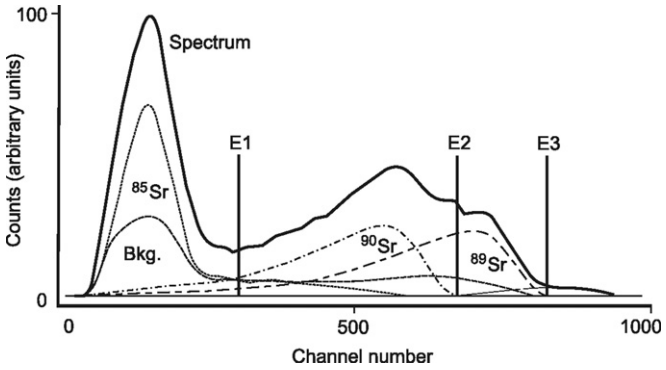

FIGURE 7.58 Spectra deconvolution: ^{85}Sr, ^{89}Sr, and ^{90}Sr in model waste. The solid line is the smoothed sample spectrum, Bkg, is the background spectrum. E1, E2 (channel 690), and E3 (channel 815) are the energy limits of the component spectra. Pulse events arising exclusively from ^{90}Y beta emissions (not identified in the figure) occur beyond E3 in channels 816−950. *(From Heilgeist, 2000. Reprinted with kind permission from Springer Science + Business Media © 2000 Akadémiai Kiadó Budapest)*

Background events are automatically subtracted by the liquid scintillation analyzer. A computer evaluation program adjusts the reference spectra to the positions of the measured sample composite spectrum and optimizes the positions of the window discriminators of ^{90}Sr/^{89}Sr at E2 and ^{89}Sr/^{90}Y at E3. The contribution of ^{90}Y to the composite spectrum is calculated first on the basis of its share in channels 816−950, which is a counting region free of any pulse events from other radionuclide emissions. Once the contribution of ^{90}Y is subtracted from the composite spectrum, the contribution from ^{89}Sr is determined from its share in the region defined by channels 691 to 815. Finally, the ^{90}Sr share is obtained after the deduction of the ^{90}Y and ^{89}Sr contributions. The contribution of ^{85}Sr due to its overlapping spectrum with ^{90}Sr was eliminated by spectral subtraction using a reference spectrum of ^{85}Sr. Quench effects are avoided by the constant composition of the scintillator solutions. Heilgeist (2000) reported recovery rates of 93.8% and a limit of detection of 0.1 Bq/kg.

Mietelski and Gaca (2002) separated numerically ^{90}Sr and ^{90}Y spectra using a fitting function with a PerkinElmer/Wallac Guardian liquid scintillation analyzer. The analysis could be performed after the separation of strontium on a column of Sr-Spec™ (Eichrom Industries) resin. There was no need to wait for secular equilibrium to be achieved. The overlapping spectra of ^{90}Sr and ^{90}Y are deconvoluted by the fitting function within 2% error, and the integrals of the ^{90}Sr and ^{90}Y parts of the combined spectrum would provide their count rates.

Nebelung et al. (2009) applied spectral peak functions with a PerkinElmer 1414 Liquid scintillation analyzer to deconvolute dual-, triple-, and multiple- (up to seven) radionuclide combinations for activity determinations. They used the peak fitting module of the graphic program Origin 5.0 (originally Microcal Inc., now OriginLab Corp.), which contains several internal peak fit functions (Nebelung and Baraniak, 2007 and Nebelung et al., 2009). Radionuclide standards of each nuclide were used to determine the spectral shape of each nuclide, which was required for the spectral fitting and analysis of multinuclide samples. The results of activity determinations of combinations of only two or three radionuclides by the curve fitting and

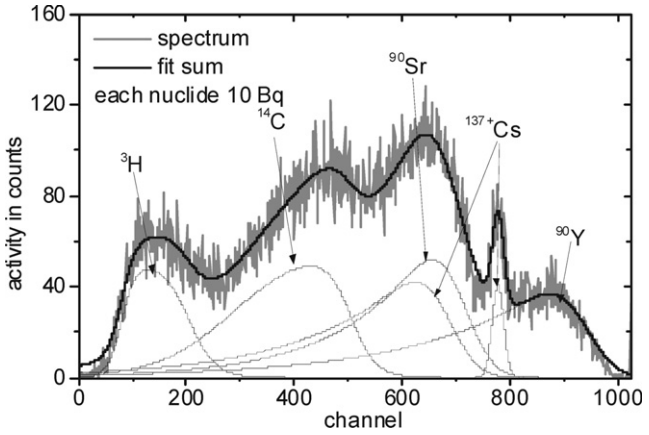

FIGURE 7.59 Liquid scintillation spectrum of a mixture of 5 radionuclides and the spectra deconvolution measured with a PerkinElmer 1414 liquid scintillation analyzer. *(From Nebelung et al., 2009. reprinted with permission from Radiocarbon, University of Arizona, © 2009 Arizona Board of Regents on behalf of the University of Arizona)*

deconvolution method yielded similar results obtained by the conventional two- and three-window counting method with a PerkinElmer TriCarb 3100 liquid scintillation analyzer. The uncertainty for activity measurements of 3 or more nuclides in one sample was $< 10\%$. An example of the deconvoluted spectra of a mixture of 10 Bq each of ^{3}H/^{14}C/$^{137+}$Cs/^{90}Sr/^{90}Y is illustrated in Fig. 7.59.

A spectral deconvolution method was applied by Altzitzoglou (2008) to the activity analysis of radionuclides from liquid scintillation spectra of two or more radionuclides. The spectral deconvolution method is based first on the mathematical expression for the count rate y in each channel i of the LSA multichannel analyzer for the measured spectrum of n radionuclides or

$$y_i = \sum_n c_n \cdot S_{n,i} \tag{7.86}$$

where c_n is the unknown count rate of the radionuclide n in the sample, and $S_{n,i}$ is the content of the corresponding channel i of a pure reference spectrum of radionuclide n. In other words, S_n is the normalized spectrum of radionuclide n, whereby the total number of counts in the spectrum for radionuclide n would equal unity. Thus, for a complete spectrum of m number of channels, there would be m number of equations similar to Eqn 7.86.

The spectrum deconvolution described by Altzitzoglou (2008) utilizes the shape of the sample spectrum on resolving its components by fitting a pure reference spectrum for each component to the measured composite spectrum. This was performed by a least-squares fitting, whereby the unknown count rates c_n for each radionuclide n were found by minimizing the sum of the squared differences between the measured (y_i) and predicted (y_i') rates for all channels of the spectra, or

$$\sum_i^m (y_i - y_i')^2 = \sum_i^m (y_i - \sum_n c_n \cdot S_{n,i})^2 \tag{7.87}$$

Altzitzoglou (2008) applied an iterative fitting using the Levenberg–Marquardt algorithm, which is a nonlinear least-squares fitting. The radionuclide activities (DPM) were calculated by c_n/ε_n where c_n is the count rate of nuclide n and ε_n is its detection efficiency. Eqns 7.86 and 7.87 are valid when the pure and composite spectra have the same quench levels. Altzitzoglou (2008) applied the method to the logarithmic spectra as determined with a PerkinElmer Quantulus 1220 liquid scintillation analyzer; but the method is also applicable to the linear pulse-height spectra as provided by the PerkinElmer TriCarb liquid scintillation counters. Figure 7.60 is an example of a typical measured liquid scintillation composite spectrum of ^{90}Sr (^{90}Y) at secular equilibrium and the component spectra as calculated by the deconvolution method. The deconvolution method was demonstrated to yield satisfactory results with low-activity samples as tested with the measurement of ^{90}Sr (^{90}Y) in milk and soil samples. The advantages over traditional methods of multiple radionuclide analysis are no counting windows need to be set, the method is rapid and straightforward and, in the case of ^{90}Sr/^{90}Y, it is not necessary to attain parent–daughter equilibrium for the activity analysis.

A method was developed by Remetti and Sessa (2011) that is capable of deconvoluting complex liquid scintillation pulse-height spectra without any preliminary knowledge of the peak shapes of the component radionuclides. They used a PerkinElmer Quantulus 1220 liquid scintillation analyzer with spectral deconvolution by Fourier series fitting with MATLAB software (The MathWorks Inc., version R2009B) according to Eqns. 7.65 and 7.66 described earlier. The calculation algorithm was structured according to the following path:

i. Identification of the portion of the pulse-height spectrum that is due to the radionuclides of highest E_{max}, and the selection of a group of channels for interpolation.

The radionuclide that possesses the highest energy emission will yield a pulse-height spectrum where a limited portion of the upper (highest pulse heights) part of the spectrum will be free of any overlap of pulse events from lower-energy-emitting nuclides. Once the channels are identified, that contain pulse events (counts) attributable only to that radionuclide, the algorithm can proceed with the next step, that of the interpolation of its contribution to the entire complex spectrum.

ii. Interpolation of the high-energy radionuclide contribution with the model "Cubic Spline."

The model "Cubic Spline," as described by Remetti and Sessa (2011), is a nonparametric interpolation model available among the functions of MATLAB. The interpolation of the high-energy radionuclide contribution to the spectrum is obtained by imposing the condition of passage of the function through the group of points of the above Step i and through zero in the first channel.

iii. Subtraction of the contribution by the high-energy radionuclide to the entire spectrum, and repetition of the procedure (steps i and ii) for the remaining radionuclide contributions to the spectrum.

Once the shape of the spectrum, attributed to the radionuclide of highest E_{max}, is obtained, it can be subtracted from the entire composite spectrum. This leaves behind a spectrum of the

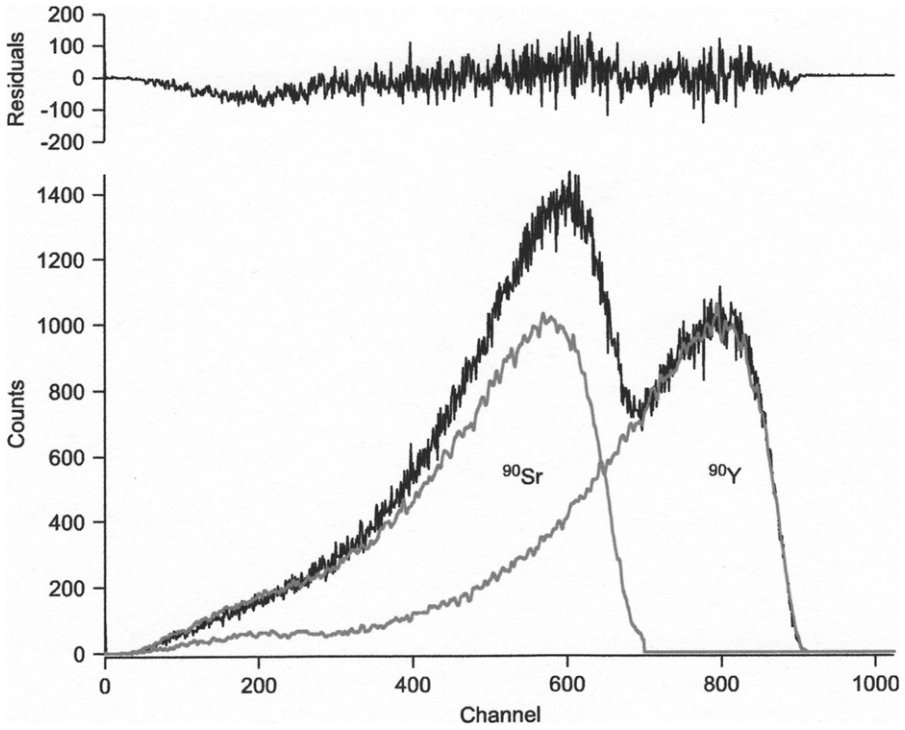

FIGURE 7.60 Typical composite spectrum of ^{90}Sr (^{90}Y) at equilibrium as measured with a liquid scintillation analyzer, and the component spectra as calculated by the deconvolution method. The upper spectrum is the plot of the residuals of the fit. *(From Altzitzoglou, 2008, reprinted with permission from Elsevier © 2008)*

remaining radionuclides of lower E_{max}. Then steps i and ii are repeated by subtracting singularly, *i.e.*, the pulse-height spectrum of one nuclide at a time, until all of the contributing pulse-height spectra of each radionuclide are unfolded from the composite spectrum.

iv. Activity calculation.

A simple integration of the unfolded pulse-height spectra of each radionuclide provides the counts attributable to each radionuclide. The count rate (CPM), of course, will depend on the time needed to achieve the composite pulse-height spectrum. The disintegration rate (DPM) of each radionuclide can easily be calculated with a measurement of the detection efficiency, which would be characteristic of the radionuclide emissions, quench level, and counter.

Figure 7.61 provides an example of the spectral deconvolution obtained by this technique. The discrepancies of the deconvoluted activities of the ^{90}Sr, ^{90}Y, and ^{241}Am from the expected values were reported to be within 5%.

4. Modeling from Spectral Library

A different approach to multiple radionuclide analysis involves the establishment of a library of radionuclide spectra constituting different mixtures of radionuclides at varying levels of quench. The spectral library, which is stored as computer data, must be prepared from radionuclide standards in various mixtures and activity ratios including also spectral distortions caused by the wall effect. Kashirin et al. (2000) describe this approach, which they have tested for complex mixtures of up to eight radionuclides including ^{3}H, ^{14}C, ^{60}Co, ^{63}Ni, ^{90}Sr + ^{90}Y, ^{125}I, ^{137}Cs, and ^{241}Am. They applied algorithms described in patents by Belanov et al. (1997, 1998) to minimize deviations between real and model spectra regardless of linear or logarithmic scales used for the presentation of spectra.

Continued research along these lines reported by Malinovsky et al. (2002a,b), Kashirin et al. (2003), and Ermakov et al. (2006) has culminated in the establishment of a software package RadSpecDec for the deconvolution of complex pulse-height spectra consisting of combinations of numerous (six or more) alpha- and beta-emitting radionuclides. As described by Ermakov et al. (2006), the deconvolution algorithm is based on the modeling of spectra, which are transformed when convoluted by the superposition of individual reference spectra taken from a previously created radionuclide library of spectra. The spectra library consists of at least 10 spectra at different quench levels. The model spectrum is calculated as a sum of the individual radionuclide spectra with weight coefficients (c_j) that are adjusted during the modeling procedure with the objective that the model spectrum coincides with the sample composite spectrum to a maximum degree.

The model method was proposed by Malinovsky et al. (2002a,b) to be based on the modeling of spectra that are transformed when convoluted into a group by the superpositioning of individual radionuclide spectra taken from the spectral library. As described by Ermakov et al. (2006), the model spectrum is created from a linear combination of normalized spectra of various radionuclides according to the equation

$$M_i = \sum_{i=1}^{j} c_j M_{i,j}(T) \tag{7.88}$$

where M_i is the model spectrum, $M_{i,j}(T)$ is the library spectra of each radionuclide as a function of the quench parameter T, and c_j is the proportion or weight coefficient of each radionuclide

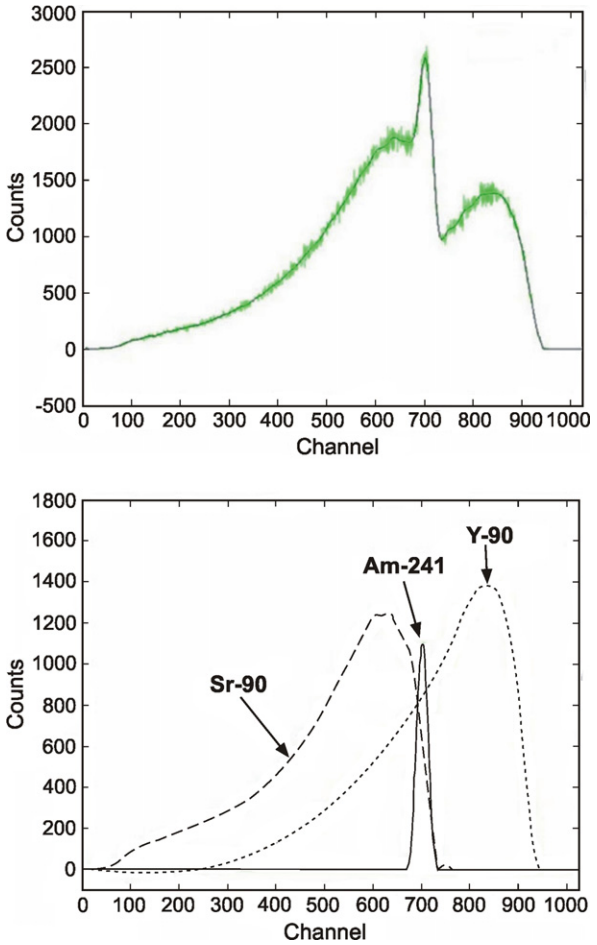

FIGURE 7.61 (Upper graph) Fourier series fitting of a composite spectrum ($^{90}Sr + {}^{90}Y + {}^{241}Am$). The continuous line represents the fitted function. (Lower graph) Total unfolding of the shapes of ^{90}Sr, ^{90}Y, and ^{241}Am. For the color version of the figure, the reader is referred to the online version of the book. *(From Remetti and Sessa, 2011. Reprinted with kind permission from Springer Science + Business Media © 2011 Akadémiai Kiadó, Budapest)*

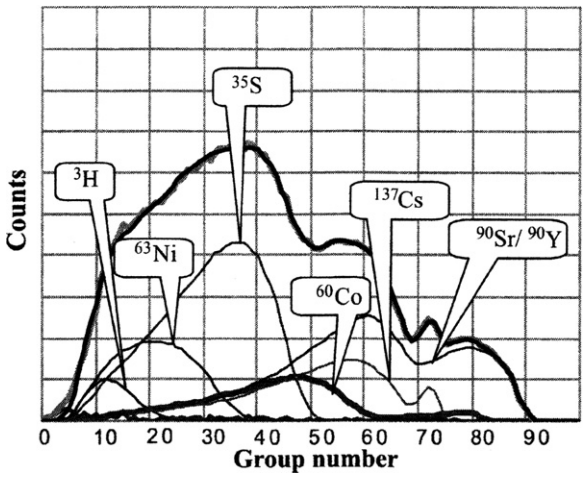

FIGURE 7.62 The spectrum decoding of a mixture (^{3}H, ^{63}Ni, ^{35}S, ^{60}Co, $^{90}Sr/^{90}Y$, and ^{137}Cs) measured with a PerkinElmer Quantulus liquid scintillation analyzer. *(From Malinovsky et al., 2002, reprinted with permission from Radiocarbon, University of Arizona, © 2002 Arizona Board of Regents on behalf of the University of Arizona)*

specie. The weight coefficients, c_j, of each radionuclide are adjusted to make the model spectrum coincide with the sample spectrum to a maximum degree. Ermakov et al. (2006) describes the solution to the model as generated by a recursive minimization of a function representing the difference between a model spectrum and the real sample composite spectrum.

The modeling is carried out with groups of channels rather than the individual channels. For liquid scintillation spectrometers equipped with a logarithmic analog-to-digital converter (*e.g.*, PerkinElmer Quantulus or Hidex Triathler), a combination of 10 channels forms a group. Thus, the composite sample spectrum and the deconvoluted spectra are depicted as plots of counts versus group number or relative activity versus group number, rather than the conventional counts versus channel number, as illustrated in Fig. 7.62. Liquid scintillation spectrometers equipped with a linear analog-to-digital converter (*e.g.*, PerkinElmer TriCarb) have channel numbers grouped by means of an arithmetic progression. Both logarithmic and linear pulse-height spectra are resolved by the modeling technique, whereby the spectral channels become "channel groups". The activity in disintegrations, A_j of the jth radionuclide in the composite spectrum will be a function of the total counts, N, the background-subtracted or net counts, $N - N_{bkg}$, the weight coefficient, c_j, of the jth radionuclide, and the detection efficiency ε_j of the jth radionuclide at quench level T or

$$A_j = \frac{(N - N_{bkg})c_j}{T\varepsilon_j} = \frac{N_j}{T\varepsilon_j} \tag{7.89}$$

where $T\varepsilon_j$ is the detection efficiency of the jth radionuclide at quench level T. Malinovsky et al. (2002a) and Ermakov et al. (2006) report tests on this deconvolution method with a wide variety of sample types and radionuclide combinations including low-level mixtures with good recoveries of the deconvoluted activities compared to the known radionuclide activities.

5. Spectral Unfolding by Region Count Ratios

Often the LSA of radionuclide mixtures is complicated by the need to analyze low-energy beta-emitters, such as ^{3}H, contaminated by much greater activities of high-energy beta impurities. Verrezen and Hurtgen (1996, 2000) describe a multiple-window spectrum unfolding technique for the analysis of low-energy ^{3}H in the presence of up to 10-fold higher activities of high-energy beta emitters over a wide range of quench (*e.g.*, tSIE $\geq$ 100). The method is based on the fact that the ratio of the net count rates in two fixed counting regions for a single radionuclide is a constant at a given quench level. Consequently, any spectral shape (*e.g.*, impurity spectrum) can be reconstructed using the established ratio and a pure reference spectrum. On the basis of this hypothesis, Verrezen and Hurtgen (2000) calculate the spectral contribution of the impurity in the low-energy part of the liquid scintillation pulse-height spectrum and correct for the impurity interference on the measured low-energy sample spectrum. The method was demonstrated successfully over a wide range of quenching and activity ratios with mixtures of ^{99}Tc and ^{63}Ni contaminated with ^{60}Co and ^{137}Cs, respectively (Verrezen and Hurtgen, 1996), mixtures of $^{63}Ni/^{3}H$, $^{14}C/^{3}H$, $^{99}Tc/^{3}H$, and $^{60}Co/^{99}Tc$ (Verrezen and Hurtgen, 2000), and mixtures of $^{3}H/^{90}Sr/^{90}Y$ (Dobrin et al., 2011).

The spectral deconvolution method described here is particularly useful for the analysis of a low-energy beta-emitting nuclide that is contaminated with a higher-energy beta emitter. Verrezen and Hurtgen (2000) and Dobrin et al. (2011) demonstrate that the method is particularly useful in the analysis of nuclear waste streams of pressurized water reactors where activity ratios of 10^3–10^6 are encountered between impurities and the nuclide of interest. The overlapping character of liquid scintillation pulse-height spectra can mask the presence of contaminating radionuclides low in activity relative to the nuclide of interest. The method is based on the hypothesis that the activity ratios of a beta-emitting radionuclide in two counting regions of the liquid scintillation pulse-height spectrum is a constant at a constant level of quench regardless of the total activity of the radionuclide. This was demonstrated to be true by Verrezen and Hurtgen (2000) and Dobrin et al. (2011) by counting various activities of a beta-emitting radionuclide in two counting regions at identical quench levels. At a given quench level, the ratio of count rates in two counting regions due to the beta emissions of a radionuclide is a constant.

As described by Verrezen and Hurtgen (2000), the method is based on the following deconvolution algorithm:

$$\mathrm{NOI(net,\ low)} = \mathrm{SMP(net,\ low)} - \sum_{k=1}^{n} K'_k(Q,\ \mathrm{high}) \cdot \mathrm{REF}_k(\mathrm{net,\ low}) \tag{7.90}$$

where

$$K'_k(Q,\ \mathrm{high}) = \frac{\mathrm{SMP(net,\ high)}}{\mathrm{REF}_k(\mathrm{net,\ high})} \tag{7.91}$$

In the above equations, SMP(net, i) represents the net contribution calculated as the difference between the gross contribution SMP(gross, i) and the background contribution BGD(i) of a sample in a specified counting region of interest ROI(i) as obtained from the spectral data. NOI(net, i) and REF_k(net, i) are the net contributions of the nuclide of interest and that of a reference spectrum of an impurity k to the beta spectrum in the same region of interest (i). The variable n refers to the number of radionuclide impurities in the sample. The term *low* represents a region of interest (ROI) in the low-energy range of the spectrum, whereas the term *high* represents a ROI in the high-energy range, set behind or beyond the endpoint of the spectrum on the nuclide of interest in such a way that NOI(net, high) = 0, or in other terms SMP(net, high) = IMP(net, high). This is illustrated in Fig. 7.63 where the pulse-height spectrum of ^{3}H, the nuclide of interest (NOI), is found only in the ROI *low*, whereby NOI(net, high) = 0 and SMP(net, high) = IMP(net, high).

As described by Verrezen and Hurtgen (2000), Eqn 7.91 relies on the fact that the ratio of the net count rate in two fixed regions of the pulse-height spectrum for a single radionuclide is a constant for a given level of quenching and that any spectral shape (in this case the spectrum of the impurity, IMP) can be reconstructed using the established ratio and a pure reference spectrum if both are at the same level of quench, that is, if both possess the same quench-indicating parameter, or

$$\frac{\mathrm{IMP(net,\ low)}}{\mathrm{IMP(net,\ high)}} = \frac{\mathrm{REF(net,\ low)}}{\mathrm{REF(net,\ high)}} = K(Q) \tag{7.92}$$

Verrezen and Hurtgen (2000) and Dobrin et al. (2011) used the above equations to recalculate the spectral contribution of the impurity in the low-energy region of the spectrum (ROI, low), thereby correcting for the impurity in the measured sample spectrum. The technique is not confined to resolving the interference caused by only one radionuclide impurity. Samples containing n impurities require $n+2$ pulse-height spectra to solve Eqn 7.90, namely, the background spectrum, the sample spectrum, and n reference spectra (one for each radionuclide impurity). Thus, the analysis of the contaminated samples by this method requires the preparation of the following counting vials: a background vial, a sample vial, and one internal reference vial for each radionuclide known to be present in the sample. The final mixtures in the counting vials must possess

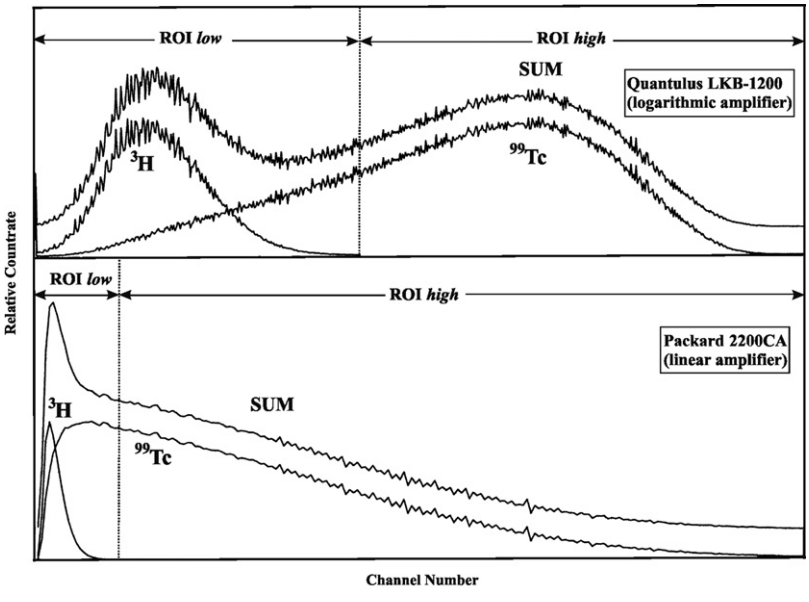

FIGURE 7.63 Effect of contamination of a ^{3}H sample with ^{99}Tc on the spectral shape as measured with a logarithmic amplifier (PerkinElmer/LKB Quantulus 1200, above) and a linear amplifier (PerkinElmer/Packard TriCarb 2200CA, below). Two regions of interest (ROI *low* and ROI *high*) are illustrated defined by a discriminator setting behind or beyond the endpoint of the nuclide of interest (^{3}H) pulse-height spectrum. *(From Verrezen and Hurtgen, 2000, reprinted with permission from Elsevier © 2000)*

identical chemistry to assure that they all are characterized by the same quench-indicating parameter. To assure this was achieved, Dobrin et al. (2011) analyzed the nuclide of interest (NOI) ^{3}H contaminated with the impurity (IMP) ^{90}Sr/^{90}Y by preparing the following counting vials with identical chemistry: (1) a background vial containing 10 mL of distilled water and 10 mL of Ultima Gold XR cocktail; (2) a sample vial containing 1 mL of sample (aqueous), 9 mL of distilled water, and 10 mL of Ultima Gold XR cocktail; and (3) reference vials, each containing 1 mL of sample, 1 mL of aqueous reference solution of the appropriate radionuclide present in the sample, 8 mL of distilled water, and 10 mL of Ultima Gold XR cocktail. For the analysis of ^{3}H contaminated with the impurity ^{90}Sr/^{90}Y Dobrin et al. (2011) corrected all spectra for the contribution due to background. They subsequently reconstructed the spectrum of the impurity (^{90}Sr/^{90}Y) in the lower-energy range using the spectral shape of the reference spectrum and the calculated ratio $K'_k(Q,\ \text{high})$of Eqn 7.91. Lastly, the net spectrum of the nuclide of interest, i.e., ^{3}H, in the lower energy range of the spectrum (ROI low) was restored by subtracting the net spectrum of the impurity from the net sample spectrum. If the reference vials were prepared with known activity concentrations of the radionuclides, the detection efficiencies can be obtained for each radionuclide, and the count rates converted to disintegration rates.

6. Multivariate Calibration

The application of multivariate calibration for the determination of ^{14}C activities was discussed in Section V.F.4. It has been applied by Toribio et al. (1995, 1996) in the liquid scintillation analysis of mixtures containing the three main α-emitting isotopes of plutonium, ^{238}Pu, ^{239}Pu, and ^{240}Pu. The multivariate methods used were principal component regression (PCR) and partial least-squares regression (PLSR). As explained by Toribio et al. (1995), these methods can estimate the concentration of radionuclide of interest without the need to consider the other radionuclides present in the system that affect the experimental signal, provided the isotopes are present in both the unknown samples and the calibration set. The advantage here is that the methods are suitable for the analysis of samples with unknown interferences, thereby avoiding the need of a separation step.

For the PCR and PLSR analysis Toribio et al. (1995) used a program written in FORTRAN 77 run on a personal computer with a DOS operating system described by Tauler et al. (1991), and the programs were validated by comparison with the PLS-Toolbox package for MATLAB written by Wise (1992). The α-emissions of ^{239}Pu and ^{240}Pu have overlapping energies, and the predicted error for the PCR or PLSR separation of these two nuclides was about 35%. These two nuclides are determined together as one component or analyte, $^{240+239}$Pu , which is similar to other established procedures using surface barrier detectors. Samples containing standards and unknowns of low-level activity (3.42−174 DPM) were counted for 5 hours and data analyzed by relating known plutonium activities to alpha disintegrations registered in energy channels of a PerkinElmer Tri-Carb CA/LL liquid scintillation analyzer. Relationships were sought between two matrices $\mathbf{R}(M,N)$ and $\mathbf{C}(M,K)$. Matrix $\mathbf{R}(M,N)$ contained the instrumental responses, number of counts at N measuring channels for M calibration samples, and the other matrix $\mathbf{C}(M,K)$ contained the activities of the K analytes in the M samples. The important step in the data treatment in PCR and PLSR models, emphasized by Toribio et al. (1995), is the number of factors chosen as noted previously in Section V.F.4. When the number is chosen correctly, the data compression step filters out noise and useless data without sacrificing significantly the desired information. One approach to the proper selection of factors is to start with a probable number of factors. The analysis is repeated using a different number of factors until the optimum number that fits the data is found. The optimum number of factors in this case was found to be four, all attributable to sample activities. No factor was attributed to background, as predictions did not improve when background was subtracted.

The values obtained for $^{240+239}$Pu and ^{238}Pu activities for samples containing varying amounts of these radionuclides in mixtures over the range of 2.43−174 DPM had errors of about 7% and 10% for the high- and low-activity samples, respectively. Background (blank) subtraction is not required. This approach to radionuclide analysis is still at its early stages of development; however, Toribio et al. (1995) conclude that the multivariate calibration technique provides a detection limit one order of magnitude higher than that obtained with a surface barrier detector. However, the detection limit would be expected to drop with the use of α/β-discrimination and active shielding in LSA. With α/β-discrimination in many liquid scintillation analyzers the β-emitting isotope ^{241}Pu could also be included in the mixture, and activity measurements of mixtures containing the α- and β-emitting isotopes of plutonium in the same sample, as ^{238}Pu + $^{239+240}$Pu + ^{241}Pu, would be possible.

Organic extracting agents are often used to improve the alpha spectral resolution in the liquid scintillation analysis of alpha emitters. However, subsequent to extraction, alpha peaks are reported to display a continuous shift along their axis with time for periods in excess of 200 hour. (Toribio et al. 1997). To overcome error due to the instability of alpha spectral peak positions, Toribio et al. (1997, 1999) report the application of moving curve fitting (MCF) to the multivariate calibration analysis of mixtures of the four alpha-emitting isotopes ^{242}Pu, $^{239+240}$Pu, and ^{238}Pu with $<$15% relative errors of predicted values and an activity quantification threshold of 15 DPM.

Mellado et al. (2005) applied multivariate calibration, which constitutes a set of chemometric techniques, to the activity analysis of various combinations, quench levels, and ratios of ^{90}Sr/^{90}Y, ^{99}Tc, ^{63}Ni, ^{137}Cs, and ^{55}Fe within 15% relative error within the range covered by the calibration matrix. Chemometrics including artificial neural network (ANN) and partial least squares (PLS) as complimentary tools are reported by Khayatzadeh Mahani et al., (2008, 2009) for the analysis of ^{226}Ra and uranium as well as thorium and uranium in aqueous samples. Relative errors of prediction for PLS and ANN in synthetic mixtures of ^{226}Ra and uranium were 18.0 and 24.8%, respectively.

Now that the application of plastic scintillator microspheres to LSC is making rapid development (see Section XVI), Bagán et al. (2011a) report the use of plastic scintillator microspheres

together with multivariate calibration (PLS) to detect and measure the activities of α- and β-emitting radionuclides in mixtures. They quantified mixtures of ^{241}Am, ^{137}Cs, and ^{90}Sr/^{90}Y without the need of pulse-height discrimination with errors under 10% in most cases. Measurement time is reduced, as the counting of background blanks is not necessary. The use of plastic scintillator microspheres also obviates the need for liquid scintillation cocktail and thus reduces the disposal costs that occur with mixed radioactive waste.

IX. RADIONUCLIDE STANDARDIZATION

Radionuclide standardization is included here as an altogether different specialty of liquid scintillation analysis, as it pertains to the purest form of measurement of the activity or disintegration rates (DPM) of radionuclides. It includes the methods used for the absolute activity of radionuclides as reference sources from which other radionuclide activities may be calibrated. The standardization of radionuclides is important in many fields, among which one of the most demanding has been radionuclide standardization for applications and research in therapeutic nuclear medicine (Coursey et al., 1991, 1994 and Zimmerman, 2006b). This section will include some of the most popular techniques applied to the standardization of radionuclides.

A. CIEMAT/NIST Efficiency Tracing

This method of radionuclide standardization, in its historical context, was first conceived by Augustín Grau Malonda in 1978 with the objective of developing a model/procedure applicable to any liquid scintillation analyzer, any scintillation cocktail, and any radionuclide (Grau Malonda, 1999). As the procedure could not be based solely on theoretical calculations of counting efficiency, Grau Malonda devised a model that combined theoretical calculations based on the radionuclide to be analyzed and experimental data provided by the liquid scintillation analyzer. Early descriptions of the method applied to the activity analysis of pure beta-particle emitting radionuclides are provided by Grau Malonda (1982a), Grau Malonda and García-Toraño (1982a,b), and Grau Malonda et al. (1985), and for radionuclides decaying by electron capture by Grau Malonda (1982b).

The name CIEMAT/NIST currently attributed to the method is the result of collaboration on the method that started in 1984 (Coursey et al., 1986 and Grau Malonda and Coursey, 1987) between the Centro de Investigaciones Energéticas Medioambientales y Tecnológicas (CIEMAT) in Madrid (the affiliation of Agustín Grau Malonda) and the National Institute of Standards and Technology (NIST), Gaithersburg, which at that time was called the National Bureau of Standards (the affiliation of Bert M. Coursey). Collaboration between the two institutions was intended to develop the method into one that could be used as a reference method for the standardization of radionuclides by any laboratory in the world with a conventional liquid scintillation analyzer. The principles of the method and many of the major references to this technique will be presented here. Comprehensive treatments on the procedures and calculations involved are available from books by Grau Malonda (1995, 1999). A paper by García-Toraño et al. (1991) also provides a good summary of the method. Excellent reviews on this liquid scintillation radionuclide standardization method as well as other related methods of standardization by liquid scintillation are provided by Grau Malonda (1999), Günther (2002a,b), Zimmerman (2006b), Broda et al., 2007, Collé, 2009, and Grau Carles and Grau Malonda, 2010.

1. Theory and Principles (^{3}H as the Tracer)

As noted by Grau Malonda (1995, 1999) the original plan, conceived in 1978, was to develop a procedure for the standardization of radionuclides, which is applicable to any commercial liquid scintillation analyzer available in most laboratories, any liquid scintillation cocktail, and any radionuclide. To achieve this goal the method had to be based on a combination of theoretical calculations related to the particular radionuclide under measurement and its emissions as well as theoretical calculations related to a primary standard tracer nuclide (*e.g.*, ^{3}H) and its emissions together with experimental data from the liquid scintillation analyzer which provides information concerning the instrument, scintillation cocktail, and radionuclide (*e.g.*, count rate and quench-indicating parameter).

The method is centered on the theoretical computer-based calculations of the counting efficiency of the radionuclide to be analyzed and that of a reference primary standard, such as tritium, for different values of figure of merit (M) and an experimental quench-correction curve obtained from a set of ^{3}H quench standards. The figure of merit (M) is a term used in this technique, which is defined as the β-particle energy in keV required to produce one photoelectron by the photocathode or, in other words, one photoelectron that reaches the first dynode of the photomultiplier tube. The relationship of radionuclide counting efficiency and figure of merit for pure β-emitters and liquid scintillation systems comprised of two photomultiplier tubes in coincidence is defined by

$$\varepsilon = \int_{0}^{E\max} N(E)\left\{1 - \exp\left[\frac{-E \cdot X(E)}{2 \cdot M}\right]\right\}^{2} dE \qquad (7.93)$$

where $E_{\max}$ is the maximum β-particle energy, $N(E)$ is the theoretical β-particle energy distribution, $X(E)$ is the correction for ionization quenching and wall losses (wall effect), and M is the figure of merit (Grau Malonda, 1982b; Grau Malonda and García-Toraño, 1982a,b; Grau Malonda and Los Arcos, 1983; Grau Malonda et al., 1985; and Coursey et al., 1986, 1989).

The objective of the method is to obtain the counting efficiency of a nuclide under investigation (*e.g.*, ^{14}C) from the counting efficiency of an absolute or primary standard of ^{3}H. Hence, the term 'efficiency tracing' is used in naming the technique. Because the ^{3}H is a primary standard, its efficiency is taken as experimental data, while that of the nuclide under measurement (*e.g.*, ^{14}C) is obtained via a theoretical calculation and experiment. It was essential, therefore, that the calculation model for the counting efficiency, as envisaged by Grau Malonda, be so complete and accurate that the final results of

the counting efficiency of the nuclide under investigation would be better than the precision limits of the experiment and instrumentation.

The term 'figure of merit' in this section has a totally different meaning than that used in other parts of this book, where the reader will find reference to figure of merit relating counting efficiency to background in low activity samples. In this section, figure of merit refers exclusively to the quantitative yield of the photomultiplier dynode and its relation to counting efficiency. To avoid confusion, the term 'free parameter' or λ has been adopted instead of figure of merit (M) when relating photomultiplier dynode yield and counting efficiency in this radionuclide standardization technique. Consequently, Eqn 7.93 for the expression of the theoretical counting efficiency is often written as

$$\varepsilon = \int_0^{E_{\max}} N(E)\left\{1 - \exp\left[\frac{-EQ(E)}{2\lambda}\right]\right\}^2 dE \qquad (7.94)$$

where $Q(E)$ is the ionization quenching correction factor or $X(E)$ of Eqn 7.93, and λ is the free parameter or figure of merit M of Eqn 7.93.

The calculation model relies on the decay schemes of the nuclide of interest, and for this purpose, tables of beta-particle and positron spectra were published by Grau Malonda and García-Toraño (1978 and 1981a) from which the spectral area over any given energy range may be obtained. Also, tables of calculated counting efficiencies as a function of the free parameter were published for numerous radionuclides decaying by pure beta-particle emission (Grau Malonda and García-Toraño, 1981b, Grau Malonda et al., 1985), electron capture decay (Grau Malonda, 1982b), positron emission (Grau Malonda and García-Toraño,1982b), beta−gamma-ray emission (García-Toraño and Grau Malonda, 1988), and electron capture decay with gamma-ray emission (Grau Malonda and Fernández, 1985).

As the calculation of the theoretical counting efficiency must account for all beta transitions, Eqn 7.94 is modified accordingly. For example, ^{125}Sb undergoes 8 beta-decay transitions to the daughter nuclide ^{125m}Te. Consequently, to account for all beta-decay transitions, Grau Carles et al. (1998) used the following expression, according to Grau Malonda (1995, 1999), for the calculation of ^{125}Sb counting efficiency:

$$\varepsilon = \sum_{i=1}^{8} p_i \int_0^{(E_m)_i} N_i(E)\left\{1 - \exp\left[\frac{-EQ(E)}{2\lambda}\right]\right\}^2 dE \qquad (7.95)$$

where p_i, $(E_m)_i$, and $N_i(E)$ are respectively the eight beta-particle transition intensities, endpoint energies ($E_{\max}$), and Fermi (beta-particle energy) distributions; E, $Q(E)$, and λ are as previously described. The calculated counting efficiency of ^{125}Sb as a function of the free parameter is, therefore, a sum of the calculated efficiencies for each of the eight beta-decay transitions.

The calculation of the theoretical counting efficiency can be yet more complex when numerous beta- and gamma transitions are part of the radionuclide decay scheme. The standardization of ^{110m}Ag described by García-Toraño et al. (2000) is an interesting example. It decays to ^{110}Cd by β^- emission (98.65%) and isomeric de-excitation by γ emission (1.35%) to ^{110}Ag. The decay scheme comprises more than 12 β branches and 50 gamma rays. García-Toraño et al. (2000) used the CIEMAT/NIST method to standardize samples of ^{110m}Ag, which required the calculation of the Fermi spectra of all β branches, as well as the Compton spectra produced by the γ-ray interactions with the scintillator. A total of 128 decay pathways are possible, and the researchers calculated their probabilities and counting efficiencies to obtain the overall counting efficiency. The expression used for the calculation of the theoretical counting efficiency, in this case, was that described by García-Toraño et al. (1991) for a radionuclide that undergoes β decay followed by a cascade of n γ transitions:

$$\varepsilon = \int_0^{E_\beta}\int_0^{E_{\gamma 1}}\cdots\int_0^{E_{\gamma n}} N(E)S_1(E_1)\cdots S_n(E_n) \times\left\{1 - \exp\left[\frac{-E_\beta Q(E_\beta) - \sum_{i=1}^{n} E_{\gamma i}Q(E_{\gamma i})}{2\lambda}\right]\right\}^2 dE dE_1\cdots dE_n \qquad (7.96)$$

where $N(E)$ and $S_i(E)$ are the β spectrum and Compton spectrum of a given γ transition, respectively, $Q(E)$ is the ionization quenching factor, λ is the free parameter or figure of merit, and E_β, $E_{\gamma 1}$, … $E_{\gamma n}$ are the maximum energies of the β and γ transitions, respectively. García-Toraño et al. (2000) factorized the integral expressions of Eqn 7.96 so that single integrals could be solved and the results combined to yield the complete counting efficiency.

Computer programs or codes have been developed for the rapid computation of counting efficiency as a function of the figure of merit (*i.e.*, free parameter) as described by Grau Malonda (1995, 1999) and Grau Malonda et al. (1987). The computer programs BETA (García-Toraño and Grau Malonda, 1985), BETA3 (Grau Malonda, 1999), EFFY (García-Toraño and Grau Malonda, 1981, 1985), and PTB code (Physikalisch-Technische Bundesanstalt), which is a modified EFFY4 code (Kossert and Schrader, 2004), have been written for computations involving pure beta (negatron or positron) emitters, and the programs EFFY2, EFFY4 (García-Toraño and Grau Malonda, 1981, 1985 and Kossert, 2003), and CN2001A (Günther, 2001 and Zimmerman et al., 2002) are available for the computation of counting efficiency as a function of free parameter for complex-decay beta emitters, and CN2004 code for a positron emitter (Cessna et al., 2008) and for series of beta and alpha decays (Cessna and Zimmerman, 2010). The programs calculate the beta spectra using the theory of radioactive beta decay, taking into account the shape factors (*e.g.*, Grau Carles, 1995, 2005; Grau Carles and Kossert, 2006, 2007; Grau Carles et al. 2008; and Kossert, Nähle and Grau Carles, 2011a). The total detection probability is obtained by dividing the spectrum into bands, calculating the partial detection probabilities of each of them, and summing. The average and mean energies in the spectra are also calculated. Because of the

different decay processes involved, special programs have been written to compute the counting efficiency as a function of free parameter such as EFYGA for X-ray and gamma emitters (García-Toraño and Grau Malonda, 1987), EBEGA for beta-gamma emitters (García-Toraño et al., 1988), and VIASKL (Los Arcos et al., 1987) and VIAS1 (Grau Malonda, 1999) for K-L shell electron capture nuclides, and EMI (Grau Carles et al., 1994b) and EMI2 (Grau Malonda et al., 1999) for electron capture-gamma and isomeric transition nuclides, and EMIS (Grau Malonda, 1999) for radionuclides decaying by electron capture, electron capture coincident with a gamma transition, and pure isomeric transition, and ADDI (Grau Malonda, 1999) computes the counting efficiency of a radionuclide decaying by electron capture and beta-decay transition. An updated program, EMILIA (Grau Carles, 2006a), is applied to counting efficiency calculations for electron-capture and capture-gamma-emitting nuclides. A paper by Los Arcos et al., (1991) provides a detailed treatment of the method applied to multi-gamma electron-capture radionuclides. The computer programs are available from CIEMAT, Avda. Complutense 22, 28040 Madrid, Spain. Also, the program CIENIST99 written in Visual Basic 5 reported by Günther (2000) combines the CIEMAT/NIST codes BETA, EBEGA, and EMI to accommodate multi-beta/multi-gamma transitions.

The procedure integrates theoretical calculations with experimental measurements. The free parameter (figure of merit) is an essential component in the theoretical calculation of the counting efficiency, while the quench-indicating parameter (QIP) of a particular liquid scintillation analyzer (*e.g.*, tSIE, SQP(E), or H#) is required for the experimental aspect of this method. However, as explained by Grau Malonda and García-Toraño (1982a,b), the figure of merit cannot be obtained directly from experiment and the quenching parameter is not theoretically computable. Therefore, the method makes use of a plot that relates the figure of merit (free parameter) with the quench-indicating parameter. Such a plot is obtained by integrating an experimental quench-correction curve of a primary standard, such as ^{3}H (*e.g.*, counting efficiency vs. a QIP), with a theoretically computed curve of counting efficiency versus figure of merit.

Tritium is the most suitable standard for this method when the analysis of beta-emitters is required. It is readily available as an absolute standard as tritiated water or in organic form, it has a relatively long half-life and, as noted by Coursey et al. (1998), it provides for more sensitive extrapolations to the low-energy portions of the beta-particle spectra than higher-energy standards. Radioactive standards of tritiated water disseminated by the Laboratoire Primaire des Ionizants (LPRI), France, and the National Institute of Standards and Technology (NIST), USA, were intercompared by Zimmerman and Collé (1997a) and demonstrated an apparent mean disagreement between standards of $<0.4\%$ on a relative basis. As a standard for the CIEMAT/NIST method, ^{3}H has the advantage that any uncertainties on the efficiency curve of this radionuclide are reduced for the efficiency calculations of the more energetic β-emitters. See Grau Malonda and García-Toraño (1982a,b) and Grau Malonda (1995, 1999) for calculations demonstrating the uncertainty propagations for tritium.

The objective is to obtain a counting efficiency quench-correction curve for any radionuclide, which may decay by β-, β/γ, X-ray and γ-photon emissions, EC decay, and isomeric transition. The counting efficiency quench-correction curve is then used to determine the absolute activity (DPM) of a radionuclide sample under investigation from its experimental quench-indicating parameter.

2. Procedure

The procedure for obtaining the counting efficiency quench-correction curve for any nuclide under investigation with ^{3}H as the standard is outlined next. The sequence of steps in the procedure is illustrated in Fig. 7.64 and the curves established as a result of each step are illustrated in Fig. 7.65:

a. A set of ^{3}H quenched standards is counted in the liquid scintillation analyzer and a quench-correction curve of tritium counting efficiency versus the quench-indicating parameter is plotted. See curve (a) of Fig. 7.65.
b. The theoretical counting efficiency of ^{3}H (ε_T) as a function of figure of merit is computed. See curve (b) of Fig. 7.65.
c. From the preceding two relationships, the figure of merit as a function of the quench-indicating parameter is obtained. Although these two relationships are determined from ^{3}H standards, the figure of merit as a function of quench-indicating parameter is independent of any radionuclide. It is a "universal" curve, which may be applied to any radionuclide, but is suitable only for the particular liquid scintillation analyzer and scintillator used. See curve (c) of Fig. 7.65.
d. The theoretical counting efficiency of the nuclide under investigation (ε_{nuc}) as a function of figure of merit is calculated. See curve (d) of Fig. 7.65.

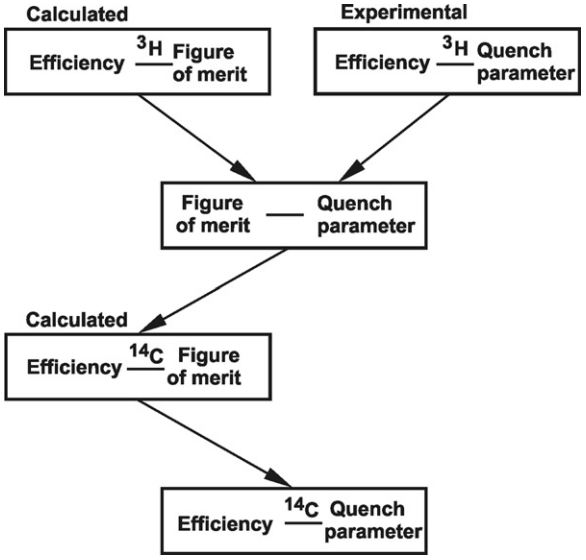

FIGURE 7.64 Outline of the CIEMAT/NIST ^{3}H efficiency tracing method of radionuclide standardization. The diagram illustrates the sequence of calculated and experimental relationships, which are defined to yield the quench-correction curve of any radionuclide under investigation. Tritium is the standard (or tracer nuclide) in all cases, while ^{14}C, illustrated here as an example, is the radionuclide under investigation. *(From Grau Malonda and García-Toraño, 1982a, reprinted with permission from Elsevier ©1982)*

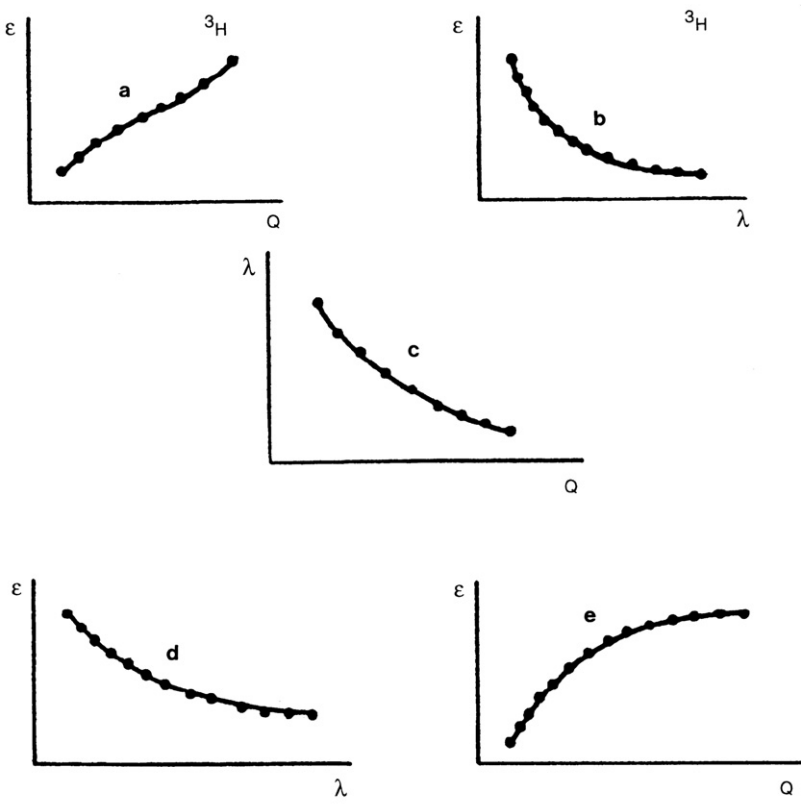

FIGURE 7.65 Calculated and experimental calibration curves obtained in the radionuclide standardization method of CIEMAT/NIST ^{3}H efficiency tracing. The curves are described in the sequence by which they are obtained as follows: (a) experimental quench-correction curve of ^{3}H counting efficiency (ε_T) vs. quench-indicating parameter (Q); (b) computed ^{3}H counting efficiency (ε_T) vs. figure of merit or free parameter (λ); (c) "universal" curve of figure of merit (free parameter, λ) vs. quench-indicating parameter (Q) derived from the above two relationships; (d) computed curve of the counting efficiency of the nuclide under investigation (ε_{nuc}, *e.g.*, ^{14}C) vs. the figure of merit or free parameter (λ); and (e) quench-correction curve of counting efficiency of the nuclide under investigation (ε_{nuc}, *e.g.*, ^{14}C) vs. the instrumental quench-indicating parameter (Q) derived from curves (c) and (d). *(From Grau Malonda, 1995, 1999, reprinted with permission from CIEMAT © 1995−1999)*

e. Consequently, the relationship between the counting efficiency of the nuclide under investigation (ε_{nuc}) and the quench-indicating parameter can be obtained. This plot is obtained from the two preceding relationships, that of the universal curve of figure of merit versus the quench-indicating parameter and the computed curve of ε_{nuc} versus figure of merit. See curve (e) of Fig. 7.65.

f. The final curve obtained in step 5 can be used to determine the counting efficiencies of experimental samples. The experimental sample of the nuclide under investigation is counted and the count rate (CPM) and quench-indicating parameter are recorded. From the quench-indicating parameter and the quench-correction curve of ε_{nuc} versus QIP [Curve (e) of Fig. 7.65], the counting efficiency of the experimental sample ε_{nuc} is obtained.

g. The activity (DPM) of the nuclide under investigation is then calculated as

$$A = \frac{\text{CPM}}{\varepsilon_{nuc}} \tag{7.97}$$

The computer calculations of counting efficiency as a function of figure of merit (M) were reported by Grau Malonda et al. (1985) for 35 pure β-emitting radionuclides. These fitted data of counting efficiency as a function of figure of merit are reported as polynomial coefficients to the fifth degree according to the equation

$$\ln \varepsilon = A_0 + A_1 \ln M + A_2 (\ln M)^2 + \ldots \tag{7.98}$$

The coefficients are listed in Table 7.8. The computer programs for calculating these coefficients and those of many other radionuclides are described in the publications cited in the previous section under theory and principles, and the entire programs are available from Grau Malonda (CIEMAT, Avda. Complutense 22, 28040 Madrid, Spain) or Grau Malonda (1999). The figure of merit of the standard ^{3}H is obtained from the relationship of (ε_T) versus M. The good fit for these data is reported by Grau Malonda et al. (1985) according to the following fifth-degree polynomial:

$$\ln M = B_0 + B_1 (\ln \varepsilon) + B_2 (\ln \varepsilon)^2 + \ldots, \tag{7.99}$$

where the values of B_i for ^{3}H are reported to be $B_0 = 3.11669$, $B_1 = -0.585619$, $B_2 = 0.137378$, $B_3 = -0.148844$, $B_4 = 0.0540364$, and $B_5 = -0.00705037$. Finally, the quench curve of ε_{nuc} versus a QIP for 34 of the radionuclides listed in Table 7.8 can be obtained from the experimental quench-correction curve for ^{3}H (*i.e.*, ε_T versus QIP) and the data obtained using Eqns 7.98 and 7.99 and the respective polynomials.

An example of the CIEMAT/NIST method using ^{3}H as the primary standard tracer nuclide can be taken from the work of Capogni et al. (2006) on the standardization of [^{18}F]fluorodeoxyglucose, a radiopharmaceutical used in positron emission tomography (PET). The procedure used by Capogni et al. (2006) was the following:

1. The counting efficiency of the tracer nuclide, ^{3}H, as a function of the quench-indicating parameter, SQP(E), was determined experimentally with a PerkinElmer "Wallac

TABLE 7.8 Polynomial Coefficients for Fitting Counting Efficiency as a Function of the Figure of Merit

	Polynomial coefficients						
Nuclide	A_0	A_1	A_2	A_3	A_4	A_5	Maximum disc (%)
^{3}H	0.405213+1	−0.519852	−0.238284	−0.542988 − 1	0.233709 − 1	−0.229258 − 2	0.2
^{10}Be	0.460257 + 1	−0.833326 − 3	−0.14108 − 2	−0.369043 − 2	0.239038 − 2	−0.675201 − 3	0.07
^{14}C	0.456074 + 1	−0.498280 − 1	−0.212707 − 1	0.599262 − 2	−0.114070 − 1	0.955890 − 3	0.3
^{31}Si	0.460386 + 1	−0.996311 − 3	−0.651159 − 3	−0.102653 − 2	0.592699 − 3	−0.174146 − 3	0.02
^{32}Si	0.456478 + 1	−0.405983 − 1	−0.175982 − 1	0.923926 − 3	−0.493393 − 2	−0.792020 − 4	0.1
^{32}P	0.460414 + 1	−0.759601 − 3	−0.494713 − 3	−0.795852 − 3	0.460529 − 3	−0.133668 − 3	0.01
^{33}P	0.457255 + 1	−0.319945 − 1	−0.144253 −1	−0.128012 − 2	−0.230966 − 2	−0.452069 − 3	0.07
^{35}S	0.454759 + 1	−0.580615 − 1	−0.236917 − 1	0.373332 − 2	−0.928844 − 2	0.654008 − 3	0.2
^{39}Ar	0.459712+1	−0.619246 − 2	−0.340035 − 2	−0.367905 − 2	0.187337 − 2	−0.608778 − 3	0.06
^{45}Ca	0.457021 + 1	−0.338821 − 1	−0.151187 − 1	−0.174736 − 2	−0.212018 − 2	−0.456534 − 3	0.06
^{63}Ni	0.441361 + 1	−0.166749	−0.657592 − 1	−0.176547 − 1	−0.139047 − 1	0.280594 − 2	0.07
^{66}Ni	0.455387 + 1	−0.504729 − 1	−0.212871 − 1	0.588624 − 3	−0.573001 − 2	0.103022 − 3	0.2
^{69}Zn	0.459965 + 1	−0.455061 − 2	−0.239135 − 2	−0.231221 − 2	0.110588 − 2	−0.369529 − 3	0.03
^{79}Se	0.457489 + 1	−0.375947 − 1	−0.161750 − 1	0.961543 − 2	−0.109656 − 1	0.656409 − 3	0.3
^{85}Kr	0.459722 + 1	−0.682161 − 2	−0.340506 − 2	−0.288481 − 2	0.123660 − 2	−0.433468 − 3	0.04
^{87}Rb	0.459557 + 1	−0.777543 − 2	−0.575931 − 2	−0.465487 − 2	0.291824 − 2	−0.128978 − 2	0.06
^{89}Sr	0.460272 + 1	−0.237735 − 2	−0.119424 − 2	−0.101322 − 2	0.438239 − 3	−0.154756 − 3	0.01
^{90}Sr	0.459429 + 1	−0.892563 − 2	−0.451710 − 2	−0.390183 − 2	0.172480 − 2	−0.597759 − 3	0.06
^{90}Y	0.460413 + 1	−0.106759 − 2	−0.558493 − 3	−0.520378 − 3	0.242267 − 3	−0.808739 − 4	0.008
^{91}Y	0.460279 + 1	−0.218860 − 2	−0.110022 − 2	−0.945244 − 3	0.409650 − 3	−0.143794 − 3	0.01
^{99}Tc	0.457235 + 1	−0.312754 − 1	−0.140836 − 1	−0.330923 − 2	−0.891300 − 3	−0.555615 − 3	0.03
^{106}Ru	0.426331 + 1	−0.279785	−0.120473	−0.527075 − 1	0.389097 − 2	0.928245 − 3	0.4
^{109}Pd	0.446763 + 1	−0.156553	−0.109538	−0.755600 − 1	0.902461 − 2	0.629885 − 3	0.6
^{113m}Cd	0.459211 + 1	−0.114637 − 1	−0.560371 − 2	−0.371747 − 2	0.133895 − 2	−0.579840 − 3	0.04
^{115}In	0.460051 + 1	−0.234863 − 2	−0.216760 − 2	−0.437909 − 2	0.277809 − 2	−0.799807 − 3	0.08
^{121}Sn	0.458112 + 1	−0.214372 − 1	−0.100221 − 1	−0.422650 − 2	0.702033 − 3	−0.677667 − 3	0.03
^{123}Sn	0.460229 + 1	−0.283529 − 2	−0.139369 − 2	−0.108105 − 2	0.430745 − 3	−0.161408 − 3	0.02
^{135}Cs	0.457944 + 1	−0.268855 − 1	−0.129479 − 1	0.900326 − 3	−0.278706 − 2	−0.546387 − 3	0.1
^{143}Pr	0.459885 + 1	−0.551151 − 2	−0.275820 − 2	−0.223641 − 2	0.930999 − 3	−0.342315 − 3	0.03
^{185}W	0.458369 + 1	−0.191761 − 1	−0.898716 − 2	−0.414450 − 2	0.842663 − 3	−0.645690 − 3	0.03
^{187}Re	0.167732 + 1	−0.165469 + 1	−0.152546	0.391800 − 1	−0.572250 − 2	0.368647 − 3	0.01
^{188}W	0.457681 + 1	−0.256581 − 1	−0.117439 − 1	−0.394376 − 2	0.558416 − 4	−0.620994 − 3	0.01
^{209}Pb	0.459299 + 1	−0.109936- 1	−0.529640 − 2	−0.334930 − 2	0.112054 − 2	−0.511350 − 3	0.04
^{241}Pu	0.394623 + 1	−0.535624	−0.217935	−0.533980 − 1	0.206078 − 1	−0.184730 − 2	0.2
^{249}Bk	0.450771 + 1	−0.938177 − 1	−0.365791 − 1	0.258343 − 2	−0.141435 − 1	0.176016 − 2	0.3

(From Grau Malonda et al., 1985, reprinted with permission from Elsevier © 1985).

1414 WinSpectral" liquid scintillation counter using a set of tritium standards at various quench levels. The plot of % detection efficiency of the tracer nuclide versus SQP(E), *i.e.*, ε_T versus SQP(E) is illustrated in Fig. 7.66 [with the heading ^{3}H (experimental)].

2. The counting efficiency of the tracer nuclide (^{3}H) is calculated as a function of the free parameter (M), defined as the effective energy necessary to create one photoelectron at the photocathode. For this calculation, Capogni et al. (2006) used the CN2001 code reported by Günther (2002a). The plot of M versus % detection efficiency of the tracer nuclide, *i.e.*, M versus ε_T, is illustrated in Fig. 7.66 [with the heading ^{3}H (theoretical)].
3. The independent nuclide relationship between the free parameter (M) and the quench-indicating parameter SQP(E) was then derived from the functions previously determined in steps (1) and (2), that is, ε_T versus SQP(E) and M versus ε_T. The relationship is not illustrated as a plot in Fig. 7.66, but it would be a plot analogous to curve c of Fig. 7.65.
4. The counting efficiency of the nuclide of interest, ε_{nuc}, (in this case ^{18}F) as a function of the free parameter (M) was calculated using the CN2001 code. The plot of % detection efficiency of the nuclide of interest (^{18}F) versus the calculated free parameter (M), *i.e.*, ε_{nuc} versus M, is illustrated in Fig. 7.66 [with the heading ^{18}F (theoretical)].
5. Finally, the counting efficiency of the nuclide of interest (^{18}F) as a function of the quench-indicating parameter [SQP(E)], which is the curve illustrated in Fig. 7.66 [with the heading ^{18}F (experimental)], is obtained from the calculated counting efficiency of ε_{nuc} versus M of the previous step (4) and the derived function or relationship between the free parameter (M) and the quench-indicating parameter [SQP(E)], determined in step (3).
6. From the quench-indicating parameter as measured by the liquid scintillation counter, the detection efficiency is then obtained directly from the derived curve illustrated in Fig. 7.66, labeled ^{18}F (experimental). The activity of the nuclide of interest A_{nuc} in DPM can then be calculated according to the basic relationship $A_{nuc} = \text{CPM}/\varepsilon_{nuc}$. In the case of ^{18}F and other short-lived nuclides, correction for decay during counting is required.

The CIEMAT/NIST efficiency tracing with ^{3}H as the tracer nuclide has become a very popular method for radionuclide standardization, as no special equipment is required. A common modern liquid scintillation analyzer and personal computer are all that is needed. The principal advantage of the CIEMAT/NIST efficiency tracing method is that only standards of ^{3}H are required, that is, no standards of the nuclide under investigation are needed. This is particularly relevant when the activities of short-lived nuclides must be determined very accurately and on-site, such as those utilized in nuclear medicine or radiotherapy. Also, the calculated uncertainties reported in the activity analysis of a broad range of radionuclides are low. The following are some examples of radionuclides reported in the literature as standardized by this method with the unsurpassed calculated standard uncertainties of the determinations expressed as a percent in parenthesis; the computer codes used for the calculations of the detection efficiencies against the figure of merit can be obtained from the references cited herewith: ^{10}Be ($\pm$0.15%) reported by Chmeleff et al., (2010); ^{14}C ($\pm$0.20%) reported by Coursey et al. (1986); ^{18}F ($\pm$0.30%) reported by Capogni et al. (2006),

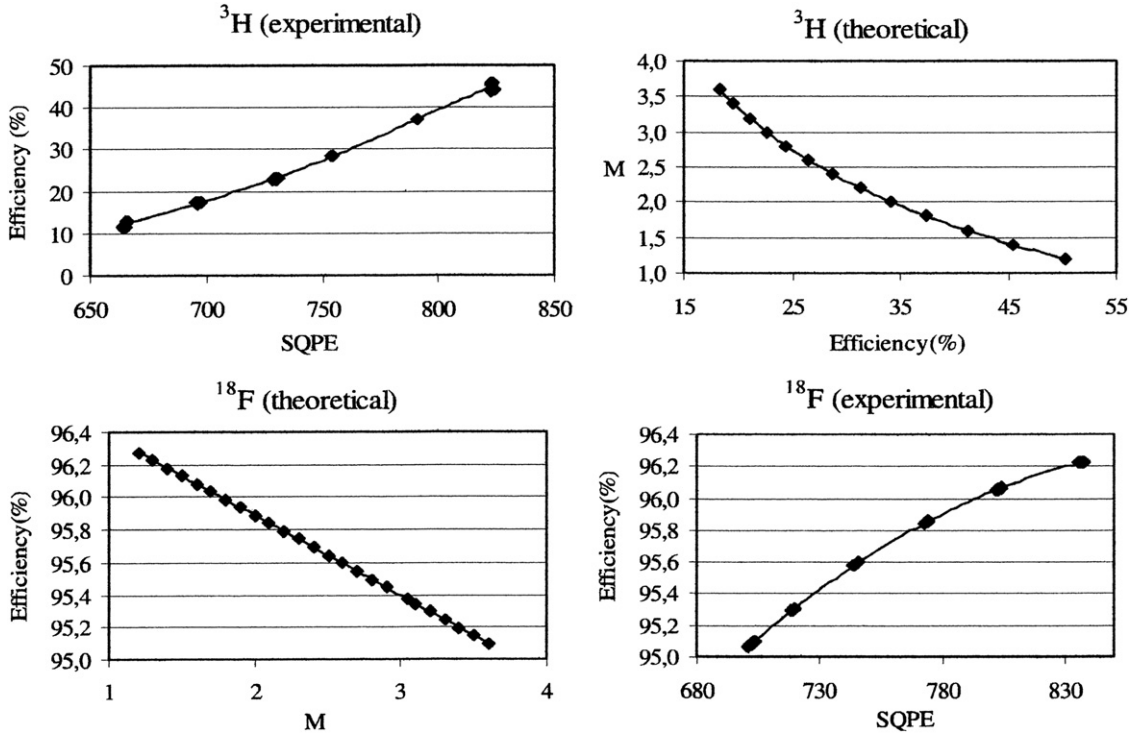

FIGURE 7.66 CIEMAT/NIST method applied to the standardization of ^{18}F. *(From Capogni et al., 2006, reprinted with permission © 2006 IOP Publishing Ltd)*

Roteta et al. (2006), Schrader et al. (2007), Cessna et al. (2008), and Nedjadi et al. (2010); ^{32}P (± 0.4 %) reported by Rodríguez Barquero et al. (2004), da Cruz et al. (2004), and Cessna (2002); ^{35}S (± 1.0%) reported by Calhoun et al. (1991); ^{36}Cl (± 0.3%) reported by Rodríguez Barquero et al. (1989); ^{40}K (± 0.1%) reported by Grau Carles and Grau Malonda (1997) and Grau Malonda and Grau Carles (2002); ^{41}Ca (± 0.38%) reported by Kossert et al. (2009) and Rodríguez Barquero and Los Arcos (1996); ^{45}Ca (± 0.4%) reported by Rodríguez Barquero et al. (1994); ^{45}Ca (± 0.25%) and ^{55}Fe (± 0.6%) reported by Ortiz et al. (1993); ^{54}Mn (<0.7%) reported by Rodríguez et al. (1992), Kossert and Grau Carles (2006), and Cassette et al. (2006); ^{59}Fe (± 0.4%) and ^{131}I (± 0.4%) reported by Günther (1994); ^{62}Cu (± 0.01%) reported by Zimmerman and Cessna (1999); ^{63}Ni (± 1.1%) and ^{241}Pu (± 3.0%) reported by Coursey et al. (1989); ^{64}Cu (± 0.49%) reported by Wanke et al. (2010) and Bakhshandeiar et al. (2011); ^{68}Ge/^{68}Ga (± 0.73%) reported by Zimmerman et al. (2008); ^{79}Se (± 0.48%) reported by Bienvenu et al. (2007) and Jörg et al. (2010); ^{85}Sr (± 1.5%), ^{109}Cd (± 1.5%), and ^{125}I (± 1.5%) reported by Grau Carles et al. (1994c); ^{87}Rb (± 0.64%) reported by Kossert (2003); ^{89}Sr (± 0.23%) reported by Altzitzoglou et al. (2002), Coursey et al. (1998), and Cruz et al. (2002); and ^{89}Sr (± 0.2%) reported by Altzitzoglou et al. (2002); ^{90}Sr (^{90}Y) (± 2%) reported by Grau Malonda and Los Arcos (1983); ^{90}Sr (± 1.1%) reported by Altzitzoglou et al. (1998) for low-level activities (~45 Bq/kg) in dry bone ash and Spasova et al. (2008) for ^{90}Sr in milk; ^{90}Y (± 0.12%) reported by Kossert and Schrader (2004), Zimmerman et al. (2004), Mo et al. (2005), Schultz et al. (2008), and Xiques Castillo et al. (2010); ^{93m}Nb (± 0.56%) reported by Günther and Schötzig (1992); ^{93}Zr (± 3.8%) reported by Cassette et al. (2010); ^{99}Tc (± 0.02%) reported by Laureano-Perez et al. (2010); ^{99m}Tc (± 3.4%) reported by Grau Malonda and Coursey (1987); ^{110m}Ag (± 0.29%) reported by García-Toraño et al. (2000); ^{113m}Cd (± 0.34%) reported by Kossert et al. (2011b); ^{124}Sb (± 0.37%) reported by Chauvenet et al. (2010); ^{125}Sb (^{125m}Te) (± 1.5%) reported by Grau Carles et al., (1997, 1998); ^{131}I (± 0.22%) reported by Oropesa Verdecia and Kossert (2009); ^{134}Cs (± 0.19%) reported by García-Toraño et al. (2002) and Wätjen et al. (2006); ^{138}Cs (± 0.74%) reported by Wätjen et al. (2006); ^{153}Sm (± 0.19%) reported by Schötzig et al. (1999); ^{177}Lu (± 0.8%) reported by Zimmerman et al. (2001); ^{186}Re (± 1.61%) reported by Coursey et al. (1991); ^{188}W/^{188}Re (± 0.4%) reported by Zimmerman et al. (2002); ^{204}Tl (± 0.24%) reported by Rodríguez Barquero et al. (2004), da Cruz et al. (2004), Hult et al. (2000), Johansson, et al. (2002), and Lee et al. (2004); ^{210}Pb (± 2.4%) reported by Laureano-Perez et al. (2007) and Collé and Laureano-Perez (2009); ^{223}Ra (± 0.27%) reported by Cessna and Zimmerman (2010); ^{229}Th (± 0.65%) reported by Fitzgerald et al. (2010); ^{237}Np (± 0.2%) reported by Günther (2000); and ^{241}Pu (± 1.06%) reported by Kossert et al. (2011a).

3. Sample, Cocktail, and Spectrometer Stability

Liquid scintillation cocktail volume can have a significant effect on the count rate of weak β-emitters such as ^{63}Ni ($E_{max} = 67$ keV). A study by Zimmerman and Collé (1997b) demonstrated that a 7% variation in the liquid scintillation counting efficiency of ^{63}Ni can be observed over the scintillation cocktail volume range of 1−20 mL. However, they demonstrate that the CIEMAT/NIST method is able, nevertheless, to trace the observed ^{63}Ni activity to about 0.1%. To assure precise standardizations when employing the CIEMAT/NIST efficiency tracing method some researchers will centrifuge the liquid scintillation counting vial to assure that no significant amount of nuclide and cocktail remain adhered to the inner surface of the counting vial cap. Gravimetric dispensing of radionuclide solutions is also a common practice.

The physical and chemical stability of samples in scintillation cocktail is a priority. Terlikowska et al. (1998) identified the causes of instability of samples which include (1) degradation of the scintillator or cocktail, (2) adsorption of the nuclide on the walls of the counting vial, (3) settlement of the aqueous phase of the nuclide source, (4) change in the physical characteristics (*e.g.*, size) of the aqueous micelles in cocktail mixtures, and (5) evolution of quenching in the cocktail due to a chemical change in its composition (*e.g.*, an increase of dissolved oxygen in the cocktail with time). A quench-indicating parameter measured with an external radiation source may not provide any evidence of a problem in the cases of the above instabilities 2 and 4. Consequently, the stability of cocktails must be studied thoroughly for each nuclide standardized. It is recommended also that standardizations of any particular nuclide be carried out in accord with previously tested and recommended cocktails and procedures cited in the literature. Carrier is used by some researchers in radionuclide standardization to avoid error that might occur due to adsorption of nuclide on the walls of counting vials. For example, the following carriers have been added to nuclide samples for this purpose: 0.25 mL of Sr carrier solution containing 4 mg Sr/g in l mol/L HCl in the standardization of ^{89}Sr (Coursey et al., 1998), 0.1 mg Mn or Zn carrier in 1 mL of 0.05 mol/L of EDTA solution (Günther, 1998), vials previously saturated with a carrier solution containing 100 μg/g of $NiCl_2$ in 0.1 M HCl in the standardization of ^{63}Ni (Terlikowska et al., 1998), and ^{177}Lu solution in carrier containing approximately 0.06 g of $LuCl_3$ per mL of 1 mol/L HCl (Zimmerman et al., 2001).

Rodríguez Barquero and Los Arcos (2004) carried out a thorough long-term study that monitored the stability of samples and drift in electronic components of the spectrometer over time intervals that extended to up to 4 years. The tests were carried out with low-energy beta emitters, namely, ^{3}H, ^{14}C, and ^{63}Ni where detection efficiency could be more susceptible to disturbing changes in sample and cocktail stability or spectrometer response. Their findings were that the CIEMAT/NIST method can compensate for count losses and quench parameter compensation values, provided the experimental quench curve of the tracer nuclide, *i.e.*, ε_T versus QIP, is prepared close to the time of nuclide measurements. If this requirement is not met, significant discrepancies of up to 5.6% for ^{3}H, 1.5% for ^{63}Ni, and 0.35% for ^{14}C can be obtained for a 1-year time difference.

4. Universal Application.

In the preceding treatment on the theory and experimental procedure involved in the CIEMAT/NIST method, it was established that the counting efficiency as a function of the

'figure of merit' (M) or 'free parameter' (λ), is found for both the standard (tracer) nuclide (ε_T) and the radionuclide under investigation (ε_{nuc}). Under such circumstances, as noted by Grau Malonda et al. (1985), the ratio of the counting efficiencies ($\varepsilon_{\text{T}}/\varepsilon_{\text{nuc}}$) is also known as a function of M. Consequently, as the counting efficiency of the tracer nuclide (*e.g.*, ^{3}H) is known, the other can be computed. Tritium is considered, therefore, not only as a standard nuclide, but also as a tracer nuclide, because the counting efficiency of the nuclide of interest is found against that of the reference nuclide, ^{3}H in this case. (Most often ^{3}H is used as the tracer for the standardization of beta-emitters, but we will see in the next section that another tracer nuclide, ^{54}Mn, may be used for the standardization of radionuclides that decay by pure electron capture.) With this in mind and in view of the curves illustrated in Fig. 7.65, we can see that the curves ε_T vs. QIP (obtained from a series of quenched standards of the tracer nuclide, *e.g.*, ^{3}H) and ε_{nuc} vs. QIP (obtained from the relationships of ε_T vs. M, M vs. QIP, and ε_{nuc} vs. M) can be integrated to provide a curve directly relating the counting efficiency of the nuclide under investigation (ε_{nuc}) and that of the tritium standard or tracer nuclide (ε_T). Such a curve is illustrated in Fig. 7.67. With this relationship, the counting efficiency of a given nuclide (ε_{nuc}) at a certain QIP could be determined from the counting efficiency of tracer nuclide (ε_T) at the same QIP.

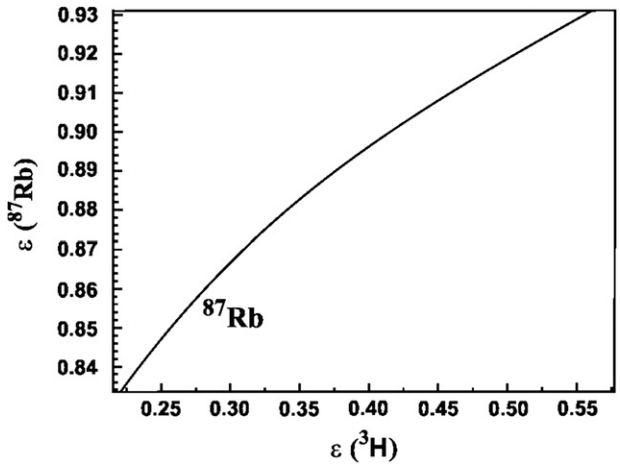

FIGURE 7.67 LSC detection efficiencies of ε_{nuc} versus ε_{T}; that is, the detection efficiencies of the nuclide to be analyzer ^{87}Rb versus the detection efficiency of the tracer nuclide ^{3}H, referred to as the 'efficiency curve'. *(Curve from Kossert, 2003, reprinted with permission from Elsevier © 2003)*

To facilitate the application of the CIEMAT/NIST efficiency tracing method Günther (1996) proposed the following procedure:

a. Calculation of the efficiencies. Calculating the efficiencies of radionuclides versus the corresponding tritium efficiency can be done in a national standards laboratory. The results should be parameterized as coefficients k_i of the polynomial in Eqn 7.100. Tables 7.9 and 7.10 summarize the results obtained at the Physikalisch-Technische Bundesanstalt (PTB) for a variety of pure β-emitters and $\beta-\gamma$-emitters:

$$\varepsilon_{\text{nuc}} = \sum_{i=0}^{n} k_i \varepsilon_T^i \tag{7.100}$$

TABLE 7.9 For β Emitters, Coefficients k_i of the Polynomial Eqn 7.100 Correlating the Nuclide Counting Efficiencies (ε_{nuc}) with Tritium Counting Efficiencies (ε_T), and a Comparison of the Standardization by Efficiency Tracing with Tritium to Other Methods.

	Coefficients of the least-squares fit[a]					Efficiency[b] (%)	Comparison[c]	
Nuclide	k_0	k_1	k_2	k_3	k_4	($\varepsilon_T = 50\%$)	Method	Δ (%)
^{14}C	72.21	0.9538	− 1.4846E-2	0.917E−4	0	94.25	I	<0.5
^{32}P	99.39	0.0145	−0.0102E-2	0	0	99.86	IC, B	<0.5
^{33}P	80.97	0.6279	−0.9657E-2	0.598E−4	0	95.70	—	
^{35}S	69.35	0.9633	− 1.4284E-2	0.868E−4	0	92.65	—	
^{45}Ca	80.43	0.6377	−0.9737E-2	0.602E−4	0	95.50	—	
^{63}Ni	22.76	2.4709	−4.8562E-2	5.603E−4	−2.633E-6	78.48	—	
^{89}Sr	96.97	0.0685	−0.0472E-2	0	0	99.22	B	<0.5
^{90}Sr	90.20	0.3099	−0.4652E-2	0.286E−4	0	97.64	—	<0.5
^{90}Y	98.39	0.0378	−0.0263E-2	0	0	99.62	B	<0.5
^{90}Sr/^{90}Y	190.09	0.2222	−0.1567E-2	{}	0	197.29	IC, B	<0.5
^{99}Tc	81.10	0.6123	− 0.9312E-2	0.575E−4	0	95.62	I	<0.5
^{147}Pm	74.15	0.8224	− 1.2363E-2	0.7596E−4	0	93.86	ET	1.4
^{204}Tl	92.96	0.1436	−0.0914E-2	0	0	97.86	B	~1

[a] *The coefficients are from Eqn 7.100 If* k_4 *is not listed, the valve is 0.*
[b] *A typical efficiency of unquenched samples with a tritium efficiency of 50%.*
[c] *The methods used to determine the activity of the standard solutions and the differences Δ from the result obtained with these methods. C, 4πβ−γ coincidence counting, IC, calibrated ionization chamber; B, 4πβ proportional counting; I, intercomparison; G, 4πγ counting; ET, efficiency tracing with coincidence counting.*
(From Günther, 1996, reprinted with permission from Radiocarbon, University of Arizona © 1996 Arizona Board of Regents on behalf of the University of Arizona).

TABLE 7.10 For β−γ Emitters, Coefficients k_i of the Polynomial Eqn 7.100 Correlating the Nuclide Counting Efficiencies (ε_{nuc}) with Tritium Counting Efficiencies (ε_T), and a Comparison of the Standardization by Efficiency Tracing with Tritium to Other Methods[a]

Nuclide	Coefficients of the least-squares fit				Efficiency (%)	Comparison	
	ko	k_1	k_2	k_3	($\varepsilon_T = 50\%$)	Method	Δ (%)
^{59}Fe	87.30	0.3778	−0.5006E-2	0.2580E−4	6.9	IC, C	<0.5
^{60}Co	86.06	0.4489	−0.6756E-2	0.4126E−4	96.78	IC, C, I	<0.5
^{129}I	79.90	0.7893	−1.2180E-2	0.6958E−4	97.61	IC, I	<0.5
^{131}I	93.86	0.1408	−0.1015E-2	0	98.36	IC, C, I	<0.5
^{137}Cs/^{137}Ba	107.90	0.179	−0.1284E-2	0	113.65	IC, G	<0.5
^{134}Cs	82.81	0.5048	−0.7181E-2	0.4313E−4	95.49	IC, C, I	<0.5
^{141}Ce	93.13	0.1424	−0.0995E-2	0	97.76	IC, C, I	<0.5
^{203}Hg	79.43	0.6568	−0.9905E-2	0.6100E−4	95.13	IC, I	0.6

[a]*See footnotes, Table 7.9.*
(From Günther, 1996, reprinted with permission from Radiocarbon, University of Arizona © 1996 Arizona Board of Regents on behalf of the University of Arizona).

b. Verifying the results. This step is also best done at one of the national standards laboratories, because they have a stock of standard solutions. An experimental comparison of the results with those obtained with other methods is necessary. Tables 7.9 and 7.10 show some results.

c. Laboratory procedure. The user must determine the quench-indicating parameter Q automatically with each single measurement, calculating the corresponding tritium efficiency ε_T of the individual measurement using his/her own tritium quench curve, and calculating the efficiency ε_{nuc} with this efficiency and the coefficients of Table 7.9 or 7.10. This can be shortened by a computer program. The tritium efficiency measurements obtained with the individual LSC device as well as the polynomial coefficients k_i can be combined and included in a program (LSCAL, available from E. W. Günther, PTB, Bundesallee 100, D-38116 Braunschweig, Germany) to obtain and use an efficiency curve

$$\varepsilon_{nuc} = \sum_{i=0}^{n} m_i Q^i \qquad (7.101)$$

with new coefficients m_i.

As explained by Günther (1996), with this procedure, only the count rate and the quench parameter Q (same as the quench-indicating parameter, QIP) are necessary to obtain the sample activity, *i.e.*, the activity of the nuclide of interest. If the liquid scintillation counter is equipped with a self-normalization procedure, the repetition of the determination of the tritium quench-correction curve need not be carried out except over longer intervals of time. Best results are obtained when the quenched standards of the tracer nuclide (^{3}H) are counted in a time span close to that of counting the nuclide of interest as reported by Rodríguez Barquero and Los Arcos (2004). The procedure proposed by Günther (1996) is summarized in Fig. 7.68.

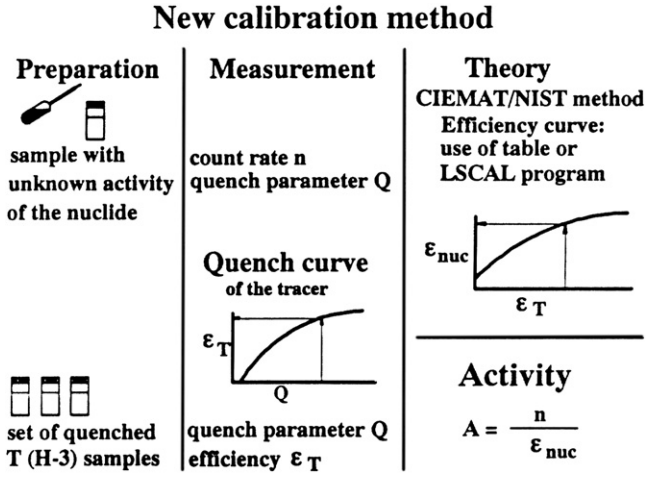

FIGURE 7.68 The new calibration method. The counting efficiency of the nuclide to be measured (ε_{nuc}) is obtained with the quench parameter (Q) of the measurement, the tritium quench curve (ε_T versus Q), and the tabulated coefficients of an efficiency curve of the nuclide (ε_{nuc} versus ε_T). *(from Günther (1996), reprinted with permission from Radiocarbon. University of Arizona © 1996 Arizona Board of Regents on behalf of the University of Arizona)*

All of the previous treatments on the CIEMAT/NIST radionuclide standardization method dealt with the use of standard ^{3}H as the tracer nuclide. Standard tritium has proven to be the best tracer for the standardization of β- or β/γ-emitting nuclides, and it has been the standard of choice since the inception of this technique. However, for the standardization of ^{55}Fe and ^{65}Zn, Günther (1998) has demonstrated ^{54}Mn to be a more robust tracer. Iron-55 decays by pure electron capture and ^{65}Zn decays by 98.6% by electron capture and the remaining 1.4% by positron emission. Günther (1998) demonstrates that the use of standard ^{54}Mn, which decays by pure electron capture, as the tracer nuclide provides radionuclide activities for ^{55}Fe with a total relative uncertainty of only

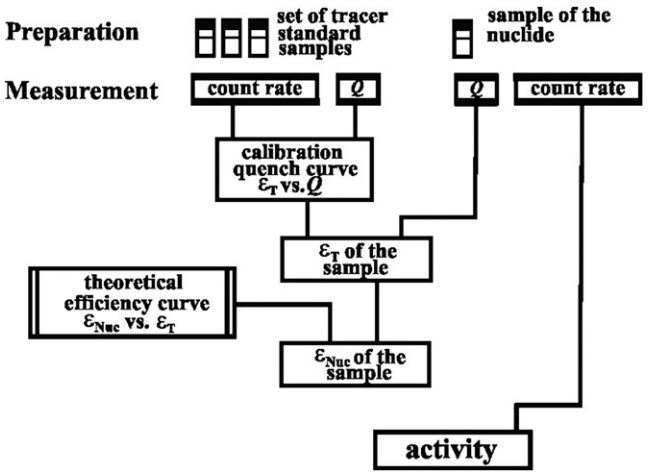

FIGURE 7.69 Principle of the CIEMAT/NIST method. Q is the quench-indicating parameter measured, ε_T is efficiency of the tracer, and ε_{Nuc} the efficiency of the nuclide to be measured. *(From Günther, 1998, reprinted with permission from Elsevier © 1998)*

0.44%, whereas the uncertainty when using tritium as the tracer was 1.67%. Likewise, the total uncertainty in the standardization of ^{65}Zn using ^{54}Mn as the tracer nuclide was only 0.44%, while the uncertainty when using ^{3}H as the tracer increased to 0.93%. Calculations of the detection efficiency by the CIEMAT/NIST method require a good knowledge of the energy transferred to the scintillator, and a good knowledge of the photon absorption coefficients of X-rays emitted by electron-capture decaying nuclides is necessary. Cassette et al. (2006) report new experimental data on X-ray photon absorption coefficients of liquid scintillators in the energy range of 5−12 keV, which could prove helpful in the standardization of EC nuclides, such as ^{55}Fe. The use of ^{54}Mn as a tracer nuclide is discussed further in the next section.

Further streamlining of the CIEMAT/NIST efficiency tracing standardization method is described by Günther (1998, 2000, 2002b). As described previously, the methodology involves the calculated theoretical efficiency curve of the efficiency of the nuclide under investigation (ε_{Nuc}) versus the theoretical efficiency curve of the tracer nuclide (ε_T). The procedure, as portrayed by Günther (1998, 2000), is reduced to the following steps, which are also depicted in Fig. 7.69:

a) The liquid scintillation analyzer is calibrated with a set of quenched standards of a tracer nuclide (usually ^{3}H) by producing an instrument-measured quench curve of counting efficiency, ε_T, versus a quench-indicating parameter, Q, [*e.g.*, SQP(E) or tSIE].

b) The count rate (CPM) and quench-indicating parameter, Q, are determined for a sample of the nuclide to be measured (*i.e.*, a sample of the nuclide of which the counting efficiency and activity are unknown). From this measured value of the quench-indicating parameter of the nuclide under investigation, a fictitious tracer efficiency for this individual measurement is obtained from the tracer calibration curve produced in step 1.

c) The efficiency of the nuclide of the sample under measurement is taken from the calculated theoretical curve of efficiency of the nuclide under investigation (ε_{Nuc}) versus the theoretical efficiency curve of the tracer nuclide (ε_T) and/or taken from a database containing the polynomial equation for the curve.

The experimentally determined quench-correction curve prepared with quenched standards of the tracer nuclide (*e.g.*, ^{3}H) in step 2) can be useful for a long period of time (several months or more) with modern liquid scintillation analyzers that are properly cared for in terms of normalization and calibration, and monitored frequently with automated instrument performance assessments (IPAs). The monitoring of instrument stability by regular automated IPAs is discussed further on in this chapter. However, the CIEMAT/NIST method depends highly on the fact that the tracer nuclide and the nuclide under investigation are measured in a cocktail that possesses the same physical and chemical characteristics. Thus, Rodríguez Barquero and Los Arcos (2004) demonstrate that best results are obtained when the quenched standards of the tracer nuclide are measured close in time to the measurement of the sample of the nuclide under investigation, as the physical and chemical characteristics of a sample in cocktail can change in time.

The theoretically calculated counting efficiencies of the nuclide under investigation and the tracer nuclide are carried out via computer programs (codes) already elaborated for specific nuclide decay schemes as previously described in this chapter or available from databases containing the polynomial for the relationship of the theoretical calculated nuclide efficiency and the tracer efficiency described by the equation

$$\varepsilon_{\mathrm{Nuc}} = \sum_{i=0}^{n} k_i \varepsilon_T^i \tag{7.102}$$

which is the general equation for the polynomial of the least-squares best fit for the relationship, as described previously (Eqn 7.100) with n number of coefficients. With the above two curves or relationships established, it becomes a simple matter to determine the counting efficiency of a sample (ε_{nuc}) and thereby standardize a radionuclide sample simply from its count rate (CPM) and its quench-indicating parameter (Q). Broda et al. (2007) provide an excellent description of the CIEMAT/NIST method, which is illustrated in Fig. 7.70. The first step, as illustrated in the figure, is the theoretical calculations of the detection efficiency of the tracer nuclide as a function of the free parameter, M, [ε_{tracer} (M), *e.g.*, ^{3}H] and of the nuclide under investigation [$\varepsilon_{nuclide}$ (M)] where $M = \lambda$ of Eqn 7.94. This leads to the establishment of the relationship between the two detections efficiencies, that is, the detection efficiency of the nuclide under investigation as a function of the detection efficiency of the tracer nuclide or $\varepsilon_{nuclide}(\varepsilon_{tracer})$ as illustrated in Fig. 7.69, which is also referred to as the 'efficiency curve'. The next step, as illustrated in Fig. 7.70 of Broda et al. (2007), involves the counting of a set of quench standards of the tracer nuclide (*e.g.*, ^{3}H). The quenched standards, as previously described in this chapter, are prepared with primary standard ^{3}H in a series of counting vials containing scintillation cocktail and increasing amounts quenching agent (see Section V.D). The count rates (CPM) and quench-indicating parameters (QIPs) of each vial are recorded. As the tracer nuclide is of a known

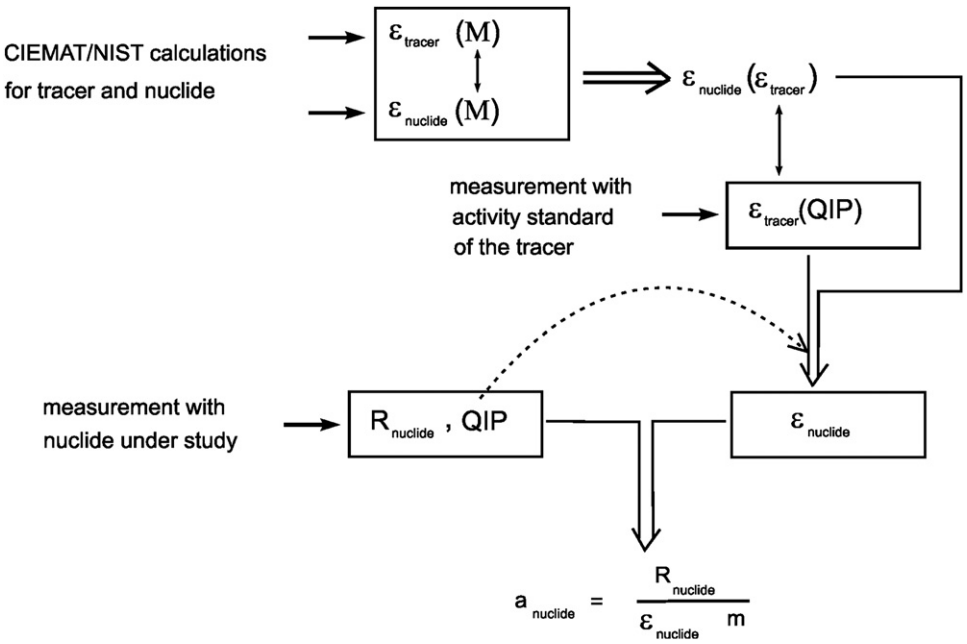

FIGURE 7.70 Illustration of the CIEMAT/NIST method: R denotes the measure count rate, M is the free parameter, QIP is the quench-indicating parameter, ε is the counting efficiency, a_{nuclide} is the solution activity concentration, and m is the mass of the solution in an LSC sample. *(From Broda et al., 2007. Reprinted with permission © 2007 IOP Publishing, Ltd)*

activity (DPM), the detection efficiency of each vial is calculated (CPM/DPM), and the quench-correction curve of the detection efficiency of the tracer nuclide as a function of the quench-indicating parameter is obtained, *i.e.*, $\varepsilon_{\text{tracer}}(QIP)$. The next step is the preparation of a sample of the nuclide under investigation for counting in liquid scintillation cocktail. The sample in the liquid scintillation counting vial must possess the sample physical and chemical characteristics (*i.e.*, same cocktail, cocktail volume, and chemical composition as the quench standards of the tracer nuclide). The count rate (CPM) of the sample and its quench-indicating parameter (QIP) are measured. The value of the QIP is then used to determine the efficiency of the tracer nuclide (see curved arrow in Fig. 7.70) from the curve or function $\varepsilon_{\text{tracer}}(QIP)$. With the corresponding tracer efficiency thus obtained, the corresponding nuclide efficiency ($\varepsilon_{\text{nuclide}}$) is obtained from the efficiency curve, $\varepsilon_{\text{nuclide}}(\varepsilon_{\text{tracer}})$. Finally, the efficiency of the nuclide under investigation, so determined, is used to convert its count rate (CPM), R_{nuclide} of Fig. 7.70, to the activity of the nuclide, according to the equation illustrated in Fig. 7.70, namely, $a_{\text{nuclide}} = R_{\text{nuclide}}/(\varepsilon_{\text{nuclide}}m)$, where m is the sample mass. The samples are generally added gravimetrically to the liquid scintillation cocktail. Consequently, including the sample mass m in the calculation of the sample activity will yield the sample activity concentration (*e.g.*, DPM/g) which can be converted to units of Bq/g.

This approach has been tested by other researchers with excellent results using ^{3}H as the tracer nuclide including the standardization of ^{22}Na with 0.17% uncertainty by Nähle et al. (2008), ^{32}P with 0.30% uncertainty by Nähle and Kossert (In Press), ^{41}Ca with 0.38% uncertainty by Kossert et al. (2009), ^{63}Ni with 0.60% uncertainty by Collé et al. (2008) and Nähle and Kossert (2011), ^{87}Rb with 0.64% uncertainty by Kossert (2003), ^{89}Sr with 0.15% uncertainty by Nähle and Kossert (2011), ^{90}Y with 0.12% uncertainty by Kossert and Schrader (2004), ^{125}Sb (^{125m}Te) in equilibrium with <1.5% uncertainty by Grau Carles et al. (1998), ^{153}Sm with 0.19% uncertainty by Schötzig et al. (1999), ^{177}Lu and ^{188}Re with 0.22% and 0.3% uncertainty, respectively by Schötzig et al. (2001), ^{237}Np with <0.2% uncertainty by Günther (2000), ^{204}Tl with <0.3% uncertainty by Hult et al. (2000), ^{210}Pb with 2.4% uncertainty by Laureano-Perez et al. (2007), and ^{241}Pu with 1.06% uncertainty by Kossert et al. (2011a), among others. Günther (2002b) reports excellent agreement between the CIEMAT/NIST and $4\pi\beta-\gamma$ standardization method with the following deviations between the two methods expressed as a percent: ^{134}Cs (<0.3%), ^{153}Sm (<0.2%), ^{169}Er (<0.2%), ^{177}Lu (0.6%), and ^{188}Re (0.2−1.0%). It is a common practice for researchers to employ more than one liquid scintillation standardization method together with the CIEMAT/NIST method in the standardization of a radionuclide, such as the TDCR method or $4\pi\beta-\gamma$ coincidence counting technique. This further demonstrates the robustness of the methods used and reconfirms the standardization determinations.

5. Ionization Quenching and Efficiency Calculations (^{3}H or ^{54}Mn as the Tracer)

The theoretical calculation of the counting efficiency of the nuclide under investigation and of the tracer nuclide (usually ^{3}H for β- and β/γ-emitters or potentially ^{54}Mn for nuclides of low atomic number that decay by electron capture) is carried out using the basic equation of Grau Malonda and coworkers, Eqn 7.93 or 7.94, and variations of the equation depending on the decay scheme of the radionuclide under measurement (*e.g.*, Eqns 7.95 and 7.96). A key factor in the theoretical calculation is the computation of the ionization quench function $Q(E)$, which has been revisited by several researchers including Los Arcos and Ortiz (1997), Cassette et al. (1998), Günther (1998),

Rodríguez Barquero et al. (1998), Ceccatelli and DeFelice (1999), Grau Malonda (1999), Grau Malonda and Grau Carles (1999, 2000, 2008), Grau Carles and Grau Malonda (2001, 2006), and García and Grau Malonda (2002), Grau Carles et al. (2004), Grau Carles et al. (2006), Zimmerman (2006a,b), Grau Malonda et al. (2006), Grau Carles (2006a,b), Kossert and Grau Carles (2006), Bagán et al. (2008), Kossert and Grau Carles (2008, 2010), and Bignell et al. (2010a,b).

Ionization quenching is defined and discussed in detail in Section IV. In brief, as described by Bignell et al. (2010a,b), ionization quenching in scintillators is a reduction in the luminosity (photon intensity) associated with a high density of excited molecules caused by a large LET to the scintillant. The high density of excited molecules results in a transfer of energy from one excited molecule to another resulting in super-excitation of a molecule and its ionization. Thus, this ionization, caused by the nuclear radiation as it travels through the scintillator solvent, results in a reduction in the amount of energy transferred from the charged particle to the fluor molecules and a consequent reduction in the photon intensity emitted by the scintillation fluor. As described by Grau Malonda (1999), the fluorescence yield or number of photons $L(E)$ produced by an ionizing particle traveling through a liquid scintillator is a nonlinear function of the particle energy (E). The nonlinearity increases with the linear energy transfer (LET) or stopping power of the particle. Therefore, a low-energy electron or beta particle will cause higher ionization quenching than a higher-energy beta particle. Radionuclides decaying by electron capture undergo, as a consequence of the capture of an atomic electron by the nucleus, a cascade of atomic electron transitions resulting in the emission of X-rays, Auger electrons, and Coster–Kronig electrons. The Auger and Koster–Cronig electrons are of low energy (See Chapter 1) and relatively high LET, and the X-rays can produce Compton and photoelectrons, all of which have a high LET relative to the higher-energy beta particles emitted by most beta-emitting radionuclides.

According to Birks (1964), the specific fluorescence or number of photons produced per particle path length of travel, dL/dx, is defined by

$$\frac{dL}{dx} = \frac{\eta_o \dfrac{dE}{dx}}{1 + kB\dfrac{dE}{dx}} \tag{7.103}$$

where η_0 is the scintillation efficiency or number of fluorescence photons emitted per unit of absorbed energy, dE/dx is the radiation stopping power (*i.e.*, stopping power of the scintillator for one beta particle of energy E) in units of MeV/cm or MeV cm^2/g (see Chapter 1, Section XIV), and kB is the ionizing quench parameter or constant with units of cm/MeV or g/MeV cm^2.

In the absence of ionization quench the specific fluorescence would be defined as

$$\frac{dL}{dx} = \eta_0 \frac{dE}{dx} \tag{7.104}$$

and the term $[1 + kB(dE/dx)]^{-1}$ of Eqn 7.103 is the reduction in fluorescence due to ionization quenching. The formula usually used for the ionization quench function in the CIEMAT/NIST calculation of counting efficiency is the formula of Birks (1964):

$$Q(E) = \frac{1}{E}\int_0^{E_{\max}} \frac{dE}{1 + kB(dE/dx)} \tag{7.105}$$

According to Grau Malonda and Grau Carles (1999), the ionization quench function $Q(E)$ is determined by applying the Birks formula (Eqn 7.105) of which the stopping power is approximated to a polynomial equation. Also, the ionization quench function is evaluated analytically whereby $Q(E)$ is expressed in terms of kB. An empirical equation for $Q(E)$ is expressed by Grau Malonda and Grau Carles (1999) as a quotient of polynomial equations, that are fitted for different kB values between 0.001 and 0.020 g/MeV cm^2. They also analyzed the influence of the tracer nuclide (*i.e.*, ^{3}H or ^{54}Mn) and demonstrated that ^{3}H remains the recommended tracer for the analysis of nuclides that undergo beta decay, while ^{54}Mn provides a more robust standardization of certain nuclides that decay by electron capture and possess a low atomic number close to that of iron. Also, they note that the calculated formula for $Q(E)$ and kB value must be the same for the tracer nuclide and the radionuclide under measurement. Computer programs BETAKB and EMISKB are provided by Grau Malonda (1999) for the calculation of the theoretical counting efficiencies of radionuclides that undergo beta-decay or electron capture decay, respectively, with subroutines for the computation of the ionization quench function $Q(E)$ for a given Birks parameter kB (see also Los Arcos and Ortiz, 1997). Günther (1998) also demonstrated the improved accuracy of standardization of the electron-capture nuclides ^{55}Fe and ^{65}Zn when ^{54}Mn is used as the tracer.

In a review of the CIEMAT/NIST and TDCR methods, Grau Carles and Grau Malonda (2001) present new concepts to improve the robustness of the radionuclide standardization methods. Currently, in all of the models, the counting efficiency is computed on the basis of the photoelectron output of the photomultiplier (PM) photocathode. Although the results of the model calculations agree well with the experimental results, they propose that the correct calculated theoretical counting efficiency should be based on the final PM anode output rather than on the photocathode or any dynode outputs. Consequently, modifications to the theoretical counting efficiency calculations and determinations of the optimum kB parameter are proposed (Grau Carles and Grau Malonda, 2001, and García and Grau Malonda, 2002). Günther (2002a) provides a review of the prospects for the universal application of the CIEMAT/NIST method. In general, the Visual Basic CN2001 program has been useful for the calculation of theoretical counting efficiencies of the nuclide under measurement versus the efficiency of the ^{3}H tracer of nuclides decaying by β, β/γ, EC, EC-γ, and for isomers and nuclides with mixed decay schemes. It is available from the Physikalisch-Technische Bundesanstalt (PTB), Bundesalee 100, 38116 Braunschweig, Germany, and it is based on the CIEMAT programs EFFY (García Toraño and Grau Malonda, 1985), EMI (Grau Carles et al., 1994b), CEGA2, and KB (Los Arcos and Ortiz, 1997). In his review, Günther (2002a)

summarizes that pure beta emitters present no problem with activities determined with uncertainties within 0.2% and 0.5%. The standardization of some pure gamma emitters (*e.g.*, ^{93m}Nb are determined with 100% efficiency). Beta/gamma emitters are determined with as high precision as pure beta emitters. The EC nuclides do present a problem with higher levels of uncertainty; however, better models such as those proposed by Grau Malonda and Grau Carles (2000), the EMI2 program of Grau Malonda et al., (1999), and the use of ^{54}Mn as a tracer for some EC nuclides (not mentioned in the review) were designed to reduce uncertainties in the standardization of electron-capture nuclides. The CIEMAT/NIST method is, in most cases, not called for when the activities of alpha emitters are needed, as the liquid scintillation counting efficiency of alpha emitters are generally close to unity. However, when the alpha emission is part of a complex decay scheme, such as ^{237}Np/^{233}Pa, alpha transitions are included in the CN2001 program of the CIEMAT/NIST method (Günther, 2000, 2002a).

The higher levels of uncertainty in the standardization of electron-capture radionuclides by the CIEMAT/NIST or low-energy beta emitters by the TDCR method have motivated much research toward improving the efficiency calculations. (The TDCR method is discussed further on in this chapter; it is a model-based method similar to the CIEMAT/NIST method in that both methods involve theoretical calculations of the detection efficiency.) With the objective of reducing the uncertainties in the activity determinations, Grau Carles et al. (2004, 2006) and Grau Carles and Grau Malonda (2006) revisited the problem of ionization quenching and photoionization-reduced energy in liquid scintillation counting of electron-capture decaying radionuclides such as ^{55}Fe, ^{51}Cr, and ^{54}Mn. Their studies provided a more detailed simulation of the photoionization process in the atomic rearrangement detection model for these electron-capture nuclides. Further studies were focused on Monte Carlo calculations of spectra and photon interaction probabilities in liquid scintillators (Zimmerman, 2006a,b and Cassette et al., 2006) for X-ray and gamma-ray-emitting nuclides, such as the electron-capture nuclide ^{54}Mn. Also, atomic electron rearrangement pathways were modeled and the MOYEN computer program developed (Grau Malonda et al., 2006) for the computation of the energy emissions in LMM Auger transitions upon which the counting efficiency calculations depend strongly. The energy of these transitions was computed for the EC nuclides ^{55}Fe and ^{125}I. A computer program, EMILIA, that includes the computation of the counting efficiency for the atomic rearrangement detection models, is reported by Grau Carles (2006a), which improved the computed counting efficiency of low-Z electron-capture nuclides under moderate quenching. Kossert and Grau Carles (2006) utilized EMILIA to compute the detection efficiency of the low-Z EC nuclides ^{54}Mn, ^{55}Fe, and ^{65}Zn. They also demonstrated that ^{54}Mn could be used as a tracer nuclide for the standardization of ^{55}Fe. They consider a future application would be to standardize ^{3}H by the CIEMAT/NIST method using ^{54}Mn as the tracer nuclide, as the uncertainty of ^{54}Mn activity standards ($< \pm 0.7\%$) is lower than for ^{3}H standards. The standardization of ^{3}H using ^{54}Mn as a tracer was reported with a relative standard uncertainty of $\pm 1.01\%$ by Nähle et al. (2010). Also, Ratel (2008) underscored the potential of ^{54}Mn as a tracer nuclide instead of ^{3}H to increase the precision of the liquid scintillation standardization of EC nuclides, such as ^{55}Fe. The computer program, MICELLE, reported by Grau Carles (2008), extends the computation of the liquid scintillation counting efficiency to electron-capture radionuclides of atomic number $30 \leq Z \leq 54$. The program considers all subshells involved in the atomic electron rearrangements following electron capture. MICELLE also simulates samples in the gel phase, as the micelle size of gel scintillators can have an effect on the counting efficiency. The micelle program applied to the standardization of EC radionuclides ^{109}Cd and ^{125}I yielded considerable improvements in the relative standard uncertainties, particularly for ^{109}Cd ($\pm 0.5\%$) when a kB value of 0.0110 cm/MeV was used for the Birks parameter. They report a reduction in the uncertainty in the standardization of ^{125}I, although there was a large dependence of the analysis on the kB value. The uncertainty in the determination of ^{125}I was improved by about 1% (Grau Malonda and Grau Carles, 2008) when models of the simultaneous interactions of electrons in liquid scintillator were included in the efficiency calculation. The simultaneous interaction of electrons produces an overlap of distributions of excited solvent molecules and an increase in the excitation density, which required a modification of the ionization quenching factor in the calculations.

A new approach to the problem of elevated uncertainties in the standardization low-energy beta emitters when the TDCR method is applied and in the standardization of some electron-capture radionuclides when the CIEMAT/NIST method is applied was presented by Grau Carles and Grau Malonda (2010). This work considers the need to expand the TDCR and CIEMAT/NIST methods by generalizing the equations used in the model and to analyze the influence of ionization and chemical quench on the spectra and counting efficiency. They studied the influence of photomultiplier response in one, two, and three PMT systems. Particularly the effect of electronic noise discriminator level on both experimental spectra and counting efficiency is considered. In a personal communication of the writer with Grau Malonda (2010), many of the problems with the model arise from the discrepancy between the experimental spectra and the computed one. In other words, when the total efficiency is calculated for beta emitters, the full spectral area is computed; however, when the experimental radionuclide is counted, only the pulses with pulse heights greater than the noise discriminator level are counted. Thus, for example, the counts for the tritium spectrum turn out to be lower than the computed total spectrum. Low counts yield low efficiency; and a lower efficiency yields a higher figure of merit and consequently a higher figure of merit for the radionuclide to be standardized (*e.g.*, ^{125}I) yielding finally a higher activity determination. Accordingly, an improvement in the accuracy of the liquid scintillation standardization of radionuclides rests with the spectral analysis (personal communication with Grau Malonda, 2010).

The CIEMAT/NIST method has been applied to the standardization of radionuclide mixtures. Early work by Grau Carles (1994) describes computer programs for the

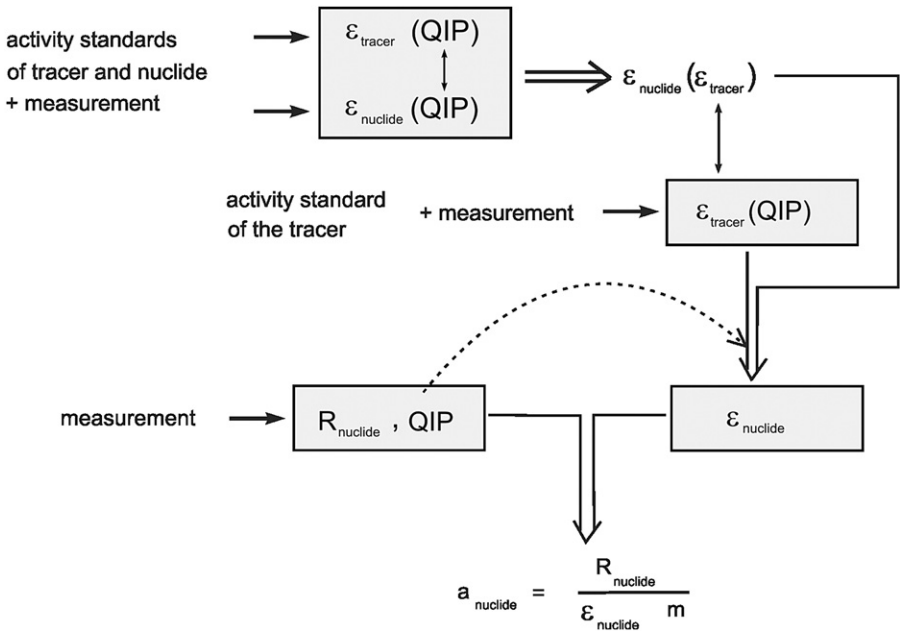

FIGURE 7.71 Secondary standard measuring procedure. *R* denotes the count rate, *QIP* the quench-indicating parameter, ε the counting efficiency, a_{nuclide} is the solution activity concentration of the nuclide under investigation, and *m* is the source mass. *(From Kossert, 2006. Reprinted with permission from Elsevier © 2006)*

deconvolution of ^{89}Sr, ^{90}Sr, and ^{90}Y mixtures with the liquid scintillation standardization of the components by the CIEMAT/NIST method. This was expanded and improved to include the standardization of more complex mixtures of several (up to five) radionuclides (Grau Carles, 1996). Günther (2002c) and Rodríguez Barquero et al. (2004) measured ^{32}P and ^{33}P activities where ^{33}P is an impurity. The relative standard uncertainties for the determination were 0.32% for ^{32}P and 1.6% for ^{33}P impurity. A triple exponential mathematical expression is described by Altsitzoglou (2004) to standardize ^{32}P in the presence of ^{33}P and ^{35}S. Van Wyngaardt and Simpson (2006a) and Van Wyngaardt et al. (2008) applied the liquid scintillation TDCR and CIEMAT/NIST standardization methods to resolved mixtures of ^{14}C and ^{63}Ni and to dual component mixtures of ^{32}P, ^{33}P, and ^{35}S, respectively. Mixtures of short-lived components were resolved for the CIEMAT/NIST standardization of ^{18}F (Capogni et al., 2006) and ^{64}Cu (Capogni et al., 2008).

B. New Method of Secondary Standardization by LSC

A new secondary standard measurement method, which utilizes liquid scintillation counting, was reported by Kossert (2006). The method is based on the CIEMAT/NIST method; however, it is distinctly different from the CIEMAT/NIST method in that the efficiency curve, *i.e.*, the counting efficiency of the nuclide under investigation as a function of the tritium counting efficiency or $\varepsilon_{\text{nuclide}}(\varepsilon_{\text{tracer}})$, is not calculated, but rather, it is determined experimentally. The method is illustrated in Fig. 7.71. Notice the similarity between Fig. 7.70, that of the CIEMAT/NIST method, and Fig. 7.71, that of the new secondary standardization method. In the new method of secondary standardization, there is no calculation of figure of merit (*M*); there is instead, the experimental determination of the quench-indicating parameter (*QIP*).

The new method of secondary standardization of Kossert (2006) is described, in a stepwise fashion, as follows:

1. The first step, as illustrated in Fig. 7.71, involves the measurement of the counting efficiency of the nuclide under investigation, $\varepsilon_{\text{nuclide}}$, as a function of a quench-indicating parameter (*QIP*). To achieve this, a set of quench standards of the nuclide under investigation is prepared. This requires the preparation of a few vials (approx. 10 vials), each containing the scintillation cocktail and a known amount of an activity standard solution. Increasing amounts of quenching agent (*e.g.*, nitromethane) are added to each counting vial, with the exception of the first vial, to provide counting vials with decreasing detection efficiencies (see Section V.D). Counting of these standards in a liquid scintillation analyzer will provide the net count rates, (*e.g.*, CPM) and values of a quench-indicating parameter (QIP), such as H#, SQP(E), or tSIE, depending on the instrument used and its external standard. From the net count rates and the known activities (DPM) in each vial, the detection efficiencies of each vial are easily calculated (*i.e.*, $\varepsilon_{\text{nuclide}} = \text{CPM/DPM}$). The same procedure is carried out with a set of quenched standards prepared with ^{3}H, which serves as the tracer nuclide. The counting of the tritium nuclide standards will yield distinct counting efficiencies, $\varepsilon_{\text{tracer}}$, for each vial as well as varying QIP values.
2. The two functions $\varepsilon_{\text{nuclide}}(QIP)$ and $\varepsilon_{\text{tracer}}(QIP)$ obtained from step (1) above are linked by the quench-indicating parameter *QIP* to provide a working 'efficiency curve' of $\varepsilon_{\text{nuclide}}(\varepsilon_{\text{tracer}})$ as illustrated in Fig. 7.72 for the case of ^{125}I as an example of a nuclide under investigation. The best fit for the function $\varepsilon_{\text{nuclide}}(\varepsilon_{\text{tracer}})$ for the working 'efficiency curve' is obtained via a fourth- order polynomial, which provides the counting efficiency of the nuclide, $\varepsilon_{\text{nuclide}}$, for a specific counting efficiency of the tritium tracer, $\varepsilon_{\text{tracer}}$, given by the equation

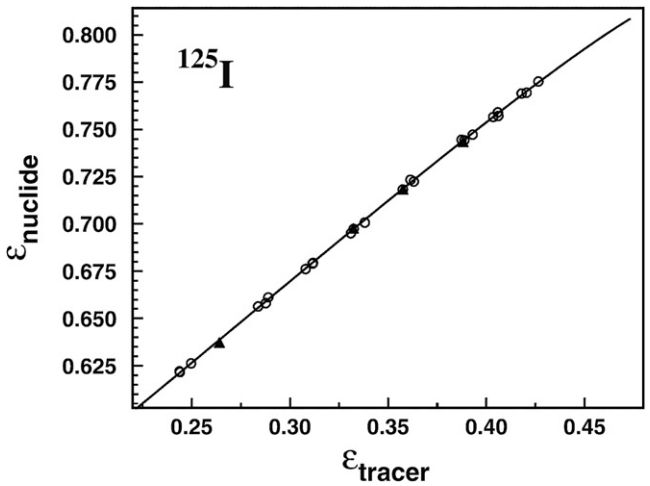

FIGURE 7.72 'Efficiency curve' of $\varepsilon_{\text{nuclide}}(\varepsilon_{\text{tracer}})$ for ^{125}I in 15 mL of Ultima Gold™ cocktail plus 1 mL of water. The empty circles represent the determined efficiencies, and the 'efficiency curve' was used to calibrate another solution of ^{125}I, which was also calibrated by coincidence counting. The solid triangles represent the results of efficiencies determined with the second solution of ^{125}I. *(From Kossert, 2006. Reprinted with permission from Elsevier © 2006)*

$$\varepsilon_{\text{fit}} = \varepsilon_{\text{nuclide}}(\varepsilon_{\text{tracer}}) = \sum_{i=0}^{4} p_i(\varepsilon_{\text{tracer}})^i \qquad (7.106)$$

Notice the similarity of Eqn 7.106, which uses the experimentally determined QIP as a link between the two detection efficiencies for this new secondary standardization method and Eqn 7.102, which uses the calculated figure of merit (M) as the link in the CIEMAT/NIST primary standardization method.

3. This following step need not be carried out during the same period of time as the above preparation of the 'efficiency curve'. As pointed out by Kossert (2006), this next step can be performed even years later. This next step involves the preparation of the ^{3}H 'calibration curve', which is the repeated measurement of the counting efficiency of the tracer nuclide, $\varepsilon_{\text{tracer}}$, expressed as a function of the quench-indicating parameter (QIP). The newly measured 'calibration curve', $\varepsilon_{\text{tracer}}(QIP)$ is required to account for any instability of the liquid scintillation counter in the event of and changes in time of the instrument response and measured spectra.
4. The sample of the nuclide under investigation is now counted, and the sample count rate, R_{nuclide}, and sample quench-indicating parameter (QIP) are measured and recorded. From the magnitude of the QIP, the corresponding value of the tracer counting efficiency can be obtained from the ^{3}H 'calibration curve' prepared in step (3). From the known tracer efficiency, the corresponding nuclide efficiency, $\varepsilon_{\text{nuclide}}$, can be obtained from the 'efficiency curve' measured in step (2).
5. With the efficiency of the nuclide under investigation, $\varepsilon_{\text{nuclide}}$, obtained from the 'efficiency curve' and the nuclide count rate, R_{nuclide}, the activity concentration of the nuclide, a_{nuclide}, is calculated as illustrated in Fig. 7.71 according to the equation $a_{\text{nuclide}} = R_{\text{nuclide}}/(\varepsilon_{\text{nuclide}}m)$, where m is the mass of the sample counted.

There are certain specifics of this secondary standardization method of Kossert (2006), which should be considered, and these are the following:

a. The sample scintillation cocktail composition (*i.e.*, cocktail and sample chemistry) and the sample geometry (*i.e.*, vial size and type and sample−cocktail volume or mass) must be very similar for all measurements.
b. The period between the measurements the tracer nuclide, and the nuclide under investigation should be short (*i.e.*, within a period of only a few days).
c. The duration between the determination of the 'efficiency curve' and the measurements of the tracer nuclide and the nuclide under investigation is unlimited. The 'efficiency curve' is even valid for application with other liquid scintillation counters.
d. The 'calibration curve' of $\varepsilon_{\text{tracer}}(QIP)$, *e.g.*, $\varepsilon_{\text{tritium}}$ vs. SQP(E) or $\varepsilon_{\text{tritium}}$ vs. tSIE, is easily measured with weighed aliquots of a standard solution of tritiated water added to cocktail in a set of about ten vials to which increasing amounts of nitromethane are added.
e. This following point is one of the key advantages of this method: The uncertainty of the tracer activity (*e.g.*, tritium) cancels out, if the aliquots used for the determination of the 'efficiency curve' and the 'calibration curve' stem from the same standard solution. In other words, if the same standard solution of the tracer is used to prepare the 'efficiency curve' and the 'calibration curve', this method of secondary standardization can be applied even if the true value of the activity concentration of the tracer nuclide is unknown.
f. The method can be applied to the activity determinations of radionuclides with low activity concentrations (*e.g.*, 10 Bq/g).

Kossert (2006) tested this secondary standard method against several nuclides standardized by accepted primary standardization methods. This secondary standardization method tested against ^{125}I primary standard yielded an uncertainty of the activity determination lower by only 0.03% of that of the primary standard. Likewise, the activity of ^{65}Zn was measured by this secondary standardization with an uncertainty of only 0.05% lower than that determined by primary standardization. Other nuclides tested by this secondary standardization method were ^{54}Mn, ^{57}Co, ^{67}Ga, ^{85}Sr, ^{88}Y, ^{109}Cd, and ^{111}In. The reader is invited to refer to the work of Kossert (2006) for specifics on these radionuclides. In a subsequent work, Kossert et al. (2006) reported the secondary standardization of ^{65}Zn by this method with an uncertainty of 0.4%.

C. Triple-to-Double Coincidence Ratio (TDCR) Efficiency Calculation Technique

The early works of Steyn (1956), Flynn and Glendenin (1959) and Radoszewski (1964) can be given the credit of initiating the possibility of utilizing a liquid scintillation analyzer for the absolute measurement of beta-emitting radionuclides (personal communication of the writer with Ryszard Broda, 2004). The first triple photomultiplier liquid scintillation counting system

with an electronic circuit having two different coincident outputs was reported originally by Schwerdtel (1965, 1966a,b); however, the method for the determination of the absolute activities of radionuclides was yet to be developed. An important contribution was made by Kolarov, Le Gallic, and Vatin (1970), who proposed a liquid scintillation detection efficiency model used in the current triple-to-double coincidence ratio (TDCR) efficiency calculation technique. Pochwalski (1978) presented the TDCR method as his thesis; he worked many years in Radoszewski's nuclear metrology laboratory in the Institute of Nuclear Research at Świerk, Poland. A triple PMT detector design and the original version of the method of radionuclide standardization now referred to as the TDCR efficiency calculation technique were published in a national report in 1979 by Pochwalski and Radoszewski and in the international journals by Pochwalski, Broda, and Radoszewski (1988). Thus, the TDCR efficiency calculation technique was invented in Poland. The integration of theoretical calculations of counting efficiency based on the radiation emissions of the radionuclide under investigation with the experimental data obtained from the LSA, somewhat similar to the approach taken in the CIEMAT/NIST efficiency tracing method described earlier, was reported by Broda et al. (1988), Grau Malonda and Coursey (1988), and Grau Carles and Grau Malonda (1989). These papers formed the basis for subsequent research and development in this method, which is described subsequently.

1. Principles

The liquid scintillation analyzer (LSA), in this case, is different from the conventional and more common commercially available equipment, described previously in this chapter. The TDCR efficiency calculation technique requires an LSA equipped with three photomultiplier (PM) tubes and two different coincident outputs. Such equipment is generally designed and manufactured by those laboratories dedicated to radionuclide standardization, such as national institutes of standards and research. Numerous national laboratories have reported the construction and installation of 3-PM liquid scintillation counting systems for radionuclide standardization in numerous countries of the world including Pochwalski et al. (1988), Cassette and Vatin (1992), Cassette and Bouchard (2003), Zimmerman et al. (2004), Lee et al. (2004), Hwang et al. (2004), Razdolescu et al. (2006), Ivan et al. (2008), Qin et al. (2008), Johansson and Sephton (2010), and Nähle et al. (2010). A commercially available liquid scintillation analyzer, the Hidex 300 SL (Hidex, Turku, Finland) manufactured with three photomultiplier tubes, which utilizes the TDCR technique, was released in 2008 (Haaslahti, 2010). The performance of the Hidex 300 SL is described by Kharitonov et al., (2011). A schematic diagram of the workings of an instrument, referred to as the TDCR liquid scintillation counter, which is applied to the standardization of radionuclides, is illustrated in Fig 7.73, and an illustration of a commercially available three-photomultiplier detector arrangement is illustrated in Fig. 7.74. The optical chamber of the LSA accommodates a standard 20-mL liquid scintillation counting vial, and facing the vial are three photomultiplier tubes at 120° angles to each other. With such an arrangement, dual and triple phototube coincidence outputs are possible as a requirement for the TDCR method. For example, the two coincident outputs used by Pochwalski, Broda, and Radoszewski (1988) from photomultiplier tubes A, B, and C were the count rates from the triple coincidences (ABC), the three double coincidences AB, BC, and AC, and the count rate from the logic sum of the three different double coincidences (AB+BC+CA). Since this initial report of the TDCR method, many developments have been made. Advances following the development of the TDCR radionuclide standardization method are described by Simpson and Meyer (1992b and 1994b), and reviews on the theory and

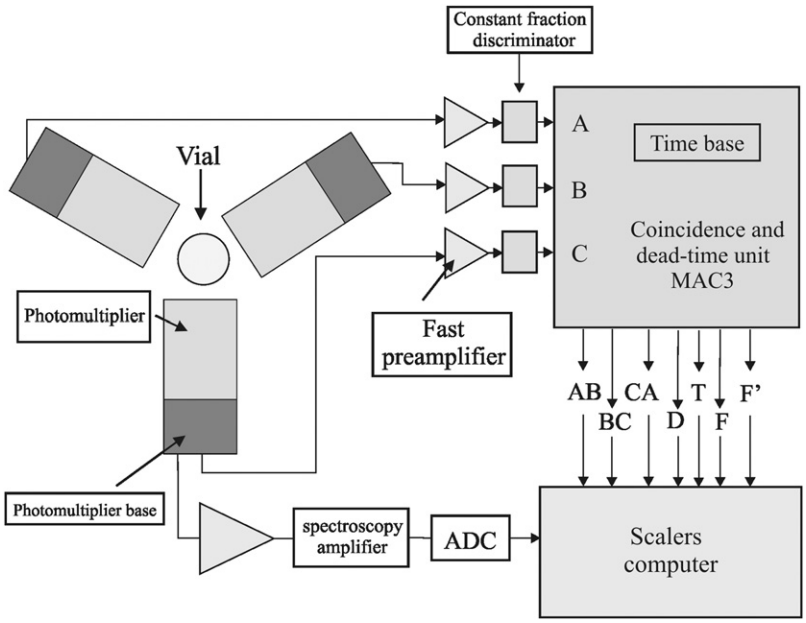

FIGURE 7.73 Diagram of the TDCR system at the Radioisotope Metrology Laboratory, CNEA, Argentina. MAC3 is the electronic coincidence module of Bouchard and Cassette (2000) for the processing of the pulses delivered by the three photomultipliers including double coincidence outputs AB, BC, and CA, the logical sum of the double coincidences D, and the triple coincidences T. *(From Arenillas and Cassette 2006. Reprinted with permission from Elsevier © 2006)*

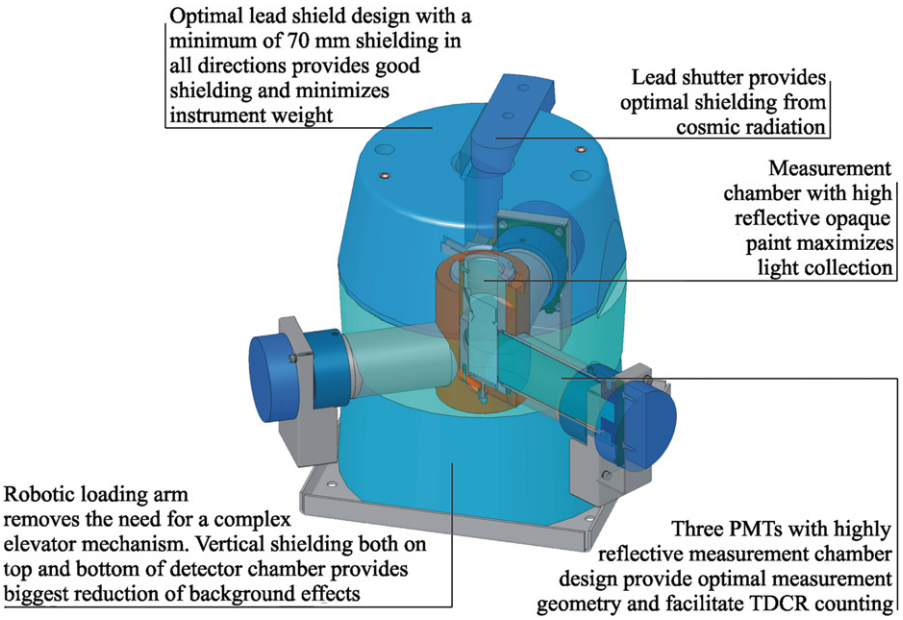

FIGURE 7.74 Hidex 300 SL detector structure. *(Courtesy of Hidex, Turku, Finland. Printed with permission)*

practice of TDCR are available from Broda (2003), Lee et al. (2004), Broda et al. (2007), Nähle and Kossert (2011), and Cassette (2011) from which the subsequent treatment and mathematical notation utilized in TDCR are taken.

The triple-to-double coincidence ratio (TDCR) method was developed for the direct determination of the absolute activities of beta- and EC-decaying radionuclides in liquid scintillator cocktail. Like the CIEMAT/NIST method, described previously in this chapter, the TDCR technique combines experimental data with theoretical calculations of the radionuclide detection efficiency. Complete data of the radionuclide decay scheme is used to calculate the counting efficiencies based on a physical and statistical model of the beta-, Auger-, and Compton electron interactions with scintillation cocktail. The TDCR method utilizes a physical and statistical model of the distribution of scintillation photons and their detection probabilities in a three-photomultiplier detector system (Broda, 2003). The ionization quenching phenomena, which is the nonlinearity of the scintillator response as a function of the linear energy transfer (LET) or stopping power of the interacting electrons in fluor cocktail, discussed previously in the CIEMAT/NIST method, is also required in the TDCR technique for the theoretical calculations of counting efficiencies.

In the case of a pure β-emitting source on which are viewed simultaneously three normalized photomultiplier tubes, the double-tube coincidence count rate N_d and the triple-tube coincidence count rate N_t are defined as

$$N_d = N_0\varepsilon_d \tag{7.107}$$

$$\text{and } N_t = N_0\varepsilon_t \tag{7.108}$$

where N_0 is the disintegration rate of the radionuclide source and ε_d and ε_t are the true double-tube and triple-tube counting efficiencies, respectively. The detection efficiencies are determined without recourse to prior instrumental calibration or the use of any reference standards. Rather, the detection efficiencies are determined in an absolute manner by combining experimental measurement with theory (Simpson and Morris, 2004b). The detection efficiencies, ε_d and ε_t of Eqns 7.107 and 7.108, are unknown; however, the ratio (R) of the count rates N_t/N_d is determined or measured experimentally with the liquid scintillation counter. For a large number of disintegration rates, the ratio of the experimentally determined triple coincidence count rate to double coincidence count rate, N_t/N_d, converges toward the ratio of counting efficiencies, as described by Broda et al. (2007). Thus, using the notation of Simpson and Morris (2004b) and Lee et al. (2004), the experimentally determined ratio (R) can be written as

$$R = \frac{N_t}{N_d} = \frac{N_0\varepsilon_t}{N_0\varepsilon_d} = \frac{\varepsilon_t}{\varepsilon_d} \tag{7.109}$$

where N_0 is the radionuclide activity, and the product of activity and detection efficiency (*i.e.*, $N_0\varepsilon_t$ and $N_0\varepsilon_d$) is count rate. As in the previously described CIEMAT/NIST radionuclide standardization method of efficiency tracing (Section IX.A), theoretical counting efficiencies are calculated and these are fitted to experimental data. The theoretical counting efficiencies ε_d and ε_t for a pure β-emitter are described, according to a 'free parameter' model by Grau Malonda and Coursey (1988) and Simpson and Meyer (1992a–c) as

$$\varepsilon_2 = \int_0^{E_{\max}} N(E)[1 - \exp\{-P\cdot F(E)\cdot E\}]^2 dE, \tag{7.110}$$

$$\text{and } \varepsilon_3 = \int_0^{E_{\max}} N(E)[1 - \exp\{-P\cdot F(E)\cdot E\}]^3 dE, \tag{7.111}$$

where ε_2 and ε_3 are the double- and triple-photomultiplier tube efficiencies, respectively, $N(E)$ represents the number of

β particles of energy between E+dE of the β-particle spectrum calculated according to the Fermi theory of decay (Fermi spectrum), E_{max} is the maximum β-particle energy, $F(E)$ is the relative scintillation efficiency Gibson (1968) and P is the figure of merit or free parameter, the only unknown variable of the theoretical efficiency equations. The figure of merit (free parameter) was defined previously in Section IX.A concerning the CIEMAT/NIST efficiency tracing technique where a "system" figure of merit M or λ was used, whereby $P = 1/2M$ for a double-phototube system and $P = 1/3M$ for a triple-phototube system (Simpson and Meyer, 1992b), and $M = \lambda$. The theoretical efficiencies, therefore, are a function of a single unknown parameter P. Thus, as described by Simpson and Morris (2004a,b) and Van Wyngaardt and Simpson (2009), the efficiencies can be expressed theoretically as a function of a single floating parameter P, the so-called 'figure-of-merit', which is effectively a measure of the electron emission process and the consequent photon output. Thus, a single value of P must be found iteratively to fit the experimentally measured count ratio to solve the equation

$$R = \frac{N_t}{N_d} = \frac{\varepsilon_t(P)}{\varepsilon_d(P)} \tag{7.112}$$

The theoretical counting efficiencies as a function of the figure of merit, P, are calculated and the value of P is obtained by mathematical iteration to best fit the experimentally determined triple-to-double count ratio of Eqn 7.112. As noted by Simpson and Meyer (1994b) and Simpson and Morris (2004a,b), the figure of merit P should be single-valued for a given value of R. With the determined value of P for a given experimental sample, the activity of the radionuclide source can then be calculated using Eqns 7.107 and 7.108 or

$$N_0 = \frac{N_d}{\varepsilon_d} = \frac{N_t}{\varepsilon_t} \tag{7.113}$$

2. Free-Parameter Model

The calculation of the theoretical efficiencies according to Eqns 7.110 and 7.111 are similar to Eqn 7.94 previously described in Section IX.A. According to Grau Carles and Grau Malonda (2001), Lee et al. (2004), Nähle and Kossert (2011), and Cassette (2011), the equations applicable to the theoretical counting efficiency calculations for beta-particle emitters and radionuclides that decay by electron capture (EC) in a two- or a three-photomultiplier system are the following:

$$\varepsilon_2 = \int_0^{E_{max}} S(E)(1 - e^{-EQ(E)/2M})^2 dE \tag{7.114}$$

for two photomultipliers working in coincidence, and

$$\varepsilon_T = \int_0^{E_{max}} S(E)(1 - e^{-EQ(E)/3M})^3 dE \tag{7.115}$$

for three photomultipliers in coincidence, whereas the logic sum of double coincidences in a 3-PM counter is calculated as

$$\varepsilon_D = \int_0^{E_{max}} S(E)[3(1 - e^{-EQ(E)/3M})^2 - 2(1 - e^{-EQ(E)/3M})^3] dE \tag{7.116}$$

Thus, the triple-to-double coincidence ratio (TDCR) is expressed as

$$\frac{N_T}{N_D} = \frac{\varepsilon_T}{\varepsilon_D} = \frac{\int_0^{E_{max}} S(E)(1 - e^{-EQ(E)/3M})^3 dE}{\int_0^{E_{max}} S(E)[3(1 - e^{-EQ(E)/3M})^2 - 2(1 - e^{-EQ(E)/3M})^3] dE} \tag{7.117}$$

where the variables are the same as those defined previously for Eqs. 7.93 and 7.94 in Section IX.A, namely, E_{max} is the maximum beta-particle energy, $S(E)$ is the normalized energy spectrum transferred to the liquid scintillation cocktail, including energy from beta particles as well as Auger-, Coster–Kronig-, and conversion electrons, and photo- and Compton electrons arising from X-ray- and gamma-ray-interactions in LS cocktail [the term $S(E)$ was previously referred to as $N(E)$ Eqns 7.93 and 7.94], $Q(E)$ is the ionization quenching correction factor, and M is the free parameter. The free parameter was expressed in Eqns 7.93 and 7.94 as λ; the expression for the free parameters M or λ depends on the user (*i.e.*, $M = \lambda$). The above calculations are based on a definition of the figure of merit (free parameter) as a computation of the β-particle energy in keV required to produce one photoelectron at the output of the photocathode or the photoelectron yield at the first dynode. The free parameter has units of electrons/keV.

The ionization quench function $Q(E)$ of Eqn 7.117 is determined by applying the Birks formula described previously by Eqn 7.105. The Birks formula expresses the reduction in fluorescence due to ionization quenching $[1 + kB(dE/dx)]^{-1}$ where kB is the ionization quench parameter or constant with units of cm/MeV or g/MeV cm^2, and dE/dx is the radiation stopping power of the scintillator with units of MeV/cm or MeV cm^2/g, as discussed previously with respect to Birks definition of specific fluorescence and ionization quenching according to Eqns 7.103 to 7.105. As described by Cassette (2011), Broda et al. (2007), and Lee et al. (2004), the left term of Eqn 7.117 (N_T/N_D) is measured experimentally, and the right term ($\varepsilon_T/\varepsilon_D$) is calculated. As the beta-particle energy distribution $N(E)$ for a given radionuclide is known, and the kB ionization quench parameter is an assumed constant, the value of the free parameter must be found, whereby the calculated $\varepsilon_T/\varepsilon_D = N_T/N_D$, which is the experimentally measured triple-to-double count ratio.

3. Experimental Conditions

The practical aspects of the TDCR method are dealt with in detail by Broda et al. (2007). Some of the major points of the TDCR method are presented here.

Simpson and Meyer (1994b) demonstrated that any change in the counting efficiency due to any altered chemical

quenching state of the sample will manifest itself in the measured triple and double counting rates, thereby producing a different value of R. They demonstrated, therefore, that the figure of merit P extracted by this method for a given sample includes effects due to chemical quenching so that the calculated sample activity N_0 is independent of chemical quench effects. Using wide ranges of $CHCl_3$ as a quenching agent (18−2287 mg $CHCl_3$ load), they demonstrated no significant quench effect on the calculated activity of ^{14}C. Also, smaller $CHCl_3$ quenching agent loads (13−409 mg) had no effect on the calculated activity of ^{63}Ni, and chloroform loads of up to 60 μL and 270 μL produced no effect on the calculated activities of ^{99}Tc and ^{3}H, respectively.

The calculation of the counting efficiencies ε_d and ε_t can be carried out with computer codes, such as EFFY2 written by García-Toraño and Grau Malonda (1985) previously described in this chapter. Simson and Meyer (1994b) and Simpson and Van Wyngaardt (2006) report the use of a modified EFFY2 program to operate on a personal computer, which calculates the ratio R of the triple-to-double efficiencies as a function of figure of merit. They note that in practice, Eqn 7.112 is solved by incrementally varying the figure of merit, P, in the computer calculation, which in effect reads the counting efficiencies corresponding to the measured ratio R from plots of efficiency curves such as those illustrated in Fig. 7.75. Simpson and Morris (2004a,b) and Simpson and Van Wyngaardt (2006) report the use of EFFY2 in the TDCR standardization of high-energy beta-emitters. Broda et al. (2000) describe a computer program, TDCRB-1, to calculate the radioactive concentration of a solution based on the TDCR method. Also, the DETECSZ program is described by Razdolescu et al. (2002) for the TDCR calculation of the activity concentration of pure beta emitters. Similar analysis codes, such as TDCRB-02, TDCR-11 among others, are cited by Zimmerman et al. (2010). The program SPECBETA, first reported by Cassette (1992) and Cassette and Vatin (1992), is used for the calculation of the beta spectrum, *i.e.*, $N(E)$ or what is also referred to as $S(E)$, the deposited spectrum in the scintillation cocktail, a required component of the TDCR efficiency calculation. The use of SPECBETA is reported by several researchers including Collé et al. (2008), Zimmerman et al. (2008), Fitzgerald et al. (2010), and Laureano-Perez et al. (2010). The calculation of efficiencies of EC nuclides requires data on interaction probabilities of electron-generating X-ray and γ-ray photons with scintillator, and the Monte Carlo code PENELOPE, first reported by Baró et al. (1995), has been used for this purpose (*e.g.*, Cassette et al., 2004, Zimmerman, 2006a,b, and Razdolescu et al., 2008). For the same purpose the simulation code Geant4 was developed (Agostinelli et al., 2003 and Allison et al., 2006) and utilized to acquire X-ray and gamma-ray energy deposition spectra and interaction probabilities with scintillant for the analysis of EC and beta-gamma-emitting radionuclides (*e.g.*, Bignell et al., 2010a,b). An updated MICELLE2 code, reported by Kossert and Grau Carles (2010), was prepared to facilitate the computation of counting efficiencies of radionuclides with complex decay schemes, such as EC nuclides, that require a treatment of the ejection of photoelectrons and a detailed model of the subsequent atomic electron rearrangement processes. Rodrigues et al. (2008) describe a non-radionuclide-specific computer code, TDCR-AR, for the analysis of data, calculation of detection efficiency, and radionuclide activity in a TDCR system. The TDCR-AR code was satisfactorily tested for the analysis of ^{3}H, ^{14}C, ^{55}Fe, ^{54}Mn, and ^{60}Co. Other simulation codes and programs are available from the literature, and it is common for laboratories to use programs developed 'in-house' for the analysis of data (*e.g.*, Collé et al., 2008). These programs may be obtained by direct contact with the authors of the published results.

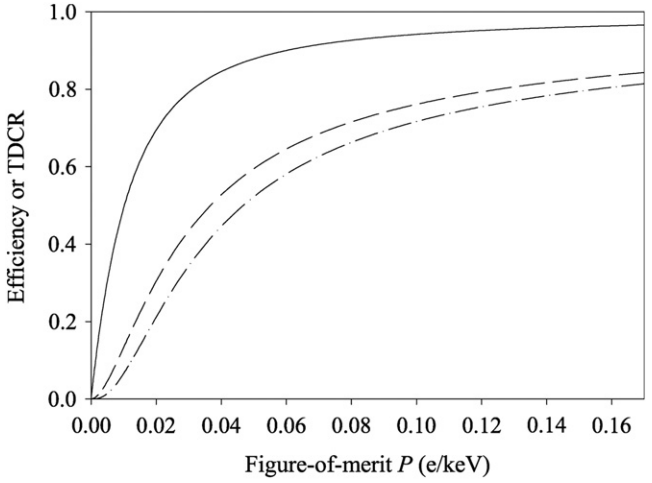

FIGURE 7.75 Results of calculations for ^{35}S of the double-coincidence efficiency ε_d (dashed line). Triple-coincidence efficiency ε_t (dashed-dotted line), and the TDCR $\varepsilon_t/\varepsilon_d$ (solid line) are plotted as a function of the figure of merit. A value for kB = 0.0100 g/(cm^2 MeV) was adopted in the calculation of the ionization quench function. *(From Van Wyngaardt and Simpson, 2009. Reprinted with permission from Radiocarbon, University of Arizona © 2009 Arizona Board of Regents on behalf of the University of Arizona, Tucson)*

The computer programs, such as those described previously in Section IX.A, may include subroutines for the calculation of the ionization quench function $Q(E)$ for any given Birks ionizing quench parameter kB (See Eqn 7.105 of this chapter.). Cassette et al. (2000) demonstrated that the Birks kB factor is independent of the cocktail chemistry and optical design of the TDCR system, the influence of the kB factor is negligible for high-energy nuclides (*e.g.*, ^{14}C and higher-energy beta emitters), and the optimum value of the kB factor is independent of the high-energy nuclide. Also, for low-energy electron-capture (EC) nuclides decaying toward the fundamental level, such as ^{55}Fe, the counting efficiency is almost independent of the kB value, because the energy emission is almost monoenergetic and the nonlinearity of the scintillator (ionization quenching), in this case, has no effect on the light emission (Broda et al. (2007). However, for low-energy beta-emitting nuclides, such as ^{3}H, ^{63}Ni, and ^{241}Pu, the calculated counting efficiency is highly dependent on the kB value (Broda et al., 2007 and Kossert et al., 2011a). The optimum kB value can be determined using different counting conditions described by Broda et al. (2007). The proper fitting of the kB ionization quench parameter in the TDCR model, as noted by Broda et al. (2002), is vital to improving the accuracy of this standardization method.

If the quantum efficiencies of the three photomultiplier tubes are different, a set of the following three equations, as described by Arenillas and Cassette (2006), Broda et al. (2007),

Van Wyngaardt and Simpson, 2009), Simpson et al. (2010), and Cassette (2011), is solved for the free parameters of each phototube A, B, and C:

$$\frac{\varepsilon_T}{\varepsilon_{AB}} = \frac{\int_0^{E_{max}} S(E)(1-e^{-EQ(E)/3M_A})(1-e^{-EQ(E)/3M_B})(1-e^{-EQ(E)/3M_C})dE}{\int_0^{E_{max}} S(E)(1-e^{-EQ(E)/3M_A})(1-e^{-EQ(E)/3M_B})dE} \tag{7.118}$$

$$\frac{\varepsilon_T}{\varepsilon_{BC}} = \frac{\int_0^{E_{max}} S(E)(1-e^{-EQ(E)/3M_A})(1-e^{-EQ(E)/3M_B})(1-e^{-EQ(E)/3M_C})dE}{\int_0^{E_{max}} S(E)(1-e^{-EQ(E)/3M_B})(1-e^{-EQ(E)/3M_C})dE} \tag{7.119}$$

$$\frac{\varepsilon_T}{\varepsilon_{AC}} = \frac{\int_0^{E_{max}} S(E)(1-e^{-EQ(E)/3M_A})(1-e^{-EQ(E)/3M_B})(1-e^{-EQ(E)/3M_C})dE}{\int_0^{E_{max}} S(E)(1-e^{-EQ(E)/3M_A})(1-e^{-EQ(E)/3M_C})dE} \tag{7.120}$$

Eqns 7.118 to 7.120 are solved using the multidimensional minimization Downhill Simplex algorithm (Broda et al., 2007), and the function, which must be minimized, is

$$\Delta = \left(\frac{\varepsilon_T}{\varepsilon_{AB}} - \frac{T}{AB}\right)^2 + \left(\frac{\varepsilon_T}{\varepsilon_{BC}} - \frac{T}{BC}\right)^2 + \left(\frac{\varepsilon_T}{\varepsilon_{AC}} - \frac{T}{AC}\right)^2 \tag{7.121}$$

where ε_T is the efficiency of the triple coincidence signals (T), and ε_{AB}, ε_{BC}, and ε_{AC} are the efficiencies of three double coincidence signals AB, BC, and CA, respectively. The solution gives the free-parameter variables M_A, M_B, and M_C or λ_A, λ_B, and λ_C (*i.e.*, $M = \lambda$) for each kB value, allowing the counting efficiency of each coincident event (Broda et al. (2007).

An interesting approach to the inequality of photomultiplier tube quantum efficiencies is reported by Van Wyngaardt and Simpson (2009). They describe a TDCR detector comprised of three high-gain electron-multiplier phototubes in an asymmetric arrangement (each at a 90° angle to the other). Matching of the PMTs was performed by adjusting the position of the source relative to the three phototube faces until all three double-coincidence count rates are the same to within some tolerance, taking variation due to counting statistics into account. In this manner, the photon intensity incident on each phototube face is adjusted to compensate for the inherent unequal phototube efficiencies. This resulted in equivalent double tube rates, which imply an equivalent figure of merit for each PMT detector.

In a review on the TDCR method, Broda (2003) demonstrated a complication in the efficiency determination of EC-decaying radionuclides. He noted, that the TDCR parameter (denoted as K) or

$$K = \varepsilon_t/\varepsilon_d \tag{7.122}$$

is single-valued for each value of K (*i.e.*, TDCR) only in the case of beta-emitting radionuclides, such as ^{3}H, ^{14}C, and ^{89}Sr, as illustrated in Fig. 7.76. However, in the case of radionuclides, that undergo electron-capture (EC) decay, such as ^{55}Fe, ^{54}Mn, and ^{139}Ce, there can be more than one counting efficiency; there can be two or even three counting efficiencies for a given TDCR, as illustrated in Fig. 7.76. Broda (2003) explains that this phenomenon is the result of the differences in the shape of the decay spectra. In the case of EC-nuclides, the decay spectra are not continuous, and two or more separated groups of scintillation energy can be distinguished, such as, K-shell, L-shell, γ, and conversion electron events. This discontinuity in the

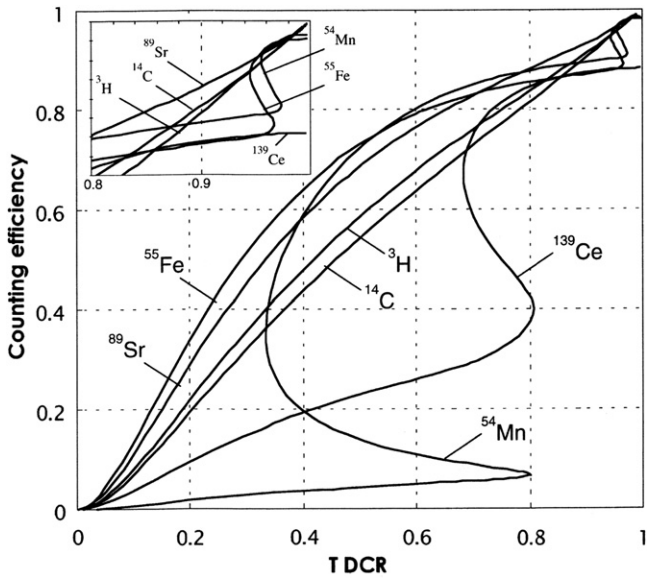

FIGURE 7.76 Calculated counting efficiencies, ε_d, as a function of the TDCR for some β- and EC-emitters. *(From Broda, 2003. Reprinted with permission from Elsevier © 2003)*

efficiency curve is a result of the probability of the appearance of these distinct groups of scintillation. Thus, in the case of EC-nuclides, the convoluted shape of the $\varepsilon_d(K)$ function complicates the calculation of the counting efficiency for each experimental measurement of K (*i.e.*, TDCR). Broda et al. (1998) and Broda (2003) describe the introduction of a parameter into the algorithm of counting efficiency determination to simplify the problem. The new parameter is $K3$, which is the ratio of a triple-coincidence efficiency ε_t to the efficiency of a sum of double coincidences ε_d to the third power, which was derived to the following expression:

$$K3 = \frac{\varepsilon_t}{\varepsilon_d^3} = \frac{N_0^2 N_t}{N_d^3} \tag{7.123}$$

The new efficiency function $\varepsilon_d(K3)$ yielded efficiency curves for EC nuclides that are single-valued.

For those interested in routine analysis of beta-emitting nuclides, a liquid scintillation counter with three photomultiplier tubes can be useful. The TDCR value can serve as the quench indicator, that is, there is no need to monitor quench with an external standard (Cassette, 2011). As described previously in this chapter, an external standard is used generally for the measurement of quench-indicating parameters with liquid scintillation counters equipped with only two photomultipliers. The three-photomultiplier liquid scintillation counter, that is available commercially, is the Hidex 300 SL illustrated previously in Fig. 7.74.

4. TDCR Progress and Development

The TDCR efficiency calculation technique is a proven method for radionuclide standardization. Since the publication of the 2nd Edition of the "Handbook of Radioactivity Analysis" in 2003, the national radionuclide metrology laboratories that now apply the TDCR efficiency calculation method for the primary standardization of radionuclides have become more widespread (Cassette, 2011).

Numerous reports on the standardization of specific radionuclides have been published. Each radionuclide presents a specific challenge with respect to the efficiency calculation due to its characteristic decay scheme, and the reader may refer to the published reports for further information on the specific calculation codes and parameters utilized for each radionuclide. With this in mind, some of the published radionuclide standardizations by the TDCR efficiency calculation method with typical standard uncertainties of the determination in percent are the following: ^{3}H with an uncertainty of 0.75% by Razdolescu and Cassette (2004), Zimmerman et al. (2004), Stanga et al. (2006), Qin et al. (2008), Ivan et al. (2008, 2010), Steele et al. (2009), Mo et al. (2010), and Nähle et al. (2010); ^{14}C with an uncertainty of 0.84% by Simpson and Meyer (1994b), Hwang et al. (2004), Qin et al. (2008) and Ivan et al. (2010); ^{32}P with an uncertainty of 0.5% and containing up to 10% impurities of ^{33}P and ^{35}S by Jaubert and Cassette (2004); ^{33}P with an uncertainty of 0.39% by Simpson and Morris (2004a,b); ^{36}Cl by Ivan et al. (2010); ^{54}Mn by Broda and Pochwalski (1993) and Zimmerman et al. (2004); ^{55}Fe with an uncertainty of 0.55% by Broda and Pochwalski (1993), Ratel (2008), Razdolescu et al. (2008), Johansson and Sephton (2010), Simpson et al. (2010) and Ivan et al. (2008); ^{63}Ni with an uncertainty of 0.60% by Simpson and Meyer (1994b), Zimmerman et al. (2004), Razdolescu et al. (2006), and Collé et al. (2008); ^{68}Ge/^{68}Ga with an uncertainty of 0.39% by Zimmerman et al. (2008); ^{89}Sr with an uncertainty of 0.41% by Simpson and Van Wyngaardt (2006), and Razdolescu et al. (2002); ^{90}Y with an uncertainty of 0.32% by Simpson and Van Wyngaardt (2006); ^{99}Tc with an uncertainty of 0.13% by Laureano-Perez et al. (2010), Zimmerman et al. (2010), and Simpson and Meyer (1994b); ^{113m}Cd with an uncertainty of 0.39% by Kossert et al. (2011); ^{139}Ce with an uncertainty of 0.51% by Broda et al. (1998); ^{186}Re with an uncertainty of 0.22% by Jaubert (2008); ^{204}Tl with an uncertainty of 0.81% by Simpson and Meyer (1996), Hwang et al. (2002, 2004), and Razdolescu and Cassette (2004); and ^{229}Th with an uncertainty of 0.40% by Fitzgerald et al. (2010).

Ivan et al. (2010) tested channel photomultiplier tubes in lieu of the traditional photomultiplier equipped with electron multiplier dynodes in a three-PM detector TDCR liquid scintillation analyzer. They observed significantly lower detection efficiencies, but excellent agreement in activity determinations of ^{3}H, ^{55}Fe, ^{63}Ni, and ^{90}Sr/^{90}Y when compared to the conventional counter equipped with the traditional electron dynode multiplier PM tubes.

A new TDCR liquid scintillation counter equipped with six photomultiplier tube detectors was tested with several beta emitters and, for comparative measurements, of tritiated water for validation studies by Ivan et al. (2010). The six photomultipliers were connected in pairs and arranged in a symmetrical pattern about the liquid scintillation vial in the optical chamber of the liquid scintillation counter. The counter can be operated in two modes: as a single system with three CPMs and a double system with six CPMs, connected in pairs in summation mode. The double system with six photomultipliers resulted in a significant improvement in the detection efficiencies over the classical TDCR counter.

The development of FASEA (field programmable gate array based acquisition and software event analysis) system was developed by Steele et al. (2009), which is capable of replacing the traditional MAC3 (see Fig. 7.73) for coincidence pulse processing in the TDCR efficiency calculation method. Tests carried out on the measurements of ^{3}H and ^{89}Sr activities confirm that the FASEA is able to emulate the behavior of the MAC3 unit, which provides a validation for the technique of separate data acquisition and post-analysis systems in TDCR radionuclide standardization measurements.

A recent development reported by Tarancón Sanz and Kossert (2011) is the application of a free-parameter model to samples containing solid plastic scintillation microspheres and radioactive aqueous solutions. Several beta-emitting radionuclide activities were measured in a TDCR system. The deviations between the determined activity concentrations and the reference values were $< 3\%$.

D. $4\pi\beta-\gamma$ Coincidence Counting

$4\pi\beta-\gamma$ coincidence counting is a direct method of activity determination, as it is independent of any quench-indicating

parameters and no reference standards are required for counting efficiency determinations. An additional advantage of this method is that the activity of a nuclide can be determined from experimental counting data only without the need for detector efficiencies.

As may be construed from the name applied to this method, it involves the coincidence detection of two types of radiations from a given radionuclide. The methods can be applied, therefore, to radionuclides that emit in coincidence more than one distinguishable type of radiation. Two types of detectors are required in coincidence to distinguish exclusively two types of radiation emissions, such as a liquid scintillation detector (or gas proportional counter) to measure a beta emission and a solid scintillation (or semiconductor detector) capable of measuring a gamma emission. Because the technique involves, in most cases, the use of a solid scintillation counter as one of the detectors, this method of radionuclide standardization is discussed in Chapters 14 and 16, where more detailed information is available on this topic.

X. NEUTRON/GAMMA-RAY MEASUREMENT AND DISCRIMINATION

The same year that Lieselott Herforth (1948) under the leadership of Hartmut Kallmann documented in her thesis the discovery that beta and gamma radiation produced scintillation in certain organic compounds, P. R. Bell (1948) demonstrated that fast neutrons could be detected in an anthracene scintillator by the proton recoils produced by neutron−proton collisions. Although neutrons have no charge and consequently cannot produce ionization or excitation directly in a scintillation fluor, the essentially equal mass of the neutron and protons (hydrogen atoms) in organic compounds facilitate transfer of energy from the neutron to protons via elastic scattering as described in Chapter 1. Because of the almost equal mass of the neutron and proton, the maximum fraction of the kinetic energy that a fast neutron can lose in a single head-on collision with a proton is calculated as 0.999 or 99.9% (see Table 1.16, Chapter 1). Although partial energy transfers also occur through less direct neutron−proton collisions, it is clear that fast neutron energy is absorbed more easily by a substance rich in protons (hydrogen atoms) compared to another substance possessing atoms of higher atomic numbers. The recoil protons with their acquired kinetic energy produce ionization until their energy is dissipated in the medium and they come to a full stop. A liquid scintillation cocktail, rich in protons (high H:C ratio), can be used to measure fast neutron radiation. The energy of the recoil protons dissipated in the scintillation cocktail solvent will excite the solute fluor molecules, resulting in the emission of visible light similar to the effect of alpha- and beta-particle interactions discussed previously.

Another radiation type, which does not carry charge but does interact in a liquid scintillation fluor cocktail, is gamma radiation. Like X-radiation described previously, gamma rays will interact with liquid scintillation cocktail via principally Compton interactions with atomic electrons. The transfer of gamma-ray photon energy to atomic electrons will result in the liberation of Compton electrons. The energy of these electrons will be absorbed by the liquid scintillation solvent in the same way as beta-particles described previously. Compton-electron energy absorption will result in fluor excitation and the emission of visible light of intensity proportional to the amount of energy absorbed in the scintillation cocktail.

The two mechanisms of fluor excitation via recoil proton or Compton-electron energy absorption form the basis for the discrimination of neutron and gamma radiation, respectively, by liquid scintillation. The liquid scintillation discrimination of the two radiation types will be discussed further on in this section.

Only a brief description of the scintillation detection of neutrons and neutron/gamma-ray discrimination will be presented here. More detailed information can be obtained from references specific to the subject (Harvey and Hill, 1979; Rausch, et al., 1993, Brooks, 1993, 1997, Poenaru and Greiner, 1997, Peurrung, 2000, Klein and Neumann, 2002, Pozzi et al., 2007, Enqvist and Pázsit, 2010, and Thomas, 2010) and from Chapter 16.

A. Detector Characteristics and Properties

The liquid scintillation cocktails used for the detection and measurement of neutrons are organic solutions generally high in hydrogen content to enhance the efficiency of trapping the neutron kinetic energy through neutron−proton collisions, which results in the production of recoil protons. Because high gamma-ray backgrounds are often present, the ability of discriminating between incident neutron and gamma radiation through pulse shape discrimination (PSD) becomes important and some liquid scintillation cocktails are most suitable for this purpose. Also, some organic scintillation cocktails are devoid of hydrogen, such as BC-509 or EJ-313 (equivalent to NE226) or BC-537 or EJ-315 (equivalent to NE230), which contain deuterated benzene (C_6D_6). Such cocktails have reduced sensitivity for neutrons and can be used for the measurement of gamma radiation in the presence of neutron radiation. Examples of commercially available cocktails for the detection of neutrons and gamma radiation or for neutron/gamma-ray discrimination as well as other applications such as neutrino detection are provided in Table 7.11. These liquid scintillators are used devoid of oxygen gas. Dissolved atmospheric oxygen reduces their light output by about 30%, and eliminates any pulse shape discrimination properties that the cocktails might possess. These cocktails are purged thoroughly with nitrogen gas prior to use.

Liquid scintillation neutron detectors vary in size from small to medium size (4−12 cm in diameter by 4−12 cm in length) up to large volume detectors comprising several cubic meters depending on the research objectives (See Table 7.11 and Zecher et al., 1997, Vartsky et al., 2003, Černý et al., 2004, and Lavagno, et al., 2010). The efficiency and energy resolution of the detector will be governed by its size. Energy is deposited by fast neutrons in the liquid scintillation cocktail by collisions for the most part with hydrogen atoms (n−p collisions) and to a lesser degree with the carbon atoms (see Table 1.16 in Chapter1), and, as a consequence, recoil proton excitation of

TABLE 7.11 Properties and Applications of Liquid Scintillators Used for Neutron Radiation Measurements or Neutron/Gamma Radiation Discrimination among other Applications[a]

Scintillator	Properties	Applications
BC-501A[b] EJ-301[c] NE213[d]	Xylene[e] (>90%) Aromatic fluors (<10%)[f] Atomic ratio, H/C: 1.212 λ_{max}: 425 nm[g] Light output: 78% anthracene[h] Decay time: 3.2 nsec[i] Density: 0.874 g/cm^3 Refractive index, $\mathbf{n}_D$: 1.505 Flash point: 26°C	Yields excellent n/γ pulse shape discrimination (PSD) over a wide energy range up to ~100 MeV (Horwáth et al., 2000, and Nakao et al., 2001, Klein and Neumann, 2002, D'Melloe et al., (2007), Aspinall et al., 2007a, Enqvist et al., (2008), Liu et al., 2009, Yousefi et al., 2009, Braizinha et al., 2010 and Lavagno et al., 2010).
BC-505 EJ-305 NE224	1,2,4-trimethylbenzene[e] (97.5%) Aromatic fluors (<0.5%) Atomic ratio, H/C: 1.331 λ_{max}: 425 nm Light output: 80% anthracene Decay time: 2.5 nsec Density: 0.977 g/cm^3 Refractive index, $\mathbf{n}_D$: 1.505 Flash point: 48°C	Exhibits high light output and transmission; fast neutron detectors; suitable for large volume, including anti-Compton and anti-coincidence shields; high flash point makes it safer to use and transport than xylene or toluene-based scintillators; (Hong et al., 2002).
EJ-309	Solvent (proprietary): aromatic hydrocarbon (>99%) Organic fluors (<1%) Atomic ratio, H/C: 1.25 λ_{max}: 424 nm Light output: 75% anthracene Decay time: 3.5 nsec[h] Density: 0.96 g/cm^3 Refractive index, $\mathbf{n}_D$: 1.57 Flash point: 144°C	New liquid scintillator developed as an alternative to the more commonly used for pulse-shape discrimination (PSD), such as BC-501A, NE213 and EJ-301, which contain xylene solvent with low flash point and high degree of solvent action. EJ-309 exhibits slightly poorer PSD characteristics, but possesses more environmentally favorable chemical properties and higher flash point (Pozzi et al.,2009, Clarke et al., 2009, Enqvist et al., 2010, and Zak et al., 2010)
BC-509 EJ-313 NE226	Hexafluorobenzene[e] Formula: C_6F_6 λ_{max}: 425 nm Light output: 20% anthracene Decay time: 3.1 nsec Density: 1.61 g/cm^3 Refractive index, $\mathbf{n}^D$: 1.38 Boiling point: 80°C Flash point: 10°C	Essentially free of hydrogen atoms (with exception of fluor molecules) only 0.18 atom % of hydrogen atoms; low sensitivity to fast and moderated neutrons, gamma-ray detection in a fast neutron flux; neutron insensitivity increased with pulse shape discrimination to enhance gamma-ray detection in n/γ discrimination; can be used to detect neutrons when it is desirable to avoid thermalizing properties of Hydrogen (Wolle et al., 1999, Davies et al., 1994, and Cecil and Medlet, 1988).
BC-517H EJ-321H NE235H	1,2,4-trimethylbenzene (<30%) Mineral oil (>70%) Aromatic fluors (<0.3%) Atomic ratio, H/C: 1.89 λ_{max}: 425 nm Light output: 52% anthracene Mean free path: >5 meters[j] Decay time: 2.5 nsec Density: 0.86 g/cm^3 Refractive index, $\mathbf{n}_D$: 1.476 Flash point: 81°C	Mineral oil-based scintillator where long mean free paths are required and high light output important; large volume detectors; compatible with acrylic plastics such as Plexiglas® and Perspex®, as well as many metals and reflective coatings; pulse shape discrimination capability (Braizinha et al., 2010).
BC-519 EJ-325 NE235C	1,2,4-trimethylbenzene (<40%) Mineral oil (<60%) Fluors (0.5%) Density 0.86 g/cm^3 Atomic ratio, H/C: >NE213 Flash point: >62°C Boiling point: >204°C	Provides excellent n/γ pulse shape discrimination for neutron energies up to 100 MeV (Horwáth et al., 2000).

(*Continued*)

TABLE 7.11 Properties and Applications of Liquid Scintillators Used for Neutron Radiation Measurements or Neutron/Gamma Radiation Discrimination among other Applications[a]—cont'd

Scintillator	Properties	Applications
BC-521 EJ-331 NE323	1,2,4-trimethylbenzene (>85%) Gadolinium (0.5%) Light output: 68% anthracene Atomic ratio, H/C: 1.314 λ_{max}: 424 nm Decay time: 3.6 nsec Density: 0.89 g/cm^3 section. Refractive index, $\mathbf{n}_D$: 1.50 Flash point: 44°C	Utilized for neutron spectrometry with pulse shape discrimination and neutrino research; fast neutrons leave a unique signature in Gd-loaded scintillator; they produce a prompt recoil proton pulse and, once thermalized, they are easily captured by Gd, which has an extremely high thermal neutron capture cross section. Neutron capture by Gd is signaled by the emission of three gamma rays totally ~8MeV. Available at 0.25% w/w Gd (EJ-335) with mineral oil to increase hydrogen content and use in large tanks; produced at Gd content of 0,5 % (BC-525) with mineral oil component for increased light transmission, hydrogen content, and higher flash point. Neutron capture by Gd results in a cascade of conversion electrons, X-rays, and γ-rays. BC-525 is used in neutron spectrometry and neutrino research. (Banerjee et al., 2007).
BC-523A EJ-339 NE311	1,2,4-trimethylbenzene (>30%) Methyl borate (<60%) 1-methylnaphthalene (10%) Light output: 65% anthracene Atomic ratio, H/C: 1.74 Natural ratio ^{10}B/^{11}B: 0.245 Enriched ratio ^{10}B/^{11}B: 9.0 λ_{max}: 424 nm Decay time: 3.7 nsec Density: 0.916 g/cm^3 Refractive index, $\mathbf{n}_D$: 1.4 Boiling point: 68.9°C	Available at natural ^{10}B isotope abundance or enriched; EJ-339A contains boron loading compound enriched to 90% atom percent in ^{10}B and thus contains 4.6% ^{10}B by weight; useful for total neutron absorption spectrometry; fast neutrons produce a prompt recoil proton pulse with initial scatterings in the cocktail; thermalized neutrons may undergo the ^{10}B(n,α)^{7}Li capture; the capture pulse is in delayed coincidence with the prompt pulse; useful in identifying neutron events; useful for n/γ separation by PSD. (Vartsky et al., 2003, Jastaniah and Sellin, 2004, and Flaska and Pozzi, 2009).
BC-537 EJ-315 NE230	Deuterated benzene (>98%) Formula: (C_6D_6) Aromatic fluors (<2%) Light output: 61% anthracene Atomic ratio, D/H: 141:1 Atomic ratio, D/C: 0.99 λ_{max}: 425 nm Decay time: 1.8 nsec Density: 0.954 g/cm^3 Refractive index, $\mathbf{n}_D$: 1.50 Boiling point: 79.1°C	Useful for n/γ separation as sensitivity to fast neutrons is reduced by deuterium. A nondeuterated version of the scintillator (EJ-315H) is available for comparative research. (Marrone et al., 2002, and Villano et al., 2011).

[a]*Data from ELJEN Technology, 1300 W. Broadway, Sweetwater, TX 79556, USA, and Saint-Gobain Corp., 750 E. Swedesford Road, Valley Forge, PA 19482, USA, and Compagnie de Saint-Gobain, Les Miroirs, 18, avenue d'Alsace, 92400 Courbevoie, France.*
[b]*Bicron scintillator (scintillators listed as a group are commercial equivalents).*
[c]*Eljen Technology scintillator (scintillators listed as a group are commercial equivalents).*
[d]*NE Technology scintillator (scintillators listed as a group are commercial equivalents).*
[e]*Solvent.*
[f]*Solute (fluor).*
[g]*Wavelength of fluorescence peak*
[h]*Percentage of anthracene light output.*
[i]*Short component of de-excitation light.*
[j]*Light transmission.*

cocktail solvent and fluor molecules is predominant. Gamma radiation will deposit energy mainly via Compton interactions resulting in Compton-electron excitation of cocktail and fluor. Since both neutrons and gamma rays are generally intermixed, both radiations should be considered. The neutrons will encounter a wide range of collisions with protons including direct head-on collisions and complete transfer of energy to less-direct collisions even just a glancing with a proton resulting in various scattering interactions and only partial energy transfers to protons (see Chapter 1). Likewise, Compton electrons will vary in energy depending on the energy of the incident gamma radiation.

If the liquid scintillation detector is very small or the neutron or γ-ray energies very high, a considerable number of recoil protons or Compton electrons can escape from the detector. This results in an incomplete deposition of either proton-recoil or Compton-electron energy in the cocktail referred to as the 'wall effect' (Thomas, 2010). When the wall effect is significant, the event (n—p or γ—e) recorded by the photomultiplier tube as a pulse height would be smaller than what would be expected had the recoil proton or Compton electron deposited all its energy in the cocktail. Consequently, the 'response function', which is the pulse height registered per neutron or gamma-ray energy, would be shifted to lower pulse heights.

For example, in the analysis of γ-ray photons of energy over the range of 7−20 MeV, Navotny et al. (1997) chose NE213 scintillation detectors large enough (*e.g.*, 5 cm in diameter by 10 cm in length, 206 cm^3 in volume) taking into account the maximum range of Compton electrons to be detected to avoid a distortion of the pulse-height response by wall effects. Likewise, for the measurement of neutron radiation Nakao et al. (2001) demonstrated, that for a NE213 liquid scintillator of 12.7-cm diameter and 12.7-cm length the proton-escape probability ranges from approximately 1% to more than 50% of the recoil protons generated for neutrons over the energy range of 25 MeV to over 300 MeV. The neutron detection efficiencies were determined by Nakao et al. (2001) by integrating the pulse-height response functions at various calibrated pulse-height thresholds. At a lower-limit discriminator settings or pulse-height threshold of 1.15 MeV (calibrated with a ^{60}Co source) the neutron detection efficiencies varied from 24% to 10% over the neutron energy range of 23−132 MeV. Satoh et al. (2001) developed a Monte Carlo code, designated SCINFUL-QMD, for the calculation of neutron detection efficiencies for neutron energies up to 3 GeV in liquid scintillators such as NE213. Other Monte Carlo and analytical models of neutron scatterings in liquid scintillation cocktail and detector response are provided by Patronis et al. (2007), Pozzi et al. (2007), and Enqvist and Pázsit, 2010).

It is important to note here that for heavy particles (*e.g.*, protons and α particles) the light output from the liquid scintillator is nonlinear with energy. Unlike electrons or β particles, which produce a relatively linear light output with energy over the range of 0.100−1.6 MeV (Novotny et al., 1997 and Horwáth et al., 2000) heavy particles exhibit high values of stopping power (d*E*/d*x*) in scintillator (see Chapter 1) and thereby produce higher specific ionization and a saturation effect that yields less light per particle energy loss. The nonlinearity of light output per particle energy loss for protons results in recoil proton energies occurring at lower pulse heights in the pulse-height spectrum. Consequently, the use of computer codes to unfold neutron and photon energy spectra require accurate measurement of the light output response as a function of energy deposited in the scintillator (Klein and Neumann, 2002, Neumann et al., 2002, Reginatto et al., 2002, Schmidt et al., 2002, Kornilov et al., 2009, and Enqvist and Pázsit, 2010). Radionuclide sources with well-separated γ-ray energies are used to establish the pulse-height scale in terms of electron energies. Gamma-photon sources produce Compton edges in the scintillator where the Compton-electron energies can be used to convert light outputs into electron equivalent energies or MeVee (Horwáth et al., 2000, Nakao et al., 2001, Klein and Neumann, 2002, and Guerrero et al., 2008, Hawkes, et al., 2010, Zak et al., 2010, and Villano et al., 2011).

The detector size will govern the number of multiple neutron scatterings. Neutron scattering can result in a broad range of energy transfers to recoil protons, from very little neutron energy when a neutron is simple glanced off a proton (near hit) up to the maximum neutron energy resulting from a head-on collision with a hydrogen atom. Recoil protons from a given neutron after multiple collisions and scatterings will produce photons, which are detected by the photomultiplier tube as they occur within the coincidence time gate of the scintillation analyzer. The sum of the photons produced by the recoil protons from the multiple scatterings of one neutron will produce a pulse height from the photomultiplier proportional to the light output. Due to the summation of photons from multiple scatterings, the resultant pulse heights will be higher than what would occur at reduced scattering.

Neutrons are also scattered by carbon atoms in the scintillator; however, carbon recoils do not produce any significant light output in liquid scintillator (Klein and Neumann, 2002). The H:C atomic ratios in liquid scintillator may vary from 1.2 to 1.9 (Table 7.11). The higher the ratio or greater the atom % H in the scintillator, the higher will be the probability of n−p collisions and the production of proton recoils. However, carbon scattering will cause neutron energy loss and consequently a reduction in pulse-height response as a function of energy. As illustrated in Table 1.16 of Chapter 1, the maximum fraction of kinetic energy that may be lost by a neutron collision with ^{12}C is 28.6% resulting from a head-on n−^{12}C collision. A neutron may lose, therefore, anywhere between zero and 28.6% of its energy in a single collision with carbon. For example, a scattered neutron, that had an initial head-on collision with a ^{12}C atom, may then collide with a proton, but the maximum energy of the recoil proton in this case would be 71.4% of the original neutron energy. Consequently, carbon atoms in the scintillator will reduce the pulse-height response as a function of neutron energy.

At lower neutron energies, particularly where neutrons may become thermalized in the liquid scintillator, special detectors may be employed, such as BC-523, that contain natural or enriched ^{10}B in the scintillation cocktail (Table 7.11) to enhance detection efficiencies. The incident neutrons are moderated by n−p collisions in the cocktail and then undergo ^{10}B(n,α)^{7}Li capture according to Eqn 1.244 of Chapter 1 and more specifically as follows:

$$ {}_0^1n + {}_5^{10}\mathrm{B} \rightarrow \alpha + {}_3^7\mathrm{Li}\ (\mathrm{g.s.}) + 2.790\ \mathrm{MeV}\ (6.3\%) \qquad (7.124) $$

$$ \rightarrow \alpha + {}_3^7\mathrm{Li}^* + \gamma(0.478\ \mathrm{MeV}) + 2.312\ \mathrm{MeV}(93.7\%) \qquad (7.125) $$

The branching ratios for the two reactions are 6.3% and 93.7%, respectively. The branch described by Eqn 7.124 leaves the ^{7}Li at the ground state, whereas the other branch (Eqn 7.125) leaves the ^{7}Li at an excited state, and the α particles plus ^{7}Li* ions create scintillation light equivalent to light produced by 65-keV electrons or beta particles. Yen et al. (2000) report the use of 4-cm-diameter detectors of ^{10}B-enriched scintillator joined together in a circular array of 55 detectors. They report detector efficiencies of 95%, 85%, and 71% at neutron energies of 10, 100, and 1000 eV, respectively.

Gd-loaded liquid scintillators, described in Table 7.11, have excellent neutron detection properties, because of the very high thermal neutron capture cross section of Gd (see Table 1.17 of Chapter 1). As described by Banerjee et al. (2007), the mechanism of neutron detection in a Gd-loaded scintillator consists of two stages. First, the fast neutron that enters the liquid scintillator will undergo multiple scatterings primarily with hydrogen atoms in a few tens of nanoseconds producing a prompt signal. After several collisions with atomic nuclei of the scintillator, the neutron slows down and is thermalized, *i.e.*,

it reaches the low thermal energy stage, provided the neutron does not escape from the scintillator. The second stage consists of the capture of the thermal neutron by a Gd nucleus, because of its extremely high thermal neutron capture cross section. Neutron capture by Gd results in the emission of three γ-rays with a total energy of ~8MeV. The detection of the capture gamma rays provides a measure of the total number of neutrons emitted.

B. Neutron/Gamma-ray (n/γ) Discrimination

The detection of neutrons is often complicated with background gamma radiation. The neutron detector can be shielded from radiation background arising from charged particles by the use of absorber material between the source and detector or via magnetic field deflection. This leaves only gamma rays, which remain undeflected by magnetic fields and relatively unattenuated by absorbers.

1. Pulse Shape Discrimination (PSD)

Neutron and γ-ray interactions in a liquid scintillator may be separated by pulse shape discrimination (PSD) according to principles that are similar to alpha- and beta-particle (α/β) discrimination in liquid scintillation described further on in this chapter and in Chapter 9. The principles behind (n/γ) discrimination rest on different degrees of excitation caused by heavy charged particles versus lighter charged particles in the liquid scintillation cocktail. Neutron interactions produce the relatively heavy recoil protons, whereas γ-rays produce much lighter Compton electrons in scintillation cocktail. The heavier charged particles produce greater specific ionization (higher LET) in cocktail than electrons and, consequently, cocktail fluors reach higher excited states that take longer for de-excitation to occur. De-excitation is manifested as fluorescence. The fluorescence is analyzed by the electric pulse it produces in the photomultiplier tube (PMT). The shape of the pulse is a function of the specific ionization of the particle (heavy particle versus lighter particle), and the shape can be defined in two components, namely, a fast (prompt) component or rise time and a slow or delayed component also referred to as the tail. The prompt component of fluorescence has a decay time of only a few nanoseconds, while the delayed component or tail may last a few hundred nanoseconds. The differences in pulse shapes produced by neutron and γ-ray interactions in a liquid scintillator are illustrated in Fig. 7.77. A heavy charged particle, such as a proton arising from neutron interactions, will produce a larger fraction of its fluorescence in the slow component, while a much lighter charged particle, such as the electron arising from γ-ray interactions, will cause fluorescence with a much smaller portion of the light in the slow component. Guerrero et al. (2008) demonstrate, with an Am−Be neutron source, that the slower neutrons exhibit a longer delayed component or tail than faster neutrons. This could be explained by the fact that protons of lower energy have a higher LET producing more high-excitation states of scintillator cocktail. The Am−Be source produces neutrons with energies up to ~10MeV with an average neutron energy of 4 MeV and various gamma lines.

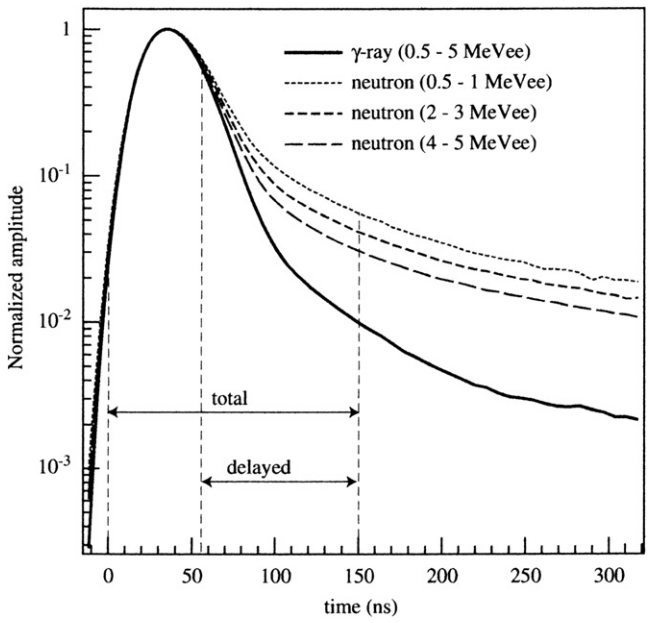

FIGURE 7.77 Neutron and γ-ray true pulse shapes recorded with BC501A liquid scintillator. The shape of the neutron signals shows a dependence on the energy of the recoil nuclei. The emission mechanism exhibits a prompt component, which starts within the first 5 ns and a delayed component, which occurs after a subsequent ~25 ns. *(From Guerrero et al., 2008. Reprinted with permission from Elsevier © 2008)*

To exploit the phenomena of differing pulse shapes, the method of Heltsley et al. (1988) is commonly used. As described by Zecher et al. (1997) the PSD method entails the use of two analog-to-digital converters (ADCs), one that integrates the total charge of the pulse and the other integrates the charge from some fixed time fraction (portion) of the pulse (*i.e.*, either the first prompt component or the longer tail component). By comparing the magnitude of the charge collected in the fraction of the pulse to the total charge collected in the pulse, one can determine which species created the pulse, proton or electron, and consequently, neutron or γ-ray. Similar n−γ discrimination techniques, that compare the 'short' and 'long', or 'total' and 'delayed', or 'total' and 'tail' components of the scintillation pulse, have been utilized by numerous researchers including Černý et al. (2004), Rochman et al. (2004), D'Mellow et al. (2007), Guerreo et al. (2008), Clarke et al. (2009), Flaska and Pozzi (2009), Hamel et al. (2009a,b), Pozzi et al. (2009), Enqvist et al. (2010), Hawkes et al. (2010), Lavagno et al. (2010), Schiffer et al. (2011), and Villano et al. (2011). An example may be taken from the work of Lavagno et al. (2010), who utilized a Canberra Nuclear Instrumentation Module (NIM) 2160A Charge-to-Digitial Converter (QDC), to exploit the difference in the intensity of the slow or delayed component of the light pulse (see Fig. 7.77) to the space density of the charge carriers produced by the different types of ionizing particles (*i.e.*, protons and electrons), which yields excellent n−γ discrimination. As described by Lavagno et al. (2010), the charge comparison method compares directly the intensity of the slow component to the total light pulse by incident ionizing radiation, *i.e.*, the recoil protons and Compton electrons. A block diagram of the experimental setup and time relation

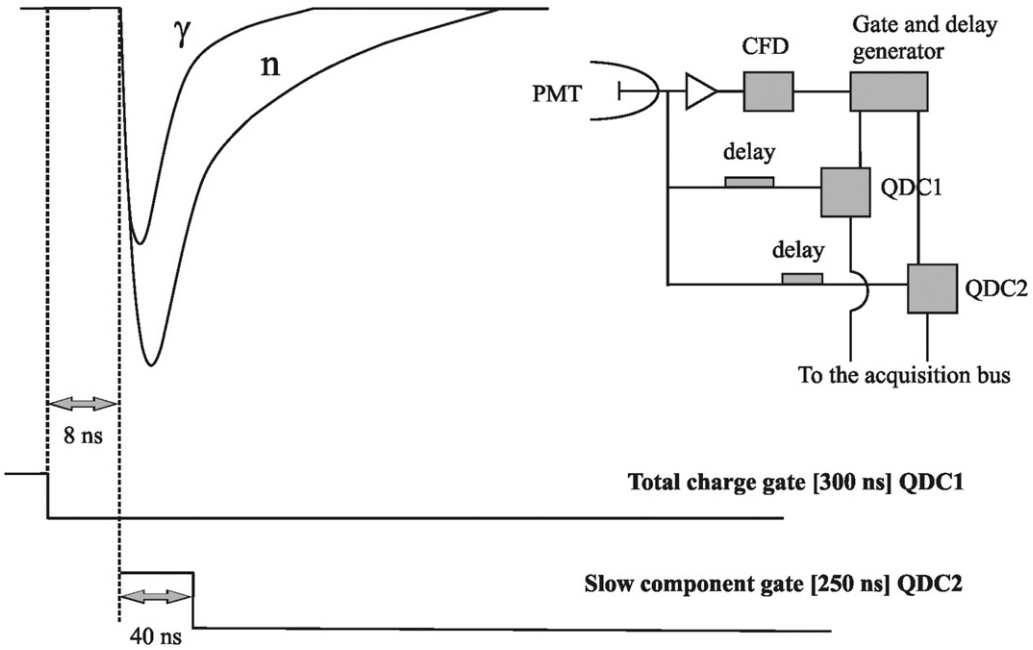

FIGURE 7.78 NIM electronic block diagram and time relation between photomultiplier pulse and gates at the input if QDCs. *(From Lavagno et al., 2010. Reprinted with permission from Elsevier © 2010)*

between photomultiplier pulse and gates at the input of the QDCs are illustrated in Fig. 7.78. One QDC at the opening of the gate signal integrates the charge corresponding to the total pulse, and another QDC, triggered by the delay gate signal, collects only the charge from the slow or delayed component. The prompt component of the pulse starts after the first ~5 ns following excitation, and the delayed or slow component in the subsequent 20−25 ns.

The signals arising from γ-ray and neutron interactions may be distinguished by plotting the integrated intensities of the two components of the pulse against each other as illustrated in Fig. 7.79. As described by Guerrero et al. (2008), the integration of the digitized signals is carried out in two different time intervals, and the particle type of each signal is evaluated by a comparison between the two signals. Each signal arising from an electron or proton in the scintillator, as a consequence of a γ-ray or neutron interaction, respectively, is characterized by its time, amplitude, and the two integrals I_{total} and I_{delayed}. Fig. 7.79 illustrates well-separated signal intensities corresponding to γ-rays and neutrons, which was reported by Geurrero et al. (2008) to be obtained from the integration of signals (see Fig. 7.77) over the 0−150-ns interval for I_{total} and from 55 to 150 ns for I_{delayed}.

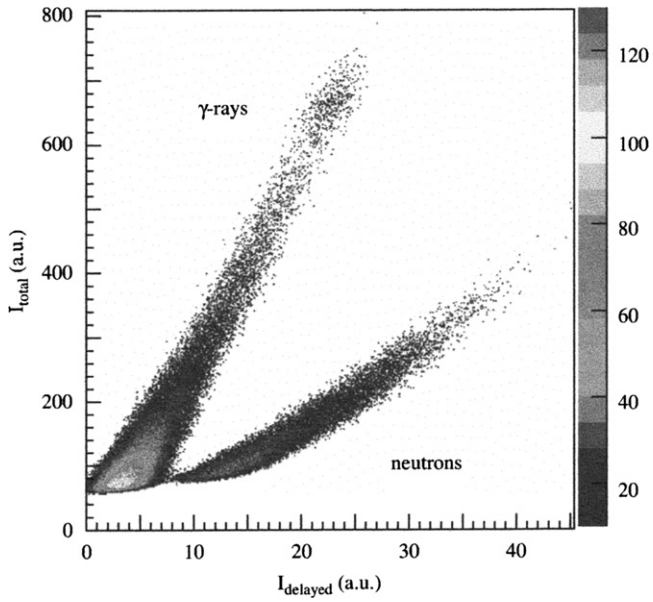

FIGURE 7.79 Distribution of I_{total} and I_{delayed} values in a measurement of an Am/Be source. The two well-separated regions correspond to γ-ray and neutron signals. *(From Guerrero et al., 2008. Reprinted with permission from Elsevier © 2008)*

2. Pulse Gradient Analysis (PGA)

The digital discrimination of neutrons and γ-rays in mixed radiation fields was described by D'Mellow et al. (2007). This digital discrimination method is referred to as pulse gradient analysis (PGA), which is somewhat distinct from the PSD method described previously. D'Mellow et al. (2007) note that the principal difference between the pulse produced by a neutron and that produced by a γ-ray is the neutron pulse, which exhibits a slower decay to the baseline, illustrated in Fig. 7.80. This is characterized by a gradient that is shallower on the trailing edge of the pulse. It is this feature that is exploited in the PGA method for n−γ discrimination, *i.e.*, to determine which radiation produced the pulse, neutron or γ-ray.

The PGA method developed by D'Mellow et al. (2007) does not require any measurement of the actual pulse decay rate for the n−γ discrimination. Rather, only a relative measurement of the gradient is found from two suitable samples of the digitized representation of the pulse. These digitized samples are the following: (1) The first sample is the peak magnitude of the pulse and (2) the second sample measured 20 ns after the first

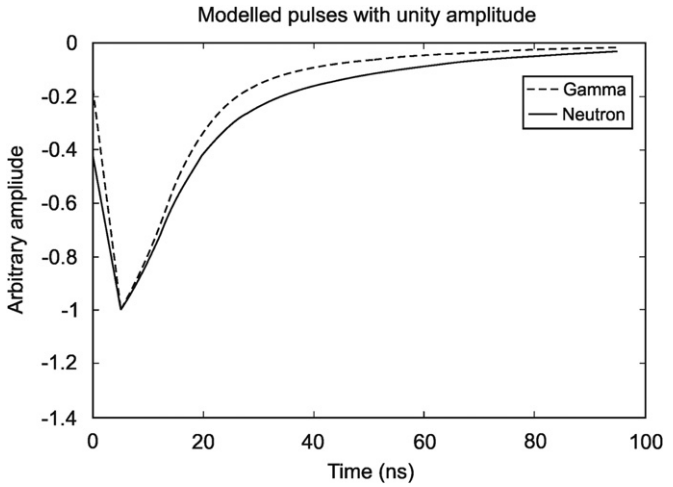

FIGURE 7.80 A plot of amplitude versus time (ns) for model pulses of a neutron and γ-ray in an organic liquid scintillator. When both pulses are attributed the same amplitude, it is clearly seen that the neutron pulse decays more slowly than the γ-ray pulse. *(From D'Mellow et al., 2007. Reprinted with permission from Elsevier © 2007)*

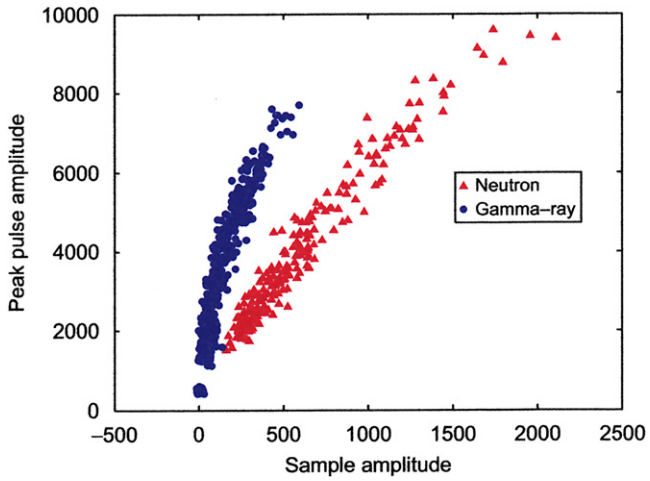

FIGURE 7.81 A scatter plot with data recorded with an Am−Be source. The peak amplitude of the pulse is plotted against the amplitude of the sample for n−γ discrimination by pulse gradient analysis (PGA). For the color version of the figure, the reader is referred to the online version of the book. *(From D'Mellow et al., 2007. Reprinted with permission from Elsevier © 2007)*

sample. The optimum time for the measurement of the second sample generally occurs 15−25 ns after the peak, and it will depend on the liquid scintillator and PMT properties (D'Mellow, 2006). The second sample, which measures the pulse gradient, is strongly affected by the pulse amplitude, which requires normalizing the pulse to remove this adverse effect. For n−γ discrimination, the amplitude of the pulse is plotted against another parameter proportional to the pulse decay rate. In the PGA algorithm, the pulse decay rate is measured by the amplitude of the second sample. Thus, two distinct groups of events are measured, namely, the peak pulse amplitude and the sample amplitude corresponding to either γ-rays or neutrons. Events labeled as γ-rays had a ratio of peak amplitude to sample greater than 11.41, and those labeled as neutrons for ratios below that value. A scatter plot of γ-ray and neutron events discriminated by the PGA method is illustrated in Fig. 7.81. The optimum ratio of peak amplitude to second sample should be determined for each detection system utilized. Aspinall et al. (2007a) describe the application of algorithms to improve the digital pulse shape discrimination techniques.

Hawkes et al. (2010) developed miniature digitizing electronics with various n−γ discrimination algorithms, which enabled the implementation and testing of the PSD, and PGA methods, previously described as well as a model pulse method described by Marrone et al., 2002 and Guerrero et al., 2008). The model pulse method constructs two model pulse shapes, one for neutrons and the other for γ-rays; the unknown pulses from a mixed neutron/gamma field are characterized according to which of the two models the pulses fit best using a χ^2 criterion. The PSD and PGA methods were implemented with a charge comparison algorithm and a pulse grade amplitude (PGA) algorithm, respectively, and the model pulse method with a model pulse algorithm. The charge comparison algorithm was found to have a small but definite figure of merit (FOM) advantage of the other two methods for the neutron fields tested; however, Hawkes et al. (2010) underscore that the FOMs of the other two methods were not much smaller and that each method has its advantages. The charge comparison algorithm integrates the pulse over two different intervals, namely, 'long' and 'short', which are similar to previously described 'total' and 'delayed' intervals (see Fig. 7.77) although not identical in their time span. The 'long integral' spanned the entire pulse and was proportional to the total light output, whereas the short integral was set to capture just the tail of the pulse. The ratio of the two integrals, *i.e.*, short integral/long integral, was used as the discrimination parameter. The charge comparison algorithm described by Hawkes et al. (2010) would determine the optimum starting time for the pulse integration by maximizing the figure of merit (FOM) derived from the probability distribution, which shows two peaks, one corresponding to the γ-rays and the other to neutrons, as illustrated in Fig. 7.82. The FOM was calculated according to

$$\text{FOM} = \frac{\text{peak separation}}{\gamma \text{ peak FWHM} + \text{neutron peak FWHM}} \tag{7.126}$$

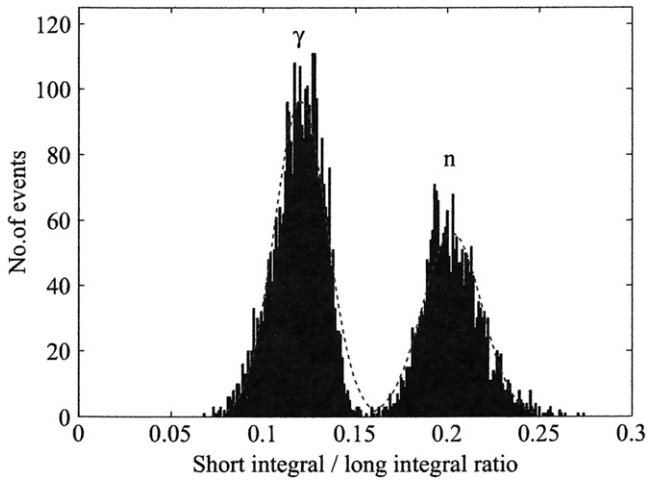

FIGURE 7.82 FOM plot for the optimum value of the short integral starting time in the charge comparison Algorithm. The dotted curves show the Gaussian fits used to determine the positions and widths of the peaks. *(From Hawkes et al., 2010. Reprinted with permission from Elsevier © 2010)*

as described by Winyard et al. (1971) and Begin et al. (2006). The optimum time for the short integral starting time was determined by maximizing the FOM, which is calculated over a range of different starting times. A FOM plot, from the work of Hawkes et al. (2010), obtained with the optimized starting time together with Gaussian fits used to measure the peak positions and widths is illustrated in Fig. 7.82.

A new approach to the discrimination of n−γ events in an organic scintillator are methods based on artificial neural networks (ANN), which were reported by Liu et al. (2009) and Ronchi et al. (2009). The methods were verified with mixed neutron/gamma field data assessed by time-of-flight measurement.

3. Time-of-Flight (TOF) Spectrometry

Another method used to discriminate neutrons and γ-ray photons is via time-of-flight (TOF) spectrometry. A γ-ray travels at the speed of light, whereas neutrons travel slower. For example, a 2.0-MeV neutron travels at only 0.065*c* or 6.5% of the speed of light (see Fig. 1.51 and 1.52 of Chapter 1). Consequently, a γ-ray that undergoes multiple Compton scattering in a scintillation cocktail would produce a pulse event in the PMT before a neutron that also undergoes multiple scattering. The n−γ discrimination is enhanced in TOF spectrometry by separating the neutron source from the liquid scintillation detector by a suitable distance that may extend to several meters. As noted by Thomas (2010), time-of-flight (TOF) spectrometry requires a measurement of the time taken for the particle (*i.e.*, neutron or γ-ray) to travel a known distance (*e.g.*, the distance from the n−γ source to the detector). Thus, there is a need for two timing signals, a start signal that is triggered when the neutrons or γ-rays are created or when they pass a particular point and an arrival signal that is triggered when the neutron or gamma rays arrive at and are detected by the liquid scintillator. Thomas (2010) outlines three ways that a start signal can be produced. These are provided below together with some examples added by the writer:

a. *A pulsed source, such as an accelerator with beam pulsing capabilities*. For example, a proton beam may strike a target material, producing neutrons and γ-rays, situated at a fixed and known distance from the liquid scintillation detector (See Fig. 7.83). Such an experimental arrangement is described by Rochman et al. (2004), Aspinall et al. (2007b), and Liu et al. (2009).

b. *The detection of radiation (e.g., γ-ray) that accompanies the formation of a neutron*. Any suitable detector for time-correlated emissions for the start signal from a radiation source may be used. For example, a BaF_2 detector is commonly placed next to a ^{252}Cf source to signal the onset of fission by detecting one of the γ-rays that accompanies the emission of neutrons in ^{252}Cf spontaneous fission (Banerjee, et al., 2007, Ronchi et al., 2009). An ionization chamber was used by Flaska and Pozzi (2007) to provide a start signal for a digitizer to determine the time zero for the measurement of neutron pulses, and a plastic scintillator next to a ^{252}Cf source was used by Venkataraman (2008). A liquid scintillator detector is placed at a distance away from the source to detect both the neutrons and γ-rays and provide a time-of-flight discrimination. For example, Ronchi et al. (2009) placed a BC-501 liquid scintillator detector 75 cm away from the source. The detected correlated fission events produce a signal in the BC-501 scintillation detector after a time-of-flight delay (t_{TOF}) with respect to the start signal from the BaF_2 detector.

c. A detector used to signal neutron scattering.

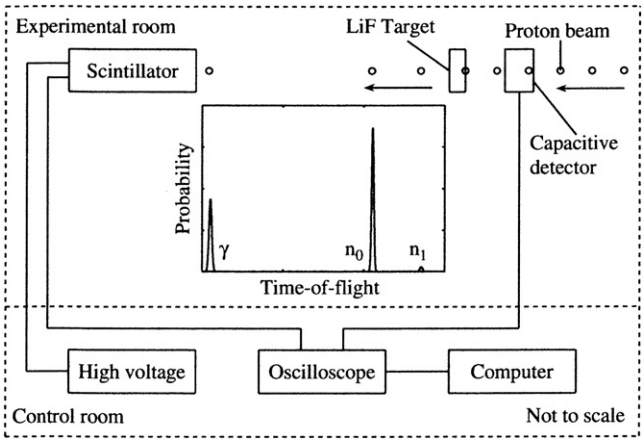

FIGURE 7.83 Schematic diagram of the experimental arrangement for the digital time-of-flight discrimination of γ-rays and neutrons produced by a proton beam striking an LiF target according to the reaction $^7Li(p,n)^7Be$ with a flight path of 1.614 m between the target and detector. A digital time-of-flight spectrum included in the center of the diagram illustrates the peaks for the intensities of the early arriving γ-rays followed by the 1.225-MeV neutrons (strong peak at n_0) and 0.745-MeV neutrons (weak peak at n_1). *(From Aspinall et al., 2007b. Reprinted with permission from Elsevier © 2007)*

The work of Aspinall et al. (2007a,b) serves as an example of digital time-of-flight (TOF) measurements in n−γ discrimination using pulse gradient analysis (PGA). The application of PGA in n−γ discrimination is described in the previous section. Aspinall et al. (2007b) used an accelerator to direct a 2.924-MeV proton beam onto a thin 60 μg/cm^2 LiF target, which produces neutrons via the reaction $^7Li(p,n)^7Be$ with neutron energies of 1.225 and 0.745 MeV corresponding to transitions to the ground and first excited states, respectively, of the product nucleus. A capacitive-type detector was placed in the proton beam line, as illustrated in Fig. 7.83, at a distance of 1.6 m from the LiF target. In this arrangement, the capacitive detector provided Aspinall et al. (2007b) with the start or proton beam pick-up signal needed to provide timing information for the TOF measurement and information on the proton pulse duration and frequency. Because the beam is monoenergetic and the target very thin, the transit time from the capacitive detector to the LiF target was constant. This provided a constant delay between the beam pick-up signal and the emission of neutrons from the LiF target. Therefore, the beam pick-up signal could be used as the start signal, as well as identify the pulse duration and period of the neutron pulses. The detector containing LS-301 organic liquid scintillator, illustrated in Fig. 7.83, was positioned 1633 mm from the LiF target. The scintillator pulses trigger the arrival or acquisition of γ-rays and neutrons, and the

pulses are sent to an oscilloscope and computer to enable n−γ discrimination by pulse gradient analysis and TOF measurements. The acquisition and digital recording of scintillation pulse and corresponding beam pick-up pulse enable all detected events, *i.e.*, γ-rays and neutrons, to be sorted in terms of their time of arrival relative to the initial beam pick-up signal (Aspinall et al., 2007b). The discrimination of the γ-rays and neutrons as a function of their time-of-flight, graphically depicted in Fig. 7.83, illustrates the early arrival of the γ-rays followed by two well-discriminated peaks for neutrons, with a strong peak for neutrons n_0 of 1.225 MeV and a weak peak for neutrons n_1 of 0.745 MeV.

XI. DOUBLE BETA ($\beta\beta$) DECAY DETECTION AND MEASUREMENT

The discovery, principles, and current research on double beta decay are reviewed in Chapter 1. Only a brief treatment of the liquid scintillation techniques employed in the search for neutrinoless double beta decay will be given here.

The first observation of double beta decay was made by Steven R. Elliott, Alan A. Hahn, and Michael K. Moe at the University of California, Irvine in 1987. They measured double beta decay in a sample of ^{82}Se enriched from its natural abundance of 8.7% to an isotope abundance of 97% to provide more source material for the double beta decay as well as reduce contamination from other sources (Eliott et al., 1986, 1987, Moe, 1986, and Moe and Rosen, 1989). The decay scheme is written as follows:

$$^{82}_{34}\mathrm{Se} \xrightarrow{t_{1/2} = 9.2 \times 10^9 \text{ years}} {}^{82}_{36}\mathrm{Kr} + 2\beta^- + 2\,\overline{\nu} \qquad (7.127)$$

where the parent nucleus decays to a daughter nucleus of the same mass number A, but with an increase in atomic number Z by two. In general terms, the double beta decay process is expressed in terms of the nuclear atomic and mass numbers as

$$(Z,\ A) \rightarrow (Z+2,\ A)\ +\ 2\mathrm{e}^-\ +\ 2\overline{\nu} \qquad (7.128)$$

Thus, in accord with the beta decay scheme, within the nucleus of the parent nuclide, two neutrons decay to two protons with the simultaneous emission of two beta particles and two antineutrinos. This type of beta decay is abbreviated as $2\nu\beta\beta$ to signify the simultaneous emission of two neutrinos and two beta particles.

Double beta decay is a rare event manifested by very long half-lives from 10^{18} to 10^{24} years. Because of the rarity of the event, the measurement of double beta decay is extremely difficult requiring highly enriched radionuclide sources and sophisticated coincidence counting instrumentation, which may include very large liquid scintillation detectors, with the capability of extreme suppression or vetoing of background radiation (Caccianiga and Giammarchi, 2000, Zuber, 2000, Fiorini, 2001, Chen, 2005, Elliott, et al., 2006, Gomez et al., 2007, Campbell, et al., 2008, Gehman et al., 2010, and McGrath et al., 2010). The National Nuclear Data Center of the Brookhaven National Laboratory (NNDC-BNL, 2011) currently lists ten nuclides that are known to undergo double beta decay: $^{48}_{20}$Ca, $^{76}_{32}$Ge, $^{82}_{34}$Se, $^{96}_{40}$Zr, $^{100}_{42}$Mo, $^{116}_{48}$Cd, $^{128}_{52}$Te, $^{130}_{52}$Te, $^{150}_{60}$Nd, and $^{238}_{92}$U. As discussed in Chapter 1, beta decay is not confined to negatron emission. There also exist positron and electron capture (EC) decay processes, which are other forms of beta decay. Research is underway with very large detectors including liquid scintillation detectors for the measurement of $\beta^+\beta^+$, β^+/EC, and double EC decay processes (Zuber, 2000, Barabash et al., 2007, 2008 and Kolhinen et al., 2010).

There is much research underway in numerous laboratories around the world directed toward the search for the detection of neutrinoless double beta decay utilizing liquid scintillation detectors and other detection methods, and only a few of the reports on this work are cited here (Caccianiga and Giammarchi, 2000, Zuber, 2000, Fiorini, 2001, Klapdor-Kleingrothaus, et al., 2004, Chen, 2005, Kraus, 2006, Hwang et al., 2007, 2009, Cremonesi, 2010, Gehman et al., 2010, Ejiri, 2010, and Kraus and Peeters, 2010). Beyond the standard model, there exists the possibility that the neutrino could be its own antiparticle referred to as a Majorana neutrino. According to this theory, if the neutrino possesses a rest mass (now estimated to have a mass upper limit of 2.3 eV/c^2) and is its own antiparticle, a neutrino emitted in one beta decay could be reabsorbed in the second beta decay resulting in a double beta decay in which no neutrinos are emitted. *i.e.*, a neutrinoless double beta decay often abbreviated as $0\nu\beta\beta$ (see Chapter 1). Current research in the search for neutrinoless double beta decay is important, because it would affirm the mass of the neutrino, as only a particle with a definite rest mass can oscillate from one form into another.

A reported observation of $0\nu\beta\beta$ in ^{76}Ge was made by Klapdor-Kleingrothaus et al. (2004) and confirmed (Klapdor-Kleingrothaus, 2006 and Klapdor-Kleingrothaus and Krivosheina, 2006) after data collection over a period of 13 years with high-purity p-type germanium detectors enriched in ^{76}Ge to 86−88%. Such a detection arrangement is optimum in terms of yielding maximum detection efficiency for a given detection method, because the source (^{76}Ge) is the detector. *i.e.*, source = detector.

Other methods, for the detection of neutrinoless double beta decay, include the incorporation of the nuclide source into the liquid scintillation detector. Some nuclides that undergo double beta decay and are easily loaded into liquid scintillators are being studied to observe the neutrinoless double beta decay. For example, Caccianiga and Giammarchi (2000) discuss the methods and sensitivity for a liquid scintillation double beta decay experiment based on ^{136}Xe in Borexino and the Borexino counting test facility, which is constructed in the Laboratorio Nazionale del Gran Sasso, Italy. The Borexino detector design is illustrated in Fig. 7.84. The detector has a capacity for 300 tons of liquid scintillator viewed by 2200 photomultipliers, and the detector is shielded by 3300 tons of radiopure liquids. Caccianiga and Giammarchi (2000) underscore the critical factors upon which the detection of double beta decay depends, which are (i) the signal detection efficiency, (ii) the number of candidate atoms (which for calorimetric detectors is related to the mass of the detector and to the enrichment of the sample), (iii) on the time or duration of collection of data, and (iv) on the background counts per unit time in the relevant energy window.

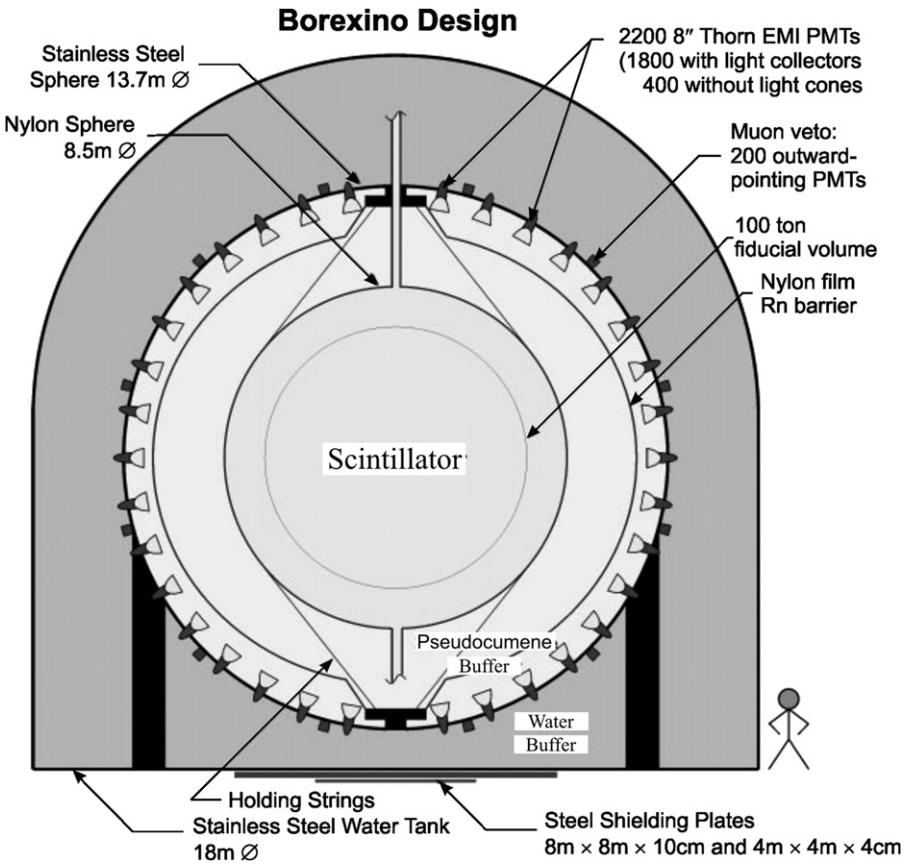

FIGURE 7.84 Schematics of the Borexino detector. An abstract figure of a person is drawn on the right side to provide an idea of the relative size of the detector. Inside an external water tank (18 m in diameter), a stainless steel sphere supports 2200 photomultiplier tubes (PMTs) directed toward the internal part of the detector containing the liquid scintillator. An additional 200 PMTs view the water shield acting as muon tagging. The scintillating volume is enclosed in a 8.5-m nylon sphere at the center containing a mass of 300 tons of scintillator. *(From Arpesella et al., 2008, Ranucci, 2007, and Ianni, 2011). Reprinted with permission from Elsevier © 2007)*

We may take the case of ^{136}Xe as an example. The double beta decay of ^{136}Xe could occur by either of the following two processes:

$$^{136}_{54}\text{Xe} \rightarrow {}^{136}_{56}\text{Ba} + 2\beta^- + 2\overline{\nu} \text{ “two neutrino double beta decay”or “}2\nu\beta\beta\text{”} \quad (7.129)$$

or

$$^{136}_{54}\text{Xe} \rightarrow {}^{136}_{56}\text{Ba} + 2\beta^- \text{ “neutrinoless double beta decay”or “}0\nu\beta\beta\text{”} \quad (7.130)$$

The $Q_{\beta\beta}$ value for the ^{136}Xe is 2.479 MeV. In the case of $2\nu\beta\beta$, the 2.479 MeV decay energy would be shared among four particles, namely, the two beta particles and the two antineutrinos. However, in the case of $0\nu\beta\beta$, the 2.479 MeV decay energy would be shared only among the two beta particles. Thus, the $2\nu\beta\beta$ double beta (*i.e.*, two electron) spectrum, for the ^{136}Xe decay would encompass a broad spectrum of energies, as illustrated in Fig. 7.85, because the two beta particles must share the decay energy with the antineutrinos, whereas $0\nu\beta\beta$ double beta (*i.e.*, two electron) spectrum would be a line spectrum centered at the decay energy of 2.479 MeV, as illustrated in Fig. 7.85, as the two beta particles are emitted simultaneously and share the entire decay energy. In the search for two neutrino double beta decay ($2\nu\beta\beta$), two beta particles would be detected simultaneously, and the sum of their energies would always be less than the decay energy. However, evidence for neutrinoless double beta decay ($0\nu\beta\beta$) would be provided by the simultaneous detection of two beta particles with combined energies equal to the decay energy. The advantage of using liquid scintillation for the detection of double beta decay of ^{136}Xe is that the xenon gas can be dissolved directly into the liquid

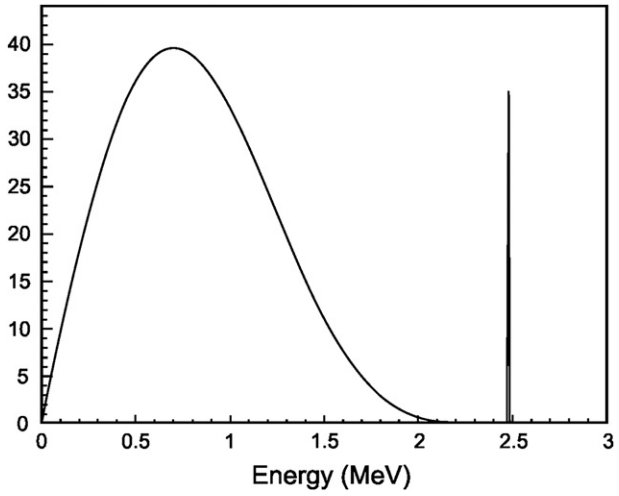

FIGURE 7.85 Double beta decay two-electron spectra for the case of Xenon-136. The broad spectrum on the left is that of the double beta energies for the $2\nu\beta\beta$ decay and the line spectrum on the right is that of $0\nu\beta\beta$ decay. The vertical scale is in arbitrary units and the proportion between the neutrinoless line and the $^{136}\text{Xe} \rightarrow {}^{136}\text{Ba} + 2e^- + 2\,\overline{\nu}$ is arbitrary as well. The $Q_{\beta\beta}$ value is 2.479 MeV. *((From Caccianiga and Giammarchi, 2000. Reprinted with permission from Elsevier © 2000). The reader may compare this isotope-specific figure with the general one illustrated in Fig. 1.44 of Chapter 1)*

scintillator permitting the detection of the two beta-particle kinetic energies. In addition, 10 kg of the xenon is available enriched at 64% in ^{136}Xe (Caccianiga and Giammarchi, 2000 and Fiorini, 2001).

An alternative approach to the detection of neutrinoless double beta decay in ^{136}Xe is to convert the source into the detector (*i.e.*, source = detector). In other words, rather than add the ^{136}Xe to liquid scintillator, the approach would be to take advantage of the fact that liquid xenon itself undergoes excitation with the emission of scintillation light photons at 175 nm wavelength in the vacuum ultraviolet (VUV) region (see Section XVII). Thus, liquid xenon enriched in ^{136}Xe would serve as both the source of the decay emissions and the detector. This technique is currently taken by the EXO-200 collaboration, which involves the construction of a 200-kg detector of liquid xenon enriched in ^{136}Xe to 80%. Construction of the detector was carried out at the SLAC National Accelerator Laboratory of Stanford University, Menlo Park, CA, USA, and it is being installed at the Waste Isolation Power Plant (WIPP) near Carlsbad, NM, USA. The detector consists of a cylindrical chamber containing the 200 kg of liquid xenon enriched in ^{136}Xe to 80% surrounded by a cylindrical wall of VUV Teflon reflectors and two walls of avalanche photodiodes (APDs) for the detection and gain multiplication of the scintillation photons. When a double beta decay event occurs in the ^{136}Xe, the beta particles will interact with the liquid xenon. The liquid xenon will emit scintillation photons that are detected by the APDs. In the planning stage is the EXO Collaboration, which is a 1-ton detector of liquid xenon enriched in ^{136}Xe including the tagging of the ^{136}Ba daughter nuclides, which would provide a complete elimination of background. Detailed descriptions of the EXO-200 detector and the techniques used to detect neutrinoless double beta decay in ^{136}Xe are provided by Leonard et al. (2008), Ueshima et al. (2008), and Neilson et al. (2009).

Another example is the conversion of the Sudbury Neutrino Observatory (SNO) in Canada into a liquid scintillation detector (named SNO+) for double beta decay measurement with ^{150}Nd (Chen, 2005, Kraus, 2006, and Kraus and Peeters, 2010). The SNO+ detector yields low backgrounds and can hold 1000 tons of liquid scintillator; and the scintillator is viewed with about a 60% effective area coverage with photomultiplier tubes. A large quantity of ^{150}Nd can be loaded into the liquid scintillator. A 1% load in the scintillator would amount to 10 tons of material. The ^{150}Nd has a high $Q_{\beta\beta}$ value of 3.37 MeV and 5.6% natural abundance. A high $Q_{\beta\beta}$ value is important, because it would place the $0\nu\beta\beta$ peak well above external background pulses. Chen (2005) calculates that, for an effective neutrino mass of 0.150 eV/c^2, the $0\nu\beta\beta$ decay rate of ^{150}Nd, at its natural abundance, would be 1000 events/year. A simulated spectrum of double beta decay events in the SNO+ detector is provided in Fig. 7.86. The measurement of neutrinoless double beta decay will be made by measuring the distortion in the energy spectrum of decays at the endpoint. Kraus and Peeters (2010) report that the study will be carried out 6800 ft (2072 m) underground providing a low background environment with 6010 m water equivalent of shielding from cosmic rays. The main goal is the measurement of the neutrinoless double beta decay. The option

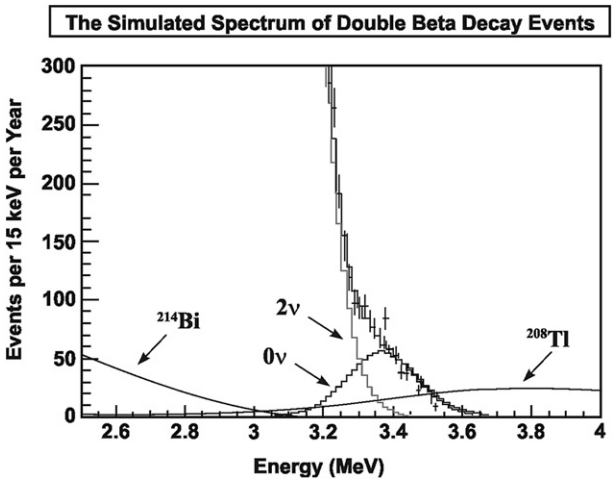

FIGURE 7.86 Double beta decay measurements with the SNO+ detector with natural Nd loaded at 1% in liquid scintillator. High statistics enables separation of 0ν from 2ν $\beta\beta$ events, despite the poor energy resolution. *(From Chen, 2005. Reprinted with permission from Elsevier © 2005)*

of loading enriched ^{150}Nd into the scintillator, which would increase the sensitivity, is under consideration. The scintillator will consist of a linear alkylbenzene solvent with 2 g/L of 2,5-diphenyloxazole (PPO), and the Nd will be loaded into the scintillator at a 1% concentration as a carboxylate. It is reported that the filling of the scintillator into the SNO+ detector will start in early 2011, and the collection of data will commence in the Spring of 2011.

Other interesting examples of the application of liquid scintillation to the measurement of double beta decay are (i) the proposed use of large-scale Yb-loaded liquid scintillator to measure $\beta\beta$ decay of ^{176}Yb (Zuber, 2000), (ii) studies of Sn-loaded liquid scintillator to study $\beta\beta$ decay of ^{124}Sn (Hwang et al. 2007, 2009), and (iii) the proposed use of Mo-loaded scintillator to study $\beta\beta$ decay of ^{100}Mo (Gehman et al. (2010) as well as (iv) loading liquid scintillator with ^{82}Se and ^{116}Cd, among others (Ejiri, 2010).

XII. DETECTION AND MEASUREMENT OF NEUTRINOS

In a letter addressed to the participants of a Regional Meeting on Radioactivity at Tübingen, Germany, on 4 December 1930, Wolfgang Pauli postulated the existence of an elusive neutral particle of near-zero rest mass, which would accompany beta decay (see Chapter 1). The particle remained elusive and unproven as to its existence for over 25 years. Nevertheless, during that time, the particle remained an essential component in our understanding of beta decay. In 1934, Enrico Fermi coined this particle as the 'neutrino' from the Italian language meaning "little neutral one" in his elaboration of the beta-decay theory.

A. Reines and Cowan Reaction

The neutrino remained elusive until 1956, when its existence was demonstrated finally by Nobel Laureate Frederick Reines and Clyde Cowan, Jr. (Reines and Cowan, Jr, 1953, 1956, 1957).

They confirmed the existence of the neutrino using liquid scintillation detectors to demonstrate inverse beta decay where an antineutrino interacts with a proton to yield a neutron and positron, *i.e.*,

$$\overline{\nu} + p^+ \rightarrow n + e^+ \tag{7.131}$$

They constructed a liquid scintillation detector next to a 700-MW nuclear reactor at the Savannah River Plant in Aiken, SC, USA, to detect the abundant antineutrinos emitted by the beta decay of fission products. Their detector was composed of a target chamber consisting of 200 liters of water containing 40 kg of dissolved $CdCl_2$ sandwiched between two tanks of 1400 liters of liquid scintillation solution schematically illustrated in Fig. 7.87. Each end of the scintillator tanks was viewed by 55 photomultiplier tubes (not illustrated). The water provided target protons for the antineutrinos. As illustrated in Fig. 7.87, the interaction of an antineutrino with a water proton would create a neutron (n) and a positron (β^+). The positron would be annihilated when coming to rest and in contact with an electron, and the resulting annihilation radiation (two 0.51-MeV gamma-ray photons emitted in opposite directions) would be detected in coincidence by the two liquid scintillation detectors above and below the water tank (Fig. 7.87). The neutron produced by the antineutrino interaction would slow down quickly (~10 μsec) in the water and be captured by a cadmium nucleus in the water target chamber. The characteristic multiple gamma rays following the neutron capture would be detected in coincidence by the two liquid scintillation detectors. The antineutrino signature therefore consisted of a delayed coincidence between the prompt scintillation pulses produced by the β^+ annihilation and the scintillation pulses produced microseconds later by the neutron capture in cadmium. With the unique signature for the antineutrino provided by the detector design devised by Reines and Cowan, the high neutron flux produced by the Savannah River reactor (1.2×10^{13}/cm^2 sec), and reduced cosmic ray backgrounds from massive shielding 11 meters from the reactor and 12 meters underground were essential to the success of their experiment. Nevertheless, a detector running time of 100 days over a period of about one year was required to provide sufficient conclusive signals from the antineutrino signature.

A more complete account of Pauli's hypothesis of the existence of the neutrino and the work of Reines and Cowan, which culminated in the discovery of the neutrino, is provided in a previous book by the author (L'Annunziata, 2007).

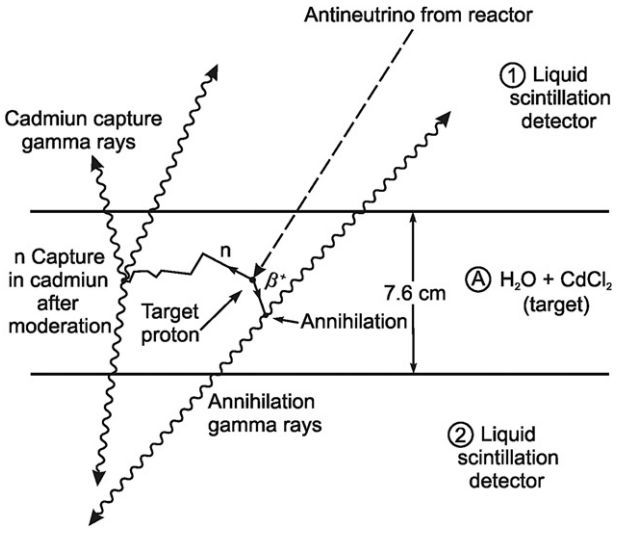

FIGURE 7.87 Detection scheme used by Reines and Cowan for the antineutrino signature signal (from Reines, 1995, Nobel Lecture with permission from The Nobel Foundation ©1995). An antineutrino is illustrated entering the tank of aqueous $CdCl_2$ solution and striking a target proton. The proton converts to a neutron and positron. The positron annihilates on an electron with the emission of two 0.511-MeV gamma rays in opposite directions detected by the liquid scintillator in tanks above and below the water target tank. The neutron produced by the antineutrino interaction slows down in the water and is captured by a cadmium nucleus, and the resulting gamma rays are detected by the liquid scintillator in the adjacent tanks approximately 10 microseconds after the positron annihilation.

B. Liquid Scintillation Schemes for Neutrino Detection and Measurement

The detection scheme of Reines and Cowen described above is one among others used today for the liquid scintillation detection and measurement of neutrinos. Among the schemes available for neutrino detection and measurement by liquid scintillation are the following:

1. Neutrino-Electron Scattering

The neutrino-electron elastic scattering reaction, $\nu e^- \rightarrow \nu e^-$, due to charged current (CC) and neutral (NC) weak current interactions, is detected in a large mass (>100 tons) of liquid scintillator. Solar neutrinos can be detected via this elastic scattering reaction, such as planned in the Borexino and SNO+ collaborations for the measurement of solar neutrinos described below. The scattered electron can receive any kinetic energy from the neutrino less than or equal to the kinetic energy of the neutrino (Kraus, 2006). A wide spectrum of pulse heights from the different scattering reactions will be produced in the liquid scintillator, but for monoenergetic neutrinos characteristic of certain nuclear reactions inside the sun, a liquid scintillation spectral 'Compton-like' edge can serve as a signature for a ν-line energy (Alimonti et al., 2002). For example, the solar neutrinos that are a result of the ^{7}Be electron capture reaction in the sun produce a mono-energetic ν line at 0.86 MeV. As described by Alimonti et al. (2002) and illustrated in Fig. 7.88, the ^{7}Be$-\nu$ line at 0.86 MeV produces a profile of the recoil electrons in the liquid scintillator in the form of a 'flat box' with a spectral 'Compton-like edge' at 0.66 MeV. This serves as a spectroscopic signature for the solar ^{7}Be neutrinos. Alimonti et al. (2002) provides an estimate of the neutrino event rate that would be expected from 100 tons of liquid scintillator target material (*e.g.*, 0.17% PPO fluor in 100 tons of pseudocumene solvent). With a 100-ton scintillator detector, based on the standard solar model with ^{7}Be neutrino flux arriving at Earth of $4800 \pm 430 \times 10^6$/cm^2 sec and an energy window of 250−800 keV (See Fig. 7.88), an event rate of 55/day is expected due to CC interactions. If the solar electron neutrinos (ν_e) from the ^{7}Be reaction are fully converted to other active flavors by the time they arrive at Earth (*e.g.*, ν_μ and μ_τ) the liquid scintillation event

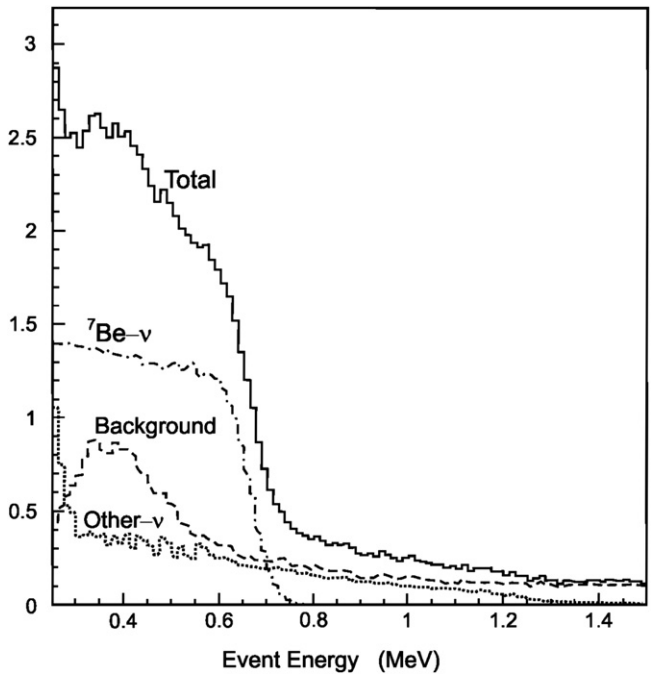

FIG. 7.88 Monte Carlo simulation of liquid scintillation ν signals and backgrounds (in arbitrary units). Plotted are the ^{7}Be$-\nu$ signal expected from the standard solar model (dotted-dashed), the signal from all other neutrino sources together (dotted), the background (dashed), and the sum spectrum from all events (solid line). The background is calculated for liquid scintillation cocktail purified to uranium level of 10^{-16} gU/g, an α/β discrimination of 90%, and 1 σ statistical cuts. *(From Alimonti et al. and the Borexino Collaboration, 2002. Reprinted with permission from Elsevier © 2002)*

rate would drop to ~20%, because these other flavors cause neutrino-electron scattering only via the NC weak interactions, which has a lower effective cross section. Thus, it is predicted that, if all of the solar electron neutrinos change flavor, the event rate that would be detected with 100 tons of scintillator would drop to 11/day. Years of data taking and extreme measures of background reduction are required for conclusive detection and measurement of solar neutrinos.

2. Reines–Cowan Inverse Beta Decay Reaction.

The Reines–Cowan reaction described previously is commonly used for the detection and measurement of anti-neutrinos, where fission product beta-decay is abundant, emitting electron anti-neutrinos ($\overline{\nu}_e$). The anti-neutrinos are detected by inverse beta decay

$$\overline{\nu}_e + \mathrm{p}^+ \rightarrow \mathrm{n} + e^+ \tag{7.132}$$

with a threshold energy $Q = 1.80$ MeV (Alimonti et al., 2002 and Kraus, 2006). The positron (e^+), that is emitted, will possess a kinetic energy equal to the neutrino energy (E_ν) $- Q$, which is deposited in the liquid scintillator. In addition, the positron almost immediately undergoes annihilation in contact with an electron of the scintillation cocktail (e^+e^- annihilation energy = 1.02 MeV). The positron signal created in the liquid scintillator will be the sum of its kinetic energy + 1.02 MeV annihilation energy (Alimonti et al., 2002 and Kraus, 2006). Neutrino spectroscopy is therefore possible, as the energy deposited (E_{dep}) and the pulse height produced (PH) in the liquid scintillator by the positron is proportional to the anti-neutrino energy or

$$\begin{aligned} \mathrm{PH} \propto E_{\mathrm{dep}} &= E_\nu - 1.80\ \mathrm{MeV} + 1.02\ \mathrm{MeV} \\ &= E_\nu - 0.78\ \mathrm{MeV} \end{aligned} \tag{7.133}$$

Even at the anti-neutrino threshold energy where $E_\nu = Q = 1.80$ MeV, the inverse decay reaction produces a liquid scintillation pulse signal at 1.02 MeV, which corresponds to the annihilation radiation. A delayed coincidence pulse resulting from the capture of the neutron serves as a tag or signature for the inverse beta decay reaction. Alimonti et al. (2002) point out that the $\overline{\nu}_e$ tag is made possible by a delayed coincidence signal produced by a 2.2-MeV γ-ray emitted by the capture of the neutron by a proton. The delayed coincidence pulse occurs ~200 μsec after the emission of a neutron from the inverse beta decay, which is the delay caused by the moderation of the neutron to thermal energies and its capture by a proton of the liquid scintillator. The delayed coincidence of ~200 μs of the positron annihilation signal and the 2.2-MeV gamma-ray signal produced by a neutron capture on a proton serves at the $\overline{\nu}_e$ tag. The unique $\overline{\nu}_e$ tag reduces background by a factor of ~100 (Alimonti et al., 2002).

The Reines–Cowan reaction in Gd-loaded liquid scintillator is reported by Dai et al. (2011) for the measurement of reactor anti-neutrinos as a tool in nuclear safeguards, which is currently implemented at the San Onofre Nuclear Generating Station, USA. Ding et al. (2008) also report the use of Gd-loaded scintillator for reactor antineutrino ($\overline{\nu}_e$) detection at the Daya Bay Nuclear Power Plant. Research is underway to improve the quality, purity, and performance of Gd-loaded scintillators for large neutrino detectors (Yeh et al., 2010). Gadolinium has a very high thermal neutron capture cross section (see Table 1.17 of Chapter 1); the delayed signal due to neutron capture in Gd is shorter (~30 μsec) than that produced in conventional liquid scintillator (~200 μsec), and it is identified with the emission of an ~8-MeV gamma ray. The strong gamma-radiation provides a unique signature, for the incident anti-neutrino and thus improved background reduction. The measurement of the anti-neutrino production by reactors can be used to reveal the fissile composition of reactor fuel, thereby providing continuous, nonintrusive, and unattended measurements important to nuclear safeguards Dai et al. (2011).

3. Inverse Beta Decay Yielding Negatrons and Unstable Nuclei

In contrast to the detection of anti-neutrinos discussed in the previous Reines–Cowan reaction, neutrinos can be detected by inverse beta decay producing negatrons or

$$\nu_e + \mathrm{n} \rightarrow \mathrm{p}^+ + e^- \tag{7.134}$$

where the neutrino interacts with a neutron of a nucleus in the liquid scintillator yielding a proton and a beta particle or negatron. If the product nucleus is unstable, the energy deposited in the scintillator by the nuclear decay can provide a tag for the neutrino interaction. Several nuclei may be used for neutrino interactions, which would yield an unstable nucleus and suitable tag for the neutrino inverse beta decay. Raghaven (1976) was first to indicate that inverse beta decay

on ^{115}In would make for an efficiency solar neutrino detector and In-loaded liquid scintillators with up to 15 wt % In have been developed for solar neutrino detection (Motta et al., 2005, Raghaven, 2001, Suzuki et al., 1990, and Payne and Booth, 1990). The reverse beta decay reaction of a neutrino with ^{115}In is written as

$$\nu_e + {}^{115}_{49}\mathrm{In} \rightarrow {}^{115}_{50}\mathrm{Sn}^* + e^- \tag{7.135}$$

where the ^{115}Sn product nucleus is unstable indicated by an asterisk superscript. This reaction has a low threshold energy of 128 keV, which provides the measurement of the incident neutrino energy as

$$E_{\nu_e} = E_{e^-} + 128\ \mathrm{keV} \tag{7.136}$$

where E_{ν_e} is the incident neutrino energy and E_{e^-} is the beta particle or negatron energy deposited in the liquid scintillator (Suzuki et al., 1990). The low threshold (128 keV) of the indium reaction provides a high sensitivity of this scintillator to neutrinos from the solar proton−proton fusion reaction ($\leq$430 keV) and to solar neutrinos produced by electron capture (EC) in ^{7}Be (860 keV) as pointed out by Payne and Booth (1990). The ^{115}Sn daughter nucleus decays with a very short half-life (3.2 μsec) by isomeric transition emitting three gamma rays at 101, 116, and 498 keV, which provide a unique signature for the incident neutrino.

Other examples of reactions in liquid scintillator that have potential for the detection and measurement of solar neutrinos by inverse beta decay are the following:

$$\nu_e + {}^{160}_{64}\mathrm{Gd} \rightarrow {}^{160}_{65}\mathrm{Tb}^* + e^- \tag{7.137}$$

$$\text{and } \nu_e + {}^{176}_{70}\mathrm{Yb} \rightarrow {}^{176}_{71}\mathrm{Lu}^* + e^- \tag{7.138}$$

The excited states of ^{160}Tb*and ^{176}Lu*de-excite with very short lifetimes of 75 nsec and 50 nsec, respectively, emitting gamma rays of 63.7 keV and 72 keV, respectively. Gratta and Wang (1999) point out that the low threshold for these reactions of 240 keV and 300 keV are well below the maximum solar proton−proton fusion neutrino energy. Also, the very fast (nsec) correlation time between beta-particle energy (e^-) deposition in the scintillator and γ-ray emission by the daughter nuclides provides a powerful signature for the solar neutrino event and background reduction. Lightfoot et al. (2004) report the development of 10 wt % Gd-loaded liquid scintillator for solar neutrino detection as well as neutron measurements.

4. Neutrino Charged Current Interactions with ^{13}C

The charged current interaction of solar neutrinos with ^{13}C nuclei naturally occurring in liquid scintillator can be used to detect the high-energy solar neutrinos derived from the ^{8}B reaction in the sun, which yields neutrino energies $\leq$15 MeV (Ianni et al., 2005). The ^{13}C isotope occurs naturally with an abundance of 1.1%. When very large neutrino detectors are involved, which utilize hundreds or even thousands of tons of liquid scintillator (*e.g.*, KamLAND, Borexino, SNO+, and LENA collaborations for solar neutrino detection and measurement), the mass of ^{13}C in the scintillator will measure in tons. The charged current interaction of a neutrino with a ^{13}C nucleus with the transition of the unstable ^{13}N product nucleus to the ground state is the following:

$$\nu_e + {}^{13}_{6}\mathrm{C} \rightarrow {}^{13}_{7}\mathrm{N}_{\mathrm{grd}} + e^- \tag{7.139}$$

The reaction threshold is $Q = 2.22$ MeV, and the kinetic energy of the electron or negatron (T_e) can be expressed as $T_e = E_\nu - Q$ neglecting the small recoil energy of the ^{13}N nucleus, which is of the order of a few keV (Ianni et al., 2005). The pulse height produced by the negatrons can thus provide spectrometry of solar neutrinos derived from the ^{8}B reaction in the sun, which are of energy in excess of the 2.22 MeV threshold energy. Ianni et al. (2005) point out the advantage of this mode of detection is that the process of ^{13}N decay to its ground state by positron emission according to

$${}^{13}_{7}\mathrm{N} \rightarrow {}^{13}_{6}\mathrm{C} + \nu_e + e^+ \tag{7.140}$$

can be used to monitor the solar neutrino interactions with the ^{13}C nuclei, as the visible energy released in the ^{13}N decay is the sum of the positron kinetic energy and the energy released in the e^+e^- annihilation.

C. Collaborations for LS Neutrino Detection and Measurement

There are several international collaborations underway with the objective of measuring the neutrino flux and its properties from the sun and other sources by means of liquid scintillation. The advantage of liquid scintillation is the possibility of preparing hundreds and even tens of thousands of tons of scintillator. Such liquid scintillators provide tons of target material for the elusive neutrino. Even with such large detectors, years of scintillator signal collection and extreme measures of background reduction are required. Ianni et al. (2005) provides a good review of high-energy ^{8}B solar neutrinos and the international collaborations for the liquid scintillation measurement of neutrinos that are underway or planned for the future. Among the international collaborations are the following:

KamLAND Collaboration. The Kamioka Liquid Scintillator Anti-Neutrino Detector (KamLAND) is a 1-kiloton (kt) detector located in the Kamioka mine of Japan at a depth of 2700 m.w.e. of rock. It has been operating continuously since 2002. The main goal of the KamLAND collaboration is the measurement of the electron anti-neutrino ($\overline{\nu}_e$) flux from the nuclear power plants of Japan. The KamLAND collaboration has also provided data on geoneutrinos and the upper limits on the speculative nuclear reactor operating in the Earth's core (the so-called georeactor), as well as information on solar neutrinos. The electron anti-neutrinos are detected by the inverse beta-decay reaction discussed in Section XII.B.2, that is,

$$\overline{\nu}_e + \mathrm{p}^+ \rightarrow \mathrm{n} + e^+ \tag{7.141}$$

$$\text{and } \mathrm{n} + \mathrm{p} \rightarrow \mathrm{d} + \gamma(2.2\ \mathrm{MeV}) \tag{7.142}$$

The electron anti-neutrino event is identified by the correlated signals produced by the prompt positron and the delayed

2.2 MeV arising from the thermal neutron capture reaction. Reviews on the work of the KamLAND Collaboration are provided by Yoshida et al. (2010), Araki et al. (2005), and Folgi et al. (2005).

Borexino Collaboration. Borexino is a 300-ton liquid scintillation detector close to being commissioned for operation at the underground National Gran Sasso Laboratory in Italy. The detector was described in detail in Section XI (see Fig. 7.84). The main goal of Borexino is the measurement of ^{7}Be solar neutrinos by the neutrino scattering off of electrons of the scintillator (*i.e.*, $\nu + e^{-} \rightarrow \nu + e^{-}$), described in more detail in Section XII.B.1. Reviews on the work of the Borexino Collaboration are provided by Alimonti et al. (2009, 2002), Arpesella et al. (2008), and Ranucci (2007).

SNO+ Experiment. The SNO+ experiment is a neutrino experiment, which will involve the reutilization of the underground detector hardware of the Sudbury Neutrino Observatory (SNO) located in Vale Inco's Creighton mine, Sudbury, ON, Canada. The current heavy water neutrino target of SNO will be replaced with a liquid scintillator for the experiment renamed as SNO+. The main goal of SNO+ will be the search for neutrinoless double beta ($0\nu\beta\beta$) decay discussed previously in Section XI. However, the experiment will have capability to research neutrinos including lower-energy solar neutrinos, geo- and reactor anti-neutrinos, and supernova neutrinos. A review on SNO+ is given by Kraus and Peeters (2010).

LENA. A low-energy neutrino astrophysics (LENA) detector is in the planning stage. It would be the largest of all neutrino liquid scintillation detectors. The detector would consist of 50 kilotons of PXE (Phenyl-ortho-xylylethane) or LAB (linear alkyl benzene)-based scintillator with a diameter of 30 m and a height of 100 m. The scintillator would be surrounded with 30,000 photomultiplier tubes. The outer part of the detector would be surrounded with water shielding, which would serve as a Cherenkov detector for cosmic muons. LENA would be placed underground at a depth of 4000 m.w.e. or greater. The detector would serve as a unique instrument capable of low-energy neutrino measurement and the search for rare events. Possible locations for the LENA detector are the Pyhäsalmi mine in Finland at a depth of 150 m (~4000 m.w.e.) or underwater in the site of Pylos, Greece. Reviews on the progress of LENA and its objectives are available from Lachenmaier et al. (2010), Hochmuth et al. (2007), and Marrodán Undagoitia (2006).

XIII. MICROPLATE SCINTILLATION AND LUMINESCENCE COUNTING

Many applications use radioactivity as a method of screening numerous compounds or reactions in an effort to find a new therapeutic agent, drug candidate, or to assess a molecular biology function. In these types of applications, many thousands of samples may be counted each week. Because of the numerous samples involved, large amounts of scintillation vials and cocktail are required for traditional liquid scintillation analysis, which add cost to the sample analysis. This large number of samples also creates a large amount of radioactive waste. Consequently, microplate scintillation counting instruments have been developed to reduce waste, increase sample throughput via the simultaneous analysis of several samples with multiple detectors, provide automation capabilities, and reduce the cost of consumable materials and waste disposal.

The microplate scintillation counter uses a microplate sample format, which was developed to provide for the analysis of large numbers of samples. A microplate is a small container with many sample wells. It is about the size of a postal card measuring approximately $5 \times 3.4 \times 0.75$ inches (L × W × H). The microplate comes in three sample-well formats, namely, 24-well plates (6×4 wells), 96-well plates (12×8 wells), and 384-well plates (24×16 wells). The 24-well microplate sample wells hold up to 375 and 1500 μL of sample plus scintillation cocktail per well for shallow- and deep-well plates, respectively. The 96-well microplate sample wells hold 75 and 350 μL of sample per well for shallow- and deep-well plates, respectively, and the 384-well microplate sample wells hold up to 80 μL of sample per well. It is clear that only relatively small samples can be analyzed in these microplates; however, the footprint is small, compact, and easy to automate. As a result of the small sample size and small amount of scintillation cocktail required, the activity analysis of many samples, often encountered in biological research, can be carried out without producing a large amount of radioactive waste. The second major feature of the microplate scintillation counter is the ability to count up to 12 samples simultaneously (*i.e.*, up to 12 detectors) in one microplate.

Only a brief description of the microplate scintillation analyzer is provided here. Additional information on this instrumentation is available in Chapter 16. The microplate scintillation and luminescence instrument can be of single- or multiple-detector design (up to 12 detectors). Some commercial microplate scintillation counters are the TopCount™ and MicroBeta™ counters available from PerkinElmer, Inc., Waltham, MA, USA and the Chamelion V™ available from HIDEX, Turku, Finland.

A. Detector Design and Background Reduction

The microplate scintillation and luminescence instrument can be of single- or multiple-detector design with up to 12 detectors all packed in close proximity in a very small area. The microplate instrument can count samples directly in microplate wells using one of two mechanisms: single or dual photomultiplier tube (PMT) detectors. In the single PMT detector arrangement, illustrated in Fig. 7.89, the PMT detectors are placed directly above the sample wells, whereas in the dual PMT arrangement there are two photomultipliers, one above and one below each sample well. With the single PMT arrangement a white reflective and opaque microplate is utilized, whereby light produced by the radioactivity in the liquid scintillator is reflected back toward the phototube; a unique method of background reduction, namely, time-resolved liquid scintillation counting (TR-LSC) is utilized. Microplate counters with two PMTs per sample can use coincidence counting to reduce background in addition to TR-LSC.

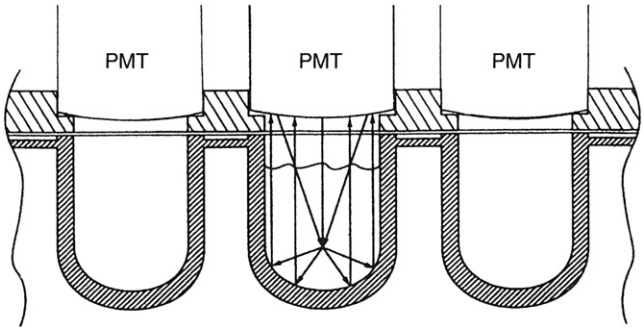

FIGURE 7.89 Single PMT detector design in microplate scintillation counting. A cross section of a microplate segment is illustrated showing three white opaque sample wells and three photomultiplier tubes (PMTs) aligned above each sample well whereby up to 12 PMTs analyze simultaneously as many as 12 samples. *(© 1998 Perkin Elmer, Inc. Printed with permission)*

The single-PMT time-resolved liquid scintillation counting (TR-LSC) technique uses pulse counting to distinguish between true scintillation pulse events and background noise. This obviates the need for a second PMT per sample and reduces lead shielding requirements. Single-PMT counting with TR-LSC uses scintillators with relatively long decay periods. A scintillator with a long decay constant emits photons, after β-particle excitation, over a longer period of time. Each scintillation pulse produces a photon packet followed by a series of pulses, as illustrated in Fig. 7.90, whereas PMT noise creates single pulse events. In TR-LSC the characteristics of a pulse are determined over a period of time (*e.g.*, 200 ns) after the initial photon packet is detected. If it is followed by one or more additional pulses within the resolving time period of 200 ns, the pulse is accepted as a true scintillation event. If no additional pulses are detected within the resolving time period, the initial pulse is rejected as background noise. The resolving time circuit to initiate pulse decay discrimination is triggered when a pulse height exceeds the single-photon event (SPE) threshold. The number of pulses above the SPE threshold is counted during the resolving time period. Multiple pulses detected in the resolving time are accepted as a valid event, which is further analyzed in the pulse-height analyzer of the LSA. If multiple pulses are not detected in the resolving time interval, the triggering pulse is rejected as background noise.

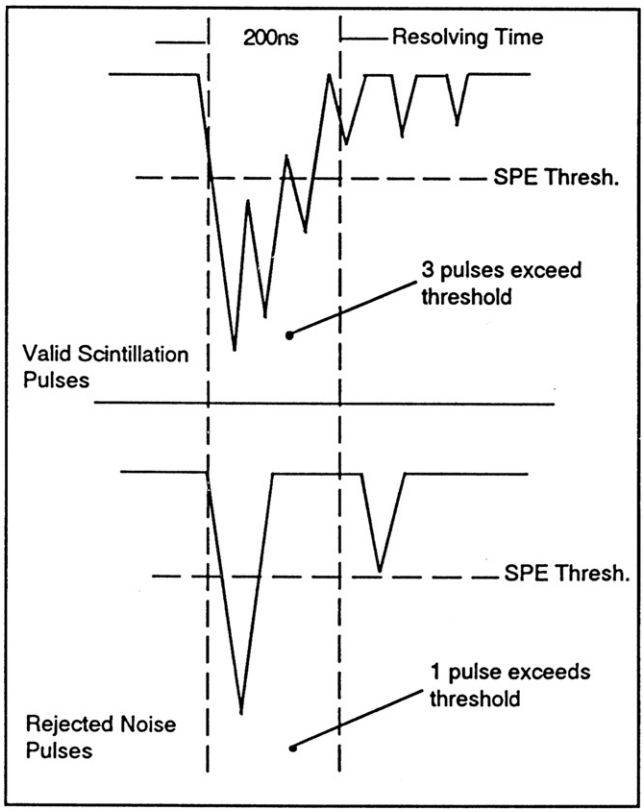

FIGURE 7.90 Time-resolved liquid scintillation counting (TR-LSC) employed in PerkinElmer microplate scintillation and luminescence counters. *(© 1998 Perkin Elmer, Inc. Printed with permission)*

B. Applications

A microplate scintillation and luminescence counter has broad applications, and with these are distinct sample preparation methods that are used for radioactivity analysis or luminescence counting. All of these applications are intended for small sample volume and high sample throughput analysis. Some of these are discussed briefly below.

1. Liquid scintillation analysis

When liquid scintillation counting is required with the microplate analyzer, scintillation cocktail and sample are added to each well of the microplate. This method is used for counting organic or aqueous samples directly in the microplate wells. An example of this can be taken from enzyme activity studies in which sample is extracted or filtered directly into the liquid scintillation cocktail and counted. Microplate liquid scintillation counting applications are numerous. Many examples of applications in the biosciences can be taken from the literature. Among these, a few will be cited including the analysis of ^{3}H, ^{35}S, and ^{125}I in biological samples with specific microplate liquid scintillation counters, namely, the TopCount™ (PerkinElmer, Inc., Waltham, MA, USA) liquid scintillation and luminescence counter (Rauly-Lestienne et al., 2011, He et al., 2011, Abdrakhmanova, et al., 2010, and Runyon et al., 2009), the MicroBeta™ (PerkinElmer, Inc., Waltham, MA, USA) liquid scintillation and luminescence counter (Heffernan et al., 2011, Kilander et al., 2011, Ooi et al., 2010, Skrlin et al., 2010), and the Chameleon V™ (HIDEX, Turku, Finland) liquid scintillation and luminescence counter (Matta, et al., 2011, 2008, López et al., 2010, Fraser and Strzeżek, 2007, and Yu et al., 2006).

2. Solid Scintillator Microplate Counting

Solid scintillation counting in microplates involves depositing a sample into the well of a special plastic microplate (*e.g.*, LumaPlate™, Scintiplate™, and Cytostar-T™), which contains a solid scintillator at the bottom of the well. The material is dried and then counted in a microplate scintillation counter. By this technique, the activities (DPM) of small volumes of any nonvolatile samples labeled with beta particle- or Auger electron-emitting nuclide may be determined. The small samples involved are particularly applicable to cytotoxicity, immunoassay, receptor binding, enzyme activity, and other metabolic

studies. In certain circumstances, the technique can replace conventional liquid scintillation analysis in counting vials when nonvolatile forms of the radionuclides and small volumes need to be analyzed. See Chapter 16 for additional information on this solid scintillation counting technique with microplate scintillation analyzers.

3. Scintillation Proximity Assay

Scintillation proximity assay (SPA) is a technology for the analysis of binding reactions, commonly studied in the medical and biochemical sciences, which circumvents the need to separate bound from free fractions. Glass or plastic solid scintillator microspheres are used in this assay together with an isotope-labeled (^{3}H or ^{125}I) ligand. With the use of modern liquid handling equipment and an automatic scintillation counter for samples in a microplate format, hundreds of samples may be prepared and analyzed in a single day, because traditional processes for the separation of bound and free fractions are not required. See Chapter 16 for additional information on the use of microplate scintillation counters for scintillation proximity assays.

4. Luminescence Assays

The microplate scintillation and luminescence counters are automated microplate luminometers suitable for use with all glow-type or enhanced flash-type luminescent chemistries. Bio- and chemiluminescence assays are carried out in the 96- or 384-well microplate format via single-photon counting (SPC). Applications include immunoassays, DNA probe assays, cell growth assays, and reporter gene assays. High-throughput automated and unattended assays are carried out with multiple-phototube detectors as previously described, while 96- or 384-well microplates are stacked in the instrument in quantities of 30 or more. Automated liquid handling systems and other robotic systems can allow unattended high-throughput screening utilizing glow luminescence as reported by Walton (1996). The background is approximately 20 counts per second (CPS) and accurate measurements of over 20×10^{6} CPS are possible.

Some examples of typical assays include reporter gene assays (Benísek et al., 2011, Mei et al., 2011, Aizenman et al., 2010, Paultz et al., 1996, and Scheirer et al., 1994), chemiluminescence assay of polymerase chain reaction products (de Castro Pazos et al., 2007, Rodríguez et al., 2006, Garson and Whitby, 1994, Kaneko et al., 1992, and Brilanti et al., 1991), neutrophil activation studies (Daou et al., 2011, Seki et al., 2011, Li et al., 2010, and Lieberman, 1995), and cell proliferation and cytotoxicity assays (Poerschke and Moos, 2011, Mei et al., 2011, Sughrue et al., 2010, and Roeland and Burns, 1995).

5. Receptor Binding and Cell Proliferation Assays

These techniques require filtration of the bound or reacted radionuclide from the free. There are two methods of performing this and both involve using a cell harvester. The cell harvester is a special instrument that can filter samples from each well of the microplate, deposits them onto a filter or membrane, and washes away the nonreacted or unbound radiolabeled material. Harvesters are available that can filter harvest from 6 to 96 samples simultaneously in a microplate format. The harvesting can be performed directly on a filter or membrane and cocktail added to the filter in a special "bag" or directly onto the filter in a holder. The second method is to use a filter-integrated microplate (*e.g.*, UniFilter plate) onto which harvesting can be performed directly using this microplate and cocktail added to each well prior to counting in a microplate scintillation counter. The most common assays of this type include receptor binding, which are used routinely for the evaluation of pharmaceutical agents by assessing their ability to interfere with the specific binding of a radiolabeled ligand to its receptor. See Chapter 16 for additional information on receptor-binding assays.

C. Advantages and Disadvantages

The microplate scintillation and luminescence counter has the basic advantage of high sample throughput, as up to 12 samples can be analyzed simultaneously for radioactivity or luminescence. Hands-off fully automated analysis of thousands of samples is possible, particularly in the simplest case of a microplate analyzer with 32 microplates stacked for counting, each microplate containing 96 samples wells, which provides for 3072 unattended analyses. Microplates containing 384 sample wells each with 80-μL capacity can be stacked up to 40 microplates at one time, which provides for over 15,000 samples of unattended analysis. The cost reduction in microplate counting compared with conventional liquid scintillation counting due to the reduced cocktail consumption and consequent reduction in radioactive waste expense and vial cost is a definite advantage. Microplates offer also a format that is easy to handle, leaving less chance for error caused from placing samples out of order, as sample wells cannot be mixed up or intermixed. Once samples are prepared on a microplate, they are kept in place on the microplate as a fingerprint. Microplates are easily portable and stored without occupying much space.

A disadvantage of the microplate scintillation analyzer is the small volumes of sample that can be accommodated in the sample wells. A 20 mL liquid scintillation vial can accept approximately 10 mL of aqueous sample mixed with 10 mL of suitable liquid scintillation cocktail. However, the largest sample well of a 24-well microplate has a capacity of only 1.5 mL (1500 μL), of which approximately 0.75 mL at most can be aqueous sample and 0.75 mL suitable cocktail − that is a 13-fold difference in sample size between the two methods of analysis. Therefore, for low sample activities in microplate scintillation counting longer counting times are required.

XIV. PERALS AND LS ALPHA-SPECTROMETRY WITH LAAPDS

Photon electron-rejecting alpha liquid scintillation (PERALS®) spectrometry was developed to provide an instrument that could measure α-particle radiation with good resolution, high counting efficiency, and low background.

A. PERALS Spectrometry

The interaction of alpha particles with liquid scintillation cocktail was described earlier in Section II.B. Of particular interest is that alpha particles are generally detected at a very

high counting efficiency of about 100% even with high degrees of quench in the scintillation cocktail. However, alpha particles produce only about one-tenth the light intensity (*i.e.* scintillation light output) as beta particles or gamma radiation per unit of radiation energy. A 5-MeV alpha particle will produce a pulse-height spectral peak at approximately 500 keV when liquid scintillation pulse heights are calibrated on a scale equivalent to particle energy in keV. (Such pulse-height energy scales are calibrated with beta particles or electrons, as electrons yield a linear light output per particle energy dissipated in the liquid scintillator as discussed previously in Section X.A.) This posed a problem in the liquid scintillation analysis of α-emitters when found in the presence of β-emitters or β−γ-emitters, because their pulse-height spectra would overlap even though the energy of the α-particle radiation was ten times that of the β-particle radiation. For example, the overlapping liquid scintillation pulse-height spectrum of the α-emitter ^{210}Po ($E = 5.30$ MeV) and the β-emitter ^{90}Sr ($E_{max} = 546$ keV) are illustrated in Fig. 7.2 in Section II.B. Therefore, since the early 1970s, research has gone into the development of liquid scintillation spectrometers that could reject the pulses produced by β and γ radiation and provide an instrument that could measure α-particle radiation with good resolution, high counting efficiency, and low background. This led to the development of photon electron-rejecting alpha liquid scintillation (PERALS®) spectrometry. The history of the work that led to the development of PERALS® spectrometry is described by McDowell and McDowell (1991). A description of the instrumentation, its performance, and applications will be provided here.

The development of PERALS® spectrometry had to solve two problems of α-particle liquid scintillation spectrometry: (1) the poor energy resolutions obtained with α-emitters in quenching aqueous-accepting scintillation cocktails in conventional liquid scintillation analyzers and (2) the interference caused by overlapping spectra from β- and γ-emitters in the same sample. The problem of resolution of α pulse-height spectra was solved by modifying the following elements of the liquid scintillation system as described by McDowell and McDowell (1993): (1) the α-emitters of interest had to be placed into a nonquenching, organophilic complex in a completely organic and highly efficient scintillator; (2) the detector assembly had to be modified with an efficient reflector arrangement and light-coupling optics to transmit the maximum amount of scintillation light to the photocathode of the PMT, and (3) a diffuse reflector had to be used in the detector assembly so that the scintillation light from an α event, anywhere in the sample would appear the same to the PMT, because of the nonuniform response of PMTs.

The basic design of the high-resolution α liquid scintillation spectrometer, known as the PERALS® spectrometer, is illustrated in Fig. 7.91. The PERALS spectrometer is produced by ORDELA, Inc, Oak Ridge, TN, USA. The α-emitters are first placed into an organic "extractive scintillator" often via some solvent extraction process that enables the radionuclides to pass from the aqueous sample phase into the organic scintillator phase. The extractive scintillator contains an organic extractant (extractive molecule) capable of forming selective complexes with certain alpha emitters to facilitate their removal from aqueous solutions and transfer into the organic scintillator phase. The organic extractants chosen must be pure, exhibit a minimum of quenching, and be high in the extractive power for the target element(s) as described by McDowell and McDowell (1993) and McDowell (1996). Popular extractive scintillators consist of a combination of scintillator (*e.g.*, PPBO), solvent (*e.g.*, toluene), and an extractant. Some commercial extractive scintillators used for PERALS® spectrometry are provided by ETRAC, Knoxville, TN, USA, among which are ALPHAEX® (actinide extracting scintillator),

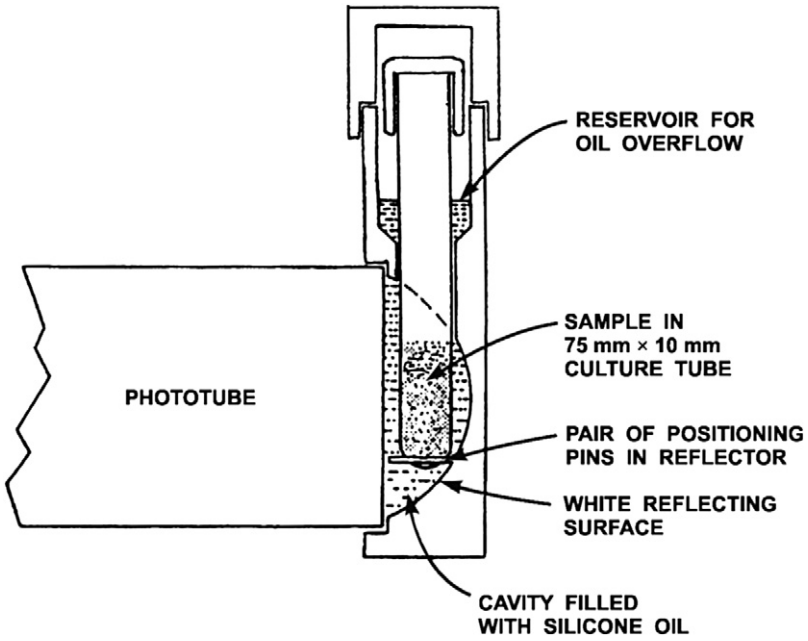

FIGURE 7.91 Cross section of a PERALS® spectrometer detector. *(From McDowell and McDowell, 1993, Reprinted with permission from Radiocarbon, University of Arizona, © 1993 Arizona Board of Regents on behalf of the University of Arizona)*

THOREX® (thorium extracting scintillator), URAEX® (uranium extracting scintillator), POLEX® (polonium extracting scintillator), and RADAEX® (radium extracting scintillator, and RADONS® (radon extracting scintillator). Extractive scintillators generally contain an organic extractant, such as di(2-ethyl-hexyl)-phosphoric acid (HDEHP), 1-nonyldecylamine sulfate, tri-*n*-octylamine sulfate (TNOA), or tri-octylphosphine oxide (TOPO).

A culture tube measuring 10×75 mm containing 1 mL of the radionuclide sample in the extractive scintillator is placed in the detecting chamber of the PERALS spectrometer (Fig. 7.91). The instrument contains only one photomultiplier tube. Dual photomultiplier tubes are not needed, in contrast to conventional liquid scintillation analysis, because the thermal electron noise in the phototubes is always well below the pulse heights produced by α particles (McKlveen, and McDowell, 1984). Light-coupling silicone oil and a white reflecting surface made of barium sulfate and binder are important to meet the light transfer requirements from sample tube to the photocathode for optimum resolutions of α-particle pulse height spectra.

To provide for clean α-particle pulse-height spectra without the interference from β-particle smear, the PERALS spectrometer discriminates the α- from β-particle events in the liquid scintillator. The instrument makes use of pulse shape discrimination (PSD), which can take advantage of the longer decay time of light produced by α-particle interactions in scintillation fluor and reject the faster decaying light produced by β-particle or γ-ray interactions. Fig. 7.92 illustrates the light pulse shapes of alpha and beta events in a liquid scintillator. Depending on the scintillator used, the decay times of α-particle interactions can be 30−40 ns longer than β-particle interactions. As explained by Cadieux (1990), each input pulse to the system generates an amplified voltage pulse for pulse-height analysis and a pulse shape signal with a voltage proportional to the time length of the incoming pulse. A discriminator generates a gating signal for only the alpha particles after analyzing the pulse shape voltages. The proper discriminator gating signal is set by use of a microcurie γ-ray source outside of the PERALS sample chamber, which generates Compton electrons that simulate β-particle interactions inside the scintillation fluor cocktail, whereby the discriminator can be adjusted to reject pulse events from the Compton electrons. Following pulse shape discrimination, a multichannel analyzer collects and analyzes pulse-height spectra from the α-particle interactions.

Applications of extractive scintillators to PERALS alpha spectrometry of Pu isotopes are reviewed by Vajda and Kim (2010). PERALS spectrometry has proven to be a valuable tool in the measurement of ^{226}Ra and ^{222}Rn in drinking water with detection limits of 0.006 Bq/L of ^{226}Ra using only 6 mL of sample (Aupiais et al., 1998) and 0.68 Bq/L of ^{222}Rn with the extraction of 1 L of water (Hamanaka et al., 1998). A fast sample preparation method for PERALS analysis of radium in water samples is reported by Aupiais (2005) yielding detection limits of 0.04 Bq/L of ^{226}Ra for 5 mL of sample and 240,000 s counting times. An example of the α-particle discrimination achievable by PERALS with low-activity water samples is provided by Fig. 7.93 illustrating the pulse-height spectra of ^{226}Ra, ^{222}Rn, and ^{218}Po with α-particle emissions at 4.78, 5.49, and 6.00 MeV, respectively. PERALS spectrometry has demonstrated to be a practical method for the analysis of the actinides with high resolution and at low levels of activity. For example, the following studies can be cited: the analysis of ^{232}U—^{234}U—^{238}U at resolutions of 266, 233, and 200 keV FWHM reported by Dacheux et al. (2000), limits of detection as low as 1 mBq/L with extraction of uranium, thorium, plutonium, americium, and curium in aqueous solutions of up to 250 mL (Dacheux and Aupiais, 1997 and Dacheux and Aupiais, 1998). Aupiais (2004a,b) provides alpha spectra deconvolution methods for PERALS analysis of actinide elements in water including the rapid PERALS analysis of uranium activities in water with detection limits of 0.2 μg/kg or 0.003 Bq/kg with a counting time of 240,000 sec. Measurements of ^{237}Np by PERALS spectrometry at levels as low as 23.7 and 9.5 pg/L after counting times of 3 and 10 days, respectively, were demonstrated by Aupiais et al. (1999).

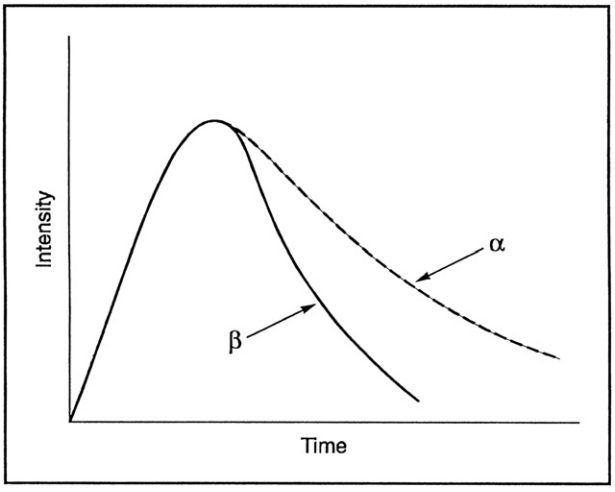

FIGURE 7.92 Alpha and beta pulse decay in a liquid scintillator. The decay time of light produced by the α particle in certain scintillators is about 35−40 ns longer than that of the faster decaying light produced by the β particle. *(© 1998 PerkinElmer, Inc. Printed with permission)*

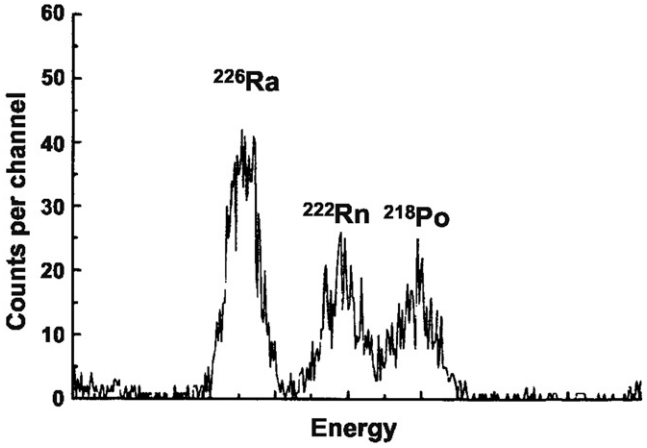

FIGURE 7.93 Radium spectrum of La Bourbouls-Choussy thermal water (3000 ± 200 mBq activity and 88650 s counting time. *(From Aupiais et al., 1998, reprinted with permission © 1998 American Chemical Society)*

Selective extraction of ^{210}Po for PERALS spectrometry by Véronneau et al., (2000) and Aleissa et al., (2006) yielded detection limits bellow 1 mBq/L for 200 mL of solution and 1000 min counting times, and 0.5 L samples and 180 min counting times, respectively. Because of the relatively high spectral resolutions achieved by PERALS spectrometry the normal Gaussian shape of alpha peaks sometimes display a high-energy tail in addition to the pure Gaussian function. Aupiais and Dacheux (2000) demonstrated that this asymmetry is due to internal conversion. They conclude that for the accurate PERALS analysis of some radionuclides, such as isotopes of actinide elements, it is necessary to account for L- and M-shell internal conversion contributions in the activity measurements. In the spectral deconvolution of actinide elements, Aupiais (2004a) demonstrated the need to account for contributions due to internal conversion.

The PERALS spectrometer can be considered as one of the most sensitive liquid scintillation α-spectrometic methods available. As reported by McDowell and McDowell (1993), the PERALS spectrometer rejects 99.99% of ambient and sample β and γ counts from the α spectrum providing ambient radiation backgrounds of 0.001 CPM or less. An alpha pulse-height energy resolution of 4.2% FWHM is achievable, which is limited by the quality of contemporary PMTs. The lower limits of detection are estimated at 0.17 mBq (0.01 DPM). The α counting efficiency is 99.7%, as a small 0.3% is lost through α-particle collisions with the sample tube. The use of PERALS instruments in mobile laboratories to diagnose radionuclide contamination for radiological or nuclear events was proposed by Castagnet et al. (2007).

The major disadvantage of PERALS spectrometry is that it is specific for the spectrometric analysis of α-emitters only, that is, this instrument or method cannot be applied to determine α and β activities simultaneously as reviewed by Pates et al. (1996a). Other conventional liquid scintillation analyzers equipped with automatic sample changers are available commercially, that provide α/β separation by pulse decay analysis or pulse shape analysis and spectrometric analysis of both α- and β-emitters in the same sample, albeit at a lower α-particle energy resolution than obtained by PERALS spectrometry. However, much improved alpha spectral energy resolutions are possible with conventional LSAs when certain detergent-free and moisture-free extraction cocktails and short optical path (small vials) are used (Aupiais et al., 2003). The simultaneous liquid scintillation measurement of α- and β-emitters in the same sample by conventional liquid scintillation analysis is described in Section XV.

B. LS Alpha-Spectrometry with LAAPDs

An improvement in liquid scintillation alpha-spectrometry with energy resolutions of 5% for ^{232}Th (200 keV FWHM) and 3.9% for ^{216}Po (260 keV FWHM) was reported by Reboli et al. (2005) by the use of a silicon large-area avalanche photodiode (LAAPD) in lieu of the standard photomultiplier tube.

Energy resolutions for alpha-emitters further improved over those obtained by the PERALS spectrometer are reported by Reboli et al. (2005) with the use of a large-area avalanche photodiode (LAAPD) rather than the photomultiplier used in PERALS. They demonstrate that the LAAPD can be used for alpha liquid scintillation spectrometry and yield better energy resolutions than photomultiplier tubes. The improved energy resolution obtained with the photodiode is reported due to the uniformity of the large spectral response of the APD. The experimental arrangement used by Reboli et al. (2005) for the measurement of the liquid scintillation alpha spectra with the LAAPD is illustrated in Fig. 7.94. Actinides are counted in scintillation cocktails containing fluors in diisopropylnaphthalene isomers (DIN) solvent containing HDEHP (di-(2-ethylhexyl)phosphoric acid) actinide extractant contained within

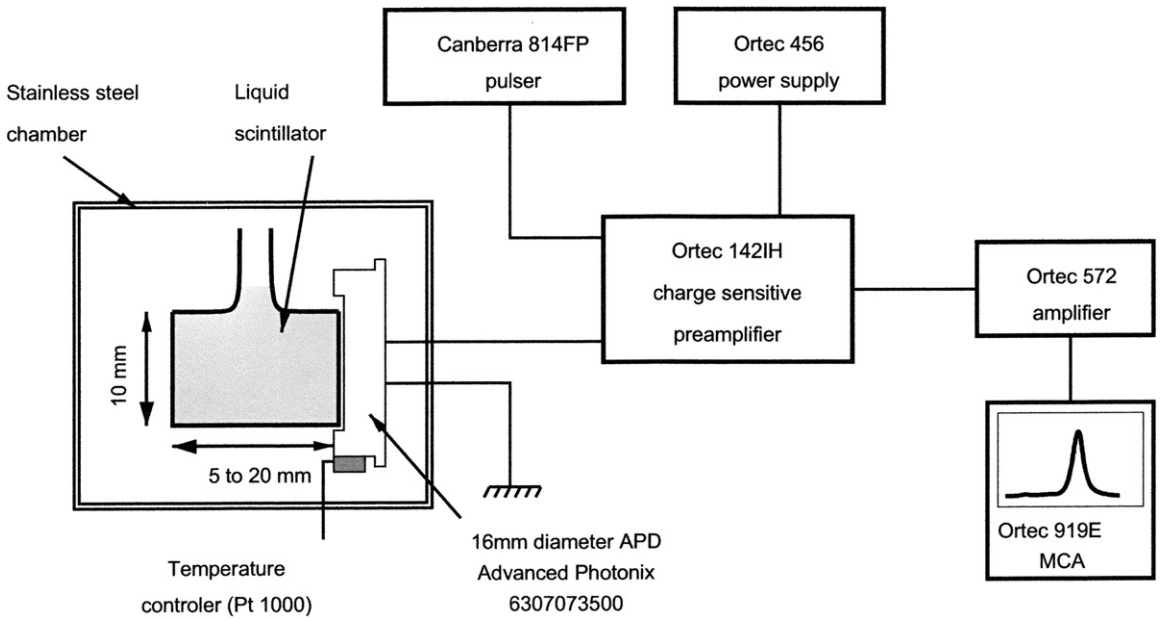

FIGURE 7.94 Experimental arrangement for the determination of liquid scintillation alpha spectra with an avalanche photodiode (APD). *(From Reboli et al., 2005; reprinted with permission from Elsevier © 2005)*

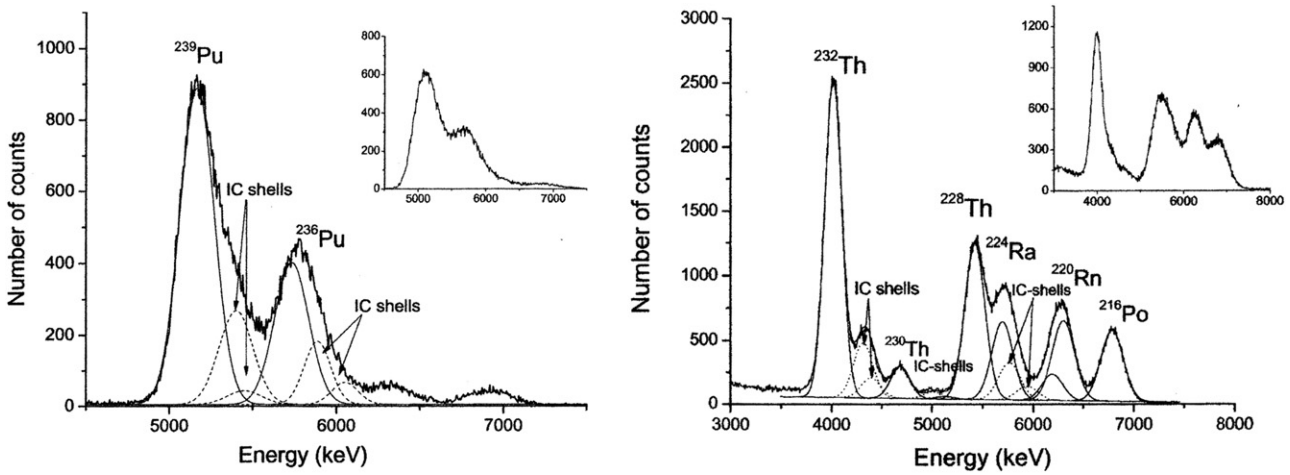

FIGURE 7.95 (Left) Pulse-height spectra of ^{239}Pu and ^{236}Pu at −40 °C obtained with the liquid scintillation−APD detector. The resolution is equal to ~240 keV for the two isotopes. The ^{236}Pu and ^{239}Pu activities are 4 and 8 Bq, respectively, and the counting time is 17 hours. The plot in the upper right shows the ^{239}Pu and ^{236}Pu spectrum measured with the PERALS® spectrometer. (Right) Pulse-height spectra of ^{232}Th and daughters at −40 °C obtained with the liquid scintillation−APD. The resolution is equal to 200 keV for ^{232}Th and 262 keV for ^{216}Po. The ^{232}Th activity is 2 Bq, and the counting time is 6 hours. The straight lines represent the main α-particle spectra and the dashed lines represent the pileup of the main α-particle + IC shell peaks. The plot in the upper right shows the ^{232}Th and daughters spectrum measured with the PERALS® spectrometer. *(From Reboli et al., 2005; reprinted with permission from Elsevier © 2005)*

a 10-mm diameter cylindrical fused silica cuvette (See Fig. 7.94). The cuvette containing 400 μL of sample in liquid scintillator is optically coupled to a windowless avalanche photodiode (APD) with silicone fluid or immersion oil. The cuvette is wrapped with Teflon tape with the exception of the face coupled to the APD, which is etched externally to provide uniformity of light collection on the photosensitive surface of the APD. Optimum resolutions of alpha spectra are obtained by cooling of the sample and APD down to constant temperature, as low as −40 °C, and a small cuvette length of 5 mm.

Typical liquid scintillation alpha spectra with the APD detector compared to spectra obtained by PERALS spectrometry are illustrated in Fig. 7.95. Improvement in energy resolution over PERALS is clearly discernable from the spectra. As described by Reboli et al. (2005) the liquid scintillation−APD spectra show a fine structure. The alpha decay of the plutonium isotopes (^{239}Pu and ^{236}Pu) and the thorium isotopes (^{232}Th, ^{230}Th, and ^{228}Th) do not lead to the ground state, and undergo further deexcitation via internal conversion (IC) mainly on L and M shells. The liquid scintillation−APD spectra of Fig. 7.95 offer sufficient energy resolution to illustrate the spectral displacement of the energy peaks of the α-transitions towards higher energy values.

The precise differences in energy resolution between spectra produced by the liquid scintillation−APD and PERALS spectrometers are provided in Table 7.12. The improvement in energy resolution of the liquid scintillation−APD detector is reported by Reboli et al (2005) to be due to higher quantum efficiency and more uniform active area than that provided by photomultiplier tubes to this date. The silicon photodiodes have a larger spectral response than PMTs, which facilitates the matching of the fluorescence spectra of scintillators with the APD spectral response.

TABLE 7.12 Comparison of Energy Resolutions (*R*) for Different α-emitters as Obtained using a Home-Made Liquid Scintillator with an APD as Detector and a Commercial Spectrometer PERALS® Equipped with a PMT[a]

		APD	PMT
Isotope	Energy (keV)	*R* (keV)	*R* (keV)
^{232}Th	4010	200 ± 13	210 ± 13
^{239}Pu	5157	242 ± 13	256 ± 14
^{228}Th	5423	235 ± 11	306 ± 14
^{236}Pu	5768	243 ± 11	293 ± 17
^{216}Po	6785	262 ± 14	448 ± 20

[a]*From Reboli et al., 2005; reprinted with permission from Elsevier © 2005.*

XV. SIMULTANEOUS α/β ANALYSIS

As described in Sections II.B and XIV, α and β pulse-height spectra often overlap. The pulse-height spectra of the α- and β-emitters ^{210}Po + ^{90}Sr(^{90}Y), respectively, illustrated in Fig. 7.2, are a good example of this spectral overlap. However, many contemporary liquid scintillation analyzers are equipped with the circuitry capable of analyzing α- and β-emitting radionuclides in the same sample. These instruments may use pulse decay analysis (PDA) or pulse shape analysis (PSA), first reported by Buchtela et al. (1974) and Thorngate et al. (1974), to differentiate alpha from beta decay events. In pulse decay analysis, a pulse decay time discriminator often referred to as the pulse decay discriminator (PDD), monitors the length of time for the decay of a pulse event originating from photon emission due to fluor cocktail excitation. As described in Section XIV and illustrated in Fig. 7.92, fluor excitation events originating from α-particle interactions have 35−40 ns longer decay lifetimes than events originating from β-particle interactions. This is due to the longer deexcitation and light

emission processes in scintillation fluors after α-particle interactions, which exhibit higher linear energy transfer (LET). In PDA, the differences in the lengths of pulse decay events resulting from α- and β-particle interactions can be measured by the charge differences collected at the photomultiplier output at the tail portion of the pulse events (see also Sections X.B.1 and X.B.2 on the similarity with pulse shape discrimination used to discriminate n/γ interactions with liquid scintillators). The fluorescence decay resulting from an α-particle interaction displays a longer tail (Fig. 7.92), and consequently produces a higher charge at the PMT output for the tail portion of the pulse event when compared to a fluorescence decay pulse event produced by a β-particle. The actual difference in decay lifetimes between the α and β events depends on the chemical composition of scintillation fluor cocktail used and particle energies (Pujol and Sanchex-Cabeza, 1997, Pates et al., 1998, and Rodriguez Barquero and Grau Carles, 1998).

Instruments that use pulse shape analysis (PSA) to discriminate between α and β events also take advantage of the greater length of the α-produced pulse compared to the β-produced pulse. In PSA, the ratio of the area of the tail of a pulse, beginning at 50 nsec after pulse initiation, is compared to the total pulse area (McDowell, 1966 and Rodriguez Barquero and Grau Carles, 1998), which provides a method of assigning a pulse to a β event (short pulse) or α event (long pulse). This is also referred to as pulse shape discrimination (PSD).

The liquid scintillation analyzer, which is equipped with pulse decay discrimination or pulse shape discrimination for α/β analysis, is also equipped with two multichannel analyzers (MCAs). All of the pulse events originating from scintillation photon emissions with a decay time longer than the PDD setting are sent to the α-MCA and those events which have a shorter lifetime are sent to the β-MCA. It is necessary, therefore, to find the optimum PDD setting to get the best separation of α- and β-radionuclide activities into separate MCAs.

A. Establishing the Optimum PDD Setting

The optimum pulse decay discriminator setting is found by counting a pure α-emitter source and a pure β-emitter source in the liquid scintillation analyzer in the same fluor cocktail, sample composition, sample volume, and type of vial used as the experimental samples to be measured. The optimum PDD setting is affected by sample quench level, the specific quenching agents (chemical and color) in the sample, and the E_{max} of the β-emitter (Pates et al., 1998 and DeVol et al., 2007). The β-particle energy is an influencing factor, because the PMT pulse event has a specific length for a given β-particle energy, and the pulse length increases with increasing event energy. Also, as noted by Pates et al. (1998), the delayed component (tail) of pulse events is a function of the amount of π-electron singlet and triplet excitation states in the scintillation solvent produced by the ionizing radiation. Alpha particles (or heavy charged particles with high LET) will produce more triplet-state excitation than the lighter beta particles. The triplet states take longer to undergo deexcitation fluorescence. However, the solvents as well as quenching agents present in the sample can affect the delayed component of deexcitation. Some components in cocktails can inhibit deexcitation and prolong triplet-state excitation, while other chemicals in the cocktail (*e.g.*, O_2, CCl_4, and $CHCl_3$) are electron scavengers, and able therefore, to interact with higher energy states and reduce the delayed component. When gross α and gross β determinations are needed and the radionuclides in the experimental samples may not be known, one uses an α- and β-standard of similar energy to that of the α- and β-radionuclides in the samples (Passo and Cook, 1994). The following calibration steps are required:

1. The pure β-emitter standard dissolved in a suitable liquid scintillation cocktail is placed into the LSA for counting. The chemical composition of this standard should be the same as those of the unknown experimental samples. During this calibration procedure, the instrument automatically counts the pure β-emitter standard at various pulse decay discriminator settings. At each PDD setting, the instrument selects and sends all pulses of duration longer than the PDD setting to an α-multichannel analyzer (α-MCA) and pulses of shorter duration to the β-multichannel analyzer (β-MCA). For each PDD setting the LSA calculates the percent spillover of the β events into the α-MCA. A curve of the percent spillover versus the PDD setting as illustrated in Fig. 7.96 is then plotted automatically.
2. The pure α-emitter standard dissolved in a suitable cocktail of the same chemistry as the previously described β-emitter (step 1) is placed into the LSA for counting. Its chemical composition should also be the same as the unknown experimental samples. As in step 1, the instrument automatically counts the pure α-emitter standard at various pulse decay discriminator settings. At each PDD setting, the instrument selects and sends all pulses of duration longer than the PDD setting to an α-multichannel analyzer (α-MCA) and pulses of shorter duration to the β-multichannel analyzer (β-MCA). For each PDD setting the LSA calculates the percent spillover of the α events into the β-MCA. A curve of the percent spillover versus the PDD setting as illustrated in Fig. 7.96 is then plotted automatically by the LSA.
3. The pulse decay discriminator setting at which the two spillover curves cross is selected as the optimum PDD setting for simultaneous α/β analysis in the same sample (*e.g.*, PDD = 171 of Fig. 7.96). The two spillover curves plotted in this fashion are referred to as crossover plots. At the crossover PDD setting, there is minimum spillover of α events into the β-MCA and β events into the α-MCA, when the activities of both α and β events must be determined. However, if only the α-emitter activity is of interest in a sample containing both α- and β-emitters, a higher PDD setting can be selected, well above the crossover setting (*e.g.*, PDD = 199 of Fig. 7.96), where the spillover of β events into the α-MCA approaches zero. Alternatively, if only the β-emitter activity is of interest in a sample containing both α and β-emitters, a lower PDD setting can be selected, well below the crossover setting (*e.g.*, PDD = 122 of Fig. 7.96), where the spillover of α events into the β-MCA is lowest.

De Vol et al. (2007) provide a thorough study on the effects of chemical and color quench and radionuclides used to calibrate

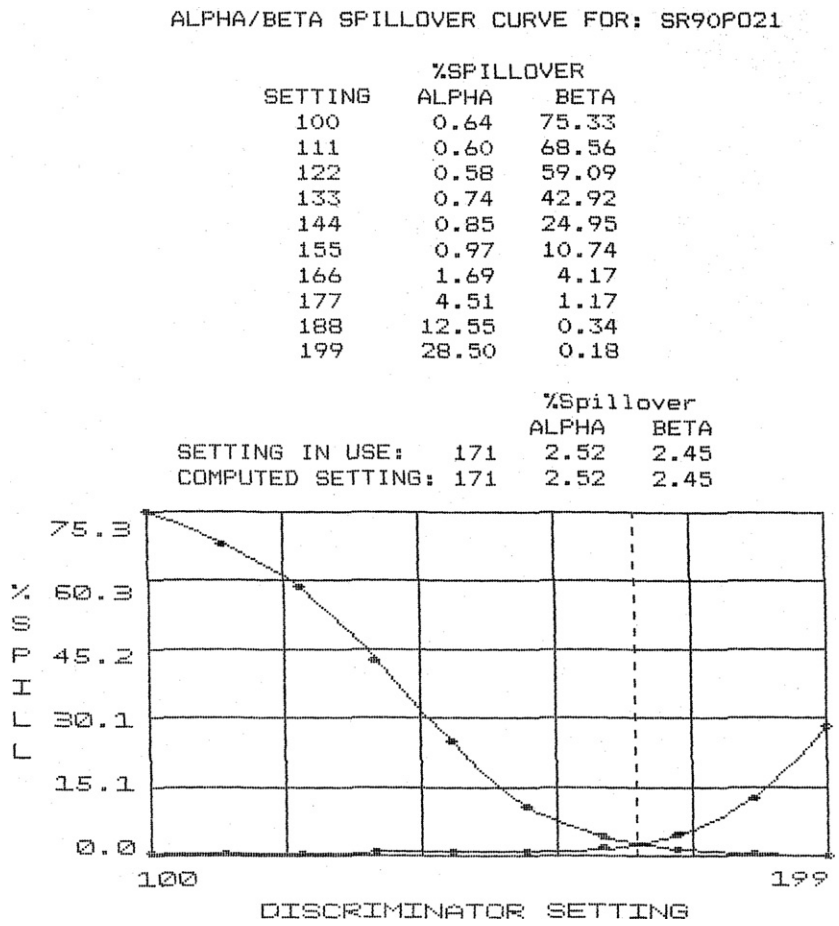

FIGURE 7.96 Alpha/beta misclassification curve for an aqueous sample of $^{210}Po + {}^{90}Sr$ (^{90}Y) in Ultima Gold AB scintillation cocktail, measured by a PerkinElmer 2700TR liquid scintillation analyzer. This crossover curve was made from the same sample, which produced the pulse-height spectra in Fig. 7.2. *(From L'Annunziata, M.F., 1997, unpublished work)*

instrumentation for α/β discrimination. Among these findings, it is important to note that the quenching agent will have a direct effect on spillover. In other words, a liquid scintillation analyzer may determine that two samples in two distinct counting vials have the same level of quench [*i.e.*, same quench-indication parameter, tSIE or SQP(E)]; however, if different chemical agents are producing the quench, the spillover can be different between the two samples. It is important therefore, that the matrix of the experimental samples be constant and that the liquid scintillation analyzer be programmed for minimum spillover under the same conditions as the experimental samples. DeVol et al. (2007) also point out that pure alpha emitters may yield different spillovers than nuclides that emit alpha with gamma cascade events, such as ^{241}Am. Nuclides with gamma cascade events are more likely to be classified by the pulse shape discriminator as alpha events, because of the pulse duration. Gamma cascade events are common with alpha emitters. Salonen (2006) was first to report that alpha spillover is a function also of the energy of the alpha particle. The alpha spillover of lower-energy alpha particles is greater than the spillover of high-energy alpha particles when samples are measured at a constant PDD setting (*i.e.*, constant pulse shape analysis). In summary, the sample matrix should be as close as possible in chemical and physical properties to the alpha and beta standards used to determine the optimum PDD setting for minimum spillover.

B. α/β Spillover Corrections and Activity Calculations

Once the optimum PDD setting is determined, the detection efficiency of the α particles in the α-MCA and that of the β particles in the β-MCA must be measured. This may be best determined by the use of internal standardization as described in Section V.A. The α-MCA and β-MCA will provide net (background-subtracted) count rates (CPM) for α and β particles, respectively. The net count rates must be corrected for spillover or misclassification and the net count rates converted to α and β activities (disintegration rates). The calculations required for the determination of α and β count rates corrected for spillover are derived by Bhade et al. (2010). The following equations described by Bakir and Bem (1995) provide the sample gross α and β activity concentrations in units of Bq/L taking into account sample volume (V) and concentration factor (C), for samples concentrated prior to counting:

$$A_\alpha = \frac{I_\beta E_\beta - I_\alpha S_{\beta/\alpha}}{(E_\alpha E_\beta - S_{\alpha/\beta} S_{\beta/\alpha}) VC60} \tag{7.143}$$

$$A_\beta = \frac{I_\alpha E_\alpha - I_\beta S_{\alpha/\beta}}{(E_\alpha E_\beta - S_{\alpha/\beta} S_{\beta/\alpha}) VC60} \quad (7.144)$$

where A_α and A_β are the gross α particle and gross β particle activities, respectively, in units of Bq/L, I_α and I_β are the net (background subtracted) count rates in the α and β multichannel analyzers, respectively, $S_{\alpha/\beta}$ and $S_{\beta/\alpha}$ are the percent spillover of α events into the β MCA and β events into the α MCA, respectively, E_α and E_β are the detection efficiencies for α particles in the α MCA and β particles in the β MCA, respectively, V is the volume of analyzed sample in liters, C is the concentration factor or the degree of concentration of the sample prior to analysis, and 60 is a conversion factor to change count rate from CPM to CPS.

The backgrounds, count rates, and detection efficiencies in the α MCA and β MCA will depend on the pulse-height discriminator settings used in the α and β channels, respectively, and instrumental background-reducing count mode used (*e.g.*, LLCM or NCM) as described in Section XX.C. The optimum PDD setting must be determined at the same pulse-height discriminator and background-reducing count mode settings as those used for the experimental sample analysis.

C. Optimizing α/β Discrimination in PDA

The chemistry of the sample, which includes the scintillation cocktail used and all of the quenching agents present in the sample, plays a crucial role in α/β discrimination in pulse decay analysis. The following are some guidelines to follow to enhance α/β separation performance:

1. The cocktail−sample mixture must be homogeneous. The chemistry of the sample including the scintillation cocktail and kinds and amounts of quenching agents present should be the same as those of the α and β standards used to plot the crossover curves for determination of the optimum PDD setting. The sample must be completely solubilized in the liquid scintillation cocktail. Acids are often necessary to keep α-emitter salts in solution in the cocktail. Organic samples and filters are often processed through ashing followed by acid dissolution of salt residues (Yang and Guo, 1995). Table 7.13 provides some guidelines on the acid loading capacity (mL acid/10 mL cocktail) at room temperature (20−22°C) of certain cocktails. The minimum α/β misclassification (at crossover point from spillover curves) for small sample sizes ($\leq$0.5 mL acid) is also provided. Water-soluble paper for smear tests is a sample type that might be used to avoid excessive acids in cocktail (Takiue et al., 1989a), although glass fiber filter is also demonstrated as a good swipe material for α/β contamination assays.
2. Minimize the sample quench. The sample volume (*e.g.*, aqueous solution) will dilute the scintillation fluor cocktail and also introduce quenching agents. Minimum α/β spillover is obtained generally at lowest levels of quench.
3. Use organic acceptor cocktails rather than cocktails that have surfactants or emulsifiers. Table 7.13 lists liquid scintillation cocktails that provide excellent α/β discrimination performance. They all use diisopropylnaphthalene (DIN) as a solvent with the exception of Insta-Gel XF, which has pseudocumene as a solvent. Pseudocumene and the alkylbenzenes are "fast" solvents, which are less efficient for α/β separation. Naphthalene is added to Insta-Gel XF in a proportion of 20 % w/v to improve α/β separation by acting as an intermediate in the energy transfer process between solvent and fluor increasing the production of π-electron triplet excitation states produced by α-particle interactions (Passo and Cook, 1994). Naphthalene is not required with the Ultima Gold Cocktails, as the DIN solvent serves the same purpose (Thomson, 1991). The DIN solvent-based cocktails, particularly Ultima Gold AB, have been demonstrated to provide excellent α/β separations, while increasing surfactant concentration degrades the cocktail performance for α/β analysis (Pates et al., 1993, 1996b).
4. Use organic extractive scintillators that are selective for the α-emitters of interest. The use of organic (water-immiscible) extractive scintillators was described in Section XIV. This is recommended when only the α-activity is desired, as after extraction of the dissolved aqueous sample with the selective organic scintillator, the α-emitters transfer from the aqueous phase to the organic scintillator leaving most of the β-emitters behind in the aqueous phase. Organic extractive scintillators are useful when only α-emitters are of interest, when there is an overwhelming β-emitter activity with α-emitters of interest, and to improve the energy resolution of α pulse-height spectra. The works of Yang et al. (1992,

TABLE 7.13 Acid Loading Performance of α/β Compatible Liquid Scintillation Cocktails[a]

Cocktail (10 mL)	H_2O (mL)	1 M HCl (mL)	2 M HCl (mL)	1 M HNO_3 (mL)	2 M HNO_3 (mL)	% Misclassification (minimal sample loads)
Ultima Gold	3.50	0.25	0.10	0.70	0.30	0.6
Ultima Gold XR	10.0	2.00	0.90	3.00	1.75	2.2
Ultima Gold AB	10.0	5.50	2.25	3.2.5	2.25	0.5
Insta-Gel XF + 20% w/v naphthalene	1.5	1.3	1.1	1.4	1.4	0.5

[a]*The loading capacity of the acids are mL acid per 10 mL of cocktail.*

1994) and Aupiais et al. (2003) are recommended as additional resources on this topic.

5. Use specific extractive resins to concentrate the radionuclides of interest. For example, actinide extractive resin, available from Eichrom Technologies, Inc., Darien IL, USA or Eichrom Europe, S.A.R.L., Paris, France, is used to extract elements of high atomic number (*e.g.*, Th, U, Pu, Am, and Cm) from aqueous solutions. The extraction of the actinides together with α/β pulse shape discrimination provides improved limits of detection (Horwitz et al., 1997 and Eikenberg et al., 1999).
6. Purging the dissolved oxygen from the cocktail with argon gas will improve α/β separation by reducing quench. This is not commonly performed except in research to obtain unquenched samples, as the additional step is time consuming and the gain in α/β separation is relatively small.
7. Time-resolved pulse decay analysis (TR-PDA) significantly improves α/β separation or, in other words, reduces misclassification of α as β and β as α (Passo, 1996). TR-PDA, available with PerkinElmer liquid scintillation analyzers, is PDA combined with time-resolved background discrimination (TR-LSC), which is described briefly in Section XX.C.5.d. This effect, as described by Passo (1996), is due to enhanced α rejection from the β-MCA and associated lowering of the β spillover into the α-MCA due to a change in the shape of the α misclassification curve.

D. Quenching Effects in α/β Discrimination

As noted previously in Section C, the α/β discrimination is improved by minimizing quench in the sample, which is accomplished by reducing the sample volume as the amount of water and acids among other substances in the sample can cause quench. The following are important affects of quench on α/β separation and guidelines to follow in controlling the effects of quench or even taking advantage of these affects, when they occur:

1. Alpha misclassification increases with quench. Once the optimum PDD setting is determined for a given sample quench level as described in Section B, any increase in quench level causes an increase in the misclassification of α events into the β-MCA. This can be seen from the alpha into beta curve of Fig. 7.97, which was prepared by measuring first the optimum PDD setting for a given value of quench (*e.g.*, tSIE = 620 in this example) and then measuring the percent spillover at various quench levels after adding incremental amounts of quenching agent. The degree of change in misclassification is a function of the type of quenching agent present in the sample. Some quenching agents are strong electron scavengers (*e.g.*, O_2, $CHCl_3$, and CCL_4), and these are able to interact more easily with π-electron triplet states reducing the delayed component of fluorescence deexcitation (Pates et al., 1998). Therefore, it is important that the chemistry of the α and β standards used to determine the optimum PDD setting be identical to the chemistry of samples under investigation.
2. Counting efficiency of α-emitters is expected to remain at 100% (Aburai et al., 1981; Takiue et al., 1989a; Parus et al., 1993); however, loss of α-events into the β-MCA occurs with increased quench. Caution should be taken in assuming 100% detection efficiency, and the detection efficiency should be determined in all cases. Reduced counting efficiencies can occur with instruments that count afterpulses to discriminate against background as described in Section XX.C.
3. Beta misclassification decreases with an increase in quench as illustrated in Fig. 7.97. However, the percent misclassification and counting efficiency are a function of the E_{max} of the β-particle emitter (Pates et al., 1998). Therefore, to assure accurate measurement of misclassification and optimum PDD setting, it is best to plot a crossover curve using the same β-emitter or one of similar E_{max} as that of the β-emitter expected in the samples to be analyzed.
4. The best α/β separation performance is maintained by keeping the quench level (sample chemistry), sample volume, and vial type the same as the α- and β-standards used to determine the optimum PDD setting. This is done by maintaining the sample chemical composition, sample size, fluor cocktail type and volume, and vial type the same for the standards as the experimental samples. If it is not possible to predict the quench level of the experimental samples, the optimum PDD settings for a wide range of

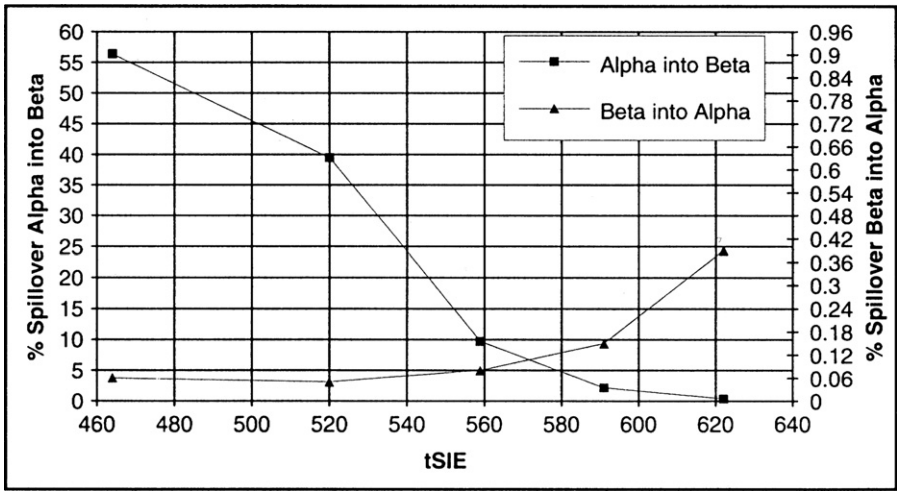

FIGURE 7.97 Percent misclassification curves of alpha and beta events as a function of quench level (tSIE) measured at a constant PDD setting determined at tSIE 620. *(© 1998 PerkinElmer, Inc. Printed with permission)*

quench levels should be determined using quenching agents that are identical to those found in the samples to be analyzed. Yang (1996) clearly demonstrates this by plotting a curve of optimum PDD setting versus tSIE.

For additional information on quench effects on α/β separation, see Pates et al., (1996c, 1998).

E. Practical Applications of α/β Discrimination and Analysis

PERALS spectrometry was discussed in the previous Section XIV as a method that yields the highest resolution of alpha spectra energy lines by liquid scintillation. However, conventional liquid scintillation analyzers with α/β discrimination and the use of appropriate nonaqueous and nondetergent scintillation cocktails can yield very good and practical energy resolutions. There are numerous applications of the alpha spectrometric analysis of radionuclides, or combined analysis of alpha- and beta-emitting radionuclides with conventional liquid scintillation analyzers equipped with α/β discrimination. Some of these applications will be cited in the following.

Aupiais et al. (2003) demonstrated that the energy resolution of a conventional liquid scintillation analyzer (*i.e.*, a PerkinElmer Tri Carb™ 2770) equipped with α/β discrimination could be enhanced by 200% by using specific no-water-miscible cocktails and a short optical path. Under such conditions, an energy resolution of about 200 keV for the 4.2 MeV energy line of ^{238}U could be obtained with either the Tri Carb™ or the PERALS™ spectrometers. Also, under such conditions, the sensitivity of the Tri Carb liquid scintillation analyzer was 40% lower than that of the PERALS spectrometer, because of the higher α/β discrimination of PERALS and its shorter optical path. Figs. 7.98 and 7.99 illustrate the improvement in alpha spectral energy resolution obtained with the PerkinElmer Tri Carb LSA compared to the PERALS spectrometer when detergent-free Ultima Gold AB® cocktail or Alphaex® cocktail (an actinide extracting scintillator specific for alpha measurement) is used. When the sample light path in the Tri Carb LSA is reduced further by employing a 1-mL sample vial ($\phi = 16$ mm), the energy resolution is improved significantly close to that obtained with the PERALS spectrometer. In conclusion, the energy resolution on liquid scintillation alpha spectrometry can be improved by using a lower or shorter optical path and no-water-miscible cocktails, such as the toluene−naphthalene-based cocktails (*e.g.*, Alphaex®) or detergent-free diisopropylnaphthalene (DIN-based) cocktails (*e.g.*, detergent-free Ultima Gold® AB). The preparation of the detergent-free Ultima Gold® AB cocktail is described by Aupiais et al. (2003) and the Alphaex® cocktail is available from ETRAC, Knoxville, TN, USA. Both cocktails contain HDEHP as a nuclide extractant and primary and secondary fluors.

As noted earlier, the % spillover of alpha pulse events into the βMCA and beta pulse events into the αMCA will be a function of quench level. In addition, as the quench level of a sample increases, the alpha pulse-height spectra will shift from higher to lower pulse heights (*i.e.*, higher to lower channel numbers) and the resolutions of the spectral energy lines will deteriorate with peak broadening (*i.e.*, increase in FWHM). Such an effect is observed in Fig. 7.100, which illustrates the liquid scintillation alpha spectra of ^{226}Ra and its daughter nuclides in equilibrium at various levels of quench (*i.e.*, tSIE = 462, 374, 283, and 218) where the least quenched sample has the highest tSIE. For the alpha spectrometric analysis of ^{226}Ra and isotopes of uranium, Stamoulis et al. (2010) established a spectral deconvolution technique, which involved the correlation of the peak's centroids, corresponding to different radionuclides, to the characteristic energies at different degrees of quenching. Values of the centroids of the peaks and the corresponding FWHMs were used as initial parameters for fitting the spectra with overlapping Gaussians using the Origin® analysis program. The derived values of peaks' centroids and FWHMs for each radionuclide were correlated to the quench-indicating parameter tSIE.

Among the applications of α/β discrimination is the determination of gross alpha and gross beta activities of samples such as drinking water, as governmental regulatory agencies often place limits and regularly monitor groundwater

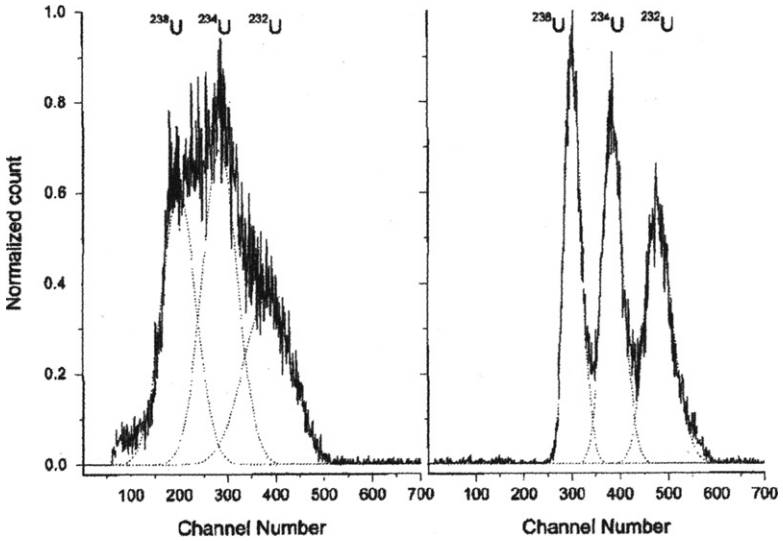

FIGURE 7.98 Uranium isotopes spectra: (left) Ultima Gold AB cocktail in standard PerkinElmer vial ($V = 20$ mL, $\phi = 26$ mm, resolution of E_α of ^{238}U at 4.2 MeV = 509 keV) spectrometer Tri-Carb; (right) Alphaex cocktail in standard culture tube ($V = 1$ mL, $\phi = 10$ mm, resolution of E_α of ^{238}U at 4.2 MeV = 260 keV), spectrometer PERALS. *(From Aupiais et al., 2003 © 2003 Oldenbourg Wissenschaftsverlag, München, Reprinted with permission)*

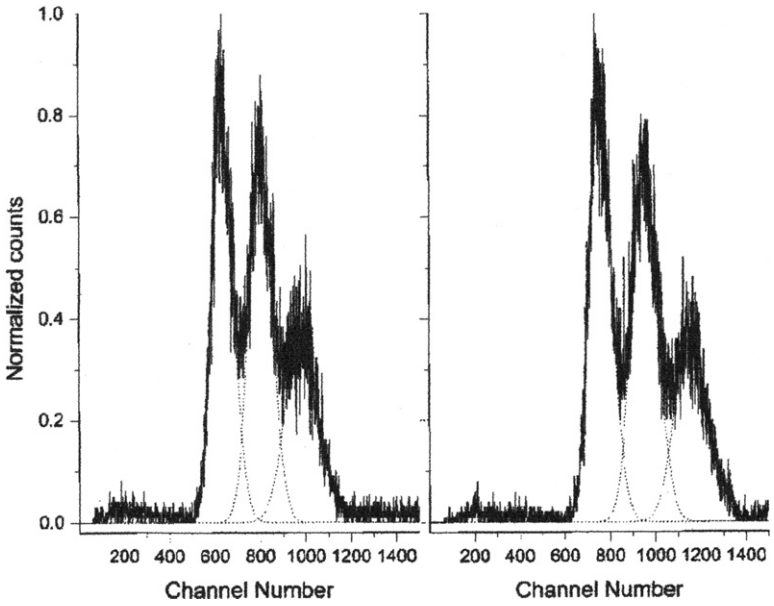

FIGURE 7.99 Improved uranium isotopes spectra: (left) detergent-free Ultima Gold AB cocktail in standard PerkinElmer vial ($V = 5$ mL, $\phi = 26$ mm, resolution of E_α of ^{238}U at 4.2 MeV = 322 keV) spectrometer Tri-Carb; (right) Alphaex cocktail in standard PerkinElmer vial ($V = 5$ mL, $\phi = 26$ mm, resolution of E_α of ^{238}U at 4.2 MeV = 342 keV) spectrometer Tri-Carb *(From Aupiais et al., 2003 © 2003 Oldenbourg Wissenschaftsverlag, München, Reprinted with permission)*

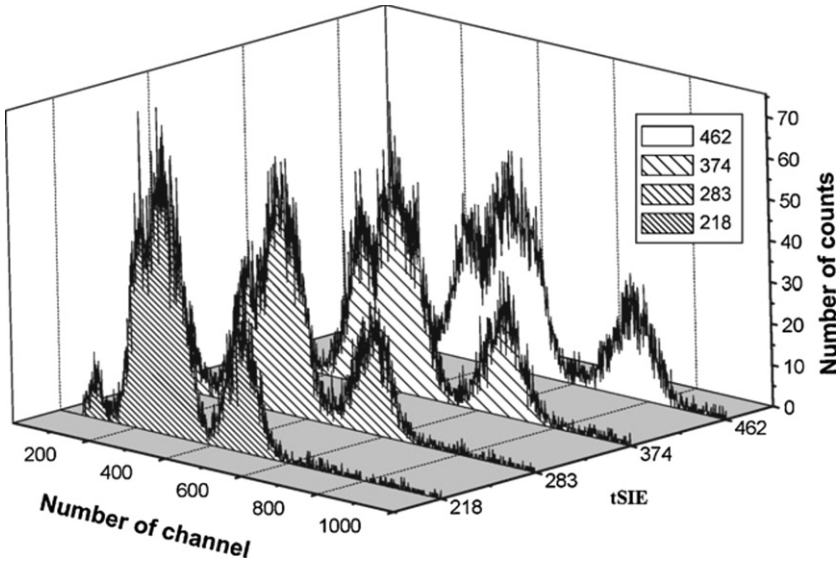

FIGURE 7.100 Alpha spectra of ^{226}Ra and its daughters in equilibrium. These spectra correspond to four degrees of quenching with the tSIE index value varying from 218 (highest quench level) to 482 (lowest quench level). *(From Stamoulis et al., 2010. Reprinted with permission from Elsevier © 2010)*

supplies and drinking water. Some example of gross alpha and gross beta activity determinations of water supplies are the works of Bakir and Bem (1995), Warrick and Croudace (2002), Kleinschmidt (2004), Happel et al. (2004), Wong et al. (2005), Wisser et al. (2006), Staffová et al. (2006), Ruberu et al. (2008), Bhade et al. (2010), and Forte (2011). Gross alpha and gross beta activity measurements have also been applied to the rapid analysis of aerosol filters for environmental monitoring (Sas et al., 2010), urine analysis for terrorism preparedness in the possible event of population exposure (Piraner and Jones, 2009), and the assessment of gross alpha and beta emitters in nuclear fuel processes (Lara-Robustillo and Rodríguez Alcalá, 2006).

Other common applications of α/β separation (*i.e.*, discrimination) liquid scintillation spectrometry are the analysis of ^{222}Rn in drinking water (Galán López et al., 2004, Pates and Mullinger, 2007, and Salonen, 2010), the spectrometric analysis of isotopes of the ^{238}U and ^{232}Th decay series (Bem et al., 2004, Bianchi et al., 2005, Kim *et al*, 2008, and Stamoulis et al., 2010), the alpha-emitting nuclides $^{234,238}U$, $^{238-240}Pu$, ^{241}Am, and ^{244}Cm and the beta-emitting nuclides $^{90}Sr/^{90}Y$ and ^{241}Pu (Versilov et al., 2002 and Eikenberg et al., 2002), isotopes of Np in nuclear waste (Diodati and Sartori, 2007), analysis of ^{241}Am and ^{243}Am (El Mrabet et al., 2004 and Alamelu et al., 2006), analysis of ^{237}Np, $^{238-240}Pu$, and ^{241}Am (Feng and He, 2009), and the simultaneous determination of ^{226}Ra, ^{233}U, and ^{237}Np (Nebelung and Baraniak, 2007).

An interesting approach to α/β discrimination was applied by Groppi et al. (2005b) to the alpha spectrometry of $^{211}At/^{211g}Po$ nuclides, which are prepared by α-cyclotron irradiation of ^{209}Bi target material according to the reaction $^{209}Bi(\alpha,2n)^{211}At$. The ^{211}At product nuclide decays

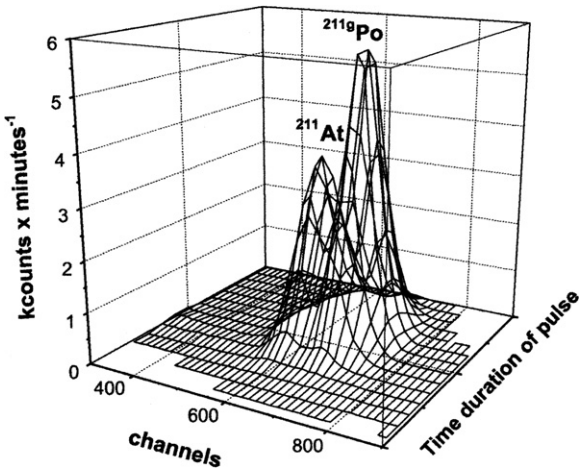

FIGURE 7.101 Liquid scintillation spectrum of ^{211}At/^{210g}Po in extracted organic phase measured with the Triathler™ (Hidex, Turku, Finland) liquid scintillation counter with pulse shape discrimination as a function of channel number and time duration of pulses. The counts in appropriate windows are used to obtain the decay curves of the two nuclides in secular equilibrium. *(From Groppi et al., 2005b. Reprinted with permission from Elsevier © 2005)*

($t_{1/2} = 7.21$ hours) by alpha emission to ^{207}Bi daughter with the main alpha at 5.87 MeV 41.8% and by EC (58.2%) to the very short-lived ^{211}Po daughter ($t_{1/2} = 0.516$ m sec). The ^{211}Po daughter also decays by alpha emission with the main alpha at 7.45 MeV. The ^{211}At/^{211}Po parent−daughter nuclides at secular equilibrium are used in radiotherapy. The high LET and short range of the alpha particles from both nuclides attribute to these nuclides the power to eradicate tumor cells in the treatment of cancer. At secular equilibrium, both nuclides decay at the half-life of the parent, *i.e.*, 7.21 hours. Thus, the alpha-emissions remain in the patient long enough to irradiate the cancer cells, and do not remain for any excessive period of time. Alpha/beta discrimination of the ^{211}At/^{211}Po assigns the alpha emissions to the αMCA and pulse events from Auger and conversion electrons to the βMCA. The alpha spectra produced by the ^{211}At/^{211}Po in a Triathler™ liquid scintillation analyzer (Hidex, Turku, Finland) with α/β pulse shape discrimination is illustrated in Fig. 7.101. The alpha spectra of the two nuclides decay at the same half-life, and the spectra were used to measure quantitatively the activities of the alpha-emitters.

XVI. PLASTIC SCINTILLATORS IN LSC

Plastic scintillators are a solid solution of fluorescent solutes in a polymeric aromatic solvent (Bagán et al., 2010). The potential of plastic scintillator as a detector for the analysis of radionuclides in a liquid scintillation counter was investigated by Tarancón et al. (2002a,b, 2003, 2004). They utilized Bicron® BC-400 plastic scintillator beads of diameter between 250 and 500 μm. The advantages that plastic scintillator beads would provide are as follows: (i) liquid scintillation cocktail costs would be eliminated, (ii) there would be no mixed-waste disposal costs, (iii) the plastic beads could be reused innumerable times, if washed properly, (iv) the absence of chemical quenching with plastic scintillators, (v) the possibility of counting samples with very high salt matrices, even salt concentrations that are difficult or impossible to mix suitably with liquid fluor cocktails, and (vi) a conventional liquid scintillation counter could be used.

The pulse-height spectra produced by beta emitters in the plastic scintillator beads in a liquid scintillation counter display a similarity to those produced by liquid scintillation, as illustrated in Fig. 7.102, This might be expected, as the beta-particle travels through the plastic beads, energy is absorbed by the polymeric aromatic compounds proportional to the beta-particle energy deposited, as discussed in Chapter 16. The polymeric aromatic compounds at various excited energy states then

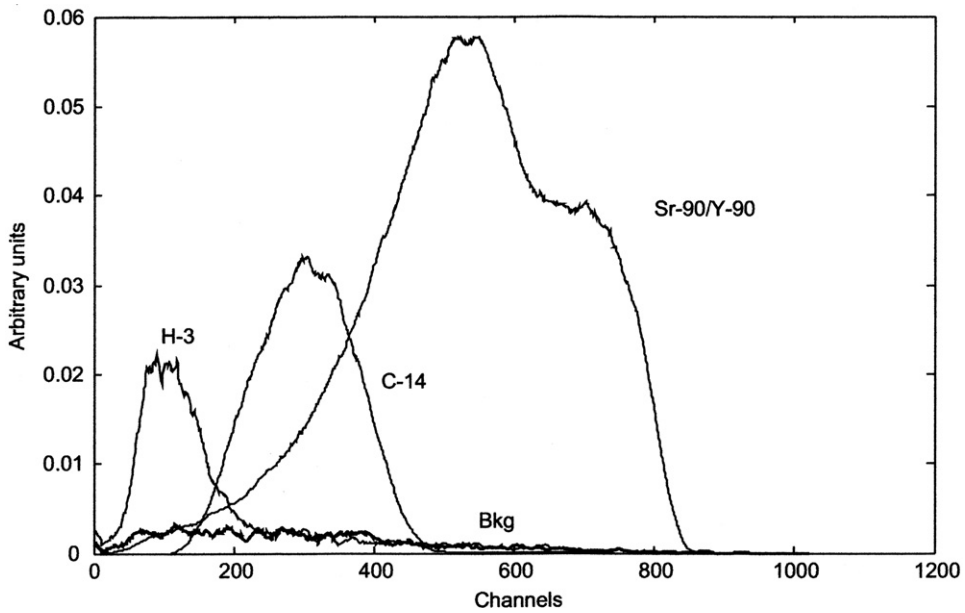

FIGURE 7.102 Pulse-height spectra from ^{3}H, ^{14}C, and ^{90}Sr/^{90}Y and background spectra produced with plastic scintillator beads with a conventional PerkinElmer Quantulus™ counter in 7-mL counting vials. *(From Tarancón et al., 2004. Reprinted with permission from Elsevier © 2004)*

transfer this energy to the fluor solutes in the plastic beads. Full-spectrum detection efficiencies for ^{3}H, ^{14}C, and $^{90}Sr/^{90}Y$ with plastic scintillator beads and aqueous radionuclide solution in 7 mL polyethylene counting vials were reported by Tarancón et al. (2004) to be 0.13% ± 0.04, 17.79% ± 0.54, and 90.02% ± 0.02, respectively, and full-spectrum backgrounds were 1.09 ± 0.04, 0.47 ± 0.04, and 1.43 ± 0.07 cpm. The low background count rates are very favorable for this counting method, and optimized counting windows produced remarkably yet much higher figures of merit (E^2/B), where E if the % detection efficiency and B the background count rate. Thus, routine low-level counting (*i.e.*, low activity samples) was demonstrated with relative errors <5 % for medium and high-energy beta emitters. The low detection efficiency for ^{3}H is understandable, as the low-energy beta particles ($E_{max} = 18.6$ keV) must travel through the aqueous solution and penetrate the plastic bead to produce a scintillation pulse event. The reusability of the plastic beads after washing in citric acid was demonstrated (Tarancón et al. (2003).

Cherenkov detection efficiencies for $^{90}Sr/^{90}Y$ in plastic beads were reported by Tarancón et al. (2002b) to be 60.1% ± 1.0 in an optimized counting window with a background of 5.0 ± 0.1 cpm. The high Cherenkov detection efficiency is due to the high-energy beta particles emitted by ^{90}Y ($E_{max} = 2280$ keV). Excellent Cherenkov detection efficiencies in plastic are expected, as the index of refraction (n) of plastics (polystyrene, $n = 1.52-1.59$, polyethylene, $n = 1.52$) are generally higher than that of water ($n = 1.332$), which is the medium normally used for Cherenkov counting of radionuclides. The higher index of refraction of the polystyrene will reduce the electron (*i.e.*, beta-particle) threshold energy for the production of Cherenkov photons, as described in Chapter 15.

Smaller-sized plastic scintillator beads (<100 nm), also referred to as nanosuspensions, were tested by Weekley et al. (2004) for the analysis of ^{14}C also to reduce costs of organic liquid scintillation cocktails and cost of mixed organic radioactive waste disposal. They reported a ^{14}C counting efficiency of 45.1%. Zhu and Jay (2007) synthesized fluor-containing nanoparticles (nanosuspensions) from styrene-in-water microemulsions to determine ^{14}C activities in various sample matrices by aqueous LSA. The average diameter of the nanoparticles was ~30 nm. Several α- and β-particle-emitting nuclides were tested and the relative counting efficiencies are listed in Table 7.14. The low detection efficiencies of the low-energy β-emitters (*e.g.*, ^{3}H and ^{63}Ni) are considered by Zhu et al. (2006) and Zhu and Jay (2007) to be offset by the positive environmental effects and reduced costs of mixed (organic) waste disposal.

The size or diameter of the plastic scintillator beads will affect the detection efficiency as reported by Tarancón et al. (2007), particularly for low-energy beta-emitting radionuclides and alpha-emitters (see Table 7.15). Higher detection efficiencies are reported with the smaller-diameter plastic beads (100−250 μm) compared to beads of larger diameter (500−1000 μm) for all beta- and alpha-emitters tested. This is expected, as the smaller diameter beads would be more compact, that is, there would be less space between beads occupied by solution within which the beta- and alpha-particles must travel before reaching the plastic beads. There is thus a loss of particle energy during travel of the particle in the medium prior to arrival of the particle at the plastic scintillator microsphere. Santiago et al. (In Press) refers to such loss of particle energy due to the interaction of the particle with the medium as "particle quenching".

TABLE 7.14 Quantification of Various α and β-Emitting Radionuclides by Liquid Scintillation Counting Using Fluor-Containing Nanoparticles. Relative Counting Efficiency is Defined as CPM from the Nanosuspensions/CPM from Conventional Organic LSC

Isotope	Mode of Decay (E_{max}) (MeV)	Relative counting efficiency (%)
^{3}H	β^- (0.018)	3.2
^{63}Ni	β^- (0.066)	8.19
^{14}C	β^- (0.156)	45.3
$^{90}Sr/^{90}Y$[a]	β^- (0.546/2.28)	82.5
^{204}Tl	β^- (0.763)	71.3
^{32}P	β^- (1.71)	100
^{241}Am	α (5.49)	96.2
^{239}Pu	α (5.15)	100

[a] *^{90}Sr samples contain progeny isotope ^{90}Y, which is likely why this sample exhibited greater counting efficiency than ^{204}Tl.*
(From Zhu and Jay, 2007. Reprinted with permission from IOP Publishing Ltd. © 2007).

Another advantage that plastic scintillator beads can offer is the analysis of aqueous samples containing high salt matrices, which can be difficult to mix with conventional liquid scintillation fluor cocktails. Using ^{14}C as a test nuclide and Detec™ (UPS-89) polystyrene plastic scintillation beads between 180 and 250 μm diameter provided by Detec (Detec.com), Gatineau, QB, Canada or Detec-Europe, F-56000 Vannes, France, Bagán et al. (2009) demonstrated that samples high in salt content (up to 2.8 M $NaClO_4$) could be analyzed efficiently, and the plastic beads can be reused after a simple citric acid wash. The high salt concentrations, however, added a new dimension to the detection efficiency calculations, as the increase in sample density with salt concentration would diminish slightly the detection efficiency. Thus, two quench parameters should be considered, color quenching and salt concentration quenching, as illustrated in Fig. 7.103. There is no chemical quenching, as the solvent and fluor molecules are components of the plastic beads and sample chemicals do not penetrate the beads to produce any chemical quenching effects. The slight decrease in detection efficiency of the ^{14}C with increased sample density is expected, as the relatively weak beta particles must travel from the solution to plastic beads before excitation of plastic and fluor molecules. As two detection efficiency factors are involved, the overall detection efficiency of the radionuclide (E_{unk}) is calculated as

$$E_{unk} = E_C \times E_S \times E_0 \quad (7.145)$$

TABLE 7.15 Detection Efficiencies and Spectrum Position for Beta-Gamma and Alpha Emitters

			(500–1000 μm) Beads		(100–250 μm) Beads	
Isotope	Activity (Bq g^{-1})	Energy (Mev)	Peak (channel)	Detection efficiency (%)	Peak (channel)	Detection efficiency (%)
$^{90}Sr/^{90}Y$	3.2	0.546 (100%) 2.274 (100%)	517 ± 3	156.5 ± 4.0[a]	490 ± 4	185.6 ± 1.4[a]
^{14}C	3.3–3.8	0.156	312 ± 6	17.5 ± 1.5	301 ± 7	41.8 ± 1.0
^{3}H	16.5	0.0186	103 ± 4	0.24 ± 0.01	100 ± 3	0.53 ± 0.04
^{60}Co	5.2–6.8	0.318 (99%) 1.491 (1%)	410 ± 7 646 ± 6	29.4 ± 2.5	377 ± 3 654 ± 4	49.8 ± 0.4
^{137}Cs	86.5	0.512 (95%) 1.174 (5%)	500 ± 4	69.9 ± 1.7	464 ± 2	91.5 ± 0.6
^{238}Pu	1.0–1.1	5.5 (100%)	647 ± 6	56.9 ± 1.0	629 ± 8	63.3 ± 1.8

[a]*Maximum value corresponding to ^{90}Sr ^{90}Y is 200% ($^{90}Sr + {}^{90}Y$).*
(From Tarancon et al., 2007, © Elsevier. Reprinted with permission)

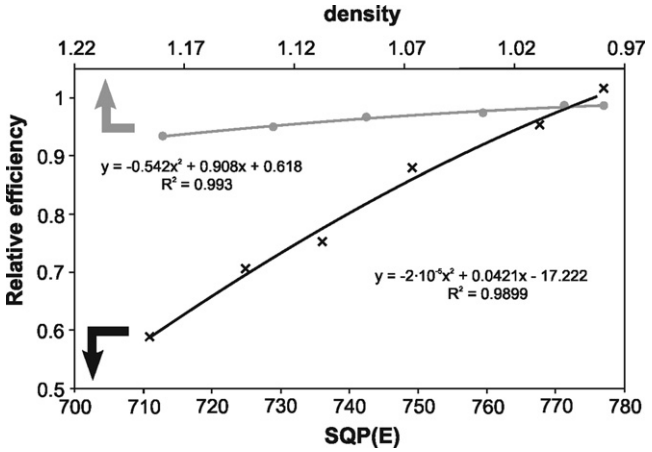

FIGURE 7.103 Relative counting efficiencies of ^{14}C as a function of color quenching (lower curve) measured with an external standard quench-indicating parameter [SQP(E)] and salt concentration quenching, *i.e.*, sample density (upper curve). *(From Bagán et al., 2009. Printed with permission from Elsevier © 2009)*

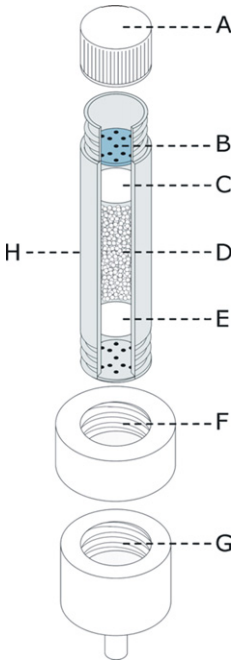

FIGURE 7.104 Cross section of column counting vial. A: top cap, B: perforated round plastic disc, C: paper filter, D: DtBuCH18C6-impregnated polystyrene microspheres, E: paper filter, F: bottom cap, G: pump connector, H: counting vial body. *(From Bagán et al., 2011b. Printed with permission from Elsevier © 2011)*

where E_C is the relative efficiency caused by color quenching, *i.e.*, the efficiency of the color-quenched sample divided by the efficiency of the standard without quenching agent E_0, and E_S is the relative efficiency caused by the salt concentration, *i.e.*, the efficiency of the salt-quenched standard divided by the efficiency of the standard without quenching agent, E_0.

The relatively high detection efficiencies and low backgrounds for ^{90}Sr (^{90}Y) provide the plastic scintillator with the required attributes to serve as a detector for the measurement of ^{90}Sr in environmental samples without the costs of mixed waste. Bagán et al. (2011a,b) impregnated the polystyrene beads with a 1-M solution of 4,4′(5′)-di-t-butylcyclohexano-18-crown-6 (DtBuCH18C6) to act as an extractant for Sr, in a similar fashion as Sr-specific resins, to extract strontium from solution. The extractant-impregnated polystyrene beads are added to a converted 6-mL plastic counting vial, which acts as a Sr extraction column, as illustrated in Fig. 7.104. The ^{90}Sr is retained by the extractant-impregnated polystyrene beads, and the ^{90}Y remains with the rinse solution. The top and bottom of the column can be capped and the column counted directly in the liquid scintillation analyzer. Drinking water, seawater, and river waters were tested, and a minimum detectable activity of 0.46 Bq/L for a 10-mL sample is reported with sample errors <4% (Bagán et al. (2011a,b).

The potential of polystyrene scintillator beads (microspheres) as a detector for α/β pulse shape discrimination in conventional liquid scintillation counters was investigated by Bagán et al. (2010). Again, the study was implemented in light

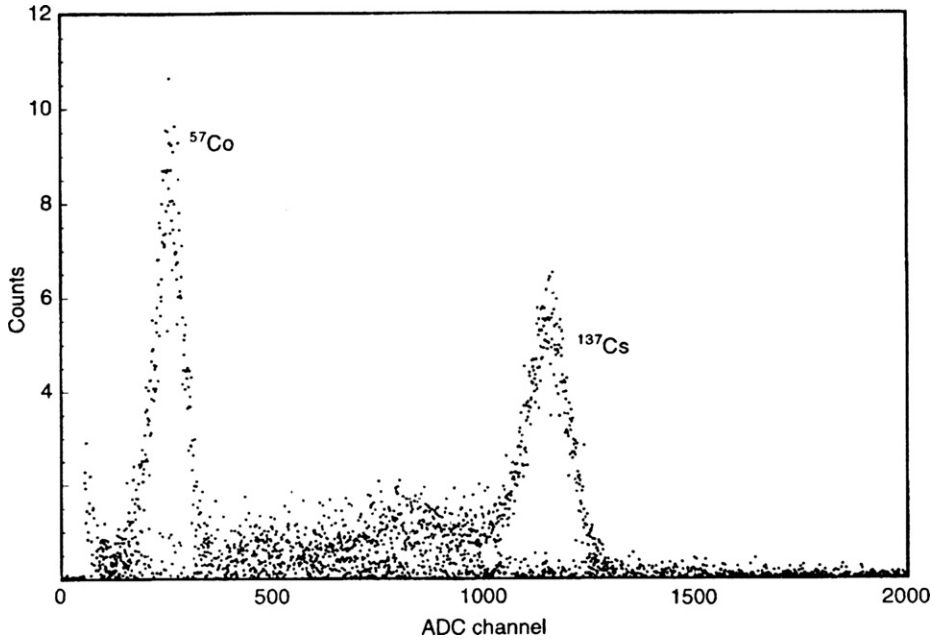

FIGURE 7.105 Liquid xenon scintillation light spectrum of ^{57}Co and ^{137}Cs. *(From Arneodo et al., 2000. Printed with permission from Elsevier © 2000)*

of the advantage of avoiding the use of organic liquid scintillation cocktails and the disposal costs of mixed waste. In a comparison of the performance of the plastic scintillator beads to the conventional use of organic fluor cocktails in α/β discrimination, Bagán et al. (2010) demonstrated that the detection efficiency and pulse heights produced by the beta emitters with plastic scintillator microspheres were lower yielding improved beta discrimination. On the other hand, the analysis of alpha emitters with the plastic scintillator microspheres yielded a poorer alpha discrimination. The α/β discrimination capability of the plastic scintillator is apparently related to the particle energy loss during travel to the plastic microspheres. Bagán et al. (2010) postulate that this energy loss would reduce the excitation of the polystyrene and consequently reduce the number of triplet excitation states key to the pulse shape discrimination of alpha particles from beta particles. A new approach to the α/β discrimination taken by Aboudou et al. (2011), which would avoid the energy loss by both alpha and beta particles, is to evaporate the samples to dryness with the scintillator beads.

The possibility of applying plastic scintillator microspheres for the standardization of beta-emitting radionuclides using the free-parameter model in lieu of organic liquid scintillation fluor cocktails was demonstrated by Tarancón Sanz and Kossert (2011) and Tarancón Sanz et al. (2011). The free-parameter model applied to efficiency tracing and TDCR techniques of radionuclide standardization are discussed in detail in Section IX. Employing the free-parameter model with the TDCR technique and efficiency tracing with ^{63}Ni, Tarancón Sanz et al. (2011) demonstrated the standardization of several beta-emitters with deviations from known reference activities between 0.1 and 2.5%.

Plastic scintillator of cylindrical shape, capable of fitting in a conventional liquid scintillation counting vial, was demonstrated by Furuta et al. (2009) to be a powerful tool for the identification of beta-emitting radionuclides. This is discussed further on in Section XVIII.

XVII. SCINTILLATION IN NOBLE LIQUIDS

Liquid noble gases, such as helium, neon, argon, and xenon, have properties of high scintillation yield as a medium for the detection of ionizing radiation and nuclear recoil energy. In particular, liquid xenon is considered most suitable for γ-ray detection, because of its high atomic number and short decay constants of the scintillation light ($\tau_1 = 4.3$ ns, $\tau_2 = 22$ ns for short and long components, respectively), which comes close to that of plastic scintillators (Hitachi et al., 1983; Tanaka et al., 2001, and Aprile and Doke, 2010). The efficiency of liquid xenon as a scintillator is reported by Aprile et al. (1990) to be similar to that of NaI(Tl) solid scintillation detector, but with a shorter scintillation decay time. Both liquid argon (LAr) and liquid xenon (LXe) are widely studied as efficient liquid scintillation detectors for (i) alpha particles and internal conversion electrons (Aprile et al., 1990, 2005; Miyajima, et al., 1992; Tanaka et al., 2001; Ni et al., 2005, and Kastens et al., 2009), (ii) α/γ and n/γ pulse-height discrimination (Benetti et al., 1993; Peiffer et al., 2008), and (iii) γ-radiation and neutron spectrometry from the scintillation efficiency of electron and nuclear recoil events (Arneodo et al., 2000; Akimov et al., 2002; and Aprile et al., 2005). Liquid rare gas detectors are currently being studied for their utility in various fields including (i) nuclear medicine as imaging detectors in positron emission tomography, *i.e.*, PET (Doke et al., 2006, Gallin-Martel et al., 2006, 2009, Grignon et al., 2007, Amaudruz et al., 2009 and Retière, 2010), (ii) tomography imaging telescopes (time projection chambers) for research in medium-energy gamma-ray astrophysics (Aprile et al., 1990; Cennini et al., 1999; and Aprile and Doke, 2010), (iii) galactic dark matter search consisting of weakly interacting massive particles (Akimov et al., 2002;

Neves et al., 2005, 2007, Aprile et al., 2006b; and Sorensen et al., 2009), (iv) relativistic heavy ion detection (Tanaka, et al., 2001), (v) the search for the rare muon decay, *i.e.*, $\mu^+ \rightarrow e^+ + \gamma$ (Adam et al., 2010; Uchiyama, 2010; Iwamoto, 2010; Sawada, 2010; and Nishimura and Natori, 2011), and (vi) the EXO (Enriched Xenon Observatory for $0\nu\beta\beta$, *i.e.*, neutrinoless double beta decay (Leonard et al., 2008; Ueshima et al., 2008; Arisaka et al., 2009; and Neilson et al., 2009). Applications of liquid xenon are numerous in light of the advantageous detector characteristics of high atomic number, scintillation efficiency, and short fluorescence decay times.

The mechanisms of scintillation in liquid argon and liquid xenon are similar and have been investigated thoroughly (Kubota et al., 1978a,b, 1979; Doke, 1981; Doke et al., 1990). As described by Cennini et al. (1999), Mei et al. (2008), and Aprile and Doke (2010), scintillation light in liquid argon (LAr) is produced by ionizing radiation either by direct ionization of an Ar atom followed by excimer formation and de-excitation according to

$$Ar^* + Ar \rightarrow Ar_2^* \rightarrow 2Ar + h\nu(128\ nm) \qquad (7.146)$$

or via ionization, recombination, excimer formation, and de-excitation as

$$Ar^{\oplus} + Ar \rightarrow Ar_2^{\oplus} + e \rightarrow Ar_2^* \rightarrow 2Ar + h\nu(128\ nm) \qquad (7.147)$$

Deexcitation from the Ar_2^* to the dissociated ground state 2Ar gives rise to fluorescence displaying fast and slow decay components of about 5 ns and 1 μs, respectively, with relative yields of 23% and 77% at an emission of approximately 128 nm wavelength. The light emission is abundant with approximately one photon emitted per 25 eV of energy dissipated in LAr by ionizing radiation or 40,000 photons per MeV. In the case of liquid xenon (LXe) excitation, light emission is at 175 nm and the lifetimes of the singlet and triplet states of the excited dimer Xe_2^* are 4 ns and 22 ns, which makes liquid xenon the fastest of the noble liquid scintillators (Hitachi et al., 1983 and Aprile et al., 2005).

The wavelength of light emission is in the vacuum ultraviolet (VUV) region. Consequently, glass-faced photomultipliers are used with wavelength shifters. Metal-channel photomultipliers (PMTs) are fabricated by Hamamatsu Photonics to efficiently detect the fast scintillation light from LXe. These PMTs are designed to operate within the LXe to efficiently detect the 175-nm Xe light photons (Giboni et al., 2005). Other photomultipliers with MgF_2 or CaF_2 windows have been used. The addition of liquid xenon in small concentrations ($\leq$100 ppm) into LAr serves as a wavelength shifter from 128 to 173 nm permitting photomultipliers with quartz windows (Cennini et al., 1999). The scintillation mechanism for liquid xenon is similar to that described above for LAr with an average of one photon emitted per 14.7 eV of energy dissipated by ionizing α-particles (Tanaka et al., 2001). Avalanche photodiodes (APD) and silicon photomultipliers are researched as alternatives to the photomultiplier tube for liquid rare gas scintillation detectors (Solovov et al. 2000; Aprile et al., 2006a; and Shagin et al., 2009).

Arneodo et al. (2000) demonstrated the excellent linear response of scintillation fluorescence versus energy deposited in liquid xenon using several γ-ray sources. Typical energy distribution in liquid Xe with ^{57}Co and ^{137}Cs γ-ray sources placed outside the LXe scintillation detector measuring 5.0 cm and 4.6 cm for the top and bottom diameters and 4.0 cm in height are illustrated in Fig. 7.105. The width of each energy distribution is dominated by a light collection efficiency that varies from 5% to 12% depending on the point of interaction of the γ-ray within the LXe detector volume. The overall detector efficiency was estimated by Arneodo et al. (2000) to be approximately 1.5% for the 175-nm UV photons from the LXe scintillation taking into account the average light collection efficiency of 8%, PMT quantum efficiency of 19%, and photoextraction potential of LXe of 15 eV.

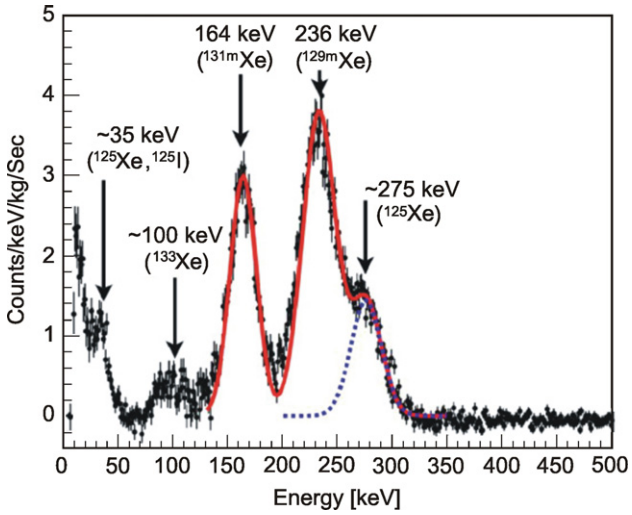

FIGURE 7.106 Background subtracted spectra from activated Xenon 12 hours after a 5-day neutron activation The energy resolutions for the 164- and 236-keV peaks are 7.0% and 5.1%, respectively. *(From Ni et al., 2007. Printed with permission from Elsevier © 2007)*

Calibration of LiXe detectors can be performed from the decay of xenon metastable states, illustrated in Fig. 7.106, produced by fast neutron activation. All of the short-lived metastable states decay within a few days leaving no longtime activity in the detector after the neutron activation as demonstrated by Ni et al. (2007). The characterization of the response of noble liquid scintillation detectors at low energies can be performed with ^{83m}Kr as a calibration source (Kastens et al., 2009). The ^{83m}Kr decays via isomeric transition with emission of 9.4 and 32.1 keV conversion electrons and with a half-life of 1.83 hours. The spectral energy peaks, illustrated in Fig. 7.107, at 9.4 and 32.1 keV are reported to have a 23% and 14 % resolution, respectively. Such a source with short half-life leaves no long-lived residue in the detector.

XVIII. RADIONUCLIDE IDENTIFICATION

It is possible to use a liquid scintillation analyzer to identify automatically an unknown pure β-emitting radionuclide sample; once it is identified, the LSA can automatically determine the activity (DPM) of that same sample.

One of the obstacles encountered in identifying β-emitting radionuclides by LSA is that the pulse-height spectrum of all

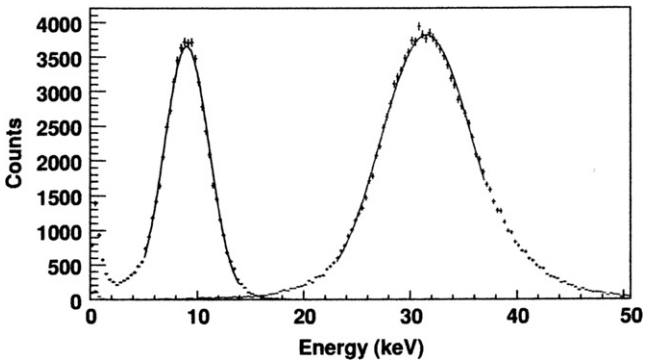

FIGURE 7.107 Activities of energy peaks due to 9.4- and 32.1-keV conversion electrons after doping ^{83m}Kr into the liquid xenon detector. The 9.4- and 32.1-keV peaks have a resolution of 23 and 14%, respectively. *(From Kastens et al., 2009. Reprinted with permission © 2009 The American Physical Society)*

β-emitters are broad over the range from 0 keV to the end point energy corresponding to the E_{max} of the β-emissions. Also, the pulse-height spectrum of a given β-emitter changes in pulse-height distribution and endpoint energy according to the level of quench in a sample. Consequently, the pulse-height distribution of a higher-energy β-emitter under a high degree of quench could resemble that of a lower-energy β-emitter under a low degree of quench.

By means of a double-ratio technique, Takiue et al. (1989b) developed a method for identifying unknown β-emitters. The technique is based on combining the information provided by two quench-indicating parameters, tSIE and SIS, which were described previously in this chapter. The tSIE is produced by the external standard, and it provides information defining the level of quench in the sample−scintillation fluor cocktail mixture. The SIS is a sample-spectrum quench-indicating parameter, which depends not only on the degree of quench in the sample but also on the β-particle energy spectrum. The two quench-indicating parameters together, therefore, provide information, that reflects the pulse-height distribution and shape of a particular pulse-height spectrum at any given quench level. The combined information provided by the two quench-indicating parameters is used to identify pure β- or β/γ-emitting radionuclides.

The technique developed by Takiue et al. (1989a,b) requires the preparation of a series of quenched "standards" of all of the pure radionuclides that may need to be identified as unknown samples. The word "standards" is enclosed in quotation marks, because the activity need not be known in the series of quenched standards. The activities of the quenched standards should be high enough to determine accurately the SIS of each of the standards, and they are used only once to prepare a double-ratio curve for a particular radionuclide.

Once the series of quenched standards has been prepared for each radionuclide of interest, the SIS and tSIE of each quenched standard are determined and plotted as illustrated in Fig. 7.108. The family of curves, illustrated in the figure, becomes separated from the lowest curve for ^{3}H to the uppermost curve for ^{32}P according to the maximum energy (E_{max}) and average energy (E_{av}) of each radionuclide, because the SIS plotted along the ordinate reflects both E_{max} and E_{av}. The curves, therefore, provide a definition of the magnitudes of the pulse-height spectral distributions as a function of quench, which are radionuclide specific.

To apply this technique, an unknown sample is monitored for its SIS and tSIE value and then compared with the double-ratio curves, such as those illustrated in Fig. 7.108, which were prepared in advance. From the tSIE and SIS of an unknown sample, the radionuclide can be identified using the double-ratio curves, provided the deviation $\Delta S/S$ of the experimental plotted point of the unknown sample is less than ± 0.02, or

$$\frac{\Delta S}{S} = \frac{(\log Y_1 - \log Y_0)}{S} < \pm 0.02 \qquad (7.148)$$

where ΔS is the difference in ordinate $(\log Y_1 - \log Y_0)$ between the plotted point Y_1 and the corresponding value Y_0 on the double-ratio curve, and S is the logarithm of the SIS value $(\log Y_0)$ on the curve. Takiue et al. (1989b) demonstrated that the activities of the unknown samples can also be determined automatically, if the double-ratio curves are linked by computer program to the quench-correction curve of the appropriate radionuclide. In essence, therefore, an unknown pure β-emitter in scintillation fluor cocktail could be placed in an LSA for both automatic identification and activity analysis.

The above procedure was demonstrated to work for several radionuclides with the exception of ^{14}C and ^{35}S. The close

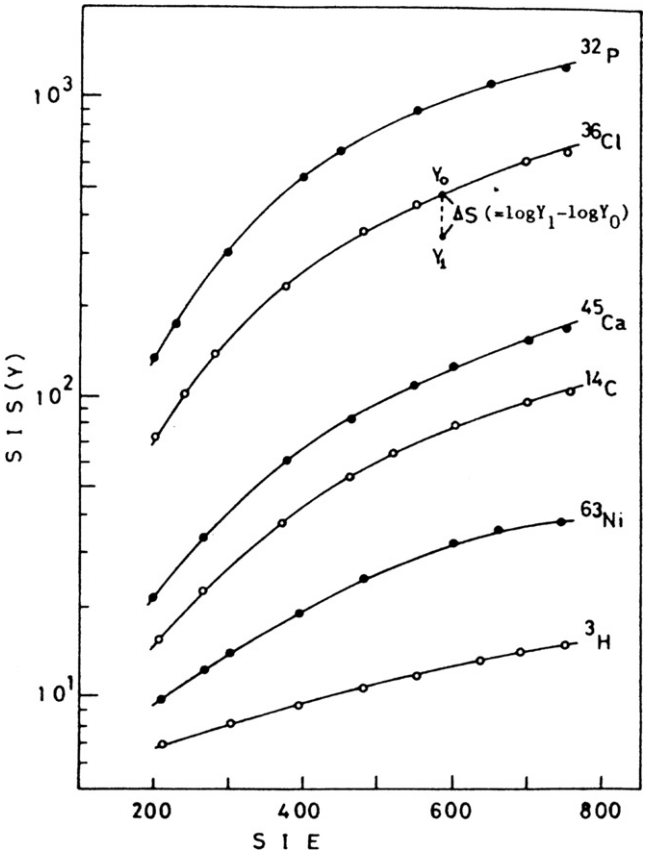

FIGURE 7.108 Double ratio curves for identifying an unknown radionuclide. Each curve is constructed from the SIS and SIE of a series of quenched "standards" of each nuclide. *(From Takiue et al., 1989b. Printed with permission from Elsevier © 1989)*

similarities of the β-particle energy spectra of ^{14}C ($E_{max} = 156$ keV) and ^{35}S ($E_{max} = 167$ keV) produce overlapping double-ratio curves, which prevents the identification of these two radionuclides in unknown samples. However, Natake et al. (1996) showed that pulse-height analysis could be used to identify ^{14}C and ^{35}S in unknown samples. The slight difference in the pulse-height distributions could be distinguished using the sample channels ratio (SCR), which is the ratio of two counts in two measurement channels. The optimum channel settings were selected to obtain as great a difference between the two radionuclides as possible for a given quench level. The SCR for a series of quenched "standards" of ^{14}C and ^{35}S are then plotted against the H number in what is referred to as a double-quench parameter (DQP) curve. The H number is an external standard quench-indicating parameter (QIP) described previously in this chapter. Other external standard QIPs, such as tSIE or SQP(E), can also be used in this technique. To apply the technique, the SCR and the H number are determined for the unknown sample and the two QIP values are plotted on the previously prepared DQP curve. The radionuclide is then identified when the plot of that point lies in the neighborhood of either the ^{14}C or ^{35}S DQP curve.

In another approach to identify unknown pure $\beta-$emitters, Dodson (1996) developed the technique of characterizing the pulse-height spectrum according to the following three properties: E_{max}, the isotope center number I, and the spectral resolution (FWHM or F). The isotope center number I is defined as

$$I = \frac{\sum(N_i E_i)}{\sum(N_i)} \tag{7.149}$$

where E_i is the energy of the N_i electron. For quenched sets of radionuclide standards, both I and F are found to be linearly dependent on E_{max}. The slopes and intercepts of the linear equations defining I and F as a function of E_{max} over a range of quench levels are tabulated for each radionuclide. The measurement of I, E_{max}, and FWHM of an unknown nuclide's sample spectrum coupled with a relevant algorithm permits the identification of the unknown nuclide within the parameters of the defined reference set.

Alpha-particle emitters were identified by Kaihola (2000) of Wallac Instruments (now PerkinElmer, Inc.) who demonstrated that the external standard quench-indicating parameter SQP(E) could be used to correlate the alpha-particle sample pulse-height distribution with its emission energy as a function of quench level. Two known energy calibration lines as a function of quench are required to verify the emission energy and identify the radionuclide in liquid scintillation alpha spectroscopy.

A new approach to the identification of pure beta-emitting radionuclides with a conventional liquid scintillation counter was taken by Furuta et al. (2009). They measured the pulse-height spectra of 6 pure beta-emitting radionuclides using plastic scintillator (Saint-Gobain BC-400) that is placed into glass counting vials. Three different instruments were used including Beckman Coulter LS-6000S, LS-6500, and PerkinElmer Tri-Carb 3270TR/SL liquid scintillation analyzers. The radionuclides were dried onto separate plastic scintillator sheets, which were inserted into plastic scintillator cylinders or containers. The plastic scintillator containers were then placed inside a conventional glass LSC vial. After calibrating the x-axis of the pulse-height spectra to read 0.5 keV per channel, the channel of the spectrum endpoint for ^{3}H, ^{14}C, ^{35}S, ^{45}Ca, and ^{33}P yielded the theoretical maximum beta energy (E_{max}) of each radionuclide, as illustrated in Fig. 7.109. The absolute nuclide decay energy is not measured with the plastic scintillator; however, the plastic scintillator permitted the identification of the nuclides by the endpoints and shapes of the spectra. The endpoint of the pulse-height spectrum of the high-energy ^{32}P ($E_{max} = 1710$ keV) is not illustrated in Fig. 7.109. Furuta et al., (2009) demonstrated that the endpoint of this spectrum was reported to reach up to 1612 keV, because the plastic scintillator

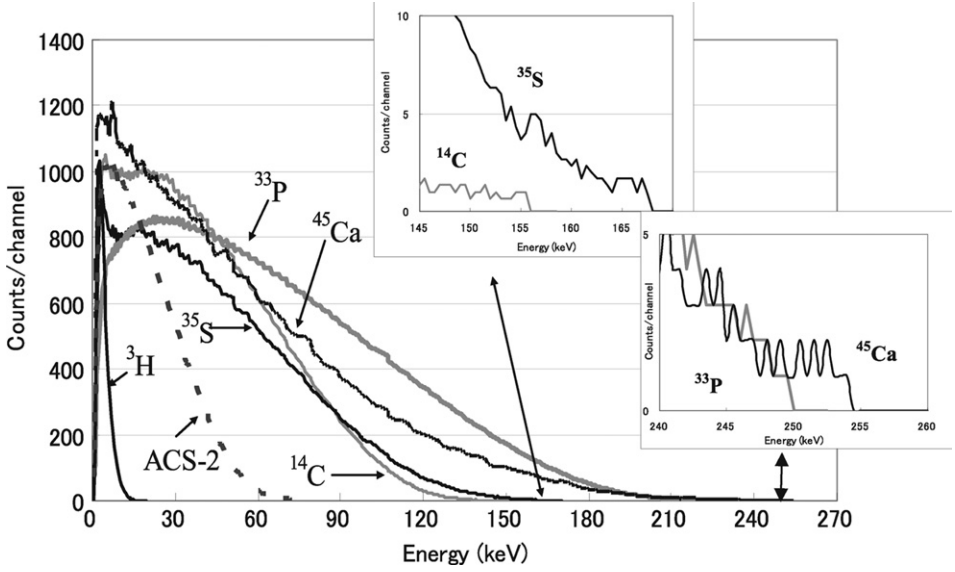

FIGURE 7.109 Spectra of five nuclides measured with plastic scintillator and a quenched spectrum of ^{14}C measured with ACS-2 liquid scintillator (dashed line). *(From Furuta et al., 2009, Printed with permission from Radiocarbon, University of Arizona © 2009 Arizona Board of Regents on behalf of the University of Arizona)*

was not thick enough to absorb all of the beta-particle energy in this case.

XIX. AIR LUMINESCENCE COUNTING

An innovative approach to α-particle counting is the use of a liquid scintillation counter to detect luminescence events caused by the α-particle excitation of N_2 in air. The technique was devised by Takiue and Ishikawa (1979b). As explained by these investigators, the alpha particle passing through air dissipates its energy, forming excited nitrogen molecules N_2^*, excited nitrogen molecular ions N_2^{+*}, and excited nitrogen atomic ions N^{+*} as follows with relative energy consumptions as given in parenthesis:

$$N_2 + W_\alpha \longrightarrow N_2^* \quad (50\%)$$
$$N_2^{+*} + e^- \quad (45\%)$$
$$N^{+*} + N + e^- \quad (5\%)$$

where W_α is the α-particle energy dissipated in air, e^- is an electron, and N is the nitrogen atom. The emission spectra are derived from entirely N_2^* and N_2^{+*} bands. Emission wavelengths of the air luminescence are found in the region of 220−520 nm, which is within the range of sensitivity of photomultiplier tubes used in conventional liquid scintillation analyzers.

The oxygen in air (21%) does not contribute to the air luminescence but rather acts as a quencher by forming a complex with N_2^*, leading to a radiationless deactivation of excited molecular nitrogen. Argon, with a natural concentration in air of only 1%, undergoes luminescence. However, its photon emissions make little contribution to the overall nitrogen luminescence because of the low concentration of argon in air compared to that of nitrogen (78%).

The sample preparation and counting procedure recommended by Takiue and Ishikawa (1979) are simple and relatively inexpensive. Approximately 0.1 g of a solution of α-particle-emitting nuclide is deposited onto a 0.84-mg/cm^2-thick Tetoran film (Toray, Inc.), dried with an infrared lamp, and inserted into an empty liquid scintillation glass counting vial so that the film and sample remain suspended in the air around the center of the vial.

The sample may be counted as such without further preparation, or the air in the vial may be purged with pure nitrogen as a gas scintillator.

When the nuclides are counted in air, counting efficiencies of 72 and 74% for ^{210}Po and ^{241}Am, respectively, are obtained, and purging with pure nitrogen leads to an increase of 10−15% in counting efficiency. The method offers several advantages: (1) there is no concern about quenching except for that of oxygen, which remains constant from sample to sample; (2) there is no need to be concerned about the preparation and handling of costly scintillators, as air is the only medium of detection; (3) the technique offers excellent reproducibility from sample to sample because of the absence of variable quenching agents; (4) the spectral emissions of nitrogen overlap well with the spectral response of photomultiplier tubes used in liquid scintillation analyzers, obviating the need for wavelength shifters; and (5) normal air containing 78 % nitrogen may be used as the detection medium.

The main disadvantages of the air luminescence method are (1) reduced counting efficiency, as liquid scintillation with fluor cocktail provides 100% counting efficiency for α-emitters even under high levels of quench; (2) there is no α-radionuclide spectroscopy capabilities, since the pulse-height spectrum is a peak produced by the air luminescence photons; (3) the limitation of the sample size to about 0.1 mL of radioactive solution that is deposited and dried on the transparent film; and (4) there is no possibility of analyzing β-emitters in the sample, that is, simultaneous α/β discrimination and analysis is not feasible.

These original findings of Takiue and Ishikawa were expanded by Takiue (1980) for the routine analysis of α-emitters on smear (swipe) paper in air without scintillation cocktail. The technique involves swiping a 100-cm^2 contaminated area with a smear paper (25-mm diameter, 30 mg/cm^2) at a pressure of about 0.2 kg/cm^2. The contaminated smear sample, thus obtained, is placed directly in an empty glass scintillation counting vial with the contaminated side of the paper facing upward and measured without adding a liquid scintillation cocktail, as illustrated in Fig. 7.110.

The α-particle counting efficiency is reduced because of the 2π counting geometry with the smear sample at the bottom of the counting vial. Takiue (1980) observed variation in smear removal efficiencies from different contaminated surfaces. The counting efficiencies of ^{210}Po or ^{241}Am as smear samples on paper varied between 10 and 20% from sample to sample. The following advantages of the air luminescence method for monitoring α-emitter radioactive contamination can be cited: (1) sample preparation for α-contamination surface monitoring is simple and inexpensive, because no scintillation cocktail is required or cocktail waste produced, and (2) low backgrounds are achieved (~9 CPM with the instrumentation used by Takiue), providing a detection limit of 1×10^{-7} μCi/cm^2 for loose contamination. Disadvantages of the air luminescence method are (1) much lower and more variable counting efficiencies (10−20%) are obtained in air luminescence analysis of smear samples,

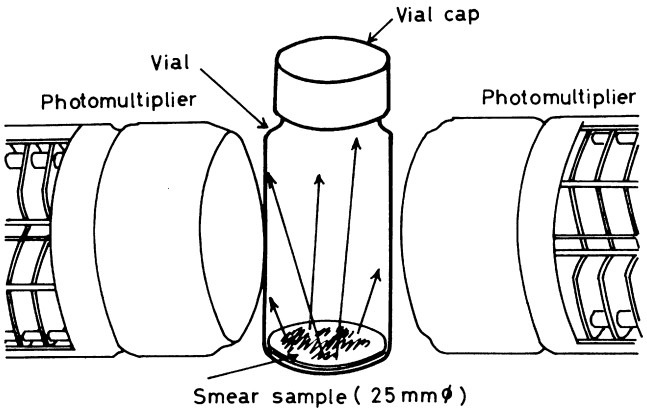

FIGURE 7.110 Measurement geometry for a smear sample in air (contaminated side of paper is facing upward) and detector photomultiplier tubes of a liquid scintillation spectrometer). *(From Takiue, 1980. Printed with permission from Wolters Kluwer Health/Lippincott, Williams & Wilkins © 1980 Health Physics Society)*

compared to a constant 100% counting efficiency obtained by liquid scintillation analysis and (2) β-emitters cannot be analyzed by air luminescence, that is, simultaneous α/β discrimination and analysis with air luminescence is not possible.

Caution must be taken to assure that there are no significant activities of β-particles with energies in excess of 180 keV, which is the threshold energy for the production of Cherenkov radiation by β-particles (electrons) in glass. For samples containing high-energy β-emitters, Takiue (1980) demonstrates that a double-region counting technique could be used to discriminate between pulses produced by Cherenkov photons and air luminescence.

Further studies by Homma et al. (1987) demonstrated the possibilities of measuring ^{222}Rn and its daughter nuclides in air in the gaseous phase by air luminescence counting. A counting efficiency of 42% was achieved. The endpoint of the air luminescence spectrum produced by ^{222}Rn is about 18 keV; hence, a preset counting region normally used for ^{3}H liquid scintillation analysis could be used for the air luminescence analysis.

In the liquid scintillation analysis of ^{222}Rn, Murase et al. (1989a) demonstrated that air luminescence produced by ^{222}Rn and its daughters in the gaseous phase above the liquid scintillator can give rise to significant air luminescence counts. Therefore, to avoid error caused by air luminescence in the LSA of ^{222}Rn, currently approved methods require filling the liquid scintillation vial to a total volume of 20 mL with sample and fluor cocktail. For example, the procedure used by the U.S. EPA (EPA/EERF-Manual-78−1) for the analysis of radon in water (see Passo and Cook, 1994) calls for the injection of 10 mL of freshly sampled water into 10 mL of an organic accepting liquid scintillation cocktail (*e.g.*, Opti-Fluor O). The ^{222}Rn partitions into the organic fluor phase, and insignificant gaseous space remains in the standard 20-mL liquid scintillation counting vial for any significant air luminescence interference. To avoid any interference from luminescence by ^{222}Rn alpha particles in the air above the liquid scintillation cocktail, Murase et al. (1999) selected a lower-level discriminator setting of 25 keV. Thus, all pulse events that may originate from air luminescence would be rejected, as these are found in the 0−18-keV region only.

Murase et al. (1989b) demonstrated the air luminescence analysis of ^{210}Po, ^{238}U, and ^{241}Am. The technique involves spotting small amounts (0.1 mL) of aqueous solutions of the α-emitters on the bottom of glass liquid scintillation vials and evaporating the samples to dryness with an infrared lamp. The counting efficiencies obtained were between 33.3 and 33.7 $\pm$ 0.23%. The air luminescence pulse-height spectra correspond to the region of 0−18 keV for pulse height calibrated on an energy scale. Therefore, a counting region preset for the analysis of ^{3}H by LSA can be used for the air luminescence counting. Following air luminescence counting, the samples can be recovered from the vials for other studies. The counting efficiencies for the air luminescence determinations are easily determined by subsequent liquid scintillation analysis of samples. These can be carried out at random or for as many vials as desired. Liquid scintillation analysis after air luminescence was carried out by Murase et al. (1989b) after dissolving the radionuclide residue by wetting the bottom of the vial with 0.5 mL H_2O followed with liquid scintillation cocktail. The liquid scintillation analysis of α-emitters is 100%. Therefore, simply the activities (DPM) of samples obtained by liquid scintillation analysis can be used to calculate the air luminescence counting efficiency, as the count rate by LSA is also the disintegration rate. A disadvantage of the air luminescence analysis is the very small sample size of 0.1 mL that can be analyzed. Larger samples might leave too thick a residue at the bottom of the scintillation vial after drying, which would produce samples with significant self-absorption.

Air luminescence counting was used by Homma et al. (1996) to standardize ^{222}Rn samples that are applied to calibrate detectors utilized for the determination of ^{222}Rn in air. The standardization of ^{222}Rn as described by Homma et al. (1996) involves collecting a sample of ^{222}Rn from approximately 20 mL of sample of a 0.1-M HCl solution of 20 kBq $^{226}RaCl_2$ with a syringe and then transferring the ^{222}Rn gas to a standard liquid scintillation counting vial, which was filled with air and closed with a silicon rubber stopper. The ^{222}Rn in the vial is allowed to sit for 3.5 hours before measurement to allow the daughters ^{218}Po, ^{214}Pb, ^{214}Bi, and ^{214}Po to reach transient equilibrium with the ^{222}Rn. This sample is referred to as the ^{222}Rn "standard." The ^{226}Ra solution from which the ^{222}Rn is taken does not have to be a standardized solution, because the ^{222}Rn determination is not based on secular equilibrium between ^{226}Ra and ^{222}Rn. It is not even necessary to know how much ^{222}Rn from the ^{226}Ra solution was actually removed. It is necessary only to standardize the ^{222}Rn that is transferred into the rubber stopper-sealed scintillation counting vial. Standardization of the gaseous ^{222}Rn is done by air luminescence counting. The air luminescence counting efficiency of the ^{222}Rn was determined by using the counting efficiency of a standardized ^{210}Po source. The ^{210}Po counting efficiency (E) was determined by calculating $E = \alpha/A$, where α is the air luminescence count rate of a ^{210}Po source and A is the α-particle emission rate of the ^{210}Po source expressed in α-particles per second in a solid angle of 2π steradians. Homma et al. (1996) underscore the importance of measuring the air luminescence counting efficiency of ^{222}Rn, as instrument models may vary in optical properties, PMT properties, and circuit properties. Morita-Murase et al. (2001, 2003) have pursued further the application of air luminescence counting to the measurement of ^{222}Rn. They standardized a ^{222}Rn sample collected with a syringe from the air space above a $^{226}RaCl_2$ solution. The ^{222}Rn was injected into a small quartz tube (7 mm in diameter by 40 mm in length) sealed at both ends with silicon rubber stoppers. After 3.5 hours, transient equilibrium of ^{222}Rn with its daughters ^{218}Po, ^{214}Pb, ^{214}Bi, and ^{214}Po is reached. The activity of the ^{222}Rn was then determined via analysis of the daughter ^{214}Pb γ-rays with a Ge semiconductor well detector. The small quartz tube with known ^{222}Rn activity was placed into a standard empty liquid scintillation vial, and the vial agitated until the quartz tube was broken, liberating the ^{222}Rn into the air of the vial. The ^{222}Rn was counted with a liquid scintillation analyzer to provide the air luminescence counting efficiency of ^{222}Rn for the particular liquid scintillation analyzer used. An air luminescence counting efficiency of 42.6 $\pm$ 0.2% for ^{222}Rn was reported. Morita-Murase et al. (2003) report that the low-level count mode (LLCM) of the PerkinElmer TriCarb 3170 TR/SL should not be used for air luminescence counting, because the

LLCM rejects pulse events that are not produced in liquid scintillator. Instead, the normal count mode (NCM) may be used with the PerkinElmer Tri-Carb instruments.

XX. LIQUID SCINTILLATION COUNTER PERFORMANCE

This chapter so far has dealt with the basic principles and procedures of liquid scintillation analysis. The remainder of the chapter will review the methods used to optimize the performance of the LSA. This is particularly important when sensitivity is key to our measurements. In addition, we need methods that can be used to assess the performance of the LSA to ensure that the instrument is providing reliable and reproducible data.

A. Instrument Normalization and Calibration

The first item to be addressed is that of assessing performance and calibration of the LSC to be sure that the activity data (DPMs) are accurate and reproducible. The first area to review is the calibration methods that are used for LSCs. One method is to use a flame sealed standard in scintillation cocktail, usually a ^{14}C source as the calibration normalization source for the LSC. This sealed standard should be a calibrated standard such as one traceable to a primary standard from a national institute of standards so that its DPM is accurately known and it produces light pulses similar to those found in real samples. Jaubert et al. (2006) report that flame-sealed purely organic liquid scintillation sources can be used as reference sources for periods of more than 10 years, provided the sources are stored at ambient temperature in reduced light.

The calibration procedure of liquid scintillation analyzers varies according to the manufacturer of commercial instrumentation. One method of calibration (*e.g.*, PerkinElmer Tri-Carb LSAs) involves loading an unquenched ^{14}C standard source into the counting chamber, the high voltage for each of the PMTs is set automatically to obtain the optimum ^{14}C efficiency, and the ^{14}C endpoint energy of the standard is fixed at 156 keV with the minimum background. Such a calibration should be performed at least weekly as long as the instrument is being used.

B. Assessing LSA Performance

Assessing the performance of the LSA on a routine basis is important to have assurance that the instrument is operating within acceptable parameters and to have a standing record over time of the instrument performance. To maintain good laboratory practice and satisfy regulatory agencies, it is often necessary to have records of the instrument performance on a routine basis, such as daily, weekly, or monthly, to provide proof that deviations in instrument performance do not have any effect on the analytical results. Instrument performance assessment (IPA) is carried out generally with a set of standards that are traceable to a primary standard from a national institute of standards. These standards can be the same as those used for calibrating the instrument.

The IPA is normally carried out on a regular basis and the results stored and printed in a tabular and/or graphic form with a time and date stamp. Eight parameters should be assessed using a set of three unquenched standards (*e.g.*, purged with argon in a flame-sealed counting vial), namely, (i) a tritium standard, (ii) a ^{14}C standard, and (iii) a background standard, *i.e.* a standard consisting only of scintillation cocktail. The three standards can measure the following instrument performance: (1) tritium efficiency, (2) tritium background, (3) tritium figure of merit, (4) tritium chi-square, (5) ^{14}C efficiency, (6) ^{14}C background, (7) ^{14}C figure of merit, and (8) ^{14}C chi-square. The tritium and ^{14}C efficiencies are determined by the LSA using two sealed standards counted in predefined counting regions. This requires approximately 1 minute for each sample, as these samples are generally of sufficiently high activity that only short count times are needed. This test should be performed daily. The backgrounds are determined using a sealed background standard with two preset counting regions for tritium and ^{14}C. This requires approximately 60 minutes because an accurate CPM value of the background needs to be obtained to assure reproducibility. Background assessment should be performed at least weekly. The ^{3}H figure-of-merit and ^{14}C figure-of-merit performance values are determined using the E^2/B calculation, which is the percent counting efficiency squared divided by the background count rate in CPM. This is an excellent indicator of any change in performance for the LSC. It can be calculated using the ^{3}H and ^{14}C standards, and it should be performed daily. The final performance parameters are the ^{3}H chi-square and ^{14}C chi-square. This is a monitor of short-term stability in the LSA and involves counting the ^{3}H and ^{14}C sealed radionuclide standards 20 times for 0.5 minutes each. The chi-square tests are used to confirm that the count rate measurements vary within the normal and expected deviations; that is, the count rates are neither too consistent nor too variable to be true. The chi-square tests should be performed weekly. By monitoring and recording these eight parameters, good laboratory practices (GLP) can be satisfied.

The instrument performance assessment (IPA) can be performed either manually by the LSC users with the data placed into a spreadsheet or automatically by an LSC that has automatic IPA and instrument calibration. Figure 7.111 shows a plot of the data obtained with an automatic IPA program on a PerkinElmer Tri-Carb LSA. This type of graph can be displayed, stored in computer memory, and printed for each of the eight IPA parameters described previously. In any given graph for any of the eight parameters, such as the example in Fig. 7.111a, an average line is calculated and the one, two, and three sigma values are provided so that the user can evaluate any trends or outlying points. If an outlying point is observed, this information is printed on the final data output. In addition, a series of suggestions can be provided so that the user can assess the problem further and take preventative action if any parameters are too frequently outside of recommended limits. An example is provided in Fig. 7.111b. Possible problems that might be indicated are counting contamination, PMT failure, dirty PMTs, and electronic failures. Jaubert et al. (2006) and Chałupnik and Mielnikow (2009) provide thorough treatments of the importance of instrument performance assessment or the

(a)

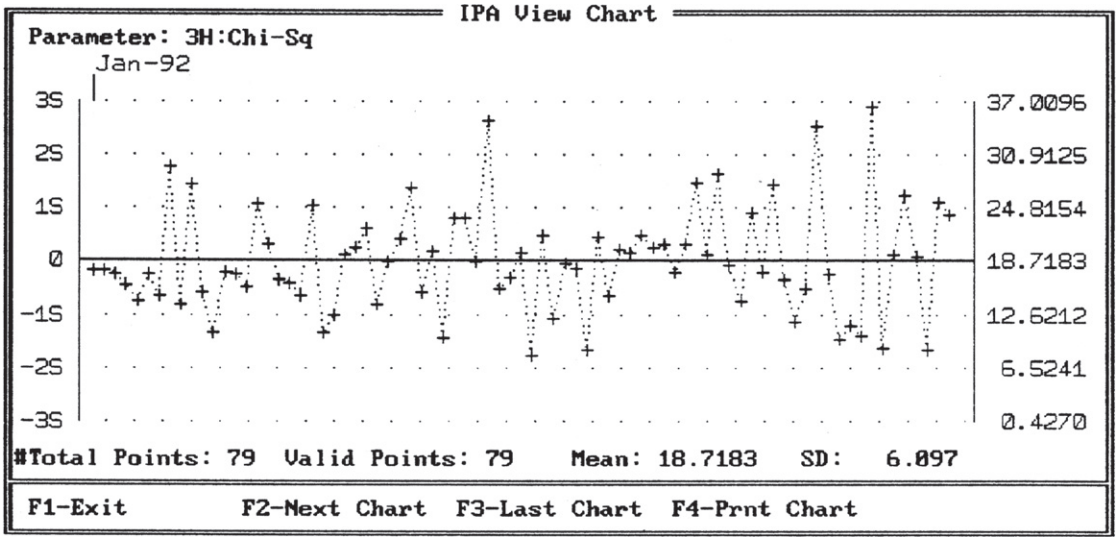

(b)

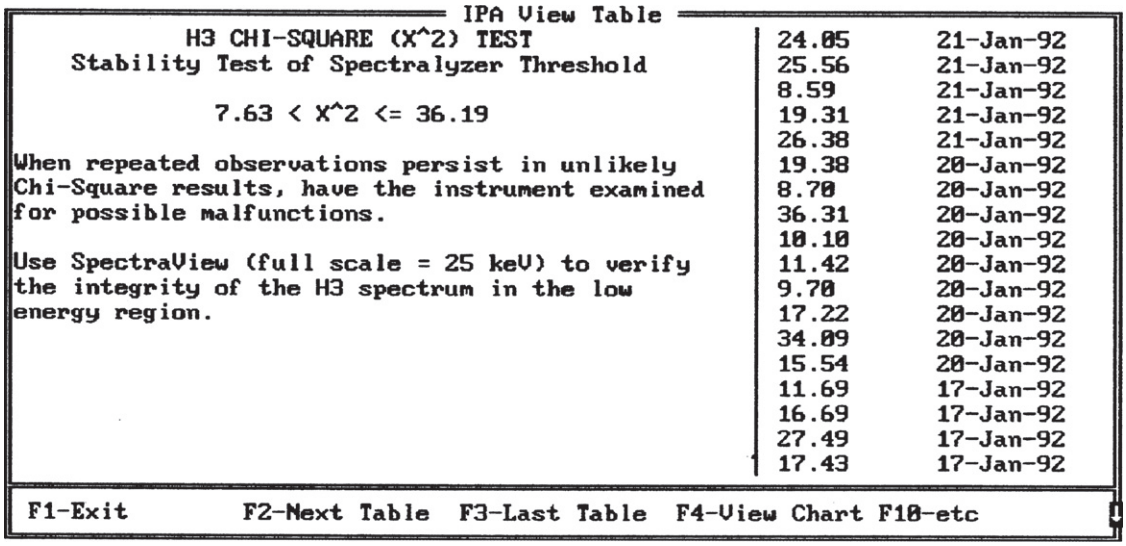

FIGURE 7.111 Chi-square instrument performance assessment (IPA) data displayed on the computer monitor of a liquid scintillation analyzer (a, upper chart) as a chart and (b, lower table) as a table with instructions if measured parameters are obtained too frequently outside of recommended limit. *(© 1998 PerkinElmer, Inc. Printed with permission)*

implementation of a quality assurance system for the monitoring of the long-term stability of LSAs.

C. Optimizing LSC Performance

The procedures for determining sample activities in DPM in routine sample analysis are dealt with in detail in previous parts of this chapter. This section will describe methods used to optimize performance particularly for low-count-rate samples when LSA sensitivity is most important. There are several methods of optimizing performance, and these will be described in detail in this section.

1. Counting Region Optimization

If a radionuclide, such as ^{14}C, is to be analyzed and a low level of detection is required, the counting region, defined by lower-level (LL) and upper-level (UL) pulse-height discriminators, must be optimized for best performance measured by the figure of merit (E^2/B). The figure of merit is calculated as the square of the percent counting efficiency of the radionuclide of interest divided by the background count rate expressed in CPM. Optimizing the counting sensitivity (E^2/B) with spectrum analysis of sample and background is achieved by the following procedure:

a. Count a known activity (DPM) of the radionuclide of interest and store the sample spectrum, as illustrated in Fig. 7.112 (upper plot), in the computer memory. The sample size, sample chemistry, and amount of cocktail used should be similar to those of the experimental samples.

b. Prepare a blank sample (no radionuclide) plus cocktail in a counting vial to measure background. Count the blank

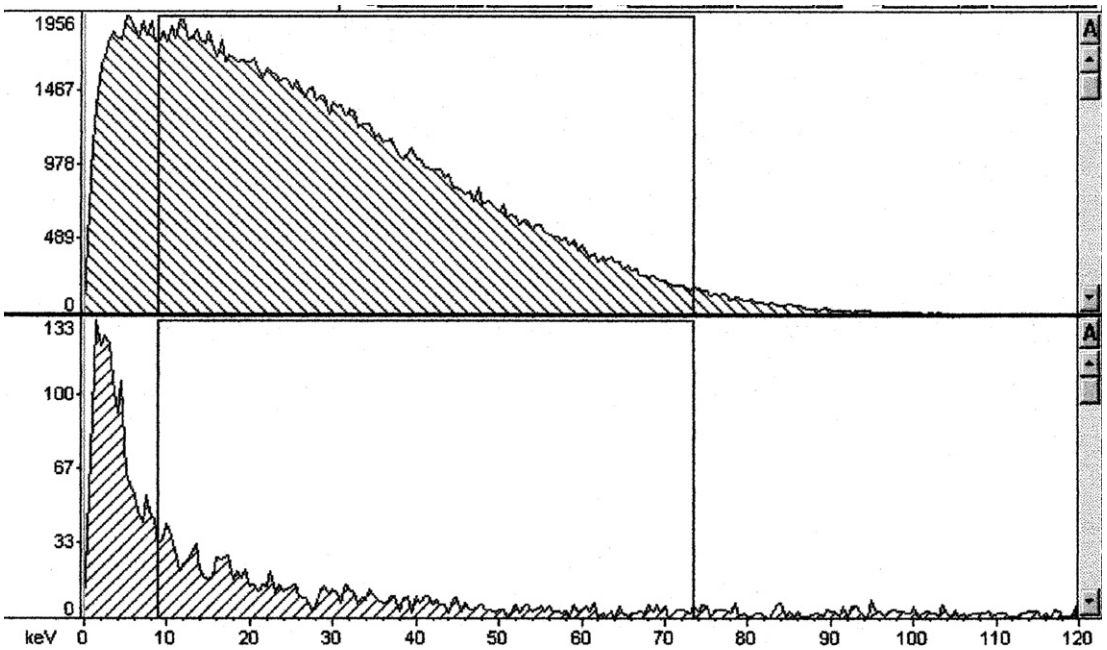

FIGURE 7.112 Pulse-height spectra of a ^{14}C sample (above) and a background or blank sample (below). For this particular sample and blank, chemical composition, sample load, cocktail, and vial type, the LL (left) and UL (right) discriminator settings of 9.0−73.5 were found to provide region optimization. In this example, the reduced counting region produced a sacrifice of 18% in the ^{14}C counting efficiency but a reduction of 54% in the background counts. Region optimization is specific to radionuclide, sample−cocktail chemistry or quench level, and vial type and size. *(L'Annunziata, M.F., 1996, unpublished work)*

sample and store the background spectrum, as illustrated in Fig. 7.112 (lower plot). It is important to prepare the sample and background (blank) counting vials in steps 1 and 2 with the same cocktail and any other chemical components in identical amounts to provide the same chemistry and the same quench levels in both counting vials. For example, if the experimental samples will have a 50% water load (*e.g.*, 10 mL H_2O + 10 mL cocktail), then the blank background vial should be prepared similarly, but without radioisotope. Ideally, the background counting vial should have the same chemical composition and QIP, that is, the same tSIE, SQP(E) or H#, as the sample vial with the exception that the background vial will not contain any added radionuclide.

c. Start with a wide-open counting region defined with the LL discriminator at 0 keV and the UL discriminator at the sample pulse-height spectrum endpoint, and measure the count rates from the sample and background vials in the wide-open counting region. From the count rate data from the sample and background calculate the figure of merit E^2/B.

d. Repeat step 3 by increasing the LL discriminator by suitable increments and calculating the E^2/B after each change of the LL discriminator setting.

e. Decrease the UL discriminator by suitable increments and measure the E^2/B for each setting of the LL discriminator already tested. Record the E^2/B for each of the LL−UL counting regions tested.

f. Select the optimum counting region as that region defined by the LL−UL settings that gave the highest E^2/B.

The above procedure can be carried out using a "Replay" option that is included with many liquid scintillation analyzers. This allows the variation of the LL and UL discriminator settings to obtain new count rates from computer-stored pulse-height spectra without having to recount the sample or background. Also, certain liquid scintillation analyzers are equipped with SpectraWorks™ or similar computer program that will (1) process automatically the sample and background spectra, (2) calculate the optimum LL−UL discriminator settings for a counting region, and (3) provide a value of the E^2/B for that optimum region. SpectraWorks will also calculate the lower limits of detection (LLD) or minimal detectable activity (MDA) for a particular radionuclide, counting efficiency, and background obtained. The LLD or MDA is defined further on in this chapter. For more information on SpectraWorks™, see Floeckher (1995), which is a reference available on-line.

An example of results obtained with region optimization can be taken from the following case:

A sample of ^{14}C and a background blank were prepared similarly in liquid scintillation counting vials with the exception that the background vial had no radionuclide added. For a wide-open counting region of 0−156 keV defined where LL and UL discriminators are calibrated in keV, the instrument gave a 95% counting efficiency for the ^{14}C, a background count rate of 25.0 CPM, and a calculated E^2/B of 361. After region optimization according to the foregoing procedure, an optimum counting region of 18−102 keV was found, which gave a ^{14}C counting efficiency of only 63.1% but a background of 3.38 CPM, and a calculated E^2/B of 1178. Region optimization caused a reduction by more than 30% in the counting efficiency from 95% to 63.1% but an even greater reduction of more than 10-fold in the background. The counting region of 18−102 keV is the optimum counting region for the particular sample and instrument used in this example. Region optimization is

important when sample count rates are low (close to background) and low levels of detection are required.

It is important to emphasize here that an optimum counting region so determined is good only for the particular radionuclide, sample size, vial type, cocktail−sample chemistry (*i.e.*, quench level), and liquid scintillation analyzer used. Therefore, we should keep in mind that when samples vary in quench, the optimized counting regions (window) vary as well. If the quench level between samples varies only slightly, one can widen slightly the optimum counting region to accommodate small changes in spectral shifts.

2. Vial Size and Type

Optimization of performance for the LSC is achieved also by selection of the proper size of vial and vial material (*e.g.*, glass or plastic). The data in Table 7.16 provide ^{3}H counting efficiencies, backgrounds, and figures of merit (E^2/B) for a standard (wide-open) counting region and an optimized counting region for two counting vial types and sizes. The data in this table provide evidence of some well-known generalities that should be considered when optimizing counting performance. First, plastic vials produce a lower background count than the corresponding glass vials. In this example, a 15−30% improvement in performance (E^2/B) was obtained with plastic vials. Second, small vials for low-volume samples provide a lower background with about the same counting efficiency as large vials. Third, the optimized counting region gives a better performance than the standard counting region. From the example taken in Table 7.16 the total performance was enhanced with small plastic vials over large glass vials in an optimized counting region by almost a factor of 3 (E^2/B 103.9−306.0). The only problem with using smaller vials is that the sample capacity is lower, and, if maximum sample size is required, the larger vials should be used.

3. Cocktail Choice

Choosing the proper liquid scintillation fluor cocktail optimizes counting performance. When sample counts are low, it is best to choose a cocktail that can hold as much sample as possible and still provide the maximum counting efficiency with a minimum amount of background. Chapter 8 provides a great deal of information that can be helpful in selecting a cocktail as a function of sample chemical properties to optimize counting performance.

4. Counting Time

The error associated with the measurement of sample counts and count rate is a function of counting time. As demonstrated in Chapter 2, the standard deviation of the counts collected and the calculation of the associated count rate are reduced according to the length of the counting time. This is particularly relevant when the sample counts are very close to background, and accurate measurements of sample counts and background counts must be made to distinguish their difference in magnitude within reasonable error limits. Therefore, liquid scintillation counting performance can be optimized by increasing the sample and background counting times. The longer the counting time, the lower is the detection level or minimal detectable activity (MDA). The MDA also referred to as the lower limits of detection (LLD) in units of Bq/L can be calculated by the following equation from Prichard et al. (1992) as described by Passo and Kessler (1993), Passo and Cook (1994), and Biggen et al. (2002):

$$LLD = \frac{L_D}{60EVTX} \tag{7.151}$$

where LLD is the lowest activity concentration in Bq/L, that yields a net count above background with a 95% probability; the detection limit, L_D , according to Currie (1968) and Hurtgen et al. (2000), is the true net signal, that can be detected with a given probability; 60 is a factor for conversion of DPM to Bq (*i.e.*, 60DPM/1 Bq); E is the fractional detection efficiency (CPM/DPM); V is the sample volume in liters, T is the count time in minutes; and X is any factor that is relevant, such as decay correction or chemical yield. As described by Passo and Cook (1994), when the background and sample are counted as pairs, that is, at the same counting time, and the background counts (B) collected are >70, the detection limit, at a 95% confidence level, may be written as

$$L_D = 4.65\sqrt{B} \tag{7.152}$$

Other working expressions of detection limits (L_D) may be used and these are described by Prichard et al. (1992) and Passo and Cook (1994). When the lower limit of detection (LLD) is

TABLE 7.16 Tritiated Water in Ultima Gold LLT Scintillation Cocktail in Glass and Plastic, Large and Small Vials, Performance Comparison

			Counting region 0−18.6 keV			Counting region 0.5−5.0 keV		
Vial size (mL)	Vial material	Water (%)	Efficiency[a] (%)	Background (CPM)	E^2/B	Efficiency[a] (%)	Background (CPM)	E^2/B
20	Glass	0.5	30.95	16.87	56.8	28.91	8.04	103.9
20	Plastic	0.5	31.71	10.15	99.1	29.31	3.88	221.1
7	Glass	0.5	29.55	12.81	68.1	27.75	5.92	130.1
7	Plastic	0.5	30.10	7.82	115.8	28.10	2.58	306.1

[a] *% Counting efficiency = (CPM/DPM)(100).*

expressed in the less common units of pCi/L, the conversion factor 60 of Eqn 7.151 is replaced with the factor 2.22 for the conversion of DPM to pCi (*i.e.*, 2.22 DPM/pCi).

To illustrate the application and interpretation of calculated lower limits of detection (*LLD*) and detection limits (L_D) let us take the following example to calculate the *LLD* and, from these calculations, determine how many sample counts must be acquired to reach a calculated *LLD*:

If a particular LSA counting region and cocktail chemistry in the analysis of ^{3}H yielded a total of 1300 background counts in a 500-minute counting time, that is, $B = 1300$ and background = 2.60 CPM, the counting efficiency for ^{3}H was 35% or 0.35, and the sample volume analyzed was 10 mL, the lower limit of detection according to Eqn 7.151 would be

$$LLD = \frac{4.65\sqrt{1300\text{ counts}}}{(60\text{ DPM/Bq})(0.35)(0.01\text{L})(500\text{ minutes})} = 1.60\text{Bq/L} \quad (7.153)$$

In the above calculation the limit of detection is

$$L_D = 4.65\sqrt{1300\text{ counts}} = 168\text{ counts} \quad (7.154)$$

Therefore, to achieve the calculated *LLD* of 1.60 Bq/L, a minimum number of sample counts defined by

$$L_D + B = 168 + 1300 = 1468\text{ counts} \quad (7.155)$$

must be registered with a 10-mL sample in a 500-minute counting time to conclude that 1.60 Bq/L are detected with a 95% confidence level.

The denominator of Eqn 7.153 may include additional factors, such as chemical yield, if an extraction of a radionuclide is less than 100% or decay corrections, which is the variable *X* in Eqn 7.151. Detailed treatments of calculations involved in the determination of limits of detection are available from Currie (1968), Prichard et al. (1992), and Passo and Cook (1994). From Eqns 7.151 and 7.152 and the calculation 7.153, we can see that increasing the counting time and reducing the background will reduce the lower limit of detection or minimal detectable activity. This is illustrated by Fig. 7.113 where we can see that, by reducing the background count rate, we can achieve a desired *LLD* with a shorter counting time.

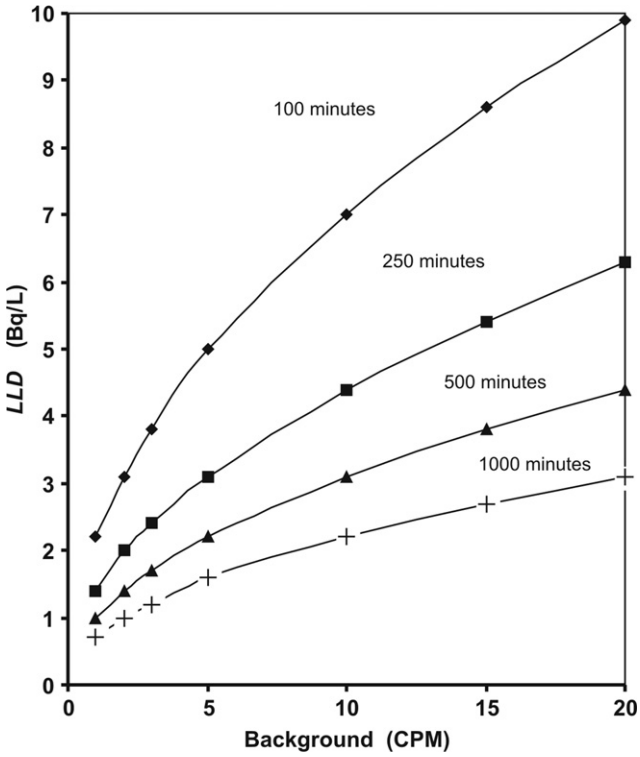

FIGURE 7.113 The calculated *LLD* or *MDA* in Bq/L as a function of sample background in CPM for 4 different sample and background counting times: 100, 250, 500, and 1000 minutes for ^{3}H tritium analysis with a counting efficiency of 35% or 0.35 and sample volume of 10 mL.

5. Background Reduction

Often the easiest method of optimizing LSC performance is to reduce the background. As described previously in this chapter, region optimization, vial size, and vial material are important variables to control in the reduction of background. This section will discuss five other methods that can be used to reduce background and enhance performance for liquid scintillation analysis.

a. Temperature Control
The original purpose of temperature control or cooling during the early years of liquid scintillation counting was to reduce background counts from thermal noise from the PMTs. Modern bialkali photomultiplier tubes are manufactured to have a low noise even at room temperature. The purpose of temperature control in contemporary liquid scintillation counting is to control and maintain the sample temperature, sometimes required for optimizing sample chemistry even at extremes of external temperatures. The sample chemistry in some cocktails requires lower temperature to accept more sample, and, as a result, temperature control is necessary.

b. Underground Counting Laboratory
This method of background reduction can be used for very low level counting and this extreme measure has been taken more often in the past for the measurement of very low levels of naturally occurring radionuclides such as ^{3}H in ground water and ^{14}C dating. This involves building a special counting room below the ground to reduce high-energy cosmic radiation that may cause background counts in the liquid scintillation counter. However, modern pulse discrimination electronics, described briefly in Part d following, will reduce instrument backgrounds to levels at which underground laboratories are generally not needed for the conventional measurement of environmental radioactivity. The placement of detectors deep underground is still utilized for the liquid scintillation measurement of rare events, such as double-beta ($\beta\beta$) decay and the detection and measurement of neutrinos, etc., as described in Sections XI and XII.

c. Shielding
Shielding the instrument from external radiation can reduce background. There are two types of shielding, passive and active shielding.

Passive shielding is the "brute force" approach. This may require lead (up to 1000 kg) barriers to reduce background. The extra lead reduces background from environmental gamma photons associated with building materials and instrument construction materials. In addition, this extra lead can reduce the "soft" cosmic muon components of background. The lead shielding is usually lined internally with cadmium and/or copper to absorb any secondary X-rays and cosmic components.

Active shielding can be one of two types, a guard detector with or without anticoincidence circuitry and components. The guard detector is an external detector [*e.g.*, bismuth germanate (BGO)] that surrounds the area between the PMTs and the sample. The BGO has special properties described in detail in Chapter 16. BGO is a solid crystal scintillator with a high density and high atomic number. The high density and atomic number give BGO excellent "stopping power" for the detection of highly penetrating radiation. BGO can be used to discriminate against gamma and muon components of cosmic background. This property of BGO in combination with time-resolved LSC (TR-LSC™) pulse discrimination electronics (described subsequently) can discriminate more background events.

Another approach to active shielding to reduce background is to manufacture a detector shield above, below, and surrounding the sample vial and PMTs consisting of an external counting chamber of a liquid or solid scintillator, such as mineral oil scintillator, plastic scintillator (*e.g.*, NE110), or even a NaI(Tl) crystal. In addition to the guard material, PMTs and an anti-coincidence circuit are added. The detector guard rejects much of the environmental gamma radiation, as well as soft and hard cosmic radiation.

d. Pulse Discrimination Electronics

Three different pulse discrimination methods are used, namely, pulse shape analysis (PSA), pulse amplitude comparison (PAC), and time-resolved LSC (TR-LSC).

PSA relies on the fact that a true nuclear decay signal produces a very prompt pulse in the LSC, whereas a background event produces a pulse with a longer decay time. By setting up the instrument to discriminate pulses on the basis of their shape, background can be discriminated from a true nuclear decay signal. This discrimination is specific and must be optimized for each vial material, vial size, and sample−cocktail chemistry.

The second method is PAC, which compares the amplitude of the pulse from each of the two PMTs. If the event occurs in the scintillation vial, photons of approximately the same intensity will be seen by both PMTs, but if the event originates from outside the sample, it will produce pulses in each of the PMTs of different pulse heights. If the PAC deviates significantly from unity, the pulse is discriminated as background.

The third method, TR-LSC™, is a patented method of reducing background by discriminating against pulses on the basis of the number of afterpulses that occur following an initial pulse event over a given period of time. These afterpulses are most commonly created by background events. Afterpulses are generally more numerous among nonquenchable background events and less numerous with events originating from the scintillation cocktail. With the TR-LSC technique, the liquid scintillation analyzer can be manufactured or programmed to count afterpulses, known as pulse index discrimination, which can identify background events by counting afterpulses with varying degrees of sensitivity. Therefore, among various liquid scintillation analyzers, the amount of pulse index discrimination for background rejection can be factory set or programmed to provide different sensitivities for the reduction of background (*e.g.*, high-sensitivity count mode, low-level count mode, and ultra-low-level count mode with BGO detector guard). Tables 7.17 and 7.18 illustrate how significantly background can be reduced and performance enhanced using this latter technique of background reduction. The data shown in these two tables might typically be found in a low-level counting laboratory. The samples are placed in the optimum counting geometry, optimum vial size and vial material, optimum cocktail, and counted in the optimum counting region with the TR-LSC method of electronic discrimination at various levels of pulse index discrimination with and without an active guard.

The data of Table 7.17 illustrate that the use of TR-LSC alone and in combination with an active BGO guard detector greatly increases the performance of the LSC for ^{14}C samples. This is also the case for many other radionuclide

TABLE 7.17 Radiocarbon Dating Samples as 3.5 mL Benzene with PPO/POPOP Scintillator[a]

Amount of pulse index discrimination	Detector guard	^{14}C efficiency (%)	Background (CPM)	Figure of merit (E^2/B)
None	No	83.45	9.67	720
Normal TR-LSC	No	81.87	7.07	948
High-sensitivity TR-LSC	No	78.51	4.74	1,300
Low-level TR-LSC	No	70.10	1.38	3,560
Ultra-low-level TR-LSC + BGO Active Guard	Yes	65.01	0.33	12,675

[a]*The optimized counting region is 10–102 keV with various levels of TR-LSC pulse index discrimination applied to the pulse events.*

TABLE 7.18 Environmental Tritium Water Samples as 10 mL Water in 10 mL Ultima Gold LLT Scintillation Cocktail[a]

Amount of Pulse Index Discrimination	Detector Guard	^{3}H efficiency (%)	Background (CPM)	Figure of Merit (E^2/B)
None	No	26.50	18.45	38
Normal TR-LSC	No	26.24	12.75	54
High-sensitivity TR-LSC	No	24.68	9.25	66
Low-level TR-LSC	No	22.59	3.33	153
Ultra-low-level TR-LSC + BGO Active Guard	Yes	20.01	1.00	400

[a]*The optimized counting region is 0.5–5.0 keV with various levels of TR-LSC pulse index discrimination applied to the pulse events.*

samples with low count rates. For the case of ^{14}C about 15–20 times better performance is obtained with the ultra-low-level TR-LSC and the BGO guard detector.

The data of Table 7.18 illustrate that the use of TR-LSC alone and in combination with a BGO active guard detector greatly increases the performance of the LSC for tritium samples in general with low count rates. For the case of tritium about a 10-fold better performance is achieved with the use of ultra-low-level TR-LSC in combination with the BGO guard detector.

For additional information on time-resolved liquid scintillation counting (TR-LSC), see papers by Roessler et al. (1991) and Passo and Roberts (1996).

e. Conclusions

In conclusion, the best ways of optimizing performance of the LSC for low-level samples are to (1) optimize counting geometry, such as optimum sample size, vial size, and vial material; (2) increase counting time; (3) optimize counting region; (4) optimize cocktail selection, and (5) use shielding together with electronic discrimination and an active guard detection method to reduce background.

REFERENCES

Abdrakhmanova, G.R., Blough, B.E., Nesloney, C., Navarro, H.A., Damaj, M.I., Carroll, F.I., 2010. *In vitro* and *in vivo* characterization of a novel negative allosteric modulator of neuronal nAChRs. Neuropharm. 59, 511–517.

Aboudou, B., Bagán, H., Tarancón Sanz, A., Rauret, G., García, J. F. (2011). Plastic scintillation and dryness evaporation: A new procedure for alpha/beta determination in water samples. In "LSC 2010, Advances in Liquid Scintillation Spectrometry". Radiocarbon, University of Arizona, Tucson.

Aburai, T., Takiue, M., Ishikawa, H., 1981. Quantitative measurement method of α-emitters by using liquid scintillation counter connected with multichannel pulse-height analyzer. Radioisotopes 30, 579–583.

Adam, J., et al., For the MEG Collaboration, 2010. A limit for the μ → eγ decay from the MEG experiment. Nucl. Phys. B 834, 1–12.

Agostinelli, S., Allison, J., Amako, K., Apostolakis, J., Araujo, H., Arce, P., et al., 2003. Geant4–a simulation toolkit. Nucl. Instrum. Methods Phys. Res. Sect. A 506, 250–303.

Aizenman, E., McCord, M.C., Saadi, R.A., Hartnett, K.A., He, K., 2010. Complex role of zinc in methamphetamine toxicity in vitro. Neurosci. 171, 31–39.

Akimov, D., Bewick, A., Davidge, D., Dawson, J., Howard, A.S., et al., 2002. Measurements of scintillation efficiency and pulse shape for low energy recoils in liquid xenon. Phys. Lett. B 524, 245–251.

Alamelu, D., Aggarwal, S.K., 2009. Determination of ^{235}U/^{238}U atom ratio in uranium samples using liquid scintillation counting. Talanta 77, 991–994.

Alamelu, D., Bhade, S.P.D., Reddy, P.J., Narayan, K.K., Shah, P.M., Aggarwal, S.K., 2006. Determination of ^{243}Am by pulse shape discrimination liquid scintillation spectrometry. Appl. Radiat. Isot. 64, 579–583.

Aleissa, K.A., Islam, M.S., Alshammari, H. (2006). Measurement of ^{210}Po and ^{210}Pb in groundwater using an alpha liquid scintillation counter. pp 197–209, In "LSC 2005, Advances in Liquid Scintillation Spectrometry". (S. Chatupnik, F. Schönhofer, J. Noakes. (Eds.), Radiocarbon, University of Arizona, Tucson. pp. 449.

Al-Haddad, M.N., Fayoumi, A.H., Abu-Jarad, F.A., 1999. Calibration of a liquid scintillation counter to assess tritium levels in various samples. Nucl. Instrum. Methods Phys. Res. Sect. A 438, 356–361.

Alimonti et al. For the Borexino Collaboration (2002). Science and technology of Borexino: a real-time detector for low energy solar neutrinos. Astropart. Phys. 16, 205–234.

Alimonti et al. for the Borexino Collaboration (2009). The liquid handling systems for the Borexino solar neutrino detector. Nucl. Instrum. Methods Phys. Res. Sect. A 609, 58–78.

Allison, J., Amako., K., Apostolakis, J., Araujo, H., Dubois, P.A., Asai, M., et al., 2006. Geant4 developments and applications. IEEE Trans. Nucl. Sci. 53, 270–278.

Alongi, D.M., Chong, V.C., Dixon, P., Sasekumar, A., Tirendi, F., 2003. The influence of fish cage aquaculture on pelagic carnon flow and water chemistry in tidally dominated mangrove estuaries of peninsular Malaysia. Marine Environ. Res. 55, 313–333.

Altzitzoglou, T., 2004. Analysis of triple-label samples by liquid scintillation spectrometry. Appl. Radiat. Isot. 60, 487–491.

Altzitzoglou, T., 2008. Radioactivity determination of individual radionuclides in a mixture by liquid scintillation spectra deconvolution. Appl. Radiat. Isot. 66, 1055–1061.

Altzitzoglou, T., Larosa, J.L., Nicholl, C., 1998. Measurement of ^{90}Sr in bone ash. Appl. Radiat. Isot. 49 (9–11), 1313–1317.

Altzitzoglou, T., Deneke, B., Johansson, L., Sibbens, G., 2002. Standardization of ^{89}Sr using three different methods. Appl. Radiat. Isot. 56, 447–452.

Amaudruz, P., Bryman, D., Kurchaninov, L., Lu, P., Marshall, C., Martin, J.P., Muennich, A., Retiere, F., Sher, A., 2009. Simultaneous reconstruction of scintillation light and ionization charge produced by 511 keV photons in

liquid xenon: Potential application to PET. Nucl. Instrum. Methods Phys. Res. Sect. A 607, 668–676.

Aprile, E., Doke, T., 2010. Liquid xenon detectors for particle physics and astrophysics. Rev. Mod. Phys. 82 (3), 2053–2097.

Aprile, E., Mukherjee, R., Suzuki, M., 1990. A study of the scintillation light induced in liquid xenon by electrons and alpha particles. IEEE Trans. Nucl. Sci. 37 (2), 553–558.

Aprile, E., Giboni, K.L., Majewski, P., Ni, K., Yamashita, M., Hasty, R., Manzur, A., McKinsey, D.N., 2005. Scintillation response of liquid xenon to low energy nuclear recoils. Phys. Rev. D 72, 072006.

Aprile, E., Cushman, P., Ni, K., Shagin, P., 2006a. Detection of liquid xenon scintillation light with a silicon photomultiplier. Nucl. Instrum. Methods Phys. Res. Sect. A 556, 215–218.

Aprile, E., Dahl, C.E., de Viveiros, L., Gaitskell, R.J., Giboni, K.L., Kwong, J., Majewski, P., Ni, K., Shutt, T., Yamashita, M., 2006. Simultaneous measurement of ionization and scintillation from nuclear recoils in liquid xenon for a dark matter experiment. Phys. Rev. Lett. 97, 081302.

Araki, T. et al. KamLAND Collaboration. (2005). Measurement of neutrino oscillation with KamLAND: evidence of spectral distortion. Phys. Rev. Lett. 94(8), 081801.

Arenillas, P., Cassette, P., 2006. Implementation of the TDCR liquid scintillation method at CNEA-LMR, Argentina. Appl. Radiat. Isot. 64, 1500–1504.

Arisaka, K., Wang, H., Smith, P.F., Cline, D., Teymourian, A., Brown, E., Ooi, W., Aharoni, D., Lam, C.W., Lung, K., Davies, S., Price, M., 2009. XAX: a multi-ton, multi-target detection system for dark matter, double beta decay and pp solar neutrinos. Astropart. Phys. 31, 63–74.

Arneodo, F., Baiboussinov, B., Badertscher, A., Benetti, R., Bernardini, E., et al., 2000. Scintillation efficiency of nuclear recoil in liquid xenon. Nucl. Instrum. Methods Phys. Res. Sect. A 449, 147–157.

Arpesella, C. et al. for the Borexino Collaboration (2008). First real time detection of ^{7}Be solar neutrinos by Borexino. Phys. Lett. B 658, 101–108.

Aspinall, M.D., D'Mellow, B., Mackin, R.O., Joyce, M.J., Jarrah, Z., Peyton, A.J., 2007a. The empirical characterization of organic liquid scintillation detectors by the normalized average of digitized pulse shapes. Nucl. Instrum. Methods Phys. Res. Sect. A 578, 261–266.

Aspinall, M.D., D'Mellow, B., Mackin, R.O., Joyce, M.J., Hawkes, N.P., Thomas, D.J., Jarrah, Z., Peyton, A.J., Nolan, P.J., Boston, A.J., 2007b. Verification of the digital discrimination of neutrons and γ rays using pulse gradient analysis by digital measurement of time of flight. Nucl. Instrum. Methods. Phys. Res. Sect. A 583, 432–438.

Attie, M.R.P., Koskinas, M.F., Dias, M.S., Fonseca, K.A., 1998. Absolute disintegration rate measurements of Ga-67. Appl. Radiat. Isot. 49 (9–11), 1175–1177.

Aupiais, J., 2004a. Deconvolution of alpha liquid scintillation spectra for quantitative analysis of actinide elements in water samples. Radiochim. Acta 92, 125–132.

Aupiais, J., 2004b. Rapid determination of uranium activity and concentration in water by alpha liquid scintillation with α/β discrimination. Anal. Chim. Acta 517, 221–228.

Aupiais, J., 2005. Radium measurement in water samples by α-liquid scintillation counting with α/β discrimination. Anal. Chim. Acta 532, 199–207.

Aupiais, J., Dacheux, N., 2000. Understanding the peak asymmetry in alpha liquid scintillation with β/γ discrimination. Radiochim. Acta 88, 391–398.

Aupiais, J., Fayolle, C., Gilbert, P., Dacheux, N., 1998. Determination of ^{226}Ra in mineral drinking waters by α liquid scintillation with rejection of $\beta-\gamma$ emitters. Anal. Chem. 70, 2353–2359.

Aupiais, J., Dacheux, N., Thomas, A.C., Matton, S., 1999. Studt oif neptunium measurement by alpha liquid scintillation with rejection of β-γ emitters. Anal. Chim. Acta 398, 205–218.

Aupiais, J., Aubert, C., Dacheux, N., 2003. Some rules to improve the energy resolution in alpha liquid scintillation with beta rejection. Radiochim. Acta 91, 63–69.

Baerg, A.P., 1973. The efficiency extrapolation method in coincidence counting. Nucl. Instrum. Methods 112, 143–150.

Bagán, H., Tarancón, A., Rauret, G., García, J.F., 2008. Classical vs. evolved quenching parameters and procedures in scintillation measurements: the importance of ionization quenching. Nucl. Instrum. Methods. Phys. Res. Sect. A 592, 361–368.

Bagán, H., Hartvig, S., Tarancón, A., Rauret, G., García, J.F., 2009. Plastic vs. liquid scintillation for ^{14}C radiotracers determination in high salt matrices. Anal. Chim. Acta 631, 229–236.

Bagán, H., Tarancón, A., Rauret, G., García, J.F., 2010. Alpha/beta pulse shape discrimination in plastic scintillation using commercial scintillation detectors. Anal. Chim. Acta 670, 11–17.

Bagán, H., Tarancón, A., Rauret, G., García, J.F., 2011a. Mixture quantification using PLS in plastic scintillation measurements. Appl. Radiat. Isot. 69, 898–903.

Bagán, H., Tarancón, A., Rauret, G., García, J.F., 2011b. Radiostrontium separation and measurement in a single step using plastic scintillators plus selective extractants. Application to aqueous sample analysis. Anal. Chim. Acta 686 (1–2), 50–56.

Bakhshandeiar, E., Johansson, L., Pearce, A., Keightley, J. (2011). Standardization of ^{64}Cu using two liquid scintillation methods. In "LSC 2010, Advances in Liquid Scintillation Spectrometry". Radiocarbon, University of Arizona, Tucson.

Bakir, Y.Y., Bem, H. (1995). Application of pulse decay discrimination liquid scintillation counting for routing monitoring of radioactivity in drinking water. pp. 293–299, In "Liquid Scintillation Spectrometry 1994". (G.T. Cook, D.D. Harkness, A.B. MacKenzie, B.F. Miller, E.M. Scott. (Eds.) Radiocarbon, University of Arizona, Tucson, pp. 396.

Banerjee, K., Kundu, S., Mukhopadhyay, S., Rana, T.K., Bhattacharya, S., Bhattacharya, C., Banerjee, S.R., Ghosh, T.K., Mukherjee, G., 2007. Characteristics of Gd-loaded liquid scintillators BC521 and BC525. Nucl. Instrum. Methods Phys. Res. Sect. A 580, 1383–1389.

Barabash, A.S., Hubert, Ph., Nachab, A., Umatov, V., 2007. Search for β^{+}EC and ECEC processes in ^{74}Se. Nucl. Phys. A 785 (3–4), 371–380.

Barabash, A.S., Hubert, Ph., Nachab, A., Konovalov, S.I., Vanyushin, I.A., Umatov, V., 2008. Search for β^{+}EC and ECEC processes in ^{112}Sn and $\beta^{-}\ \beta^{-}$decay of ^{124}Sn to the excited states of ^{124}Te. Nucl. Phys. A 807 (3–4), 269–281.

Baró, J., Sempau, J., Fernández-Varea, J.M., Salvat, F., 1995. PENELOPE: an algorithm for Monte Carlo simulation of the penetration and energy loss of electrons and positrons in matter. Nucl. Instrum. Methods Phys. Res. Sect. B 100 (1), 31–46.

Barosi, G., Cazzola, M., Perugini, S., 1980. In: Liquid Scintillation Counting, Recent Applications and Development, Vol. II. Academic Press, New York and London, pp. 517–523.

Basson, J.K., Steyn, J., 1954. Absolute alpha standardization with liquid scintillators. Proc. Phys. Soc. A 67, 297–298.

Batistoni, P., Angelone, M., Carconi, P., Ochiai, K., Schäfer, I., Seidel, K., Verzilov, Y., Zappa, G., Pillon, M., 2005. International comparison of measuring techniques of tritium production for fusion neutronics experiments. Status and preliminary results. Fision Eng. Design 75–79, 911–915.

Batistoni, P., Angelone, M., Bettinali, L., Carconi, P., Fischer, U., Kodeli, I., Leichtle, D., Ochiai, K., Perel, R., Pillon, M., Schäfer, I., Seidel, K., Verzilov, Y., Villari, R., Zappa, G., 2007. Neutronics experiment on a helium cooled pebble bed (HCPB) breeder blanket mock-up. Fision Eng. Design 82, 2095–2104.

Beebe, K.R., Kowalski, B.R., 1987. An introduction to multivariate calibration and analysis. Anal. Chem. 59, 1007A–1017A.

Begin, F., Assaillit, G., Groetz, J.E., 2006. New shapes for liquid scintillation detectors used in neutron spectrometry. Nucl. Instrum. Methods Phys. Res. Sect. A 562, 351–357.

Belanov, S.V., Kashirin, I.A., Malinovskiy, S.V., Egorova, M.E., Efimov, K.M., Tikhomirov, V.A., Sobolev, A. I. (1997). The method of identifying radionuclides with the use of a liquid scintillation counter. RF Patent No. 2, 120, 646.

Belanov, S.V., Kashirin, I.A., Malinovskiy, S.V., Ermakov, A.I., Efimov, K.M., Tikhomirov, V.A., Sobolev, A. I. (1998). The method of identifying radionuclides with the use of a liquid scintillation counter. RF Patent No. 98, 106, 407.

Bell, P.R., 1948. The use of anthracene as a scintillation counter. Phys. Rev. 73 (11), 1405–1406.

Bem, H., Olszewski, M., Kaczmarek, A., 2004. Concentration of selected natural radionuclides in the thermal groundwater of Uniejów, Poland. Nikleonika 49 (1), 1−5.

Benetti, P., Calligarich, E., Dolfini, R., et al., 1993. Detection of energy deposition down to the keV region using liquid xenon scintillation. Nucl. Instrum. Methods Phys. Res. Sect. A 327, 203−206.

Benísek, M., Kubincová, P., Luděk, B., Hilscherová, K., 2011. The effects of PAHs and N-PAHs on retinoid signaling and Oct-4 expression in vitro. Toxicol. Letts. 200, 169−175.

Benitez-Nelson, C.R., Buessler, K.O., 1998. Measurement of cosmogenic ^{32}P and ^{33}P activities in rainwater and seawater. Anal. Chem. 70, 64−72.

Bhade, S.P.D., Reddy, P.J., Narayanan, A., Narayan, K.K., Babu, D.A.R., Sharma, D.N., 2010. Standardization of calibration procedures for quantification of gross alpha and gross beta activities uning liquid scintillation counter. J. Radioanal. Nucl. Chem. 284, 367−375.

Bianchi, D., Cortese, P., Dellacasa, G., Merlano, I., 2005. Determination of the isotope ratio ^{234}U/^{238}U in liquid scintillation and environmental applications. Nucl. Instrm. Methods Phys. Res. Sect. A 553, 543−549.

Bienvenu, P., Cassette, P., Andreoletti, G., Bé, M.-M., Comte, J., Lépy, M.-C., 2007. A new determination of ^{79}Se half-life. Appl. Radiat. Isot. 65, 355−364.

Biggen, C.D., Cook, G.T., MacKenzie, A.B., Pates, J.M., 2002. Time-efficienct method for the determination of ^{210}Pb, ^{210}Bi, and ^{210}Po activities in seawater using liquid scintillation spectrometry. Anal. Chem. 74, 671−677.

Bignell, L.J., Mo, L., Alexiev, D., Hashemi-Nezhad, S.R., 2010a. The effect of multiple γ-ray interactions on ionization quenching corrections in liquid scintillants. Nucl. Instrm. Methods Phys. Res. Sect. A 614, 231−236.

Bignell, L.J., Mo, L., Alexiev, D., Hashemi-Nezhad, S.R., 2010b. Sensitivity and uncertainty analysis of the simulation of ^{123}I and ^{54}Mn gamma and X-ray emissions in a liquid scintillation vial. Appl. Radiat. Isot. 68, 1495−1502.

Birks, J.B., 1964. The Theory and Practice of Scintillation Counting. Pergamon Press, Oxford.

Bobin, C., Bouchard, J., Hamon, C., Iroulart, M.G., Plagnard, J., 2007. Standardization of ^{67}Ga using a 4π(LS) $\beta-\gamma$ anti-coincidence system. Appl. Radiat. Isot. 65, 757−763.

Bonardi, M.L., Birattari, C., Groppi, F., Gini, L., Mainardi, C.H.S., Menapace, E., 2004. Determination of ^{125}I impurities in [^{123}I]labelled radiopharmaceuticals, by liquid scintillation counting: sensitivity of the method. Nucl. Instrum. Methods Phys. Res. Sect. B 213, 348−350.

Borthwick, L.A., Neal, A., Hobson, L., Gerke, V., Robson, L., Muimo, R., 2008. The annexin 2-S100A10 complex and its association with TRPV6 is regulated by cAMP/PKA/CnA in airway and gut epithelia. Cell Calcium 44, 147−157.

Bouchard, J., Cassette, P., 2000. MAC3: and electronic module for the processing of pulses delivered by a three photomultiplier liquid scintillation counting system. Appl. Radiat. Isot. 52, 669−672.

Bradshaw, C., Kumblad, L., Fagrell, A., 2006. The use of tracers to evaluate the importance of bioturbation in remobilising contaminants in Baltic sediments. Estuarine Coastal Shelf Sci. 66, 123−134.

Braizinha, B., Esterline, J.H., Karwowski, H.J., Tornow, W., 2010. Determination of the proton and alpha-particle light-response functions for the KamLAND, BC-501A and BC-517H liquid scintillators. Nucl. Instrum. Methods Phys. Res. Sect. A 623 (3), 1046−1049.

Bransome Jr., E.D., 1973. Liquid scintillation counting in nuclear medicine. Semin. Nucl. Med. 3 (4), 389−399.

Breitholtz, M., Wollenberger, L., 2003. Effects of three PBDEs on development, reproduction and population growth rate of the harpacticoid copepod *Nitocra spinipes*. Aquatic Toxicol. 64, 85−96.

Brillanti, S., et al., 1991. Effect of alpha Interferon therapy on hepatitis C viremia in community-acquired chronic non-A non B hepatitis A quantitative polymerase chain reaction study. J. Med. Virol. 34, 136−141.

Broda, R., 2003. A review of the triple-to-double coincidence ratio (TDCR) method for standardizing radionuclides. Appl. Radiat. Isot. 58, 585−594.

Broda, R., Pochwalski, K. (1993). The ETDCR method of standardizing ^{55}Fe and ^{54}Mn. In"Liquid Scintillation Spectrometry 1992" (J.E. Noakes, F. Schönhofer, H.A. Polach. (Eds.), pp. 255−260. Radiocarbon, University of Arizona, Tucson.

Broda, R., Pochwalski, K., Radoszewski, T., 1988. Calculation of liquid-scintillation detector efficiency. Appl. Radiat. Isot. 39, 159−164.

Broda, R., Péron, M.N., Cassette, P., Terlikowska, T., Hainos, D., 1998. Standardization of ^{139}Ce by the liquid scintillation counting using the triple to double coincidence ratio method. Appl. Radiat. Isot. 49 (9−11), 1035−1040.

Broda, R., Cassette, P., Maletka, K., Pochwalski, K., 2000. A simple computing program for application of the TDCR method to standardization of pure-beta emitters. Appl. Radiat. Isot. 52, 673−678.

Broda, R., Maletka, K., Terlikowska, T., Cassette, P., 2002. Study of the influence of the LS-cocktail composition for the standardization of radionuclides using the TDCR model. Appl. Radiat. Isot. 56, 285−289.

Broda, R., Cassette, P., Kossert, K., 2007. Radionuclide metrology using liquid scintillation counting. Metrologia 44, S36−S52. http://iopscience.iop.org/0026-1394/44/4/S06.

Brooks, F.D., 1993. Developments in neutron detection. In: Vourvopoulos, G., Raradellis, T. (Eds.), "Nuclear Techniques for Analytical and Industrial Applications". Western Kentucky University, Bowling Green, pp. 151−170.

Brooks, F.D., 1997. Neutron detectors and spectrometers. Proc. SPIE 2867, 538−549.

Broser, I., Herforth, L., Kallmann, H., Martius, U., 1948. Über den Elementarprozeβ der Lichtanregung von Leuchtstoffen III. Die Anregung des Naphthalins (Weitere Versuche mit dem Leichtmassenzähler). Zeitschrift f. Naturforsch. 3a, 6−15.

Buchtela, K., Tschurlovits, M., Unfried, E., 1974. Eine Methode zur Unterschiedung von α- und β-Strahlen in einem Flüssigszintillationsmessgerät. Int. J. Appl. Radiat. Isot. 25, 551−555.

Bukowski, T.R., Moffett, T.C., Revkin, J.H., Ploger, J.D., Bassingthwaighte, J.B., 1992. Triple-label β liquid scintillation counting. Anal. Biochem. 204, 171−180.

Caccianiga, B., Giammarchi, M.G., 2000. Neutrinoless double beta decay with Xe-136 in BOREXINO and the BOREXINO counting test facility. Astropart. Phys. 14, 15−31.

Cadieux, J.R., 1990. Evaluation of a photoelectron-rejecting alpha liquid-scintillation (PERALS) spectrometer for the measurement of alpha-emitting radionuclides. Nucl. Instrum. Methods Phys. Res. Sect. A 299, 119−122.

Calhoun, J.M., Coursey, B.M., Gray, D., Karam, L., 1991. The standardization of ^{35}S methionine by liquid scintillation efficiency tracing with ^{3}H. In: Ross, Harley, Noakes, John E., Spaulding, Jim D. (Eds.), "Liquid Scintillation Counting and Organic Scintillators". Lewis Publishers, Chelsea, MI 48118, pp. 317−323.

Campbell, D.B., Vetter, K., Henning, R., Lesko, K., Chan, Y.D., Poon, A.W.P., Perry, M., Hurley, D., Smith, A.R., 2008. Evaluation of radioactive background rejection in ^{76}Ge neutrino-less double-beta decay experiments using a highly segmented HPGe detector. Nucl. Instrum. Methods Phys. Res. Sect. A 587, 60−67.

Capogni, M., De Felice, P., Fazio, A., Simonelli, F., D'Ursi, V., Pecorale, A., Giliberti, C., Abbas, K., 2006. Development of a primary standard for calibration of [^{18}F]FDG activity measurement systems. J. Phys: Conf. Ser. 41, 506−513. http://iopscience.iop.org/1742-6596/41/1/057.

Capogni, M., De Felice, P., Fazio, A., Latini, F., Abbas, K., 2008. Development of a primary standard for calibration of ^{64}Cu activity measurement systems. Appl. Radiat. Isot. 66, 948−953.

Cassette, P., 1992. SPECBETA programme de calcul du spectre en énergie des électrons émis par des radionucléides émetteurs beta. CEA Technical Note (Saclay: CEA/DAMRI/LPRI).

Cassette, P. (2003). Evaluation of the influence of wall effects on the liquid scintillation counting detection effuiciency for the standardization of high energy beta and alpha radionuclides. In "LSC 2001. Advances in Liquid Scintillation Spectrometry". pp. 45−55. (S. Mobius, J.E. Noakes, J.E. Schönhofer. (Eds.). Radiocarbon, University of Arizona, Tucson, pp. 456.

Cassette, P. (2011). TDCR in a nutshell. In "LSC 2010, Advances in Liquid Scintillation Spectrometry". Radiocarbon, University of Arizona, Tucson.

Cassette, P., Vatin, R., 1992. Experimental evaluation of TDCR models for the 3 PM liquid scintillation counter. Nucl. Instrum. Methods Phys. Res. Sect. A 312, 95–99.

Cassette, P., Bouchard, J., 2003. The design of a liquid scintillation counter based on the triple to double coincidence ratio method. Nucl. Instrum. Methods Phys. Res. Sect. A 505, 72–75.

Cassette, P., Altzitzoglou, T., Broda, R., Collé, R., Dryak, P., De Felice, P., Günther, E., Los Arcos, J.M., Ratel, G., Simpson, B., Verregen, F., 1998. Comparison of activity concentration measurement of ^{63}Ni and ^{55}Fe in the framework of the EUROMET 297 project. Appl. Radiat. Isot. 49, 1403–1410.

Cassette, P., Broda, R., Hainos, D., Terlikowska, T., 2000. Analysis of detection-efficiency variation techniques for the implementation of the TDCR method in liquid scintillation counting. Appl. Radiat. Isot. 52, 643–648.

Cassette, P., Bé, M.M., Jaubert, F., Lépy, M.C., 2004. Measurement of a ^{103}Pd solution using the TDCR method by LSC. Appl. Radiat. Isot. 60, 439–445.

Cassette, P., Ahn, G.H., Altzitzoglou, T., Aubineau-Lanièce, I., Bochud, F., García Toraño, E., Grau Carles, A., Grau Malonda, A., Kossert, K., Lee, K.B., Laedermann, J.P., Simpson, B.R.S., Van Wyngaardt, W.M., Zimmerman, B.E., 2006. Comparison of calculated spectra for the interaction of photons in a liquid scintillator. Example of 54Mn 835 keV emission. Appl. Radiat. Isot. 64, 1471–1480.

Cassette, P., Tartes, I., Maguet, F., Plagnard, J., Lépy, M.C., Jaubert, F., 2006. Measurement of photon absorption coefficients of liquid scintillators in the 5- to 12-keV energy range using a monochromatic x-ray source. In: Chałupnik, S., Schönhofer, F., Noakes, J. (Eds.), LSC 2005, Advances in Liquid Scintillation Spectrometry. Radiocarbon, University of Arizona, Tucson, p. 449. 125–133.

Cassette, P., Chartier, F., Isnard, H., Fréchou, C., Laszak, I., Degros, J.P., Bé, M.M., Lépy, M.C., Tartes, I., 2010. Determination of ^{93}Zr decay scheme and half-life. Appl. Radiat. Isot. 68, 122–130.

Castagnet, X., Amabile, J.C., Cazoulat, A., Lecompte, Y., de Carbonnières, H., Laroche, P., 2007. Diagnosis of internal radionuclide contamination by mobile laboratories. Radiat. Prot. Dosim. 125 (1–4), 469–471.

Ceccatelli, A., De Felice, P., 1999. Standardisation of ^{90}Sr, ^{63}Ni and ^{55}Fe by the 4πβ liquid scintillation spectrometry method with 3H-standard efficiency tracing. Appl. Radiat. Isot. 51, 85–92.

Cecil, F.E., Medlet, S.S., 1988. Gamma ray measurements during deuterium and ^{3}He discharges in TFTR. Nucl. Instrum. Methods. Phys. Res. Sect. A 271, 628–635.

Cennini, P., Revol, J.P., Rubbia, C., Sergiampietri, F., Bueno, A., et al., 1999. Detection of scintillation light in coincidence with ionizing tracks in a liquid argon time projection chamber. Nucl. Instrum. Methods. Phys. Res. Sect. A 432, 240–248.

Černý, J., Doležal, Z., Ivanov, M.P., Kuzmin, E.S., Švejda, J., Wilhelm, I., 2004. Study of neutron response and n–γ discrimination by charge comparison method for small liquid scintillation detector. Nucl. Instrum. Methods. Phys. Res. Sect. A 527, 512–518.

Cessna, J.T., 2002. The measurement of activity contained in a ^{32}P stainless-steel stent by destructive assay. Appl. Radiat. Isot. 56, 337–342.

Cessna, J.T., Zimmerman, B.E., 2010. Standardization of radium-223 by liquid scintillation counting. Appl. Radiat. Isot. 68, 1523–1528.

Cessna, J.T., Schultz, M.K., Leslie, T., Bores, N., 2008. Radionuclide calibrator measurements of ^{18}F in a 3 mL plastic syringe. Appl. Radiat. Isot. 66, 988–993.

Chałupnik, S., Mielnikow, A. (2009). Long-term stability of Quantulus LSC counter. pp, 211–218, In "LSC 2008, Advances in Liquid Scintillation Spectrometry". Radiocarbon, University of Arizona, Tucson, pp. 445.

Chandrasekaran, E.S., 1981. Measurement of iodine-125 by liquid scintillation counting method. Health Phys. 40 (6), 896–898.

Chauvenet, B., Bé, M.-M., Amiot, M.-N., Bobin, C., Lépy, M.-C., Branger, T., Laniècе., I., Luca, A., Sahagia, M., Wätjen, A.C., Kossert, K., Ott, O., Nähle, O., et al., 2010. International exercise on ^{124}Sb activity measurements. Appl. Radiat. Isot. 68, 1207–1210.

Chen, M.C., 2005. The SNO liquid scintillator project. Nucl. Phys. B (Proc. Suppl.) 145, 65–68.

Cheng, K.Y., Wong, J.W.C., 2008. Fate of ^{14}C–Pyrene in soil–plant system amended with pig manure compost and Tween 80: a growth chamber study. Bioresource Techn. 99, 8406–8412.

Chobola, R., Mell, P., Daróczi, L., Vincze, A., 2006. Rapid determination of radiostrontium isotopes in samples of NPP origin. J. Radioanal. Nucl. Chem. 267 (2), 297–304.

Chmeleff, J., von Blanckenburg, F., Kossert, K., Jakob, D., 2010. Determination of the ^{10}Be half-life by multicollector ICP-MS and liquid scintillation counting. Nucl. Instrum. Methods Phys. Res. Sect B 268, 192–199.

Clarke, S.D., Flaska, M., Pozzi, S.A., Peerani, P., 2009. Neutron and gamma-ray cross-correlation measurements of plutonium oxide powder. Nucl. Instrum. Methods Phys. Res. Sect A 604, 618–623.

Collé, R., 1997a. Systematic effects of total cocktail mass (volume) and H_2O fraction on 4 $\pi\beta$ liquid scintillation spectrometry of ^{3}H. Appl. Radiat. Isot. 48 (6), 815–831.

Collé, R., 1997b. Cocktail mismatch effects in 4 $\pi\beta$ liquid scintillation spectrometry of ^{3}H: implications based on the systematics of ^{3}H detection efficiency and quench indicating parameter variations with total cocktail mass (volume) and H_2O fraction. Appl. Radiat. Isot. 48 (6), 833–842.

Collé, R., 2009. Radionuclide standardization by primary methods: an overview. J. Radioanal. Nucl. Chem. 280 (2), 265–273.

Collé, R., Laureano-Perez, L. (2009). On the standardization of ^{209}Po and ^{210}Pb. pp. 77–85 In "LSC 2008, Advances in Liquid Scintillation Spectrometry". (J. Eikenberg, M. Jäggi, H. Beer, H. Baehrle. (Eds.), Radiocarbon, University of Arizona, Tucson, pp. 445.

Collé, R., Zimmerman, B.E., Cassette, P., Laureano-Perez, L., 2008. ^{63}Ni, its half-life and standardization: revisited. Appl. Radiat. Isot. 66, 60–68.

Cosolito, F.J., Cohen, N., Petrow, H.G., 1968. Simultaneous determination of iron-55 and stable iron by liquid scintillation counting. Anal. Chem. 40 (1), 213–215.

Coursey, B.M., Mann, W.B., Grau Malonda, A., Garcia-Toraño, E., Los Arcos, J.M., Gibson, J.A.B., Reher, D., 1986. Standardization of carbon-14 by 4$\pi\beta$ liquid scintillation efficiency tracing with hydrogen-3. Appl. Radiat. Isot. 37, 403–408.

Coursey, B.M., Lucas, L.L., Grau Malonda, A., Garcia-Toraño, E., 1989. The standardization of plutonium-241 and nickel-63. Nucl. Instrum. Methods Phys. Res. Sect. A 279, 603–610.

Coursey, B.M., Cessna, J., Garcia-Toraño, E., Golas, D.B., Grau Molanda, A., Gray, D.H., Hoppes, D.D., Los Arcos, J.M., Martin-Casallo, M.T., Schima, F.J., Unterweger, M.P., 1991. The standardization and decay scheme of Rhenium-186. Appl. Radiat. Isot. 42, 865–869.

Coursey, B.M., Calhoun, J.M., Cessna, J., Golas, D.B., Schima, F.J., 1994. Liquid-scintillation counting techniques for the standardization of radionuclides used in therapy. Nucl. Instrum. Methods Phys. Res. Sect. A 339, 26–30.

Coursey, B.M., Schima, F.J., Golas, D.B., Palabrica, O.T., Suzuki, A., Dell, M.A., 1998. Measurement standards for strontium-89 for use in bone palliation. Appl. Radiat. Isot. 49 (4), 335–344.

Cramer, C.F., Nicholson, M., Moore, C., Teng, K., 1971. Computer programs for calculation of liquid scintillation data from long-lived and short-lived radionuclides used in single or dual labeling. Int. J. Appl. Radiat. Isot. 22, 17–20.

Cremonesi, O. (2010). Neutrino masses and neutrinoless double beta decay: Status and exprectations. Presented at the "European Strategy for Future Neutrino Physics" Workshop, CERN, October 1-3, 2009, CERN Report No. arXiv: 1002.1437 9 Feb. 2010.

Cruz, P.A.L., Loureiro, J.S., Bernardes, E.M.O., 2002. Standardization of ^{89}Sr solution from a BIPM intercomparison using a liquid scintillation method. Appl. Radiat. Isot. 56, 457–459.

Currie, L.A., 1968. Limits for qualitative detection and quantitative determination – application to radiochemistry. Anal. Chem. 40, 586–593.

Dacheux, N., Aupiais, J., 1997. Determination of uranium, thorium, plutonium, americium, and curium ultratraces by photon electron rejecting α liquid scintiullation. Anal. Chem. 69, 2275–2282.

Dacheux, N., Aupiais, J., 1998. Determination of low concentrations of americium and curium by photon/electron rejecting alpha liquid scintillation. Anal. Chim. Acta 363, 279–294.

Dacheux, N., Aupiais, J., Courson, O., Aubert, C., 2000. Comparison and improvement of the determinations of actinide low activities using several α liquid scintillation spectrometers. Anal. Chem. 72, 3150−3157.

Da Cruz, P.A.L., Iwahara, A., Bernardes, E.M.O., da Silva, C.J., 2004. The absolute standardization of ^{32}P and ^{204}Tl at LNMRI. Appl. Radiat. Isot. 60, 415−418.

Dahlberg, E., 1982. Quench correction in liquid scintillation counting by a combined internal standard-samples channels ratio technique. Anal Chem. 54 (12), 2082−2085.

Dai, X., Jonkmans, G., Cui, Y., Sur, B., 2011. Gadolinium-loaded liquid scintillator for an anti-neutrino detector. In "LSC 2010, Advances in Liquid Scintillation Spectrometry". Radiocarbon, University of Arizona, Tucson.

Daou, S., El Chemaly, A., Christofilopoulos, P., Bernard, L., Hoffmeyer, P., Demaurex, N., 2011. The potential role of cobalt ions released from metal prosthesis on the inhibition of Hv1 proton channels and the decrease in *Staphyloccocus* epidermidis killing by human neutrophils. Biomat. 32, 1769−1777.

Davies, G.J., Spooner, N.J.C., Davies, J.D., Pyle, G.J., Bucknell, T.J., Squier, G.T.A., Lewin, J.D., Smith, P.F., 1994. The scintillation efficiency for calcium and fluorine recoils in CaF_2 and carbon and fluorine recoils in C_6F_6 for dark matter searches. Phys. Letts. B 322, 159−165.

de Castro Pazos, M., Ricci, R., Simioni, A.R., Lopes, C.C., Tedesco, A.C., Nader, H.B., 2007. Putative role of heparan sulfate proteoglycan expression and shedding on the proliferation and survival of cells after photodynamic therapy. Int. J. Biochem. Cell Biol. 39, 1130−1141.

De Filippis, S., 1991. ^{55}Fe and ^{59}Fe: a qualitative comparison of four methods of liquid scintillation activity analysis. Radioactivity Radiochem. 2, 14R&R−21R&R.

Dern, R.J., Hart, W.L., 1961a. Doubly labeled iron. I. Simultaneous liquid scintillation counting of isotopes ^{55}Fe and ^{59}Fe as ferrous perchlorate. J. Lab. Clin. Med. 57, 322−330.

Dern, R.J., Hart, W.L., 1961b. Doubly labeled iron. II. Separation of iron from blood samples and preparation of ferrous perchlorate for liquid scintillation counting. J. Lab. Clin. Med. 57, 460−467.

DeVol, T.A., Brown, D.D., Leyba, J.D., Fjeld, R.A., 1996. A comparison of four aqueous-miscible liquid scintillation cocktails with an alpha/beta discriminating Wallac 1415 liquid scintillation counter. Health Phys. 70 (1), 41−46.

DeVol, T.A., Theisen, C.D., DiPrete, D.P., 2007. Effect of quench on alpha/beta pulse shape discrimination of liquid scintillation cocktails. Operational Radiat. Safety 92 (Suppl.2), S105−S111.

DeVries, D., Griffin, H., 2008. X- and γ-ray emissions observed in the decay of ^{237}Np and ^{233}Pa. Appl. Radiat. Isot. 66, 668−675.

Dianu, M., Podină, C., 2007. The safety of environment in final disposal of ultima gold scintillation liquid cocktail used for determination of the radioactive content in various samples at Cernavoda nuclear power plant. Rev. Roumaine Chim. 52 (2), 509−519.

Ding, Y., Zhang, Z., Liu, J., Wang, Z., Zhou, P., Zhao, Y., 2008. A new gadolinium-loaded liquid scintillator for reactor neutrino detection. Nucl. Instrum. Methods Phys, Res. Sect. A 584, 238−243.

Diodati, J.M., Sartori, F.M., 2007. ^{239}Np as a tracer of ^{237}Np in effluent samples and low level nuclear waste. J. Radioanal. Nucl. Chem. 272 (1), 11−15.

D'Mellow, B. (2006). "Digital Processing in Neutron Spectrometry". Ph.D. Thesis, Lancaster University.

D'Mellow, B., Aspinall, M.D., Mackin, R.O., Joyce, M.J., Peyton, A.J., 2007. Digital discrimination of neutrons and γ-rays in liquid scintillators using pulse gradient analysis. Nucl. Instrum. Methods Phys, Res. Sect. A 578, 191−197.

Dobbs, H.E., 1965. "Dispersing Solutions for Liquid Scintillation Counting", Memorandum No. AERE-M1574. UK Atomic Energy Research Establishment, Harwell.

Dobrin, R.I., Pavelescu, M., Dulama, C.N., Toma, A.L., 2011. Measurement of multiple labeled samples by beta spectrum unfolding. Romanian J. Phys. 56 (1−2), 93−102.

Dodson, C. L. (1996). Radionuclide identification in liquid scintillation spectrometry. In "Liquid Scintillation Spectrometry 1994" (G.T. Cook, D.D. Harkness, A.B. MacKenzie, B.F. Miller E.M. Scott. (Eds.), Radiocarbon, University of Arizona, Tucson, pp. 361−364.

Doke, T., 1981. Fundamental properties of liquid argon, krypton, and xenon as radiation detector media. Port. Phys. 12 (1−2), 9−48.

Doke, T., Masuda, K., Shibamura, E., 1990. Estimation of absolute photon yields in liquid argon and xenon for relativistic electrons. Nucl Instrum. Methods, Sect. A 291, 617−620.

Doke, T., Kikuchi, J., Nishikido, F., 2006. Time-of-flight positron emission tomography using liquid xenon scintillation. Nucl. Instrum. Methods Phys, Res. Sect. A 569, 863−871.

Eakins, J.D., Brown, D.A., 1966. An improved method for the simultaneous determination of iron-55 and iron-59 in blood by liquid scintillation counting. Int. J. Appl. Radiat. Isot. 17, 391−397.

Eardly, D.F., Carton, M.W., Gallagher, J.M., Patching, J.W., 2001. Bacterial abundance and activity in deep-sea sediments from the eastern North Atlantic. Prog. Oceanogr. 50, 245−259.

Edler, R., 2004. Efficiency Tracing and Direct DPM. PerkinElmer, Germany. http://las.perkinelmer.de/Content/applicationnotes/app_de-efftracingunddirectdpm.pdf, Applikationsnote 13, p. 9.

Effertz, R., Neuman, K., Englert, D., 1993. Single photomultiplier technology for scintillation counting in microplates. In: Noakes, J.E., Schönhofer, F., Polach, H.A. (Eds.), Liquid Scintillation Spectrometry 1992, pp. 37−42. Radiocarbon.

Eikenberg, J., Zumsteg, I., Rüthi, M., Bajo, S., Fern, M.J., Passo, C.J., 1999. Fast radiochemical screening of transuranium radionuclides in urine using actinide extractive resin and low-level α/ β LSC. Radioact. Radiochem. 10, 19−30.

Eikenberg, J., Bajo, S., Rüthi, M., Gann, C., Beer, H., Butterweck, G. (2002). A rapid procedure for determining $^{239+240}$Pu and ^{241}Pu in environmental samples using α/β LSC. pp. 351−362, In "LSC 2001, Advances in Liquid Scintillation Spectrometry". (S. Möbius, J. Noakes, F. Schönhofer. (Eds.), Radiocarbon, University of Arizona, Tucson, pp. 456.

Eikenberg, J., Beer, H., Rüthi, M., Zumsteg, I., Vetter, A. (2006). Precise determination of ^{89}Sr and ^{90}Sr/^{90}Y in various matruces: The LSC 3-window approach. pp. 237−249. In "LSC 2005, Advances in Liquid Scintillation Spectrometry". (S. Chałupnik, F. Schönhofer, J. Noakes. (Eds.), Radiocarbon, The University of Arizona, Tucson, pp. 449.

Eikenberg, J., Jäggi, M., Rüthi, M. (2011). Determination of H-3 and C-14 in the frame of decommissioning projects at the Paul Scherrer Institute. In "LSC 2010, Advances in Liquid Scintillation Spectrometry". (P. Cassetle, Ed.) Radiocarbon, University of Arizona, Tucson.

Ejiri, H., 2010. Double beta decays and neutrino nuclear responses. Progr. Part. Nucl. Phys. 64, 249−257.

Elliott, J.C., 1984. Effect of vial composition and diameter on determination of efficiency, background, and quench curves in liquid scintillation counting. Anal. Chem. 56, 758−761.

Elliot, J.C., van Mourik, B., 1987. A performance comparison of select akylbenzene and detergent based liquid scintillation cocktails. Appl. Radiat. Isot. 38 (8), 629−633.

Elliott, S.R., Hahn, A.A., Moe, M.K., 1986. Experimental investigation of double-beta decay in ^{82}Se. Phys. Rev. Lett. 56, 2582−2585.

Elliott, S.R., Hahn, A.A., Moe, M.K., 1987. Direct evidence for two-neutrino double-beta decay in ^{82}Se. Phys. Rev. Lett. 59, 2020−2023.

Elliott, S.R., Gehman, V.M., Kazkaz, K., Mei, D.-M., Young, A.R., 2006. Pulse shape analysis in segmented detectors as a technique for background reduction in Ge double-beta decay experiments. Nucl. Instrum. Methods Phys, Res. Sect. A 558, 504−510.

El Mrabet, R., Abril, J.M., Manjón, G., Garcí Tenorio, R., 2004. Experimental and modeling study of ^{241}Am uptake by suspended matter in freshwater environment from southern Spain. J. Radioanal. Nucl. Chem. 261 (1), 137−144.

Enqvist, A., Flaska, M., Pozzi, S., 2008. Measurement and simulation of neutron/gamma-ray cross-correlation functions from spontaneous fission. Nucl. Instrum. Methods Phys. Res. Sect. A 595, 426−430.

Enqvist, A., Pázsit, I., 2010. Calculation of the light pulse distributions induced by fast neutrons in organic scintillation detectors. Nucl. Instrum. Methods Phys. Res. Sect. A 618, 266−274.

Enqvist, A., Pozzi, S.A., Flaska, M., Pázsit, I., 2010. Initial evaluation for a combined neutron and gamma ray multiplicity counter. Nucl. Instrum. Methods Phys. Res. Sect. A 621, 493−497.

Ermakov, A.I., Malinovsky, S.V., Kashirin, I.A., Tikhomirov, V.A., Sobolev, A. I. (2006). Rapid analysis of radionuclide composition (screening) of liquid samples via deconvolution of their LS spectra. pp. 89−98. In "LSC 2005.

Advances in Liquid Scintillation Spectrometry". (S. Chałupnik, F. Schönhofer, J. Noakes. (Eds.), RADIOCARBON, The University of Arizona, Tucson, pp. 449.

Everett, L.J., Ring, J.G., Nguyen, D.C., 1980. In: Peng, C.-T., Horrocks, D.L., Alpen, E.L. (Eds.), Liquid Scintillation Counting, Recent Applications and Development. Physical Aspects, Vol. I. Academic Press, New York and London, pp. 119−128.

Feng, X., He, Q., 2009. Simultaneous determination of ^{237}Np, $^{238-240}$Pu and ^{241}Am in HNO_3 solution by combining extraction, liquid scintillation counting, and α spectrometry. Nucl. Instrum. Methods Phys. Res. Sect. A 609, 165−171.

Fiorini, E., 2001. Double beta decay: the future. Nucl.Phys. B (Proc. Suppl.) 91, 262−269.

Fischer, A.C., Kroon, J.J., Verburg, T.G., Teunissen, T., Wolterbeek, H. Th., 2007. On the relevance of iron adsorption to container materials in small-volume experiments on iron marine chemistry: 55Fe-aided assessment of capacity, affinity and kinetics. Marine Chem. 107, 533−546.

Fitzgerald, R., Collé, R., Laureano-Pérez, L., Pibida, L., Hammond, M.M., Nour, S., Zimmerman, B.E., 2010. A new primary standardization of ^{229}Th. Appl. Radiat. Isot. 68, 1303−1308.

Flaska, M., Pozzi, S.A., 2007. Identification of shielded neutron sources with the liquid scintillator BC-501A using a digital pulse shape discrimination method. Nucl. Instrum. Methods Phys. Res. Sect. A 577, 654−663.

Flaska, M., Pozzi, S.A., 2009. Digital pulse shape analysis for the capture-gated liquid scintillator BC-523A. Nucl. Instrum. Methods Phys. Res. Sect. A 599, 221−225.

Flynn, K.F., Glendenin, L.E., 1959. Half-life and beta spectrum of Rb-87. Phys. Rev. 116, 744−748.

Floeckher, J., 1995. SpectraWorks™ for windows spectrum analysis software. Cronical Software Notes SC-003. PerkinElmer, Inc., Waltham, MA, USA. http://las.perkinelmer.com/Content/applicationnotes/app_spectraworkswinspectrumanalysis.pdf, pp. 4.

Fogli, G.L., Lisi, E., Palazzo, A., Rotunno, A.M., 2005. KamLAND neutrino spectra in energy and time:Indications for reactor power variations and constraints on the georeactor. Phys. Lett. B 623, 80−92.

Forte, M. (2011). Gross alpha and beta measurements by LSC in waters: advantages, problems and limitations. In "LSC 2010, Advances in Liquid Scintillation Spectrometry". Radiocarbon, University of Arizona, Tucson (In Press).

Fraser, L., Strzeżek, J., 2007. Is there a relationship between the chromatin status and DNA fragmentation of boar spermatozoa following freezing−thawing. Theriogen. 68, 248−257.

Fujii, H., Takiue, M., 2001. Foggy scintillation counting technique. Appl. Radiat. Isot. 55, 517−520.

Fujii, H., Takiue, M., Ishikawa, H., 1986. Activity determination of disc samples with liquid scintillation efficiency tracing technique. Appl. Radiat. Isot. 37, 1147−1149.

Fujii, H., Matsuno, K., Takiue, M., 1999. Construction of analytical beta ray monitor for liquid waste. Radioisotopes 48, 465−471.

Fujii, H., Matsuno, K., Takiue, M., 2000. Hybrid radioassay of multiple radionuclide mixtures in waste solutions by using liquid and NaI(Tl) scintillation monitors. Health Phys. 79 (3), 294−298.

Funck, E., Nylandstedt Larsen, A., 1983. The influence from low energy x-rays and Auger electrons on $4\pi\ \beta-\gamma$ coincidence measurements of electron-capture-decaying nuclides. Int. J. Appl. Radiat. Isot. 34 (3), 565−569.

Fujii, H., Takiue, M., 1988a. Radioassay of dual-labeled samples by sequential Cherenkov counting and liquid scintillation efficiency tracing technique. Nucl. Instrum. Methods Phys. Res. Sect. A 273, 377−380.

Fujii, H., Takiue, M., 1988b. Radioassay of alpha-and beta-emitters by sequential Cherenkov and liquid scintillation counting. Appl. Radiat. Isot 39, 327−330.

Furuta, E., Yokota, S., Watanabe, Y. (2009). Identification of beta nuclides measured by using plastic scintillator and liquid sciontillation counter. pp. 19−26, In "LSC 2008, Advances in Liquid Scintillation Spectrometry". (J. Eikenberg, M. Jäggi, H. Beer, H. Baehrle. (Eds.), Radiocarbon, University of Arizona, Tucson, pp. 445.

Galán López, M., Martín Sánchez, A., Gómez Escobar, V., 2004. Application of ultra-low level liquid scintillation to the determination of ^{222}Rn in groundwater. J. Radioanal. Nucl. Chem. 261 (3), 631−636.

Gallin-Martel, M.-L., Martin, Ph., Mayet, F., Ballon, J., Barbier, G., Barnoux, C., Berger, J., Bondoux, D., Bourrion, O., Collot, J., et al., 2006. Experimental study of a liquid xenon PET prototype module. Nucl. Instrum. Methods Phys. Res. Sect. A 563, 225−228.

Gallin-Martel, M.-L., Gallin-Martel, L., Grondin, Y., Rossetto, O., Collot, J., Grondin, D., Jan, S., Martin, Ph., Mayet, F., Petit, P., Vezzu, F., 2009. A liquid xenon positron emission tomograph for small animal imaging: first experimental results of a prototype cell. Nucl. Instrum. Methods Phys. Res. Sect. A 599, 275−283.

García, G., Grau Malonda, A., 2002. The influence of stopping power on the ionization quench factor. Appl. Radiat. Isot. 56, 295−300.

García, J.F., Izquierdo-Ridorsa, A., Toribio, M., Rauret, G., 1996. Classical versus multivariate calibration for a beta emitter (^{14}C) activity determination by liquid scintillation counting. Anal. Chim. Acta 331, 33−41.

García-Toraño, E., Grau Malonda, A., 1981. EFFY, a program to calculate the counting efficiency of beta particles in liquid scintillators. Comput. Phys. Commun. 23, 385−391.

García-Toraño, E., Grau Malonda, A., 1985. EFFY2, a new program to compute the counting efficiency of beta particles in liquid scintillators. Comput. Phys. Commun. 36, 307−312.

García-Toraño, E., Grau Malonda, A., 1987. EFYGA, a Monte Carlo program to compute the interaction probability and the counting efficiency of gamma rays in liquid scintillators. Comput. Phys. Commun. 47, 341−347.

García-Toraño, E., Grau Malonda, A., 1988. Cálculo de la eficiencia de recuentro de nucleidos que experimentan desintegración beta y desexcitación gamma simple. Report CIEMAT 616, Madrid.

García-Toraño, E., Grau Malonda, A., Los Arcos, J.M., 1988. EBEGA-the counting efficiency of a beta-gamma emitter in liquid scintillators. Comput. Phys. Commun. 50, 313−319.

García-Toraño, E., Martin Cassallo, M.T., Rodríguez., L., Grau, A., Los Arcos, J.M., 1991. On the standardization of beta-gamma-emitting nuclides by liquid scintillation counting. In: Ross, Harley, Noakes, John E., Spaulding, Jim D. (Eds.), Liquid Scintillation Counting and Organic Scintillators. Lewis Publishers, Chelsea, MI, pp. 307−316.

García-Toraño, E., Roteta, M., Rodríguez Barquero, L., 2000. Standardization of ^{110m}Ag by liquid scintillation and 4 $\pi\beta-\gamma$ coincidence counting. Appl. Radiat. Isot. 52, 637−641.

García-Toraño, E., Rodríguez Barquero, L., Roteta, M., 2002. Standardization of ^{134}Cs by three methods. Appl. Radiat. Isot. 56, 211−214.

Garson, J., Whitby, K., 1994. Nucleic acid quantification by chemiluminescence assay of polymerase chain reaction products. TopCount Topics, TCA-020. PerkinElmer, Inc, Waltham, MA, USA. http://las.perkinelmer.com/Content/applicationnotes/app_topcountnucleicacidquantchemilumin.pdf. pp.4.

Gehman, V.M., Doe, P.J., Robertson, R.G.H., Will, D.I., Ejiri, H., Hazama, R., 2010. Solubility, light output and energy resolution studies of molybdenum-loaded liquid scintillators. Nucl. Instrum. Methods Phys. Res. Sect. A 622, 602−607.

Geladi, P., Kowalski, B.R., 1986. Partial least-squares regression: a tutorial. Anal. Chim. Acta 185, 1−17.

Giboni, K.-L., Aprile, E., Majewski, P., Ni, K., Yamashita, M., 2005. Fast timing measurements of gamma-ray events in liquid xenon. IEEE Trans. Nucl. Sci. 52 (5), 1800−1804.

Gibson, J.A.B., Gale, H.J., 1968. Absolute standardization with liquid scintillation counters. J. Sci. Instrum. 1 (2), 96−106.

Goldstein, G., 1965. Absolute liquid-scintillation counting of beta emitters. Nucleonics 23, 67−69.

Gómez, H., Cebrián, S., Morales, J., Villar, J.A., 2007. Background reduction and sensitivity for germanium double beta decay experiments. Astroparticle Phys. 28, 435−447.

Grahek, Ž, Mačefat, M.R., 2004. Isolation of iron and strontium from liquid samples and determination of ^{55}Fe and ^{89,90}Sr in liquid radioactive waste. Anal. Chim. Acta 511, 339−348.

Grahek, Ž, Mačefat, M.R., 2006. Extraction chromatographic separation of iron from complex liquid samples and the determination of ^{55}Fe. J. Radioanal. Nucl. Chem. 267 (1), 131−137.

Gratta, G., Wang, Y.F., 1999. Towards low-threshold, real-time solar neutrino detectors. Nucl. Instrum. Methods Phys. Res. Sect. A 438, 317–321.

Grau Carles, A., 1993. A new linear spectrum unfolding method applied to radionuclide mixtures in liquid scintillation spectrometry. Appl. Radiat. Isot. 45, 83–90.

Grau Carles, A., 1994. SRLOG, the simultaneous standardization of $^{90}Sr + {}^{90}Y + {}^{89}Sr$ mixtures. Comp. Phys. Commun. 82, 17–22.

Grau Carles, A., 1995. New methods for the determination of β-spectra shapefactor coefficients. Appl. Radiat. Isot. 46, 125–128.

Grau Carles, A., 1996. MLOG, the simultaneous standardization of multi-nuclide mixtures. Comp. Phys. Commun. 93, 48–52.

Grau Carles, A., 2005. Beta shapefactor determinations by the cutoff energy yield method. Nucl. Instrum. Methods Phys. Res. Sect. A 551, 312–322.

Grau Carles, A., 2006a. EMILIA, the LS counting efficiency for electron-capture and capture-gamma emitters. Comp. Phys. Commun. 174 (1), 35–46.

Grau Carles, A., 2006b. Synergic quenching effects of water and carbon tetrachloride in liquid scintillation gel samples. Appl. Radiat. Isot. 64, 1505–1509.

Grau Carles, A., 2008. MICELLE, the micelle size effect on the LS counting efficiency. Comp. Phys. Commun. 176, 305–317.

Grau Carles, A., Grau Malonda, A., 1989. Electron-capture standardization with a triple phototube system. Anales de Física, Ser. B 85, 160–176.

Grau Carles, A., Grau Malonda, A., 1991. A new procedure for multiple isotope analysis in liquid scintillation counting. In: Ross, Harley, Noakes, John E., Spaulding, Jim D. (Eds.), Liquid Scintillation Counting and Organic Scintillators. Lewis Publishers, Chelsea, MI 48118, pp. 295–306.

Grau Carles, A., Grau Malonda, A. (1992). "Precise System for the Determination of the Quench Parameter of Radioactive Samples in Liquid Phase", Patent P. 9202639, December 29, 1992, Registry of Industrial Property, Madrid, Spain.

Grau Carles, A., Grau Malonda, A., 1997. Calibración del ^{40}K por centelleo líquido. Determinación del periodo de semidesintegración. Report CIEMAT 831, Madrid.

Grau Carles, A., Grau Malonda, A., 2001. Free parameter, figure of merit and ionization quench in liquid scintillation counting. Appl. Radiat. Isot. 54, 447–454.

Grau Carles, A., Grau Malonda, A., 2006. Computational aspects in modelling the interaction of low-energy X-rays with liquid scintillators. Appl. Radiat. Isot. 64, 1515–1519.

Grau Carles, A., Grau Malonda, A., 2010. Liquid scintillation high resolution spectral analysis, Informes Técnicos Ciemat 1208, June 2010, pp. 28 (in English). Editorial CIEMAT, Madrid.

Grau Carles, A., Kossert, K., 2006. New advances in the determination of the ^{87}Rb shape factor function. Nucl. Phys. A 767, 248–258.

Grau Carles, A., Kossert, K., 2007. Measurement of the shape-factor functions of the long-lived radionuclides ^{87}Rb, ^{40}K and ^{10}Be. Nucl. Instrum. Methods Phys. Res. Sect. A 572, 760–767.

Grau Carles, A., Kossert, K., 2009. Monte Carlo simulation od Auger-electron spectra. Appl. Radiat. Isot. 67, 192–196.

Grau Carles, A., Martin-Casallo, M.T., Grau Malonda, 1991. Spectrum unfolding and double window methods applied to standardization of ^{14}C and ^{3}H mixtures. Nucl. Instrum. Methods Phys. Res. Sect. A 307, 484–490.

Grau Carles, A., Grau Malonda, A., Rodríguez Barquero, L., 1993a. Cherenkov radiation effects on counting efficiency in extremely quenched liquid scintillation samples. Nucl. Instrum. Methods Phys. Res. Sect. A 334, 471–476.

Grau Carles, A., Rodríguez Barquero, L., Grau Malonda, A., 1993b. Standardization of ^{14}C and ^{35}S mixtures. Nucl. Instrum. Methods Phys. Res. Sect. A 335, 234–240.

Grau Carles, A., Rodríguez Barquero, L., Grau Malonda, A., 1993c. A spectrum unfolding method applied to standardization of ^{3}H and ^{55}Fe mixtures. Appl. Radiat. Isot. 44, 581–586.

Grau Carles, A., Rodríguez Barquero, L., Grau Malonda, A., 1993d. Standardization of multi-nuclide mixtures by a new spectrum unfolding method. J. Radioanal. Nucl. Chem. Letters 176, 391–403.

Grau Carles, A., Rodríguez Barquero, L., Grau Malonda, A., 1993e. Simultaneous standardization of ^{90}Sr–^{90}Y and ^{89}Sr mixtures. Appl. Radiat. Isot. 44, 1003–1010.

Grau Carles, A., Rodríguez Barquero, L., Grau Malonda, A. (1993f). Double-label counting of heterogeneous samples. pp. 239–249, In "Liquid Scintillation Spectrometry 1992" (J.E. Noakes, F. Schönhofer, H.A. Polach. (Eds.), Radiocarbon, University of Arizona, Tucson.

Grau Carles, A., Rodríguez Barquero, L., Grau Malonda, A., 1994a. Deconvolution of $^{204}Tl/^{36}Cl$ and $^{147}Pm/^{45}Ca$ dual mixtures. Nucl. Instrum. Methods Phys. Res. Sect. A 339, 71–77.

Grau Carles, A., Grau Malonda, A., Grau Carles, P., 1994b. EMI, the counting efficiency for electron capture, electron capture-gamma and isomeric transition. Comput. Phys. Commun. 79, 115–123.

Grau Carles, A., Grau Malonda, A., Rodríguez Barquero, L., 1994c. Standardization of ^{125}I, ^{85}Sr and ^{109}Cd by CIEMAT/NIST method. Appl. Radiat. Isot. 45, 461–464.

Grau Carles, A., Grau Malonda, A., Gómez Gil, 1996. Standardization of $U(X_1 + X_2)$: The $^{234}Th + {}^{234m}Pa + {}^{230}Th$ mixture. Nucl. Instrum. Methods Phys. Res. Sect. A 369, 431–436.

Grau Carles, A., Rodriguez Barquero, L., Jimenez De Mingo, A., 1997. ^{125}Sb to ^{125m}Te branching ratio. ICRM '97, 1–12. Biennial Conference, 19–23 May 1997. National Institute of Standards and Technology, Gaithersburg, Maryland, USA.

Grau Carles, A., Rodriguez Barquero, L., Jimenez De Mingo, A., 1998. ^{125}Sb to ^{125m}Te branching ratio. Appl. Radiat. Isot. 49 (9–11), 1377–1381.

Grau Carles, A., Gunther, E., García, G., Grau Malonda, A., 2004. Ionization quenching in LSC. Appl. Radiat. Isot. 60, 447–451.

Grau Carles, A., Gunther, E., Grau Malonda, A., 2006. The photoionization-reduced energy in LSC. Appl. Radiat. Isot. 64, 43–54.

Grau Carles, A., Kossert, K., Grau Malonda, A., 2008. Determination of the shape factor of ^{90}Sr by means of the cutoff energy yield method. Appl. Radiat. Isot. 66, 1021–1025.

Grau Malonda, A. (1982a). Measurement of beta radioactivity by liquid scintillation counting. (in Spanish), Doctoral Thesis No. 171/82. Universidad Complutense de Madrid, Madrid.

Grau Malonda, A., 1982b. Counting efficiency for electron-capturing nuclides in liquid scintillator solutions. Int. J. Appl. Radiat. Isot. 33, 371–375.

Grau Malonda, A., 1995. Modelos de Parámetro Libre en Centelleo Líquido. Editorial. CIEMAT, Madrid, ISBN: 84-7834-287-7, pp. 387.

Grau Malonda, A., 1999. Free Parameter Models in Liquid Scintillation Counting. Editorial. CIEMAT, Madrid, ISBN: 84-7834-350-4, pp. 416.

Grau Malonda, A., Coursey, B.M., 1987. Standardization of isomeric-transition radionuclides by liquid-scintillation efficiency tracing with hydrogen-3: Application to Technetium-99 m. Appl. Radiat. Isot. 38, 695–700.

Grau Malonda, A., Coursey, B.M., 1988. Calculation of beta-particle counting efficiency for liquid-scintillation systems with three phototubes. Appl. Radiat. Isot. 39, 1191–1196.

Grau Malonda, A., Fernández, A., 1985. Cálculo de la eficiencia de detección de nucleidos que se desintegran por captura electrónica y emission gamma. Informe Junta de Energía Nuclear, JEN, 575, Madrid.

Grau Malonda, A., García-Toraño, E., 1978. Espectros beta, I. Espectros simples de negatrons. Informe Junta de Energía Nuclear, JEN, 427, Madrid.

Grau Malonda, A., García-Toraño, E., 1981a. Cálculo de la eficiencia de detección en liquidos centelleadores. I. Nucleidos que se desintegran por emission simple de negatrons. Informe Junta de Energía Nuclear, JEN, 488, Madrid.

Grau Malonda, A., García-Toraño, E., 1981b. Espectros beta, II. Espectros simples de positrons. Informe Junta de Energía Nuclear, JEN, 489, Madrid.

Grau Malonda, A., García-Toraño, E., 1982a. Evaluation of counting efficiency in liquid scintillation counting or pure β-ray emitters. Int. J. Appl. Radiat. Isot. 33, 249–253.

Grau Malonda, A., García-Toraño, E., 1982b. Cálculo de la eficiencia de detección en liquidos centelleadores. II. Nucleidos que se desintegran por emission simple de positrons. Informe Junta de Energía Nuclear, JEN, 518, Madrid.

Grau Malonda, A., Grau Carles, A., 1999. The ionization quench factor in liquid-scintillation counting standardizations. Appl. Radiat. Isot. 51, 183–188.

Grau Malonda, A., Grau Carles, A., 2000. Standardization of electron-capture radionuclides by liquid scintillation counting. Appl. Radiat. Isot. 52, 657−662.

Grau Malonda, A., Grau Carles, A., 2002. Half-life determination of ^{40}K by LSC. Appl. Radiat. Isot. 56, 153−156.

Grau Malonda, A., Grau Carles, A., 2008. The ionization quenching function for coincident electrons. Appl. Radiat. Isot. 66, 1043−1048.

Grau Malonda, A., Los Arcos, J.M., 1983. Un nuevo procedimiento para la Calibración del ^{90}Sr y del ^{90}Y mediante centelleo en fase liquido. Anales de Física B 79, 5−9.

Grau Malonda, A., García-Toraño, E., Los Arcos, J.M., 1985. Liquid-scintillation counting efficiency as a function of the figure of merit for pure beta-particle emitters. Int. J. Appl. Radiat, Isot. 36, 157−158.

Grau Malonda, A., García-Toraño, E., Los Arcos, J.M., 1987. Free parameter codes to compute the counting efficiency in liquid scintillators. Trans. Amer. Nucl. Soc. 55, 55−56.

Grau Malonda, A., Rodriguez Barquero, L., Grau Carles, A., 1994. Radioactivity determination of ^{90}Y, ^{90}Sr and ^{89}Sr mixtures by spectral deconvolution. Nucl. Instrum. Methods Phys. Res. Sect. A 339, 31−37.

Grau Malonda, A., Grau Carles, A., Grau Carles, P., 1994b. EMI, the counting efficiency for electron capture, electron capture-gamma and isomeric transitions. Comput. Phys. Commun. 79, 115−123.

Grau Malonda, A., Grau Carles, A., Grau Carles, P., Galiano Casas, G., 1999. EMI2, the counting efficiency for electron capture by a $KL_1L_2L_3M$ model. Comput. Phys. Commun. 123, 114−122.

Grau Malonda, A., Grau Carles, A., Garcia, G., 2006. Mean values of the LMM Auger transition in a KLM model. Appl. Radiat. Isot. 64, 1485−1491.

Grignon, C., Barbet, J., Bardiès, M., Carlier, T., Chatal, J.F., Couturier, O., Cussonneau, J.P., Faivre, A., Ferrer, L., Girault, S., et al., 2007. Nuclear medical imaging using β^+ γ coincidence from ^{44}Sc radio-nuclide with liquid xenon as detection medium. Nucl. Instrum. Methods Phys. Res. Sect. A 571, 142−145.

Grigorescu, L., 1963. Mesure absolue de l'activité des radionucléides par la méthode des coïncidences beta-gamma. Corrections des coincidences instrumentals et de temps morts. MESUCORA Congress, Paris.

Grigorescu, L., 1973. Accuracy of coincidence measurements. Nucl. Instrum. Methods 112 (1−2), 151−155.

Grigorescu, E.L., Sahagia, M., Razdolescu, A., Luca, A., Radwan, R.M., 1998. Standardization of ^{110m}Ag and ^{75}Se by the beta-efficiency extrapolation method. Appl. Radiat. Isot. 49 (9−11), 1165−1170.

Groppi, F., Mainardi, H.S., Martinotti, A., Morzenti, S., Bonardi, M.L., 2005a. The use of liquid scintillation spectrometry as a very sensitive radio-analytical tool for the determination of alpha, beta and monchromatic electron emitting impurities in radiopharmaceutical compounds. J. Radioanal. Nucl. Chem. 263 (2), 521−525.

Groppi, F., Bonardi, M.L., Birattari, C., Menapace, E., Abbas, K., Holzwarth, U., Alfarano, A., Morzenti, S., Zona, C., Alfassi, Z.B., 2005b. Optimization study of α-cyclotron production of At-211/Po-211 g for high-LET metabolic radiotherapy purposes. Appl. Radiat. Isot. 63, 621−631.

Gudelis, A., Druteikiené, R., Lukšiené, B., Gvozdaité, R., Nielsen, S.P., Hou, X., Mažeika, J., Petrošius, R., 2010. Assessing deposition levels of ^{55}Fe, ^{60}Co and ^{63}Ni in the Ignalina NPP environment. J. Environ. Radioact. 101, 464−467.

Gudjonsson, G., Theodórsson, P., Sigurdsson, K., Kozak, K., Grzadziel, D. (2009). A study of the simple open-vial liquid scintillation method for measurement of radon in air. pp. 361-366. In "LSC 2008. Advances in Liquid Scintillation Spectrometry". (J. Eikenberg, M. Jäggi, H. Beer, H. Baehrle. (Eds.), Radiocarbon, The university of Arizona, Tucson, pp. 445.

Guerrero, C., Cano-Ott, D., Fernández-Ordóñez, M., González-Romero, E., Martínez, T., Villamarín, D., 2008. Analysis of the BC501A neutron detector signals using the true pulse shape. Nucl. Instrum. Methods Phys. Res. Sect. A 597, 212−218.

Günther, E.W., 1994. Standardization of ^{59}Fe and ^{131}I by liquid scintillation counting. Nucl. Instrum. Methods Phys. Res. Sect. A 339, 402−407.

Günther, E. W. (1996). A simple method for transferring the tritium calibration of an LSC system to other radionuclides. pp. 373−379, In "Liquid Scintillation Spectrometry 1994" (G.T. Cook, D.D. Harkness, A.B. MacKenzie, B.F. Miller E.M. Scott. (Eds.), Radiocarbon, University of Arizona, Tucson.

Günther, E., 1998. Standardization of the EC nuclides ^{55}Fe and ^{65}Zn with the CIEMAT/NIST LSC tracer method. Appl. Radiat. Isot. 49 (9−11), 1055−1060.

Günther, E., 2000. Standardization of ^{237}Np by the Ciemat/NIST LSC tracer method. Appl. Radiat. Isot. 52, 471−474.

Günther, E., 2001. Computer program CN2001A. Physikalisch-Technische Bundesanstalt, Braunschweig, Germany.

Günther, E., 2002a. What can we expect from the CIEMAT/NIST method? Appl. Radiat. Isot. 56, 357−360.

Günther, E. (2002b) Determination of the activity of radionuclide sources emitting beta and gamma radiation using the CIEMAT/NIST method. pp. 57-63, In "LSC 2001, Advances in Liquid Scintillation Spectrometry". (S. Möbius, J.E. Noakes, F. Schönhofer. (Eds.), Radiocarbon, The University of Arizona, Tucson, pp. 456.

Günther, E., 2002c. Determination of the ^{32}P activity in angioplastic balloons by LSC. Appl. Radiat. Isot. 56, 291−293.

Günther, E., Schötzig, U., 1992. Activity determination of ^{93m}Nb. Nucl. Instrum. Methods Phys. Res. Sect. A 312, 132−135.

Haaslahti, V. (2010). LSC 2010 − Hidex, Products for Liquid Scintillation Counting. Presented at the International Conference "LSC 2010 Advances in Liquid Scintillation Spectrometry" held at the Cité Internationale Universitaire de Paris, France, 6−10 September 2010.

Hamanaka, S., Shizuma, K., Wen, X., Iwatani, K., Hasai, H., 1998. Radon concentration measurement in water by means of α liquid scintillation spectrometry with a PERALS spectrometer. Nucl. Instrum. Methods Phys. Res. Sect. A 410, 314−318.

Hamel, M., Normand, S., Frelin, A.-M., Simic, V. (2009a). Novel 1,8-naphthamides for fast neutron/gamma discrimination in liquid scintillators. pp. 13-18, In "LSC 2008, Advances in Liquid Scintillation Spectrometry". (J. Eokenberg, M. Jäggi, H. Beer, H. Baehrie. (Eds.), Radiocarbon, University of Arizona, Tucson, pp. 445.

Hamel, M., Frelin-Labalme, A.-M., Simic, V., Normand, S., 2009b. *N*-(2′,2′-di-t-butylphenyl)-4-ethoxy-1,8-naphthalimide: a new fluorophore highly efficient for fast neutrons/gamma-rays discrimination in liquid media. Nucl. Instrum. Methods Phys. Res. Sect. A 602, 425−431.

Happel, S., Letessier, P., Ensinger, W., Eikenberg, J.H., Thakkar, A.H., Horwitz, E.P., 2004. Gross alpha determination in drinking water using a highly specific resin and LSC. Appl. Radiat. Isot. 61, 339−344.

Harms, A.V., Jerome, S.M., 2004. Development of an organically bound tritium standard. Appl. Radiat. Isot. 61, 389−393.

Harvey, J.A., Hill, N.W., 1979. Scintillation detectors for neutron physics research. Nucl. Instrum. Methods 162, 507−529.

Harwood Jr., H.J., 1995. Protein farnesyltransferase: Measurement of enzymatic activity in a 96-well format using TopCount microplate scintillation counting technology. Anal. Biochem. 226, 268−278.

Hawkes, N.P., Gamage, K.A.A., Taylor, G.C., 2010. Digital approaches to field neutron spectrometry. Radiat. Meas. 45, 1305−1308.

Hawkins, B.T., Sykes, D.B., Miller, D.S., 2010. Rapid, reversible modulation of blood−brain barrier P-glycoprotein transport activity by vascular endothelial growth factor. J. Neurosci. 30 (4), 1417−1425.

He, Z.-H., Zhou, R., He, M.-F., Lau, C.B.-S., Yue, G.G.-L., Ge, W., But, P.P.-H., 2011. Anti-angiogenic effect and mechanism of rhein from Rhizoma Rhei. Phytomed. 18 (6), 470−476.

Heffernan, M.J., Zaharoff, D.A., Fallon, J.K., Schlom, J., Greiner, J.W., 2011. In vivo efficacy of a chitosan/IL-12 adjuvant system for protein-based vaccines. Biomat. 32, 926−932.

Heilgeist, M., 2000. Use of extraction chromatography, ion chromatography and liquid scintillation spectrometry for rapid determination of strontium-89 and strontium-90 in food in cases of increased release of radionuclides. J. Radioanal. Nucl. Chem. 245 (2), 249−254.

Heltsley, J.H., Brandon, L., Galonsky, A., Heilbronn, L., Remington, B.A., Vandes Molen, A., Yurkon, J., Kasagi, J., 1988. Nucl. Instrum. Methods Phys. Res. Sect. A 263, 441−445.

Hendee, W.R., Ibbott, G.S., Crisha, K.L., 1972. ^{3}H-toluene, ^{3}H-water and ^{3}H-hexadecane as internal standards for toluene- and dioxane-based liquid scintillation cocktails. Int. J. Appl. Radiat. Isot. 23, 90−95.

Herforth, L. (1948). "Die Fluoreszensanregung organischer Substanzen mit Alphateilchen, schnellen Elektronen und Gammastrahlen." Thesis presented Sept. 13, 1948, Technical University, Berlin-Charlottenburg.

Herforth, L., Kallmann, H., 1948. Die Fluoreszensanregung von festem und flüssigem Naphthalin, Diphenyl und Phenanthren durch Alphateilchen, schnelle Elektronen und Gammastrahlung. Ann. der Physik 6 (4), 231–245.

Hino, Y., Ohgaki, H., 1998. Absolute measurement of ^{192}Ir. Appl. Radiat. Isot. 49 (9–11), 1179–1183.

Hitachi, A., Takahashi, T., Funayama, N., Masuda, K., Kikuchi, J., Doke, T., 1983. Effect of ionization density on the time dependence of luminescence from liquid argon and xenon. Phys. Rev. B 27 (9), 5279–5285.

Hochmuth, K.A., v. Feilitzsch, F., Fields, B.D., Marrodán Undagoitia, T., Oberauer, L., Potzel, W., Raffelt, G.G., Wurm, M., 2007. Probing the Earth's interior with a large-volume liquid scintillator detector. Astropart. Phys. 27, 21–29.

Holst, P.B., Christophersen, C., Engvild, K.C., 2000. In vivo incorporation of radioactive ^{36}Cl, a method for monitoring chloro compounds in biological material. J. Chromat. A 903, 267–270.

Homma, Y., Murakami, Y., 1977. Study on the applicability of the integral counting method for the determination of ^{226}Ra in various sample forms using a liquid scintillation counter. J. Radioanal. Chem. 36, 173–184.

Homma, Y., Murase, Y., Takiue, M., 1987. Determination of ^{222}Rn by air luminescence method. J. Radioanal. Nucl. Chem. Letters 119, 457–465.

Homma, Y., Murase, Y., Handa, K. (1993a). Comparison of a modified integral counting method and efficiency tracing method for the determination of ^{222}Rn by liquid scintillation counting. pp. 59–62, In "Liquid Scintillation Spectrometry 1992" (J.E. Noakes, F. Schönhofer, F. and H.A. Polach. (Eds.), Radiocarbon, University of Arizona, Tucson.

Homma, Y., Murase, Y., Handa, K. (1993b). Determination of atmospheric radioactivity using a membrane filter and liquid scintillation spectrometry. pp. 63–67, In "Liquid Scintillation Spectrometry 1992" (J.E. Noakes, F. Schönhofer, F. H.A. Polach. (Eds.), Radiocarbon, University of Arizona, Tucson.

Homma, Y., Murase, Y., Handa, K., 1994a. The zero detection threshold of a liquid scintillation spectrometer and its application to liquid scintillation counting. Appl. Radiat. Isot. 45, 341–344.

Homma, Y., Murase, Y., Handa, K., 1994b. Absolute liquid scintillation counting of ^{35}S and ^{45}Ca using a modified integral counting method. J. Radioanal. Nucl. Chem. 187, 367–374.

Homma, Y., Murase, Y., Handa, K., 1994c. A modified integral counting method and efficiency tracing method for measuring ^{222}Rn by liquid scintillation counting. Appl. Radiat. Isot. 45, 699–702.

Homma, Y., Murase, Y., Handa, K., Koyama, S., Suzuki, N., Horiuchi, K. (1996). Rapid calibration of detectors for determining ^{222}Rn using air luminescence counting. pp. 111–116, In "Liquid Scintillation Spectrometry 1994" (G.T. Cook, D.D. Harkness, A.B. MacKenzie, B.F. Miller, E.M. Scott. (Eds.), Radiocarbon, University of Arizona, Tucson.

Hong, J., Craig, W.W., Graham, P., Hailey, C.J., Spooner, N.J.C., Tovey, D.R., 2002. The scintillation efficiency of carbon and hydrogen recoils in an organic liquid scintillator for dark matter searches. Astropart. Phys. 16, 333–338.

Hong, K.H., Cho, Y.H., Lee, M.H., Choi, G.S., Lee, C.W., 2001. Simultaneous measurement of ^{89}Sr and ^{90}Sr in aqueous samples by liquid scintillation counting using the spectrum unfolding method. Appl. Radiat. Isot. 54, 299–305.

Horrocks, D.L., 1971. Obtaining the possible maximum of 90 percent efficiency for counting of ^{55}Fe in liquid scintillator solutions. Int. J. Appl. Radiat. Isot. 22, 258–260.

Horrocks, D.L., 1974. Applications of Liquid Scintillation Counting. Academic Press, New York, pp. 340.

Horrocks, D.L., 1976a. The mechanism of the liquid scintillation process. In: Noujaim, A.A., Ediss, C., Wiebe, L.I. (Eds.), Liquid Scintillation Science and Technology. Academic Press, New York and London, pp. 1–16.

Horrocks, D.L., 1976b. Absolute disintegration rate determination of beta-emitting radionuclides by the pulse height shift extrapolation method. In: Noujaim, A.A., Ediss, C., Wiebe, L.I. (Eds.), Liquid Scintillation Science and Technology. Academic Press, New York and London, pp. 185–198.

Horrocks, D.L., 1976c. Measurement of ^{125}I by liquid scintillation methods. Nucl. Instrum. Methods 133, 293–301.

Horrocks, D.L., 1977. The H-Number Concept", Publication No. 1095 NUC-77-IT. Beckman Instruments Inc. Irvine, pp. 26.

Horrocks, D.L., 1978a. A new method of quench monitoring in liquid scintillation counting: the H number concept. In: Crook, M.A., Johnson, P. (Eds.), Liquid Scintillation Counting, Vol. 5. Heyden, London, pp. 145–168.

Horrocks, D.L., 1978b. A new method of quench monitoring in liquid scintillation counting: the H number concept. J. Radioanal. Chem. 43, 489–521.

Horrocks, D.L., 1980. Effect of quench on the pulse height distribution for tritium-containing samples – high quench levels. In: Peng, C.-T., Horrocks, D.L., Alpen, E.L. (Eds.), Liquid Scintillation Counting, Recent Applications and Development, Vol. I. Academic Press, New York and London, pp. 199–210.

Horrocks, D.L., Kolb, A.J., 1981. Instrumental methods for detecting some common problems in liquid scintillation counting. Lab. Pract. 30, 485–487.

Horváth, Á, Ieki, K., Iwata, Y., Kruse, J.J., Seres, Z., Wang, J., Weiner, J., Zecher, P.D., Galonsky, A., 2000. Comparison of two liquid scintillators used for neutron detection. Nucl. Instrum. Methods Phys. Res. Sect. A 440, 241–244.

Horwitz, E.P., Chiarizia, R., Dietz, M.L., 1997. DIPEX: a new extraction chromatographic material for the separation and preconcentration of actinides from aqueous solution. Reactive & Functional Pol. 33, 25–36.

Hou, X., 2005. Rapid analysis of ^{14}C and ^{3}H in graphite and concrete for decommissioning of nuclear reactor. Appl. Radiat. Isot. 62, 871–882.

Hou, X., Frøsig Østergaard, L., Nielsen, S.P., 2005. Determination of ^{63}Ni and ^{55}Fe in nuclear waste samples using radiochemical separation and liquid scintillation counting. Anal. Chim. Acta 535, 297–307.

Houtermans, H., Miguel, M., 1962. 4π- β- γ coincidence counting for the calibration of nuclides with complex decay schemes. Int. J. Appl. Radiat. Isot. 13, 137–142.

Hueber-Becker, F., Nohynek, G.J., Dufour, E.K., Meuling, W.J.A., de Bie, A., Th.H.J., Toutain, H., Bolt, H.M., 2007. Occupational exposure of hairdressers to [^{14}C]- *para*-phenylenediamine-containing oxidative hair dyes: a mass balance study. Fd. Chem. Toxicol. 45, 160–169.

Hughes, K.T., Ireson, J.C., Jones, N.R.A., Kivela, P., 2001. Color quench correction in scintillation proximity assays using Paralux Count Mode, Application Note, pp. 12. PerkinElmer Life Sciences, Boston, MA.

Hui, S.K., Sharma, M., Bhattacharyya, M.H., 2012. Liquid scintillation based quantitative measurement of dual radioisotopes (^{3}H and ^{45}Ca) in biological samples for bone remodeling studies. Appl. Radiat. Isot. 70 (1), 63–68.

Hult, M., Altzitzoglou, T., Denecke, B., Persson, L., Sibbens, G., Reher, D.F.G., 2000. Standardization of ^{204}Tl at IRMM. Appl. Radiat. Isot. 52, 493–498.

Huntington, C.E., Veum, T.L., Morris, J.S., 2008. Zinc uptake in swine intestinal brush border membrane vesicles using a ^{65}Zn/^{69m}Zn duel isotopre experiment. J. Radioanal. Nucl. Chem. 276 (1), 129–134.

Hurtado, S., Villa, M., Manjon, G., Garcia-Tenorio, R. (2009). Monte Carlo simulation of a liquid scintillation counter using GEANT4 code. pp. 155–159. In "LSC 2008, Advances in Liquid Scintillation Spectrometry". (J. Eikenberg, M. Jäggi, H. Beer, H. Baehrle. (Eds.), Radiocarbon, University of Arizona, Tucson, pp. 445.

Hurtgen, C., Jerome, S., Woods, M., 2000. Revisiting Curie – how low can you go? Appl. Radiat. Isot. 53, 45–50.

Hwang, H.-Y., Park, J.H., Park, T.S., Lee, J.M., Cho, Y.H., Byun, J.I., Choi, O., Jun, J.-S., Lee, M.H., Lee, C.W., 2002. Development of MCTS technique for 3-PM liquid scintillation counting. Appl. Radiat. Isot. 56, 307–313.

Hwang, H.-Y., Kwak, S.-I., Lee, H.Y., Lee, J.-M., Lee, K.-B., Park, T.S., 2004. Development of 3-PM liquid scintillation counting system with geometrical efficiency variation. Appl. Radiat. Isot. 60, 469–473.

Hwang, M.J., Kwon, Y.J., Kim, H.J., Kwak, J.W., Kim, S.C., Kim, S.K., Kim, T.Y., Kim, S.Y., Lee, H.S., Lee, J. et al., KIMS Collaboration (2007). Development of tin-loaded liquid scintillator for the double beta decay experiment. Nucl. Instrum. Methods Phys. Res. Sect. A 570, 454–458.

Hwang, M.J., Kwon, Y.J., Kim, H.J., Kwak, J.W., Kim, S.C., Kim, S.K., Kim, T.Y., Kim, S.Y., Lee, H.S., Lee, J. et al., KIMS Collaboration (2009).

A search for $0\nu\beta\beta$ decay of ^{124}Sn with tin-loaded liquid scintillator. Astropart. Phys. 31, 412–416.

Ianni, A., 2011. Neutrino physics with Borexino. Prog. Part. Nucl. Phys. 66, 405–411.

Ianni, A., Montanino, D., Villante, F.L., 2005. How to observe ^{8}B solar neutrinos in liquid scintillator detectors. Phys. Lett. B 627, 38–48.

Ishikawa, H., Takiue, M., 1973. Liquid scintillation measurement for β-ray emitters followed by γ-rays. Nucl. Instrum. Methods 112, 437–442.

Ishikawa, H., Takiue, M., Aburai, T., 1984. Radioassay by an efficiency tracing technique using a liquid scintillation counter. Int. J. Appl. Radiat. Isot. 35, 463–466.

Ishimori, K., Kameo, Y., Matsue, H., Ohki, Y., Nakashima, M., Takahashi, K., 2010. Carbon-14 analysis in solidified product of non-metallic solid waste by a combination of alkaline fusion and gaseous CO_2 trapping. Appl. Radiat. Isot. 69 (2), 506–510.

Itaya, M., Inagaki, T., Iwata, T., Lim, G.Y., Oishi, H., Okuno, H., Tajima, Y., Yoshida, H.Y., Yoshimura, Y., 2004. Development of a new photomultiplier tube with high sensitivity for a wavelength-shifter fiber readout. Nucl. Instrum. Methods Phys. Res. Sect. A 522, 477–486.

Ivan, C., Cassette, P., Sahagia, M., 2008. A new TDCR-LS counter using channel photomultiplier tubes. Appl. Radiat. Isot. 66, 1006–1011.

Ivan, C., Wätjen, A.C., Cassette, P., Sahagia, M., Antohe, A., Grigorescu, E.L., 2010. Participation in the CCRI(II)-K2.H-3 comparison and study of the new TDCR-LS counter with 6 CPMs. Appl. Radiat. Isot. 68, 1543–1545.

Iwamoto, T., 2010. System overview of liquid xenon calorimeter for the MEG experiment. Nucl. Instrum. Methods Phys. Res. Sect. A 617, 92–95.

Jastaniah, S.D., Sellin, P.J., 2004. Digitial techniques for n/γ pulse shape discrimination and capture-gated neutron spectroscopy using liquid scintillators. Nucl. Instrum. Methods Phys. Res. Sect. A 517, 202–210.

Jaubert, F., 2008. Standardization of a ^{186}Re sodium perrhenate radiochemical solution using the TDCR method in liquid scintillation counting. Appl. Radiat. Isot. 66, 960–964.

Jaubert, F., Cassette, P., 2004. Standardization of a ^{32}P solution containing pure-beta impurities using the TDCR method in liquid scintillation counting. Appl. Radiat. Isot. 60, 601–606.

Jaubert, F., Tartès, I., Cassette, P., 2006. Quality control of liquid scintillation counters. Appl. Radiat. Isot. 64, 1163–1170.

Johansson, L.C., Sephton, J.P., 2010. Validation of a new TDCR system at NPL. Appl. Radiat. Isot. 68, 1537–1539.

Johansson, L., Sibbens, G., Altzitzoglou, T., Denecke, B., 2002. Self-absorption correction in standardization of ^{204}Tl. Appl. Radiat. Isot. 56, 199–203.

Johansson, L., Altzitzoglou, T., Sibbens, G., Pommé, S., Denecke, B., 2003. Standardization of ^{238}Pu using four methods of measurement. Nucl. Instrum. Methods Phys. Res. Sect. A 505, 699–706.

Johansson, L.C., Harms, A.V., Keightley, J.D., Pearce, A.K., Woods, D.H., Woods, M.J., 2004. Primary standardization of ^{204}Tl using the efficiency tracing method. Appl. Radiat. Isot. 60, 347–351.

Jónsson, G., Theodórsson, P., Sigurdsson, K. (2006). Auto-radon: A new automatic liquid scintillation system for monitoring radon in water and air. pp. 119-123. In "LSC 2005. Advances in Liquid Scintillation Spectrometry". (S. Chałupnik, F. Schönhofer, J. Noakes. (Eds.), Radiocarbon, The University of Arizona, Tucson, pp. 449.

Jordan, W.C., Spiehler, V., Haendiges, R., Helman, E.Z., 1974. Evaluation of alternative counting methods for radioimmunoassay of hepatitis-associated antigen (HB Ag). Clin. Chem. 20 (7), 733–737.

Jörg, G., Bühnemann, R., Hollas, S., Kivel, N., Kossert, K., Van Winckel, S., Lierse v. Gostomski, C., 2010. Preparation of radiochemically pure ^{79}Se and highly precise determination of its half-life. Appl. Radiat. Isot. 68, 2339–2351.

Kaihola, L., 2000. Radionuclide identification in liquid scintillation alpha-spectroscopy. J. Radioanal. Nucl. Chem. 243 (2), 313–317.

Kallmann, H., 1950. Scintillation counting with solutions. Phys. Rev. 78 (5), 621–622.

Kaneko, S., et al., 1992. Quantification of hepatitis C RNA by competitive polymerase chain reaction. J. Med. Virol. 37, 278–282.

Kashirin, I.A., Ermakov, A.I., Malinovsky, S.V., Belanov, S.V., Sapozhnikov, Yu., A., Efimov, K.M., Tikhomirov, V.A., Sobolev, A.I., 2000. Liquid scintillation determination of low level components in complex mixtures of radionuclides. Appl. Radiat. Isot. 53, 303–308.

Kashirin, I.A., Ermakov, A.I., Malinovsky, S.V., Efimov, K.M., Tikhomirov, V.A., Sobolev, A. I. (2003). LSC: from routine counter to the real spectrometer. pp. 174–184. In "Environmental Radiochemical Analysis II". (P. Warwick, Ed.), Royal society of Chemistry, Cambridge, pp. 420.

Kastens, L.W., Cahn, S.B., Manzur, A., McKinsey, D.N., 2009. Calibration of a liquid xenon detector with ^{83}Kr^{m}. Phys. Rev. C 80 (4), 045809.

Publ. No. 169–3052Kessler, M.J. (Ed.), Liquid Scintillation Analysis, Science and Technology. PerkinElmer Life and Analytical Sciences, Boston.

Kessler, M.J., 1991a. Applications of quench monitoring using transformed external standard spectrum (tSIE). In: Ross, Harley, Noakes, John E., Spaulding, Jim D. (Eds.), Liquid Scintillation Counting and Organic Scintillators. Lewis Publishers, Chelsea, MI 48118, pp. 343–364.

Kessler, M.J., 1991b. Absolute activity liquid scintillation counting: an attractive alternative to quench-corrected DPM for higher energy isotopes. In: Ross, Harley, Noakes, John E., Spaulding, Jim D. (Eds.), Liquid Scintillation Counting and Organic Scintillators. Lewis Publishers, Chelsea, MI 48118, pp. 647–653.

Kharitonov, I., Shilnikova, T., Haaslahti, J. (2011). Uncertainty of a result of tritium activity measurement carried out with counter SL-300 at simplified and conventional processing of measurement results. In "LSC 2010, Advances in Liquid Scintillation Spectrometry". Radiocarbon, University of Arizona, Tucson.

Khayatzadeh Mahani, M., Chaloosi, M., Khanchi, A.R., Ghannadi Maragheh, M., Salimi, B., Asgharizadeh, F., 2008. A new method for simultaneous determination of ^{226}Ra and uranium in aqueous samples by liquid scintillation using chemometrics. J. Radioanal. Nucl. Chem. 275 (2), 427–432.

Khayatzadeh Mahani, M., Khanchi, A.R., Ghannadi Maragheh, M., Chaloosi, M., Salimi, B., Asgharizadeh, F. (2009). Application of chemometrics for simultaneous determination of thorium and uranium in aqueous samples by liquid scintillation. pp. 203–210. In "LSC 2008. Advances in Liquid Scintillation Spectrometry". (J. Eikenberg, M. Jäggi, H. Beer, H. Baehrle. (Eds.), Radiocarbon, University of Arizona, Tucson, pp. 445.

Kilander, M.B.C., Dijksterhuis, J.P., Sri Ganji, R., Bryja, V., Schulte, G., 2011. WNT-5A stimulates the GDP/GTP exchange at pertussis toxin-sensitive heterotrimeric G proteins. Cell. Sign. 23, 550–554.

Kim, C.-K., Martin, P., Fajgelj, A., 2008. Quantification of measurement uncertainty in the sequential determination of ^{210}Pb and ^{210}Po by liquid scintillation counting and alpha-particle spectrometry. Accred. Qual. Assur. 13, 691–702.

Kim, C.K., Al-Hamwi, A., Törvényi, A., Kis-Benedek, G., Sansone, U., 2009. Validation of rapid methods for the determination of radiostrontium in milk. Appl. Radiat. Isot. 67, 786–793.

Kim, Y.J., Kim, C.S., Kang, S.H., Row, J.W., Lee, D.M., Kim, C. K. (2006). Determination of 129I using liquid scintillation counting. In "LSC 2005. Advances in Liquid Scintillation Spectrometry." pp. 273–276. (S. Chałupnik, F. Schönhofer, J. Noakes. (Eds.). Radiocarbon, University of Arizona, Tucson, pp. 449.

Kits, J., Látalová, M., Látal, F., Zich, O., 1985. Determination of the activity of ^{125}I by liquid scintillation measurement. Int. J. Appl. Radiat. Isot. 36, 320.

Klapdor-Kleingrothaus, H.V., 2006. Lessons after the evidence for $0\nu\beta\beta$ decay. Phys. Scr. T 127, 40.

Klapdor-Kleingrothaus, H.V., Krivosheina, I.V., 2006. The evidence for the observation of $0\nu\beta\beta$ decay: the identification of $0\nu\beta\beta$ events from the full spectra. Mod. Phys. Letts. A 21 (20), 1547–1566.

Klapdor-Kleingrothaus, H.V., Krivosheina, I.V., Dietz, A., Chkvorets, O., 2004. Search for neutrinoless double beta decay with enriched ^{76}Ge in Gran Sasso 1990–2003. Phys. Letts. B 586, 198–212.

Klein, H., Neumann, S., 2002. Neutron and photon spectrometry with liquid scintillation detectors in mixed fields. Nucl. Instrum. Methods Phys. Res. Sect. A 476, 132–142.

Kleinschmidt, R.I., 2004. Gross alpha and beta activity analysis in water—a routine laboratory method using liquid scintillation analysis. Appl. Radiat. Isot. 61, 333–338.

Kobayashi, Y., Maudsley, D.V., 1970. Practical aspects of double isotope counting. In: Bransome Jr., E.D. (Ed.), Current Status of Liquid Scintillation Counting. Grune and Stratton, New York, pp. 76–78.

Kobbe, D., Focke, M., Puchta, H. (2009). Purification and characterization of RecQ heliocases of plants. pp 195-209, In "Heliocases, Methods and protocols". (M.M. Abdelhaleem, Ed.), Humana Press, pp. 404.

Kolarov, V., Le Gallic, Y., Vatin, R., 1970. Mesure absolue directe de l'activité des emetteurs β purs par scintillation liquide. Int. J. Appl. Radiat. Isot. 21, 443−452.

Kolhinen, V.S., Elomaa, V.-V., Eronen, T., Hakala, J., Jokinen, A., Kortelainen, M., Suhonen, J., Äystö, J., 2010. Accurate Q value for the ^{74}Se double-electron-capture decay. Phys. Letters B 684 (Issue 1), 17−21.

Kornilov, N.V., Fabry, I., Oberstedt, S., Hambsch, F.-J., 2009. Total characterization of neutron detectors with a ^{252}Cf source and a new light output determination. Nucl. Instrum. Methods Phys. Res. Sect. A 599, 226−233.

Kossert, K., 2003. Half-life measurements of ^{87}Rb by liquid scintillation counting. Appl. Radiat. Isot. 59, 377−382.

Kossert, K., 2006. A new method for secondary standard measurements with the aid of liquid scintillation counting. Appl. Radiat. Isot. 64, 1459−1464.

Kossert, K., Grau Carles, A., 2010. Improved method for the calculation of the counting efficiency of electron-capture nuclides in liquid scintillation samples. Appl. Radiat. Isot. 68 (7−8), 1482−1488.

Kossert, K., Grau Carles, A., 2008. Study of a Monte Carlo rearrangement model for the activity of electron-capture nuclides by means of liquid scintillation counting. Appl. Radiat. Isot. 66, 998−1005.

Kossert, K., Grau Carles, A., 2006. The LSC efficiency for low-*Z* electron-capture nuclides. Appl. Radiat. Isot. 64, 1446−1453.

Kossert, K., Schrader, H., 2004. Activity standardization by liquid scintillation counting and half-life measurements of ^{90}Y. Appl. Radiat. Isot. 60, 741−749.

Kossert, K., Janβen, H., Klein, R., Schneider, M., ans Schrader, H., 2006. Standardization and nuclear decay data of ^{65}Zn. Appl. Radiat. Isot. 64, 1420−1424.

Kossert, K., Jörg, G., Lierse von Gostomski, Ch., 2009. Activity standardization of ^{41}Ca by means of liquid scintillation counting. Radiochim. Acta 97, 1−8.

Kossert, K., Jörg, G., Nähle, O., Lierse v. Gostomski, C., 2009. High-precision measurement of the half-life of ^{147}Sm. Appl. Radiat. Isot. 67, 1702−1706.

Kossert, K., Nähle, Grau Carles, A. (2011a). Beta shape-factor function and activity determination of ^{241}Pu. In "LSC 2010, Advances in Liquid Scintillation Spectrometry". Radiocarbon, University of Arizona, Tucson.

Kossert, K., Nähle, O., Warwick, P.E., Wershofen, H., Croudace, I.W., 2011b. Activity determination and nuclear decay data of ^{113m}Cd. Appl. Radiat. Isot. 69, 500−505.

Kouru, H. (1991). A new quench curve fitting procedure: fine tuning of a spectrum library. pp. 247−255, In "Liquid Scintillation Counting and Organic Scintillators" (Harley Ross, John E. Noakes, Jim D. Spaulding. (Eds.), Lewis Publishers, Chelsea, MI 48118.

Kouru, H., Rundt, K. (1991). Multilabel counting using digital overlay technique. pp. 239−246, In "Liquid Scintillation Counting and Organic Scintillators" (H, Ross, J.E. Noakes, J.D. Spaulding. (Eds.), Lewis Publishers, Chelsea, MI 48118.

Krajcar Bronić, I., Horvatinčić, N., Barešić, J., Obelić, B., 2009. Measurement of ^{14}C activity by liquid scintillation counting. Appl. Radiat. Isot. 67, 800−804.

Kraus, C., for the SNO+ Collaboration. (2006). SNO with liquid scintillator: SNO+. Progr. Part. Nucl. Phys. 57, 150−152.

Kraus, C., Peeters, S.J.M., 2010. The rich neutrino programme of the SNO+ experiment. Progr. Part. Nucl. Phys. 64, 273−277.

Kubota, S., Nakamoto, A., Takahashi, T., Hamada, T., Shibamura, E., Miyajima, M., Masuda, K., Doke, T., 1978a. Recombination luminescence in liquid argon and in liquid xenon. Phys. Rev. B 17 (6), 2762−2765.

Kubota, S., Hishida, M., Ruan, J.-Z., 1978b. Evidence for a triplet state of the self-trapped excitation states in liquid argon, krypton and xenon. J. Phys. C 11, 2645−2651.

Kubota, S., Hishida, M., Suzuki, M., Ruan, J.-Z., 1979. Dynamical behavior of free electrons in the recombination process in liquid argon, krypton, and xenon. Phys. Rev. B 20 (8), 3486−3496.

Kumblad, L., Bradshaw, C., Gilek, M., 2005. Bioaccumulation of ^{51}Cr, ^{63}Ni and ^{14}C in Baltic Sea benthos. Environ. Poll. 134, 45−56.

Lachenmaier, T., von Feilitzsch, F., Göger-Neff, M., Lewkea, T., Marrodán Undagoitia, T., Meindl, Q., Möllenberg, R., Oberauer, L., Peltoniemi, J., Potzel, W., Tippmanna, M., Winter, J., Wurm, M., 2010. Physics with the large liquid-scintillator detector LENA. Prog. Part. Nucl. Phys. 64, 381−383.

Laney, B.H., 1976. External standard method of quench correction: advanced techniques. In: Noujaim, A.A., Ediss, C., Wiebe, L.I. (Eds.), Liquid Scintillation Science and Technology. Academic Press, New York and London, pp. 135−152.

Laney, B.H., 1977. Two-parameter pulse height analysis in liquid scintillation. In: Crook, M.A., Johnson, P. (Eds.), Liquid Scintillation Counting, Vol. 4. Heyden, London, pp. 74−84.

L'Annunziata, M.F., 1971. Birth of an unique parent-daughter relation: secular equilibrium. J. Chem. Educ. 48, 700−703.

L'Annunziata, M.F., 1979. Radiotracers in Agricultural Chemistry. Academic Press, London, pp. 536.

L'Annunziata, M.F., 1984a. The detection and measurement of radionuclides. In: L'Annunziata, M.F., Legg, J.O. (Eds.), Isotopes and Radiation in Agricultural Sciences, Vol 1. Academic Press, London, pp. 141−231.

L'Annunziata, M.F., 1984b. Agricultural biochemistry: reaction mechanisms and pathways in biosynthesis. In: L'Annunziata, M.F., Legg, J.O. (Eds.), Isotopes and Radiation in Agricultural Sciences, Vol 2. Academic Press, London, pp. 105−182.

L'Annunziata, M.F., 1987. Radionuclide Tracers, Their Detection and Measurement. Academic Press, San Diego, pp. 505.

L'Annunziata, M.F., 1997a. Efficiency tracing DPM (ET-DPM) and Direct-DPM − Instrument performance data. Tri-Carb LSC Application Note. Packard BioScience Co., Meriden, CT, pp. 8.

L'Annunziata, M.F., 1997b. Comparison of conventional and full spectrum DPM (FS-DPM) analysis of ^{33}P−^{32}P double labels − Instrument performance data. Tri-Carb LSC Application Note. PerkinElmer Inc. http://las.perkinelmer.com/Content/applicationnotes/app_tricarbconventnlfsdpm.pdf, pp. 6. Available via.

L'Annunziata, M.F., 2007. Radioactivity: Introduction and History. Elsevier, Amsterdam and Boston, pp. 609.

Lara-Robustillo, E., Rodríguez Alcalá, M. (2006). Simultaneous determination of alpha and beta emitters by liquid scintillation counting. pp. 41−49, In "LSC 2005, Advances in Liquid Scintillation Spectrometry". (S. Chałupnik, F. Schönhofer, J. Noakes. (Eds.) Radiocarbon, University of Arizona, Tucson, pp. 449.

Larsson, J., Wingårdh, K., Berggård, T., Davies, J.R., Lögdberg, L., Strand, S.-E., Åkerström, B., 2001. Distribution of iodine-125-labeled α1-microglobulin in rats after intravenous injection. J. Lab. Clin. Med. 137 (3), 165−175.

Laureano-Perez, L., Collé, R., Fitzgerald, R., Outola, I., Pibida, L., 2007. A liquid-scintillation-based primary standardization of ^{210}Pb. Appl. Radiat. Isot. 65, 1368−1380.

Laureano-Perez, L., Collé, R., Fitzgerald, R., Zimmerman, B.E., Cumberland, L., 2010. Investigation into the standardization of ^{99}Tc. Appl. Radiat. Isot. 68, 1489−1494.

Lavagno, A., Gervino, G., Marino, C., 2010. High efficiency large volume multiparametric neutron detector. Nucl. Instrum. Methods Phys. Res. Sect. A 617, 492−494.

Lazare, L., Crestey, C., Bleistein, C., 2009. Measurement of ^{90}Sr in primary coolant of pressurized water reactor. J. Radioanal. Nucl. Chem. 279 (2), 633−638.

Lee, K.B., Lee, J.M., Park, T.S., 2004. Implementation of CIEMAT/NIST LSC efficiency tracing method in KRISS: ^{204}Tl standardization. Appl. Radiat. Isot. 60, 893−897.

Lee, K.B., Lee, J.M., Park, T.S., Hwang, H.Y., 2004. Implementation of TDCR method in KRISS. Nucl. Instrum. Methods Phys. Res. Sect. A 534, 496−502.

Lee, M.H., Chung, K.H., Lee, C. W. (2002a). Sequential radiochemical separation of ^{90}Sr and ^{99}Tc in aqueous samples and measurement by liquid scintillation counting. pp. 397−403. In "LSC 2001. Advances in Liquid Scintillation Spectrometry". (S. Möbius, J.E. Noakes, F. Schönhofer. (Eds.), Radiocarbon, University of Arizona, Tucson, pp. 456.

Lee, M.H., Chung, K.H., Choi, G.K., Lee, C.W., 2002b. Measurement of ^{90}Sr in aqueous samples using liquid scintillation counting with full spectrum DPM method. Appl. Radiat. Isot. 57 (2), 257−263.

Leonard, D.S., et al. and the EXO-200 Collaboration (2008). Systematic study of trace radioactive impurities in candidate construction materials for EXO-200. Nucl. Instrum. Methods Phys. Res. Sect. A 591, 490–509.

Leppänen, M.T., Kukkonen, J.V.K., 2006. Evaluating the role of desorption in bioavailability of sediment-associated contaminants using oligochaetes, semipermeable membrane devices and Tenax extraction. Environ. Poll. 140, 150–163.

Li, C., Blencke, H.-M., Smith, L.C., Karp, M.T., Stensvåg, K., 2010. Two recombinant peptides, SpStrongylocins 1 and 2, from *Strongylocentrotus purpuratus*, show antimicrobial activity against Gram-positive and Gram-negative bacteria. Develop. Comp. Immun. 34, 286–292.

Lieberman, M.M., 1995. Determination of neutrophil activation by chemiluminescence using the Packard TopCount™ microplate scintillation and luminescence counter. TopCount Topics, TCA-022. PerkinElmer, Inc. Waltham, MA, USA, pp. 2.

Lightfoot, P.K., Kudryavtsev, V.A., Spooner, N.J.C., Liubarsky, I., Luscher, R., Smith, N.J.T., 2004. Nucl. Instrum. Methods Phys. Res. Sect. A 522, 439–446.

Lin, R., Ye, L., Yang, Y., Liao, J., Mo, S., Liu, N., 2008. Calcium antagonistic effects of *Bambusa Rigida* investigated by ^{45}Ca and its protection on myocardial ischemia in rats. Nucl. Sci. Technol. 19, 99–104.

Liu, G., Aspinall, M.D., Ma, X., Joyce, M.J., 2009. An investigation of the digital discrimination of neutrons and γ rays with orgainic scintillation detectors using an artificial neural netwrok. Nucl. Instrum. Methods Phys. Res. Sect. A 607, 620–628.

Liu, N., Yang, Y., Mo, S., Liao, J., Jin, J., 2005. Calcium antagonistic effects of Chinese crude drugs: Preliminary investigation and evaluation by ^{45}Ca. Appl. Radiat. Isot. 63, 151–155.

Little, R.J., Rodríguez, C.G., 2005. Modeling of human corticosteroid binding globulin. Use of structure–activity relations in soft steroid binding to refine the structure. Pharmac. Res. 22 (11), 1783–1792.

Liyanage, J.A., Yonezawa, C., 2003. A new analytical method for ^{32}P: liquid scintillation counting with solvent extraction. J. Radioanal. Nucl. Chem. 256 (2), 279–282.

López, M.L., Vommaro, R., Zalis, M., de Souza, W., Blair, S., Segura, C., 2010. Induction of cell death on *Plasmodium falciparum* asexual blood stages by Solanum nudum. Parasit. Int. 59, 217–225.

Lorber, A., Wangen, L.E., Kowalski, B.R., 1986. A theoretical foundation for the PLS algorithm. J. Chemom. 1 (1), 19–31.

Los Arcos, J.M., Ortiz, F., 1997. kB: a code to determine the ionization quench function $Q(E)$ as a function of the kB parameter. Comp. Phys. Commun. 103, 83–94.

Los Arcos, J.M., Grau Molanda, A., Fernandez, A., 1987. VIASKL: a computer program to evaluate the liquid scintillation counting efficiency and its associated uncertainty for K-L-atomic shell electron-capture nuclides. Comput. Phys. Commun. 44, 209–220.

Los Arcos, J.M., Grau, A., García-Toraño, E., 1991. LSC standardization of multigamma electron-capture radionuclides by the efficiency tracing method. In: Harley Ross, Noakes, John E., Spaulding, Jim D. (Eds.), Liquid Scintillation Counting and Organic Scintillators. Lewis Publishers, Chelsea, MI 48118, pp. 611–622.

Malinovsky, S.V., Kashirin, I.A., Ermakov, A.I., Tikhomirov, V.A., Sobolev, A.I., Kaihola, L.L., Fedotov, A. A. (2002a). New software for analyzing complex spectra obtained with ultra low level liquid scintillation spectrometer 'Quantulus'. pp. 119–126. In "LSC 2001. Advances in Liquid Scintillation Spectrometry." (S. Möbius, J.E. Noakes, F. Schönhofer. (Eds.), Radiocarbon, University of Arizona, Tucson, pp. 456.

Malinovsky, S.V., Kashirin, I.A., Ermakov, A.I., Tikhomirov, V.A., Belanov, S.V., Sobolev, A. I. (2002b). Mathematical aspects of decoding complex spectra applied to liquid scintillation counting. pp. 127–135. In "LSC 2001. Advances in Liquid Scintillation Spectrometry." (S. Möbius, J.E. Noakes, F. Schönhofer. (Eds.), Radiocarbon, University of Arizona, Tucson, pp. 456.

Malkov, V.A., Panyutin, I.G., Neumann, R.D., Zhurkin, V.B., Camerini-Otero, R.D., 2000. Radioprobing of a recA-three-stranded DNA complex with iodine-125: evidence for recognition of homology in the major groove of the target duplex. J. Molec. Biol. 299 (3), 629–640.

Mann, W.B., Rytz, A., Spernol, A., McLaughlin, W.L., 1988. Radioactivity Measurements, Principles and Practice. Pergamon Press, Oxford, pp. 937.

Marrodán Undagoitiaa, T., von Feilitzsch, F., Göger-Neffa, M., Hochmuth, K.A., Oberauera, L., Potzela, W., Wurm, M., 2006. Low energy neutrino astronomy with the large liquid scintillation detector LENA. Prog, Part. Nucl. Phys. 57, 283–289.

Marrone, S., Cano-Ott, D., Colonna, N., Domingo, C., Gramegna, F., Gonzalez, E.M., Gunsing, F., et al., 2002. Pulse shape analysis of liquid scintillators for neutron studies. Nucl. Instrum. Methods Phys. Res. Sect. A 490, 299–307.

Martens, H., Næs, T., 1992. Multivariate Calibration. Wiley, p. 419.

Martins, S.I.F.S., van Boekel, M.A.J.S., 2003. Malanoidins extinction coefficient in the glucose/glycine Maillard reaction. Food Chem 83, 135–142.

Matsui, Y., Takiue, M., 1991. Liquid scintillation radioassay of multi-labeled beta-emitters. Appl. Radiat. Isot. 42, 841–845.

Matta, C., Juhász, T., Szíjgyártó, Z., Kolozsvári, B., Somogyi, C., Nagy, G., Gergely, P., Zákány, R., 2011. PKCdelta is a positive regulator of chondrogenesis in chicken high density micromass cell cultures. Biochim. 93, 149–159.

McDowell, W. J. (1996). Recent applications of PERALS® spectrometry. In "Liquid Scintillation Spectrometry 1994" (G.T. Cook, D.D. Harkness, A.B. MacKenzie, B.F. Miller E.M. Scott. (Eds.), Radiocarbon, University of Arizona, Tucson, pp. 157–165.

McDowell, W.J., McDowell, B.L., 1991. Liquid scintillation alpha spectrometry: A method for today and tomorrow. In: Ross, Harley, Noakes, John E., Spaulding, Jim D. (Eds.), Liquid Scintillation Counting and Organic Scintillators. Lewis Publishers, Chelsea, MI 48118, pp. 105–122.

McDowell, W.J., McDowell, B. L. (1993). The growth of a radioanalytical method: alpha liquid scintillation spectrometry. pp. 193–200, In "Liquid Scintillation Spectrometry 1992" (J.E. Noakes, F. Schönhofer, H.A. Polach. (Eds.), Radiocarbon, University of Arizona, Tucson.

McGrath, J., Fulton, B.R., Joshi, P., Davies, P., Muenstermann, D., Schulz, O., Zuber, K., Freer, M., 2010. Detecting multi-hit events in a CdZnTe coplanar grid detector using pulse shape analysis: a method for improving background rejection in the COBRA 0 $\nu\beta\beta$ experiment. Nucl. Instrum. Methods Phys. Res. Sect. A 615, 57–61.

McKlveen, J.W., McDowell, W.J., 1984. Liquid scintillation alpha spectrometry techniques. Nucl. Instrum. Methods Phys. Res. 223 (2–3), 372–376.

McQuarrie, S.A., Wiebe, L.I., Ediss, C., 1980. Observations of the performance of ESP and H# in liquid scintillation counting. In: Peng, C.-T., Horrocks, D.L., Alpen, E.L. (Eds.), Liquid Scintillation Counting, Recent Applications and Development. Academic Press, New York and London, pp. 291–299.

McQuarrie, S.A., Noujaim, A.A., Ediss, C., Wiebe, L.I., 1981. Liquid scintillation counting of positron emitters. ANS 1981 Winter Meeting, San Francisco, CA, November 29-December 3, 1981. Trans. Amer. Nucl. Soc. 39, 27–28.

McQuarrie, S.A., Noujaim, A.A., 1983. ^{67}Ga: a novel internal standard for LSC. In: McQuarrie, S.A., Ediss, C., Wiebe, L.I. (Eds.), Advances in Scintillation Counting. University of Alberta Printing Services, Edmonton, pp. 57–65.

Medeiros, R.B., Godinho, R.O., Mattos, M.F.S.S., 2003. Comparison of the efficacy of biodegradable and non-biodegradable scintillation liquids on the counting of tritium- and [^{14}C]-labeled compounds. Braz. J. Med. Biol. Res 36 (12), 1733–1739.

Mei, D.M., Yin, Z.B., Stonehill, L.C., Hime, A., 2008. A model of nuclear recoil scintillation efficiency in noble liquids. Astropart. Phys. 30, 12–17.

Mei, H., Ho, M.K.C., Yung, L.Y., Wu, Z., Ip, N.Y., Wong, Y.H., 2011. Expression of Gαz in C2C12 cells restrains myogenic differentiation. Cell. Sign. 23, 389–397.

Mellado, J., Tarancón, A., García, J.F., Rauret, G., Warwick, P., 2005. Combination of chemical separation and data treatment for ^{55}Fe, ^{63}Ni, ^{99}Tc, ^{137}Cs and ^{90}Sr/^{90}Y activity determination in radioactive waste by liquid scintillation. Appl. Radiat. Isot. 63, 207–215.

Mendonça, M.L.T.G., Godoy, J.M., P. da Cruz, R., Perez, R.A.R., 2006. Radiocarbon dating of archaeological samples (*sambaqui*) using CO_2

absorption and liquid scintillation spectrometry of low background radiation. J. Environ. Radioact. 88, 205–214.

Mietelski, J.W., Gaca, P. (2002). Measurements of 90Sr and 241Pu in various matrices. pp. 373–378. In "LSC 2001, Advances in Liquid Scintillation Spectrometry". (S. Möbius, J.E. Noakes, F Schönhofer. (Eds.), RADIOCARBON, The University of Arizona, Tucson, p. 456.

Mikelic, L., Orescanin, V., Lulic, S., 2007. Determination of ^{55}Fe in waste waters of the Krsko nuclear power plant measured simultaneously by liquid scintillation spectrometer (LSC) and X-ray spectrometer (XRS). Nucl. Instrum. Methods Phys. Res. Sect. B 263, 95–98.

Miller, M., Kereiakes, J.G., Friedman, B.I., 1969. Determination of iron-59 and iron-55 in [blood] plasma using liquid scintillation counting. Int. J. Appl. Radiat. Isot. 20 (2), 133–135.

Mingote, R.M., Barbeira, P.J.S., Rocha, Z., 2006. Methodoly for rapid tritium determination in urine. J. Radioanal. Nucl. Chem. 269 (2), 475–479.

Miyajima, M., Sasaki, S., Tawara, H., Shibamura, E., 1992. Absolute number of scintillation photons in liquid xenon by alpha-particles. IEEE Trans. Nucl. Sci. 39 (4), 536–540.

Mo, L., Avei, B., James, D., Simpson, B., Van Wyngaardt, W.M., Cessna, J.T., Baldock, C., 2005. Development of activity standard for ^{90}Y microspheres. Appl. Radiat. Isotopes 63, 193–199.

Mo, L., Bignell, L.J., Steele, T., Alexiev, D., 2010. Activity measurement of ^{3}H using the TDCR method and observation of source stability. Appl. Radiat. Isotopes 68, 1540–1542.

Moe, M.K., 1986. Double-beta decay in ^{82}Se, ^{128}Te, and ^{130}Te. AIP Conf. Proc. 150, 1012–1016.

Moe, M.K., Rosen, S.P., 1989. Double-beta decay (November). Scient. Amer. 48–55.

Mordaunt, C.J., Gevao, B., Jones, K.C., Semple, K.T., 2005. Formation of non-extractable pesticide residues: observations on compound differences, measurement and regulatory issues. Environm. Poll. 133, 25–34.

Morita-Murase, Y., Murakami, I., Homma, Y., 2001. The air luminescence count for the rapid determination of ^{222}Rn in a liquid scintillation spectrometer. Chem. Lett. 2001, 238–239.

Morita-Murase, Y., Murakami, I., Homma, Y., 2003. Counting efficiency for rapid preparation of known amounts of ^{222}Rn by the air luminescence method. J. Nucl. Radiochem. Sci. 4 (2), 23–26.

Motta, D., Buck, C., Hartmann, F.X., Lasserre, Th., Schönert, S., Schwan, U., 2005. Prototype scintillator cell for an In-based solar neutrino detector. Nucl. Instrum. Methods Phys. Res. Sect. A 547, 368–388.

Murase, Y., Homma, Y., Takiue, M., 1989a. Effect of air luminescence counts on determination of ^{222}Rn by liquid scintillation counting. Appl. Radiat. Isotopes 40, 295–298.

Murase, Y., Homma, Y., Takiue, M., Aburai, T., 1989b. Determination of air luminescence spectra for alpha-emitters with liquid scintillation spectrometers. Appl. Radiat. Isotopes 40, 291–294.

Murase, Y., Homma, Y., Murakami, I., Handa, K., 1998. Assay of ^{222}Rn in water samples by a modified integral counting method. Appl. Radiat. Isot. 49 (7), 861–865.

Murase, Y., Homma, Y., Murakami, I., Handa, K., Horiuchi, K., 1999. Indoor ^{222}Rn measurements using an activated charcoal detector. Appl. Radiat. Isot. 50, 561–565.

Næs, T., 2002. User Friendly Guide to Multivariate Calibration and Classification. NIR Publications, pp. 352.

Nähle, O., Kossert, K., 2011. Comparison of the TDCR method and the CIEMAT/NIST method for the activity determination of beta emitting nuclides. In "LSC 2010, Advances in Liquid Scintillation Spectrometry". Radiocarbon, University of Arizona, Tucson.

Nähle, O., Kossert, K., Klein, R., 2008. Activity standardization of ^{22}Na. Appl. Radiat. Isot. 66, 865–871.

Nähle, O., Kossert, K., Cassette, P., 2010. Activity standardization of ^{3}H with the new TDCR system at PTB. Appl. Radiat. Isot. 68, 1534–1536.

Nakanishi, T., Kusakabe, M., Aono, T., Yamada, M., 2009. Simultaneous measurements of cosmogenic radionuclides ^{32}P, ^{33}P and ^{7}Be in dissolved and particulate forms in the upper ocean. J. Radioanal. Nucl. Chem. 279 (3), 769–776.

Nakao, N., Kurosawa, T., Nakamura, T., Uwamino, Y., 2001. Absolute measurements of the response function of an NE213 organic liquid scintillator for the neutron energy range up to 206 MeV. Nucl. Instrum. Methods Phys. Res. Sect. A 463, 275–287.

Natake, T., Takiue, M., Fujii, H., 1996. Nuclide identification for pure beta-emitting radionuclides with very similar beta end-point energies using a liquid scintillation spectrometer. Nucl. Instrum. Methods Phys. Res. Sect. A 378, 506–510.

Navotny, T., Büermann, L., Guldbakke, S., Klein, H., 1997. Response of N213 liquid scintillation detectors to high-energy photons (7 Mev $< E_r <$ 20 MeV). Nucl. Instrum. Methods Phys. Res. Sect. A 400, 356–366.

Nayak, D., 2001. Multitracer techniques: applications in chemical and life sciences. Appl. Radiat. Isot. 54, 195–202.

NCRP (1985). "A Handbook of Radioactivity Measurements Procedures". Report No. 64. National Council on Radiation Protection and Measurements, Washington, D.C. 20014.

Nebelung, C. (2003). Separation of 14C, 234U and 226Ra in liquid scintillation spectra. Report FZR-373, 53, Rossendorf.

Nebelung, C., Baraniak, L., 2007. Simultaneous determination of ^{226}Ra, ^{233}U and ^{237}Np by liquid scintillation spectrometry. Appl. Radiat. Isot. 65, 209–217.

Nebelung, C., Henniger, J., Mann, G. (2001). Schnelles Freimessverfahren für alpha-aktive Nuklide in Bauschutt durch Direktmessung von großflächigen dünnen Messpräparaten. Final Report BMBF Project 02 S 7768, Rossendorf.

Nebelung, C., Jähnigen, P., Bernhard, G. (2009). Simultaneous determination of beta nuclides by liquid scintillation spectrometry. pp. 193–201. In "LSC. 2008. Advances in Liquid Scintillation Spectrometry". (J. Eikenberg, M. Jäggi, H. Beer, H. Baehrle. (Eds.), Radiocarbon, University of Arizona, Tucson, pp. 445.

Nedjadi, Y., Bailat, C., Caffari, Y., Bochud, F., 2010. Standardization of ^{18}F by a coincidence method using full solid angle detectors. Appl. Radiat. Isot. 68, 1309–1313.

Neilson, R. et al. and the EXO-200 Collaboration (2009). Characterization of large area APDs for the EXO-200 detector. Nucl. Instrum. Methods Phys. Res. Sect. A 608, 68–75.

Nejjari, M., Kryza, D., Poncet, G., Roche, C., Perek, N., Chayvialle, J.A., Le Bars, D., Scoazec, J.-Y., Janier, M., Borson-Chazot, F., 2008. In vitro and in vivo studies with [^{18}F]fluorocholine on digestive tumoral cell lines and in an animal model of metastasized endocrine tumor. Nucl. Med. Biol. 35, 123–130.

Neumann, K.E., Roessler, N., ter Wiel, J., 1991. Safe scintillation chemicals for high efficiency, high throughput counting. In: Ross, Harley, Noakes, John E., Spaulding, Jim D. (Eds.), Liquid Scintillation Counting and Organic Scintillators. Lewis Publishers, Chelsea, MI 48118, pp. 35–41.

Neumann, S., Böttger, R., Guldbakke, S., Matzke, M., Sosaat, W., 2002. Neutron and photon spectrometry in monoenergetic neutron fields. Nucl. Instrum. Methods Phys. Res. Sect. A 476, 353–357.

Neves, F., Chepel, V., Solovov, V., Pereira, A., Lopes, M.I., Pinto de Cinha, J., Mendes, P., Lindote, A., Silva, C.P., Ferreira Marques, R., Policarpo, A.J.P.L., 2005. Performance of a chamber for studying the liquid xenon response to γ-rays and nuclear recoils. IEEE Trans. Nucl. Sci. 52 (6), 2793–2800.

Neves, F., Solovov, V., Chepel, V., Lopes, M.I., Pinto de Cinha, J., Lindote, A., Silva, C., 2007. Position reconstruction in a liquid xenon scintillation chamber for low-energy nuclear recoils and γ-rays. Nucl. Instrum. Methods Phys. Res. Sect. A 573, 48–52.

Newell, S.Y., Krambeck, C., 1995. Responses of bacterioplankton to tidal inundations of a saltmarish in a flume and adjacent mussel enclosures. J. Exp. Marine Biol. Ecol. 190, 79–95.

Ni, K., Aprile, E., Day, D., Giboni, K.L., Lopes, J.A.M., Majewski, P., Yamashita, M., 2005. Performance of a large area avalanche photodiode in a liquid xenon ionization and scintillation chamber. Nucl. Instrum. Methods Phys. Res. Sect. A 551, 356–363.

Ni, K., Aprile, E., Giboni, K.L., Majewski, P., Yamashita, M., 2006. Gamma ray spectroscopy with scintillation light in liquid xenon. J. Instrum. (JINST) 1, P09004.

Ni, K., Hasty, R., Wongjirad, T.M., Kastens, L., Manzur, A., McKinsey, D.N., 2007. Preparation of neutron-activated xenon for liquid xenon detector calibration. Nucl. Instrum. Methods Phys. Res. Sect. A 582, 569–574.

Niese, S., 1999. The discovery of organic solid and liquid Scintillators by H. Kallmann and L. Herforth 50 years ago. J. Radioanal. Nucl. Chem. 241 (3), 499–501.

Niese, S. (2003). The discovery of the excitation of liquid biphenyl and phenanthrene fluorescence by fast electrons; laudatio on the inauguration of the German Society for Liquid Scintillation Spectrometry (DGFS). pp. 447–450. In "LSC 2001. Advances in Liquid Scintillation Spectrometry". The University of Arizona, Tucson, p. 456.

Nishimura, Y., Natori, H., 2011. Performance of the liquid xenon detector for the MEG experiment. Nucl. Instrum. Methods Phys. Res. Sect. A 628 (1), 376–380.

NNDC (2011). National Nuclear Data Center, Brookhaven National Laboratory, "Nuclear Decay Data (NuDat)". Decay Radiation Data, NuDat 2.5, http://www.nndc.bnl.gov/nudat2/.

NNDC-BNL (2011). National Nuclear Data Center, Brookhaven National Laboratory, "Double Beta (ββ) Decay Data". http://www.nndc.bnl.gov/bbdecay/.

Noor, A., Kasim, N., L'Annunziata, M.F., 1995. Application of pulse height spectral analysis to double-label counting of ^{35}S-^{32}P. Appl. Radiat. Isot. 46, 791–797.

Noor, A., Zakir, M., Burhanuddin, , Maming, R., L'Annunziata, M.F., 1996a. Cerenkov and liquid scintillation analysis of the triple label ^{86}Rb–^{35}S–^{33}P. Appl. Radiat. Isot. 47, 659–668.

Noor, A., Zakir, M., Burhanuddin, R., Kasim, N., Nurr, L.A., Anthony, Maming, Agung, M., L'Annunziata, M.F., 1996b. Pulse height spectral analysis of ^{3}H:^{14}C ratios. Appl. Radiat. Isot. 47, 767–775.

Novotny, T., Büermann, L., Guldbakke, S., Klein, H., 1997. Response of nE213 liquid scintillation detectors to high-energy photons (7 MeV $< E_\gamma <$ 20 MeV). Nucl. Instrum. Methods Phys. Res. Sect. A 400, 356–366.

Ogata, Y., 2007. Radioactivity measurement with a plastic scintillation vial. J. Radioanal. Nucl. Chem. 273 (1), 253–256.

Okita, G.T., Kabara, J.J., Richardson, F., LeRoy, G.V., 1957. Assaying compounds containing ^{3}H and ^{14}C. Nucleonics 15, 111–114.

Ooi, Y.Y., Ramasamy, R., Rahmat, Z., Subramaiam, H., Tan, S.W., Abdullah, M., Israf, D.A., Vidyadaran, S., 2010. Bone marrow-derived mesenchymal stem cells modulate BV2 microglia responses to lipopolysaccharide. Int. Immunopharm. 10, 1532–1540.

Oropesa Verdecia, P., Kossert, K., 2009. Activity standardization of ^{131}I at CENTIS-DMR and PTB within the scope of a bilateral comparison. Appl. Radiat. Isot. 67, 1099–1103.

Ortiz, J.F., Los Arcos, J.M., Grau Malonda, A. (1993). CIEMAT/NIST standardization method extended to anode outputs for beta and electron-capture nuclides. pp. 261–267, In "Liquid Scintillation Spectrometry 1992" (J.E. Noakes, F. Schönhofer H.A. Polach. (Eds.), Radiocarbon, University of Arizona, Tucson.

Palomo, M., Peñalver, A., Aguilar, C., Borrull, F., 2007. Tritium activity levels in environmental water samples from different origins. Appl. Radiat. Isot. 65, 1048–1056.

Park, T.S., Hwang, H.Y., Lee, J.M., 1998. An improved coincidence counting technique for standardization of radionuclides. Appl. Radiat. Isot. 49 (9–11), 1147–1151.

Parus, J.L., Raab, W., Radoszewski, T. (1993). Liquid scintillation counting of plutonium and/or americium concentrations. In "Liquid Scintillation Spectrometry 1992" (J.E. Noakes, F. Schönhofer, H.A. Polach. (Eds.), Radiocarbon, University of Arizona, Tucson.

Passo, Jr., C. J. (1996). Time-resloved pulse decay analysis (TR-PDA): A refinement for alpha/beta discrimination. In "Liquid Scintillation Spectrometry 1994" (G.T. Cook, D.D. Harkness, A.B. MacKenzie, B.F. Miller, E.M. Scott. (Eds.), Radiocarbon, University of Arizona, Tucson, pp. 37–41.

Passo Jr., C.J., Cook, G.T., 1994. Handbook of Environmental Liquid Scintillation Spectrometry, A Compilation of Theory and Methods. Publ. No. PMC0387. PerkinElmer Life and Analytical Sciences, Boston.

Passo, Jr., C.J., Kessler, M. J. (1993). Selectable delay before burst - a novel feature to enhance low-level counting performance. pp. 51–57, In "Liquid Scintillation Spectrometry 1992" (J.E. Noakes, F. Schönhofer, H.A. Polach. (Eds.), Radiocarbon, University of Arizona, Tucson.

Passo, Jr., C.J., Roberts, D. J. (1996). Expanded energy for time-resolved liquid scintillation counting: an enhancement for programmable TR-LSC®. pp. 67–74, In "Liquid Scintillation Spectrometry 1994" (G.T. Cook, D.D. Harkness, A.B. MacKenzie, B.F. Miller, E.M. Scott. (Eds.), Radiocarbon, University of Arizona, Tucson.

Pates, J.M., Mullinger, N.J., 2007. Determination of ^{222}Rn in fresh water: Development of a robust method of analysis by α/β separation liquid scintillation spectrometry. Appl. Radiat. Isot. 65, 92–103.

Pates, J.M., Cook, G.T., MacKenzie, A.B., Thomson, J., 1993. The development of alpha/beta separation liquid scintillation cocktail for aqueous samples. J. Radioanal. Nucl. Chem. Articles 172, 341–348.

Pates, J.M., Cook, G.T., MacKenzie, A. B. (1996a). Alpha/beta separation liquid scintillation spectrometry: current trends. pp. 267–281, In "Liquid Scintillation Spectrometry 1994" (G.T. Cook, D.D. Harkness, A.B. MacKenzie, B.F. Miller, E.M. Scott. (Eds.), Radiocarbon, University of Arizona, Tucson.

Pates, J.M., Cook, G.T., MacKenzie, A.B., Thomson, J. (1996b). The effect of cocktail fluors on pulse shapes and alpha/beta separation liquid scintillation spectrometry. In "Liquid Scintillation Spectrometry 1994" (G.T. Cook, D.D. Harkness, A.B. MacKenzie, B.F. Miller, E.M. Scott. (Eds.), Radiocarbon, University of Arizona, Tucson, pp. 317–326.

Pates, J.M., Cook, G.T., MacKenzie, A.B., Passo, Jr., C. J. (1996c). Quenching and its effect on alpha/beta separation liquid scintillation spectrometry. pp. 75–85, In "Liquid Scintillation Spectrometry 1994" (G.T. Cook, D.D. Harkness, A.B. MacKenzie, B.F. Miller, E.M. Scott. (Eds.), Radiocarbon, University of Arizona, Tucson.

Pates, J.M., Cook, G.T., MacKenzie, A.B., Passo Jr., C.J., 1998. Implications of beta energy and quench level for alpha/beta liquid scintillation spectrometry calibration. Analyst 123, 2201–2207.

Patronis, N., Kokkoris, M., Giantsoudi, D., Perdikakis, G., Papadopoulos, C.T., Vlastou, R., 2007. Aspects of GEANT4 Monte-Carlo calculations of the BC501A neutron detector. Nucl. Instrum. Methods Phys. Res. Sect. A 578 (1), 351–355.

Payne, A.G.D., Booth, N.E., 1990. Tests of some prototype indium-loaded scintillators for solar neutrino detection. Nucl. Instrum. Methods Phys. Res. Sect. A 288, 632–640.

Peiffer, P., Pollmann, T., Schönert, S., Smolnikov, A., Vasiliev, S., 2008. Pulse shape analysis of scintillation signals from pure and xenon-doped liquid argon for radioactive background identification. J. Instrum. (JINST) 3, P08007.

Peng, C.T., 1976. Chemiluminescence. In: Noujaim, A.A., Ediss, C., Wiebe, L.I. (Eds.), Liquid Scintillation Science and Technology. Academic Press, New York and London, pp. 313–329.

Perry, S.W., Warner, G.T., 1963. A method of sample preparation for the estimation of ^{55}Fe in whole blood by the liquid scintillation counting technique. Int. J. Appl. Radiat. Isot. 14, 397–400.

Peurung, A.J., 2000. Recent development in neutron detection. Nucl. Instrum. Methods Phys. Res. Sect. A 443, 400–415.

Piraner, O., Jones, R. L. (2009). Urine gross alpha/beta analysis by liquid scintillation counting for terrorism preparedness. pp. 41–46, In "LSC 2008, Advances in Liquid Scintillation Spectrometry". (J. Eikenberg, M. Jäggi, H. Beer, H. Baehrie. (Eds.), Radiocarbon, University of Arizona, Tucson, p. 445.

Plautz, J.D., Strayer, C.A., Kay, S.A., 1996. Automated Recording of Luciferase-Reported Gene Transcription in Living Seedlings and Fruit Flies. TopCount Topics, TCA-025. PerkinElmer, Inc., Waltham, MA, USA, p. 4.

Pochwalski, K. (1978). Measurement of the activity of pure β-emitters in liquid scintillator by use of the new triple-to-double coincidence ratio method. Thesis, unpublished, Institute of Nuclear Research, Warsaw (in Polish).

Pochwalski, K., Broda, R., Radoszewski, T., 1988. Standardization of pure beta emitters by liquid-scintillation counting. Appl. Radiat. Isot. 39, 165–172.

Poenaru, D.N., Greiner, W., 1997. In: Experimental Techniques in Nuclear Physics. Walter de Gruyter, Berlin.

Poerschke, R.L., Moos, P.J., 2011. Thioredoxin reductase 1 knockdown enhances selenazolidine cytotoxicity in human lung cancer cells via mitochondrial dysfunction. Biochem. Pharmacol. 81, 211–221.

Pommé, S., Altzitzoglou, T., Van Ammel, R., Sibbens, G., 2005. Standardisation of ^{125}I using seven techniques for radioactivity measurement. Nucl. Instrum. Methods Phys. Res. Sect. A 544, 584–592.

Pozzi, S.A., Flaska, M., Enqvist, A., Pázsit, I., 2007. Monte Carlo and analytical models of neutron detection with organic scintillation detectors. Nucl. Instrum. Methods Phys. Res. Sect. A 582, 629–637.

Pozzi, S.A., Clarke, S.D., Flaska, M., Peerani, P., 2009. Pulse-height distributions of neutron and gamma rays from plutonium-oxide samples. Nucl. Instrum. Methods Phys. Res. Sect. A 608, 310−315.

Prichard, H.M., Venso, E.A., Dodson, C.L., 1992. Liquid scintillation analysis of ^{222}Rn in water by alpha-beta discrimination. Radioact. Radiochem. 3 (1), 28−36.

Pujol, L., Sanchez-Cabeza, J.-A., 1997. Role of quenching on alpha/beta separation in liquid scintillation counting for several high capacity cocktails. Analyst 122, 383−385.

Qin, M.J., Mo, L., Alexiev, D., Cassette, P., 2008. Construction and implementation of a TDCR system at ANSTO. Appl. Radiat. Isot. 66, 1033−1037.

Radoszewski, T. (1964). An absolute measurement of ^{14}C by the 4π scintillation counter method. Thesis, unpublished (In Polish).

Raghaven, R.S., 1976. Inverse β decay of ^{115}In $\rightarrow$ ^{115}Sn*: a new possibility for detecting solar neutrinos from the proton-proton reaction. Phys. Rev. Lett. 37 (5), 259−262.

Raghaven, R.S., 2001. pp-Solar neutrino spectroscopy: return of the indium detector. Phys. Rev. Lett. arXiv:hep-ex/0106054v1.

Ranucci, G., 2007. Borexino. Nucl. Phys. B (Proc. Suppl.) 168, 111−114.

Ratel, G., 2008. Analysis of the results of the international comparison of activity measurements of a solution of ^{55}Fe. Appl. Radiat. Isot. 66, 729−732.

Rauly-Lestienne, I., Lestienne, F., Ailhaud, M.-C., Binesse, J., Newman-Tancredi, A., Cussac, D., 2011. Competitive interaction of 5-HT_{1A} receptors with G-protein subtypes in CHO cells demonstrated by RNA interference. Cell. Sign. 23, 58−64.

Rausch, C., Bucherl, T., Gaehler, R., Von Seggern, H., Winnaker, A., 1993. Recent developments in neutron detection. Proc. SPIE 1737, 255−263.

Ray, B., Simon, J.R., Lahiri, D.K., 2009. Determination of high-affinity choline uptake (HACU) and choline acetyltransferase (ChAT) activity in the same population of cultured cells. Brain Res. 1297, 160−168.

Razdolescu, A.C., Cassette, Ph, 2004. Standardization of tritiated water and ^{204}Tl by TDCR liquid scintillation counting. Appl. Radiat. Isot. 60, 493−497.

Razdolescu, A.C., Grigorescu, E.L., Sahagia, M., Luca, A., Ivan, C., 2000. Standardization of ^{169}Yb by the $4\pi\beta$-γ method. Appl. Radiat. Isot. 52, 505−507.

Razdolescu, A.C., Sahagia, M., Cassette, Ph., Grigorescu, E.L., Luca, A., Ivan, C., 2002. Standardization of ^{89}Sr. Appl. Radiat. Isot. 56, 461−465.

Razdolescu, A.C., Broda, R., Cassette, P., Simpson, B.R.S., Van Wyngaardt, W.M., 2006. The IFIN-HH triple coincidence liquid scintillation counter. Appl. Radiat. Isot. 64, 1510−1514.

Razdolescu, A.C., Cassette, Ph., Sahagia, M., 2008. Measurement of ^{55}Fe solution activity by LSC-TDCR method. Appl. Radiat. Isot. 66, 750−755.

Reboli, A., Aupiais, J., Mialocq, J.C., 2005. Application of large area avalanche photodiodes for alpha liquid scintillation counting. Nucl. Instrum. Methods Phys. Res. Sect. A 550, 593−602.

Reddy, P.J., Bhade, S.P.D., Narayan, K.K., Narayanan, A., Babu, D.A.R., Sharma, D.N., 2009. Comparative study of different methods for the activity quantification of ^{3}H and ^{14}C radionuclides in dual labeled samples using liquid scintillation analyzer. Appl. Radiat. Isot. 67, 1945−1951.

Reginatto, M., Goldhagen, P., Neumann, S., 2002. Spectrum unfolding, sensitivity analysis and propagation of uncertainties with the maximum entropy deconvolution code MAXED. Nucl. Instrum. Methods Phys. Res. Sect. A 476, 242−246.

Reines, F., Cowan Jr., C.L., 1953. Detection of the free neutrino. Phys. Rev. Lett. 92, 330.

Reines, F., Cowan Jr., C.L., 1956. The neutrino. Nature 178, 446−449.

Reines, F., Cowan Jr., C.L., 1957. Neutrino physics. Phys. Today 10 (8), 12−18.

Remetti, R., Sessa, A., 2011. Beta spectra deconvolution for liquid scintillation counting. J. Radioanal. Nucl. Chem. 287 (1), 107−111.

Ren, Y.L., Mahon, D., 2007. Evaluation of ^{35}S-residues in grains and grain fractions fumigated with ^{35}S-labelled carbonyl sulfide. J Stored Prod. Res. 43, 356−361.

Retière, F., 2010. A liquid xenon detector for micro-PET. Nucl. Instrum. Methods Phys. Res. Sect. A 623, 591−593.

Reynolds, G.T., Harrison, F.B., Salvini, G., 1950. Liquid scintillation counters. Phys. Rev. 78 (4), 488.

Rhodes, B.A., 1965. Liquid scintillation counting of radioiodine. Anal. Chem. 37 (8), 995−997.

Ring, J.G., Nguyen, D.C., Everett, L.J., 1980. In: Peng, C.T., Horrocks, D.L., Alpen, E.L. (Eds.), Liquid Scintillation Counting, Recent Applications and Development. Physical Aspects, Vol. I. Academic Press, New York and London, pp. 89−104.

Roberts, D., Moore, H.M., Berges, J., Patching, J.W., Carton, M.W., Eardly, D.F., 2001. Sediment distribution, hydrolytic enzyme profiles and bacterial activities in the guts of *Oneirophanta mutabilis, Psychropotes longicauda* and *Pseudostichopus villosus*: what do they tell us about digestive strategies of abyssal holothurians? Prog. Oceanogr. 50, 443−458.

Rochman, D., Haight, R.C., O'Donnell, J.M., Devlin, M., Ethvignot, T., Granier, T., 2004. Neutron-induced reaction studies at FIGARO using a spallation source. Nucl. Instrum. Methods Phys. Res. Sect. A 523, 102−115.

Rodrígues, D., Arenillas, P., Capoulat, M.E., Balpardo, C., 2008. General data analysis code for TDCR liquid scintillation counting. Appl. Radiat. Isot. 66, 1049−1054.

Rodríguez, M., Piña, G., Lara, E., 2006. Radiochemical analysis of ^{36}Cl. Czech. J. Phys. 56 (Suppl.4), D211−D217.

Rodríguez, M.C., Monti, M.R., Argaraña, C.E., Rivas, G.A., 2006. Enzymatic biosensor for the electrochemical detection of 2,4-dinitrotoluene biodegradation derivatives. Talanta 68, 1671−1676.

Rodríguez Barquero, L., Grau Carles, A., 1998. The influence of the primary solute on alpha/beta discrimination. Appl. Radiat. Isot. 49 (9−11), 1065−1068.

Rodríguez Barquero, L., Los Arcos, J.M., 1996. ^{41}Ca standardization by the CIEMAT/NIST LSC method. Nucl. Instrum. Methods Phys. Res. Sect. A 369, 353−358.

Rodríguez Barquero, L., Los Arcos, J.M., 2000. Measurement of ^{49}V half-life. Appl. Radiat. Isot. 52, 569−571.

Rodríguez Barquero, L., Los Arcos, J.M., 2004. Compensation by the CIEMAT/NIST-method of long-term effects in LSC measurements of beta emitters. Appl. Radiat. Isot. 61, 1403−1411.

Rodríguez Barquero, L., Grau Malonda, A., Los Arcos Merino, J.M., Suarez Contreras, C., 1989. Preparación y calibración por centelleo liquido de una muestra de Cl-36. Anales de Física B 85, 55−69.

Rodríguez Barquero, L., Garcia-Toraño, E., Los Arcos, J.M., 2004. Standardization of ^{32}P/^{33}P and ^{204}Tl by liquid scintillation counting. Appl. Radiat. Isot. 60, 615−618.

Rodríguez, L., Los Arcos, J.M., Grau, A., 1992. LSC standardization of ^{54}Mn in inorganic and organic samples by the CIEMAT/NIST efficiency tracing method. Nucl. Instrum. Methods Phys. Res. Sect. A 312, 124−131.

Rodríguez, L., Los Arcos, J.M., Grau Malonda, A., Garcia-Toraño, E., 1994. LSC standardization of ^{45}Ca by the CIEMAT/NIST efficiency tracing method. Nucl. Instrum. Methods Phys. Res. Sect. 339, 6−13.

Rodríguez, L., Los Arcos, J.M., Ortiz, F., Jiménez, A., 1998. ^{49}V standardization by the CIEMAT/NIST LSC method. Appl. Radiat. Isot. 49 (9−11), 1077−1082.

Roelant, C.H., Burns, D.A., 1995. Introduction to CytoLite™; A chemiluminescent reagent system for cell proliferation and cytotoxicity assays. LiteGuides LGA-001. Packard BioScience Company, Meriden, CT 06450. p. 6.

Roessler, N., Valenta, R.J., van Cauter, S., 1991. Time-resolved liquid scintillation counting. In: Ross, Harley, Noakes, John E., Spaulding, Jim D. (Eds.), Liquid Scintillation Counting and Organic Scintillators. Lewis Publishers, Chelsea, MI 48118, pp. 501−511.

Ronchi, E., Söderström, P.-A., Nyberg, J., Andersson Sundén, E., Conroy, S., Ericsson, G., Hellesen, C., Gatu Johnson, M., Weiszflog, M., 2009. An artificial neural network based neutron−gamma discrimination and pile-up rejection framework for the BC-501 liquid scintillation detector. Nucl. Instrum. Methods Phys. Res. Sect. A 610, 534−539.

Roteta, M., Garcí-Toraño, E., Rodríguez Barquero, L., 2006. Stansradisation of ^{18}F by coincidence and LSC methods. Appl. Radiat. Isot. 64, 1199−1202.

Ruberu, S.R., Liu, Y.-G., Perera, S.K., 2008. An improved liquid scintillation counting method for the determination of gross alpha activity in groundwater wells. Health Phys. 95 (4), 397−406.

Rundt, K., 1991. The effect of quench curve shape of the solvent and quencher in a liquid scintillation counter. In: Ross, Harley, Noakes, John E.,

Spaulding, Jim D. (Eds.), Liquid Scintillation Counting and Organic Scintillators. Lewis Publishers, Chelsea, MI 48118, pp. 257–268.

Rundt, K., Kouru, H. (1989). Liquid scintillation counter for measuring the activity of radioactive samples containing a multiple of radioactive isotopes. US Patent No. 4,918,310.

Rundt, K., Kouru, H. (1992). Apparatus and a method for measuring the activity of radioactive samples containing a multiple of radioactive isotopes. US Patent. No. 5,134,294.

Runyon, S.P., Orr, M., Navarro, H.A., Kepler, J.A., Rogawski, M.A., Kaminski, R.M., Cook, C.E., 2009. 17β-Nitro-5α-androstan-3α-ol and its 3β-methyl derivative: Neurosteroid analogs with potent anticonvulsant and anxiolytic activities. Eur. J. Pharm. 617, 68–73.

Salonen, L. (2006). Alpha spillover depends on alpha energy: A new finding in alpha/beta liquid scintillation spectrometry. pp. 135–148, In "LSC 2005, Advances in Liquid Scintillation Spectrometry". (S. Chałupnik, F. Schönhofer, J. Noakes. (Eds.). Radiocarbon, University of Arizona, Tucson, p. 449.

Salonen, L., 2010. Comparison of two direct LS methods for measuring ^{222}Rn in drinking water using α/β liquid scintillation spectrometry. Appl. Radiat. Isot. 68, 1970–1979.

Samuels, E.R., Scott, J.E., 1995. Ca^{+2}-phosphatidylserine-dependent protein kinase C activity in fetal, neonatal and adult rabbit lung and isolated lamellar bodies. Life Sci. 57 (17), 1557–1568.

Sandhya, D., Subramanian, M.S., 1998. Radiometric determination of trace amounts of zinc using liquid scintillation counting. Talanta 46, 921–926.

Santiago, L., Bagán, H., Tarancón Sanz, A., Rauret, G., García, J.F., 2011. Systematic study of the different quenching phenomena in organic scintillators. In "LSC 2010, Advances in Liquid Scintillation Spectrometry." Radiocarbon, University of Arizona, Tucson.

Sas, D., Sládek, P., Janda, J., 2010. Measuring alpha and beta activity of filter and swab samples with LSC. J. Radioanal. Nucl. Chem. 286, 513–517.

Satoh, D., Shigyo, N., Iwamoto, Y., Kitsuki, H., Ishibashi, K., 2001. Study of neutron detection efficiencies for liquid organic scintillator up to 3 GeV. IEEE Trans. Nucl. Sci. 48 (4), 1165–1167.

Sawada, R., 2010. Performance of liquid xenon gamma ray detector for MEG. Nucl. Instrum. Methods Phys. Res. Sect. A 632 (1), 258–260.

Scheirer, W., Roelant, C., Burns, D.A., 1994. Introduction to LucLite™; A Bioluminescent Reagent System for Reporter Gene Assays. Lite-Guides LGA-002. Packard BioScience Company, Meriden, CT 06450, p. 5.

Schiffer, R.T., Flaska, M., Pozzi, S.A., Carney, S., Wentzloff, D.D., 2011. A scalable FPGA-based digitizing platform for radiation data acquisition. Nucl. Instrum. Methods Phys. Res. Sect. A 652 (1), 491–493.

Schmidt, D., Asselineau, B., Böttger, R., Klein, H., Lebreton, L., Neumann, S., Nolte, R., Pichenot, G., 2002. Nucl. Instrum. Methods Phys. Res. Sect. A 476, 186–189.

Schneider, E.W., Verbrugge, M.W., 1993. Radiotracer method for simultaneous measurement of cation, anion and water transport through ion-exchange membranes. Appl. Radiat. Isot. 44, 1399–1408.

Schötzig, U., Schönfeld, E., Günther, E., Klein, R., Schrader, H., 1999. Standardization and decay data of ^{153}Sm. Appl. Radiat. Isot. 51, 169–175.

Schötzig, U., Schrader, H., Schönfeld, E., Günther, E., Klein, R., 2001. Standardization and decay data of ^{177}Lu and ^{188}Re. Appl. Radiat. Isot. 55, 89–96.

Schrader, H., Klein, R., Kossert, K., 2007. Standardisation of ^{18}F and ionization chamber calibration for nuclear medicine. Appl. Radiat. Isot. 65, 581–592.

Schultz, M.K., Cessna, J.T., Anderson, T.L., Ponto, J.A., Petry, N., Kowalsky, R.J., Palmer, M.R., Beinlich, U.F., Baker, W., Hinkle, G.H., Hung, J.C., Quinton, T., Rice, P.A., Divgi, C., Norenberg, J.P., 2008. Appl. Radiat. Isot. 66, 252–260.

Schwerdtel, E., 1965. G.I.T. Fachzeitschrift für das Laboratorium 9, 881.

Schwerdtel, E., 1966. Recent developments in liquid scintillation counting. Kerntechnik 8, 517–520.

Schwerdtel, E., 1966. Simple method for an exact efficiency determination in liquid scintillation counting of low-energy β-emitters. Atomkernenergie 11, 324–325.

Seki, T., Fukamizu, A., Kiso, Y., Mukai, H., 2011. Mitocryptide-2, a neutrophil-activating cryptide, is a specific endogenous agonist for formyl-peptide receptor-like 1. Biochem. Biophys. Res. Comm. 404, 482–487.

Shaffer, C.L., Langer, C.S., 2007. Metabolism of ^{14}C/^{3}H-labeled $GABA_A$ receptor partial agonist in rat, dog and human liver microsomes: evaluation of a dual-radiolabel strategy. J. Pharmaceut. Biomed. Anal. 43, 1195–1205.

Shagin, P., Gomez, R., Oberlack, U., Cushman, P., Sherwood, B., McClish, M., Farrell, R., 2009. Avalanche photodiode for liquid xenon scintillation: quantum efficiency and gain. J. Instrum. (JINST) 4, P01005.

Simpson, B.R.S., 2002. Radioactivity standardization in South Africa. Appl. Radiat. Isot. 56, 301–305.

Simpson, B.R.S., Meyer, B.R., 1988. A multiple-channel 2- and 3-fold coincidence counting system for radioactivity standardization. Nucl. Instrum. Methods Phys. Res. Sect. A 263, 436–440.

Simpson, B.R.S., Meyer, B. R. (1992a). The standardization of 201Tl by liquid scintillation coincidence counting. National Accelerator Centre Report. NAC/92–01, P.O. Box 72, Faure, 7131 South Africa.

Simpson, B.R.S., Meyer, B. R. (1992b). Direct determination of the activity of non-gamma-emitting radionuclides by the TDCR efficiency calculation technique: a review of the present status. Report NAC/92-02, September 1992, National Accelerator Centre, PO Box 72, Faure, 7131 South Africa. p. 18.

Simpson, B.R.S., Meyer, B.R., 1992c. Further investigations of the TDCR efficiency calculation technique for the direct determination of activity. Nucl. Instrum. Methods Phys. Res. Sect. A 312, 90–94.

Simpson, B.R.S., Meyer, B.R., 1994a. Standardization and half-life of ^{201}Tl by the $4\pi(x,e)-\gamma$ coincidence method with liquid scintillation counting in the 4π-channel. Appl. Radiat. Isot. 45, 669–673.

Simpson, B.R.S., Meyer, B.R., 1994b. Direct activity measurement of pure beta-emitting radionuclides by the TDCR efficiency calculation technique. Nucl. Instrum. Methods Phys. Res. Sect. A 339, 14–20.

Simpson, B.R.S., Meyer, B.R., 1996. Activity measurement of ^{204}Tl by direct liquid scintillation measurements. Nucl. Instrum. Methods Phys. Res. Sect. A 369, 340–343.

Simpson, B.R.S., Morris, W.M., 2004a. Direct activity determination of ^{54}Mn and ^{65}Zn by a non-extrapolation liquid scintillation method. Appl. Radiat. Isot. 60, 475–479.

Simpson, B.R.S., Morris, W.M., 2004b. The standardization of ^{33}P by the TDCR efficiency calculation technique. Appl. Radiat. Isot. 60, 465–468.

Simpson, B.R.S., van Oordt, E. J. (1997). Data acquisition program for the NAC radioactivity standards laboratory. NAC Report NAC/97–03, National Accelerator Centre, PO Box 72, Faure, 7131 South Africa.

Simpson, B.R.S., Van Wyngaardt, W.M., 2006. Activity measurements of the high-energy pure β-emitters ^{89}Sr and ^{90}Y by the TDCR efficiency calculation technique. Appl. Radiat. Isot. 64, 1481–1484.

Simpson, B.R.S., Van Wyngaardt, W.M., Lubbe, J., 2010. Fe-55 activity measurements at the NMISA revisited. Appl. Radiat. Isot. 68, 1529–1533.

Sinor, J.D., Boeckman, F.A., Aizenman, E., 1997. Intrinsic redox properties of *N*-methyl-D-aspartate receptor can determine the developmental expression of excitotoxicity in rat cortical neurons in vitro. Brain Res. 747, 297–303.

Sirelkhatim, D.A., Sam, A.K., Hassona, R.J., 2008. Distribution of ^{226}Ra—^{210}Pb—^{210}Po in marine biota and surface sediments of the Red Sea, Sudan. J. Environ. Radioact. 99, 1825–1828.

Skrlin, A., Radic, I., Vuletic, M., Schwinke, D., Runac, D., Kusalic, T., Paskvan, I., Krsic, M., Bratos, M., Marinc, S., 2010. Biologicals 38, 557–566.

Sorensen, P. et al. and the XENON10 Collaboration (2009). The scintillation and ionization yield of liquid xenon for nuclear recoils. Nucl. Instrum. Methods Phys. Res. Sect. A 601, 339–346.

Spasova, Y., Wätjen, U., Altzitzoglou, T., 2008. European measurement comparison of ^{137}Cs, ^{40}K and ^{90}Sr in milk powder. J. Radioanal. Nucl. Chem. 277 (1), 211–215.

Staffová, P., Němec, M., John, J., 2006. Determination of gross alpha and beta activities in water samples by liquid scintillation counting. Czech. J. Phys. 56 (Suppl. D), D299–D305.

Stamoulis, K.C., Ioannides, K.G., Karamanis, D., 2010. Deconvolution of liquid scintillation alpha spectra of mixtures of uranium and radium isotopes. Anal. Chim. Acta 657, 108–115.

Stanga, D., Moreau, I., Cassette, P., 2006. Standardization of tritiaited water by two improved methods. Appl. Radiat. Isot. 64, 1203–1206.

Steele, T., Mo, L., Bignell, L., Smith, M., Alexiev, D., 2009. FASEA: a FPGA acquisition system and software event analysis for liquid scintillation counting. Nucl. Instrum. Methods Phys. Res. Sect. A 609, 217–220.

Steyn, J., 1956. Absolute standardization of beta-emitting isotopes with a liquid scintillator counter. Proc. Phys. Soc. A 69, 865–867.

Suárez, J.A., Rodríguez, M., Espartero, A.G., Piña, G., 2000. Radiochemical analysis of ^{41}Ca and ^{45}Ca. Appl. Radiat. Isot. 52, 407–413.

Sughrue, M.E., Rutkowski, M.J., Kane, A.J., Parsa, A.T., 2010. Human glioma demonstrates cell line specific results with ATP-based chemiluminescent cellular proliferation assays. J. Clin. Neurosci. 17, 1573–1577.

Suzuki, Y., Inoue, K., Nagashima, Y., Hashimoto, S., Inagaki, T., 1990. Development of indium-loaded liquid scintillators with long attenuation length. Nucl. Instrum. Methods Phys. Res. Sect. A 293, 615–622.

Sweet, I.R., Cook, D.L., Lernmark, Å, Greenbaum, C.J., Wallen, A.R., Marcum, E.S., Stekhova, S.A., Krohn, K.A., 2004. Systematic screening of potential β-cell imaging agents. Biochem. Biophys. Res. Commun. 314, 976–983.

Takiue, M., 1980. Simple and rapid measurement of α-rays on smear samples using air luminescence. Health Phys. 39 (1), 29–32.

Takiue, M., Ishikawa, H., 1974. Quenching analysis of liquid scintillation. Nucl. Instrum. Methods 118, 51–54.

Takiue, M., Ishikawa, H., 1978. Thermal neutron reaction cross section measurements for fourteen nuclides with a liquid scintillation spectrometer. Nucl. Instrum. Methods 148, 157–161.

Takiue, M., Ishikawa, H., 1979a. Absolute measurement of internal conversion electrons with a liquid scintillation spectrometer. Nucl. Instrum. Methods 164, 343–347.

Takiue, M., Ishikawa, H., 1979b. α-ray measurement due to air luminescence employing a liquid scintillation spectrometer. Nucl. Instrum. Methods 159, 139–143.

Takiue, M., Natake, T., Hayashi, M., 1983. Double ratio technique for determining the type of quenching in liquid scintillation measurement. Int. J. Appl. Radiat. Isot. 34, 1483–1485.

Takiue, M., Hayashi, M., Natake, T., Ishikawa, H., 1984. Elimination of chemiluminescence in liquid scintillation measurement. Nucl. Instrum. Methods Phys. Res. 219, 192–195.

Takiue, M., Natake, T., Hayashi, M., Yoshizawa, Y., 1985. Analytical subtraction of chemiluminescence counts for dual-labeled samples in liquid scintillation measurement. Int. J. Appl. Radiat. Isot. 36, 285–289.

Takiue, M., Natake, T., Fujii, H., Ishikawa, H., 1986a. Modification of a dual-label analysis data processing system for chemiluminescence corrections in liquid scintillation counting. Nucl. Instrum. Methods Phys. Res. Sect. A 247, 395–398.

Takiue, M., Fujii, H., Aburai, T., Ishikawa, H., 1989a. Usefulness of water-soluble paper for smear test of low-energy β- and α-emitters using a liquid scintillation technique. Health Phys. 56, 367–371.

Takiue, M., Natake, T., Fujii, H., 1989b. Nuclide identification of β-emitter by a double ratio technique using a liquid scintillation counter. Nucl. Instrum. Methods Phys. Res. Sect. A 274, 345–348.

Takiue, M., Fujii, H., Homma, Y., 1990a. Reliability of the activity determined by the quenching correction method for two groups of emulsion scintillators. Appl. Radiat. Isot. 41, 195–198.

Takiue, M., Matsui, Y., Natake, T., Yoshizawa, Y., 1990b. A new approach to analytical radioassay of multiple beta-labeled samples using a liquid scintillation spectrometer. Nucl. Instrum. Methods Phys. Res. Sect. A 293, 596–600.

Takiue, M., Matsui, Y., Fujii, H., 1991a. Activity determination of simultaneously chemical and color quenched samples using a liquid scintillation counter. Appl. Radiat. Isot. 42 (3), 241–244.

Takiue, M., Matsui, Y., Fujii, H., 1991b. Liquid scintillation radioassay for multiple radionuclide mixtures by the most probable value theory. J. Radioanal. Nucl. Chem. 152, 227–236.

Takiue, M., Fujii, H., Natake, T., Matsui, Y., 1991c. Analytical measurements of multiple beta-emitter mixtures with a liquid scintillation spectrometer. J. Radioanal. Nucl. Chem. Letters 155, 183–193.

Takiue, M., Matsui, Y., Natake, T., Fujii, H., 1992. Nuclide identification of pure-beta emitter mixtures with liquid scintillation spectrometry. Appl. Radiat. Isot. 43, 853–857.

Takiue, M., Natake, T., Fujii, H., 1995. Liquid scintillation radioassay for low-activity beta-emitter mixtures by the method of least squares. J. Radioanal. Nucl. Chem. Letters 200, 247–258.

Takiue, M., Natake, T., Fujii, H., 1999. A hybrid radioassay technique for multiple beta-emitter mixtures using liquid and NaI(Tl) scintillation spectrometers. Appl. Radiat. Isot. 51, 429–434.

Takiue, M., Yoshizawa, Y., Fujii, H., 2004. Cerenkov counting of low-energy beta-emitters using a new ceramic with high refractive index. Appl. Radiat. Isot. 61, 1335–1337.

Tanaka, M., Doke, T., Hitachi, A., Kato, T., Kikuchi, J., Masuda, K., Murakami, T., Nishikido, F., Okada, H., Ozaki, K., Shibamura, E., Yoshihira, E., 2001. LET dependence of scintillation yields in liquid xenon. Nucl. Instrum. Methods Phys. Res. Sect. A 457, 454–463.

Tarancón, A., García, J.F., Rauret, G., 2002a. Mixed waste reduction in radioactivity determination by using plastic scintillators. Anal. Chim. Acta 463, 125–134.

Tarancón, A., Alonso, E., García, J.F., Rauret, G., 2002b. Comparative study of quenching correction procedures for ^{90}Sr/^{90}Y determination by Cerenkov, liquid scintillation and plastic scintillation techniques. Anal. Chim. Acta 471, 135–143.

Tarancón, A., García, J.F., Rauret, G., 2003. Reusability of plastic scintillators used in beta emitter activity determination. Appl. Radiat. Isot. 59, 373–376.

Tarancón, A., García, J.F., Rauret, G., 2004. Determination of beta emitters (^{90}Sr, ^{14}C and ^{3}H) in routine measurements using plastic scintillation beads. Nucl. Instrum. Methods Phys. Res. Sect. A 516, 602–609.

Tarancón, A., García, J.F., Rauret, G., 2007. First approach to radionuclide mixtures quantification by using plastic scintilaltors. Influence of the diameter of the plastic beads. Anal. Chim. Acta 590, 232–238.

Tarancón Sanz, A., Kossert, K., 2011. Application of a free parameter model to plastic scintillation samples. Nucl. Instrum. Methods Phys. Res. Sect. A 648 (1), 124–131.

Tarancón Sanz, A., Bagán, H., Kossert, K., Nähle, O., 2011. Application of a free parameter model to plastic scintillation samples. In LSC 2010, Advances in Liquid Scintillation Spectrometry. Radiocarbon, University of Arizona, Tucson.

Tauler, R., Izquierdo-Ridorsa, A., Casassas, E., 1991. Comparison of multivariate calibration methods applied to the spectrophotometric study of mixtures of purine and pyrimidine bases. An. Quím. 87, 571–579.

TenBrook, P.L., Tjeerdema, R.S., 2006. Biotransformation of clomazone in rice (*Oryza sativa*) and early watergrass (*Echinochloa oryzoides*). Pest. Biochem. Physiol. 85, 38–45.

Teresa, M., Robela, C.P., Camargo, I.M.C., Oliveira, J.E., Bartolini, P., 2000. Single-step purification of recombinant human growth hormone (hGH) directly from bacterial osmotic shock fluids, for the purpose of ^{125}I-hGH preparation. Protein Expression Purif. 18 (2), 115–120.

Terlikowska, T., Cassette, P., Péron, M.N., Broda, R., Hainos, D., Tartes, I., Kempisty, T., 1998. Study of the stability of 63Ni sources in Ultima Gold® liquid scintillation cocktail. Appl. Radiat. Isot. 49 (9–11), 1041–1047.

Theodórsson, P. (2006). Determining fundamental parameters of a single-phototube liquid scintillation counter., p. 449. In "LSC 2005. Advances in Liquid Scintillation Spectrometry". (S. Chałupnik, F. Schönhofer, J. Noakes. (Eds.) Radiocarbon, The University of Arizona, Tucson, pp 99–107.

Theodórsson, P., Gudjonsson, G. I. (2006). Number of cathode electrons per absorbed energy in liquid scintillation counters, derived from resolution of radon spectra. pp 109–114. In "LSC 2005. Advances in Liquid Scintillation Spectrometry". (S. Chałupnik, F. Schönhofer, J. Noakes. (Eds.) Radiocarbon, The University of Arizona, Tucson, p. 449.

Theodórsson, P., Gudjonsson, G. I. (2003). A simple and sensitive liquid scintillation counting system for continuous monitoring of radon in water. pp. 249–252, In "LSC 2001. Advances in Liquid Scintillation Spectrometry". (S. Möbius, J.E. Noakes, F. Schönhofer. (Eds.), Radiocarbon, The University of Arizona, Tucson, p. 456.

Theodórsson, P., Skripkin, V. (2003). Measuring environmental tritium bound in benzene using a single-photomultiplier tube LSC system. pp. 41–44. In "LSC 2001. Advances in Liquid Scintillation Spectrometry". (S. Möbius, J.E. Noakes, F. Schönhofer. (Eds.), Radiocarbon, The University of Arizona, Tucson, p. 456.

Theodórsson, P., Sigurdsson, K., Jónsson, G. (2006). A portable, single-phototube liquid scintillation system with automatic sample changing. pp. 115–118. In "LSC 2005. Advances in Liquid Scintillation

Spectrometry". (S. Chałupnik, F. Schönhofer, J. Noakes. (Eds.) Radiocarbon, The University of Arizona, Tucson, p. 449.
Thomas, D.J., 2010. Neutron spectrometry. Radiat. Meas. 45, 1178–1185.
Thomas, E.V., Haaland, D.M., 1990. Comparison of multivariate calibration methods for quantitative spectral analysis. Anal. Chem. 62, 1091–1099.
Thomas, R.C., Judy, R.W., Harpvotlian, H., 1965. Dispenser for addition of internal standard in liquid scintillation counting. Anal. Biochem. 13, 358–360.
Thomson, J., 1991. Di-isopropylnaphthalene – A new solvent for liquid scintillation counting. In: Harley Ross, Noakes, John E., Spaulding, Jim D. (Eds.), Liquid Scintillation Counting and Organic Scintillators. Lewis Publishers, Chelsea, MI 48118, pp. 19–34.
Thorngate, J.H., McDowell, W.J., Christian, D.J., 1974. An application of pulse shape discrimination to liquid scintillation counting. Health Phys. 27, 123–126.
Toribio, M., García, J.F., Izquierdo-Ridorsa, A., Tauler, R., Rauret, G., 1995. Simultaneous determination of plutonium alpha emitters by liquid scintillation counting using multivariate calibration. Anal. Chim. Acta 310, 297–305.
Toribio, M., García, J.F., Izquierdo-Ridorsa, A., Rauret, G. (1996). Optimization of counting conditions and simultaneous determination of ^{238}Pu, ^{239}Pu and ^{240}Pu by liquid scintillation counting. In Liquid Scintillation Spectrometry 1994 (G.T. Cook, D.D. Harkness, A.B. MacKenzie, B.F. Miller, E.M. Scott. (Eds.), Radiocarbon 1996, 157–165.
Toribio, M., García, J.F., Izquierdo-Ridorsa, A., Rauret, G., 1997. Multivariate calibration and spectrum position correction for simultaneous determination of alpha and beta emitting plutonium isotopes by liquid scintillation. Anal. Chim. Acta 356, 41–50.
Toribio, M., Padró, A., García, J.F., Rauret, G., 1999. Determination of mixtures of alpha emitting isotopes (^{242}Pu, $^{239+240}$Pu, ^{238}Pu) by using liquid scintillation-moving curve fitting. Anal. Chim. Acta 380, 83–92.
Uchiyama, Y., 2010. Gamma ray resonstruction with liquid xenon calorimeter for the MEG experiment. Nucl. Instrum. Methods Phys. Res. Sect. A 617, 118–119.
Ueshima, K., et al. and the XMASS Collaboration. (2008). Scintillation yield of liquid xenon at room temperature. Nucl. Instrum. Methods Phys. Res. Sect. A 594, 148–154.
Vajda, N., Kim, C.-K., 2010. Determination of Pu isotopes by alpha spectrometry: a review of analytical spectrometry. J. Radioanal. Nucl. Chem. 283, 203–223.
Van Cauter, S., Roessler, N., 1991. Modern techniques for quench correction and DPM determination in windowless liquid scintillation counting: a critical review. In: Ross, Harley, Noakes, John E., Spaulding, Jim D. (Eds.), Liquid Scintillation Counting and Organic Scintillators. Lewis Publishers, Chelsea, MI 48118, pp. 219–237.
Van Wyngaardt, W.M., Simpson, B.R.S., 2006a. A simple counting technique for measuring mixtures of two pure β-emitting radionuclides. Nucl. Instrum. Methods Phys. Res. Sect. A 564, 339–346.
Van Wyngaardt, W.M., Simpson, B.R.S., 2006b. Absolute activity measurement of the electron-capture-dased radionuclides ^{139}Ce, ^{125}I, ^{192}Ir and ^{65}Zn by liquid scintillation coincidence counting. Appl. Radiat. Isot. 64, 1454–1458.
Van Wyngaardt, W.M., Simpson, B.R. S. (2009). Standardization of sulfur-35 by the TDCR efficiency calculation technique. pp. 173–181, In "LSC 2008, Advances in Liquid Scintillation Spectrometry". Radiocarbon, University of Arizona, Tucson. p. 445.
Van Wyngaardt, W.M., Simpson, B.R.S., Jackson, G.E., 2008. Further investigations of a simple counting technique for measuring mixtures of two pure β-emitting radionuclides. Appl. Radiat. Isot. 66, 1012–1020.
Varlam, C., Stefanescu, I., Duliu, O.G., Faurescu, I., Popescu, I., 2009. Applying direct liquid scintillation counting to low level tritium measurement. Appl. Radiat. Isot. 67, 812–816.
Varmuza, K., Filmoser, P., 2009. Introduction to Multivariate Statistical Analysis in Chemometrics. CRC Press, p. 336.
Varlam, C., Stefanescu, I., Duliu, O.G., Faurescu, I., Popescu, I., 2009. Applying direct liquid scintillation counting to low level tritium measurement. Appl. Radiat. Isot. 67, 812–816.
Vartsky, D., Goldberg, M.B., Breskin, A., Chechik, R., Guerard, B., Clergeau, J.F., 2003. Largearea imaging detector for neutron scattering based on boron-rich liquid scintillator. Nucl. Instrum. Methods Phys. Res. Sect. A 504, 369–373.
Venkataramanan, S., Gupta, A., Golda, K.S., Singh, H., Kumar, R., Singh, R.P., Bhowmik, R.K., 2008. A compact pulse shape discriminator module for large neutron detector arrays. Nucl. Instrum. Methods Phys. Res. Sect. A 596, 248–252.
Vera Tomé, F., Gómez Escobar, V., Martín Sánchez, A., 2002. Study of the peak shape in alpha spectra measured by liquid scintillation. Nucl. Instrum. Methods Phys. Res. Sect. A 485 (3), 444–452.
Véronneau, C., Aupiais, J., Dacheux, N., 2000. Selective determinatioin of polonium by photon electron rejecting alpha liquid scintillation (PERALS system). Anal. Chim. Acta 415, 229–238.
Verrezen, F., Hurtgen, C., 1996. Radioassay of low-level, low-energy beta activity in multilabeled samples containing high-energy beta impurities using liquid scintillation spectrometry. Radiocarbon, 381–389.
Verrezen, F., Hurtgen, C., 2000. A multiple window deconvolution technique for measuring low-energy beta activity in samples contaminated with high-energy beta impurities using liquid scintillation spectrometry. Appl. Radiat. Isot. 53, 289–296.
Verrezen, F., Loots, H., Hurtgen, C., 2008. A performance comparison of nine selected liquid scintillation cocktails. Appl. Radiat. Isot. 66, 1038–1042.
Verzilov, Y., Curtius, H., Fachinger, J. (2002). Determination of alpha/beta radionuclides in concentrated salt brines from fuel leaching by liquid scintillation spectrometry using solvent extraction. pp. 379–388, In "LSC 2001, Advances in Liquid Scintillation Spectrometry". (S. Möbius, J. Noakes, F. Schönhofer. (Eds.) Radiocarbon, University of Arizona, Tucson, p. 456.
Villano, A.N., Becchetti, F.D., Kolata, J.J., Ojaruega, M., Roberts, A., 2011. Efficiency measurements of deuterated liquid scintillators using d(d, n)^{3}He coincidence events. Nucl. Instrum. Methods Phys. Res. Sect. A 652 (1), 280–283.
Vincze, Á, Solymosi, J., Kása, I., Sáfrány, Á, 2007. Extractive-scintillating resin produced by radiation polymerization. Radiat. Phys. Chem. 76, 1395–1398.
Viteri, F.E., Kohaut, B.A., 1997. Improvement of the Eakins and Brown method for measuring ^{59}Fe and ^{55}Fe in blood and other iron-containing materials by liquid scintillation counting and sample preparation using microwave digestion and ion-exchange column purification of iron. Anal. Biochem. 244 (1), 116–123.
Walton, T.D., 1996. Implementation of a Robotics System for High Throughput Screening Utilizing Glow Luminescence. TopCount Topics, TCA-026. PerkinElmer, Inc, p. 6. available at http://las.perkinelmer.co.uk/content/applicationnotes/app_topcountimplroboticshts.pdf available at.
Wanke, C., Kossert, K., Nähle, O.J., Ott, O., 2010. Activity standardization and decay data of ^{64}Cu. Appl. Radiat. Isot. 68, 1297–1302.
Warwick, P.E., Croudace, I. W. (2002). Measurement of gross alpha and beta activities in acid leachates using alpha-beta discriminating liquid scintillation counting. pp. 75–82, In "LSC 2001, Advances in Liquid Scintillation Spectrometry". (S. Möbius, J. Noakes, F. Schönhofer. (Eds.) Radiocarbon, University of Arizona, Tucson, p. 456.
Warwick, P.E., Croudace, I.W., 2006. Isolation and quantification of ^{55}Fe and ^{63}Ni in reactor effluents using extraction chromatography and liquid scintillation analysis. Anal. Chim. Acta 567, 277–285.
Warwick, P.E., Kim, D., Croudace, I.W., Oh, J., 2010. Effective desorption of tritium from diverse solid matrices and its application to routine analysis of decommissioning materials. Anal. Chim. Acta 676, 93–102.
Wakabayashi, G., Ohura, H., Okai, T., Matoba, M., Nohtomi, A., Kakiuchi, H., Momoshima, N., Kawamura, H., 1999. Simple measurement of ^{14}C in the environment using a gel suspension method. J. Radioanal. Nucl. Chem. 239 (3), 639–642.
Wätjen, U., Szántó, Zs., Altzitzoglou, T., Sibbens, G., Keightley, J., Hult, M., 2006. EC intercomparisons for laboratories monitoring environmental radioactivity. Appl. Radiat. Isot. 64, 1108–1113.
Weekley, J.C., Wuenschel, S., Rosenstiel, P.E., Mumper, R.J., Jay, M., 2004. Aqueous liquid scintillation counting with fluor-containing nanosuspensions. Appl. Radiat. Isot. 60, 887–891.
Wells, J.M., Thomas, J., Boddy, L., 2001. Soil water potential shifts: developmental responses and dependence on phosphorus translocation by the

saprotrophic, cord-forming basidiomycete Phanerochaete velutina. Mycol. Res. 105 (7), 859–867.

Werth, M., Kuzyakov, Y., 2008. Root-derived carbon in soil respiration and microbial biomass determined by ^{14}C and ^{13}C. Soil Biol. Biochem. 40, 625–637.

Wiebe, L.I., McQuarrie, S.A., Ediss, C., 1980. In: Peng, C.-T., Horrocks, D.L., Alpen, E.L. (Eds.), Liquid Scintillation Counting, Recent Applications and Development, Vol. 1. Academic Press, New York and London, pp. 81–87.

Wiegand, C., Pehkonen, S., Akkanen, J., Penttinen, O.-P., Kukkonen, J.V.K., 2007. Bioaccumulation of paraquat by *Lumbriculus variegatus* in the presence of dissolved natural organic matter and impact on energy costs, biotransformation and antioxidative enzymes. Chemosphere 66, 558–566.

Wiesenberg, G.L.B., Gocke, M., Kuzyakov, Y., 2010. Fast incorporation of root-derived lipids and fatty acids into soil – Evidence from a short term $^{14}CO_2$ pulse labelling experiment. Organic Geochem. 41, 1049–1055.

Wigfield, D.C., Cousineau, C.M.E., 1978. Some empirical observations concerning the liquid scintillation counting of coloured solutions. Can. J. Chem. 56, 2173–2177.

Williams, M., Kookana, R., 2010. Isotopic exchangeability as a measure of the available fraction of the human pharmaceutical carbamazepine in river sediment. Sci. Total Environ. 408, 3689–3695.

Winyard, R.A., Lutkin, J.E., McBeth, G.W., 1971. Pulse shape discrimination in inorganic and organic scintillators. Nucl. Instrum. Methods 95 (1), 141–153.

Wise, B.M., 1992. PLS-Toolbox for use with MATLAB™. Center for Process Analytical Chemistry (CPAC). University of Washington, Seattle.

Wisser, S., Frenzel, E., Dittmer, M., 2006. Innovative procedure for the determination of gross-alpha/gross-beta activities in drinking water. Appl. Radiat. Isot. 64, 368–372.

Wolle, B., Beikert, G., Gadelmeier, F., 1999. Effect of anisotropic D–D fusion neutron emission on counter calibration using activation techniques. Nucl. Instrum. Methods Phys. Res. Sect. A 424, 561–568.

Wolterbeek, H., Th., van der Meer, A.J.G.M., 2002. Transport rate of arsenic, cadmium, copper and zinc in *Potamogeton pectinatus* L.: radiotracer experiments with ^{76}As, $^{109,115}Cd$, ^{64}Cu and $^{65,69m}Zn$. Sci. Total Environ. 287, 13–30.

Wong, C.T., Soliman, V.M., Perera, S.K., 2005. Gross alpha/beta analysis in water by liquid scintillation counting. J. Radioanal. Nucl. Chem. 264 (2), 357–363.

Xiques Castillo, A., Isaac Olivé, K., Casanova González, E., Beckford, D., Leyva Montaña, R., Montero Álvarez, A., Olivé Álvarez, E., 2009. An adapted purification procedure to improve the quality of ^{90}Y for clinical use. Radiochim. Acta 97, 739–746.

Xiques Castillo, A., Pérez-Malo, M., Isaac-Olivé, K., Mukhallalati, H., Casanova González, E., Torres Berdeguez, M., Cornejo Díaz, N., 2010. Production of large quantities of ^{90}Y by ion-exchange chromatography using an organic resin and a chelating agent. Nucl. Med. Biol. 37 (8), 935–942.

Yamada, Y., Yasuike, K., Itoh, M., Kiriyama, N., Komura, K., 2004. Temporal variation of tritium concentration in tree-ring cellulose. J. Radioanal. Nucl. Chem. 261 (1), 9–17.

Yan, C.G., 1996. Improvement of accuracy of efficiency extrapolation method in $4\pi\beta$-γ coincidence counting. Nucl. Instrum. Methods Phys. Res. Sect. A 369, 383–387.

Yang, D. (1996). Calibration and quench correction for alpha liquid scintillation analysis. pp. 339–344, In "Liquid Scintillation Spectrometry 1994" (G.T. Cook, D.D. Harkness, A.B. MacKenzie, B.F. Miller, E.M. Scott. (Eds.), Radiocarbon, University of Arizona, Tucson.

Yang, D., Guo, Y., 1995. Determination of Alpha Radioactivity in Vegetable Ashes with Liquid Scintillation Analysis. Alpha Beta Application Note, ABA-007. Packard BioScience Company, Meriden, CT 06450, p. 4.

Yang, D., Zhu, Y., Mobius, S., 1992. Rapid Method for Alpha Counting with Extractive Scintillator and Pulse Decay Analysis. Alpha Beta Application Note, ABA-002. Packard BioScience Company, Meriden, CT 06450, p. 8.

Yang, D., Zhu, Y., Jiao, R., 1994. Determination of Np, Pu and Am in high level radioactive waste with extraction-liquid scintillation counting. J. Radioanal. Nucl. Chem. 183, 245–260.

Yasuoka, Y., Ishii, T., Sanada, T., Nitta, W., Ishimori, Y., Kataoka, Y., Kubo, T., Suda, H., Tokonami, S., Ishikawa, T., Shinogi, M., 2005. Measurement of radon concentration in water using direct dpm method of liquid scintillation counter. Intern. Congr. Series 1276, 299–300.

Yeh, M., Cumming, J.B., Hans, S., Hahn, R.L., 2010. Purification of lanthanides for large neutrino detectors: thorium removal from gadolinium chloride. Nucl. Instrum. Methods Phys. Res. Sect. A 618, 124–130.

Yi-Fen, Y., Bowman, J.D., Bolton, R.D., Crawford, B.W., et al., 2000. A high-rate ^{10}B-loaded liquid scintillation detector for parity-violation studies in neutron resonances. Nucl. Instrum. Methods Phys. Res. Sect. A 447, 476–489.

Yoon, S., Chang, B.U., Kim, Y., Byun, J.I., Yun, J.Y., 2010. Indoor radon distribution of subway stations in a Korean major city. J. Environ. Radioact. 101, 304–308.

Yoshida, S., Ebihara, T., Yano, T., Kozlov, A., Kishimoto, T., Ogawa, I., Hazama, R., Umehara, S., Mukaida, K., Ichihara, K., Hirano, Y., Murata, I., Datemichi, J., Sugimoto, H., 2010. Light output response of KamLAND liquid scintillator for protons and ^{12}C nuclei. Nucl. Instrum. Methods Phys. Res. Sect. A 622, 574–582.

Yoshikawa, H., Nakanishi, T., Nakahara, H., 2006. Determination of thoron and radon ratio by liquid scintillation spectrometry. J. Radioanal. Nucl. Chem. 267 (1), 195–203.

Yousefi, S., Lucchese, L., Aspinall, M.D., 2009. Nucl. Instrum. Methods Phys. Res. Sect. A 598, 551–555.

Yu, C.S., Chiang, L.W., Wu, C.H., Wang, R.T., Chen, S.W., Wang, H.Y., Yeh, C.H., 2006. Synthesis of 5-radioiodoarabinosyl uridine analog for probing HSV-1 thymidine kinase gene: an unexpected chelating effect. Nucl. Med. Biol. 33, 367–370.

Zak, T., Clarke, S.D., Bourne, M.M., Pozzi, S.A., Xu, Y., Downar, T.J., Peerani, P., 2010. Neutron spectroscopy of plutonium oxide using matrix unfolding approach. Nucl. Instrum. Methods Phys. Res. Sect. A 622, 191–195.

Zecher, P.D., Galonsky, A., Kruse, J.J., Gaff, S.J., Ottarson, J., Wang, J., Deák, F., Horváth, A., Kiss, A., Seres, Z., Ieki, K., Iwata, Y., Schelin, H., 1997. A large area, position-sensitive neutron detector with neutron/γ-ray discrimination capabilities. Nucl. Instrum. Methods Phys. Res. Sect. A 401, 329–344.

Zheng, Q., Bobich, J.A., 2004. ADP-ribosylation factor6 regulates both [^3H]-noradrenaline and [^{14}C]-glutamate exocytosis through phosphatidylinositol 4,5-biphosphate. Neurochem. Internat. 45, 633–640.

Zheng, Q., McFadden, S.C., Bobich, J.A., 2004. Phosphatidylinositol 4,5-biphosphate promotes both [^3H]-noradrenaline and [^{14}C]-glutamate exocytosis from nerve endings. Neurochem. Internat. 44, 243–250.

Zhilin, C., Shixiong, X., Heyi, W., Ruimin, C., Guanyin, W., Yinhang, Z., 2010. The effect of vial type and cocktail quantity on tritium measurement in LSC. Appl. Radiat. Isot. 68, 1855–1858.

Zhu, D., Mu, Z., Mooty, C., Kovarik, M., Jay, M., 2006. Suspensions of fluor-containing nanoparticles for quantifying β^--emitting radionuclides in non-hazardous media. J. Pharm. Innov. 1 (1), 76–82.

Zhu, D., Jay, M., 2007. Aqueous polystyrene-fluor nanosuspensions for quantifying α and β^- radiation. Nanotechn. 18 (22), 225502.

Zimmerman, B.E., 2006a. Monte Carlo calculations of spectra and interaction probabilities for photons in liquid scintillators for use in the standardization of radiionuclides. Appl. Radiat. Isot. 64, 1492–1498.

Zimmerman, B.E., 2006b. Radionuclide metrology in the life sciences: recent advances and future trends. Appl. Radiat. Isot. 64, 1351–1359.

Zimmerman, B.E., Collé, R., 1997a. Comparison of the French and U.S. National ^3H (tritiated H_2O) standards by $4\pi\beta$ liquid scintillation spectrometry. Appl. Radiat. Isot. 48, 521–526.

Zimmerman, B.E., Collé, R., 1997b. Cocktail volume effects in $4\pi\beta$ liquid scintillation spectrometry with ^3H-standard efficiency tracing for low-energy β-emitting radionuclides. Appl. Radiat. Isot. 48 (3), 365–378.

Zimmerman, B.E., Cessna, J.T., 1999. The standardization of ^{62}Cu and experimental determinations of dose calibrator settings for generator-produced $^{62}CuPTSM$. Appl. Radiat. Isot. 51, 515–526.

Zimmerman, B.E., Cessna, J.T., Schima, F.J., 1998. The standardization of the potential bone palliation radiopharmaceutical ^{117m}Sn(+4)DTPA. Appl. Radiat. Isot. 49 (4), 317−328.

Zimmerman, B.E., Unterweger, M.P., Brodack, J.W., 2001. The standardization of ^{177}Lu by $4\pi\beta$ liquid scintillation spectrometry with ^{3}H-standard efficiency tracing. Appl. Radiat. Isot. 54, 623−631.

Zimmerman, B.E., Cessna, J.T., Unterweger, M.P., 2002. The standardization of ^{188}W/^{188}Re by $4\pi\beta$ liquid scintillation spectrometry with the CIEMAT/NIST ^{3}H-standard efficiency tracing method. Appl. Radiat. Isot. 56, 315−320.

Zimmerman, B.E., Collé, R., Cessna, J.T., 2004. Construction and implementation of the NIST triple-to-double coincidence ratio (TDCR) spectrometer. Appl. Radiat. Isot. 60, 433−438.

Zimmerman, B.E., Cessna, J.T., Millican, M.A., 2004. Experimental determination of calibration settings for plastic syringes containing solutions of ^{90}Y using commercial radionuclide calibrators. Appl. Radiat. Isot. 60, 511−517.

Zimmerman, B.E., Cessna, J.T., Fitzgerald, R., 2008. Standardization of ^{68}Ge/^{68}Ga using three liquid scintillation counting based methods. J. Res. Natl. Inst. Stand. Technol. 113 (5), 265−280.

Zimmerman, B.E., Altzitzoglou, T., Rodrigues, D., Broda, R., Cassette, P., Mo, L., Ratel, G., Simpson, B., van Wyngaardt, W., Wätjen, C., 2010. Comparison of triple-to-double coincidence ratio (TDCR) efficiency calculations and uncertainty assessments for ^{99}Tc. Appl. Radiat. Isot. 68, 1477−1481.

Zuber, K., 2000. Double beta decay and large scale Yb-loaded scintillators. Phys. Letts. B 485, 23−26.